

PETROLOGISCHE UND GEOCHEMISCHE UNTERSUCHUNGEN AN
MAGMATISCHEN GESTEINEN DER GARDAR-PROVINZ,
SÜDGRÖNLAND

Dissertation

zur Erlangung des Grades eines Doktors der Naturwissenschaften

der Geowissenschaftlichen Fakultät

der Eberhard-Karls-Universität Tübingen

vorgelegt von

RALF HALAMA

aus Frankenthal/Pfalz

2003

Tag der mündlichen Prüfung: 19. Dezember 2003
Dekan: Prof. Dr. Dr. h. c. M. Satir
1. Berichterstatter: Prof. Dr. G. Markl
2. Berichterstatter: Prof. Dr. H. Keppler

Einführung

Die vorliegende Arbeit entstand am Institut für Geowissenschaften der Universität Tübingen im Rahmen des von der DFG geförderten Projektes „*Differentiationsprozesse alkalischer bis peralkalischer Magmen, untersucht an Intrusivkomplexen der Gardar-Provinz in Südgrönland*“ (Antragsteller Prof. G. Markl). Basierend auf der Untersuchung unterschiedlich stark differenzierter Magmatite der Gardar-Provinz mit Hilfe moderner petrologischer, geochemischer und isotopengeochemischer Methoden wurden unter anderem die folgenden Fragestellungen bearbeitet:

- Welche spezifischen Mantelquellen können für die primären Schmelzen der Gardar-Magmatite identifiziert werden? Welchen Einfluß hat dabei krustale Kontamination auf die chemische Zusammensetzung der Ursprungsschmelzen und Differentiationsprozesse während des Aufstiegs?
- Welche Phasengleichgewichte bestimmen die Differentiation von alkalibasaltischen zu alkalisyenitischen, agpaitischen und karbonatitischen Magmen und wie hängen diese Phasengleichgewichte mit der Geochemie der Schmelzen zusammen? Wie wird die Differentiation von intensiven Parametern wie a_{SiO_2} und f_{O_2} beeinflusst?
- In welchem Zusammenhang stehen die alkalisyenitischen Gesteine des Grønnedal-Ika-Komplexes zu den Karbonatiten und welche Schlußfolgerungen ergeben sich daraus für die Genese von Kalzium-Karbonatiten im Allgemeinen?
- Wie ist die Verteilung wichtiger Haupt- und Spurenelemente zwischen der Schmelze, den verschiedenen Festphasen und der/den fluiden Phasen während unterschiedlicher Stadien der Fraktionierung?

Die Ergebnisse dieser Untersuchungen sind dabei nicht nur von regionaler Bedeutung für die Gardar-Provinz, sondern tragen allgemein zum besseren Verständnis der Genese und Differentiation alkalischer Magmen in Riftzonen bei.

Die vorliegende Arbeit umfaßt fünf Kapitel, von denen jedes einem bei einer internationalen Fachzeitschrift eingereichten oder bereits gedruckten Manuskript entspricht. Der nun folgenden Zusammenfassung und jedem Einzelkapitel ist ein spezifisches Literaturverzeichnis angeschlossen, um das Auffinden der verwendeten Literatur zu erleichtern.

Geologische Übersicht

Der südliche Teil Grönlands besteht zu einem großen Teil aus archaischen Gesteinseinheiten, die 3.75 bis 2.5 Ga alt sind und seit dieser Zeit nicht mehr von tektonischen und magmatischen Aktivitäten beeinflusst wurden (Escher & Watt, 1976). Hauptsächlich handelt es sich dabei um Orthogneise, aber es treten auch metavulkanische Amphibolite, Paragneise, Anorthosite und assoziierte mafische Magmatite auf. Südlich an den archaischen Block schließt sich der Ketilidische Gürtel an, der durch das Auftreten großer granitoider Plutone charakterisiert ist. Diese entstanden vor etwa 1.85-1.80 Ga, als ozeanische Kruste unter den archaischen Kraton subduziert wurde (van Breemen et al., 1974; Garde et al., 2002). Im Zentralbereich des Ketilidischen Gürtels dominieren kalkalkaline Granitgneise, Diorite und Granite, die zusammengefaßt als Julianehåb Batholit bekannt sind. Am nördlichen Rand des Ketilidischen Gürtels treten z.T. metamorph überprägte Sedimente und Vulkanite auf, während südlich des Julianehåb Batholits neben Graniten und Gneisen auch migmatitische Metasedimente und Metavulkanite sowie Rapakivi-Granite vorkommen.

Die erodierten Granitoide des Ketilidischen Gürtels werden überlagert von kontinentalen Sandsteinen und dazwischengeschalteten, überwiegend basaltischen Laven (Poulsen, 1964). Diese etwa 3500 m mächtige Sequenz von Suprakrustalgesteinen (Eriksfjord Formation) ist meist in von Störungen begrenzten Zonen zu finden, man nimmt aber an, dass sie viel weiter verbreitet war (Escher & Watt, 1976). Die Extrusion der Basalte wurde begleitet von der Intrusion von Gangschwärmen und einer Serie von alkalinen magmatischen Komplexen in das ketilidische und zum Teil auch in das archaische Grundgebirge. Wegmann (1938) war der erste, der die jüngeren Sedimente, Vulkanite und Intrusivkomplexe zu einer tektono-magmatischen Episode zusammenfaßte und sie Gardar-Gesteine nannte. Der Name Gardar stammt von dem alten nordischen Bistum *Gardur*, das sich dort befand, wo heute die Ortschaft Igaliko liegt.

Die präkambrischen Gesteine Südgrönlands können als Fortsetzung des kanadischen Schildes betrachtet werden, mit ähnlichen tektonischen Einheiten und orogenen Phasen zu etwa den gleichen Zeiten (Bridgwater, 1967). Beispielsweise treten im Archaischen Kraton Südgrönlands ähnliche Gesteine auf wie in Labrador. Auch die auf 1282 ± 5 Ma datierten Olivin-Dolerite der Gardar-Periode (Upton et al., 2003) können zeitlich mit dem Mackenzie Gangschwarm (LeCheminant &

Heaman, 1989) und dem Harp Gangschwarm (Cadman et al., 1993) auf dem kanadischen Schild korreliert werden. Während die heute in Kanada aufgeschlossenen Einheiten unter Drücken von 3-5 kbar kristallisierten (Fuhrmann et al., 1988; Kolker & Lindsley, 1989), ergaben entsprechende Abschätzungen für die Gardar-Gesteine ~ 1 kbar (Konnerup-Madsen & Rose-Hansen, 1984). Dementsprechend kann die Gardar-Provinz als ein in einem höheren Krustenstockwerk aufgeschlossenes Segment des kanadischen Schildes angesehen werden.

Wichtige Zusammenfassungen über die magmatischen Gesteine der Gardar-Provinz, wurden von Upton (1974), Emeleus & Upton (1976), Upton & Emeleus (1987) und Upton et al. (2003) publiziert. Die Gardar-Provinz ist eine intrakontinentale Riftzone mittelproterozoischen Alters, in der die magmatische Aktivität von etwa 1.35 bis 1.14 Ga andauerte. In den 12 größeren alkalinen Komplexen treten gabbroische, nephelin-syenitische bis granitische und untergeordnet karbonatitische Gesteine auf. Auch die Ganggesteine können sehr unterschiedliche chemische Zusammensetzungen aufweisen. Die zwei wichtigsten Gangschwärme intrudierten in den Julianehåb-Batholit entlang WSW-ENE bis SW-NE streichender Trends in den Tugtutôq-Ilímaussaq und Nunarssuit-Isortoq Zonen etwa zwischen 1.20 und 1.14 Ga.

Die basaltischen Laven der Eriksfjord Formation und die gabbroischen Ganggesteine im Isortoq-Gebiet gehören zu den geochemisch primitivsten magmatischen Gesteinen der Provinz und sind deshalb von großer Bedeutung für die geochemische Zusammensetzung von Ursprungsmagmen. Sie werden in den Kapiteln 1 und 2 untersucht, insbesondere in Hinblick auf ihre Mantelquellen und den Einfluß krustaler Kontamination. Daneben werden die detaillierten Untersuchungen an einem der „Giant Dikes“ der Isortoq-Region dargestellt. Diese voluminösen Gänge, die mehrere 100 m Mächtigkeit und viele Kilometer Länge erreichen können, zeigen eine interne Fraktionierung von gabbroider zu syenitischer Fazies und werden als Übergangsglied zwischen Ganggesteinen und Intrusivkomplexen gedeutet (Bridgwater & Coe, 1970). Eine Besonderheit der Isortoq-Ganggesteine ist das häufige Auftreten von Feldspat-Megakristallen und Anorthosit-Xenolithen in gabbroischen Gängen, was als Hinweis auf einen Anorthositkörper in größerer Tiefe gedeutet wird (Bridgwater, 1967; Bridgwater & Harry, 1968). Mit diesen Gängen, die als „Big Feldspar Dikes“ (BFDs) bekannt sind, beschäftigt sich Kapitel 3. In Kapitel 4 geht es um die Entstehung und

Entwicklung des Grønnedal-Ika Komplexes, der zu den ältesten der großen Intrusivkomplexe gehört und gleichzeitig das größte Einzelvorkommen von Karbonatit in der Gardar-Provinz darstellt. Schwerpunktmäßig wird dabei erforscht, in welcher Beziehung die syenitischen zu den karbonatitischen Gesteinen stehen und wie sich die intensiven Kristallisationsparameter in den Syeniten Grønnedals von denen der anderen Komplexe unterscheidet. Dieser letzte Punkt wird auch in Kapitel 5 diskutiert, welches die Merkmale der Spurenelementgehalte –und Muster in mafischen Mineralen von drei ausgewählten Intrusionen behandelt. Neben den Nephelin-Syeniten Grønnedals, die den Fraktionierungstrend zur Syenit-Karbonatit-Assoziation repräsentieren, werden agpaitische Gesteine der Ilímaussaq-Intrusion als Beispiel für den Trend zur SiO₂-Untersättigung und Quarz-Syenite und Alkaligranite der Puklen-Intrusion als Beispiel für den Trend zur SiO₂-Übersättigung untersucht.

Zusammenfassung der Publikationen

Kapitel 1 und 2 befassen sich mit den petrologischen und isotopengeochemischen Studien an relativ primitiven Gesteinen der Gardar-Provinz. Diese sind gut geeignet, um die geochemischen Signaturen der Mantelquellen der Magmen zu charakterisieren. Ähnliche Quellen werden vermutlich auch eine Rolle in der Entstehung der stärker fraktionierten Gardar-Magmatite gespielt haben.

Die Basalte der Eriksfjord Formation (EF) sind Gegenstand der Untersuchungen in Kapitel 1. Zwei Sm-Nd Isochronenalter für die Basalte ergaben Alter von 1.17 ± 0.03 Ga und 1.20 ± 0.03 Ga (Paslick et al., 1993), aber paläomagnetische Studien weisen auf ein Alter von 1.35-1.31 Ga hin (Piper et al., 1999), so daß das exakte Alter der EF unbekannt ist (Upton et al., 2003). In Kapitel 2 werden die Ergebnisse der Arbeiten an den Ganggesteinen der Isortoq-Region vorgestellt. Die Ganggesteine des Isortoq-Gangschwarms stehen höchstwahrscheinlich in Verbindung zu dem Bangs Havn - Gangkomplex (Bridgwater & Harry, 1968), der auf 1185 ± 22 Ma datiert wurde (Engell & Pedersen, 1974). Dies ist in Übereinstimmung mit dem Ergebnis einer Sm-Nd 3-Punkt-Isochronendatierung dieser Studie, die ein Alter von 1190 ± 44 Ma ergab. Der Isortoq-Gangschwarm setzt sich aus petrographisch unterschiedlichen Gesteinen zusammen, die von Gabbro bis Syenit reichen, und ist

deshalb besonders gut geeignet, um einen möglichen Einfluß von krustaler Assimilation auf die Zusammensetzung intrakontinentaler mafischer Magmen zu untersuchen.

Generell ist die Erforschung von basaltischem Magmatismus in Zusammenhang mit kontinentalen Riftzonen wichtig für das Verständnis der chemischen Zusammensetzung der subkontinentalen Erdmantels und für die Mechanismen, die zur Bildung von Flutbasalten, Alkalimagmatiten und Karbonatiten führen. Die Untersuchung von proterozoischen Gesteinen, die mit Rift-Magmatismus assoziiert sind, gewährt Einblick in die Zusammensetzung des Mantels und das Zusammenspiel zwischen Magmenquellen im Erdmantel und in der Kruste zu dieser Zeit (z.B. Lightfoot et al., 1991). Darüber hinaus können mafische Gangschwärme zur Identifikation von Mantelplumes genutzt werden (Ernst & Buchan, 1997, 2001).

Mehrere unterschiedliche Mantelkomponenten können zum Rift-Magmatismus beitragen (z.B. Perry et al., 1987; Paces & Bell, 1989). Dabei kann die relative Bedeutung der verschiedenen Mantelquellen in Zeit und Raum sehr variabel sein (z.B. Shirey et al., 1994, Nicholson et al., 1997). Um die geochemische Signatur der Riftgesteine zu erklären, werden im Allgemeinen drei wichtige Mantelquellen diskutiert:

- Verarmter Mantel, der die wesentliche Mantelquelle der Basalte mittelozeanischen Rücken darstellt („Depleted MORB Mantle“ = DMM). Dieser Mantel ist verarmt an allen inkompatiblen Elementen, d.h. an den Elementen, die während des Aufschmelzes des Mantels bevorzugt in die Schmelze fraktionieren und weniger in den Festphasen aufgenommen werden.
- Mantel, der von ozeanischen Inselbasalten („Ocean Island Basalts“ = OIB) bekannt ist. Diese Mantelquelle ist in ozeanischen Regionen beschränkt auf Inseln, die nicht subduktionsbezogen sind. Im Vergleich zum primitiven Mantel ist sie weniger verarmt oder sogar angereichert an inkompatiblen Elementen. Man unterscheidet mehrere Typen von OIB-Komponenten, die durch Sr-Nd-Pb Isotopenstudien definiert wurden (Zindler & Hart, 1986; Hart et al., 1992). Diese sind HIMU („high μ “, $\mu \equiv {}^{238}\text{U}/{}^{206}\text{Pb}$), angereicherter Mantel 1 (EM-1) und angereicherter Mantel 2 (EM-2).
- Subkontinentaler lithospärischer Mantel, der gewöhnlich angereichert an inkompatiblen Elementen ist. Diese Mantelquelle kann sehr heterogen und regional unterschiedlich sein.

Spurenelementdaten und Sr-Nd Isotopendaten der EF Basalte weisen darauf hin, daß ein an inkompatiblen Spurenelementen verarmter Mantel keine signifikante Rolle in ihrer Entstehung gespielt hat. Seltenerd-Element (SEE)–Daten von Klinopyroxenen und Gesamtgesteinen sind eher vereinbar mit einer OIB-ähnlichen Mantelquelle. Die primitivsten Proben der EF Basalte weisen eine ähnliche initiale Sr-Nd-Isotopensignatur auf wie heutige OIBs und wie Karbonatite der Gardar-Provinz (Pearce & Leng, 1996; Andersen, 1997). Sowohl OIBs als auch Karbonatite werden oft mit Mantelplumes assoziiert (z.B. Bell, 2001), so dass spekuliert werden kann, dass die OIB-ähnlichen Mantelkomponenten in den EF Basalten von einer Mantelplumequelle stammen. Der Einfluß einer Plume-Quelle wird auch durch geologische Argumente gestützt. Interaktion mit dem subkontinentalen lithosphärischen Mantel kann aber anhand der vorliegenden Daten nicht ausgeschlossen werden.

Um den steilen Vektor der Datenpunkte der Basalte im Sr-Nd-Isotopenkorrelationsdiagramm zu erklären, wurden Modellierungen durchgeführt, mit deren Hilfe Trends basierend auf Assimilation und fraktionierender Kristallisation (Assimilation and Fractional Crystallization = AFC; DePaolo, 1981) berechnet werden können. Es zeigte sich, daß Assimilation von weniger als 5% Unterkrustenmaterial den steilen Trend erklären kann, wohingegen Assimilation von Oberkrustenmaterial unwahrscheinlich erscheint. Sauerstoffisotopendaten sind mit diesem Ergebnis kompatibel.

Für die mafischen Ganggesteine der Isortoq-Region zeigen geochemische und Sr-Nd-Os-O isotopengeochemische Daten, dass Assimilation von krustalem Material eine bedeutendere Rolle als bei den EF Basalten gespielt haben muß. Deswegen sind die geochemischen Mantelquellencharakteristika der Isortoq-Ganggesteine weniger gut zu definieren. Dennoch spricht, ähnlich wie bei den EF Basalten, die generelle Anreicherung von inkompatiblen Elementen und die Sr-Nd Isotopenzusammensetzungen der primitivsten Gesteine gegen eine signifikante Rolle des DMM in der Magmenentstehung. SEE-Muster in Klinopyroxenen zeigen ebenfalls keine Ähnlichkeit zu Mustern von Klinopyroxenen aus MORB-ähnlichen Gabbros. Sie sind aber den Mustern von Kumulus-Klinopyroxen in gabbroischen Gesteinen, die nach einem kontinentalen

Auseinanderdriften in Zusammenhang mit dem Island-Plume in Ostgrönland entstanden sind, sehr ähnlich (Bernstein et al., 1998). Ob die relative Anreicherung in inkompatiblen Elementen auf den Einfluß des subkontinentalen lithosphärischen Mantels (z.B. Condie et al., 1987; Boily & Ludden, 1991; Molzahn et al., 1996) oder eines angereicherten Mantelplumes (z.B. Walker et al., 1997; Puchtel et al., 1999) oder einer Mischung beider Quellen (z.B. Ellam et al., 1992; Gibson et al., 1995; Thompson et al., 1998) zurückzuführen ist, ist aber aufgrund der ausgeprägten krustale Kontamination in den Isortoq Ganggesteinen nicht zu entscheiden.

Dennoch können die Daten der Ganggesteine bezüglich der kontinentalen Kruste, die sie durchquert haben, interpretiert werden (Baker et al., 1998). Generell herrscht Übereinstimmung, dass mafische Magmen aus dem Mantel ein gewisses Maß an krustaler Kontamination während des Aufstiegs oder des Verbleibs in krustalen Magmenkammern erfahren (Mohr, 1987). Die Kruste ist sowohl Dichtefilter als auch Quelle von inkompatiblen Elementen (Lightfoot et al., 1991) und kann Ort großer Kontamination und/oder partieller Kristallisation von primitiven Schmelzen sein (O'Hara & Herzberg, 2002). Beispielsweise wurde Assimilation von Krustenmaterial als signifikant in der Entstehung von Flutbasalten erkannt (Devey & Cox, 1987; Peng et al., 1992, Baker et al., 2000).

Unsere Daten von Isortoq zeigen, daß das assimilierte Material relativ Silizium-reich gewesen sein muss, da der Anstieg in der Silica-Aktivität und im SiO_2 -Gehalt in einigen der Ganggesteine höher ist als man durch fraktionierende Kristallisation allein erwarten würde. Das Fehlen signifikanter negativer Eu-Anomalien deutet darauf hin, dass das assimilierte Material reich an Plagioklas gewesen sein muss. Isotopencharakteristika der krustalen Komponente beinhalten ein sehr niedriges $^{143}\text{Nd}/^{144}\text{Nd}$ und ein mittleres bis sehr niedriges $^{87}\text{Sr}/^{86}\text{Sr}$ -Verhältnis. Außerdem sind niedrige Nb-Gehalte, mittlere $\delta^{18}\text{O}$ -Werte und extrem radiogene Os-Isotopenzusammensetzungen für den potentiellen Kontaminanten angezeigt. Alle diese geochemischen Charakteristika sind kompatibel mit der Assimilation von partiellen Schmelzen von Archaischen granulitfaziellen Gneisen der Unterkruste, wie sie im Archaischen Kraton Südgrönlands aufgeschlossen sind. Mit EC-AFC-Modellierungen (Energy Constrained – Assimilation and Fractional Crystallization; Bohrson & Spera, 2001; Spera & Bohrson, 2001) konnte eine Quantifizierung des krustalen Beitrags vorgenommen werden. Diese Ergab eine Zufuhr von Unterkrustenmaterial von maximal 10% für

die am stärksten kontaminierten Gesteine. Dagegen zeigte sich, dass Assimilation von Oberkrustenmaterial, repräsentiert durch Granitoide des Julianehåb-Batholit, bei der Genese der meisten Ganggesteine kaum bedeutend gewesen sein kann, eventuell aber bei der Entstehung eines Hornblende-Syenit-Ganges eine Rolle gespielt hat. In Übereinstimmung mit seismischen Daten (Dahl-Jensen et al., 1998) kann deshalb gefolgert werden, daß archaische Gesteine in größerer Tiefe auch in der Isortoq-Region vorkommen und sich somit weiter nach Süden fortsetzen, als das gegenwärtige Erosionsniveau vermuten läßt. Kontamination mit Unterkrustenmaterial ist auch in Übereinstimmung mit Modellen der Anorthosit-Genese (Ashwal, 1993) und somit kompatibel mit der vermuteten Existenz von massiven Anorthosit-Körpern in größerer Tiefe in der Gardar-Provinz (Bridgwater, 1967).

Kapitel 3 befaßt sich mit geochemischen und isotopischen Zonierungsmustern in den Plagioklas-Megakristallen der „Big Feldspar Dikes“ (BFDs) des Isortoq-Gangschwarms. Da die BFDs vermutlich in enger Beziehung zu den Proterozoischen massiven Anorthositkörpern stehen (Bridgwater, 1967), kann man annehmen, dass ihre Genese auch Aussagen über Magmenkammer – und Platznahme-Prozesse während der Anorthosit-Genese im Allgemeinen erlaubt. Die Gardar BFDs werden so interpretiert, dass sie ein Krustenniveau über einem massiven Anorthositkörper repräsentieren (Bridgwater, 1967; Bridgwater & Harry, 1968). Somit bietet sich ein Vergleich zu den massiven Anorthositen Kanadas, wo ein tieferes Krustenstockwerk aufgeschlossen ist, an. Die Größe des Isortoq-Gebietes, in dem zahlreiche BFDs auftreten, beträgt ungefähr 50 x 25 km, und läßt sich beispielsweise gut mit der Genese des proterozoischen Morin Anorthosit-Komplexes in Quebec vergleichen (Peck & Valley, 2000). Auch die Intrusionsalter der massiven Anorthosite wie Nain (1.29-1.35 Ga; Amelin et al., 1999) oder Lac St. Jean (1.15 Ga; Higgins & van Breemen, 1992) überlappen mit dem Zeitrahmen der magmatischen Aktivität in der Gardar Provinz.

Massive Anorthosit-Körper sind große Intrusivkörper (bis zu 17 000 km² Fläche), die überwiegend im mittleren Proterozoikum von etwa 1.6 – 1.1 Ga entstanden sind. Sie bestehen aus großen Akkumulationen von Plagioklas ($An_{50\pm 10}$) und untergeordnet mafischen Mineralen (Ashwal, 1993). Verschiedene Mechanismen wurden vorgeschlagen, um das Auftreten von derart großen Mengen an

Plagioklas zu erklären, u.a. die Bildung von Plagioklas-Kumulaten von basaltischen Magmen (z.B. Morse, 1982), Resorption und Wiederaufschmelzen von Plagioklas (Wiebe, 1990), verspätete Nukleation von Plagioklas in mafischen Schmelzen (Morse, 1982) oder Interaktion zwischen basaltischem Magma und aluminium-reicher Kruste (Dempster et al., 1999). Über die Quelle der Magmen, aus denen Anorthosite kristallisiert sind, gibt es zwei prinzipiell unterschiedliche Ideen. Zum einen gibt es Autoren, die davon ausgehen, daß die Magmen aus dem Mantel stammen (Emslie, 1978; Wiebe, 1992; Mitchell et al., 1995; Markl & Frost, 1999). Andere wiederum glauben, dass die Magmen in der Unterkruste generiert werden (Longhi et al., 1999; Schiellerup et al., 2000; Bédard, 2001). Oft wird von einer Interaktion zwischen Magmen aus dem Mantel und krustalem Material ausgegangen (z.B. Scoates & Frost, 1996; Bédard, 2001). Ein Modell von Ashwal (1993) zur Genese massiver Anorthosite, auf das im folgenden häufiger Bezug genommen wird, soll hier etwas ausführlicher erläutert werden. Demnach sammeln sich mafische Schmelzen aus dem Mantel an der Kruste-Mantel-Grenze, wo mafische Silikate kristallisieren und absinken und die Residualschmelzen in Aluminium angereichert werden. Wenn Plagioklas kristallisiert, flotiert er und bildet anorthositische Kumulate im oberen Bereich der Magmenkammer. Gravitativ instabile, plagioklas-reiche breiartige Schmelzen steigen durch die Kruste auf und bilden schließlich Anorthositkörper in der Oberkruste. Während all dieser Stadien verursacht die Kristallisationswärme eine Teilaufschmelzung der umgebenden Kruste.

In den Plagioklas-Megakristallen der BFDs treten teilweise großmaßstäbliche Oszillationsmuster im Hauptelementchemismus auf, die, soweit bekannt, noch von nirgendwo anders beschrieben wurden. Die Oszillationen haben Wellenlängen von bis zu 2500 μm und eine maximale Amplitude von bis zu 7 mol% Anorthit. Vermutlich wurden diese Muster durch Bewegungen der Kristalle in einer kompositionell variablen Magmenkammer hervorgerufen. Dieses Magmenreservoir kann sowohl an der Kruste-Mantel-Grenze als auch innerhalb der Kruste gewesen sein. Sr-Isotopendaten eines ausgewählten Plagioklases zeigen einen inneren Kernbereich mit gegenüber dem äußeren Kernbereich leicht erhöhten initialen Isotopenverhältnissen. Dies weist auf den Einfluß einer krustalen Komponente während des Beginns der Kristallisation hin. Konstante Verhältnisse von inkompatiblen Spurenelementen in den Megakristallkernen können ebenfalls durch den dominanten

Einfluß einer Unterkrustenkomponente auf das Spurenelementbudget interpretiert werden. Assimilation von krustalem Material kann in verschiedenen Stadien des Magmenaufstiegs sowohl durch Infiltration von krustalen Schmelzen als auch durch direkte Assimilation von Nebengestein stattgefunden haben (Ashwal, 1993).

Zwischen dem Kern der Plagioklaskristalle und dem relativ schmalen ($< 600 \mu\text{m}$), normal zonierten Rand tritt oft eine deutliche Resorptionsfläche auf. Diese ist durch einen scharfen Anstieg im Anorthit-Gehalt (X_{An}) gekennzeichnet. Diese Resorptionsflächen mit maximalen Anstiegen in X_{An} von bis zu 11 mol% werden einem plötzlichen Druckabfall zugeschrieben. Die Abschätzung der Druckdifferenz beruht auf experimentellen Daten von Longhi et al. (1993), welche zeigen, dass mit zunehmenden Druck bei gleichbleibendem Schmelzchemismus Albit-reichere Plagioklase kristallisieren. Das Fehlen einer signifikanten Änderung in der Sr-Isotopie zwischen dem äußeren Bereich des Kristallkerns und dem Kristallrand ist konsistent mit der Bildung eines Anorthit-reicheren Randes aufgrund einer Druckentlastung.

Die maximale Druckdifferenz zwischen der Kristallisation von Kern und Rand, abgeleitet von dem Sprung im Anorthit-Gehalt, liegt bei 10-12 kbar. Somit könnten einige der Plagioklas-Megakristalle ihren Ursprung im Bereich der damaligen Kruste-Mantel-Grenze haben, also dort, wo auch das Modell für die Anorthositgenese annimmt, dass Plagioklas beginnt auszukristallisieren (Emslie, 1978; Ashwal, 1993). Einige der Megakristalle in den Ganggesteinen repräsentieren also möglicherweise eine initiale Kristallisation im Bereich der Kruste-Mantel-Grenze, während andere mit weniger deutlichen Sprüngen im Chemismus während des Magmenaufstiegs in das jetzige Niveau kristallisierten. Unsere Daten unterstützen die Auffassung, dass initiale Kristallisation von massiven Anorthositen in ungefähr 30-35 km Tiefe begonnen hat.

Der scharfe Anstieg in X_{An} an der Kern-Rand-Resorptionsfläche in den Megakristallen weist auch auf einen relativ schnellen Magmenaufstieg hin. Einige der Megakristalle könnten direkt von der Kruste-Mantel Grenze bis in das heute aufgeschlossene Krustenniveau gestiegen sein, ohne in einem zusätzlichen Anorthosit-Reservoir aufgehalten worden zu sein. Dies scheint zunächst inkonsistent mit dem Modell Ashwals (1993), kann aber im Angesicht der tektonischen Situation in der Gardar Provinz erklärt werden. Dort können nämlich extensionaler Stress und die Entstehung von Spalten den Aufstieg von Magmen vereinfacht haben. Während des Magmenaufstiegs wurden

Feldspat-Megakristallen von verschiedenen Regionen des Magmenreservoirs aufgenommen, möglicherweise innerhalb des gesamten vertikalen Krustenprofils (Marsh, 1996). In tektonisch ruhigeren Zeiten können sich Plagioklas-Breie gebildet haben, die langsamer in mittelkrustale Niveaus (~ 9-15 km Tiefe) aufgestiegen sind, unterhalb des Platznahme-Niveaus der BFDs, wo wir erwarten würden, massive Anorthosit-Körper wie solche in Kanada zu finden. Beide Prozesse haben ihre Spuren in den BFDs hinterlassen: Es kommen sowohl einzelne Plagioklas-Megakristalle als auch Anorthosit-Xenolithe von massiven plutonischen Körpern vor. Während der Platznahme der Ganggesteine kam es zur Umverteilung des feldspatreichen Materials (Winther, 1992) und zur Konzentration von Kristallen in den Gangzentren durch Fließdifferentiation.

In der Gardar-Provinz sind die BFDs mit einer Vielzahl von anderen alkalinen Gesteinen vergesellschaftet, wie z.B. Karbonatiten (Grønnedal-Ika; Pearce et al., 1997), agpaitischen Gesteinen (Ilímaussaq; Markl et al., 2001) und peralkalinen Graniten (Puklen; Marks et al., 2003). Das gleiche gilt für den kanadischen Schild, von dem mittelproterozoische Alkaligranite (Strange Lake Complex; Boily & Williams-Jones, 1994), agpaitische Gesteine (Red Wine Intrusion, Curtis & Gittins, 1979) und Karbonatite (Seabrook Lake Carbonatite; Cullers & Medaris, 1977) bekannt sind. Außerdem sind viele der geochemischen Merkmale, die in Granitoiden, die mit massiven Anorthositen vergesellschaftete sind, auch in den Gesteinen der Gardar-Provinz ausgeprägt. Dazu gehören z.B. hohe Na + K – Gehalte, hohe Fe/Mg – Verhältnisse, hohe Konzentrationen an SEE und Halogenen sowie Fe-reiche mafische Silikate. Deshalb ist es denkbar, dass diese Assoziation von Alkaligesteinen für bestimmte Anorthositprovinzen generell typisch ist.

Ein mögliches Modell, dass die Bildung vieler verschiedener magmatischer Gesteine im Zusammenhang mit der Bildung von massiven Anorthositen erklären kann, stammt von Duchesne et al. (1999). Demnach kann es nach der Unterschiebung von mafischer Unterkruste zu lithosphärischer Delamination und anschließend zum Aufstieg von Astenosphären-Material und Aufschmelzung dieser Kruste kommen. Alkalische Magmen können dabei durch den Einfluss von Astenosphären-Material gebildet werden (Liégeois et al., 1998) und Magmenaufstieg kann entlang von lithosphärischen Diskontinuitäten stattgefunden haben. Solche Strukturen sind auch im

Grundgebirge der Gardar-Provinz vorhanden, und ihre Reaktivierung während der Gardar-Aktivität steht in Einklang mit dem Riftsetting der Provinz (Upton & Emeleus, 1987).

Kapitel 4 beinhaltet die Untersuchungen zur Entstehung und Entwicklung des bimodalen Grønnedal-Ika Karbonatit-Syenit-Komplexes im Nordwesten der Gardar-Provinz. Er befindet sich in der Grenzzone zwischen dem Ketilidischen Gürtel im Süden und dem Archaischen Kraton im Norden. Mit der Rb-Sr-Isochronenmethode wurde Grønnedal-Ika auf 1299 ± 17 Ma datiert (Blaxland et al., 1978). Die Intrusion ist rund 8×3 km groß und besteht überwiegend aus magmatisch geschichteten, SiO_2 -untersättigten Nephelin-Syeniten, die von einem xenolithisch-porphyrischen Syenit (XPS) und einem Karbonatit intrudiert wurden (Emeleus, 1964). Dort, wo mafische Gänge den Siderit-haltigen Teil des Karbonatits schneiden, treten Akkumulationen von Magnetit auf (Emeleus, 1964). In mehreren Teilen der Syenite treten Sodalith-Adern auf, die vermutlich durch ein orthomagmatisches, Na- und Cl-reiches Fluid des Karbonatits entstanden sind (Bühn et al., 2002).

Der Ursprung der Karbonatite von Grønnedal und ihre Beziehung zu den Syeniten ist noch umstritten. Hauptsächlich anhand von Gesamtgesteins-Spurenelementdaten wurde von Bedford (1989) ein Ursprung der Grønnedal-Karbonatite durch Entmischung von einer syenitischen Schmelze vorgeschlagen. Neuere C, O und Sr-Isotopendaten von Pearce et al. (1997) wurden aber dahingehend interpretiert, dass die Unterschiede in C- und O Isotopenzusammensetzung zwischen den Karbonatiten und Syeniten einen gemeinsamen Ursprung ausschließen.

Allgemein wird die Beziehung zwischen Karbonatiten und assoziierten silikatischen Gesteinen intensiv diskutiert (Bell, 1998; Bell et al., 1998). Prinzipiell gibt es drei verschiedene Modelle, um die Entstehung von Karbonatiten zu erklären:

- Direktes Aufschmelzen einer karbonathaltigen Mantelquelle (z.B. Wyllie & Huang, 1976; Dalton & Presnall, 1998; Harmer & Gittins, 1998; Moore & Wood, 1998)
- Entmischung aus einer karbonathaltigen silikatischen Schmelze (z.B. Koster von Groos & Wyllie, 1963; Freestone & Hamilton, 1980; Kjarsgaard & Hamilton, 1988; Kjarsgaard, 1998)

- Kristallfraktionierung einer karbonathaltigen alkalischen Silikatschmelze (z.B. Lee & Wyllie, 1994; Korobeinikov et al., 1998; Veksler et al., 1998a)

Die Unterscheidung zwischen karbonatitischen Schmelzen, die direkt aus dem Mantel kommen und unfraktioniert sind (primäre Karbonatite), und solchen, die durch Differentiation einer silikatischen Mutterschmelze entstanden sind, ist nicht immer eindeutig (Bell, 1998). In dieser Studie wenden wir Kriterien an, die in der Literatur diskutiert sind, und evaluieren neue geochemische und petrologische Daten, um die Entstehung des Grønnedal-Ika Nephelin-Syenit – Karbonatit Komplexes zu untersuchen. Außerdem werden die Daten der Syenite mit anderen, gut untersuchten magmatischen Komplexen der Gardar Provinz, die keine assoziierten Karbonatite aufweisen, verglichen. Damit soll evaluiert werden, welche Parameter für die Entstehung der Karbonatite wichtig gewesen sind. Als Vergleichsobjekte von besonderer Bedeutung sind dabei die SiO₂-untersättigten Gesteine der Ilímaussaq-Intrusion (Larsen, 1976; Marks & Markl, 2001; Markl et al., 2001), die SiO₂-gesättigten- und übersättigten Gesteine des Puklen Komplexes (Marks et al., 2003), und die Basalte der Eriksfjord Formation (Halama et al., 2003).

Der Grønnedal-Ika Komplex wird dominiert von magmatisch geschichteten Nephelin-Syeniten, in den Aegirin-Augit, Alkali Feldspat und Nephelin die wichtigsten Mineralphasen sind. Für die Kristallisation der Syenite konnten Temperaturen von 680-910 °C, Silica-Aktivitäten von 0.28-0.43 und Sauerstoffugazitäten von 2-5 log-Einheiten über dem Fayalit-Magnetit-Quarz (FMQ) – Puffer ermittelt werden. Die berechneten Silica-Aktivitäten der Grønnedal-Syenite sind deutlich niedriger als im Augit-Syenit von Ilímaussaq ($a_{\text{SiO}_2} = 0.4 - 0.9$; Marks & Markl, 2001) und in den Syeniten von Puklen ($a_{\text{SiO}_2} = 0.7 - 1$; Marks et al., 2003). Dagegen sind die Sauerstoffugazitäten im frühmagmatischen Stadium in Grønnedal höher als in den syenitischen Gesteinen von Ilímaussaq (1-5 log Einheiten unter dem FMQ-Puffer; Marks & Markl, 2001) und Puklen (1-3 log unter dem FMQ-Puffer; Marks et al., 2003). Basierend auf dem Argument, daß der SiO₂-untersättigte Charakter von mafisch alkalinen Laven auf niedrige Schmelzgrade unter CO₂-reichen Bedingungen zurückgeführt werden kann (Mysen & Boettcher, 1975; Wyllie & Huang, 1976; Gerlach et al., 1988), können die extrem niedrigen Silica-Aktivitäten der Grønnedal Syenite möglicherweise relativ hohe CO₂-Partialdrücke in der Schmelze widerspiegeln. Ein Anstieg des CO₂-Gehaltes wird

auch durch das Auftreten von Kalzit in den Nephelin-Syeniten angezeigt. Weitere Einschränkungen auf die Sauerstofffugazität können aus dem Gleichgewicht $\text{CH}_4 + 2 \text{O}_2 = \text{CO}_2 + 2 \text{H}_2\text{O}$ abgeleitet werden. Dabei zeigt sich, dass nur bei sehr niedrigen CH_4/CO_2 -Verhältnissen die hohen Sauerstofffugazitäten, wie sie für Grønnedal ermittelt wurden, erreicht werden. Dies ist konsistent mit der oft bei Karbonatiten beobachteten Dominanz von CO_2 - H_2O Fluid-Einschlüssen (Andersen, 1986; Samson et al., 1995; Bühn & Rankin, 1999). Andererseits deuten sich für Ilímaussaq hohe CH_4/CO_2 -Verhältnisse an, in Übereinstimmung mit dem Auftreten von Methan-haltigen Fluid-Einschlüssen (Konnerup-Madsen & Rose-Hansen, 1982). Die hohe CO_2 -Fugazität ist sicherlich als wichtige Voraussetzung für die Karbonatitentstehung in Grønnedal zu sehen und könnte auch einer der wichtigsten Unterschiede zwischen den Ursprungsschmelzen in Grønnedal und Ilímaussaq sein.

Ein Ziel der vorliegenden Studie war, geochemische Charakteristika zu finden, die eine Unterscheidung zwischen den 3 prinzipiell möglichen Entstehungsarten von Karbonatiten im Fall von Grønnedal-Ika erlauben (Bell et al., 1998). Dabei zeigte sich, dass es einige Kriterien gibt, die einen Ursprung des Karbonatits durch Entmischung aus einer syenitischen Silikatschmelze unterstützen. Diese sind im folgenden zusammengefaßt:

- Geländebefund und petrographische Merkmale, wie z.B. das Auftreten von spätmagmatischem Cancrinit (karbonat-haltiges Silikatmineral) in den Syeniten, weisen darauf hin, daß es keine signifikante zeitliche Lücke zwischen der Platznahme der silikatischen Gesteine und der Karbonatite gab.
- Gesamtgesteins- und mineralchemische Fraktionierungsindizes wie Mg# und $(\text{Mg}+\text{Fe}^{2+})/\text{Ca}$ bestätigen, dass die Karbonatite keine unfraktionierten Mantelschmelzen darstellen. Auch die syenitischen Silikatgesteine stellen naturgemäß fraktionierte Schmelzen dar, so daß klare Hinweise auf Differentiationsprozesse vor und während der Bildung des Komplexes vorliegen.
- Radiogene Isotopenzusammensetzungen (Sr, Nd) sind identisch für Karbonatite und Syenite.
- Sauerstoffisotopenzusammensetzungen der syenitischen Schmelzen, die basierend auf Mineraldaten und den passenden Fraktionierungsfaktoren zwischen Mineral und Gesamtgestein (Zhao & Zheng, 2003) berechnet wurden, liegen in dem Bereich, wo man die

Sauerstoffisotopenzusammensetzung einer silikatischen Schmelze erwarten würde, die von einer karbonatitischen Schmelze mit den Signaturen des Grønnedal-Karbonatits entmischt.

- In Übereinstimmung mit Entmischungsexperimenten (Veksler et al., 1998b) zeigen die normalisierten SEE-Muster von Kalzit der Karbonatite steilere Steigungen als Kalzit in den assoziierten silikatischen Gesteinen. Andere Spurenelementdaten von Kalzit zeigen ebenfalls Merkmale, die mit den experimentellen Daten übereinstimmen.
- Die Kristallisation von aegirin-augitischem Klinopyroxen im XPS mit erhöhten Zr/Hf und erniedrigten Y/Ho Verhältnissen weist auf die Entmischung eines CO₂-reichen Fluids hin. Dieser Prozess steht möglicherweise in Beziehung zur Entmischung einer karbonatitischen Schmelze und würde so die Idee unterstützen, dass der XPS die silikatische Schmelze in einem Entmischungsprozess darstellt (Bedford, 1989).
- Die silikatischen Gesteine, die mit den Karbonatiten assoziiert sind, sind stark SiO₂-untersättigt und entsprechen damit silikatischen Schmelzen einiger Entmischungsexperimente (Koster van Groos & Wyllie, 1973).
- Die räumlich scharf getrennte Vorkommen von Karbonatit und SiO₂-untersättigtem Syenit sprechen eher für Entmischung als für einen Zusammenhang allein durch fraktionierende Kristallisation, wo man eine kontinuierlich Serie von silikatischen zu karbonatitischen Gesteinen erwarten würde (Le Bas, 1989).
- Die Karbonatite stellen die späteste Phase im Komplex dar (Minarik, 1998).

Obwohl ein Vergleich mit weltweiten Vorkommen von Karbonatit-Syenit-Assoziationen über den Rahmen dieser Arbeit hinausgeht, können diese Kriterien auch im Allgemeinen auf andere assoziierte karbonatitische und silikatische Gesteine angewendet werden. Es wird geschlußfolgert, daß die Karbonatite Grønnedals mit den Syeniten durch Entmischung zusammenhängen. Einige der Daten weisen darauf hin, dass der XPS die entsprechende silikatische Schmelze repräsentiert.

In **Kapitel 5** werden die Ergebnisse von Spurenelementuntersuchungen an mafischen Mineralen (Klinopyroxen und Amphibol) dreier Intrusionen der Gardar-Provinz präsentiert. Spurenelementdaten können verwendet werden, um magmatische Prozesse zu modellieren und zu

interpretieren. Der Großteil der bisher gesammelten Datensätze von *in situ*-Messungen an Mineralen stammt aus Studien über basaltische Systeme (z.B. Benoit et al., 1996; Dobosi & Jenner, 1999; Coogan et al., 2000; Thompson & Malpas, 2000), ultramafische Gesteine und Mantelminerale (z.B. Nimis & Vanucci, 1995; Blundy & Dalton, 2000, Grégoire et al., 2000; Tiepolo et al., 2000). Untersuchungen über Spurenelementverteilung- und -gehalte in höher fraktionierten silikatischen Systemen (Lemarchand et al. 1987; Wood & Trigila, 2001) und insbesondere in alkalinen silikatischen Magmatiten (Larsen 1979; Wörner et al., 1983; Shearer and Larsen 1994) sind weniger häufig. Neuere Studien, die auf theoretischen Modellen basieren, haben gezeigt, dass die Kristallchemie einen bedeutenden Einfluß auf die Verteilung von Spurenelementen hat (Blundy & Wood, 1991; Blundy & Wood, 1994; Wood & Blundy, 1997). Die Ionengröße relativ zum relevanten Gitterplatz und die Ionenladung sind dabei kritische Faktoren, während der Chemismus der Schmelze als weniger wichtig angesehen wird (Blundy & Wood, 2003). Leider sind experimentelle Daten zur Spurenelementverteilung zwischen mafischen Mineralen und alkalinen silikatischen Schmelzen selten. Die vorhandenen Daten von natürlichen Gesteinen (z.B. Larsen, 1979; Wörner et al., 1983) zeigen eine Variabilität in den Verteilungskoeffizienten, die überraschend groß ist, selbst wenn man die Unterschiede in den Mineralchemismen berücksichtigt.

In dieser Studie vergleichen wir die Spurenelementgehalte von mafischen Mineralen dreier petrologisch unterschiedlicher alkaliner bis peralkaliner magmatischer Komplexe der Gardar-Provinz Südgrönlands, um die Verteilung von Spurenelementen in natürlichen alkalinen Systemen zu studieren. Alkaline plutonische Komplexe treten häufig in riftbezogenen Provinzen auf und sind oft durch eine Anreicherung von seltenen Elementen mit ökonomischer Bedeutung charakterisiert (Kramm & Kogarko, 1994; Platt, 1996; Digonnet et al., 2000). Unsere Untersuchungen fokussieren auf Klinopyroxene und Amphibole, da diese beiden Minerale große Mengen geochemisch relevanter Spurenelemente einbauen können (Wood & Blundy, 1997; Botazzi et al., 1999). Die drei untersuchten Komplexe zeigen ein fast kontinuierliches Spektrum in der Zusammensetzung der mafischen Minerale von Ca-reich und Na-arm zu Ca-arm und Na-reich. Dies ermöglicht uns, die relativen Spurenelementhäufigkeiten in den Mineralen in Bezug zu ihrer Kristallchemie zu setzen. Außerdem bestimmen wir Verteilungskoeffizienten zwischen Klinopyroxen und Amphibol für eine

große Zahl von Spurenelementen und vergleichen diese mit Literaturdaten für andere Gesteinstypen.

In situ – Analysen von Spurenelementen umgehen die Problematik von Gesamtgesteinsdaten von Plutoniten, die häufig durch Akkumulation von bestimmten Mineralen oder durch verschiedene magmatische und postmagmatische Einflüsse beeinflusst werden (z.B. Marks et al., 2003). Wir nutzen eine Spannbreite von Mineral-Schmelze Verteilungskoeffizienten aus der Literatur, die an natürlichen alkalinen Gesteinen bestimmt wurden (Larsen, 1979; Wörner et al., 1983; Lemarchand et al., 1987), um zu untersuchen, ob diese auch für die Berechnung von Schmelzzusammensetzungen in den hier untersuchten Gesteinen anwendbar sind.

Die meisten Spurenelemente in den untersuchten Klinopyroxenen und Amphibolen sind relativ zu primitiven Mantel angereichert, was in Übereinstimmung mit dem hochfraktionierten Charakter der Gesteine ist. Der Einbau einiger der HFSE („High Field Strength Elements“, z.B. Ti, Zr, Hf, Sn) scheint hauptsächlich von der Hauptelementzusammensetzung des Minerals gesteuert zu werden, die wiederum die strukturellen Eigenschaften des Minerals bestimmt. Eine überwiegend kristallchemische Kontrolle ist auch beim Einbau der SEE zu beobachten. Klinopyroxene und Amphibole zeigen eine kontinuierliche Entwicklung in ihren SEE-Mustern, beginnend mit einer Anreicherung der leichten SEE in Ca-dominierten Mineralen, über wellenförmige Muster in Ca-Na-Mineralen, bis hin zu Mustern mit einer deutlichen Anreicherung der schweren SEE in Na-dominierten Mineralen. Ebenso können die niedrigen Gehalte an LILE („Large Ion Lithophile Elements“, z.B. Ba, Sr, Pb, Eu^{2+}) so interpretiert werden, dass sie sowohl die kristallchemisch begründete Abneigung gegen den Einbau dieser Elemente als auch eine Erniedrigung der entsprechenden Absolutkonzentrationen in der Schmelze durch intensive Fraktionierung von Feldspat widerspiegeln. Zusätzlich spielen Faktoren wie die Sauerstoffugazität (Einbau von Eu) und krustale Assimilation (absolute Häufigkeit von Pb in der Schmelze) eine Rolle.

Die Verteilung der meisten Spurenelemente zwischen koexistierendem Klinopyroxen und Amphibol ist im Allgemeinen unabhängig von der Schmelzzusammensetzung oder der Hauptelementchemie der Minerale. Die meisten Spurenelemente zeigen eine leichte Bevorzugung der Amphibolstruktur, insbesondere Nb, Ta, U, Th, Rb, Ba und Li. Ausnahmen treten in Gesteinen

auf, die durch späte Zirkulation von Fluiden und der daraus resultierenden Umverteilung einiger mobiler Elemente beeinflusst worden sind. Im Vergleich mit Literaturdaten können keine systematischen Unterschiede in den $D_{\text{cpx-amph}}$ -Werten zwischen ultramafischen, basanitischen oder hochfraktionierten Gesteinen beobachtet werden.

Abschließend wird die Anwendbarkeit von publizierten Mineral-Schmelze-Verteilungskoeffizienten auf die untersuchten Alkaligesteine überprüft, indem mittels der Verteilungskoeffizienten aus den Spurenelementgehalten der Pyroxene und Amphibole Spurenelementzusammensetzungen der Schmelze berechnet werden. Eine fehlende Übereinstimmung zwischen berechneter Schmelzzusammensetzung und Gesamtgestein kann durch folgende Ursachen hervorgerufen worden sein: 1. Die Kristallisationsgeschichte der Gesteine ist sehr komplex, so daß sich die Kristallisationsparameter während der Mineralbildung ändern und die Spurenelementverteilung nicht durch einen einzigen Wert für den Verteilungskoeffizienten dargestellt werden kann. 2. Gesamtgesteinsdaten reflektieren nicht die Zusammensetzung der Schmelze. 3. Kristall –und Schmelzchemismus in dem hier untersuchten alkalinen Systemen sind teilweise so unterschiedlich von den bisher untersuchten Systemen, daß die entsprechenden Verteilungskoeffizienten hier nicht angewendet werden können. Es ist sehr wahrscheinlich, dass alle diese Begründungen zu einem gewissen Grad auf die untersuchten Alkaligesteine zutreffen. So dient beispielsweise die Beobachtung von magmatischer Schichtung und Mineralakkumulation in allen Komplexen als Hinweis, dass auch feinkörnige Gesamtgesteinsproben nicht unbedingt die ursprüngliche Schmelzzusammensetzung widerspiegeln. Die relativ großen Unterschiede zwischen den anhand von Aegirin-Augit berechneten Schmelzzusammensetzungen und den Gesamtgesteinschemismen suggeriert einen starken kristallchemischen Einfluß auf die Verteilung der Spurenelemente. Schließlich ist bekannt, dass chemische Differentiationsprozesse in magmatischen Systemen oft polythermal und polybarisch ablaufen, so dass Verteilungskoeffizienten für eine Mineralphase während der Kristallisation variieren können (Blundy & Wood, 2003). Große Kristallisationsintervalle wurden beispielsweise für Ilímaussaq beschrieben (Markl et al., 2001), und das Auftreten von chemisch unterschiedlichen Klinopyroxenkernen in Grønnedal könnte auf Druckunterschiede während der Kristallisation zurückzuführen sein. Weitere Komplexitäten in den

untersuchten Gesteinen können durch Wechselwirkungen mit spätmagmatischen oder meteorischen Fluiden (Puklen: Marks et al., 2003) oder Entmischungsprozesse (Grønnedal: Bedford, 1989) hervorgerufen werden. Auch die Eigenschaften der Schmelzphase können Verteilungskoeffizienten unabhängig von der Mineralzusammensetzung beeinflussen (z.B. Adam & Green, 2003).

Basierend auf den Mineralchemismen wurden Spurenelementgehalte in der Schmelze mit minimalen und maximalen Verteilungskoeffizienten berechnet (Larsen, 1979; Wörner et al., 1983; Lemarchand et al., 1987). Um die Genauigkeit der Verteilungskoeffizienten überprüfen zu können, muss die Spurenelementzusammensetzung der Schmelze bekannt sein. Gesamtgesteinsdaten der intrusiven Gesteine sind generell nicht sehr gut geeignet, die Schmelzzusammensetzung widerzuspiegeln, da sie von Akkumulationsprozessen beeinflusst worden sein können. Dennoch benutzen wir die publizierten Zusammensetzungen von feinkörnigen Ganggesteinen, die von den Autoren (Larsen, 1979; Upton et al., 1985) als mögliche initiale Schmelzzusammensetzungen angesehen werden. Zusätzlich vergleichen wir die berechneten Schmelzzusammensetzungen mit Gesamtgesteinsdaten der Intrusionen. Die Vergleiche zeigen, dass in hochentwickelten magmatischen Systemen wie den Alkaligesteinskomplexen der Gardar-Provinz die Berechnung von Spurenelementgehalten in der Schmelze in Abhängigkeit von der Mineralzusammensetzung betrachtet werden muss. Veröffentlichte Klinopyroxen-Schmelze-Verteilungskoeffizienten für alkaline Systeme können offensichtlich nur verwendet werden, wenn der Klinopyroxen eine ähnliche, diopsidische bis augitische, Kristallchemie aufweist. Berechnet man Schmelzzusammensetzungen von Aegirin-Augiten oder Aegirinen, so können beträchtliche Unterschiede zwischen berechneter Schmelzzusammensetzung und den Gesamtgesteinsdaten auftreten. Beispielsweise liegen die Zr- und Hf-Gehalte in aus Aegirin-Augit und Aegirin kalkulierten Schmelzen deutlich höher als in den vergleichbaren Gesamtgesteinen.

Um den Einfluß der Kristallchemie auf die Verteilungskoeffizienten besser quantifizieren zu können, wurden Verteilungskoeffizienten für die SEE nach einem theoretischen Modell zur Verteilung von Spurenelementen zwischen Klinopyroxen und Schmelze nach Wood & Blundy (1997) berechnet. Es zeigt sich, dass die Präferenz für die Kristallstruktur bei den schweren SEE relativ zu den leichten SEE zunimmt, wenn der Kristall reicher an Aegirin-Komponente wird. Dies ist in qualitativer Übereinstimmung mit den beobachteten SEE-Mustern. Die berechneten

Verteilungskoeffizienten werden mit fortschreitender kristallchemischer Entwicklung niedriger, aber sie steigen mit abnehmenden Temperaturen an. Schmelzen, die mittels der theoretisch ermittelten Verteilungskoeffizienten berechnet wurden, zeigen eine gute Übereinstimmung mit Gesamtgesteinsdaten für relativ Fe^{3+} -arme Klinopyroxen-Zusammensetzungen. Schmelzzusammensetzungen, die basierend auf Aegirin-Chemismen kalkuliert wurden, stimmen dagegen nicht mit Gesamtgesteinszusammensetzungen überein. Daraus läßt sich folgern, dass das theoretische Modell zur Berechnung von Verteilungskoeffizienten Verbesserungen benötigt, um den zuvor nicht betrachteten Einbau der $\text{NaFe}^{3+}\text{Si}_2\text{O}_6$ -Komponente zu berücksichtigen. Möglicherweise hat auch der Fluid-reiche Charakter der peralkalinen Schmelzen das Verteilungsverhalten von Spurenelementen signifikant beeinflusst. Bei den Amphibolen zeigen die berechneten Schmelzzusammensetzungen eine relativ schlechte Übereinstimmung mit Gesamtgesteinszusammensetzungen, was möglicherweise auf ihren spätmagmatische Bildung unter stärker wasserhaltigen Bedingungen zurückzuführen ist.

Danksagung

Zunächst möchte ich Prof. Gregor Markl danken, der es mir ermöglichte, die Thematik dieser Arbeit zu bearbeiten, und dessen Anregungen viel zu den Ergebnissen der Arbeit beigetragen haben. Für sein kontinuierliches Interesse am Gelingen der Arbeit bin ich ihm ebenso dankbar wie für zahlreiche stimulierende Diskussionen. Herrn Prof. Hans Keppler danke ich für die Übernahme des Koreferates.

Meinem Kollegen Dipl.-Min. Michael Marks möchte ich für die sehr angenehme Zusammenarbeit und für das Gelingen einer rundum erfolgreichen und unvergeßlichen Geländearbeit im Sommer 2001 danken. Besonderer Dank gebührt ihm für seine Hilfsbereitschaft und geduldige Unterstützung in der Anfangsphase der Arbeit, als er mich mit den vielfältigen Fragestellungen zu den Gesteinen der Gardar-Provinz vertraut machte. Für Unterstützung bei der Datengewinnung und viele konstruktive Diskussionen gebührt mein Dank PD Dr. Wolfgang Siebel (Tübingen), PD Dr. Thomas Wenzel (Tübingen), Prof. Torsten Vennemann (Lausanne), PD Dr. Gerhard Brüggemann (Mainz), Dr. Tod Waight (Kopenhagen) und Prof. Brian Upton (Edinburgh). Für ihre Hilfe bei der Vorbereitung und Durchführung der verschiedenen analytischen Verfahren sei Dr. Mathias Westphal (Mikrosonde), Dr. Bruce Paterson (Laser ICP-MS), Gaby Stoscheck, Bernd Steinhilber (Stabile Isotope), Elmar Reitter (Radiogene Isotope), Gisela Bartholomä (Mineralseparation) und Nora Groschopf (RFA) gedankt. Dank auch an alle Kollegen und Mitarbeiter des Instituts, insbesondere Frau Dagmar Dimitrovice, deren freundliche Hilfe zum Gelingen der Arbeit beigetragen haben.

Den größten Dank möchte ich meinen Eltern aussprechen für ihre uneingeschränkte Unterstützung während des gesamten Studiums und allen Phasen der Arbeit. Insbesondere meine Mutter hat sich stets für geologische Fragestellungen interessiert, aber aufgrund ihres Todes im Oktober 2001 ist es ihr leider nicht vergönnt, die Fertigstellung dieser Arbeit mitzuerleben.

Literatur

- Adam, J. & Green, T. (2003). The influence of pressure, mineral composition and water on trace element partitioning between clinopyroxene, amphibole and basanitic melts. *European Journal of Mineralogy* **15**, 831-841.
- Amelin, Y., Li, C.S., & Naldrett, A.J. (1999). Geochronology of the Voisey's Bay intrusion, Labrador, Canada, by precise U-Pb dating of coexisting baddeleyite, zircon, and apatite. *Lithos* **47**, 33-51.
- Andersen, T. (1997). Age and petrogenesis of the Qassiarsuk carbonatite-alkaline silicate volcanic complex in the Gardar rift, South Greenland. *Mineralogical Magazine* **61**, 499-513.
- Ashwal, L.D. (1993). *Anorthosites*. Berlin Heidelberg: Springer.
- Baker, J.A., MacPherson, C.G., Menzies, M.A., Thirlwall, M.F., Al-Kadasi, M., & Matthey, D.P. (2000). Resolving crustal and mantle contributions to continental flood volcanism, Yemen; constraints from mineral oxygen isotope data. *Journal of Petrology* **41**, 1805-1820.
- Baker, J.A., Menzies, M.A., Thirlwall, M.F., & Macpherson, C.G. (1998). Petrogenesis of Quaternary Intraplate Volcanism, Sana'a, Yemen: Implications for Plume-Lithosphere Interaction and Polybaric Melt Hybridization. *Journal of Petrology* **38**, 1359-1390.
- Bédard, J.H. (2001). Parental magmas of the Nain Plutonic Suite anorthosites and mafic cumulates: a trace element modelling approach. *Contributions to Mineralogy and Petrology* **141**, 747-771.
- Bedford, C.M. (1989). The mineralogy, geochemistry and petrogenesis of the Grønndal-Ika complex, south west Greenland. Ph.D. thesis, University of Durham.
- Bell, K. (1998). Radiogenic Isotope Constraints on Relationships between Carbonatites and Associated Silicate Rocks - a Brief Review. *Journal of Petrology* **39**, 1987-1996.
- Bell, K. (2001). Carbonatites; relationships to mantle-plume activity. *Special Paper - Geological Society of America* **352**, 267-290.
- Bell, K., Kjarsgaard, B.A., & Simonetti, A. (1998). Carbonatites-Into The Twenty-First Century. *Journal of Petrology* **39**, 1839-1845.
- Benoit, M., Polvé, M., & Ceuleneer, G. (1996). Trace element and isotopic characterization of mafic cumulates in a fossil mantle diapir (Oman ophiolite). *Chemical Geology* **134**, 199-214.
- Bernstein, S., Kelemen, P.B., Tegner, C., Kurz, M.D., Blusztajn, J., & Kent Brooks, C. (1998). Post-breakup basaltic magmatism along the East Greenland Tertiary rifted margin. *Earth and Planetary Science Letters* **160**, 845-862.
- Blaxland, A.B., van Breemen, O., Emeleus, C.H., & Anderson, J.G. (1978). Age and origin of the major syenite centers in the Gardar province of south Greenland: Rb-Sr studies. *Bulletin of the Geological Society of America* **89**, 231-244.
- Blundy, J. & Dalton, J. (2000). Experimental comparison of trace element partitioning between clinopyroxene and melt in carbonate and silicate systems, and implications for mantle metasomatism. *Contributions to Mineralogy and Petrology* **139**, 356-371.
- Blundy, J.D. & Wood, B.J. (1991). Crystal-chemical controls on the partitioning of Sr and Ba between plagioclase feldspar, silicate melts, and hydrothermal solutions. *Geochimica et Cosmochimica Acta* **55**, 193-209.
- Blundy, J. & Wood, B. (1994). Prediction of crystal-melt partition coefficients from elastic moduli. *Nature* **372**, 452-454.
- Blundy, J. & Wood, B. (2003). Partitioning of trace elements between crystals and melts. *Earth and Planetary Science Letters* **210**, 383-397.
- Bohrson, W.A. & Spera, F.J. (2001). Energy-constrained open-system magmatic processes; II, Application of energy-constrained assimilation-fractional crystallization (EC-AFC) model to magmatic systems. *Journal of Petrology* **42**, 1019-1041.
- Boily, M. & Ludden, J.N. (1991). Trace-element and Nd isotopic variations in Early Proterozoic dyke swarms emplaced in the vicinity of the Kapuskasing structural zone: enriched mantle or assimilation and fractional crystallization (AFC) process? *Canadian Journal of Earth Sciences* **28**, 26-36.
- Boily, M. & Williams-Jones, A.E. (1994). The role of magmatic and hydrothermal processes in the chemical evolution of the Strange Lake plutonic complex, Quebec-Labrador. *Contributions to Mineralogy and Petrology* **118**, 33-47.
- Bottazzi, P., Tiepolo, M., Vannucci, R., Zanetti, A., Brum, R., Foley, S.F., & Oberti, R. (1999). Distinct site preferences

- for heavy and light REE in amphibole and the prediction of $^{Amph/L}D_{REE}$. *Contributions to Mineralogy and Petrology* **137**, 36-45.
- Bridgwater, D. (1967). Feldspathic inclusions in the Gardar igneous rocks of South Greenland and their relevance to the formation of major Anorthosites in the Canadian Shield. *Canadian Journal of Earth Sciences* **4**, 995-1014.
- Bridgwater, D. & Coe, K. (1970). The role of stoping in the emplacement of the giant dikes of Isortoq, South Greenland. *Geological Journal, Special issue* **2**, 67-78.
- Bridgwater, D. & Harry, W.T. (1968). Anorthosite xenoliths and plagioclase megacrysts in Precambrian intrusions of South Greenland. *Meddelelser om Grønland* **185**, 243 pp.
- Bühn, B. & Rankin, A.H. (1999). Composition of natural, volatile-rich Na-Ca-REE-Sr carbonatitic fluids trapped in fluid inclusions. *Geochimica et Cosmochimica Acta* **63**, 3781-3797.
- Bühn, B., Rankin, A.H., Schneider, J., & Dulski, P. (2002). The nature of orthomagmatic, carbonatitic fluids precipitating REE, Sr-rich fluorite: fluid-inclusion evidence from the Okorusu fluorite deposit, Namibia. *Chemical Geology* **186**, 75-98.
- Cadman, A.C., Heaman, L., Tarney, J., Wardle, R., & Krogh, T.E. (1993). U-Pb geochronology and geochemical variation within two Proterozoic mafic dyke swarms, Labrador. *Canadian Journal of Earth Sciences* **30**, 1490-1504.
- Condie, K.C., Bobrow, D.J., & Card, K.D. (1987). Geochemistry of Precambrian Mafic Dykes from the Southern Superior Province of the Canadian Shield. In: Halls, H.C. & Fahrig, W.C. (Eds.), *Mafic dyke swarms*. Geological Association of Canada, Special Publication **34**, 95-107.
- Coogan, L.A., Kempton, P.D., Saunders, A.D., & Norry, M.J. (2000). Melt aggregation within the crust beneath the Mid-Atlantic Ridge: evidence from plagioclase and clinopyroxene major and trace element compositions. *Earth and Planetary Science Letters* **176**, 245-257.
- Cullers, R.L. & Medaris, G.Jr. (1977). Rare earth elements in carbonatite and cogenetic alkaline rocks; examples from Seabrook Lake and Callander Bay, Ontario. *Contributions to Mineralogy and Petrology*, **65**, 143-153.
- Curtis, L.W. & Gittins, J. (1979). Aluminous and titaniferous clinopyroxenes from regionally metamorphosed agpaitic rocks in central Labrador. *Journal of Petrology* **20**, 165-186.
- Dahl-Jensen, T., Thybo, T., Hopper, H., & Rosing, M. (1998). Crustal structure at the SE Greenland margin from wide-angle and normal incidence seismic data. *Tectonophysics* **288**, 191-198.
- Dalton, J.A. & Presnall, D.C. (1998). The continuum of primary carbonatitic-kimberlitic melt compositions in equilibrium with lherzolite: data from the system CaO-MgO-Al₂O₃-SiO₂-CO₂ at 6 GPa. *Journal of Petrology* **39**, 1953-1964.
- Dempster, T.J., Preston, R.J., & Bell, B.R. (1999). The origin of Proterozoic massif-type anorthosites: evidence from interactions between crustal xenoliths and basaltic magma. *Journal of the Geological Society of London* **156**, 41-46.
- DePaolo, D.J. (1981). Trace element and isotopic effects of combined wallrock assimilation and fractional crystallisation. *Earth and Planetary Science Letters* **53**, 189-202.
- Devey, C.W. & Cox, K.G. (1987). Relationships between crustal contamination and crystallisation in continental flood basalt magmas with special reference to the Deccan Traps of the Western Ghats, India. *Earth and Planetary Science Letters* **84**, 59-68.
- Digonnet, S., Goulet, N., Bourne, J., Stevenson, R., & Archibald, D. (2000). Petrology of the Abloviak aillikite dykes, New Quebec; evidence for a Cambrian diamondiferous alkaline province in northeastern North America. *Canadian Journal of Earth Sciences* **37**, 517-533.
- Dobosi, G. & Jenner, G.A. (1999). Petrologic implications of trace element variation in clinopyroxene megacrysts from the Nograd volcanic province, North Hungary; a study by laser ablation microprobe-inductively coupled plasma-mass spectrometry. *Lithos* **46**, 731-749.
- Duchesne, J.C., Liégeois, J.P., Vander Auwera, J., & Longhi, J. (1999). The crustal tongue melting model and the origin of massive anorthosites. *Terra Nova* **11**, 100-105.
- Ellam, R.M., Carlson, R.W., & Shirey, S.B. (1992). Evidence from Re-Os isotopes for plume-lithosphere mixing in Karoo flood basalt genesis. *Nature* **359**, 718-721.
- Emeleus, C.H. (1964). The Grønneal-Ika alkaline complex, South Greenland. The structure and geological history of the complex. *Meddelelser om Grønland* **172**, 75 pp.
- Emeleus, C.H. & Upton, B.G.J. (1976). The Gardar period in southern Greenland. In: Escher, A. & Watt, W.S. (Eds.),

- Geology of Greenland*. Copenhagen: Geological Survey of Greenland, 152-181.
- Emslie, R.F. (1978). Anorthosite massifs, rapakivi granites, and late Proterozoic rifting of North America. *Precambrian Research*, **7**, 61-98.
- Engell, J. & Pedersen, S. (1974). Rb-Sr whole rock isochron age determination from the Bangs Havn intrusion, South Greenland. *Bulletin of the Geological Society of Denmark* **23**, 130-133.
- Ernst, R.E. & Buchan, K.L. (1997). Giant Radiating Dyke Swarms: Their Use in Identifying Pre-Mesozoic Large Igneous Provinces and Mantle Plumes. In: Mahoney, J.J. & Coffin, M.E. (Eds.), *Large Igneous Provinces: Continental, Oceanic, and Planetary Flood Volcanism*. Geophysical Monograph **100**, 297-333.
- Ernst, R.E. & Buchan, K.L. (2001). The use of mafic dike swarms in identifying and locating mantle plumes. In: Ernst, R.E. & Buchan, K.L. (Eds.), *Mantle Plumes: Their Identification Through Time*. Geological Society of America Special Paper **352**, 247-265.
- Escher, A. & Watt, W.S. (1976). Summary of the geology of Greenland. In: Escher, A. & Watt, W.S. (Eds.), *Geology of Greenland*. Copenhagen: Geological Survey of Greenland, 10-16.
- Freestone, I.C. & Hamilton, D.L. (1980). The role of liquid immiscibility in the genesis of carbonatites - an experimental study. *Contributions to Mineralogy and Petrology* **73**, 105-117.
- Fuhrman, M.L., Frost, B.R., & Lindsley, D.H. (1988). Crystallization conditions of the Sybille Monzosyenite, Laramie Anorthosite Complex, Wyoming. *Journal of Petrology* **29**, 699-729.
- Garde, A.A., Hamilton, M.A., Chadwick, B., Grocott, J., & McCaffrey, K.J.W. (2002). The Ketilidian orogen of South Greenland: geochronology, tectonics, magmatism, and fore-arc accretion during Palaeoproterozoic oblique convergence. *Canadian Journal of Earth Sciences* **39**, 765-793.
- Gerlach, D.C., Cliff, R.A., Davies, G.R., Norry, M., & Hodgson, N. (1988). Magma sources of the Cape Verdes archipelago: isotopic and trace element constraints. *Geochimica et Cosmochimica Acta* **52**, 2979-2992.
- Gibson, S.A., Thompson, R.N., Dickin, A.P., & Leonardos, O.H. (1995). High-Ti and Low-Ti mafic potassic magmas: key to plume-lithosphere interactions and continental flood-basalt genesis. *Earth and Planetary Science Letters* **136**, 149-165.
- Grégoire, M., Moine, B.N., O'Reilly, S.Y., Cottin, J.Y., & Giret, A. (2000). Trace element residence and partitioning in mantle xenoliths metasomatized by highly alkaline, silicate- and carbonate-rich melts (Kerguelen Islands, Indian Ocean). *Journal of Petrology* **41**, 477-509.
- Halama, R., Wenzel, T., Upton, B.G.J., Siebel, W., & Markl, G. (2003). A geochemical and Sr-Nd-O isotopic study of the Proterozoic Eriksfjord Basalts, Gardar Province, South Greenland: Reconstruction of an OIB signature in crustally contaminated rift-related basalts. *Mineralogical Magazine* **67**, 831-854.
- Harmer, R.E. & Gittins, J. (1998). The Case for Primary, Mantle-derived Carbonatite Magma. *Journal of Petrology* **39**, 1895-1903.
- Hart, S.R., Hauri, E.H., Oschmann, L.A., & Whitehead, J.A. (1992). Mantle Plumes and Entrainment: Isotopic Evidence. *Science* **256**, 517-520.
- Higgins, M.D. & van Breemen, O. (1992). The age of the Lac-Saint-Jean anorthosite complex and associated mafic rocks, Grenville Province, Canada. *Canadian Journal of Earth Sciences* **29**, 1412-1423.
- Kjarsgaard, B.A. (1998). Phase relations of a carbonated high-CaO nephelinite at 0.2 and 0.5 GPa. *Journal of Petrology* **39**, 2061-2075.
- Kjarsgaard, B.A. & Hamilton, D.L. (1988). Liquid immiscibility and the origin of alkali-poor carbonatites. *Mineralogical Magazine* **52**, 43-55.
- Kolker, A. & Lindsley, D.H. (1989). Geochemical evolution of the Maloin Ranch pluton, Laramie Anorthosite Complex, Wyoming: petrology and mixing relations. *American Mineralogist* **74**, 307-324.
- Konnerup-Madsen, J. & Rose-Hansen, J. (1984). Composition and significance of fluid inclusions in the Ilimaussaq peralkaline granite, South Greenland. *Bulletin de Minéralogie* **107**, 317-326.
- Konnerup-Madsen, J. & Rose-Hansen, J. (1982). Volatiles associated with alkaline igneous rift activity: Fluid inclusions in the Ilimaussaq intrusion and the Gardar granitic complexes (south Greenland). *Chemical Geology* **37**, 79-93.
- Korobeinikov, A.N., Mitrofanov, F.P., Gehör, S., Laajoki, K., Pavlov, V.P., & Mamontov, V.P. (1998). Geology and copper sulphide mineralization of the Salmagorskii Ring Igneous Complex, Kola Peninsula, NW Russia. *Journal of Petrology* **39**, 2033-2041.
- Koster van Groos, A.F. & Wyllie, P.J. (1963). Experimental data bearing on the role of liquid immiscibility in the

- genesis of carbonatites. *Nature* **199**, 801-802.
- Kramm, U. & Kogarko, L.N. (1994). Nd and Sr isotope signatures of the Khibina and Lovozero agpaitic centres, Kola Province, Russia. *Lithos* **32**, 225-242.
- Larsen, L.M. (1976). Clinopyroxenes and coexisting mafic minerals from the alkaline Ilimaussaq intrusion, south Greenland. *Journal of Petrology*, **17**, 258-290.
- Larsen, L.M. (1979). Distribution of REE and other trace elements between phenocrysts and peralkaline undersaturated magmas, exemplified by rocks from the Gardar igneous province, south Greenland. *Lithos* **12**, 303-315.
- Le Bas, M.J. (1989). Diversification of carbonatite. In: Bell, K. (Ed.), *Carbonatites*, London: Unwin Hyman, 428-447.
- LeCheminant, A.N. & Heaman, L.M. (1989). Mackenzie igneous events, Canada: Middle Proterozoic hotspot magmatism associated with ocean opening. *Earth and Planetary Science Letters* **96**, 38-48.
- Lee, W.-J. & Wyllie, P.J. (1994). Experimental data bearing on liquid immiscibility, crystal fractionation, and the origin of calciocarbonatites and natrocarbonatites. *International Geology Review* **36**, 797-819.
- Lemarchand, F., Villemant, B., & Calas, G. (1987). Trace element distribution coefficients in alkaline series. *Geochimica et Cosmochimica Acta* **51**, 1071-1081.
- Liégeois, J.P., Navez, J., Hertogen, J., & Black, R. (1998). Contrasting origin of post-collisional high-K calc-alkaline and shoshonitic versus alkaline and peralkaline granitoids. *Lithos* **45**, 1-28.
- Lightfoot, P.C., Sutcliffe, R.H., & Doherty, W. (1991). Crustal contamination identified in Keweenawan Osler Group Tholeiites, Ontario: A trace element perspective. *Journal of Geology* **99**, 739-760.
- Longhi, J., Fram, M.S., Vander Auwera, J., & Montie, J.N. (1993). Pressure effects, kinetics, and rheology of anorthositic and related magmas. *American Mineralogist* **78**, 1016-1030.
- Longhi, J., Vander Auwera, J., Fram, M.S., & Duchesne, J.-C. (1999). Some Phase Equilibrium Constraints on the Origin of Proterozoic (Massif) Anorthosites and Related Rocks. *Journal of Petrology* **40**, 339-362.
- Markl, G. & Frost, B.R. (1999). The Origin of Anorthosites and Related Rocks from the Lofoten Islands, Northern Norway: II. Calculation of Parental Liquid Compositions for Anorthosites. *Journal of Petrology* **40**, 61-77.
- Markl, G., Marks, M., Schwinn, G., & Sommer, H. (2001). Phase equilibrium constraints on intensive crystallization parameters of the Ilimaussaq Complex, South Greenland. *Journal of Petrology* **42**, 2231-2258.
- Marks, M. & Markl, G. (2001). Fractionation and assimilation processes in the alkaline augite syenite unit of the Ilimaussaq Intrusion, South Greenland, as deduced from phase equilibria. *Journal of Petrology* **42**, 1947-1969.
- Marks, M., Vennemann, T., Siebel, W., & Markl, G. (2003). Quantification of Magmatic and Hydrothermal Processes in a Peralkaline Syenite-Alkali Granite Complex Based on Textures, Phase Equilibria, and Stable and Radiogenic Isotopes. *Journal of Petrology* **44**, 1247-1280.
- Marsh, B.D. (1996). Solidification fronts and magmatic evolution. *Mineralogical Magazine* **60**, 5-40.
- Minarik, W.G. (1998). Complications to carbonate melt mobility due to the presence of an immiscible silicate melt. *Journal of Petrology* **39**, 1965-1973.
- Mitchell, J.N., Scoates, J.S., & Frost, C.D. (1995). High-Al gabbros in the Laramie Anorthosite Complex, Wyoming: Implications for the composition of melts parental to Proterozoic anorthosite. *Contributions to Mineralogy and Petrology* **119**, 166-180.
- Mohr, P.A. (1987). Crustal Contamination in Mafic Sheets: a Summary. In: Halls, H.C. & Fahrig, W.C. (Eds.), *Mafic dyke swarms*. Geological Association of Canada, Special Publication **34**, 75-80.
- Molzahn, M., Reisberg, L., & Wörner, G. (1996). Os, Sr, Nd, Pb, O isotope and trace element data from the Ferrar flood basalts, Antarctica: evidence for an enriched subcontinental lithospheric source. *Earth and Planetary Science Letters* **144**, 529-546.
- Moore, K.R. & Wood, B.J. (1998). The transition from carbonate to silicate melts in the CaO-MgO-SiO₂-CO₂ system. *Journal of Petrology* **39**, 1943-1951.
- Morse, S.A. (1982). A partisan review of Proterozoic anorthosites. *American Mineralogist* **67**, 1087-1100.
- Mysen, B.O. & Boettcher, A.L. (1975). Melting of a hydrous mantle; II, Geochemistry of crystals and liquids formed by anatexis of mantle peridotite at high pressures and high temperatures as a function of controlled activities of water, hydrogen, and carbon dioxide. *Journal of Petrology* **16**, 549-593.
- Nicholson, S.W., Shirey, S.B., Schulz, K.J., & Green, J.C. (1997). Rift-wide correlation of 1.1 Ga Midcontinent rift system basalts: implications for multiple mantle sources during rift development. *Canadian Journal of Earth Sciences* **34**, 504-520.
- Nimis, P. & Vannucci, R. (1995). An ion microprobe study of clinopyroxenes in websteritic and megacrystic xenoliths

- from Hyblean Plateau (SE Sicily, Italy): constraints on HFSE/REE/Sr fractionation at mantle depth. *Chemical Geology* **124**, 185-197.
- O'Hara, M.J. & Herzberg, C. (2002). Interpretation of trace element and isotope features of basalts: relevance of field relations, petrology, major element data, phase equilibria, and magma chamber modeling in basalt petrogenesis. *Geochimica et Cosmochimica Acta* **66**, 2167-2191.
- Paces, J.B. & Bell, K. (1989). Non-depleted sub-continental mantle beneath the Superior Province of the Canadian Shield: Nd-Sr isotopic and trace element evidence from Midcontinent Rift basalts. *Geochimica et Cosmochimica Acta* **53**, 2023-2035.
- Paslick, C.R., Halliday, A.N., Davies, G.R., Mezger, K., & Upton, B.G.J. (1993). Timing of proterozoic magmatism in the Gardar Province, southern Greenland. *Bulletin of the Geological Society of America* **105**, 272-278.
- Pearce, N.J.G. & Leng, M.J. (1996). The origin of carbonatites and related rocks from the Igaliko Dyke Swarm, Gardar Province, South Greenland: field, geochemical and C-O-Sr-Nd isotope evidence. *Lithos* **39**, 21-40.
- Pearce, N.J.G., Leng, M.J., Emeleus, C.H., & Bedford, C.M. (1997). The origins of carbonatites and related rocks from the Grønneidal-Ika Nepheline Syenite complex, South Greenland: C-O-Sr isotope evidence. *Mineralogical Magazine* **61**, 515-529.
- Peck, W.H. & Valley, J.W. (2000). Large crustal input to high ^{18}O anorthosite massifs of the Southern Grenville Province: new evidence from the Morin Complex, Quebec. *Contributions to Mineralogy and Petrology* **139**, 402-417.
- Peng, Z.X., Mahoney, J., Hooper, P., Harris, C., & Beane, J. (1994). A role for lower continental crust in flood basalt genesis? Isotopic and incompatible element study of the lower six formations of the western Deccan Traps. *Geochimica et Cosmochimica Acta* **58**, 267-288.
- Perry, F.V., Baldrige, W.S., & DePaolo, D.J. (1987). Role of asthenosphere and lithosphere in the genesis of late cenozoic basaltic rocks from the Rio Grande rift and adjacent regions of the Southwestern United States. *Journal of Geophysical Research* **92**, 9193-9213.
- Piper, J.D.A., Thomas, D.N., Share, S., & Zhang Qi Rui (1999). The palaeomagnetism of (Mesoproterozoic) Eriksfjord Group red beds, South Greenland: multiphase remagnetization during the Gardar and Grenville episodes. *Geophysical Journal International* **136**, 739-756.
- Platt, R.G. (1996). Nepheline syenite complexes - an overview. In: R.H. Mitchell (Ed.), *Undersaturated alkaline rocks: mineralogy, petrogenesis, and economic potential*. Winnipeg: Mineralogical Society of Canada Short Course **24**, 63-99.
- Poulsen, V. (1964). The sandstones of the Precambrian Eriksfjord Formation in South Greenland. *Rapport Grønlands Geologiske Undersøgelse* **2**, 16 pp.
- Puchtel, I.S., Brüggmann, G.E., & Hofmann, A.W. (1999). Precise Re-Os mineral isochron and Pb-Nd-Os systematics of a mafic-ultramafic sill in the 2.0 Ga Onega plateau (Baltic Shield). *Earth and Planetary Science Letters* **170**, 447-461.
- Samson, I.M., Williams-Jones, A.E., & Weining, L. (1995). The chemistry of hydrothermal fluids in carbonatites: Evidence from leachate and SEM-decrepitate analysis of fluid inclusions from Oka, Quebec, Canada. *Geochimica et Cosmochimica Acta* **59**, 1979-1989.
- Schiellerup, H., Lambert, D.D., Prestvik, T., Robins, B., McBride, J.S., & Larsen, R.B. (2000). Re-Os isotopic evidence for a lower crustal origin of massif-type anorthosites. *Nature* **405**, 781-784.
- Scoates, J.S. & Frost, C.D. (1996). A strontium and neodymium isotopic investigation of the Laramie anorthosites, Wyoming, USA: Implications for magma chamber processes and the evolution of magma conduits in Proterozoic anorthosites. *Geochimica and Cosmochimica Acta* **60**, 95-107.
- Shearer, C.K. & Larsen, L.M. (1994). Sector-zoned aegirine from the Ilimaussaq alkaline intrusion, South Greenland: Implications for trace-element behavior in pyroxene. *American Mineralogist* **79**, 340-352.
- Shirey, S.B., Klewin, K.W., Berg, J.H., & Carlson, R.W. (1994). Temporal changes in the sources of flood basalts: Isotopic and trace element evidence from the 1100 Ma old Keweenaw Mamainse Point Formation, Ontario, Canada. *Geochimica et Cosmochimica Acta* **58**, 4475-4490.
- Spera, F.J. & Bohron, W.A. (2001). Energy-constrained open-system magmatic processes; I, General model and energy-constrained assimilation and fractional crystallization (EC-AFC) formulation. *Journal of Petrology* **42**, 999-1018.

- Stevenson, R., Upton, B.G.J., & Steenfelt, A. (1997). Crust-mantle interaction in the evolution of the Ilimaussaq Complex, South Greenland: Nd isotopic studies. *Lithos* **40**, 189-202.
- Thompson, G.M. & Malpas, J. (2000). Mineral/melt partition coefficients of oceanic alkali basalts determined on natural samples using laser ablation-inductively coupled plasma-mass spectrometry (LAM-ICP-MS). *Mineralogical Magazine* **64**, 85-94.
- Thompson, R.N., Gibson, S.A., Mitchell, J.G., Dickin, A.P., Leonardos, O.H., Brod, J.A., & Greenwood, J.C. (1998). Migrating Cretaceous-Eocene Magmatism in the Serra do Mar Alkaline Province, SE Brazil: melts from the deflected Trindade mantle plume? *Journal of Petrology* **39**, 1493-1526.
- Tiepolo, M., Vannucci, R., Oberti, R., Foley, S., Bottazzi, P., & Zanetti, A. (2000). Nb and Ta incorporation and fractionation in titanian pargasite and kaersutite: crystal-chemical constraints and implications for natural systems. *Earth and Planetary Science Letters* **176**, 185-201.
- Upton, B.G.J. (1974). The alkaline province of South-West Greenland. In: Sørensen, H. (Ed.), *The Alkaline Rocks*. New York: Wiley, 221-238.
- Upton, B.G.J., Stephenson, D. & Martin, A.R. (1985). The Tugtutôq older giant dyke complex: mineralogy and geochemistry of an alkali gabbro-augite-syenite-foyaite association in the Gardar Province of South Greenland. *Mineralogical Magazine* **49**, 624-642.
- Upton, B.G.J. & Emeleus, C.H. (1987). Mid-Proterozoic alkaline magmatism in southern Greenland: the Gardar province. In: Fitton, J.G. & Upton, B.G.J. (Eds.), *The Alkaline Rocks*. Boston: Blackwell Scientific, 449-471.
- Upton, B.G.J., Emeleus, C.H., Heaman, L.M., Goodenough, K.M., & Finch, A. (2003). Magmatism of the mid-Proterozoic Gardar Province, South Greenland: chronology, petrogenesis and geological setting. *Lithos* **68**, 43-65.
- van Breemen, O., Aftalion, M., & Allart, J.H. (1974). Isotopic and Geochronologic Studies on Granites from the Ketilidian Mobile Belt of South Greenland. *Bulletin of the Geological Society of America* **85**, 403-412.
- Veksler, I.V., Nielsen, T.F.D. & Sokolov, S.V. (1998a). Mineralogy of crystallized melt inclusions from Gardiner and Kovdor ultramafic alkaline complexes: implications for carbonatite genesis. *Journal of Petrology* **39**, 2015-2031.
- Veksler, I.V., Petibon, C., Jenner, G.A., Dorfman, A.M., & Dingwell, D.B. (1998b). Trace Element Partitioning in Immiscible Silicate-Carbonate Liquid Systems: an Initial Experimental Study Using a Centrifuge Autoclave. *Journal of Petrology* **39**, 2095-2104.
- Walker, R.J., Morgan, J.W., Hanski, E.J., & Smolkin, V.F. (1997). Re-Os systematics of Early Proterozoic ferropicrites, Pechenga Complex, northwestern Russia: Evidence for ancient ¹⁸⁷Os-enriched plumes. *Geochimica et Cosmochimica Acta* **61**, 3145-3160.
- Wegmann, C.E. (1938). On the structural divisions of southern Greenland. *Meddelelser om Grønland* **113/2**, 148 pp
- Wiebe, R.A. (1990). Evidence for unusually feldspathic liquids in the Nain complex, Labrador. *American Mineralogist* **75**, 1-12.
- Wiebe, R.A. (1992). Proterozoic Anorthosite Complexes. In: Condie, K.C. (Ed.), *Proterozoic crustal evolution*. Amsterdam: Elsevier, 215-261.
- Winther, K.T. (1992). Feldspar megacryst and anorthosite xenolith-bearing dykes in the Narssarsuaq area, South Greenland. *Rapport Grønlands Geologiske Undersøgelse* **154**, 49-59.
- Wood, B.J. & Blundy, J.D. (1997). A predictive model for rare earth element partitioning between clinopyroxene and anhydrous silicate melt. *Contributions to Mineralogy and Petrology* **129**, 166-181.
- Wood, B.J. & Trigila, R. (2001). Experimental determination of aluminous clinopyroxene-melt partition coefficients for potassic liquids, with application to the evolution of the Roman province potassic magmas. *Chemical Geology* **172**, 213-223.
- Wörner, G., Beusen, J.-M., Duchateau, N., Gijbels, R., & Schmicke, H.-U. (1983). Trace element abundances and mineral/melt distribution coefficients in phonolites from the Laacher See Volcano (Germany). *Contributions to Mineralogy and Petrology* **84**, 152-173.
- Wyllie, P.J. & Huang, W.L. (1976). Carbonation and melting relations in the system CaO-MgO-SiO₂-CO₂ at mantle pressures with geophysical and petrological applications. *Contributions to Mineralogy and Petrology* **54**, 79-107.
- Zhao, Z.-F. & Zheng, Y.-F. (2003). Calculation of oxygen isotope fractionation in magmatic rocks. *Chemical Geology* **193**, 59-80.
- Zindler, A. & Hart, S.R. (1986). Chemical geodynamics. *Annual Reviews of Earth and Planetary Sciences* **14**, 493-571.

Kapitel 1:

Geochemische und Sr-Nd-O isotopengeochemische Untersuchungen an den Eriksfjord Basalten

Manuskript-Titel:

A geochemical and Sr-Nd-O isotopic study of the Proterozoic Eriksfjord Basalts, Gardar Province, South Greenland: Reconstruction of an OIB signature in crustally contaminated rift-related basalts.

Autoren:

Ralf Halama¹, Thomas Wenzel¹, Brian G.J. Upton², Wolfgang Siebel¹, Gregor Markl¹

¹ Institut für Geowissenschaften, Eberhard-Karls-Universität Tübingen,
Wilhelmstr. 56, D-72074 Tübingen

² The University of Edinburgh, Department of Geology and Geophysics, West
Mains Road, Edinburgh, EH9 3JW, UK

Veröffentlicht bei:

Mineralogical Magazine 67: 831-854 (2003)

Gutachter:

Tom Andersen (Oslo), Alexei S. Rhuklov (Ottawa), Ian Coulson (Regina)

Eigenanteile:

a) Idee	70%
b) Datenbeschaffung	90%
c) Auswertung und Interpretation	80%
d) Ausarbeitung der Publikation	80%

Abstract

Basalts from the volcano-sedimentary Eriksfjord Formation (Gardar Province, South Greenland) were erupted at around 1.2 Ga into rift-related graben structures. The basalts have compositions transitional between tholeiite and alkaline basalt with MgO contents < 7 wt.% and they display LREE-enrichment relative to a chondritic source. Most of the trace element and REE characteristics are similar to those of basalts derived from OIB-like mantle sources. Initial $^{87}\text{Sr}/^{86}\text{Sr}$ ratios of clinopyroxene separates range from 0.70278 to 0.70383 and initial ϵ_{Nd} values vary from -3.2 to +2.1. The most unradiogenic samples overlap with the field defined by carbonatites of similar age and can be explained by mixing of isotopically depleted and enriched mantle components. Using AFC modelling equations, the Sr-Nd isotope data of the more radiogenic basalts can successfully be modelled by addition of less than 5% lower crustal granulite-facies gneisses as contaminants. $\delta^{18}\text{O}_{\text{v-smow}}$ values of separated clinopyroxene range from +5.2 to +6.0 ‰ and fall within the range of typical mantle-derived rocks. However, up to 10% mixing with an average lower crustal component are permitted by the data.

Introduction

Study of rift-related basaltic magmatism is essential for an improvement in our understanding of the chemical composition of the sub-continental mantle and also the mechanisms responsible for the generation of flood basalts, alkaline rocks and carbonatites. It has been shown that several distinct mantle components can contribute to magmatism in rift-related environments (e.g. Perry *et al.*, 1987, Paces and Bell, 1989, Heaman and Machado, 1992), but that the relative importance of these sources is highly variable in both space and time (Shirey *et al.*, 1994, Nicholson *et al.*, 1997). For example, many occurrences of recent rift-related magmatism have a mantle-plume association (e.g. Baker *et al.*, 1997, Bell and Tilton, 2001). Studies of Proterozoic continental volcanic rocks provide insight into the composition of the mantle and the interplay between mantle and crustal magma sources at that time (e.g. Lightfoot *et al.*, 1991, Shirey *et al.*, 1994). In most models, three main mantle source components have been invoked to explain the geochemical signatures of the erupted rocks: 1. Depleted MORB mantle (DMM), i.e. mantle sources of mid-ocean ridge basalts (MORBs) that are depleted in all incompatible elements. 2. OIB-like mantle, i.e. mantle known from ocean island basalts (OIBs), that is in oceanic regions restricted to islands that are not related to subduction (Hofmann, 1997). This type of mantle is less depleted or even enriched in incompatible elements compared to the primitive mantle. There are several types of OIB components well defined by Sr-Nd-Pb isotopic studies (Zindler and Hart, 1986, Hart *et al.*, 1992). These are HIMU ("high μ ", $\mu \equiv {}^{238}\text{U}/{}^{206}\text{Pb}$), enriched mantle 1 (EM-1) and enriched mantle 2 (EM-2). 3. Subcontinental lithospheric mantle (SCLM), representing the mantle below the continental crust. The SCLM is usually enriched in incompatible elements, but it can be very heterogeneous.

Interaction of an OIB-like source with lithospheric mantle (Ormerod *et al.*, 1988, Paslick *et al.*, 1995, Molzahn *et al.*, 1996) or DMM (e.g. Nicholson *et al.*, 1997) may have played a major role in magma genesis of continental volcanic rocks. Lavas chemically similar to OIBs have been observed in many continental flood basalt provinces, e.g. Deccan Traps (Mahoney, 1988), British Tertiary Volcanic Province (Fitton *et al.*, 1997) and Paraná-Etendeka (Gibson *et al.*, 1997). These are believed to represent mantle-derived melts from plumes not contaminated by lithospheric material, but they represent only a small proportion of the total magma volume erupted (Gibson *et al.*, 1999). Therefore, the SCLM has been invoked in various models either as a source of large-scale melts

(e.g. Turner *et al.*, 1996) or as assimilant in plume-derived melts (e.g. Gibson *et al.*, 1995). The SCLM appears to be especially important in the genesis of small-degree melts (Gibson *et al.*, 1999). Post-Archaean lithospheric mantle is considered to have been sufficiently fertile to have contributed to the genesis of flood basalts (Hawkesworth *et al.*, 1990).

The Gardar Province in South Greenland is a rift-related igneous province with magmatism lasting from about 1.35 to 1.14 Ga (Emeleus and Upton, 1976, Upton and Emelous, 1987, Upton *et al.*, 2003). It comprises about twelve main igneous complexes, numerous dykes of variable chemical composition, and a sequence of rift-related interlayered lavas and sediments (Eriksfjord Formation). The basaltic lavas of the Eriksfjord Formation are among the geochemically most primitive rocks of the Province. However, except for detailed palaeomagnetic investigations (Thomas and Piper, 1992, Piper *et al.*, 1999), they have been studied relatively little (Larsen, 1977, Paslick *et al.*, 1993). Due to their comparatively primitive nature, the basaltic rocks of the Eriksfjord Formation provide a good opportunity to discern the geochemical signatures of the mantle sources of the magmatic activity of the Province. Similar sources may have been involved in the petrogenesis of the Gardar anorthosites, alkali gabbros and nepheline syenites. In this study, we present new geochemical data (XRF analyses of major and trace elements, Sr, Nd and O isotopic analyses, REE analyses of whole-rock samples and *in situ* REE analyses of clinopyroxene) to constrain mantle sources and to determine the role of crustal contamination in the petrogenesis of the Eriksfjord Formation basalts. In particular, high-precision laser-fluorination oxygen isotope data have only recently become an important tool for evaluating the contribution of mantle and continental crust in suites of continental flood basalts (Baker *et al.*, 2000). Since continental intraplate basalts are the only major class of terrestrial basalts that have not yet been explored systematically using these methods (Eiler, 2001), the laser fluorination oxygen isotope data of clinopyroxene separates presented herein are an important contribution to the knowledge of oxygen isotopic compositions of continental basalts in general.

Geological setting

The Eriksfjord Formation (EF) represents a roughly 3500 m thick sequence of Precambrian supracrustal rocks comprising continental sandstones and conglomerates and eruptive rocks and

sills that range from basalt through trachyte to alkaline phonolite and carbonatite (Larsen, 1977). The rocks lie unconformably on the ketilidian Julianehåb batholith dated at 1.85 to 1.79 Ga (van Breemen *et al.*, 1974, Garde *et al.*, 2002) and are cut by the 1.16 Ga Ilímaussaq intrusion (Waight *et al.*, 2002). The type-section of the Eriksfjord Formation occurs on the Ilímaussaq peninsula, and has been subdivided into six stratigraphic groups (Thomas and Piper, 1992), originally defined as members (Poulsen, 1964) (Fig. 1). The three volcanic groups are known as, from oldest to youngest, Mussartût, Ulukasik and Ilímaussaq. The Mussartût Group is subdivided into nine sub-units and the Ilímaussaq Group is subdivided into three sub-units, called Sermilik, Tunugdliarfik and Narssaq Fjeld (Fig. 1). A sandstone unit precedes each volcanic group (Thomas and Piper, 1992). The Mussartût Group contains the Qassiarsuk carbonatite complex, dated at ~ 1.2 Ga by Rb-Sr and Pb-Pb isochrons (Andersen, 1997). Paslick *et al.* (1993) obtained two Sm-Nd isochron ages of 1.17 ± 0.03 and 1.20 ± 0.03 Ga for two samples of the Ulukasik Group. However, palaeomagnetic data indicate an age of 1.35-1.31 Ga for the entire succession (Piper *et al.*, 1999) and the exact age of the EF is as yet unresolved (Upton *et al.*, 2003). Parts of the Eriksfjord lavas have been subjected to extensive metasomatism related to the intrusion of alkaline magmas (Ranlov and Dymek, 1991, Coulson and Chambers, 1996). The local presence of epidote implies thermal metamorphism at temperatures of up to 300-350 °C (Piper *et al.*, 1999). High eruption rates are inferred for the volcanic system and the whole lifespan is considered to be less than ~ 5 Myr (Piper *et al.*, 1999).

Analytical procedures

Electron microprobe analysis

Mineral compositions were determined using a JEOL 8900 electron microprobe (EMP) at the Institut für Geowissenschaften, Universität Tübingen, Germany. An internal $\phi\rho z$ correction of the raw data was applied (Armstrong, 1991). Both natural and synthetic standards were used for major and minor elements. Measuring times were 16 s and 30 s on the peak positions for major and minor elements, respectively. The emission current was 15 nA and the acceleration voltage 15 kV. For feldspar analyses, a beam diameter of 5 μm was used to avoid errors resulting from diffusion of Na.

XRF analysis

Whole-rock analyses were performed by standard X-ray fluorescence (XRF) techniques at the Institut für Geowissenschaften at the Johannes Gutenberg-Universität Mainz, Germany, using a Philips PW 1404 spectrometer, and at the Universität Freiburg, using a Philips PW 2404 spectrometer. Prior to analysis, whole-rock samples were crushed and milled in tungsten carbide mills. The powders obtained were dried at 105°C. Loss of ignition (LOI) determinations were carried out on 1 g of pulverised sample material which was heated for 2 hours at 1000°C. Pressed powder pellets and fused glass discs were prepared to measure contents of trace and major elements, respectively. Natural standards were used for calibration. Detection limits vary between 1 and 9 ppm, depending on the specific trace element and on the instrument used.

Whole-rock REE analyses

Whole-rock REE analyses were carried out by the Natural Environment Research Council (NERC) inductively coupled plasma-atomic emission spectrometry (ICP-AES) facility at Royal Holloway, University of London. Solutions were prepared using a combined HF dissolution and alkali fusion as described in Walsh *et al.* (1981). Resultant solutions were analysed for twelve rare-earth elements and selected potential interferences using a Perkin Elmer Optima 3300RL ICP-AES.

Laser ICP-MS in-situ REE measurement of clinopyroxene

In situ laser ablation inductively coupled plasma-mass spectrometer (LA-ICP-MS) REE analyses on ~ 150 µm thick polished thin sections were performed at the EU Large-Scale Geochemical Facility (University of Bristol) using a VG Elemental PlasmaQuad 3 + S-Option ICP-MS equipped with a 266 nm Nd-YAG laser (VG MicroProbe II). The laser beam diameter at the sample surface was approximately 20 µm. All measurements were made using Thermo Elemental PlasmaLab "time-resolved analysis" (TRA) data acquisition software with a total acquisition time of 100 s per analysis, allowing about 40 s for background followed by 50 s for laser ablation. NIST 610 glass was used for instrument calibration, and NIST 612 was used as a secondary standard. Ca was used as an internal standard to correct the ablation yield differences between and during individual analyses on both standards and samples. To avoid analytical uncertainties due to variations in the

concentrations of the internal standard, Ca concentrations were quantitatively measured within 20 μm of the laser ablation pits using the EMP at the Institut für Geowissenschaften, Universität Tübingen. The precision of trace-element concentrations, based on repeated analyses of standards, is approximately $\pm 5\%$ for element concentrations >10 ppm and $\pm 10\%$ for concentrations <10 ppm. Data processing was carried out offline using the same PlasmaLab software used for data collection and various custom-designed Excel spreadsheets. The limits of detection are defined as 3.28 standard deviations above background level, which is equal to a 95% confidence that the measured signal is significantly above background. Typical detection limits for the REE in this study were 0.04 - 0.6 ppm.

Sr and Nd isotope analysis

For Sr and Nd isotope analyses, 15-20 mg samples of hand-picked clinopyroxene were spiked with mixed ^{84}Sr - ^{87}Rb and ^{150}Nd - ^{149}Sm tracers before dissolution under high pressure in HF at 180°C in poly-tetrafluor-ethylene (PTFE) reaction bombs. Rb and Sr were separated in quartz columns containing a 5 ml resin bed of AG50W-X12, 200 – 400 mesh, equilibrated with 2.5N HCl. Sm and Nd separation was performed in quartz columns, using 1.7 ml Teflon powder coated with HDEHP (Di-Ethyl Hexyl Phosphate) as the cation exchange medium, equilibrated with 0.18N HCl. All analyses were made with a multicollector Finnigan MAT 262 thermal ionisation mass spectrometer (TIMS) in static collection mode at the Institut für Geowissenschaften, Universität Tübingen. Sr was loaded with a Ta-HF activator and measured on a single W filament. Rb, Sm and Nd were measured in a double Re-filament configuration mode. $^{87}\text{Sr}/^{86}\text{Sr}$ and $^{143}\text{Nd}/^{144}\text{Nd}$ ratios were normalised for mass fractionation to $^{86}\text{Sr}/^{88}\text{Sr} = 0.1194$ and $^{146}\text{Nd}/^{144}\text{Nd} = 0.7219$, respectively. The average $^{143}\text{Nd}/^{144}\text{Nd}$ ratio obtained for the Ames Nd-standard (Geological Survey of Canada, Roddick *et al.*, 1992) was 0.512119 ± 10 ($n = 42$) and the average $^{87}\text{Sr}/^{86}\text{Sr}$ ratio for the NBS 987 Sr-standard was 0.710261 ± 16 ($n = 30$) during the course of this study. $^{143}\text{Nd}/^{144}\text{Nd}$ ratios have been cross-checked with the La Jolla Nd-standard which gave 0.511831 ± 30 ($n = 12$). Total procedural blanks (chemistry and loading) were < 200 pg for Sr and < 100 pg for Nd.

Oxygen isotope analysis

The oxygen isotope composition of hand-picked clinopyroxene separates was measured using a method similar to that described by Sharp (1990) and Rumble and Hoering (1994). 1 - 2 mg of hand-picked clinopyroxene were loaded onto a Pt-sample holder. The sample chamber was pumped out to a vacuum of about 10^{-6} mbar and pre-fluorinated overnight. Samples were then heated with a CO₂-laser in an atmosphere of 50 mbars of pure F₂. Excess F₂ is separated from O₂ by conversion to Cl₂ using KCl held at 150°C. The extracted O₂ is collected on a molecular sieve (13X). Oxygen isotopic compositions were measured on a Finnigan MAT 252 mass spectrometer at the Institut für Geowissenschaften, Universität Tübingen. The results are reported as the per mil deviation from Vienna Standard Mean Ocean Water (V-SMOW) in the standard δ -notation. Replicate oxygen isotope analyses of the NBS-28 quartz standard (Valley *et al.*, 1995) had an average precision of $\pm 0.1\%$ for $\delta^{18}\text{O}$. In each run, standards were analysed at the beginning and the end of the sample set. A correction was applied to the data equal to the average of the difference between the mean measured value and the accepted value for the standard (9.64 ‰).

Oxygen isotope compositions of powdered whole-rock samples were determined by a conventional method modified after Clayton and Mayeda (1963), using BrF₅ as reagent and converting the liberated oxygen to CO₂ before mass spectrometric analysis.

Petrography

175 samples were collected from all three volcanic units of the Eriksfjord Formation, but most of them were extensively altered. They contained secondary chlorite, Fe-talc, Ca-Fe silicates and carbonate as alteration products. Since the focus of this study was *in situ* analyses of minerals or analyses of mineral separates, only nine samples with a significant proportion of fresh clinopyroxene and relatively few alteration products were selected for analysis. Due to the limited number of suitable samples, we did not attempt to investigate the lavas in terms of their stratigraphic position. In addition to the nine samples from which pyroxene separates were obtained, REE whole-rock data of six other samples were added to the data set.

In general, the Mussartût Group lavas are olivine-free, but contain up to 50% chloritic matrix that probably results from devitrification of former glass. In contrast, the majority of Ulukasik and

Ilímaussaq Group lavas contain olivine-pseudomorphs and tend to be coarser grained and holocrystalline. Many of them contain "snow-flake" glomerocrysts of plagioclase indicating plagioclase-saturation or super-saturation at near-surface levels (Upton, 1996). The samples from which clinopyroxenes have been separated are fine-grained basalts with plagioclase laths embedded in interstitial clinopyroxene as the major and apatite and Fe-Ti oxides as subordinate primary magmatic mineral phases. The texture can be described as ophitic and is believed to result from the cotectic crystallization of plagioclase and clinopyroxene (Philpotts, 1990). Olivine has been present in a few samples, but it is now completely altered. Pyrite, pyrrhotite and chalcopyrite occur as accessory phases. Some samples contain two oxides (ilmenite + titanomagnetite), whereas others contain a single oxide exsolved into ilmenite and titanomagnetite or ilmenite and hematite. Texturally, they are mostly subhedral to anhedral, although few euhedral grains occur. Hematite is also present around both discrete and exsolved ilmenite and titanomagnetite grains and the exsolved hematite might be entirely of secondary origin formed by oxidation of titanomagnetite. Late-stage interstitial quartz occurs rarely. Sample EF 108 (Ulukasik Group) is remarkable in having an intense reddish colour unlike the other samples that are almost black.

Results

Mineral chemistry

Typical analyses of clinopyroxenes are given in Table 1. Compositions range from $En_{41}Wo_{44}Fs_{16}$ to $En_{28}Wo_{45}Fs_{27}$ and broadly overlap for all groups (Fig. 2). According to the classification of Morimoto *et al.* (1988), clinopyroxenes of the Mussartût and Ulukasik Groups are mainly augites with few diopsides present, whereas in the Ilímaussaq Group samples of diopsidic compositions dominate over augitic ones. Clinopyroxene analyses from the various samples form tight clusters on the pyroxene quadrilateral except for those from sample EF 108 that are more scattered. With only a single pyroxene phase present in all samples, clinopyroxene compositions indicate minimum crystallisation temperatures (Lindsley, 1983) of 750-1000°C (Fig. 2). Plagioclase is normally zoned and its composition typically varies between $An_{70}Ab_{29}Or_1$ and $An_{16}Ab_{72}Or_{12}$. Late interstitial albite can reach compositions of $An_0Ab_{99}Or_1$. There are no significant compositional changes among the various samples. Ilmenite from two samples (EF 024 and EF 039) which contain coexisting ilmenite

and titanomagnetite includes a significant component of pyrophanite (MnTiO_3) with up to 8.7 wt.% MnO. Its compositions vary between $\text{Ilm}_{86}\text{Hem}_5\text{Pyr}_8$ and $\text{Ilm}_{76}\text{Hem}_5\text{Pyr}_{19}$. Titanomagnetite analyses were unsatisfactory as all grains show strong alteration. They are considered unreliable and are not presented here.

Whole-rock geochemistry and classification

Concentrations of major and trace elements are summarized in Table 2. The basalts can be classified according to the TAS diagram (Le Maitre *et al.*, 1989) as basalts and trachybasalts with both alkaline and subalkaline compositions (not shown). Due to possible mobility of the Na and K, the samples were also plotted into Nb/Y vs. Zr/ P_2O_5 and P_2O_5 vs. Zr diagrams (Floyd and Winchester, 1975) which can discriminate between tholeiitic and alkaline series. These diagrams do not yield consistent discriminations for the EF basalts, but indicate that the character of the sample suite is transitional between tholeiitic and alkaline (not shown).

Mg# [$100\text{Mg}/(\text{Mg}+\text{Fe}^{2+})$], calculated assuming $\text{Fe}_2\text{O}_3/\text{FeO} = 0.2$ as recommended for basalts by Middlemost (1989), varies between 54 and 40 (Table 2). Ni concentrations range from 46 to 115 ppm and Cr contents from 29 to 126 ppm. Taking Mg# as fractionation index, a positive correlation ($r^2 = 0.61$) with Ni contents indicates fractionation of olivine (Fig. 3). The relatively poor positive correlations of Mg# with Cr ($r^2 = 0.44$) and Sc ($r^2 = 0.23$) argue against a significant fractionation of Cr-spinel or clinopyroxene. This is consistent with the lack of clinopyroxene phenocrysts and the absence of any Cr-spinel. The negative correlations of Mg# with Sr, TiO_2 and P_2O_5 suggest that fractionation of plagioclase, Fe-Ti oxides and apatite was not important in the sample set investigated, which is again consistent with the mostly subhedral Fe-Ti oxides and the ophitic texture. Ratios of incompatible trace elements, such as Zr/Y (range: 4.0-6.3) and Ti/Y (range: 385-716), are relatively uniform throughout all samples, but some scatter is evident. Notable geochemical features are high Sr contents up to 1000 ppm and very high Ba contents up to 1300 ppm.

Normative mineral compositions were determined according to the CIPW calculation scheme (Cross *et al.*, 1903; Cox *et al.*, 1979). Most samples are hypersthene-normative, some are nepheline-normative and one (EF 059) is quartz-normative (Table 2). Despite the uncertainties involved in the

CIPW norm calculation, the data indicate that some of the basalts crystallised from silica-undersaturated magmas and others from distinct silica-saturated or -oversaturated magmas.

Multi-element diagrams normalized to primitive mantle values show that the EF basalts are enriched in all incompatible elements relative to primitive mantle values (Fig. 4). The patterns of the EF basalts are characterized by a prominent Ba peak, a subordinate P peak and a decreasing element enrichment with increasing compatibility. In comparison with normal MORB (N-MORB), enriched MORB (E-MORB) and average OIB (Sun and McDonough, 1989), the patterns of the EF basalts are closest to those of OIB both in shape and normalized concentrations.

Whole-rock REE data

Whole-rock REE data are presented in Table 3 and REE concentrations, normalised to chondritic values of Boynton (1984), are shown in Fig. 5a. All samples are characterised by LREE-enriched patterns with no, or slightly positive, Eu anomalies ($\text{Eu}/\text{Eu}^* = 0.97$ to 1.13). La concentrations are roughly 20-60 times and Lu concentrations are ~ 10 times chondritic values. Normalised LREE abundances from La to Nd are fairly constant, but the patterns show a steady and smooth decline from Nd towards heavier REE. The REE patterns of the EF basalts fall in between those of typical OIB and E-MORB (Fig. 5b). They have similar patterns and absolute abundances compared to basaltic dykes from the Ivittuut area, South Greenland (Goodenough *et al.*, 2002). La_N/Sm_N , as a measure of LREE fractionation, has a restricted range from 1.30 to 1.65. The degree of HREE fractionation expressed as Gd_N/Yb_N is slightly more variable and ranges from 1.57 to 2.57. Both these ratios of the EF basalts fall generally between typical OIB and E-MORB compositions.

Clinopyroxene REE patterns

Typical analyses of REE concentrations in clinopyroxenes are given in Table 3. They show that REE concentrations in individual minerals of one particular sample can be quite variable. Chondrite-normalised REE patterns of clinopyroxenes are very similar in the samples from the Mussartût and Ulukasik Groups (Fig. 6a,b). They are enriched in all REE relative to chondritic values and the patterns show a fairly steep increase from La to Sm, followed by a gradual smooth decrease from Sm to Lu. Clinopyroxenes from sample EF 168 (Ilímaussaq Group) are distinct as

they have generally higher REE contents, especially in the LREE, and a weak Eu anomaly (Fig. 6c). The 3-10x enrichment in Nd in clinopyroxenes of EF 168 compared to the other samples (EF 024, 039 and 072) seems only partly due to a higher degree of fractionation since the Mg# value of EF 168 is only slightly lower. Thus, the LREE enrichment appears to underline the more alkaline character of this sample. A comparison with published REE patterns of clinopyroxenes (Fig. 6d) shows that the EF patterns are unlike patterns from olivine gabbros with MORB-like signatures (Benoit *et al.*, 1996), but fairly similar to clinopyroxene megacryst patterns from an OIB-like alkaline basalt (Nimis and Vannucci, 1995).

Sr, Nd and O isotopic composition

Sr, Nd and oxygen isotopic compositions of all samples are presented in Table 4. Sr and Nd isotopic compositions of the clinopyroxene separates have been recalculated to an approximate eruption age of 1.2 Ga (Paslick *et al.*, 1993) using decay constants of $1.42 \times 10^{-11} \text{ a}^{-1}$ for ^{87}Rb (Steiger and Jäger, 1977) and $6.54 \times 10^{-12} \text{ a}^{-1}$ for ^{147}Sm (Lugmair and Marti, 1978). Present day CHUR values of 0.1967 for $^{147}\text{Sm}/^{144}\text{Nd}$ (Jacobsen and Wasserburg, 1980) and 0.512638 for $^{143}\text{Nd}/^{144}\text{Nd}$ (Goldstein *et al.*, 1984) were used to calculate initial ϵ_{Nd} values. $^{87}\text{Sr}/^{86}\text{Sr}$ initial ratios are fairly constant and range from 0.70278 to 0.70383 (Table 4). $\epsilon_{\text{Nd}(i)}$ values vary from - 3.2 to + 2.1 (Table 4). On the Sr-Nd isotope diagram, the EF basalts define a relatively steep trend (Fig. 7) with initial $^{87}\text{Sr}/^{86}\text{Sr}$ ratios similar to those of the Bulk Silicate Earth (BSE). Only one sample is slightly displaced towards a more radiogenic initial $^{87}\text{Sr}/^{86}\text{Sr}$ ratio. None of the samples has an ϵ_{Nd} value close to depleted mantle values, estimated to be between $\epsilon_{\text{Nd}} = + 5.3$ (calculated after DePaolo, 1981) and $\epsilon_{\text{Nd}} = + 7.3$ (calculated after Goldstein *et al.*, 1984) at 1.2 Ga. The two alkaline basalts of the Ilímaussaq Group are within the range of the other data, but they define a restricted field around CHUR and BSE, respectively. Errors induced by the uncertainty in the age of the EF basalts are largely within the error of the isotope analyses and do not change the overall picture. In comparison with other published Sr-Nd isotope data from the Gardar Province, the initial Sr isotope ratios of the EF basalts are very similar to relatively primitive basaltic, lamprophyric and carbonatitic dyke rocks which have $(^{87}\text{Sr}/^{86}\text{Sr})_i$ of ~ 0.703 (Pearce and Leng, 1996; Andersen, 1997; Goodenough *et al.*, 2002). So far, no evidence has been presented for an isotopically enriched mantle source in the Gardar

Province as the existing $\epsilon_{\text{Nd}}(i)$ data of -0.5 to +5.2 show a isotopically depleted signature (Pearce and Leng, 1996; Andersen, 1997; Goodenough *et al.*, 2002, Upton *et al.*, 2003). Clinopyroxene from the EF samples of Paslick *et al.* (1993) yield $\epsilon_{\text{Nd}}(i)$ of + 2.2. The Nd isotope data of this study are within the lower range of published values from the Gardar Province and extend the spread to more negative $\epsilon_{\text{Nd}}(i)$ values.

Several recent oxygen isotope studies have shown that mineral separates are less sensitive to low-T alteration and secondary water take-up than whole-rock samples (e.g. Vroon *et al.*, 2001). However, only few oxygen isotope data of mineral separates from continental volcanics are available (e.g. Dobosi *et al.*, 1998; Baker *et al.*, 2000). Extensive studies of mineral separates of ocean island basalts (Eiler *et al.*, 1997) and oceanic-arc lavas (Eiler *et al.*, 2000a) demonstrated that analyses of mineral separates consistently span a narrower range than comparable whole-rock data. In our study, we used clinopyroxene because it is the only fresh mineral phase present in the samples. Oxygen isotope measurements of clinopyroxene separates from the EF basalts show a range in $\delta^{18}\text{O}_{\text{cpx}}$ from +5.2 to +6.0 ‰ with an average value of $+5.66 \pm 0.23$ (1 σ) ‰. All samples overlap the range of $\delta^{18}\text{O}_{\text{cpx}}$ values from mantle peridotites (+5.25 to +5.90 ‰, Matthey *et al.*, 1994), from continental flood basalts from Yemen (+5.5 to +6.9 ‰, Baker *et al.*, 2000) and from alkaline basalts of Hungary (+5.07 to +5.34 ‰, Dobosi *et al.*, 1998). There is a small difference between the averages of Mussartût Group ($\delta^{18}\text{O}_{\text{cpx-avg}} = +5.75 \pm 0.15$ (1 σ) ‰) and Ulukasik Group ($\delta^{18}\text{O}_{\text{cpx-avg}} = +5.75 \pm 0.09$ (1 σ) ‰) samples compared to Ilímaussaq Group ($\delta^{18}\text{O}_{\text{cpx-avg}} = +5.33 \pm 0.21$ (1 σ) ‰) samples.

$\delta^{18}\text{O}$ values of melts coexisting with clinopyroxene were calculated assuming that oxygen in pyroxene and melt were in isotopic equilibrium and T was 1100 °C. $\Delta_{\text{melt-cpx}}$ can then be calculated using the following equation of Kalamarides (1986):

$$\Delta_{\text{melt-cpx}} = - 0.0008 T + 1.43 \text{ (T in Kelvin)}$$

Although fractionation varies with magmatic temperatures, we consider the temperature of 1100 °C and the resulting $\Delta_{\text{melt-cpx}}$ of + 0.3 ‰ as sufficiently representative considering the analytical errors involved. It is similar to $\Delta_{\text{melt-cpx}}$ values used in previous studies (+ 0.39 ‰: Vroon *et al.*, 2001; + 0.2 ‰: Dobosi *et al.*, 1998). Resulting $\delta^{18}\text{O}_{\text{melt}}$ values of EF basalts range from +5.5 to +6.3 ‰. These

values can be compared to whole-rock data from continental basalts given by Harmon and Hoefs (1995). Intraplate basalts from continental rift zones show a range from +4.6 to +8.3 ‰ with a mean of +6.1‰ and continental flood basalts, which are rather poorly represented in the database, have values between +4.3 and +6.5 ‰. Calculated EF model melt oxygen isotope data are within the ranges of both groups. Compared to Igaliko dyke rocks from further SE in the Gardar Province (Pearce and Leng, 1996), the EF basalts cover a much more restricted field, possibly because $\delta^{18}\text{O}$ whole-rock analyses are more prone to secondary alteration than analyses of mineral separates (Fig. 8). Whole-rock $\delta^{18}\text{O}$ measurements of the underlying Julianehåb Granite and of the sedimentary sandstone members of the Eriksfjord Formation yield values of 7.8 ‰ and 6.8 - 11.5 ‰, respectively (Table 4), and are shown for comparison.

Discussion

Mantle source regions of the EF basalts

To reconstruct the mantle sources involved in the formation of the EF basalts, we use Sr-Nd-O isotope and incompatible trace element data. On a Sr-Nd isotope diagram, the isotopic composition of DMM was modelled for an age of 1.2 Ga (DePaolo 1981, Goldstein *et al.*, 1984, Taylor and McLennan, 1985). The fairly constant $^{87}\text{Sr}/^{86}\text{Sr}$ initial isotope ratios of the EF basalts are ~ 0.703 which falls within the range typical for mantle-derived rocks, but slightly above calculated values for DMM (Fig. 7). $\epsilon_{\text{Nd}(i)}$ values are more scattered and indicate that the rocks contain a mixture of isotopic components from both mantle and crustal reservoirs or a heterogeneous mantle source. Only one sample (EF 108) has an $\epsilon_{\text{Nd}(i)}$ value significantly above 0. This sample exhibits the largest spread of clinopyroxene compositions, which may reflect strong alteration. Goodenough *et al.* (2002) also note that the highest ϵ_{Nd} occurs in the most altered sample of their sample set. However, Paslick *et al.* (1993) report clinopyroxene data from two Ulukasik Group samples with $\epsilon_{\text{Nd}(i)} > +2$, and those samples were apparently not disturbed with regard to their Sm-Nd age information. On the other hand, Piper *et al.* (1999) suggest that the Sm-Nd systematics of those samples may be erroneous due to later disturbance by fluids derived from the Ilímaussaq intrusion. Therefore, although we are presently not able to decide whether positive $\epsilon_{\text{Nd}(i)}$ values for the EF basalts are

real, it is clear that none of those values is close to values of a 1.2 Ga old DMM source (i.e. $\epsilon_{\text{Nd}} = +5$ to $+7$).

The Sr-Nd isotopic composition for OIB-type sources in the Proterozoic is not as well constrained as DMM. Today, OIB-type mantle sources have a wide range of isotopic compositions that partly overlap with DMM, but ϵ_{Nd} values are generally lower (Hart *et al.*, 1992, Hofmann, 1997). The EM-1 mantle component is characterised by extremely low $^{143}\text{Nd}/^{144}\text{Nd}$ ratios and ϵ_{Nd} values of between 0 and -5 (Hofmann, 1997). A possible 1.2 Ga position for EM-1 is plotted in Fig. 7, calculated according to Schleicher *et al.* (1998) with $^{147}\text{Sm}/^{144}\text{Nd} = 0.18$ and $^{87}\text{Rb}/^{86}\text{Sr} = 0.10$. The present-day values used in the calculation are $^{143}\text{Nd}/^{144}\text{Nd} = 0.51234$ and $^{87}\text{Sr}/^{86}\text{Sr} = 0.7057$, taken from ocean island basalts closest to an EM-1 end-member (Hofmann, 1997). Other Sr-Nd isotope data from the Gardar Province are plotted to put further constraints on the mantle sources of the EF basalts (Fig. 7). We also added comparative data from African and Canadian carbonatites of similar age because there is a well known similarity between Sr-Nd isotopic data of OIBs and carbonatites (Bell and Blenkinsop, 1989). The linear array of the carbonatite data is considered to be the result of mixing between the two mantle components HIMU and EM-1 (Bell and Blenkinsop, 1989, Bell and Tilton, 2001). The carbonatites from the Gardar Province have similar Nd but slightly more radiogenic Sr isotopic compositions than the reference carbonatite data (Fig. 7). The least contaminated samples overlap with the linear array and the more radiogenic Sr isotopic composition can be explained by crustal contamination (Andersen, 1997). We therefore consider it possible that the Gardar carbonatites also represent mixing of hypothetical HIMU and EM-1 components of an OIB-like source. Since the isotopically most primitive EF basalt samples overlap with the Qassiarsuk carbonatites, it could be possible that the basalts also contain such mantle components, although Pb isotope data for the EF basalts that could clarify the importance of a HIMU source are lacking. Based on the Sr-Nd isotope data, the EF basalts appear to be derived from a heterogeneous OIB-like mantle source that comprises isotopically depleted and enriched components. OIB-like and carbonatitic magmatism are often attributed to mantle plume activity (Bell and Simonetti, 1996, Hofmann, 1997, Simonetti *et al.*, 1998). A plume input to the formation of the EF basalts is supported by the relative large volume of magmas and the short duration (< 5 Ma) of magmatism (Piper *et al.*, 1999). It is also compatible with the geological setting of a continental breakup.

Additionally, a plume component appears to be necessary to explain the thermal input, as it is difficult to melt a cold lithosphere section (Arndt and Christensen, 1992).

Oxygen isotope data of the EF basalts are generally consistent with a mantle derivation, including an OIB-like mantle source. On the $\delta^{18}\text{O}$ versus $\epsilon_{\text{Nd}(i)}$ diagram (Fig. 8), the overlap between the EF data, clinopyroxene data from EM-1-like oceanic basalts and the hypothetical EM-1 end-member suggests an involvement of an EM-1-type mantle source. Olivines from HIMU-like sources are known to be slightly lower in $\delta^{18}\text{O}$ than typical upper mantle values from MORBs (Eiler *et al.*, 1997), but the EF data are not sufficient to assess if the slightly lower $\delta^{18}\text{O}$ values in the Ilímaussaq Group basalts are caused by a relatively higher input from a HIMU source.

The contribution of the various mantle sources to the EF basalts can also be evaluated on the primitive mantle-normalized multi-element diagram (Fig. 4) and on the REE plots (Figs. 5 and 6). Both the whole-rock REE and the clinopyroxene REE patterns of the EF basalts are unlike those representative of N-MORB sources. We conclude again that DMM did not play a major role in the petrogenesis of the EF basalts. On the other hand, similarities with OIB-like mantle sources are more prominent. The shape of the clinopyroxene REE pattern closely resembles those from clinopyroxene of OIB-like alkaline basalts, despite differences in absolute concentrations. The whole-rock REE patterns of the EF basalts lie between E-MORB and average OIB patterns, as do the multi-element patterns. On the latter, the EF basalts have marked positive Ba and P peaks that are not present in typical OIBs. However, Ba contents should be interpreted with caution since highly variable Zr/Ba ratios from 0.14 to 0.70 are an indication that Ba was re-mobilised after emplacement of the basalts (e.g. Price *et al.*, 1991, Oliveira and Tarney, 1995). Likewise, P mobility was demonstrated in altered basaltic rocks (Winchester and Floyd, 1976). In summary, the REE and trace element data are evidence that the mantle source(s) of the EF basalts were enriched in incompatible trace elements relative to primitive mantle.

For relatively primitive *hy*-normative basaltic rocks of the Ivittuut area further north in the Gardar Province it has been argued that some of them were derived from a lithospheric mantle source previously enriched by subduction-related processes. This interpretation is based on certain geochemical characteristics such as high La/Nb ratios and negative Nb anomalies (Goodenough *et al.*, 2002). For the EF basalts, negative Nb anomalies are not clearly discernible, but La/Nb ratios

are > 1 which seems to be a characteristic feature of a lithospheric mantle source (Fitton, 1995). La/Ba, La/Rb and La/K ratios were also used to argue for a lithospheric origin of the Gardar basic magmas, although a mantle plume involvement was assumed to provide the required energy (Upton and Emeleus, 1987, Upton *et al.*, 2003). Since feldspar is the only primary magmatic mineral in the EF basalts in which Ba, Rb and K are incorporated in significant amounts and the feldspars are generally altered, these elements might have been easily mobilised and we therefore do not dare to base the interpretation of the EF basalts sources on these data. In addition, the lack of precise geochemical data on the composition of the lithosphere below the Gardar Province complicates an evaluation of the lithospheric contribution to the EF basaltic magmatism.

Certain ratios of incompatible trace elements of the EF basalts are compared to several occurrences of ocean island basalts representative for EM-1 and HIMU sources in Table 5. Ratios between highly incompatible trace elements do not change significantly during partial melting or fractional crystallisation in basaltic systems and may therefore constrain the ratios in their sources (Weaver *et al.*, 1987). The EF basalts are subdivided into the more alkaline, isotopically primitive Ilímaussaq Group samples and those samples with $\epsilon_{\text{Nd}(i)} < -1$. The Ilímaussaq Group samples have higher Sr/Nd, La/Nb and Zr/Nb ratios than HIMU and overlap with the upper range of EM-1 ratios. The EF basalts with $\epsilon_{\text{Nd}(i)} < -1$ have generally higher ratios than the oceanic island basalts and partly overlap with typical values of the lower crust. It therefore seems likely that assimilation of lower crustal material may have changed the primary trace element ratios in the basalts. Therefore, we will evaluate the possible influence of assimilation of crustal material on the geochemistry of the EF basalts in the following section.

The role of crustal contamination

Large amounts of bulk assimilation of crustal material, which is relatively SiO₂-rich compared to a basaltic melt, would drive the compositions to higher SiO₂ contents and quartz-normative compositions. Partial melts derived from crustal rocks would also be relatively SiO₂-rich (Beard *et al.*, 1993; Carroll and Wyllie, 1990) and would have the same effect. The *ne*-normative character of the EF basalts (Table 1) suggests that assimilation of crustal material, especially of silica-rich upper crustal rocks, was not significant with the possible exception of sample EF 059.

On the primitive mantle-normalized multi-element diagrams (Fig. 4), Ti troughs are typical for crustal rocks, especially for the Upper Crust (Rudnick and Fountain, 1995) and they may therefore be present in rocks extensively contaminated by continental crust. Ti troughs are generally lacking in the patterns of the EF basalts and a major upper crustal contribution to the magmas can therefore be excluded. However, small amounts of assimilation of lower crustal material cannot be ruled out because the average lower crust has higher Ti contents.

Steep trends on Sr-Nd isotope plots have been attributed to assimilation of granulite facies gneisses (e.g. Bernstein *et al.*, 1998). AFC modelling based on an equation developed by DePaolo (1981) was performed to test the hypothesis of small amounts of contamination with lower crustal material (Fig. 9). The basaltic magma which represents one end-member for the calculations has the isotopic signature of the isotopically most primitive samples from the present data set and from the literature (Table 6). Two possible contaminants representing upper and lower crustal compositions were selected for modelling (Table 6). The representative samples are a granite from the Julianeåb batholith for the upper crust (sample JG 02) and an average of five granulite-facies gneisses with low Rb/Sr ratios from the Archaean craton of West Greenland (Taylor *et al.*, 1984) for the lower crust. An influence of Archaean rocks on Gardar magmas has been demonstrated by Pb isotope studies (Taylor and Upton, 1993) and seismic data were also interpreted to reflect the existence of a wedge of Archaean crust that extends southwards to Lindenow Fjord (Dahl-Jensen *et al.*, 1998). We have shown in the previous sections, on the basis of Ni trends, that fractionation of olivine was most relevant to the major element evolution of the lavas, whereas fractionation of other phases was apparently of minor importance. We therefore modelled the AFC processes with olivine fractionation using mineral-melt partition coefficients of 0.014 for Sr and 0.0066 for Nd (Rollinson, 1993).

The modelling of AFC processes is strongly dependent on the parameter r , defined as the ratio of mass assimilation rate and fractional crystallisation rate (DePaolo, 1981). The change in isotopic signature becomes enhanced for higher values of r . Reiners *et al.* (1995) have shown that r values might be very high and even > 1 in the early stages of magmatic evolution at high temperatures since crystallisation can be suppressed by assimilation. Therefore, we calculated AFC processes with two r -values of 0.5 and 0.8 that represent a relatively high and a middle to low assimilation

rate to demonstrate the effects of variable r (Fig. 9). The results indicate that AFC processes involving upper crust similar to the Julianehåb Granite cannot explain the trend of the EF basalts because Sr isotopic compositions would shift to considerably more radiogenic values. This result is consistent with the conclusions derived from trace element data. AFC curves for assimilation of lower crust, however, agree well with the bulk of the data. The most negative ϵ_{Nd} values can be explained by AFC processes with intermediate assimilation rates ($r = 0.5$) involving assimilation of < 5% lower crustal material. With a greater degree of assimilation and an r value of 0.8, < 4% assimilation is indicated.

Lower crustal rocks of igneous origin have an average $\delta^{18}\text{O}$ value of $+7.5 \pm 1.4$ ‰ with an overall range from +5.4 to +12.5 ‰ (Fowler and Harmon, 1990). 5% to 10% bulk assimilation of lower crustal material with $\delta^{18}\text{O} = +7.5$ ‰ into a typical mantle-derived magma with $\delta^{18}\text{O} = +5.7$ ‰ results in $\delta^{18}\text{O}$ values of the contaminated magma from +5.79 to +5.88 ‰. Therefore, the $\delta^{18}\text{O}$ data cannot be used to rule out small amounts of assimilation of lower crust. To evaluate how much contamination would be permissible from the present oxygen isotope data, we calculated how much contamination of a mantle-derived magma with $\delta^{18}\text{O} = +5.7$ ‰ with a contaminant within the lower range of lower crustal xenoliths ($\delta^{18}\text{O} = +6.7$ ‰) would drive the oxygen isotopic composition to the highest value of the EF basalts ($\delta^{18}\text{O} \sim +6.3$ ‰). Although simple mixing shows that 60% assimilation are permissible, this amount would drive the whole-rock geochemistry to more silicic compositions than what is observed in the EF basalts. In Fig. 8, there is no obvious trend from the basalts towards the Ketilidian basement, suggesting again that upper crust was not assimilated in significant amounts.

Ratios of trace elements incompatible in basaltic systems can be used to distinguish between crust and mantle reservoirs (e.g. Weaver, 1991). Based on the AFC modelling, EF basalts with $\epsilon_{\text{Nd}(i)} < -1$ are those which are most likely influenced by crustal contamination. The relatively high La/Nb and Zr/Nb ratios of these samples are consistent with assimilation of lower crustal material. Sr/Nd ratios are even higher than the average lower crustal composition, but Sr/Nd ratios in those samples which were taken as representative for the lower crust in the AFC modelling can reach values of 80, i.e. well above the highest EF basalt ratios. Again, the Sr/Nd ratios support the hypothesis of some lower crustal contamination.

The absence of more primitive basaltic rocks with MgO > 8 wt.% might also indicate lower crustal assimilation. It suggests that magmas may have been retained at depth where they acquired more evolved compositions by fractional crystallisation and had the opportunity to assimilate lower crustal material during crustal underplating (Upton *et al.*, 2003).

Summary and conclusions

The new geochemical data of the Eriksfjord Formation basalts in the Gardar Province provided in this study are used to make petrogenetic constraints about the sources of their parental magmas. Based on trace element patterns and Sr-Nd isotopic constraints, there seems to be no indication that a DMM-like source played an important role in magma genesis of the EF basalts. Clinopyroxene and whole-rock REE patterns are more compatible with an OIB-like source, but we are not able to conclude whether the observed enrichment in REE reflects the source's signature or magmatic processes. The isotopically most primitive EF basalts have Sr-Nd isotopic compositions that are similar to Gardar carbonatites. Due to the isotopic similarity between carbonatites and OIBs, many are thought to be related to mantle plumes (Bell, 2001). We therefore speculate that OIB-like mantle components from a plume source were also involved in the parental EF magmas, but we cannot exclude interaction with the SCLM. Two distinct mantle components, one isotopically depleted and another one enriched, could have contributed to the EF magmas. AFC modelling of Sr-Nd isotope data indicates that assimilation of less than 5% lower crust could explain the steep vector on the Sr-Nd isotope plot, but assimilation of upper crustal material is unlikely. Oxygen isotope data of clinopyroxene separates are consistent with a mantle origin but permit some assimilation of lower crustal rocks. In summary, the data are consistent with the hypothesis that the EF magmas could have been originated from a mantle plume source, which is supported by geological arguments, and that they underwent some assimilation of lower crustal material.

Acknowledgements

We would like to thank Bruce Paterson who provided invaluable help during Laser ICP-MS measurements at the Large-Scale Geochemical Facility supported by the European Community - Access to Research Infrastructure action of the Improving Human Potential Programme, contract

number HPRI-CT-1999-00008 awarded to Prof. B.J. Wood (University of Bristol). Gabi Stoschek and Torsten Vennemann are thanked for their help with oxygen isotope measurements. Elmar Reitter expertly assisted with preparation and measurements of radiogenic isotopes and Mathias Westphal helped with microprobe measurements. REE whole-rock analyses were kindly provided by the NERC facility at Royal Holloway, University of London. Michael Marks is thanked for his pleasant company during fieldwork. Very constructive reviews by Tom Andersen and Alexei S. Rukhlov greatly helped to improve the manuscript. We also thank Ian Coulson for final editing. Financial funding of this work by the Deutsche Forschungsgemeinschaft (grant Ma-2135/1-2) is gratefully acknowledged.

References

- Andersen, T. (1997) Age and petrogenesis of the Qassiarsuk carbonatite-alkaline silicate volcanic complex in the Gardar rift, South Greenland. *Mineralogical Magazine*, **61**, 499-513.
- Armstrong, J.T. (1991) Quantitative elemental analysis of individual microparticles with electron beam instruments. Pp. 261-315 in: *Electron Probe Quantitation* (K.F.J. Heinrich and D.E. Newbury, editors). Plenum Press, New York and London.
- Arndt, N.T. and Christensen, U. (1992) The role of lithospheric mantle in continental flood volcanism: Thermal and geochemical constraints. *Journal of Geophysical Research*, **97**, 10967-10981.
- Baker, J.A., MacPherson, C.G., Menzies, M.A., Thirlwall, M.F., Al-Kadasi, M., and Matthey, D.P. (2000) Resolving crustal and mantle contributions to continental flood volcanism, Yemen; constraints from mineral oxygen isotope data. *Journal of Petrology*, **41**, 1805-1820.
- Baker, J.A., Menzies, M.A., Thirlwall, M.F., and Macpherson, C.G. (1997) Petrogenesis of Quaternary Intraplate Volcanism, Sana'a, Yemen: Implications for Plume-Lithosphere Interaction and Polybaric Melt Hybridization. *Journal of Petrology*, **38**, 1359-1390.
- Beard, J.S., Abitz, R.J., and Lofgren, G.E. (1993) Experimental melting of crustal xenoliths from Kilbourne Hole, New Mexico and implications for the contamination and genesis of magmas. *Contributions to Mineralogy and Petrology*, **115**, 88-102.
- Bell, K. (2001) Carbonatites; relationships to mantle-plume activity. *Geological Society of America Special Paper*, **352**, 267-290.
- Bell, K. and Blenkinsop, J. (1989) Neodymium and Strontium Isotope Geochemistry of Carbonatites. in: *Carbonatites - Genesis and Evolution* (K. Bell, editor). Unwin Hyman, London.
- Bell, K. and Simonetti, A. (1996) Carbonatite Magmatism and Plume Activity: Implications from the Nd, Pb and Sr Isotope Systematics of Oldoinyo Lengai. *Journal of Petrology*, **37**, 1321-1339.
- Bell, K. and Tilton, G.R. (2001) Nd, Pb and Sr Isotopic Compositions of East African Carbonatites: Evidence for Mantle Mixing and Plume Inhomogeneity. *Journal of Petrology*, **42**, 1927-1945.
- Benoit, M., Polvé, M., and Ceuleneer, G. (1996) Trace element and isotopic characterization of mafic cumulates in a fossil mantle diapir (Oman ophiolite) *Chemical Geology*, **134**, 199-214.
- Bernstein, S., Kelemen, P.B., Tegner, C., Kurz, M.D., Blusztajn, J., and Kent Brooks, C. (1998) Post-breakup basaltic magmatism along the East Greenland Tertiary rifted margin. *Earth and Planetary Science Letters*, **160**, 845-862.
- Boynton, W.V. (1984) Geochemistry of the rare earth elements: meteorite studies. Pp. 63-114 in: *Rare earth element geochemistry* (P. Henderson, editor). Elsevier, Amsterdam.
- Carroll, M.R. and Wyllie, P.J. (1990) The system tonalite-H₂O at 15 kbar and the genesis of calc-alkaline magmas. *American Mineralogist*, **75**, 345-357.
- Chauvel, C., Hofmann, A.W., and Vidal, P. (1992) HIMU-EM: The French Polynesian connection. *Earth and Planetary Science Letters*, **110**, 99-119.
- Clayton, R.N. and Mayeda, T.K. (1963) The use of bromine pentafluoride in the extraction of oxygen from oxides and silicates for isotope analysis. *Geochimica et Cosmochimica Acta*, **27**, 43-52.
- Cliff, R.A., Baker, P.E., and Mateer, N.J. (1991) Geochemistry of Inaccessible Island volcanics. *Chemical Geology*, **92**, 251-260.
- Coulson, I.M. and Chambers, A.D. (1996) Patterns of zonation in rare-earth-bearing minerals in nepheline syenites of the North Qôroq center, South Greenland. *The Canadian Mineralogist*, **34**, 1163-1178.
- Cox, K.G., Bell, J.D., and Pankhurst, R.J. (1979) *The interpretation of igneous rocks*. George, Allen and Unwin, London.
- Cross, W., Iddings, J.P., Pirsson, L.V., and Washington, H.S. (1903) *Quantitative classification of igneous rocks*. University of Chicago Press.
- Dahl-Jensen, T., Thybo, T., Hopper, H., and Rosing, M. (1998) Crustal structure at the SE Greenland margin from wide-angle and normal incidence seismic data. *Tectonophysics*, **288**, 191-198.
- DePaolo, D.J. (1981) Trace element and isotopic effects of combined wallrock assimilation and fractional crystallisation. *Earth and Planetary Science Letters*, **53**, 189-202.
- DePaolo, D.J. (1988) *Neodymium isotope geochemistry: An introduction*. Springer Verlag, New York.
- Dobosi, G., Downes, H., Matthey, D., and Embey-Isztin, A. (1998) Oxygen isotope ratios of phenocrysts from alkali

- basalts of the Pannonian basin: Evidence for an O-isotopically homogeneous upper mantle beneath a subduction-influenced area. *Lithos*, **42**, 213-223.
- Eiler, J.M. (2001) Oxygen Isotope Variations of Basaltic Lavas and Upper Mantle Rocks. Pp 319-364 in: *Reviews in Mineralogy and Geochemistry*, "Stable Isotope Geochemistry" vol. 43 (J.W. Valley and D.R. Cole, editors). The Mineralogical Society of America, Washington DC, USA.
- Eiler, J.M., Farley, K.A., Valley, J.W., Hauri, E., Craig, H., Hart, S.R., and Stolper, E.M. (1997) Oxygen isotope variations in ocean island basalt phenocrysts. *Geochimica et Cosmochimica Acta*, **61**, 2281-2293.
- Eiler, J.M., Crawford, A., Elliot, T., Farley, K.A., Valley, J.W., and Stolper, E.M. (2000a) Oxygen isotope geochemistry of oceanic-arc lavas. *Journal of Petrology*, **41**, 229-256.
- Eiler, J.M., Schiano, P., Kitchen, N., and Stolper, E.M. (2000b) Oxygen-isotope evidence for recycled crust in the sources of mid-ocean-ridge basalts. *Nature*, **403**, 530-534.
- Emeleus, C.H. and Upton, B.G.J. (1976) The Gardar period in southern Greenland. Pp 152-181 in: *Geology of Greenland* (A. Escher and W.S. Watt, editors). Geological Survey of Greenland, Copenhagen.
- Fitton, J.G. (1995) Coupled molybdenum and niobium depletion in continental basalts. *Earth and Planetary Science Letters*, **136**, 715-721.
- Fitton, J.G., Saunders, A.D., Norry, M.J., Hardarson, B.S., and Taylor, R.N. (1997) Thermal and chemical structure of the Iceland plume. *Earth and Planetary Science Letters*, **153**, 197-208.
- Floyd, P.A. and Winchester, J.A. (1975) Magma-type and tectonic setting discrimination using immobile elements. *Earth and Planetary Science Letters*, **27**, 211-218.
- Fowler, M.B. and Harmon, R.S. (1990) The oxygen isotope composition of lower crustal granulite xenoliths. Pp 493-506 in: *Granulites and Crustal Evolution* (D. Vielzeuf and P. Vidal, editors). Kluwer Academic Publishers, Dordrecht, The Netherlands.
- Garde, A.A., Hamilton, M.A., Chadwick, B., Grocott, J., and McCaffrey, K.J.W. (2002) The Ketilidian orogen of South Greenland: geochronology, tectonics, magmatism, and fore-arc accretion during Palaeoproterozoic oblique convergence. *Canadian Journal of Earth Sciences*, **39**, 765-793.
- Gibson, S.A., Thompson, R.N., Dickin, A.P., and Leonardos, O.H. (1995) High-Ti and Low-Ti mafic potassic magmas: key to plume-lithosphere interactions and continental flood-basalt genesis. *Earth and Planetary Science Letters*, **136**, 149-165.
- Gibson, S.A., Thompson, R.N., Weska, R.K., and Dickin, A.P. (1997) Late-Cretaceous rift-related upwelling and melting of the Trindade starting mantle-plume head beneath western Brazil. *Contributions to Mineralogy and Petrology*, **126**, 303-314.
- Gibson, S.A., Thompson, R.N., Leonardos, O.H., Dickin, A.P., and Mitchell, J.G. (1999) The limited extent of plume-lithosphere interactions during continental flood-basalt genesis: geochemical evidence from Cretaceous magmatism in southern Brazil. *Contributions to Mineralogy and Petrology*, **137**, 147-169.
- Goldstein, S.L., O'Nions, R.K., and Hamilton, P.J. (1984) A Sm-Nd isotopic study of the atmospheric dust and particulates from major river systems. *Earth and Planetary Science Letters*, **70**, 221-236.
- Goodenough, K.M., Upton, B.G.J., and Ellam, R.M. (2002) Long-term memory of subduction processes in the lithospheric mantle: evidence from the geochemistry of basic dykes in the Gardar Province of south Greenland. *Journal of the Geological Society of London*, **159**, 705-714.
- Harmon, R.S. and Hoefs, J. (1995) Oxygen isotope heterogeneity of the mantle deduced from global ^{18}O systematics of basalts from different geotectonic settings. *Contributions to Mineralogy and Petrology*, **120**, 95-114.
- Harris, C., Smith, H.S., and le Roex, A.P. (2000) Oxygen isotope composition of phenocrysts from Tristan da Cunha and Gough Island lavas: variation with fractional crystallization and evidence for assimilation. *Contributions to Mineralogy and Petrology*, **138**, 164-175.
- Hart, S.R., Hauri, E.H.; Oschmann, L.A. and Whitehead, J.A. (1992) Mantle Plumes and Entrainment: Isotopic Evidence. *Science*, **256**, 517-520.
- Hawkesworth, C.J., Kempton, P.D., Rogers, N.W., Ellam, R.M., and van Calsteren, P.W. (1990) Continental mantle lithosphere, and shallow level enrichment processes in the Earth's mantle. *Earth and Planetary Science Letters*, **96**, 256-268.
- Heaman, L.M. and Machado, N. (1992) Timing and origin of midcontinent rift alkaline magmatism, North America: evidence from the Coldwell Complex. *Contributions to Mineralogy and Petrology*, **110**, 289-303.
- Hofmann, A. (1997) Mantle geochemistry: the message from oceanic volcanism. *Nature*, **385**, 219-229.

- Humphris, S.E. and Thompson, G. (1983) Geochemistry of rare earth elements in basalts from the Walvis Ridge: implications for its origin and evolution. *Earth and Planetary Science Letters*, **66**, 223-242.
- Jacobsen, S.B. and Wasserburg, G.J. (1980) Sm-Nd isotopic evolution of chondrites. *Earth and Planetary Science Letters*, **50**, 139-155.
- Kalamarides, R.I. (1986) High-temperature oxygen isotope fractionation among the phases of Kiglapait intrusion, Labrador, Canada. *Chemical Geology*, **58**, 303-310.
- Larsen, J.G. (1977) Petrology of the late lavas of the Eriksfjord Formation, Gardar province, South Greenland. *Bulletin Grønlands Geologiske Undersøgelse*, **125**, 31 pp.
- Le Maitre, R.W., Bateman, P., Dudek, A., Keller, J., Lameyre Le Bas, M.J., Sabine, P.A., Schmid, R., Sørensen, H., Streckeisen, A., Woolley, A.R., and Zanettin, B. (1989) *A classification of igneous rocks and glossary of terms*. Blackwell, Oxford.
- Lightfoot, P.C., Sutcliffe, R.H., and Doherty, W. (1991) Crustal contamination identified in Keweenawan Osler Group Tholeiites, Ontario: A trace element perspective. *Journal of Geology*, **99**, 739-760.
- Lindsley, D.H. (1983) Pyroxene thermometry. *American Mineralogist*, **68**, 477-493.
- Lugmair, G.W. and Marti, K. (1978) Lunar initial $^{143}\text{Nd}/^{144}\text{Nd}$: differential evolution of the lunar crust and mantle. *Earth and Planetary Science Letters*, **39**, 349-357.
- Mahoney, J.J. (1988) Deccan traps. Pp. 151-194 in: *Continental flood basalts* (J.D. MacDougall, editor). Kluwer Academic Publishers, Dordrecht, The Netherlands.
- Mattey, D., Lowry, D., and Macpherson, C. (1994) Oxygen isotope composition of mantle peridotite. *Earth and Planetary Science Letters*, **128**, 231-241.
- McDonough, W.F. and Sun, S.S. (1995) The composition of the Earth. *Chemical Geology*, **120**, 223-253.
- Middlemost, E.A.K. (1989) Iron oxidation ratios, norms and the classification of volcanic rocks. *Chemical Geology*, **77**, 19-26.
- Molzahn, M., Reisberg, L., and Wörner, G. (1996) Os, Sr, Nd, Pb, O isotope and trace element data from the Ferrar flood basalts, Antarctica: evidence for an enriched subcontinental lithospheric source. *Earth and Planetary Science Letters*, **144**, 529-546.
- Morimoto, N., Fabrie, J., Ferguson, A.K., Ginzburg, I.V., Ross, M., Seifert, F.A., Zussman, J., Aoki, K., & Gottardi, G. (1988) Nomenclature of pyroxenes. *Mineralogical Magazine*, **52**, 535-550.
- Nicholson, S.W., Shirey, S.B., Schulz, K.J., and Green, J.C. (1997) Rift-wide correlation of 1.1 Ga Midcontinent rift system basalts: implications for multiple mantle sources during rift development. *Canadian Journal of Earth Sciences*, **34**, 504-520.
- Nimis, P. and Vannucci, R. (1995) An ion microprobe study of clinopyroxenes in websteritic and megacrystic xenoliths from Hyblean Plateau (SE Sicily, Italy): constraints on HFSE/REE/Sr fractionation at mantle depth. *Chemical Geology*, **124**, 185-197.
- Oliveira, E.P. and Tarney, J. (1995) Petrogenesis of the Late Proterozoic Curaçá mafic dyke swarm, Brazil: asthenospheric magmatism associated with continental collision. *Mineralogy and Petrology*, **53**, 27-48.
- Ormerod, D.S., Hawkesworth, C.J., Rogers, N.W., Leeman, W.P., and Menzies, M.A. (1988) Tectonic and magmatic transitions in the Western Great Basin, USA. *Nature*, **333**, 349-353.
- Paces, J.B. and Bell, K. (1989) Non-depleted sub-continental mantle beneath the Superior Province of the Canadian Shield: Nd-Sr isotopic and trace element evidence from Midcontinent Rift basalts. *Geochimica et Cosmochimica Acta*, **53**, 2023-2035.
- Paslick, C.R., Halliday, A.N., Davies, G.R., Mezger, K., and Upton, B.G.J. (1993) Timing of proterozoic magmatism in the Gardar Province, southern Greenland. *Bulletin of the Geological Society of America*, **105**, 272-278.
- Paslick, C.R., Halliday, A.N., James, D., and Dawson, J.B. (1995) Enrichment of the continental lithosphere by OIB melts: Isotopic evidence from the volcanic province of northern Tanzania. *Earth and Planetary Science Letters*, **130**, 109-126.
- Pearce, N.J.G. and Leng, M.J. (1996) The origin of carbonatites and related rocks from the Igaliko Dyke Swarm, Gardar Province, South Greenland: field, geochemical and C-O-Sr-Nd isotope evidence. *Lithos*, **39**, 21-40.
- Perry, F.V., Baldrige, W.S., and DePaolo, D.J. (1987) Role of asthenosphere and lithosphere in the genesis of late cenozoic basaltic rocks from the Rio Grande rift and adjacent regions of the Southwestern United States. *Journal of Geophysical Research*, **92**, 9193-9213.
- Philpotts, A.R. (1990) *Principles Of Igneous And Metamorphic Petrology*. Prentice Hall, New Jersey, U.S.A.

- Piper, J.D.A., Thomas, D.N., Share, S., and Zhang Qi Rui (1999) The palaeomagnetism of (Mesoproterozoic) Eriksfjord Group red beds, South Greenland: multiphase remagnetization during the Gardar and Grenville episodes. *Geophysical Journal International*, **136**, 739-756.
- Poulsen, V. (1964) The sandstones of the Precambrian Eriksfjord Formation in South Greenland. *Rapport Grønlands Geologiske Undersøgelse*, **2**, 16 pp.
- Price, R.C., Gray, C.M., Wilson, R.E., Frey, F.A., and Taylor, S.R. (1991) The effects of weathering on rare-earth element, Y and Ba abundances in Tertiary basalts from southeastern Australia. *Chemical Geology*, **93**, 245-265.
- Ranløv, J. and Dymek, R.F. (1991) Compositional zoning in hydrothermal aegirine from fenites in the Proterozoic Gardar Province, South Greenland. *European Journal of Mineralogy*, **3**, 837-853.
- Reiners, P.W., Nelson, B.K., and Ghiorso, M.S. (1995) Assimilation of felsic crust by basaltic magma: thermal limits and extents of crustal contamination of mantle-derived magmas. *Geology*, **23**, 563-566.
- Roddick, J.C., Sullivan, R.W., and Dudas, F.Ö. (1992) Precise calibration of Nd tracer isotopic composition for Sm-Nd studies. *Chemical Geology*, **97**, 1-8.
- Rollinson, H. (1993) *Using geochemical data: evaluation, presentation, interpretation*. Longman Group UK Limited, London.
- Rudnick, R. and Fountain, D.M. (1995) Nature and composition of the Continental Crust: A lower crustal perspective. *Reviews of Geophysics*, **33**, 267-309.
- Rumble, D. and Hoering, T.C. (1994) Analysis of oxygen and sulfur isotope ratios in oxide and sulfide minerals by spot heating with a carbon dioxide laser in a fluorine atmosphere. *Accounts of Chemical Research*, **27**, 237-241.
- Schleicher, H., Kramm, U., Pernicka, E., Schidlowski, M., Schmidt, F., Subramanian, V., Todt, W., and Viladkar, S.G. (1998) Enriched Subcontinental Upper Mantle beneath Southern India: Evidence from Pb, Nd, Sr, and C-O Isotopic Studies on Tamil Nadu Carbonatites. *Journal of Petrology*, **39**, 1765-1785.
- Sharp, Z.D. (1990) A laser-based microanalytical method for the in-situ determination of oxygen isotope ratios of silicates and oxides. *Geochimica et Cosmochimica Acta*, **54**, 1353-1357.
- Shirey, S.B., Klewin, K.W., Berg, J.H., and Carlson, R.W. (1994) Temporal changes in the sources of flood basalts: Isotopic and trace element evidence from the 1100 Ma old Keweenaw Mamainse Point Formation, Ontario, Canada. *Geochimica et Cosmochimica Acta*, **58**, 4475-4490.
- Simonetti, A., Goldstein, S.L., Schmidberger, S.S., Viladkar, S.G. (1998) Geochemical and Nd, Pb, and Sr Isotope Data from Deccan Alkaline Complexes – Inferences for Mantle Sources and Plume-Lithosphere Interaction. *Journal of Petrology*, **39**, 1847-1864.
- Steiger, R.H. and Jäger, E. (1977) Subcommittee on geochronology: conventions of the use of decay constants in geo- and cosmochronology. *Earth and Planetary Science Letters*, **36**, 359-362.
- Sun, S.S. and McDonough, W.F. (1989) Chemical and isotopic systematics of oceanic basalts: implications for mantle composition and processes. Pp. 313-345 in: *Magmatism in ocean basins* (A.D. Saunders and M.J. Norry, editors). Geological Society of London Special Publication vol. 42.
- Taylor, P.N., Jones, N.W., and Moorbath, S. (1984) Isotopic assessment of relative contributions from crust and mantle sources to the magma genesis of Precambrian granitoid rocks. *Philosophical Transactions of the Royal Society of London*, **A 310**, 605-625.
- Taylor, P.N. and Upton, B.G.J. (1993) Contrasting Pb isotopic compositions in two intrusive complexes of the Gardar Magmatic Province of South Greenland. *Chemical Geology*, **104**, 261-268.
- Taylor, S.R. and McLennan, S.M. (1985) *The continental crust: its composition and evolution*. Blackwell Scientific Publications, Oxford.
- Thomas, D.N. and Piper, J.D.A. (1992) A revised magnetostratigraphy for the Mid-Proterozoic Gardar lava succession, South Greenland. *Tectonophysics*, **201**, 1-16.
- Turner, S.P., Hawkesworth, C.J., Gallagher, K.G., Stewart, K., Peate, D., and Mantovani, M. (1996) Mantle plumes, flood basalts and thermal models for melt generation beneath continents: assessment of a conductive heating model. *Journal of Geophysical Research*, **101**, 11503-11518.
- Upton, B.G.J. (1996) Anorthositic and troctolitic rocks of the Gardar Magmatic Province. Pp 19-34 in: *Petrology and Geochemistry of magmatic suites of rocks in the continental and oceanic crusts. A volume dedicated to Professor Jean Michot, Université Libre de Bruxelles, Royal Museum for Central Africa (Tervuren)* (D. Demaiffe, editor).
- Upton, B.G.J. and Emeleus, C.H. (1987) Mid-Proterozoic alkaline magmatism in southern Greenland: the Gardar province. Pp. 449-471 in: *The Alkaline Rocks* (J.G. Fitton and B.G.J. Upton, editors). Geological Society of

London Special Publication vol. 30.

- Upton, B.G.J., Emeleus, C.H., Heaman, L.M., Goodenough, K.M and Finch, A.A. (2003) Magmatism of the mid-Proterozoic Gardar Province, South Greenland: chronology, petrogenesis and geological setting. *Lithos*, **68**, 43-65.
- Valley J.W., Kitchen, N., Kohn, M.J., Niendorf, C.R., and Spicuzza, M.J. (1995) UWG-2, a garnet standard for oxygen isotope ratios: strategies for high precision and accuracy with laser heating. *Geochimica et Cosmochimica Acta*, **59**, 5223-5231.
- van Breemen, O., Aftalion, M., and Allaart, J.H. (1974) Isotopic and Geochronologic Studies on Granites from the Ketilidian Mobile Belt of South Greenland. *Bulletin of the Geological Society of America*, **85**, 403-412.
- Vroon, P.Z., Lowry, D., Van Bergen, M.J., Boyce, A.J., and Matthey, D.P. (2001) Oxygen isotope systematics of the Banda Arc: Low $\delta^{18}\text{O}$ despite involvement of subducted continental material in magma genesis. *Geochimica et Cosmochimica Acta*, **65**, 589-609.
- Waight, T., Baker, J., and Willigers, B. (2002) Rb isotope dilution analyses by MC-ICPMS using Zr to correct for mass fractionation: towards improved Rb-Sr geochronology? *Chemical Geology*, **186**, 99-116.
- Walsh, J.N., Buckley, F., and Barker, J. (1981) The simultaneous determination of the rare-earth elements in rocks using Inductively Coupled Plasma Source Spectrometry. *Chemical Geology*, **33**, 141-153.
- Weaver, B.L. (1991) The origin of ocean island basalt end-member compositions: trace element and isotopic constraints. *Earth and Planetary Science Letters*, **104**, 381-397.
- Weaver, B.L., Wood, D.A., Tarney, J., and Joron, J.-L. (1987) Geochemistry of ocean island basalts from the South Atlantic: Ascension, Bouvet, St. Helena, Gough and Tristan da Cunha. Pp. 253-267 in: *The Alkaline Rocks* (J.G. Fitton and B.G.J. Upton, editors). Geological Society of London Special Publication vol. 30.
- Winchester, J.A. and Floyd, P.A. (1976) Geochemical magma type discrimination; application to altered and metamorphosed basic igneous rocks. *Earth and Planetary Science Letters*, **28**, 459-469.
- Zindler, A. and Hart, S.R. (1986) Chemical geodynamics. *Annual Reviews of Earth and Planetary Sciences*, **14**, 493-571.

Figure Captions

Fig. 1: Map of the Eriksfjord Formation on the Narssaq peninsula with sample locations (after Poulsen, 1964 and Larsen, 1977). Sample 101472 (not shown) is from a succession ~ 2 km south of the settlement of Narsarsuaq further to the NE.

Fig. 2: Clinopyroxene analyses of the Eriksfjord basalts plotted in the pyroxene quadrilateral with isotherms after Lindsley (1983).

Fig. 3: Whole-rock variation diagrams for EF basalts with Mg# as fractionation index. Mg# is calculated as $\text{Mg}/(\text{Mg}+\text{Fe}^{2+})$ with $\text{Fe}_2\text{O}_3/\text{FeO} = 0.2$ (Middlemost, 1989).

Fig. 4: Multi-element plots normalised to primitive mantle values (McDonough and Sun, 1995). Data for N-MORB, E-MORB and average OIB (Sun and McDonough, 1989) are shown for comparison.

Fig. 5: a) Whole-rock REE data of EF basalts, normalised to chondritic values from Boynton (1984). b) Typical compositions of N-MORB, E-MORB and OIB (Sun and McDonough, 1989) are shown for comparison.

Fig. 6: REE patterns of clinopyroxenes (cpx) from Mussartût (a), Ulukasik (b) and Ilímaussaq (c) Group samples, normalised to chondritic values from Boynton (1984). (d) REE patterns of cpx from MORB-type olivine gabbro (Benoit *et al.*, 1996) and OIB-type alkaline basalt (Nimis and Vannucci, 1995) for comparison (note the change of scale).

Fig. 7: $\epsilon_{\text{Nd}}(i)$ vs. $(^{87}\text{Sr}/^{86}\text{Sr})_i$ diagram, calculated for $T = 1.2$ Ga which is considered as the eruption age of the EF basalts (Paslick *et al.*, 1993). The reference line of Bulk Silicate Earth (BSE) for the Sr isotopic composition was calculated after DePaolo (1988) assuming present-day values of 0.0827 for $^{87}\text{Rb}/^{86}\text{Sr}$ and 0.7045 for $^{87}\text{Sr}/^{86}\text{Sr}$. Isotopic composition of the depleted MORB mantle (DMM) was calculated after DePaolo (1981), Goldstein *et al.* (1984) and Taylor and McLennan (1985). EM-1 was calculated after Schleicher *et al.* (1998) (see text for details). Data sources are: Goodenough *et al.* (2002), Ivittuut ($n = 6$); Pearce and Leng (1996), Igaliko ($n = 5$); Andersen (1997), Qassiarsuk ($n = 25$); Bell and Blenkinsop (1989), other carbonatites of similar age (Goudini, Schryburt Lake and Prairie Lake; $n = 6$).

Fig. 8: Oxygen isotopic compositions ($\delta^{18}\text{O}$ ‰ V-SMOW) of clinopyroxene from EF basalts, calculated melt (see text for details) and whole-rock Ketilidian basement versus $\epsilon_{\text{Nd}}(i)$. Whole-rock data for Igaliko dyke rocks ($n = 7$) are from Pearce and Leng (1996), DMM data derived from fresh MORB glasses are from Eiler *et al.* (2000b). The field of EM-1 lavas is taken from clinopyroxene data of Gough and Tristan da Cunha Island lavas (Harris *et al.*, 2000) and the EM-1 end-member composition is based on the calculations after Schleicher *et al.* (1998) for $\epsilon_{\text{Nd}}(i)$ and an average value of 5.78 ‰ ($n = 18$) from the EM-1 lavas for $\delta^{18}\text{O}$.

Fig. 9: $\epsilon_{\text{Nd}}(\text{i})$ vs. $(^{87}\text{Sr}/^{86}\text{Sr})_{\text{i}}$ diagram showing the results of AFC modelling. End-member compositions are listed in Table 6. Olivine is the only fractionating mineral. Partition coefficients for olivine/melt are from the compilation of Rollinson (1993). Curves were calculated for two values of r (r = rate of assimilation/rate of fractional crystallisation). Dashed lines and numbers in italics are for $r = 0.5$, solid lines and regular numbers are for $r = 0.8$. Values at the curves are for F values (fraction of melt remaining) with 10% tick marks.

Table 1: Typical clinopyroxene analyses of Eriksfjord Formation basalts determined by EMP.

Sample Cpx No.	EF 024 cpx 2	EF 024 cpx 3	EF 039 cpx 5	EF 059 cpx 3	EF 072 cpx 5	EF 108 cpx 7	EF 168 cpx 4	EF 174 cpx 1
SiO ₂	50.60	50.41	51.28	49.88	51.45	49.50	51.75	50.69
TiO ₂	1.73	1.76	1.21	1.69	1.40	1.62	0.96	1.21
Al ₂ O ₃	2.97	3.00	1.79	2.23	1.71	2.64	1.55	2.13
FeO	11.60	10.68	12.18	14.05	9.93	12.34	9.79	11.29
MnO	0.28	0.21	0.30	0.40	0.19	0.28	0.25	0.31
MgO	12.54	13.24	12.63	11.82	13.25	11.63	13.07	12.14
CaO	19.59	20.29	20.02	19.07	21.06	20.99	21.74	21.43
Na ₂ O	0.34	0.31	0.29	0.49	0.33	0.55	0.52	0.54
Total	99.65	99.89	99.71	99.63	99.32	99.55	99.62	99.74

Formulae based on 4 cations and 6 oxygens:

Si	1.91	1.89	1.94	1.90	1.94	1.88	1.94	1.91
Al	0.13	0.13	0.08	0.10	0.08	0.12	0.07	0.09
Ti	0.05	0.05	0.03	0.05	0.04	0.05	0.03	0.03
Fe ³⁺	-	-	-	0.03	-	0.07	0.03	0.05
Mg	0.71	0.74	0.71	0.67	0.75	0.66	0.73	0.68
Fe ²⁺	0.37	0.33	0.39	0.41	0.31	0.32	0.28	0.31
Mn	0.01	0.01	0.01	0.01	0.01	0.01	0.01	0.01
Ca	0.79	0.82	0.81	0.78	0.85	0.85	0.87	0.87
Na	0.02	0.02	0.02	0.04	0.02	0.04	0.04	0.04
Total	4.00	4.00	4.00	4.00	4.00	4.00	4.00	4.00

Pyroxene projection after Lindsley (1983):

Wo	0.39	0.41	0.41	0.41	0.43	0.43	0.45	0.44
En	0.40	0.41	0.39	0.37	0.40	0.38	0.40	0.38
Fs	0.21	0.18	0.21	0.23	0.17	0.19	0.15	0.17

Table 2: XRF whole-rock analyses of Eriksfjord Formation basalts

Sample	EF 024	EF 063	EF 061	EF 039	EF 059	EF 108	EF 072	EF 174	EF 168
Group	Mussartût	Mussartût	Mussartût	Mussartût	Mussartût	Ulukasik	Ulukasik	Ilímaussaq	Ilímaussaq
Subunit	4	4	5	6	7	Lower Unit	Upper Unit	Sermilik	Narssaq Fjeld
<i>Major elements (wt.%)</i>									
SiO ₂	45.73	45.85	46.88	46.60	48.75	46.98	46.56	46.01	45.45
TiO ₂	2.30	2.00	1.80	1.75	1.91	2.65	2.03	2.99	2.77
Al ₂ O ₃	15.78	16.30	16.00	16.12	16.45	16.82	16.68	16.45	17.19
Fe ₂ O ₃	15.10	13.56	13.31	13.83	12.25	13.94	13.21	14.38	13.92
MnO	0.28	0.18	0.18	0.18	0.17	0.14	0.17	0.18	0.17
MgO	5.25	6.83	6.53	6.73	5.68	3.96	6.47	4.40	4.80
CaO	8.42	8.49	8.72	8.57	9.20	6.41	8.08	7.46	7.37
Na ₂ O	3.49	2.74	2.89	2.76	2.36	4.48	3.03	3.23	3.76
K ₂ O	0.87	0.83	0.68	0.32	0.27	1.59	0.70	2.05	1.32
P ₂ O ₅	0.41	0.35	0.23	0.23	0.23	0.48	0.35	1.11	0.83
LOI	1.99	2.10	2.40	2.38	2.42	2.04	2.10	0.52	1.56
Total	99.62	99.23	99.62	99.47	99.69	99.49	99.38	98.78	99.14
Mg#	45.3	54.5	53.8	53.6	52.4	40.3	53.8	42.1	45.0
<i>Trace elements (ppm)</i>									
Sc	24	22	25	22	26	19	20	21	16
V	209	175	215	195	211	142	170	164	203
Cr	81	108	66	65	126	48	82	33	29
Co	63	78	70	62	71	44	68	35	46
Ni	99	115	85	85	101	58	106	46	51
Cu	65	49	46	60	97	41	59	38	41
Zn	103	102	110	97	110	93	82	122	105
Ga	20	18	21	19	20	19	16	21	19
Rb	24	26	16	< 10	< 10	38	12	39	45
Sr	504	503	512	392	373	712	507	850	992
Y	31	26	28	23	28	31	17	31	25
Zr	188	165	121	116	125	125	88	164	139
Nb	12	11	10	< 10	10	9	< 10	31	27
Ba	445	375	415	302	178	582	405	1293	900
Pb	6	7	3	4	3	4	4	3	5
La	-	-	15	-	12	11	-	37	28
Ce	-	-	40	-	38	39	-	92	71
Pr	-	-	1	-	1	2	-	9	4
Nd	-	-	16	-	15	18	-	43	34
Sm	-	-	6	-	7	6	-	5	5
<i>CIPW norm:</i>									
q	-	-	-	-	3.13	-	-	-	-
or	5.14	4.91	4.02	1.89	1.60	9.40	4.14	12.12	7.80
ab	28.07	23.19	24.45	23.35	19.97	32.07	25.64	27.33	29.81
an	24.82	29.73	28.68	30.65	33.50	21.09	29.85	24.33	26.13
ne	0.79	-	-	-	-	3.16	-	-	1.09
di	11.87	8.30	10.76	8.53	8.77	6.33	6.54	4.52	4.16
hy	-	8.90	10.59	16.50	22.17	-	10.97	3.15	-
ol	16.70	13.09	10.44	7.80	-	14.72	11.20	13.88	16.89
mt	3.65	3.28	3.22	3.35	2.96	3.36	3.19	3.48	3.36
il	4.37	3.80	3.42	3.32	3.63	5.03	3.86	5.68	5.26
ap	0.95	0.81	0.53	0.53	0.53	1.11	0.81	2.57	1.92

Mg# was calculated as $Mg\# = 100 * Mg^{2+} / (Mg^{2+} + Fe^{2+})$ using $Fe_2O_3/FeO = 0.2$. Normative mineral compositions were determined according to the CIPW calculation scheme.

Table 3: REE data of whole-rocks and clinopyroxenes, the latter determined by Laser ICP-MS.

<i>Whole-rock analyses:</i>							<i>Representative clinopyroxene analyses:</i>							
Sample No.	101231	101446	101457	101472	186389	186395	EF 024-2	EF 039-1	EF 039-2	EF 039-4	EF 072-2	EF 072-3	EF 168-3	EF 168-5
<i>REE concentrations in ppm:</i>														
La	11.65	18.06	10.29	6.61	15.54	12.28	4.40	2.66	1.99	1.50	2.73	3.04	16.55	27.59
Ce	29.03	46.05	24.96	17.13	37.81	30.08	18.04	11.46	8.68	7.17	10.50	12.60	57.23	99.67
Pr	4.34	6.7	3.88	2.68	5.27	4.33	3.31	2.16	1.81	1.28	2.49	2.62	10.29	17.43
Nd	20.06	31.71	17.64	12.49	25.09	20.16	19.02	13.82	12.22	8.98	15.64	15.72	58.51	96.06
Sm	4.75	6.97	4.04	3.21	5.91	4.82	6.66	4.19	4.28	3.27	6.07	7.06	15.82	26.59
Eu	1.74	2.5	1.57	1.07	1.97	1.72	1.83	1.49	1.11	1.21	2.00	1.94	3.87	7.07
Gd	4.82	6.58	4.04	3.55	5.8	4.99	6.96	5.61	5.24	4.32	6.15	6.05	14.75	25.27
Tb	-	-	-	-	-	-	1.35	1.01	0.77	0.71	1.11	1.21	2.31	3.61
Dy	4.47	5.22	3.61	3.56	5.35	4.81	6.86	5.93	4.78	4.25	5.99	6.86	13.10	20.52
Ho	0.92	1.04	0.73	0.73	1.1	1.01	1.48	1.40	1.00	1.00	1.21	1.29	2.39	4.24
Er	2.43	2.53	1.95	1.97	2.87	2.66	3.89	3.34	2.64	2.11	2.99	3.64	6.53	9.60
Tm	-	-	-	-	-	-	0.45	0.39	0.36	0.29	0.35	0.44	0.86	1.27
Yb	2.18	2.07	1.74	1.83	2.59	2.36	3.78	2.81	2.49	2.45	2.70	3.01	6.78	8.89
Lu	0.34	0.31	0.26	0.27	0.39	0.35	0.46	0.41	0.30	0.31	0.52	0.41	1.25	1.60
(Eu/Eu*) _N	1.11	1.13	1.19	0.97	1.03	1.07	0.82	0.94	0.72	0.99	1.00	0.91	0.77	0.83

Eu anomaly is calculated as $(Eu/Eu^*)_N = Eu_N / (Sm_N \times Gd_N)^{0.5}$, normalised to chondrite values from Boynton (1984).

Table 4: Sr, Nd and O isotopic compositions of clinopyroxene separates from Eriksfjord Formation basalts. Whole-rock analyses from the Ketilidian basement and from sedimentary rocks of the Eriksfjord Formation are given for comparison.

Sample	Member	Sr (ppm)	Rb (ppm)	$^{87}\text{Rb}/^{86}\text{Sr}$	$^{87}\text{Sr}/^{86}\text{Sr}$	$^{87}\text{Sr}/^{86}\text{Sr}_{\text{initial}}$	Sm (ppm)	Nd (ppm)	$^{147}\text{Sm}/^{144}\text{Nd}$	$^{143}\text{Nd}/^{144}\text{Nd}$	$\epsilon_{\text{Nd}}(\text{i})$	$\delta^{18}\text{O}$
<i>Basalts:</i>												
EF 024	Mussartût	64.65	0.486	0.0218	0.704201 ± 10	0.703826	7.38	22.80	0.1956	0.512467 ± 10	- 3.2	5.67
EF 063	Mussartût											5.60 ± 0.11
EF 061	Mussartût	89.95	0.999	0.0321	0.703818 ± 10	0.703266	5.74	16.39	0.2115	0.512629 ± 10	- 2.5	5.79 ± 0.28
EF 039	Mussartût	73.74	0.583	0.0229	0.703492 ± 10	0.703098	6.62	19.13	0.2092	0.512626 ± 10	- 2.2	5.71 ± 0.01
EF 059	Mussartût	54.47	0.137	0.0073	0.703375 ± 12	0.703250	6.06	16.89	0.2171	0.512727 ± 09	- 1.4	5.99 ± 0.01
EF 108	Ulukasik	66.92	1.110	0.0480	0.703741 ± 09	0.702916	10.99	36.82	0.1805	0.512617 ± 10	+ 2.1	5.81
EF 072	Ulukasik	69.41	0.322	0.0134	0.703014 ± 10	0.702784	8.18	25.19	0.1962	0.512574 ± 10	- 1.2	5.68
EF 174	Ilímaussaq	125.4	2.324	0.0536	0.703935 ± 10	0.703014	18.76	79.61	0.1424	0.512230 ± 10	+ 0.4	5.47
EF 168	Ilímaussaq	86.67	1.422	0.0475	0.703799 ± 07	0.702983	16.45	64.16	0.1550	0.512304 ± 09	- 0.1	5.18
<i>Basement and sedimentary rocks:</i>												
JG 02	Julianehåb Granite	300.1	169.7	1.6375	0.744789 ± 10	0.716647	10.53	62.28	0.1022	0.511470 ± 09	-8.3	7.8
EF 021	Quartzite											11.5
EF 028	Arkosic arenite											6.8

Samples are listed in stratigraphic order from oldest to youngest. $^{87}\text{Sr}/^{86}\text{Sr}$ initial ratios and $\epsilon_{\text{Nd}}(\text{i})$ values were calculated for an age of 1.2 Ga. Standard deviations for $\delta^{18}\text{O}$ are given for samples that were analysed twice.

Table 5: Trace element ratios of EF basalts compared to ocean island basalts (OIBs) representing EM-1 and HIMU mantle components, and the lower crust.

	Sr/Nd	La/Nb	Zr/Nb
EF basalts with $\epsilon_{\text{Nd}} < -1$	24.9 - 39.6	1.20 - 1.50	12.1 - 15.7
Ilímaussaq Group EF basalts	19.8 - 29.2	1.04 - 1.19	5.1 - 5.3
EM-1	9.0 - 20.7	0.67 - 1.11	3.9 - 10.9
HIMU	4.5 - 16.3	0.63 - 0.80	2.7 - 3.6
Lower continental crust	30	1.6	13.6

Data sources: EM-1: Humphris and Thompson (1983, Walvis Ridge) and Cliff *et al.* (1991, Inaccessible Islands); HIMU: Chauvel *et al.* (1992, Tubuai Island); Lower continental crust: Rudnick and Fountain (1995).

Table 6: End-member compositions used for AFC modelling

End-member	Sr (ppm)	$(^{87}\text{Sr}/^{86}\text{Sr})_i$ (T = 1.2 Ga)	Nd (ppm)	$\epsilon_{\text{Nd}(i)}$ (T = 1.2 Ga)	Data source
Primitive EF basaltic magma	507	0.70278	18	+ 2.2	Sample EF 072, Paslick <i>et al.</i> , 1993
Upper Crust (Julianehåb Granite)	300	0.71665	62	- 8.3	Sample JG 02
Lower Crust * (Granulite facies gneiss)	747	0.70668	63	- 23.4	Taylor <i>et al.</i> , 1984

* The composition of the granulite facies gneiss is an average of 5 samples with low Rb/Sr ratios < 0.2.

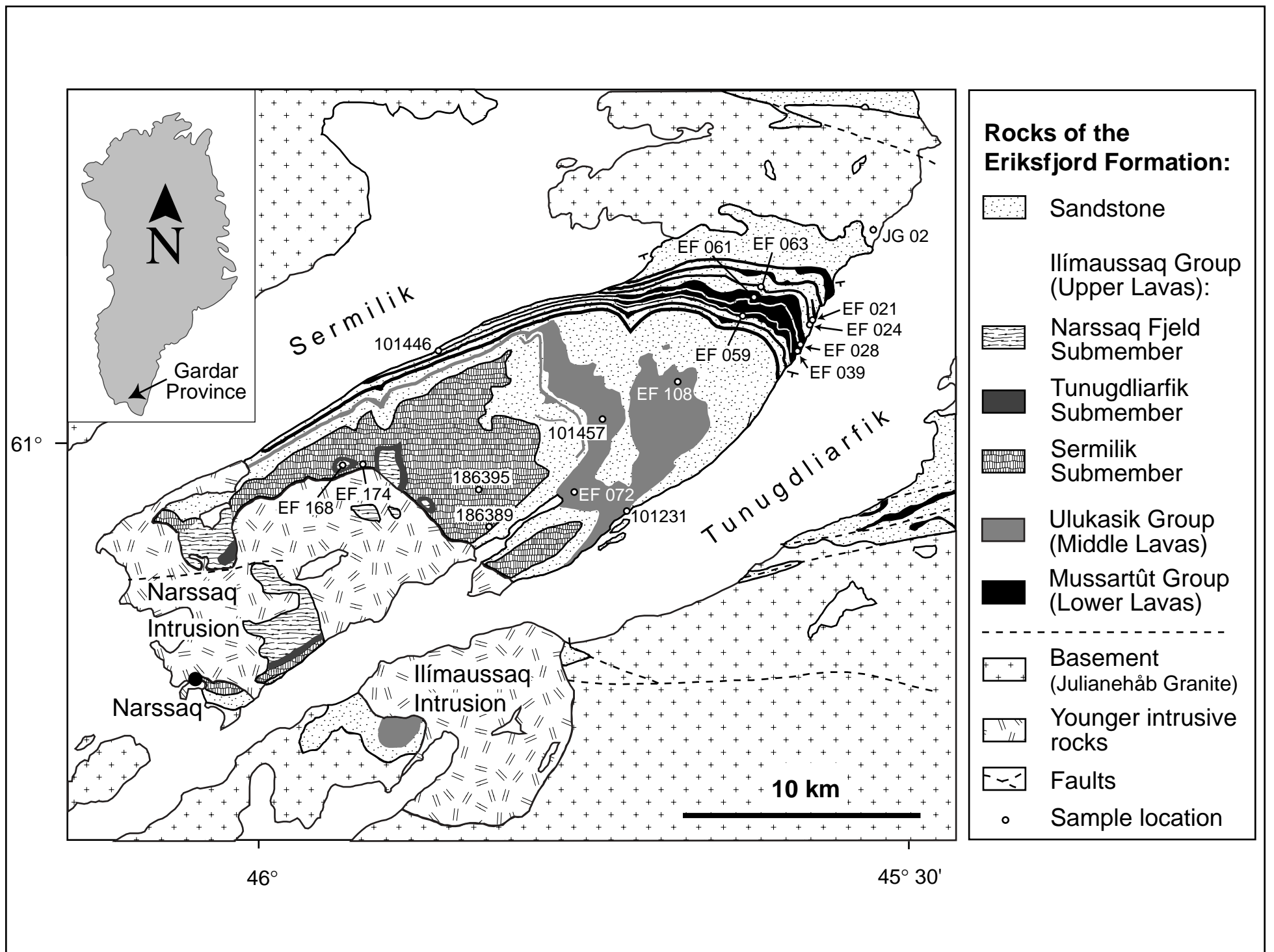


Fig. 1

Fig. 2

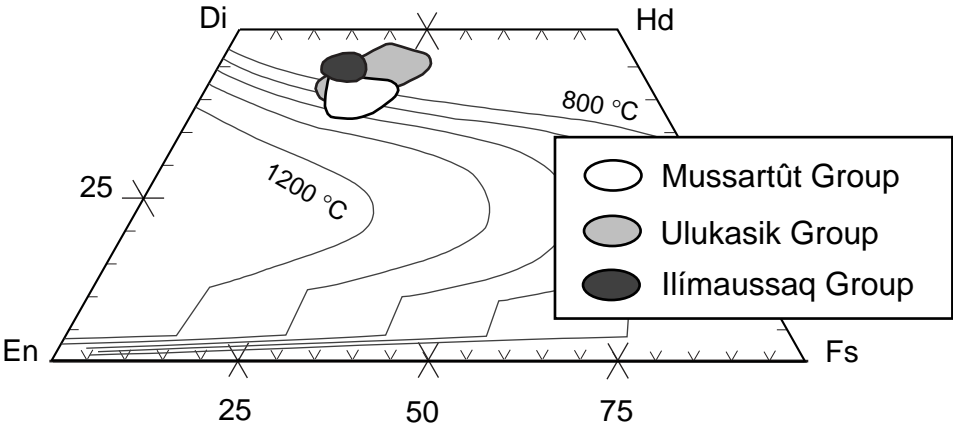


Fig. 3

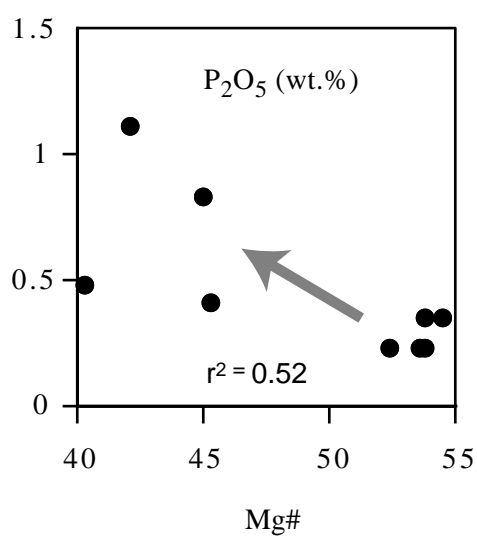
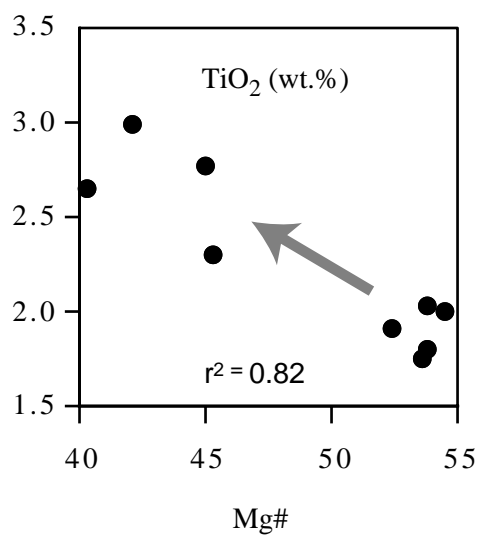
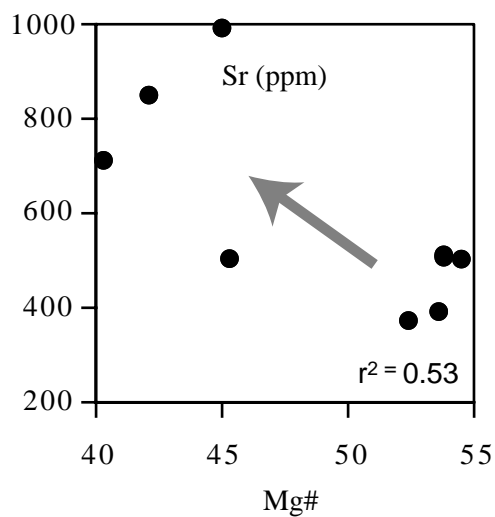
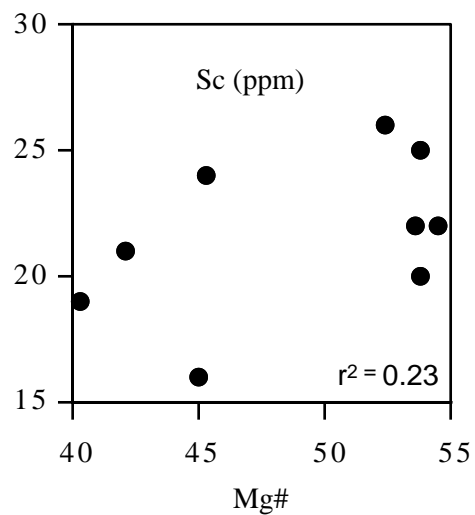
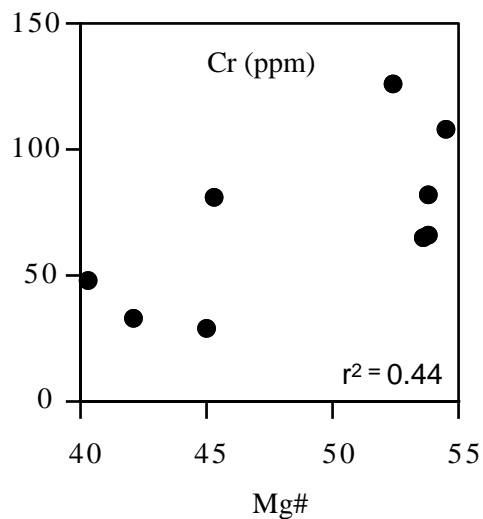
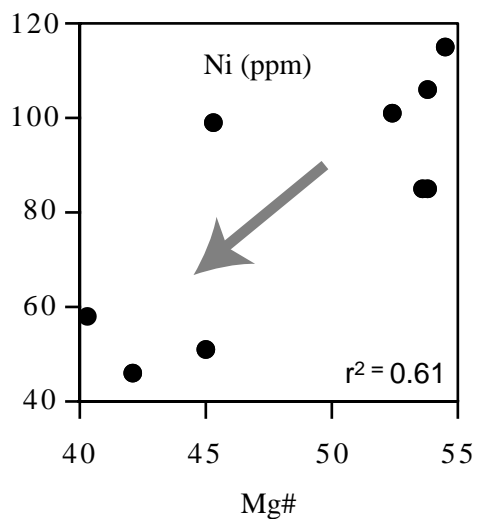


Fig. 4

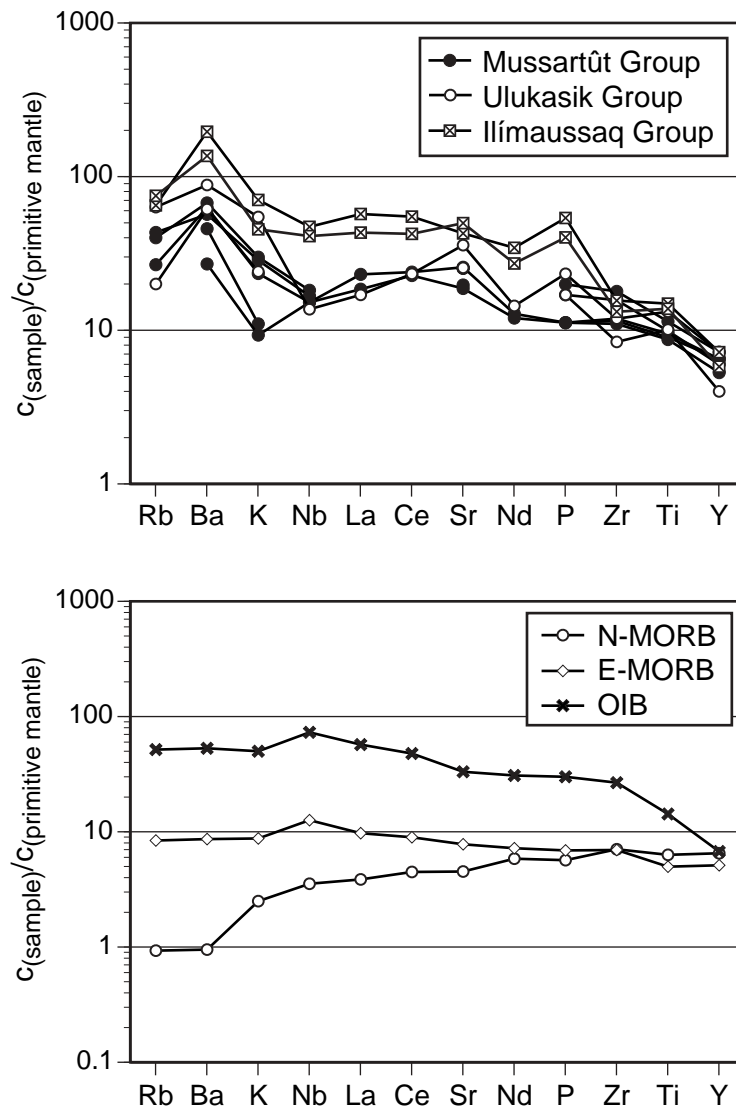
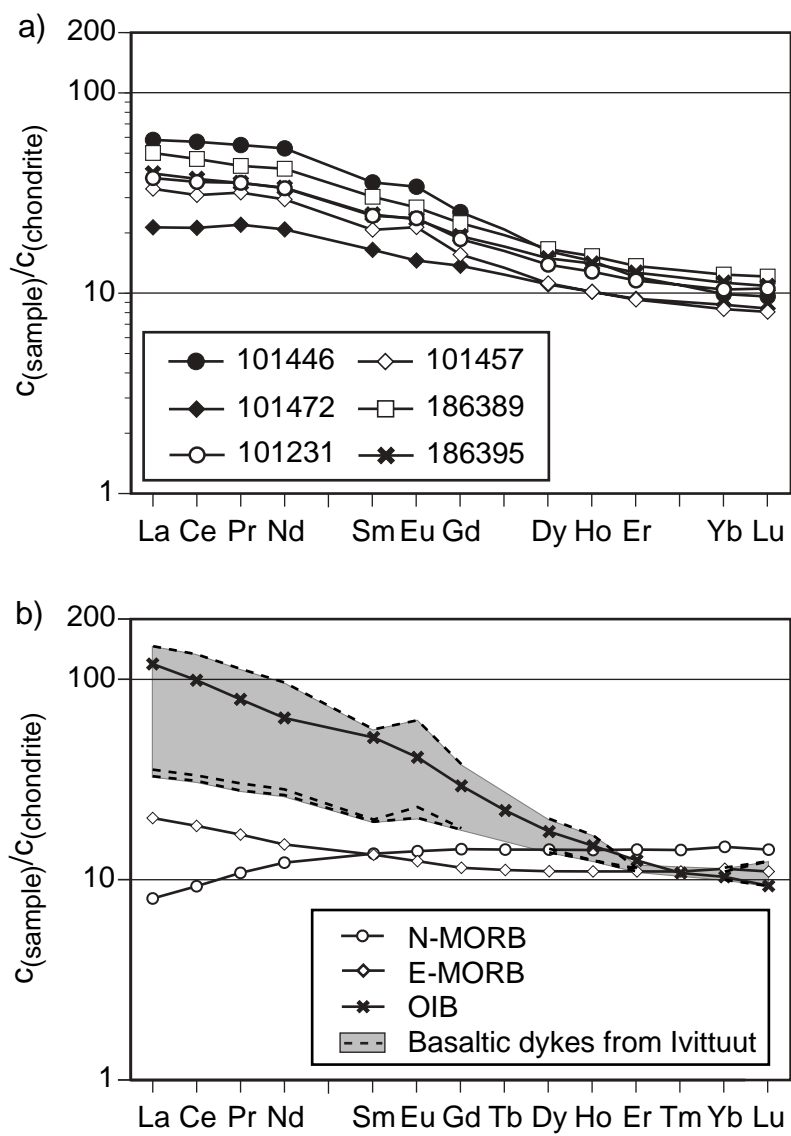


Fig. 5



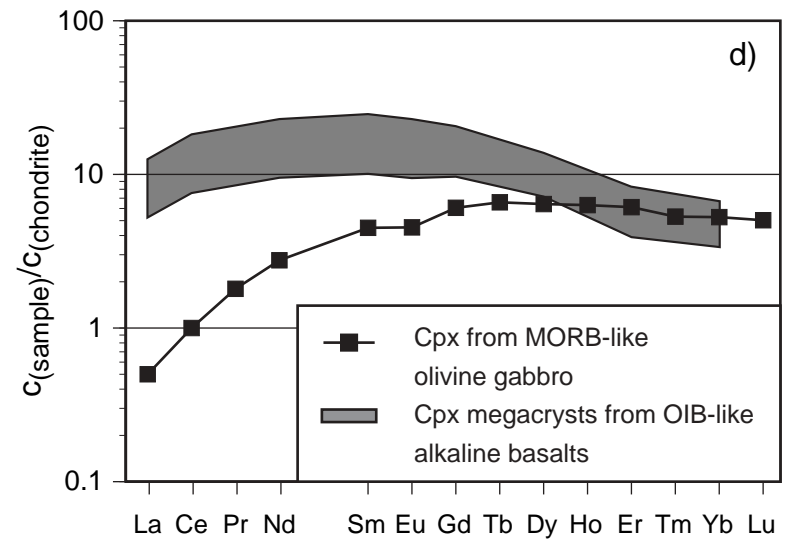
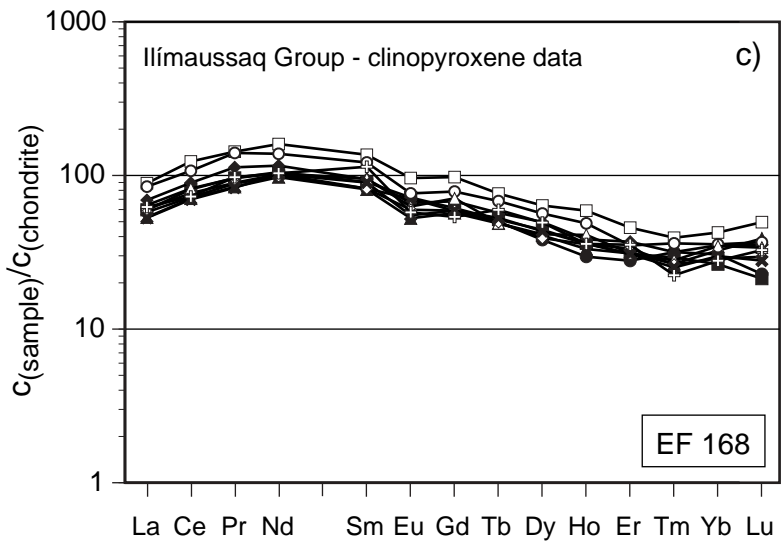
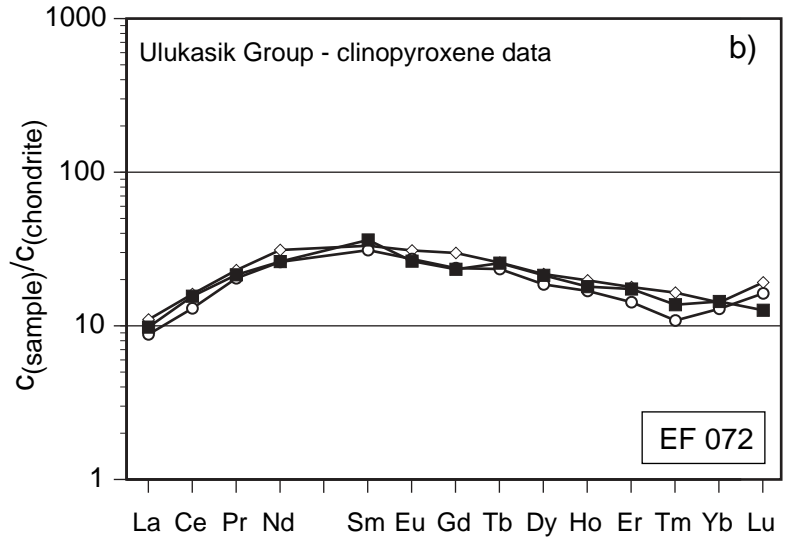
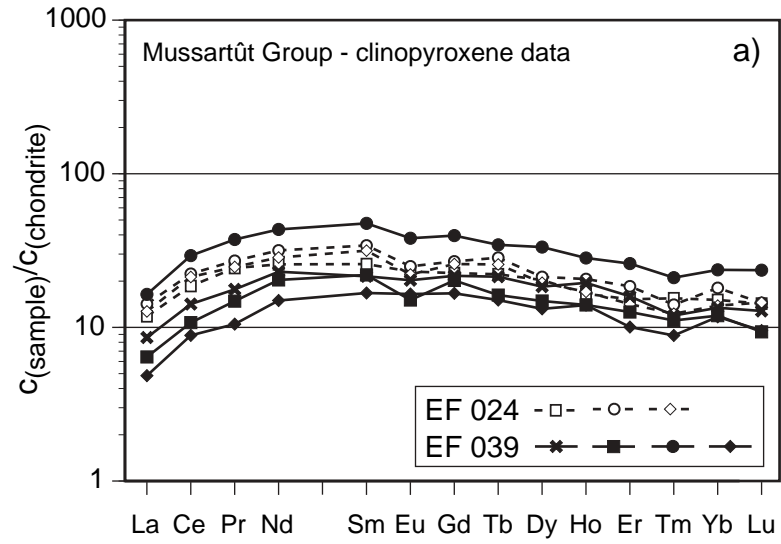


Fig. 6

Fig. 7

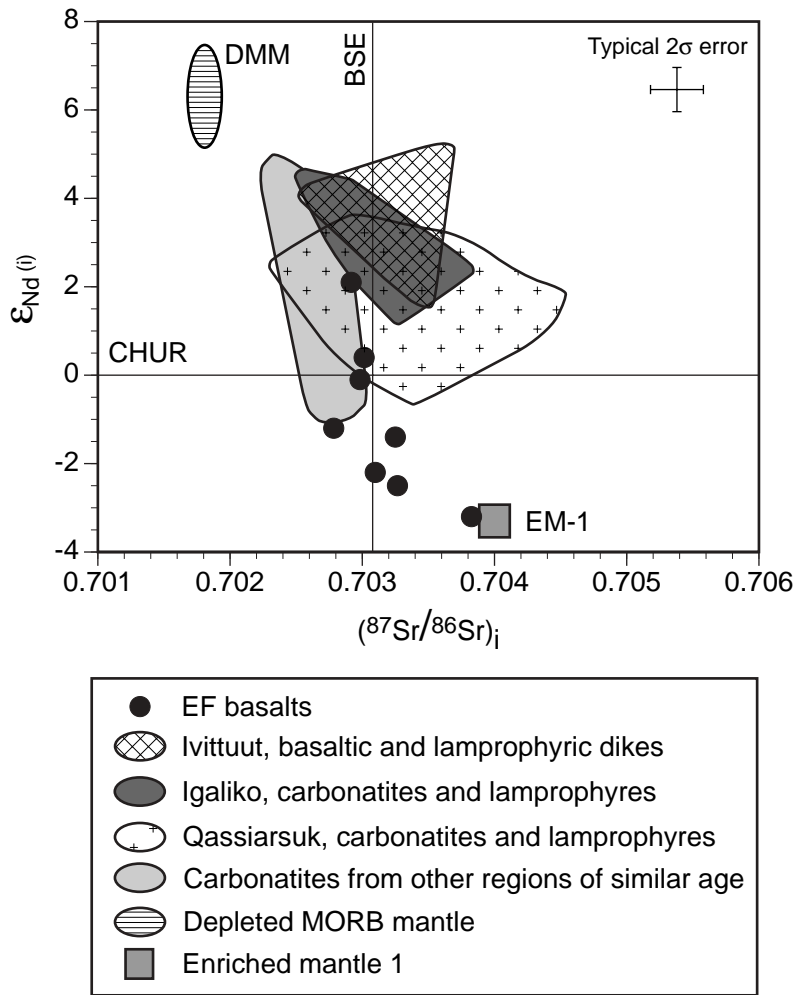


Fig. 8

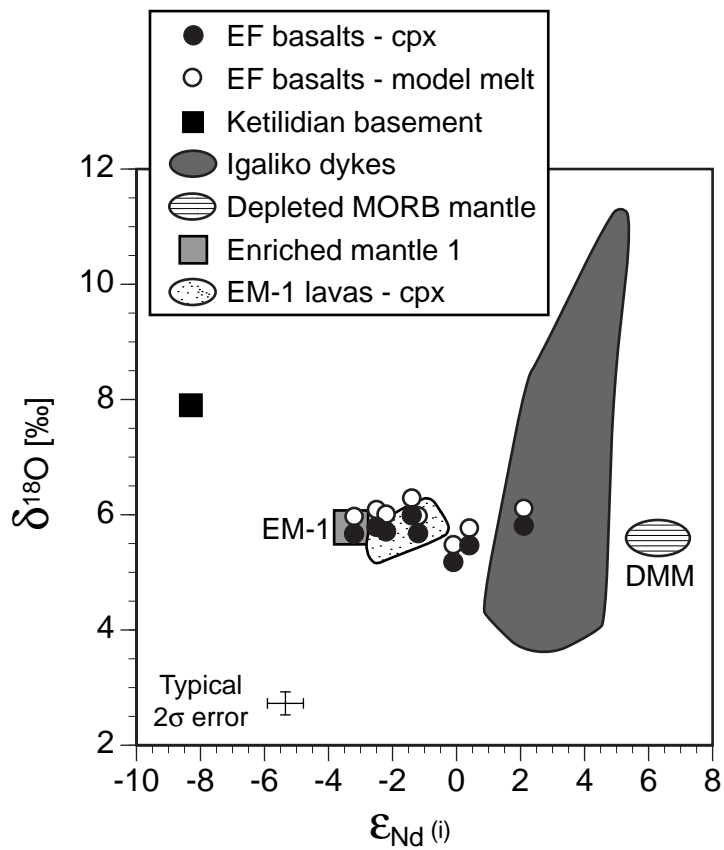
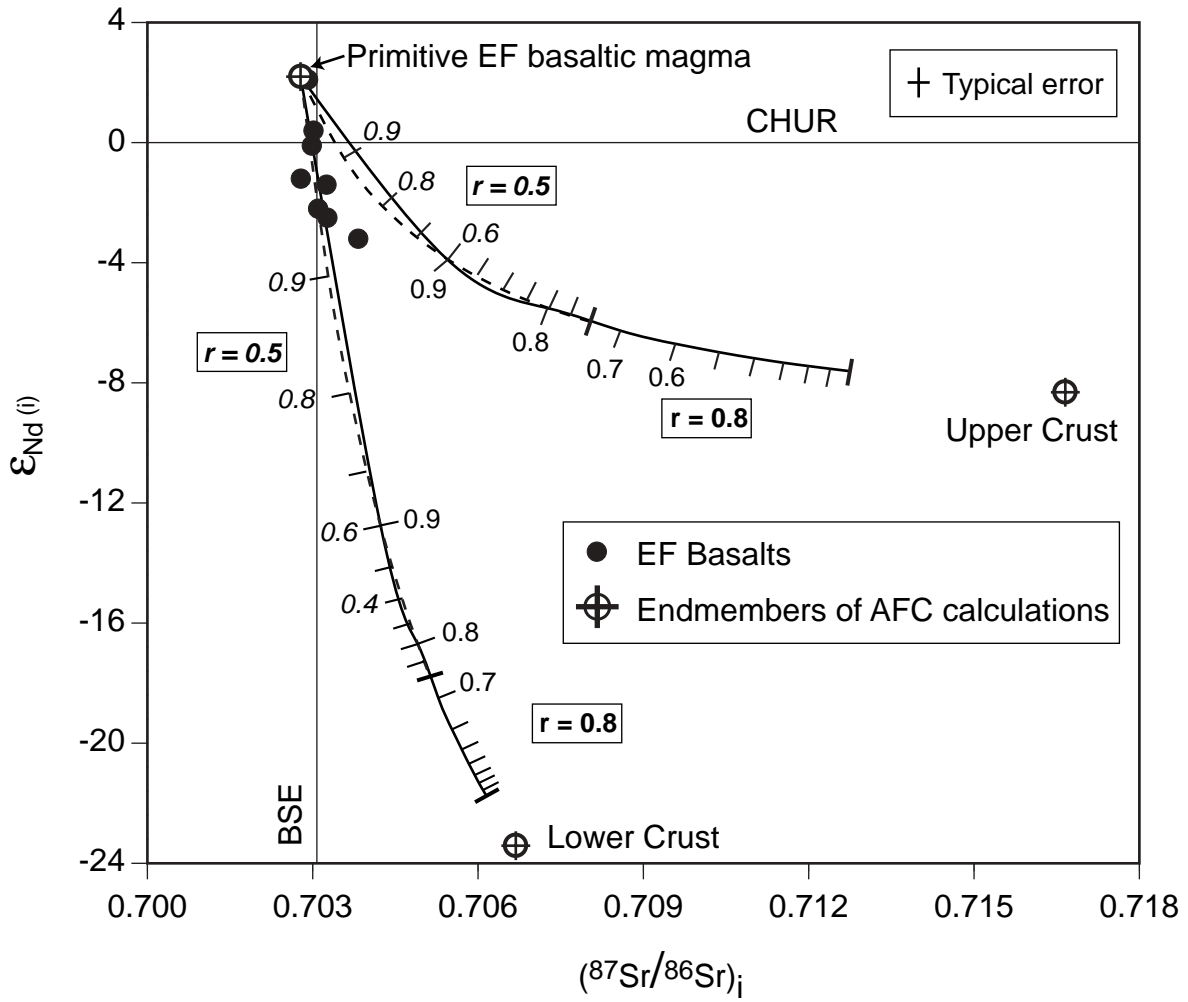


Fig. 9



Kapitel 2:

Petrologische und geochemische Untersuchungen an den Ganggesteinen von Isortoq

Manuskript-Titel:

Archean crust below South Greenland: Evidence from a petrological, geochemical and Sr-Nd-Os-O isotopic study of the Proterozoic Isortoq dike swarm

Autoren:

Ralf Halama¹, Michael Marks¹, Gerhard Brügmann², Wolfgang Siebel¹, Thomas Wenzel¹, Gregor Markl¹

¹ Institut für Geowissenschaften, Eberhard-Karls-Universität Tübingen,
Wilhelmstr. 56, D-72074 Tübingen

² Max-Planck-Institut für Chemie, Abteilung Geochemie, Postfach 3060, D-55020 Mainz

Eingereicht bei:

Lithos

Eigenanteile:

- | | |
|----------------------------------|-----|
| a) Idee | 50% |
| b) Datenbeschaffung | 70% |
| c) Auswertung und Interpretation | 70% |
| d) Ausarbeitung der Publikation | 60% |

Abstract

The mid-Proterozoic Isortoq dike swarm in the Gardar Province, South Greenland, comprises a variety of alkaline rocks ranging from gabbroic to syenitic in composition. Major magmatic mineral phases are olivine, clinopyroxene, Fe-Ti oxides, amphibole, plagioclase and alkali feldspar. Quartz occurs in some samples as a late magmatic phase. Liquidus temperatures of olivine-bearing samples range between 1120-1145 °C and solidus temperatures are 850-930 °C. Calculated silica activities are highly variable between 0.53 and unity. Oxygen fugacities vary from -3 to +1 log units relative to the fayalite-magnetite-quartz buffer.

The rocks have MgO contents < 6 wt.% with Mg# between 53 and 17. Primitive mantle-normalized trace-element patterns show a relative enrichment of LIL elements with Ba peaks and Nb troughs. Clinopyroxenes show a general enrichment in REE relative to chondritic values with variable slightly positive to prominent negative Eu anomalies. Two of the dikes were dated with Sm-Nd 3-point isochrons at 1190 ± 44 Ma and 1187 ± 87 Ma, respectively. Initial $^{87}\text{Sr}/^{86}\text{Sr}$ ratios of mafic mineral separates range from 0.70289 to 0.70432 and initial ϵ_{Nd} values vary from +0.3 to -10.7. Whole-rock initial $^{187}\text{Os}/^{188}\text{Os}$ ratios are highly variable including very radiogenic values of up to 7.967. $\delta^{18}\text{O}_{\text{v-smow}}$ values of separated clinopyroxene and amphibole range from +5.2 to +6.2 ‰ and fall within the range of typical mantle-derived rocks, although mixing with a lower crustal component is permitted by the data. Using EC-AFC modeling equations, the Sr-Nd isotope data of the more radiogenic samples can successfully be modeled by addition of up to 10 % lower crustal granulite-facies Archean gneisses as contaminants. The Os isotopic data also suggest the involvement of old radiogenic crust. In accordance with seismic data, we conclude that a wedge of Archean crust extends from West Greenland further to the south below the present erosion level.

Keywords: Sr-Nd-Os-O isotopes; QUILF; EC-AFC modeling; mafic dike swarm; Gardar Province; South Greenland;

1. Introduction

Mafic dike swarms of Proterozoic age are widespread in many Precambrian cratons and their intrusion indicates a considerable extension of the continental crust (Tarney and Weaver, 1987). Studies of rift-related mafic dike swarms are essential for understanding generation of such extensive mafic magmatism and they may be used to identify mantle plumes (Ernst and Buchan, 1997, 2001). There is general agreement that mafic mantle-derived experience some degree of crustal contamination during ascent and/or residence in crustal magma chambers (Mohr, 1987). The crust is both a density filter and a source of incompatible elements (Lightfoot *et al.*, 1991) and it may act as a site of large-scale contamination and extensive partial crystallization of primitive melts (O'Hara and Herzberg, 2002). However, there is much debate whether the trace element and isotopic characteristics of intracontinental basalts are mantle-derived or due to crustal contamination. Crustal contamination has been shown to be important in the petrogenesis of flood basalts (Devey and Cox 1987; Peng *et al.*, 1992; Chesley and Ruiz 1998; Baker *et al.*, 2000). On the other hand, a mantle source enriched in incompatible trace-elements not influenced by a major crustal input was postulated for some Proterozoic dike swarms (Tarney and Weaver 1987; Condie *et al.*, 1987; Boily and Ludden, 1991) and other flood basalts (Molzahn *et al.*, 1996). If a mantle-derived geochemical signature can be demonstrated, it remains difficult to locate the mantle source, *i.e.* whether the magmas are predominantly derived from the subcontinental lithospheric mantle (SCLM) (*e.g.* Gallagher and Hawkesworth 1992; Turner *et al.*, 1996), from an upwelling mantle plume (*e.g.* LeCheminant and Heaman, 1989; Walker *et al.*, 1997; Puchtel *et al.*, 1999) or from a mixture of both (*e.g.* Ellam *et al.*, 1992; Gibson *et al.*, 1995; Thompson *et al.*, 1998).

Here we present new petrological, geochemical and isotopic data of the Isortoq dike swarm in the mid-Proterozoic igneous Gardar Province in South Greenland. The Gardar Province represents a failed rift and comprises numerous mafic dikes of different generations. The Isortoq dike swarm is one major Gardar mafic dike swarm which has not been studied in great detail before, although the feldspathic inclusions in some of the dikes were the topic of several investigations (Bridgwater, 1967; Bridgwater and Harry, 1968; Halama *et al.*, 2002). Since the swarm comprises a variety of petrographically diverse dike rocks ranging from gabbroic to syenitic in composition, it is well suited to study the influence of crustal assimilation processes on the composition of intracontinental

mafic magmas. For that purpose, we combine petrological with Sr-Nd-O isotopic and whole-rock geochemical data. Additionally, we apply the Re-Os method which is known to have a great potential as tracer of crustal contamination (e.g. Chesley and Ruiz, 1998). The olivine-gabbroic dikes may provide information on the nature of the mantle sources for the dikes and Gardar magmatism in general.

2. Geological Setting

The mid-Proterozoic Gardar Province in South Greenland represents a rift-related igneous province with magmatic activity lasting from about 1.35 to 1.14 Ga (Emeleus and Upton, 1976; Upton and Emeleus, 1987; Upton et al., 2003) (Fig. 1a). The country rocks mainly consist of I-type calc-alkaline granitoids (Julianehåb batholith) of Early Proterozoic age (van Breemen et al., 1974; Allaart, 1976; Patchett and Bridgwater, 1984; Kalsbeek and Taylor, 1985). Recent work (Garde et al., 2002) indicates that the Julianehåb batholith was emplaced mainly between 1.85 – 1.80 Ga. In the northwestern part of the province, Archean rocks of the Border and Foreland Zones of the craton comprise the basement (Allaart, 1976). Apart from twelve major alkaline igneous complexes and a succession of supracrustal lavas and sediments (Eriksfjord Formation), a large number of dike rocks with variable chemical composition intruded the basement. Two major dike swarms were emplaced into the Julianehåb batholith along WSW-ENE to SW-NE trends in the Tugtutôq-Ilímaussaq and the Nunarssuit-Isortoq zones during the late Gardar period (~ 1.20 - 1.14 Ga). The latter of these is the topic of the present paper.

In the Isortoq area, several generations of gabbroic to intermediate dikes with variable widths from a few centimeters to several hundred meters occur (Bridgwater and Coe 1970, Fig. 1b). The earliest generation of Gardar dikes belongs to a regional dike swarm of early-Gardar olivine dolerites (“Brown Dikes” or “BD₀ dikes”) trending WNW-ESE across the Gardar province. They are dated at 1282 ± 5 Ma (Upton et al., 2003), pre-dating the main late-Gardar dike swarm of the Isortoq area. These Brown Dikes can be correlated with major dike swarms within the Canadian shield, namely the Mackenzie swarm (LeCheminant and Heaman, 1989) and the Harp dikes (Cadman et al., 1993). The late-Gardar dikes of the Nunarssuit-Isortoq region were emplaced along WSW-ENE to SW-NE trends. The most spectacular feature of the dike swarm is the abundance of anorthosite xenoliths

and feldspar megacrysts in some of the gabbroic dikes (Bridgwater and Harry, 1968; Halama *et al.*, 2002) that are informally named "Big Feldspar Dikes" (BFDs). The feldspathic material varies from single feldspar crystals (< 1 cm to 1 m in size) to anorthositic bodies up to 30 m long. It is considered as evidence for an anorthosite body underlying South Greenland (Bridgwater, 1967). BFD 1 can be traced for 30 km and is one of the dikes with the greatest volume of feldspathic material in South Greenland (Bridgwater and Harry, 1968). BFD 2 is a composite dike that consists of a 1-2 m wide marginal microsyenite enclosing a feldspathic alkaline gabbro (Bridgwater and Harry, 1968). The amount of feldspathic material is about average in BFD 3, but relatively low in BFD 4. Olivine-gabbros without excessive feldspathic material also occur. Composite dikes comprising a gabbroic, a syenitic and an intermediate syeno-gabbroic facies with maximum widths of up to 500 metres are called "Giant Dikes". They post-date all other members of the swarm (Bridgwater and Coe, 1970) and represent a connecting link between the mafic dykes and the major intrusions of the Gardar province. Giant Dike 3 is the least altered of the Giant Dikes and was therefore selected for a detailed study. Two further, petrographically distinct dikes investigated in this study include a larvikite and a hornblende-syenite. It is likely that some of the gabbroic dikes of the Isortoq swarm are connected to the Bangs Havn Giant Dike (Bridgwater and Harry, 1968) dated at 1185 ± 22 Ma (Engell and Pedersen, 1974). The swarm pre-dates the 1171 ± 5 Ma old Nunarssuit syenite (Finch *et al.*, 2001).

3. Analytical Methods

Mineral compositions were determined using a JEOL 8900 electron microprobe at the Institut für Geowissenschaften, Universität Tübingen, Germany. An internal $\rho\rho Z$ correction of the raw data was applied (Armstrong, 1991). Both synthetic and natural standards were used. Measuring times were 16 s for major elements and 30 s for minor elements. The emission current was 15 nA and the acceleration voltage 15 kV. For feldspar analyses, a beam diameter of 5 μm was used to avoid Na migration. The bulk compositions of oxy-exsolved titanomagnetite grains were reconstructed by combining image processing (NIH Image software) of back-scattered electron images of the exsolved grains with point analyses of exsolved ilmenite and broad beam analyses of exsolved magnetite (Marks and Markl, 2001).

Rare earth element contents (REE) in clinopyroxenes were measured by in-situ laser ablation inductively coupled plasma-mass spectrometry (LA-ICP-MS) at the EU Large-Scale Geochemical Facility (University of Bristol) using a VG Elemental PlasmaQuad 3 + S-Option ICP-MS equipped with a 266 nm Nd-YAG laser (VG MicroProbe II). Details of the method are described by Halama *et al.* (2002). The precision of trace-element concentrations, based on repeated analyses of standards, is approximately $\pm 5\%$ for element concentrations >10 ppm and $\pm 10\%$ for concentrations <10 ppm. Typical detection limits for the REE in this study were 0.04 - 0.6 ppm.

Whole-rock analyses were performed by standard X-ray fluorescence (XRF) techniques at the Universität Mainz, using a Philips PW 1404 spectrometer and at the Universität Freiburg, using a Philips PW 2404 spectrometer. Pressed powder pellets and fused glass discs were prepared to measure contents of trace and major elements, respectively. The raw data were processed with the standard XR-55 software of Philips. Natural standards were used for calibration. Detection limits vary between 1 and 10 ppm, depending on the specific trace element and on the instrument used.

For Sr and Nd isotope analyses, about 10 mg of hand-picked mineral separate were spiked with mixed ^{84}Sr - ^{87}Rb and ^{150}Nd - ^{149}Sm tracers before dissolution under high pressure in HF at 180°C in poly-tetrafluor-ethylene reaction bombs. Rb, Sr, Sm and Nd were separated and measured as described by Marks *et al.* (in press). Analyses of the Ames Nd-standard (Geological Survey of Canada, Roddick *et al.*, 1992) gave $^{143}\text{Nd}/^{144}\text{Nd} = 0.512119 \pm 10$ ($\pm 2\sigma$, $n = 42$) and analyses of the NBS 987 Sr standard yielded $^{87}\text{Sr}/^{86}\text{Sr} = 0.710261 \pm 16$ ($\pm 2\sigma$, $n = 30$) $^{143}\text{Nd}/^{144}\text{Nd}$ ratios were cross-checked with the La Jolla Nd-standard which gave 0.511831 ± 30 ($\pm 2\sigma$, $n = 12$). ϵ_{Nd} values were calculated using present day CHUR values of 0.1967 for $^{147}\text{Sm}/^{144}\text{Nd}$ (Jacobson and Wasserburg, 1980) and 0.512638 for $^{143}\text{Nd}/^{144}\text{Nd}$ (Goldstein *et al.*, 1984). The uncertainty in ϵ_{Nd} based on analytical errors is less than $0.5 \epsilon_{\text{Nd}}$ units.

For Re-Os isotope analyses, 2-3 g of bulk sample powder was dissolved and equilibrated with a ^{185}Re - ^{190}Os mixed spike using aqua regia digestion in sealed Carius tubes (Shirey and Walker, 1998). Details of the further analytical procedures based on the method of Birck *et al.* (1997) are described by Puchtel *et al.* (2001). Re and Os isotopic compositions were measured via negative thermal ionization mass spectrometry at the MPI für Chemie at Mainz. Effects of mass fractionation were eliminated by normalizing to $^{192}\text{Os}/^{188}\text{Os} = 3.082678$. Re isotopic ratios were not corrected for

fractionation. Analytical errors were determined by multiple analyses of internal MPI standards. They are $\pm 0.5\%$ on both Os isotopic composition and Re/Os ratio. Initial $^{187}\text{Os}/^{188}\text{Os}$ ratios were calculated using the ^{187}Re decay constant of $1.666 \times 10^{-11} \text{ a}^{-1}$ (Shirey and Walker, 1998).

Oxygen isotope compositions of powdered whole-rock basement samples were determined by a conventional method modified after Clayton and Mayeda (1963) and Vennemann and Smith (1990), using BrF_3 as reagent and converting the liberated oxygen to CO_2 . The oxygen isotope composition of 0.5 - 2 mg handpicked mineral separates was determined using a laser fluorination method adapted after Sharp (1990) and Rumble and Hoering (1994). Details of the method are described by Marks *et al.* (in press). Results are given in the standard δ -notation, expressed relative to V-SMOW in per mil (‰). Replicate oxygen isotope analyses of the NBS-28 quartz standard (Valley *et al.*, 1995) had an average precision of ± 0.1 ‰ for $\delta^{18}\text{O}$. In each run, standards were analyzed at the beginning and the end of the sample set. A correction was applied to the data equal to the average of the difference between the mean measured value and the accepted value for the standard (9.64 ‰).

4. Results

4.1. Petrography

Major mineral assemblages of the samples investigated in this study are summarized in Table 1. Abbreviations used there and in text and figures are after Kretz (1983).

Olivine-Gabbro and "Big Feldspar Dikes" (BFDs)

The major magmatic mineral phases in the olivine-gabbro and in BFDs 1, 3 and 4 are subhedral olivine, plagioclase and interstitial clinopyroxene. The excessive feldspathic material characteristic of the BFDs is absent in the olivine-gabbro, but otherwise both rock types are petrographically very similar. In BFD 2, olivine is lacking, but some quartz occurs interstitially. Minor phases are apatite, Fe-Ti oxides and sulphides. Biotite is fairly common and can occur either as single grain or surrounding Fe-Ti oxides or olivine. Titanite, amphibole and chlorite occur as secondary alteration products.

Giant Dikes

The Giant Dikes consist of a gabbroic and a syenitic facies. In the gabbroic samples primary minerals are plagioclase, alkali feldspar, anhedral olivine, interstitial clinopyroxene, titanomagnetite, ilmenite, and in some samples high amounts of apatite. In two samples (GM1761 and GM1762) olivine is rimmed by a second clinopyroxene generation. Biotite and/or chlorite overgrow olivine, clinopyroxene and Fe-Ti oxides, whereas amphibole is absent. The transition from the gabbroic to the syenitic facies is characterized by the disappearance of plagioclase, olivine and primary ilmenite, and the abundant occurrence of amphibole. Additionally, clinopyroxene in syenitic samples is euhedral to subhedral but never occurs as interstitial grains (Fig. 2a). As in the gabbroic samples, primary titanomagnetite is oxy-exsolved to ilmenite and magnetite. The exsolved ilmenite laths are selectively altered to titanite and chlorite. Most oxide grains are rimmed by amphibole, biotite and chlorite. In all syenitic samples, aggregates of sector-zoned epidote, associated with titanite, biotite and interstitial albite can be observed (Fig. 2b). In some places pumpellyite and prehnite occur as breakdown products of epidote. Sample GM1712 from the Giant Dike 1 is intermediate between the two above-mentioned facies. Primary olivine is strongly altered, titanomagnetite is the only primary Fe-Ti oxide, but plagioclase is still present in this sample. As in syenitic samples of Giant dike 3, aggregates of epidote and prehnite occur in this sample.

Larvikite

In the larvikite, olivine is very rare, and is surrounded by orthopyroxene (Fig. 2c). The major magmatic phases are clinopyroxene, plagioclase and alkali feldspar. Plagioclase is less common than alkali feldspar and is rimmed by the latter (Fig. 2d). Accessory phases in the larvikite include euhedral to subhedral amphibole, interstitial quartz, biotite, apatite, Fe-Ti oxides and sulphides. Secondary talc, titanite and chlorite are relatively rare.

Hornblende-syenite

Major minerals of this dike rock are euhedral amphibole, alkali feldspar and quartz. Accessory phases are Fe-Ti oxides, biotite, apatite and zircon. Occasional chlorite and titanite are probably of secondary origin.

4.2. Mineral Chemistry

Feldspars

Representative feldspar analyses are presented in Table 2 and illustrated in Fig. 3. In the olivine-gabbro and the BFDs, plagioclase is normally zoned and its composition varies between $An_{63}Ab_{36}Or_2$ and $An_{12}Ab_{85}Or_3$ (Fig. 3a). Plagioclase megacryst data from BFDs and the anorthosite xenoliths have been presented in Halama *et al.* (2002).

The gabbroic samples of Giant Dikes contain plagioclase evolving from $An_{59}Ab_{36}Or_5$ to $An_{15}Ab_{73}Or_{11}$ and alkali feldspar with compositions between $An_{14}Ab_{43}Or_{42}$ and $An_6Ab_{27}Or_{67}$ (Fig. 3b). Maximum anorthite content decreases from the margin to the center of the Giant Dike. In the syenitic facies, plagioclase is lacking, and alkali feldspar composition varies between $An_7Ab_{65}Or_{29}$ to $An_2Ab_{38}Or_{61}$ (Fig. 3b).

The larvikite contains plagioclase ($An_{47}Ab_{51}Or_2$ to $An_{20}Ab_{77}Or_3$) and alkali feldspar ($An_{14}Ab_{56}Or_{30}$ to $An_3Ab_{30}Or_{67}$; Fig. 3c). Large areas of alkali feldspar in the larvikite and all feldspar in the hornblende-syenite are completely exsolved to albite and orthoclase.

Olivine

Typical olivine analyses are presented in Table 3. Olivine ranges in composition from Fo_{70} to Fo_{32} , with the most Fo-rich olivine in some BFD samples and the most Fa-rich ones in the larvikite (Fig. 4). In the olivine-gabbro and the BFD samples, the compositional variability can reach 20 mol% Fo within a single grain and can be as large as in the whole sample. Some grains show growth zoning patterns with a decrease in Fo content towards the rims, but most are irregularly zoned. Olivines from Giant Dike 3 and from the larvikite are rather homogeneous with only minor chemical variation within one single grain and sample. In the gabbroic samples of Giant Dyke 3, Fo-contents of olivine decrease systematically from the margin (Fo_{57}) to the center (Fo_{38}) of the dike.

Clinopyroxene

Clinopyroxene of the whole sample suite is subcalcic augite with generally > 90% quadrilateral (Di + Hed + En + Fs) components. End-member components are calculated after Lindsley (1983) and

some typical analyses are presented in Table 4. Aegirine contents in all samples range from 2 to 10 mol %.

Augites in the olivine-gabbro, the BFDs and the matrix of the anorthosite xenoliths have all similar compositions between $\text{En}_{43}\text{Fs}_{15}\text{Wo}_{42}$ and $\text{En}_{30}\text{Fs}_{31}\text{Wo}_{39}$ (Figs. 4a, b). Some rare augite inclusions in feldspar megacrysts are relatively Ca-poor with a compositional range from $\text{En}_{51}\text{Fs}_{19}\text{Wo}_{31}$ to $\text{En}_{48}\text{Fs}_{19}\text{Wo}_{33}$ (Fig. 4a).

Augite in the gabbroic samples of the two Giant dikes is essentially unzoned and shows a relatively small compositional range within the sample suite ($\text{En}_{41}\text{Fs}_{16}\text{Wo}_{42}$ to $\text{En}_{34}\text{Fs}_{22}\text{Wo}_{44}$). Augite rims around olivine are strongly zoned showing an increase in Fs-component with increasing distance from the olivine grain ($\text{En}_{42}\text{Fs}_{11}\text{Wo}_{47}$ to $\text{En}_{31}\text{Fs}_{22}\text{Wo}_{47}$). Augites of the syenitic samples span a large range in composition ($\text{En}_{40}\text{Fs}_{19}\text{Wo}_{41}$ to $\text{En}_8\text{Fs}_{47}\text{Wo}_{45}$), partly overlapping with augites of the gabbroic samples. Due to strong chemical zoning, the compositional variation within one single grain may reach as much as 20 mol% (Fig. 4c). Among the investigated syenitic samples, three different zoning patterns can be distinguished: In most cases X_{Fe} ($=\text{Fe}^{2+}/(\text{Fe}^{2+} + \text{Mg})$), Fe^{3+} , Na and Si increase and Ti and Al(4) decrease more or less continuously from core to rim, whereas the wollastonite component is almost constant (Fig. 5a). Some samples have Mg-rich cores, and display a stepwise increase of X_{Fe} from core to rim (Fig. 5b). In other samples, partly resorbed inner cores of clinopyroxene are Fe- and Si-rich, followed by a homogeneous but significantly Fe-depleted outer rim with a normal increase of X_{Fe} towards the rim. Interestingly, Na, Al(4), Fe^{3+} and Ti contents in these crystals is more or less constant throughout the whole profile (Fig. 5c).

Clinopyroxene in the larvikite is relatively Ca-poor with a compositional range between $\text{En}_{44}\text{Fs}_{17}\text{Wo}_{39}$ and $\text{En}_{29}\text{Fs}_{32}\text{Wo}_{39}$ (Fig. 4d).

Orthopyroxene

Orthopyroxene is only present in the larvikite where it occurs as small rims around olivine (Fig. 2c).

It is chemically unzoned with a composition of $\text{En}_{52}\text{Fs}_{47}\text{Wo}_1$ to $\text{En}_{50}\text{Fs}_{49}\text{Wo}_1$.

Fe-Ti oxides

Typical compositions of exsolved and reintegrated Fe-Ti oxides are presented in Table 5. In most samples, primary titanomagnetite is oxy-exsolved to ilmenite and magnetite (Figs. 6a-d).

The olivine-gabbro contains a single oxy-exsolved titanomagnetite with very Ti-rich compositions ($\text{Usp}_{94-95}\text{Sp}_{3-4}\text{Mag}_2$), which is characterized by a very fine trellis-type exsolution texture (terminology after Buddington and Lindsley, 1964 ; Fig. 6a).

In BFD 1 and 3, more coarsely trellis-type oxy-exsolved titanomagnetite is common, but there are also Fe-Ti oxide grains where it is difficult to decide whether they represent a single oxy-exsolved grain with a granule exsolution texture or two coexisting oxides. In those cases, oxides with trellis-type exsolution were preferentially used for reintegration resulting in compositions between $\text{Usp}_{89}\text{Sp}_3\text{Mag}_7$ and $\text{Usp}_{65}\text{Sp}_4\text{Mag}_{31}$ (Fig. 6b). In BFD 4, a two-oxide assemblage comprises $\text{Usp}_{71-58}\text{Sp}_{9-5}\text{Mag}_{24-37}$ coexisting with $\text{Ilm}_{98-96}\text{Hem}_{2-4}$.

Gabbroic samples of Giant Dike 3 contain a two-oxide assemblage of titanomagnetite ($\text{Usp}_{94-70}\text{Sp}_3\text{Mag}_{4-27}$) coexisting with ilmenite ($\text{Ilm}_{99-96}\text{Hem}_{1-4}$). The intermediate sample of Giant Dike 1 contains a single exsolved titanomagnetite of the composition $\text{Usp}_{93-83}\text{Sp}_3\text{Mag}_{5-14}$. In syenitic samples primary titanomagnetite compositions could not be recalculated because both exsolved ilmenite and magnetite were strongly altered to titanite/Fe-rich chlorite and chlorite/Fe-hydroxides, respectively (Fig. 6c). However, relics of exsolved magnetite ($\text{Usp}_{19-8}\text{Sp}_{5-3}\text{Mag}_{78-87}$) still have elevated Ti contents indicating an Usp-rich primary composition of titanomagnetite.

The larvikite contains a two-oxide assemblage, but textural evidence suggests that ilmenite was overgrown by later magnetite (Fig. 6d). Both have a relatively constant composition of $\text{Ilm}_{97-94}\text{Hem}_{6-3}$ and $\text{Usp}_{27-21}\text{Sp}_{4-3}\text{Mag}_{70-76}$, respectively. The hornblende-syenite contains only primary ilmenite of the composition $\text{Ilm}_{98-89}\text{Hem}_{2-11}$.

4.3. Calculation of intensive crystallization parameters

Intensive crystallization parameters were calculated because estimates of liquidus and solidus temperatures of the dike magmas are essential for energy constrained – AFC modeling (Spera and Bohron, 2001) and calculated values of silica activity and oxygen fugacity may provide important constraints on the evolution of the dike magmas. For all calculations, pressure was fixed at 1 kbar,

assuming that crystallization of the dikes took place at approximately the same depth as of the Ilímaussaq complex further south in the Gardar Province for which a crystallization pressure of ~ 1 kbar was derived from fluid inclusion data (Konnerup-Madsen and Rose-Hansen, 1984).

Liquidus temperatures were calculated for some olivine-bearing samples, which are considered to be close to liquid compositions (GM 1803, GM 1735, GM 1805 and GD 39) after Sugawara (2000) based on the MgO content in olivine-saturated liquids. They range between 1145 and 1120 °C with an error in calculated temperatures of ± 30 °C.

Feldspar geothermometry using solvus isotherms after Elkins and Grove (1990) indicates minimum crystallization temperatures of ~ 700 °C for BFD 1 as an example for the gabbroic BFDs and the olivine-gabbro (Fig. 3a). Plagioclase-alkali feldspar pairs in the gabbroic samples of Giant Dike 3 and in the larvikite are not in equilibrium. As shown in Fig. 2d, plagioclase has reacted with the liquid to produce alkali feldspar. Ternary feldspar compositions in gabbroic and syenitic samples of Giant Dike 3 point to minimum temperatures of 950 °C - 1020 °C (Fig. 3b). A zoning profile through an alkali feldspar in the larvikite show continuously decreasing minimum temperatures from > 1000 ° in the core to about 700 °C in the outermost rim (Fig. 3 c).

Solidus temperatures, silica activity and oxygen fugacity were calculated from olivine-pyroxene-Fe-Ti oxide equilibria using the QUILF program of Andersen *et al.* (1993). The theoretical background for these calculations was given by Frost and Lindsley (1992) and Lindsley and Frost (1992). Temperature and silica activity were calculated based on Fe, Mg and Ca exchange between olivine and clinopyroxene using a range of mineral compositions. Calculated silica activities are based on a reference state of pure SiO₂ at P and T. The oxygen fugacity was calculated from equilibria among Fe-Mg silicates and Fe-Ti oxides using the full range of measured and reintegrated Fe-Ti oxide compositions. Details of the use of QUILF can be found in Marks and Markl (2001).

Calculated equilibrium temperatures for the olivine-gabbro, the BFDs, and for gabbroic samples of the Giant Dike 3 range between 930°C and 850°C. Calculated silica activities are 0.60 in the olivine-gabbro, 0.67 - 0.83 in the quartz-free BFDs, and 0.53 – 0.68 in the Giant Dike profile. The clinopyroxene rims around olivine in two gabbroic samples of Giant Dike 3 indicate an increase in silica activity. In the syenitic samples, olivine has disappeared due to a further increase in silica activity during progressive fractionation. Unreasonably low calculated temperatures (< 650 °C) for

the larvikite indicate that very rare olivine is not in chemical equilibrium with clinopyroxene. Using a calculated olivine equilibrium composition of Fo₅₆ and a range of early ilmenite compositions, the resulting silica activity is 0.83, which is within the upper range obtained for the gabbroic samples. The orthopyroxene rim around olivine indicates increasing silica activities during later stages. This is in accordance with petrography, as interstitial quartz is present and thus, final solidification of the larvikite took place at $a_{\text{SiO}_2} = 1$.

Generally, the calculated oxygen fugacity increases with increasing silica activity from about 3 log units below the fayalite-magnetite-quartz (FMQ) buffer in the olivine-gabbro to values slightly above the FMQ buffer in some BFD samples, with the gabbroic samples of Giant Dike 3 in between (Fig. 7). Oxygen fugacity for the syenitic samples of Giant Dike 3 could not be determined because it was not possible to reconstruct the primary composition of titanomagnetite. However, the absence of primary ilmenite indicates that oxygen fugacity in the syenitic samples was higher than in gabbroic samples of Giant Dike 3 (Toplis and Carroll, 1995). For the larvikite, oxygen fugacity was calculated only with ilmenite, as textural relationships (Fig. 6d) indicate that magnetite grew later. It varies between 0 and 0.9 log units below FMQ at $T = 853 \text{ }^\circ\text{C}$. Oxygen fugacity calculated with the assemblage Fe-rich clinopyroxene + titanomagnetite \pm orthopyroxene at temperatures fixed between 850-700 $^\circ\text{C}$ to simulate gradual cooling during later stages indicates more oxidizing conditions of 0.6 to 1.0 log units above the FMQ buffer.

4.4. REE data of clinopyroxenes

REE concentrations of average clinopyroxenes from the Isortoq dike rocks are presented in Table 6 and typical chondrite-normalized REE patterns of individual and average analyses are shown in Fig. 8. Since closed-system fractionation can result in considerable fractionation of the REE (Bernstein *et al.*, 1998), rims of clinopyroxenes were avoided for analyses. Clinopyroxenes of all dikes are enriched in REE relative to chondritic values. The patterns generally show an increase in normalized REE contents from La to Nd, followed by a gradual decrease from Sm to Lu. Significant Eu anomalies are lacking in the BFDs, but there is a small negative Eu anomaly in the olivine-gabbro ($\text{Eu}/\text{Eu}^* = 0.70$). In the Giant Dikes, a negative Eu anomaly is increasing from $\text{Eu}/\text{Eu}^* = 0.81$ in the relatively primitive gabbroic facies, via 0.65 in an intermediate syenogabbro

towards 0.41 in the more fractionated syenitic rocks. A similar evolution can be seen in the larvikite, where the extent of the negative Eu anomaly is positively correlated with the degree of REE enrichment, i.e. fractionation. Taking La_N/Yb_N as a measure for REE fractionation, two observations may be of importance: First, the olivine-gabbro has a less fractionated clinopyroxene REE pattern than the BFDs, but it has a more pronounced negative Eu anomaly. Second, La_N/Yb_N in the low-Ca clinopyroxene inclusions is considerably lower than in any of the dike matrix clinopyroxenes. Clinopyroxenes from all dike rocks have REE patterns similar to gabbros from the rifted East Greenland margin (Bernstein *et al.*, 1998), but distinct from gabbros derived from a MORB-like source.

4.5. Whole-rock geochemistry

XRF whole-rock data of the dike rocks are presented in Table 7 and the compositional variation with respect to Mg# as fractionation index is shown in Fig. 9. Mg-numbers ($Mg\# = 100 \text{ Mg}/(\text{Mg} + \text{Fe}^{2+})$ atomic) were calculated using a $\text{Fe}_2\text{O}_3/\text{FeO}$ ratio of 0.2 (Middlemost, 1989) for all rock types as the Ti-rich oxides from all samples indicate relatively reducing conditions even in more fractionated rocks. Mg# between 53 and 18 indicate that the samples do not represent primary melts. SiO_2 contents appear to be relatively scattered, but there is a distinct negative correlation within the BFD and the Giant Dike samples. The positive correlation of $\text{CaO}/\text{Al}_2\text{O}_3$ with Mg# suggests fractionation of clinopyroxene (Class *et al.*, 1994). The larvikite and the hornblende-syenite are characterized by higher SiO_2 and lower $\text{CaO}/\text{Al}_2\text{O}_3$ values. The high P_2O_5 and TiO_2 concentrations in Giant Dike sample GM 1760 (Table 7), combined with the high modal apatite content, indicates that this sample was affected by apatite and possibly Fe-Ti oxide accumulation.

Maximum Ni and Cr contents of 87 ppm and 70 ppm, respectively, confirm that the dikes crystallized from relatively fractionated melts. Other trace elements compatible in mafic systems (e.g. V, Sc) also have relatively low concentrations. Ni and Sc are positively correlated with Mg# suggesting fractionation of olivine and clinopyroxene. A positive correlation of Cr contents with Mg# in the BFDs is a further indication that olivine and/or clinopyroxene fractionation operated in the magmas (not shown). V, which is highly compatible in magnetite and slightly compatible in clinopyroxene, is also decreasing with decreasing Mg#, indicating fractionation of Fe-Ti oxides.

The larvikite and the hornblende-syenite have compatible trace element contents that lie in general within the trends observed for the other samples, although the latter has relatively low Ni contents. However, due to its distinct mineralogy compared with all the other dikes, the hornblende-syenite should not be combined with the other data to derive conclusions on the geochemical evolution of the magmas. Incompatible trace elements like Zr show a weak negative correlation with Mg# for the Giant Dike samples consistent with increasing degrees of differentiation, but the BFD samples are rather scattered.

Normative mineral compositions were calculated following the CIPW scheme (Cross *et al.*, 1903; Cox *et al.*, 1979) and characteristic normative minerals are listed in Table 7. The olivine-gabbro and the BFDs are variably *ne*- and *hy*-normative. In the Giant Dikes, normative compositions change from *ne*-normative in the gabbros to *hy*-normative in the syenites. The *qz*-normative larvikite and hornblende-syenite both contain modal quartz indicating that the normative compositions accurately reflect the modal mineralogy. However, BFD 2 (GM 1750) and the anorthosite xenolith (GM 1682) have late interstitial quartz, but they are quartz-free in the norm calculation. This might be due to the fact that small errors in the assumed $\text{Fe}^{2+}/\text{Fe}^{3+}$ ratio can lead to variable normative mineral compositions. In summary, the calculations of the normative mineral compositions demonstrate that the least fractionated rocks are silica undersaturated. The most fractionated rocks, represented by the syenites of the Giant Dikes, evolved towards *hy*-normative compositions. *Qz*-normative compositions of the larvikite and the hornblende-syenite are not coupled to a low Mg#.

Primitive mantle-normalized incompatible trace element diagrams for selected samples are shown in Fig. 10. The patterns are characterized by a general enrichment relative to primitive mantle values and distinct Ba peaks and Nb troughs. The Ba peak in the hornblende-syenite is considerably smaller than in all other dikes. Small negative P and Ti anomalies are present in the two syenitic samples, and the GD 3 syenite has also a negative Sr anomaly. The two BFD samples have fairly smooth patterns from La to Y with a small positive Sr anomaly in the anorthosite xenolith and a small negative one in BFD 4.

4.6. Sr and Nd isotopic compositions

Sr and Nd isotopic compositions of mineral separates from the dikes and of whole-rocks from the Julianehåb batholith are presented in Table 8. Using the Sm-Nd system on mineral separates of clinopyroxene and plagioclase and whole-rock powder (Table 8, Fig. 11), we dated sample GM 1735 from BFD 1. The age of 1190 ± 44 Ma agrees well with that of the Bangs Havn Giant Dike (1185 ± 22 Ma; Engell and Pedersen, 1974) which is thought to be of the same age. The three clinopyroxene separates from Giant Dike 3 give an age of 1187 ± 87 Ma, consistent with the BFD 1 and the Bangs Havn Giant Dike ages. These ages also agree with field evidence, as the Isortoq swarm is cut by the Nunarssuit syenite, which was dated by the U/Pb method at 1171 ± 5 Ma (Finch *et al.*, 2001), and post-dates the older “Brown dikes” dated at 1280 ± 5 Ma (Upton *et al.*, 2003). The ages of the Isortoq dike swarm overlap with a Rb-Sr age for a dike from the Narsarsuaq area (1206 ± 20 Ma; Winther, 1992), an U-Pb age for the older Giant Dike of Tugtutôq (1184 ± 5 Ma; Upton *et al.*, 2003) and Sm-Nd ages for the Eriksfjord Formation basalts (1170 ± 30 and 1200 ± 30 Ma; Paslick *et al.*, 1993). However, more precise U-Pb dating would be desirable to determine how these magmatic events are related in time.

$^{87}\text{Sr}/^{86}\text{Sr}$ initial ratios of the dikes at 1.19 Ga range from 0.70289 to 0.70432 and $\epsilon_{\text{Nd}(i)}$ values from +0.3 to -10.7 (Table 8). On the Sr-Nd isotope diagram, the data define a relatively steep trend (Fig. 12) with initial $^{87}\text{Sr}/^{86}\text{Sr}$ ratios of the isotopically more primitive samples similar to Bulk Silicate Earth (BSE). The olivine-gabbro and the Giant Dikes have $\epsilon_{\text{Nd}(i)}$ values clustering around 0 to -2, whereas the BFDs show a clear tendency towards more negative $\epsilon_{\text{Nd}(i)}$ values. None of the samples has $\epsilon_{\text{Nd}(i)}$ values close to those of the depleted MORB mantle (DMM) reservoir, estimated to be between $\epsilon_{\text{Nd}(i)} = +5.3$ (calculated after DePaolo, 1981) and $\epsilon_{\text{Nd}(i)} = +7.4$ (calculated after Goldstein *et al.*, 1984).

In comparison with other Sr-Nd data from the Gardar Province, the Isortoq dikes extend the range of $\epsilon_{\text{Nd}(i)}$ towards significantly more negative values than previously reported. The isotopically more primitive dikes overlap with data from the Eriksfjord Formation basalts (Halama *et al.*, in press), but they do not reach the positive $\epsilon_{\text{Nd}(i)}$ values of basaltic, lamprophyric and carbonatitic dikes from Ivittuut (Goodenough *et al.*, 2002) and Igaliko (Pearce and Leng, 1996). The initial $^{87}\text{Sr}/^{86}\text{Sr}$ ratios of the Isortoq dikes, however, show a broad overlap with published data.

4.7. Re-Os isotopic analyses

The Os isotopic data presented in Table 9 include 4 samples from the Isortoq dike rocks together with 4 samples from the Eriksfjord Formation basalts (Halama *et al.*, in press) and 2 samples from the Ilímaussaq intrusion (Marks and Markl, 2001). The EF basalt samples were added to the data set because they represent even more primitive Gardar melts than the Isortoq dikes and are therefore more likely to reflect the Os isotopic composition of the mantle source. The augite syenites from Ilímaussaq are the most primitive rocks of one of the major igneous complexes of the Gardar Province. Obtaining reliable geochemical information of these samples proved to be a challenging task because of the very low Os abundances and the potential Re-mobility during secondary alteration, although it has been shown that the Re-Os system can remain resistant during low-degree metamorphism and hydrothermal alteration (Puchtel *et al.*, 1999). One sample (EF 024) was omitted from data analysis because it was overspiked with respect to Os. The other samples show highly variable initial $^{187}\text{Os}/^{188}\text{Os}$ ratios ranging from -2.428 to 7.967 (Table 9). The negative $(^{187}\text{Os}/^{188}\text{Os})_i$ of the olivine-gabbro is probably due to either analytical problems or mobilization of Re. All other $(^{187}\text{Os}/^{188}\text{Os})_i$ values are much higher than those assumed for the primitive upper mantle (0.129), the subcontinental lithospheric mantle (0.105-0.129), the depleted MORB mantle (0.123-0.126) or enriched mantle components (0.130–0.152) (Shirey and Walker, 1998). The initial $^{187}\text{Os}/^{188}\text{Os}$ ratio of the two most radiogenic samples are significantly higher than the estimated average upper crustal value of 1.9256 (Esser and Turekian, 1993) and a range of values from 0.1652 to 1.8138 for lower crustal xenoliths (Saal *et al.*, 1998).

4.8. Oxygen isotope measurements

Oxygen isotope analyses of mineral separates from the dikes and whole-rock powders from the basement rocks are listed in Table 8. $\delta^{18}\text{O}$ values of clinopyroxene and amphibole separates from the dikes range from 5.2 to 6.2 ‰. The BFDs show a restricted range in $\delta^{18}\text{O}_{\text{cpx}}$ from 5.6 - 5.9 ‰ whereas the dikes without feldspathic material, i.e. the olivine-gabbro and the Giant Dikes, have lower $\delta^{18}\text{O}_{\text{cpx}}$ values in the range 5.3 - 5.6 ‰. Most of the $\delta^{18}\text{O}_{\text{cpx}}$ values from the Isortoq dike swarm overlap with $\delta^{18}\text{O}_{\text{cpx}}$ values of mantle peridotites (5.25 – 5.90 ‰, Matthey *et al.*, 1994), OIBs

(5.3 – 6.1 ‰, Harris *et al.*, 2000) and the spatially associated Eriksfjord Formation basalts (5.2 – 6.0 ‰, Halama *et al.*, in press).

The oxygen isotope equilibration temperature for fractionation between plagioclase and diopside was calculated after Zheng (1993) for sample GM 1735 (BFD 1) using $\Delta(\text{plagioclase-diopside}) = 0.89$ and $X_{\text{An}} = 0.50$. The apparent equilibration temperature is 924 °C. Allowing an error of ± 0.15 ‰ in Δ , calculated temperatures range from 832 to 1035 °C. This indicates that the equilibration of oxygen isotopes occurred at magmatic temperatures.

Mineral-melt fractionations allow the calculation of the magma oxygen isotopic compositions directly from measured values of minerals (Taylor and Sheppard, 1986). Using a $\Delta_{\text{melt-cpx}}$ value of 0.3, calculated after Kalamarides (1986) for a liquidus temperature of ~ 1130 °C, calculated $\delta^{18}\text{O}_{\text{melt}}$ values for the Isortoq dike rocks range from 5.5 to 6.5 ‰.

On the $\epsilon_{\text{Nd}(i)} - \delta^{18}\text{O}$ diagram (Fig. 12b), the Isortoq dike rocks define a weak trend of slightly increasing $\delta^{18}\text{O}$ with decreasing $\epsilon_{\text{Nd}(i)}$. This trend does not approach the trend defined by the Ketilidian basement rocks. Some of the data overlap with comparative data from the Eriksfjord Formation basalts, but none of the Isortoq data plots close to a modeled DMM source.

5. Discussion

5.1. Validity of calculations of intrinsic parameters

Liquidus temperatures calculated for the Isortoq dike samples after Sugawara (2000) (1120-1145 °C) are in agreement with experimental results from Upton (1971) and Upton and Thomas (1980), who obtained liquidus temperatures of about 1190 °C for very similar gabbroic rocks from the Tugtutoq area and assumed that the intrusion of the dike magmas took place between 1160 and 1125 °C. Toplis and Carroll (1995) obtained similar liquidus temperatures for ferro-basaltic melts of ~ 1160 °C. Minimum crystallisation temperatures derived from ternary feldspars yield temperatures in the range 950-1020 °C similar to intrusion temperatures of 1050°C inferred for more differentiated syenitic rock types (Upton and Thomas, 1980).

Temperatures determined by QUILF (Andersen *et al.*, 1993) can be subjected to subsolidus exchange (Markl *et al.*, 1998). Re-equilibration of Fe/Mg in mafic silicates takes place more readily than Na/Ca equilibration in plagioclase (Morse 1984) and restricted zoning may suggest local

homogenization (Tegner *et al.*, 1996). Fe/Mg silicates equilibrate fast when liquid is present and temperatures calculated by QUILF might reflect equilibration with a cooler, more fractionated residual melt (Markl and White 1999). Our QUILF-calculated temperatures (930-850 °C) are slightly lower compared to solidus temperatures of hawaiitic magmas (990-965 °C, Upton 1971). Therefore, QUILF temperatures calculated here are believed to reflect partly solidus temperatures and partly sub-solidus exchange temperatures. Thus, the crystallization interval for the gabbroic rocks is assumed to be 1150-900 °C, whereas the syenitic rocks probably crystallized between 1050-800 °C.

The calculated silica activities correlate positively with whole-rock SiO₂ contents, indicating that the results are reliable. Oxygen fugacities indicate conditions below the FMQ buffer curve within the range of other Gardar magmas. Low oxygen fugacities appear to be a general feature of the Gardar magmas (Powell, 1978; Upton and Thomas, 1980, Larsen and Sørensen, 1987; Marks and Markl, 2001; Marks *et al.*, in press). Albeit the range in calculated log f_{O₂} values is relatively large, there appears to be a general tendency of increasing oxygen fugacity with increasing silica activity (Fig. 7), which is confirmed by magnetite overgrowths over ilmenite in the larvikite. This feature may hint at an FMQ-type equilibrium buffering these parameters.

5.2. Evidence for closed-system fractionation in the Giant Dikes

The systematic decrease of X_{Fo} in olivine and X_{An} in plagioclase parallel to the assumed crystallization direction from the margin towards the dike center in GD 3 is interpreted to reflect fractional crystallization in an essentially closed system for the gabbroic facies of the dike. For various intrusions of the Gardar Province, in situ differentiation (e.g. Stephenson and Upton, 1982; Marks and Markl, 2001) and sidewall crystallisation (e.g. Parsons and Brown, 1988) have been proposed as crystallization processes and it seems likely that both of those processes governed the magmatic evolution of the gabbroic facies of the Giant Dikes. Whole-rock geochemical data trends and REE patterns from clinopyroxenes are consistent with a closed-system fractional crystallization in Giant Dike 3. The Nd isotopic data provide evidence that fractionation from gabbroic to syenitic rocks in GD3 took place in a closed-system because the three samples from GD3 do not show any change in ε_{Nd(i)} at various concentrations of SiO₂ (Fig. 13) and it was demonstrated earlier that they

define an isochron age. Thus, the syenitic rocks may represent a more differentiated member of the same parental melt as the gabbroic rocks. However, differentiation did probably not occur in situ as field evidence (Bridgewater and Coe, 1970, and own observations) indicates that stoping was an important emplacement mechanism in the Giant Dikes. Thereby, syenitic rocks differentiated in deeper levels as the magma rose, and intruded the partly solidified gabbroic material. Fe-rich and partly resorbed cores (Fig. 5) of augites from syenitic samples support this assumption. Possibly, these cores represent relics of crystals from gabbroic rocks which were already solidified and were incorporated into the rising magma during emplacement of the syenitic members.

5.3. Evaluation of crustal contamination and mantle heterogeneity

Variations in the Sr-Nd isotopic composition of magmatic rocks can principally be explained by either crustal contamination or heterogeneous mantle sources. Today, the different mantle components have a wide range of isotopic compositions (Hart *et al.*, 1992, Hofmann, 1997), but their projection into the Proterozoic is problematic. Generally speaking, steep trends on Sr-Nd isotope plots could be attributed to mixtures of an isotopically depleted mantle component and an isotopically enriched mantle component similar to EM-1 (e.g. Milner and Le Roex, 1996). The EM-1 component is characterized by extremely low $^{143}\text{Nd}/^{144}\text{Nd}$ ratios and negative ϵ_{Nd} values (Hofmann, 1997). Based on the Sr-Nd data alone, it seems possible that the dike magmas were derived from a source composed of two distinct mantle components, implying that the larvikite is closest to the EM-1-like end-member composition. However, mantle melts with these low initial Nd isotopic values are usually potassic, highly enriched in LREE and do not show any features indicative of crustal influences (e.g. Nelson, 1992, Schmidt *et al.*, 1999). We will show below that there are many signs for a crustal component in the dike compositions and we therefore prefer the alternative view to explain the decrease in initial ϵ_{Nd} values by increasing amounts of crustal contamination (e.g. Paces and Bell, 1989).

In the Isortoq dikes, the rough negative correlation of a_{SiO_2} with Mg# indicates that a_{SiO_2} was increasing with fractionation and/or crustal contamination (Fig. 13). One possibility to explain this is that the liquid composition for the dike rocks started on the right-hand side of the thermal boundary in the nepheline-albite-quartz system and therefore differentiation produced quartz-

saturated compositions. However, the trend towards higher a_{SiO_2} in the Isortoq dikes is not continuous as the most fractionated syenites of Giant Dike 3 are still below SiO_2 -saturation, whereas the less fractionated larvikite contains quartz. The negative correlation of a_{SiO_2} with ϵ_{Nd} (Fig. 13) is not compatible with simple fractionation trends, but suggests assimilation of relatively quartz-rich partial melts of crustal rocks that influenced the silica activities in the dikes to different degrees. Normative rock compositions agree well with the Nd isotope and QUILF data. Those rocks with relatively high ϵ_{Nd} are *ne*-normative, whereas the larvikite with the most negative ϵ_{Nd} is *qz*-normative, again consistent with assimilation of a SiO_2 -rich partial melt. Mixing with SiO_2 -rich mantle material is considered as unlikely because typical mantle-derived melts are usually poor in SiO_2 compared to crustal melts.

Geochemical data are in agreement with the assimilation hypothesis. High Ba contents typical of the Isortoq dikes (Fig. 10) resemble those in basaltic-hawaiitic lavas from Mull (Kerr *et al.*, 1995). Based on melting experiments (Thompson, 1981), the latter were explained by addition partial melts derived from Lewisian gneisses containing alkali feldspar as a source of the Ba (Kerr *et al.*, 1995). This scenario is also conceivable for the Isortoq magmas when we consider contamination with Archean lithologies which are present in the craton of southern West Greenland. There, granodioritic K-feldspar-bearing gneisses are quite common (McGregor, 1973; O'Nions and Pankhurst, 1974) and some of the gneisses are relatively Ba-rich (McGregor, 1979). Small negative Nb and Ti anomalies (Fig. 10) are consistent with contamination by crustal material modified or generated by subduction zone magmatism. In fact, they are typical features of Archean granulites (Rudnick and Presper, 1990) and negative Nb anomalies in flood basalts were previously explained by crustal contamination (McDonough, 1990). However, the presence of a negative Nb anomaly is no unequivocal evidence for crustal contamination, as it was also proposed to be characteristic for magmas derived from the SCLM (e.g. Hawkesworth *et al.*, 1992; Goodenough *et al.*, 2002).

Recent studies have shown that the Re-Os isotopic system can be particularly useful to distinguish between magmas derived from sublithospheric mantle plumes and lithospheric mantle (e.g. Ellam *et al.*, 1992; Hart *et al.*, 1997; Shirey, 1997). Additionally, Re-Os data can be a powerful tool to decipher crustal assimilation (e.g. Chesley and Ruiz, 1998) as some portions of the lower crust comprise the most radiogenic large-scale Os reservoirs within the Earth (Asmerom and Walker,

1998). Os concentrations in the Isortoq dike rocks are very low, probably because of the compatible behaviour of Os during mantle melting (Shirey and Walker, 1998), prior sulfide separation and/or Os compatibility in olivine (Brügmann *et al.*, 1987). Therefore, small amounts of crustal contamination may have a large impact on the Os isotopic composition of the magmas. On the Re-Os isochron diagram, the data points have a tendency to scatter around the 1.2 Ga reference line, which is an approximate realistic age for all samples (Fig. 14). Excluding the relatively most altered Eriksfjord Formation basalt sample (EF 174), a reasonable fit of the reference line to the data points yields an initial $^{187}\text{Os}/^{188}\text{Os}$ ratio of ~ 0.8 . Despite the large uncertainty in this estimation, this ratio is much higher than $^{187}\text{Os}/^{188}\text{Os}$ values of all known mantle reservoirs, which have a range in $^{187}\text{Os}/^{188}\text{Os}$ from 0.105 to 0.152 (Shirey and Walker, 1998). Therefore, the Os isotopic composition does not reflect a primary mantle composition. The only reservoir known to contain significant radiogenic Os is old continental crust (Chesley and Ruiz, 1998) and lower crustal xenoliths with $^{187}\text{Os}/^{188}\text{Os}$ values as high as 3.5 have been reported (Molzahn *et al.*, 1996). Accordingly, several studies postulated the assimilation of material from the lower crust in the petrogenesis of mafic continental magmas (e.g. Asmerom and Walker, 1998; Sproule *et al.*, 2002). The Os isotopic data are at least compatible with an important role of assimilation of crustal material in the petrogenesis of the Gardar magmas. The high initial $^{187}\text{Os}/^{188}\text{Os}$ ratio might suggest that almost all Os was crustally derived.

Fractionation of olivine, clinopyroxene, plagioclase and Fe-Ti oxides is known to produce small increases in melt $\delta^{18}\text{O}$ values (< 0.3 ‰) and the increase in the $\Delta_{\text{melt-cpx}}$ fractionation factor with decreasing T is about 0.1 ‰ in $\delta^{18}\text{O}$ of the clinopyroxene (Baker *et al.*, 2000). Therefore, the increase in $\delta^{18}\text{O}$ isotopic values in the Isortoq clinopyroxenes can only partly be accounted for by these processes. Since the EM-1 mantle component does not deviate significantly from average upper mantle values (Eiler *et al.*, 1997), the $\delta^{18}\text{O}_{\text{melt}}$ in the larvikite is above typical values for mantle melts and requires another explanation than a heterogeneous mantle source. The weak positive correlations of $\delta^{18}\text{O}$ with ϵ_{Nd} (Fig. 12b) and $\text{Eu}/\text{Eu}^*_{\text{cpx}}$ (Fig. 15) are consistent with an $\delta^{18}\text{O}$ increase due to crustal contamination. The Nd-O data indicate that assimilation of Ketilidian upper crustal basement is unlikely (Fig. 12b). This is supported by field evidence as granitoid xenoliths in the dikes are characterized by sharp contacts, suggesting that they did not react much with the

magmas. Lower crustal rocks of igneous origin have an average $\delta^{18}\text{O}$ value of $+7.5 \pm 1.4$ ‰ with an overall range from +5.4 ‰ to +12.5 ‰ (Fowler and Harmon, 1990) and contamination with crustal material with oxygen isotopic values of +7.0 ‰ to + 10 ‰ and low ϵ_{Nd} values is in qualitative agreement with the data.

Having established that the olivine-gabbro and the Giant Dikes are less crustally contaminated than the BFDs, the absence of a negative Eu anomaly in the BFDs needs to be explained. Intuitively, one would expect that the more pronounced the influence of the AFC process is, the larger should the negative Eu anomaly be. However, this is not the case and alternative explanations are required. A significant difference in the oxidation state of the magmas can be excluded because QUILF calculations show negative ΔFMQ values for both. A more viable explanation for the lack of negative Eu anomalies in the BFD clinopyroxenes is resorption of plagioclase in the melt either due to a pressure decrease or due to injection of new, hot magma (Markl and Frost, 1999). BFD magmas could have been mechanically enriched in plagioclase in a magma chamber possibly close to the crust-mantle boundary before the resorption started. Alternatively, interaction with lower crust can even produce positive Eu anomalies in the melts (Mitchell *et al.*, 1995). This explanation is also compatible with the negative correlation of $\text{Eu}/\text{Eu}^*_{\text{max}}$ with ϵ_{Nd} (Fig. 15) because a larger degree of assimilation as seen in the BFDs would also lead to a relative enrichment in Eu. REE data of amphibolite- and granulite-facies gneisses from the Archean craton of southern West Greenland frequently show a prominent positive Eu anomaly (Compton, 1978) and contamination of the dike magmas with similar material is therefore in agreement with the REE data. In the most primitive clinopyroxenes of the most contaminated rock (the larvikite), an Eu anomaly is also absent (Fig. 8). Negative Eu anomalies occur in more REE-enriched clinopyroxenes of the larvikite, but the size of the anomaly correlates well with the degree of REE fractionation and can therefore be best explained by plagioclase fractionation.

5.4. Quantitative modeling of crustal contamination processes

Mechanisms to explain contamination signatures in mantle-derived mafic magmas include assimilation coupled with fractional crystallization (AFC) (Bowen, 1928; Taylor, 1980; DePaolo,

1981) and assimilation of crust by the most mafic magmas during turbulent ascent (ATA) (Huppert and Sparks, 1985; Devey and Cox, 1987). Correlations of isotopic ratios and parameters of fractionation can be used to evaluate which process is more likely to have occurred. For the Isortoq magmas, the $\epsilon_{\text{Nd}}(i)$ vs. SiO_2 diagram (Fig. 13) reveals a negative correlation. This indicates that AFC processes were operating because AFC processes result in the most evolved rocks becoming the most contaminated. Quantification of the AFC processes was carried out using an energy-constrained assimilation-fractional crystallization (EC-AFC) model (Spera and Bohrson, 2001; Bohrson and Spera, 2001). Since some of the trace elements analyzed are prone to mobilization (Rb, Ba, K) or influenced by accumulation or fractionation processes (P, Ti, Sr) and the oxygen isotope data show only a limited spread, we constrained this modeling to the Sr-Nd isotopic compositions.

Several studies proposed assimilation of granulite facies gneisses by mafic magmas to explain steep trends on Sr-Nd isotope diagrams (e.g. Carter *et al.*, 1978; Bernstein *et al.*, 1998). A negative correlation between ϵ_{Nd} and SiO_2 content was suggested as further indication for assimilation of Archean granulite-facies lower crust (Heaman and Machado, 1992). Since our data point towards compositionally similar contaminants and seismic data were interpreted to reflect the existence of a wedge of Archean crust that extends southwards to Lindenow Fjord (Dahl-Jensen *et al.*, 1998), we used an average of five granulite-facies gneisses with low Rb/Sr ratios from the Archaean craton of West Greenland (Taylor *et al.*, 1984) as representative for the lower crustal composition (Table 10). The Julianehåb granitoids, in which the dikes were emplaced and which represents the most abundant country rock, are a second possible contaminant. Thus, the weighted average from the three granitoid samples of the Julianehåb batholith were used as representative for the chemical composition of an upper crustal contaminant. Sr is modeled as compatible in the assimilant because the assimilated material is thought to be plagioclase-rich based on the $\epsilon_{\text{Nd}} - \text{Eu}/\text{Eu}^*_{\text{max}}$ correlation (Fig. 15). In the magma, Sr is also modeled as slightly compatible consistent with the influence of plagioclase on the fractionating assemblage. Following Bohrson and Spera (2001), Nd is modeled as incompatible both in the magma and the upper and lower crustal assimilants.

The results indicate that AFC processes involving upper crustal Ketilidian basement cannot explain the steep trend on the Sr-Nd isotope diagram, although an upper crustal component appears to be

involved in the petrogenesis of the hornblende-syenite (Fig. 16). On the other hand, assimilation of lower crustal material is consistent with the bulk of the data and indicates a maximum mass of assimilated anatectic melt of $\sim 10\%$ (Fig. 16). However, the starting composition, chosen to be similar to the isotopically most primitive samples, might already be contaminated by some crustal material and therefore 10% is not a maximum value. We conclude that AFC processes involving magmas isotopically similar to the most primitive of the Isortoq dikes and up to $\sim 10\%$ partial melts derived from lower crustal rocks similar to Archean granulite-facies gneisses can reasonably explain the bulk of the Sr-Nd isotope data. The hornblende-syenite appears to be contaminated with both upper and lower crustal material, whereas the off-trend position of BFD 2 can be explained by assimilation of isotopically and/or chemically heterogeneous material.

5.5. Regional perspective

Contamination of Gardar magmas with crustal rocks was demonstrated previously at several localities (e.g. Taylor and Upton, 1993; Andersen, 1997; Stevenson *et al.*, 1997; Marks and Markl, 2001). However, there has been no consensus whether the Ketilidian mobile belt, in which the Isortoq dikes are emplaced, is underlain by Archean crust. This hypothesis was rejected based on isotopic and geochemical data of the Ketilidian granites (van Breemen *et al.*, 1974; Kalsbeek and Taylor, 1985), although field evidence suggested the presence of older basement in the mobile belt (van Breemen *et al.*, 1974). On the other hand, seismic data indicate that a wedge of Archean crust underlies the predominant part of the Ketilidian belt (Dahl-Jensen *et al.*, 1998) and recent studies on Gardar rocks suggest an involvement of lower crustal material in their petrogenesis (Marks *et al.*, in press; Halama *et al.*, in press). The ϵ_{Nd} data reported here are among the most negative for Gardar rocks and together with petrological and Sr-O-Os isotopic data provide compelling evidence for assimilation of partial melts from lower crustal rocks similar to granulite-facies gneisses from the Archean craton. The Nd isotopic composition of the BD₀ Brown Dike, which is roughly about 90 Ma older than the main Isortoq dike swarm, indicates that these assimilation processes in the Gardar magmas occurred already at earlier times. It is also noteworthy that the REE patterns of the clinopyroxenes and the strongly negative ϵ_{Nd} value of the anorthosite xenolith are compatible with a significant input of crustal partial melts. This is in contrast to previous observations which

concluded, based on the alkalic character of the anorthosites and the low initial $^{87}\text{Sr}/^{86}\text{Sr}$ values, that crustal assimilation was insignificant in the formation of the anorthositic rocks (Patchett *et al.*, 1976). On the other hand, the data from Giant Dike 3 show that closed-system fractional crystallization operated at near-surface levels in magmas that were contaminated prior to emplacement.

6. Conclusions

The importance of mafic rocks as probes of the continental crust they have traversed rather than as probes of the lithospheric mantle was recently stressed by Baker *et al.* (1998). Our data of the Isortoq dikes indicate that the assimilated material must have been silicic because the increase in a_{SiO_2} and SiO_2 content in some dikes is higher than expected from fractional crystallization alone. REE and Nd isotopic data require the assimilated material to be rich in plagioclase-component. Isotopic characteristics of the crustal component include a very low $^{143}\text{Nd}/^{144}\text{Nd}$ and a moderately low $^{87}\text{Sr}/^{86}\text{Sr}$ ratio. Furthermore, low Nb contents, moderate $\delta^{18}\text{O}$ values and a highly radiogenic Os isotopic composition of the assimilant are indicated. All these features are compatible with assimilation of partial melts derived from Archean granulite-facies gneisses similar to those present in the Archean craton north of the Ketilidian mobile belt. In agreement with seismic data (Dahl-Jensen *et al.*, 1998), we therefore suggest that Archean rocks occur at depth in the Isortoq region, thus continuing further south than at the present erosion level. Contamination of mafic mantle-derived magmas with lower crustal material is also compatible with models for anorthosite genesis (Ashwal, 1993 and references therein) and therefore in agreement with the assumed existence of anorthosite complexes below the present erosion surface in the Gardar Province (Bridgwater, 1967). Assimilation of upper crustal material was generally insignificant, but might have operated in the petrogenesis of the hornblende-syenite dike.

The Giant Dikes of the Isortoq dike swarm provide evidence for closed-system fractional crystallization processes with olivine, clinopyroxene, plagioclase and Fe-Ti oxides as major fractionating phases. Resorbed clinopyroxene cores in syenitic samples are probably inherited from the gabbro support the idea that stoping was the main emplacement mechanism of the Giant Dikes (Bridgwater and Coe, 1970).

Due to their crustal contamination, mantle source characteristics of the Isortoq dikes are masked. However, the general relative enrichment in incompatible elements and the Sr-Nd isotopic compositions argue against a significant role of depleted MORB mantle in the magma generation. The clinopyroxene REE patterns do also not show any similarity to patterns from MORB-like gabbros, but they are very similar to patterns from cumulus clinopyroxene in gabbroic rocks related to post-breakup magmatism caused by the proximity of the Iceland plume in East Greenland (Bernstein *et al.*, 1998). However, the importance of crustal contamination demonstrated for the Isortoq dikes makes it impossible to distinguish whether the enrichment in incompatible trace elements relative to the primitive mantle was derived from the SCLM, an enriched plume or a mixture of both.

Acknowledgements

We would like to thank Bruce Paterson who provided invaluable help during Laser ICP-MS measurements at the Large-Scale Geochemical Facility supported by the European Community - Access to Research Infrastructure action of the Improving Human Potential Programme, contract number HPRI-CT-1999-00008 awarded to Prof. B.J. Wood (University of Bristol). Gabi Stoschek and Torsten Vennemann are thanked for their help with oxygen isotope measurements. Elmar Reitter expertly assisted with preparation and measurements of radiogenic isotopes and Mathias Westphal helped with microprobe measurements. Financial funding of this work by the Deutsche Forschungsgemeinschaft (grant Ma-2135/1-2) is gratefully acknowledged.

References

- Allaart, J.H., 1976. Ketilidian mobile belt in South Greenland. In: A. Escher W.S. Watt (Editors), *Geology of Greenland. Grønlands Geologiske Undersøgelse*, Copenhagen, pp. 121-151.
- Andersen, D.J., Lindsley, D.H., Davidson, P.M., 1993. QUILF: a PASCAL program to assess equilibria among Fe-Mg-Mn-Ti oxides, pyroxenes, olivine, and quartz. *Computers and Geosciences* 19: 1333-1350.
- Andersen, T., 1997. Age and petrogenesis of the Qassiarsuk carbonatite-alkaline silicate volcanic complex in the Gardar rift, South Greenland. *Mineralogical Magazine* 61: 499-513.
- Armstrong, J.T., 1991. Quantitative elemental analysis of individual microparticles with electron beam instruments. In: K.F.J. Heinrich and D.E. Newbury (Editors), *Electron Probe Quantitation*. Plenum Press, New York and London, pp. 261-315.
- Ashwal, L.D., 1993. *Anorthosites*. Springer, Berlin Heidelberg.
- Asmerom, Y., Walker, R.J., 1998. Pb and Os isotopic constraints on the composition and rheology of the lower crust. *Geology* 26: 359-362.
- Baker, J.A., Menzies, M.A., Thirlwall, M.F., Macpherson, C.G., 1998. Petrogenesis of Quaternary Intraplate Volcanism, Sana'a, Yemen: Implications for Plume-Lithosphere Interaction and Polybaric Melt Hybridization. *Journal of Petrology* 38: 1359-1390.
- Baker, J.A., MacPherson, C.G., Menzies, M.A., Thirlwall, M.F., Al-Kadasi, M., Matthey, D.P., 2000. Resolving crustal and mantle contributions to continental flood volcanism, Yemen; constraints from mineral oxygen isotope data. *Journal of Petrology* 41: 1805-1820.
- Benoit, M., Polvé, M., Ceuleneer, G., 1996. Trace element and isotopic characterization of mafic cumulates in a fossil mantle diapir (Oman ophiolite). *Chemical Geology* 134: 199-214.
- Bernstein, S., Kelemen, P.B., Tegner, C., Kurz, M.D., Blusztajn, J., Kent Brooks, C., 1998. Post-breakup basaltic magmatism along the East Greenland Tertiary rifted margin. *Earth and Planetary Science Letters* 160: 845-862.
- Birck, J.L., Roy Barman, M., Capmas, F., 1997. Re-Os Isotopic Measurements at the Femtomole Level in Natural Samples. *Geostandard Newsletters* 20: 19-27.
- Bohrson, W.A., Spera, F.J., 2001. Energy-constrained open-system magmatic processes; II, Application of energy-constrained assimilation-fractional crystallization (EC-AFC) model to magmatic systems. *Journal of Petrology* 42: 1019-1041.
- Boily, M., Ludden, J.N., 1991. Trace-element and Nd isotopic variations in Early Proterozoic dyke swarms emplaced in the vicinity of the Kapuskasing structural zone: enriched mantle or assimilation and fractional crystallization (AFC) process? *Canadian Journal of Earth Sciences* 28: 26-36.
- Bowen, N.L., 1928. *The evolution of the Igneous Rocks*. Princeton University Press, Princeton, 332 pp.
- Boynton, W.V., 1984. Geochemistry of the rare earth elements: meteorite studies. In: P. Henderson (Editor), *Rare earth element geochemistry*. Elsevier, Amsterdam, pp. 63-114.
- Bridgwater, D., 1967. Feldspathic inclusions in the Gardar igneous rocks of South Greenland and their relevance to the formation of major Anorthosites in the Canadian Shield. *Canadian Journal of Earth Sciences* 4: 995-1014.
- Bridgwater, D., Coe, K., 1970. The role of stoping in the emplacement of the giant dikes of Isortoq, South Greenland. *Geological Journal*, special issue 2: 67-78.
- Bridgwater, D., Harry, W.T., 1968. Anorthosite xenoliths and plagioclase megacrysts in Precambrian intrusions of South Greenland. *Meddelelser om Grønland* 185.
- Brüggemann, G.E., Arndt, N.T., Hofmann, A.W., Tobschall, H.J., 1987. Noble metal abundances in komatiite suites from Alexo, Ontario and Gorgona Island, Columbia. *Geochimica et Cosmochimica Acta* 51: 2159-2169.
- Buddington, A.F., Lindsley, D.H., 1964. Iron-titanium oxide minerals and synthetic equivalents. *Journal of Petrology* 5: 310-357.
- Cadman, A.C., Heaman, L., Tarney, J., Wardle, R., Krogh, T.E., 1993. U-Pb geochronology and geochemical variation within two Proterozoic mafic dyke swarms, Labrador. *Canadian Journal of Earth Sciences* 30: 1490-1504.
- Carter, S.R., Evensen, N.M., Hamilton, P.J., O'Nions, R.K., 1978. Neodymium and Strontium Isotope Evidence for Crustal Contamination of Continental Volcanics. *Science* 202: 743-747.
- Chesley, J.T., Ruiz, J., 1998. Crust-mantle interaction in large igneous provinces: Implications from the Re-Os isotope systematics of the Columbia River flood basalts. *Earth and Planetary Science Letters* 154: 1-11.
- Class, C., Altherr, R., Volker, F., Eberz, G., McCulloch, M.T., 1994. Geochemistry of Pliocene to Quaternary alkali

- basalts from the Huri Hills, northern Kenya. *Chemical Geology* 113: 1-22.
- Clayton, R.N., Mayeda, T.K., 1963. The use of bromine pentafluoride in the extraction of oxygen from oxides and silicates for isotope analysis. *Geochimica et Cosmochimica Acta* 27: 43-52.
- Compton, P., 1978. Rare earth Evidence for the Origin of the Nûk Gneisses, Buksefjorden Region, Southern West Greenland. *Contributions to Mineralogy and Petrology* 66: 283-293.
- Condie, K.C., Bobrow, D.J., Card, K.D., 1987. Geochemistry of Precambrian Mafic Dykes from the Southern Superior Province of the Canadian Shield. In: H.C. Halls and W.C. Fahrig (Editors), *Mafic dyke swarms*. Geological Association of Canada, Special Publication 34: 95-107.
- Cox, K.G., Bell, J.D., Pankhurst, R.J., 1979. *The interpretation of igneous rocks*. George, Allen and Unwin, London.
- Cross, W., Iddings, J.P., Pirsson, L.V., Washington, H.S., 1903. *Quantitative classification of igneous rocks*. University of Chicago Press, Chicago.
- Dahl-Jensen, T., Thybo, T., Hopper, H., Rosing, M., 1998. Crustal structure at the SE Greenland margin from wide-angle and normal incidence seismic data. *Tectonophysics* 288: 191-198.
- DePaolo, D.J., 1988. *Neodymium isotope geochemistry: An introduction*. Springer Verlag, New York.
- DePaolo, D.J., 1981. Trace element and isotopic effects of combined wallrock assimilation and fractional crystallisation. *Earth and Planetary Science Letters* 53: 189-202.
- Devey, C.W., Cox, K.G., 1987. Relationships between crustal contamination and crystallisation in continental flood basalt magmas with special reference to the Deccan Traps of the Western Ghats, India. *Earth and Planetary Science Letters* 84: 59-68.
- Eiler, J.M., Farley, K.A., Valley, J.W., Hauri, E., Craig, H., Hart, S.R., Stolper, E.M., 1997. Oxygen isotope variations in ocean island basalt phenocrysts. *Geochimica et Cosmochimica Acta* 61: 2281-2293.
- Elkins, L.T., Grove, T.L., 1990. Ternary feldspar experiments and thermodynamic models. *American Mineralogist*, 75, 544-559.
- Ellam, R.M., Cox, K.G., 1991. An interpretation of Karoo picrite basalts in terms of interaction between asthenospheric magmas and the mantle lithosphere. *Earth and Planetary Science Letters* 105: 330-342.
- Ellam, R.M., Carlson, R.W., Shirey, S.B., 1992. Evidence from Re-Os isotopes for plume-lithosphere mixing in Karoo flood basalt genesis. *Nature* 359: 718-721.
- Emeleus, C.H. Upton, B.G.J., 1976. The Gardar period in southern Greenland. In: A. Escher and W.S. Watt (Editors), *Geology of Greenland*. Geological Survey of Greenland, Copenhagen, pp. 152-181.
- Engell, J., Pedersen, S., 1974. Rb-Sr whole rock isochron age determination from the Bangs Havn intrusion, South Greenland. *Bulletin of the Geological Society of Denmark* 23: 130-133.
- Ernst, R.E., Buchan, K.L., 1997. Giant Radiating Dyke Swarms: Their Use in Identifying Pre-Mesozoic Large Igneous Provinces and Mantle Plumes. In: J.J. Mahoney and M.E. Coffin (Editors), *Large Igneous Provinces: Continental, Oceanic, and Planetary Flood Volcanism*. Geophysical Monograph 100: 297-333.
- Ernst, R.E., Buchan, K.L., 2001. The use of mafic dike swarms in identifying and locating mantle plumes. In: R.E. Ernst and K.L. Buchan (Editors), *Mantle Plumes: Their Identification Through Time*. Geological Society of America Special Paper 352: 247-265.
- Esser, B.K., Turekian, K.K., 1993. The osmium isotopic composition of the continental crust. *Geochimica et Cosmochimica Acta* 57: 3093-3104.
- Finch, A.A., Mansfeld, J., Andersen, T., 2001. U-Pb radiometric age of Nunarsuit pegmatite, Greenland: constraints on the timing of Gardar magmatism. *Bulletin of the Geological Society of Denmark* 48: 1-7.
- Fowler, M.B. Harmon, R.S., 1990. The oxygen isotope composition of lower crustal granulite xenoliths. In: D. Vielzeuf and P. Vidal (Editors), *Granulites and Crustal Evolution*. Kluwer Academic Publishers, Dordrecht, pp. 493-506.
- Frost, B.R., Lindsley, D.H., 1992. Equilibria among Fe-Ti-oxides, pyroxenes, olivine, and quartz: Part II. Application. *American Mineralogist* 77: 1004-1020.
- Gallagher, K., Hawkesworth, C., 1992. Dehydration melting and the generation of continental flood basalts. *Nature* 358: 57-59.
- Garde, A.A., Hamilton, M.A., Chadwick, B., Grocott, J., McCaffrey, K.J.W., 2002. The Ketilidian orogen of South Greenland: geochronology, tectonics, magmatism, and fore-arc accretion during Palaeoproterozoic oblique convergence. *Canadian Journal of Earth Sciences* 39: 765-793.
- Gibson, S.A., Thompson, R.N., Dickin, A.P., Leonardos, O.H., 1995. High-Ti and Low-Ti mafic potassic magmas: key

- to plume-lithosphere interactions and continental flood-basalt genesis. *Earth and Planetary Science Letters* 136: 149-165.
- Goldstein, S.L., O'Nions, R.K., Hamilton, P.J., 1984. A Sm-Nd isotopic study of the atmospheric dust and particulates from major river systems. *Earth and Planetary Science Letters* 70: 221-236.
- Goodenough, K.M., Upton, B.G.J., Ellam, R.M., 2002. Long-term memory of subduction processes in the lithospheric mantle: evidence from the geochemistry of basic dykes in the Gardar Province of south Greenland. *Journal of the Geological Society of London* 159: 705-714.
- Halama, R., Waight, T., Markl, G., 2002. Geochemical and isotopic zoning patterns of plagioclase megacrysts in gabbroic dykes from the Gardar Province, South Greenland: implications for crystallisation processes in anorthositic magmas. *Contributions to Mineralogy and Petrology* 144: 109-127.
- Halama, R., Wenzel, T., Upton, B.G.J., Siebel, W., Markl, G., in press. A geochemical and Sr-Nd-O isotopic study of the Proterozoic Eriksfjord Basalts, Gardar Province, South Greenland: Reconstruction of an OIB signature in crustally contaminated rift-related basalts. *Mineralogical Magazine*.
- Harris, C., Smith, H.S., le Roex, A.P., 2000. Oxygen isotope composition of phenocrysts from Tristan da Cunha and Gough Island lavas: variation with fractional crystallization and evidence for assimilation. *Contributions to Mineralogy and Petrology* 138: 164-175.
- Hart, S.R., Hauri, E.H., Oschmann, L.A., Whitehead, J.A., 1992. Mantle Plumes and Entrainment: Isotopic Evidence. *Science* 256: 517-520.
- Hart, W.K., Carlson, R.W., Shirey, S.B., 1997. Radiogenic Os in primitive basalts from the northwestern U.S.A.: Implications for petrogenesis. *Earth and Planetary Science Letters* 150: 103-116.
- Hawkesworth, C.J., Gallagher, K., Kelly, S., Mantovani, M., Peate, D.W., Regelous, M., Rogers, N.W., 1992. Paraná magmatism and the opening of the South Atlantic. In: B.C. Storey, T. Alabaster and R.J. Pankhurst (Editors), *Magmatism and the Causes of Continental Break-up*. Geological Society of London Special Publication 68: 221-240.
- Heaman, L.M., Machado, N., 1992. Timing and origin of midcontinent rift alkaline magmatism, North America: evidence from the Coldwell Complex. *Contributions to Mineralogy and Petrology* 110: 289-303.
- Hofmann, A.W., 1997. Mantle geochemistry: the message from oceanic volcanism. *Nature* 385: 219-229.
- Huppert, H.E., Sparks, R.S.J., 1985. Cooling and contamination of mafic and ultramafic magmas during ascent through continental crust. *Earth and Planetary Science Letters* 74: 371-386.
- Jacobson, S.B., Wasserburg, G.J., 1980. Sm-Nd isotopic evolution of chondrites. *Earth and Planetary Science Letters* 50: 139-155.
- Kalamarides, R.I., 1986. High-temperature oxygen isotope fractionation among the phases of Kiglapait intrusion, Labrador, Canada. *Chemical Geology* 58: 303-310.
- Kalsbeek, F., Taylor, P.N., 1985. Isotopic and chemical variation in granites across a Proterozoic continental margin-the Ketilidian mobile belt of South Greenland. *Earth and Planetary Science Letters* 73: 65-80.
- Kerr, A.C., Kempton, P.D., Thompson, R.N., 1995. Crustal assimilation during turbulent magma ascent (ATA); new isotopic evidence from the Mull Tertiary lava succession, N.W. Scotland. *Contributions to Mineralogy and Petrology* 119: 142-154.
- Konnerup-Madsen, J., Rose-Hansen, J., 1984. Composition and significance of fluid inclusions in the Ilímaussaq peralkaline granite, South Greenland. *Bulletin minéralogique* 107: 317-326.
- Kretz, R., 1983: Symbols for rock-forming minerals. *American Mineralogist* 68: 277-279.
- Larsen, L.M., Sørensen, H., 1987. The Ilímaussaq intrusion-progressive crystallization and formation of layering in an appaitic magma. In: J.G. Fitton and B.G.J. Upton (Editors), *Alkaline Igneous Rocks*. Geological Society of London Special Publication 30: 473-488.
- LeCheminant, A.N., Heaman, L.M., 1989. Mackenzie igneous events, Canada: Middle Proterozoic hotspot magmatism associated with ocean opening. *Earth and Planetary Science Letters* 96: 38-48.
- Lightfoot, P.C., Sutcliffe, R.H., Doherty, W., 1991. Crustal contamination identified in Keweenaw Osler Group Tholeiites, Ontario: A trace element perspective. *Journal of Geology* 99: 739-760.
- Lindsley, D.H., 1983. Pyroxene thermometry. *American Mineralogist* 68: 477-493.
- Lindsley, D.H., Frost, B.R., 1992. Equilibria among Fe-Ti-oxides, pyroxenes, olivine, and quartz: Part I. Theory. *American Mineralogist* 77: 987-1003.
- Markl, G., Frost, B.R., 1999. The Origin of Anorthosites and Related Rocks from the Lofoten Islands, Northern

- Norway: II. Calculation of Parental Liquid Compositions for Anorthosites. *Journal of Petrology* 40: 61-77.
- Markl, G., White, C., 1999. Pigeonite-augite intergrowths from the Graveyard Point sill, Oregon: a record of the interplay between bulk and interstitial liquid fractionation. *Contributions to Mineralogy and Petrology* 137: 170-183.
- Markl, G., Frost, B.R., Bucher, K., 1998. The origin of Anorthosites and related rocks from the Lofoten islands, Northern Norway: I. Field relations and estimation of intrinsic variables. *Journal of Petrology* 39: 1425-1452.
- Marks, M., Markl, G., 2001. Fractionation and assimilation processes in the alkaline augite syenite unit of the Ilimaussaq Intrusion, South Greenland, as deduced from phase equilibria. *Journal of Petrology* 42: 1947-1969.
- Marks, M., Vennemann, T., Siebel, W., Markl, G., in press. Quantification of Magmatic and Hydrothermal Processes in a Peralkaline Syenite-Alkali Granite Complex based on Textures, Phase Equilibria, and Stable and Radiogenic Isotopes. *Journal of Petrology*.
- Mattey, D., Lowry, D., Macpherson, C., 1994. Oxygen isotope composition of mantle peridotite. *Earth and Planetary Science Letters* 128: 231-241.
- McDonough, W.F., 1990. Constraints on the composition of the continental lithospheric mantle. *Earth and Planetary Science Letters* 101: 1-18.
- McDonough, W.F., Sun, S.S., 1995. The composition of the Earth. *Chemical Geology* 120: 223-253.
- McGregor, V.R. 1973. The early Precambrian gneisses of the Godthaab district, West Greenland. *Philosophical Transactions of the Royal Society of London A273*: 343-358.
- McGregor, V.R., 1979. Archean gray gneisses and the origin of the continental crust; evidence from the Godthaab region, West Greenland. In: F. Barker (Editor), *Trondhjemites, dacites, and related rocks*. Elsevier, Amsterdam, pp. 169-204.
- Middlemost, E.A.K., 1989. Iron oxidation ratios, norms and the classification of volcanic rocks. *Chemical Geology* 77: 19-26.
- Milner, S.C., Le Roex, A.P., 1996. Isotope characteristics of the Okenyenya igneous complex, northwestern Namibia: constraints on the composition of the early Tristan plume and the origin of the EM 1 mantle component. *Earth and Planetary Science Letters* 141: 277-291.
- Mitchell, J.N., Scoates, J.S., Frost, C.D., 1995. High-Al gabbros in the Laramie Anorthosite Complex, Wyoming: Implications for the composition of melts parental to Proterozoic anorthosite. *Contributions to Mineralogy and Petrology* 119: 166-180.
- Mohr, P.A., 1987. Crustal Contamination in Mafic Sheets: a Summary. In: H.C. Halls and W.C. Fahrig (Editors), *Mafic dyke swarms*. Geological Association of Canada, Special Publication 34: 75-80.
- Molzahn, M., Reisberg, L., Wörner, G., 1996. Os, Sr, Nd, Pb, O isotope and trace element data from the Ferrar flood basalts, Antarctica: evidence for an enriched subcontinental lithospheric source. *Earth and Planetary Science Letters* 144: 529-546.
- Morse, S.A., 1984. Cation diffusion in Plagioclase Feldspar. *Science* 225: 505-505.
- Nelson, D.R., 1992. Isotopic characteristics of potassic rocks: Evidence for the involvement of subducted sediments in magma genesis. *Lithos* 28: 403-420.
- O'Hara, M.J., Herzberg, C., 2002. Interpretation of trace element and isotope features of basalts: relevance of field relations, petrology, major element data, phase equilibria, and magma chamber modeling in basalt petrogenesis. *Geochimica et Cosmochimica Acta* 66: 2167-2191.
- O'Nions, R.K., Pankhurst, R.J., 1974. Rare-earth element distribution in Archaean gneisses and anorthosites, Godthåb area, West Greenland. *Earth and Planetary Science Letters* 22: 328-338.
- Paces, J.B., Bell, K., 1989. Non-depleted sub-continental mantle beneath the Superior Province of the Canadian Shield: Nd-Sr isotopic and trace element evidence from Midcontinent Rift basalts. *Geochimica et Cosmochimica Acta* 53: 2023-2035.
- Parsons, I., Brown, W.L., 1988. Sidewall crystallization in the Klokken intrusion: zoned ternary feldspars and coexisting minerals. *Contributions to Mineralogy and Petrology* 98: 431-443.
- Paslick, C.R., Halliday, A.N., Davies, G.R., Mezger, K., Upton, B.G.J., 1993. Timing of proterozoic magmatism in the Gardar Province, southern Greenland. *Bulletin of the Geological Society of America* 105: 272-278.
- Patchett, J., Bridgwater, D., 1984. Origin of continental crust of 1.9-1.7 Ga age defined by Nd isotopes in the Ketilidian terrain. *Contributions to Mineralogy and Petrology* 87: 311-318.
- Patchett, P.J., Hutchinson, J., Blaxland, A.B., Upton, B.G.J., 1976. Origin of anorthosites, gabbros and potassic

- ultramafic rocks from the Gardar Province, South Greenland: Sr isotopic ratio studies. *Bulletin of the Geological Society of Denmark* 25: 79-84.
- Pearce, N.J.G., Leng, M.J., 1996. The origin of carbonatites and related rocks from the Igaliko Dyke Swarm, Gardar Province, South Greenland: field, geochemical and C-O-Sr-Nd isotope evidence. *Lithos* 39: 21-40.
- Peng, Z.X., Mahoney, J., Hooper, P., Harris, C., Beane, J., 1994. A role for lower continental crust in flood basalt genesis? Isotopic and incompatible element study of the lower six formations of the western Deccan Traps. *Geochimica et Cosmochimica Acta* 58: 267-288.
- Powell, M., 1978. The crystallisation history of the Igdlerfigssalik nepheline syenite intrusion, Greenland. *Lithos* 11: 99-120.
- Puchtel, I.S., Brüggemann, G.E., Hofmann, A.W., 1999. Precise Re-Os mineral isochron and Pb-Nd-Os systematics of a mafic-ultramafic sill in the 2.0 Ga Onega plateau (Baltic Shield). *Earth and Planetary Science Letters* 170: 447-461.
- Puchtel, I.S., Brüggemann, G.E., Hofmann, A.W., 2001. ¹⁸⁷Os-enriched domain in an Archean mantle plume: evidence from 2.8 Ga komatiites of the Kostomuksha greenstone belt, NW Baltic Shield. *Earth and Planetary Science Letters* 186: 513-526.
- Roddick, J.C., Sullivan, R.W., Dudas, F.Ö., 1992. Precise calibration of Nd tracer isotopic composition for Sm-Nd studies. *Chemical Geology* 97: 1-8.
- Rudnick, R.L., Presper, T., 1990. Geochemistry of intermediate- to high-pressure granulites. In: D. Vielzeuf and P. Vidal (Editors), *Granulites and Crustal Evolution*. Kluwer Academic Publishers, Dordrecht, pp. 523-550.
- Rumble, D., Hoering, T.C., 1994. Analysis of oxygen and sulfur isotope ratios in oxide and sulfide minerals by spot heating with a carbon dioxide laser in a fluorine atmosphere. *Accounts of Chemical Research* 27: 237-241.
- Saal, A.E., Rudnick, R.L., Ravizza, G.E., Hart, S.R., 1998. Re-Os isotope evidence for the composition, formation and age of the lower continental crust. *Nature* 393: 58-61.
- Schmidt, K.H., Bottazzi, P.V.R., Mengel, K., 1999. Trace element partitioning between phlogopite, clinopyroxene and leucite lamproite melt. *Earth and Planetary Science Letters* 168: 287-299.
- Sharp, Z.D., 1990. A laser-based microanalytical method for the in-situ determination of oxygen isotope ratios of silicates and oxides. *Geochimica et Cosmochimica Acta* 54: 1353-1357.
- Shirey, S.B., 1997. Re-Os isotopic compositions of Midcontinent rift system picrites: implications for plume-lithosphere interaction and enriched mantle sources. *Canadian Journal of Earth Sciences*, 34, 489-503.
- Shirey, S.B., Walker, R.J., 1998. The Re-Os isotope system in cosmochemistry and high-temperature geochemistry. *Annual Review of Earth and Planetary Sciences* 26: 423-500.
- Spera, F.J., Bohron, W.A., 2001. Energy-constrained open-system magmatic processes I: General model and energy-constrained assimilation and fractional crystallization (EC-AFC) formulation. *Journal of Petrology* 42: 999-1018.
- Sproule, R.A., Lambert, D.D., Hoatson, D.M., 2002. Decoupling of the Sm-Nd and Re-Os Isotopic Systems in Sulphid-Saturated Magmas in the Halls Creek Orogen, Western Australia. *Journal of Petrology* 43: 375-402.
- Stephenson, D., Upton, B.G.J., 1982. Ferromagnesian silicates in a differentiated alkaline complex: Kungnât Fjeld, South Greenland. *Mineralogical Magazine* 46: 283-300.
- Stevenson, R., Upton, B.G.J., Steinfeld, A., 1997. Crust-mantle interaction in the evolution of the Ilimaussaq Complex, South Greenland: Nd isotopic studies. *Lithos* 40: 189-202.
- Sugawara, T., 2000. Empirical relationships between temperature, pressure, and MgO content in olivine and pyroxene saturated liquid. *Journal of Geophysical Research* 105: 8457-8472.
- Tarney, J., Weaver, B.L., 1987. Geochemistry and Petrogenesis of Early Proterozoic Dyke Swarms. In: H.C. Halls and W.C. Fahrig (Editors), *Mafic dyke swarms*. Geological Association of Canada, Special Publication 34: 81-93.
- Taylor, H.P., 1980. The effects of assimilation of country rocks by magmas on ¹⁸O/¹⁶O and ⁸⁷Sr/⁸⁶Sr systematics in igneous rocks. *Earth and Planetary Science Letters* 47: 243-254.
- Taylor, H.P.J., Sheppard, S.M.F., 1986. Igneous rocks: I. Processes of isotopic fractionation and isotope systematics. In: J.W. Valley, H.P.J. Taylor and J.R. O'Neil (Editors), *Stable Isotopes*. Reviews in Mineralogy 16: 227-269.
- Taylor, P.N., Upton, B.G.J., 1993. Contrasting Pb isotopic compositions in two intrusive complexes of the Gardar magmatic province of South Greenland. *Chemical Geology* 104: 261-268.
- Taylor, P.N., Jones, N.W., Moorbath, S., 1984. Isotopic assessment of relative contributions from crust and mantle sources to the magma genesis of Precambrian granitoid rocks. *Philosophical Transactions of the Royal Society of London A* 310: 605-625.
- Tegner, C., Robins, B., Sørensen, H.S., 1996: Crystallization from stratified magmas in the Honningsvåg intrusive suite,

- Northern Norway; a reappraisal. *Mineralogical Magazine* 60: 41-51.
- Thompson, R.N., 1981. Thermal aspects of the origin of Hebridean Tertiary acid magmas. I. An experimental study of partial fusion of Lewisian gneisses and Torridonian sediments. *Mineralogical Magazine* 44: 161-170.
- Thompson, R.N., Gibson, S.A., Mitchell, J.G., Dickin, A.P., Leonardos, O.H., Brod, J.A., Greenwood, J.C., 1998. Migrating Cretaceous-Eocene Magmatism in the Serra do Mar Alkaline Province, SE Brazil: melts from the deflected Trindade mantle plume? *Journal of Petrology* 39: 1493-1526.
- Toplis, M.J., Carroll, M.R., 1995. An experimental study of the influence of oxygen fugacity on Fe-Ti oxide stability, phase relations, and mineral-melt equilibria in ferro-basaltic systems. *Journal of Petrology* 36: 1137-1170.
- Turner, S.P., Hawkesworth, C.J., Gallagher, K.G., Stewart, K., Peate, D., Mantovani, M., 1996. Mantle plumes, flood basalts and thermal models for melt generation beneath continents: assessment of a conductive heating model. *Journal of Geophysical Research* 101: 11503-11518.
- Upton, B.G.J., 1971. Melting experiments on chilled gabbros and syenogabbros. *Carnegie Institute Washington Year Book*, pp. 112-118.
- Upton, B.G.J., Emeleus, C.H., 1987. Mid-Proterozoic alkaline magmatism in southern Greenland: the Gardar province. In: J.G. Fitton and B.G.J. Upton (Editors), *The Alkaline Rocks*. Geological Society of London Special Publication 30: 449-471.
- Upton, B.G.J., Thomas, J.E., 1980. The Tugtutôq younger giant dyke complex, South Greenland: fractional crystallisation of transitional olivine basalt magma. *Journal of Petrology* 21: 167-198.
- Upton, B.G.J., Emeleus, C.H., Heaman, L.M., Goodenough, K.M., Finch, A., 2003. Magmatism of the mid-Proterozoic Gardar Province, South Greenland: chronology, petrogenesis and geological setting. *Lithos* 68: 43-65.
- Valley J.W., Kitchen, N., Kohn, M.J., Niendorf, C.R., Spicuzza, M.J., 1995. UWG-2, a garnet standard for oxygen isotope ratios: strategies for high precision and accuracy with laser heating. *Geochimica et Cosmochimica Acta* 59: 5223-5231.
- van Bremen, O., Aftalion, M., Allart, J.H., 1974. Isotopic and Geochronologic Studies on Granites from the Ketilidian Mobile Belt of South Greenland. *Bulletin of the Geological Society of America* 85: 403-412.
- Vennemann, T.W. O'Neil, J.R., 1993. A simple and inexpensive method of hydrogen isotope and water analyses of minerals and rocks based on zinc reagent. *Chemical Geology* 103: 227-234.
- Walker, R.J., Morgan, J.W., Hanski, E.J., Smolkin, V.F., 1997. Re-Os systematics of Early Proterozoic ferropicrites, Pechenga Complex, northwestern Russia: Evidence for ancient ¹⁸⁷Os-enriched plumes. *Geochimica et Cosmochimica Acta* 61: 3145-3160.
- Wendt, I., 1986. *Radiometrische Methoden in der Geochronologie*. Clausthaler Tektonische Hefte Band 23, Pilger Verlag, Clausthal-Zellerfeld.
- Winther, K.T., 1992. Feldspar megacryst and anorthosite xenolith-bearing dykes in the Narssarssuaq area, South Greenland. *Rapport Grønlands Geologiske Undersøgelse* 154: 49-59.
- Zheng, Y.-F., 1993. Calculation of oxygen isotope fractionation in anhydrous silicate minerals. *Geochimica et Cosmochimica Acta* 57: 1079-1091.

Figure captions

Fig. 1: a) Map of the Gardar Province (after Upton and Emeleus, 1987); b) Map of the Isortoq region (after Bridgwater and Coe, 1970) with sample localities.

Fig. 2: Back-scattered electron (BSE) images of a) euhedral clinopyroxene with apatite inclusions in the gabbroic facies of Giant Dike 3, b) sector-zoned epidote associated with titanite, biotite, albite, pumpellyite and prehnite in the syenitic facies of Giant Dike 3, c) olivine, overgrown by orthopyroxene and biotite, in the larvikite and d) plagioclase surrounded by alkali feldspar in the larvikite.

Fig. 3: Feldspar compositions of Isortoq dike rocks in the An-Ab-Or triangle with solvus isotherms after Elkins and Grove (1990).

Fig. 4: Olivine and pyroxene compositions of Isortoq dike rocks in the enstatite-ferrosilite-hedenbergite-diopside (En-Fs-Hd-Di) quadrilateral. Fo = forsterite, Fa = fayalite, Ks = kirschsteinite (CaFeSiO_4) and Mo = monticellite (CaMgSiO_4).

Fig. 5: Zoning profiles in clinopyroxenes of Giant Dike 3.

Fig. 6: BSE images of Fe-Ti oxides in Isortoq dike rocks. a) fine trellis-type exsolution in the olivine-gabbro; b) coarse trellis-type exsolution in BFD 1; c) alteration of Fe-Ti oxides to titanite in the syenitic facies of Giant Dike 3; d) ilmenite overgrown by magnetite in the larvikite.

Fig. 7: Oxygen fugacity vs. silica activity in Isortoq dike rocks, calculated with QUILF (Andersen *et al.*, 1993). Please note that BFD 2 and the hornblende-syenite were omitted for QUILF calculations due to the lack of suitable mineral parageneses, but they should plot at $a_{\text{SiO}_2} = 1$.

Fig. 8: REE patterns of clinopyroxenes from Isortoq dike rocks, normalized to chondritic values from Boynton (1984). Individual clinopyroxene analyses are shown in a) and c), all other diagrams show averaged values. REE patterns of clinopyroxenes from MORB-like olivine-gabbro (Benoit *et al.*, 1996) and gabbro from a rifted continental margin (Bernstein *et al.*, 1998) together with whole-rock REE data from two Archean gneisses (Compton, 1978) are shown for comparison.

Fig. 9: Whole-rock variation diagrams for Isortoq dike rocks with $\text{Mg\#} = \text{Mg}/(\text{Mg} + \text{Fe}^{2+})$ as fractionation index.

Fig. 10: Multi-element plot of selected Isortoq samples normalized to primitive mantle values from McDonough and Sun (1995).

Fig. 11: Isochron diagrams for BFD 1 and Giant Dike 3. Error bars indicate 2σ errors. Errors used in the isochron calculations are $\pm 0.5\%$ for $^{147}\text{Sm}/^{144}\text{Nd}$ and 0.002% $^{143}\text{Nd}/^{144}\text{Nd}$, based on repeated standard analyses. Isochrons were calculated after Wendt (1986).

Fig. 12: a) $\epsilon_{\text{Nd}(i)}$ vs. $(^{87}\text{Sr}/^{86}\text{Sr})_i$ diagram for mineral separates of Isortoq dike rocks and whole-rock basement samples. Reference data are from Pearce and Leng (1996), Goodenough et al. (2002) and Halama et al. (in press). The reference line of Bulk Silicate Earth (BSE) for the Sr isotopic composition was calculated after DePaolo (1988) assuming present-day values of 0.0827 for $^{87}\text{Rb}/^{86}\text{Sr}$ and 0.7045 for $^{87}\text{Sr}/^{86}\text{Sr}$. b) Oxygen isotopic compositions vs. $\epsilon_{\text{Nd}(i)}$ of separated clinopyroxenes and amphiboles from Isortoq dike rocks and whole-rock country rock samples. Oxygen isotopic composition of clinopyroxene from a DMM source was modeled using an average mantle olivine $\delta^{18}\text{O}$ value of 5.2 ‰ (Eiler et al., 1997) and an average $\Delta^{18}\text{O}_{\text{cpx-olivine}}$ fractionation of 0.4 ‰ (Mattey et al., 1994).

Fig. 13: a) $\epsilon_{\text{Nd}(i)}$ vs. SiO_2 (wt.%) diagram with general trends of fractional crystallization and AFC processes (solid arrows). Note the fractional crystallization trend for the three samples of Giant Dike 3 (dashed arrow). b) and c) Silica activities calculated with QUILF (Andersen et al., 1993) vs. $\epsilon_{\text{Nd}(i)}$ and Mg# (symbols as in Fig. 12).

Fig. 14: Maximum Eu anomalies in clinopyroxenes from Isortoq dike rocks vs. $\epsilon_{\text{Nd}(i)}$ and $\delta^{18}\text{O}$ (symbols as in Fig. 12).

Fig. 15: Re-Os isotope composition correlation diagram for four Isortoq dikes, three Eriksfjord Formation basalts and two Ilímaussaq augite-syenites.

Fig. 16: Sr-Nd isotope diagram showing the results of the AFC modeling with the parameters from Table 10 (symbols as in Fig. 12). Isotopic compositions of upper crust is an weighted average from the three basement samples and lower crust is represented by an average of 5 Archean granulite facies gneisses with low Rb/Sr ratios from Taylor et al. (1984). Numbers at EC-AFC curves indicate the percentage of mass of assimilated partial melt.

Table 1: Sample description

Dike	Type	Sample	Ol	Cpx	Feldspar	Amph	Qtz	Fe-Ti oxides
BD ₀	gabbro	GD 37	⊕	⊕	plag			mag
BFD 1	gabbro	GM 1680	⊕	⊕	plag			mag
	plagioclase megacryst	GM 1681		⊕	plag			
	anorthosite xenolith	GM 1682		⊕	plag	±	±	mag
	gabbro	GM 1729	⊕	⊕	plag			
	gabbro	GM 1735	⊕	⊕	plag			mag
BFD 2	leucogabbro from the dike center	GM 1750		⊕	plag		±	mag
BFD 3	gabbro	GM 1805	⊕	⊕	plag			mag
BFD 4	gabbro	GD 39	⊕	⊕	plag			ilm + mag
Olivine-gabbro	gabbro	GM 1803	⊕	⊕	plag			mag
Giant Dike 1	syeno-gabbro	GM 1712		⊕	plag + alk			mag
Giant Dike 3	sample traverse from center to margin in gabbroic facies	GM 1759 - 1762	⊕	⊕	plag + alk			ilm + mag
	syenite	GM 1768		⊕	alk	±		mag
	sample traverse from margin to margin in syenitic facies	GM 1769 - 1776		⊕	alk	±		mag
	syenite	GM 1778		⊕	alk	±		mag
	syenite	GM 1780		⊕	alk	±		mag
	syenite	GM 1784		⊕	alk	±		mag
Larvikite	larvikite from the dike center	GM 1684	⊕	⊕	plag + alk	±	±	ilm + mag
Hornblende-syenite	syenite	GD 38			alk	⊕	⊕	mag

⊕ = mineral is a major component of the sample, ± = minor amounts of mineral present

Table 2: Representative microprobe analyses of feldspar from Isortoq dike rocks

Dike	Olivine- gabbro	BFD 2	BFD 2	GD 3	GD 3	GD 3	GD 3	GD 3	GD 3	GD 3	GD 3	Larvikite	Larvikite	Larvikite
Sample	GM 1803	GM 1750	GM 1749	GM1760	GM 1760	GM 1761	GM 1762	GM 1762	GM 1762	GM 1774	GM 1774	GM 1684	GM 1684	GM 1684
wt.%														
SiO ₂	53.87	56.49	62.81	62.88	62.55	56.01	65.35	64.84	62.73	65.17	64.20	57.16	62.42	64.41
TiO ₂	0.25	0.08	0.05	0.04	0.05	0.05	0.01	0.00	0.05	0.07	0.01	0.08	0.12	0.03
Al ₂ O ₃	27.78	26.46	21.92	22.50	21.98	27.66	19.10	19.88	22.76	19.42	19.11	26.05	21.52	20.00
FeO	1.66	0.51	0.24	0.25	0.27	0.17	0.13	0.11	0.10	0.14	0.11	0.35	0.36	0.19
MnO	0.04	0.00	0.01	0.00	0.00	0.00	0.02	0.02	0.05	0.00	0.00	0.00	0.00	0.02
MgO	0.56	0.08	0.01	0.03	0.00	0.02	0.00	0.00	0.00	0.01	0.00	0.03	0.01	0.01
BaO	0.00	0.05	0.41	0.17	0.23	0.04	0.08	0.12	0.06	0.28	1.59	0.20	0.93	0.77
SrO	0.23	0.25	0.20	0.31	0.29	0.32	0.12	0.16	0.37	0.21	0.24	0.21	0.21	0.20
CaO	9.88	9.86	4.09	3.94	3.55	9.47	0.57	1.43	4.34	0.85	0.31	8.29	3.04	1.51
Na ₂ O	4.23	5.49	6.43	7.93	6.16	5.46	4.01	4.94	8.24	6.58	4.12	6.61	7.33	5.84
K ₂ O	0.93	0.70	3.88	1.95	4.72	0.38	10.61	8.37	0.89	6.76	10.03	0.40	3.33	6.83
Total	99.42	99.97	100.04	99.99	99.79	99.60	99.99	99.89	99.60	99.50	99.72	99.39	99.27	99.82
Formulae based on 8 oxygens														
Si	2.46	2.55	2.82	2.81	2.83	2.53	2.97	2.94	2.80	2.95	2.96	2.59	2.83	2.92
Al	1.50	1.41	1.16	1.18	1.17	1.47	1.02	1.06	1.20	1.04	1.04	1.39	1.15	1.07
Ti	0.01	0.00	0.00	0.00	0.00	0.00	0.00	0.00	0.00	0.00	0.00	0.00	0.00	0.00
Fe ²⁺	0.06	0.02	0.01	0.01	0.01	0.01	0.00	0.00	0.00	0.01	0.00	0.01	0.01	0.01
Mn	0.00	0.00	0.00	0.00	0.00	0.00	0.00	0.00	0.00	0.00	0.00	0.00	0.00	0.00
Mg	0.04	0.01	0.00	0.00	0.00	0.00	0.00	0.00	0.00	0.00	0.00	0.00	0.00	0.00
Ba	0.00	0.00	0.01	0.00	0.00	0.00	0.00	0.00	0.00	0.01	0.03	0.00	0.02	0.01
Sr	0.01	0.01	0.01	0.00	0.00	0.00	0.00	0.00	0.00	0.00	0.00	0.01	0.01	0.01
Ca	0.48	0.48	0.20	0.19	0.17	0.46	0.03	0.07	0.21	0.04	0.02	0.40	0.15	0.07
Na	0.38	0.48	0.56	0.69	0.54	0.48	0.35	0.43	0.71	0.58	0.37	0.58	0.64	0.51
K	0.05	0.04	0.22	0.11	0.27	0.02	0.62	0.48	0.05	0.39	0.59	0.02	0.19	0.39
Total	4.99	5.00	4.99	5.00	4.99	4.98	5.00	4.99	4.98	5.01	5.00	5.01	5.01	5.00
X _{An}	0.53	0.48	0.20	0.19	0.17	0.48	0.03	0.07	0.21	0.04	0.02	0.40	0.15	0.07
X _{Ab}	0.41	0.48	0.57	0.70	0.55	0.50	0.35	0.44	0.73	0.57	0.38	0.58	0.65	0.52
X _{Or}	0.06	0.04	0.23	0.11	0.28	0.02	0.62	0.49	0.05	0.39	0.61	0.02	0.20	0.40

Table 3: Representative microprobe analyses of olivine from Isortoq dike rocks

Dike	Olivine- Gabbro	Olivine- Gabbro	BFD 1	BFD 1	BFD 4	Giant Dike 3 gabbro	Giant Dike 3 gabbro	Giant Dike 3 gabbro	Larvikite	Larvikite
Sample	GM 1803	GM 1803	GM 1735	GM 1729	GD 39	GM1759	GM1761	GM1760	GM 1684	GM 1684
wt. %										
SiO ₂	36.26	33.82	37.16	33.55	35.28	33.28	35.42	34.64	32.89	32.88
TiO ₂	0.06	0.07	0.03	0.02	0.02	0.05	0.02	0.01	0.02	0.08
Al ₂ O ₃	0.01	0.01	0.10	0.05	0.02	0.01	0.00	0.00	0.01	0.00
NiO	0.03	0.03	0.06	0.03	0.03	—	—	—	0.00	0.05
FeO	33.23	47.09	29.32	48.71	39.67	48.28	37.72	42.61	52.13	51.03
MnO	0.44	0.91	0.25	0.84	0.71	0.53	0.23	0.65	1.24	1.14
MgO	29.92	17.84	32.67	16.82	24.00	17.00	26.51	21.86	14.05	15.15
CaO	0.25	0.51	0.24	0.19	0.36	0.40	0.33	0.38	0.06	0.09
Total	100.20	100.28	99.82	100.20	100.10	99.55	100.23	100.15	100.40	100.42
Formulae based on 4 oxygens:										
Si	1.00	1.00	1.00	1.00	1.00	1.00	0.99	1.00	1.00	0.99
Al	0.00	0.00	0.00	0.00	0.00	0.00	0.00	0.00	0.00	0.00
Ti	0.00	0.00	0.00	0.00	0.00	0.00	0.00	0.00	0.00	0.00
Mg	1.22	0.79	1.31	0.75	1.02	0.76	1.11	0.94	0.64	0.68
Fe	0.76	1.17	0.66	1.22	0.94	1.21	0.89	1.03	1.33	1.29
Mn	0.01	0.02	0.01	0.02	0.02	0.01	0.01	0.02	0.03	0.03
Ni	0.00	0.00	0.00	0.00	0.00	—	—	—	0.00	0.00
Ca	0.01	0.02	0.01	0.01	0.01	0.01	0.01	0.01	0.00	0.00
Sum	3.00	3.00	3.00	3.00	3.00	3.00	3.01	3.00	3.00	3.00
X _{Fo}	0.614	0.400	0.663	0.380	0.516	0.383	0.553	0.475	0.324	0.346
X _{Fa}	0.383	0.592	0.334	0.617	0.478	0.610	0.442	0.519	0.675	0.653
X _{La}	0.004	0.008	0.004	0.003	0.006	0.006	0.005	0.006	0.001	0.001

— = not determined

Table 4: Representative microprobe analyses of pyroxene from Isortoq dike rocks

Dike	Olivine-gabbro	BFD 1	BFD 1	BFD 2	GD 1	GD 3	GD 3	GD 3	GD 3	GD 3	Larvikite	Larvikite
Sample	GM1803	GM 1729	GM 1681	GM 1749	GM 1712	GM 1760	GM 1761	GM 1769	GM 1769	GM 1772	GM 1684	GM 1684
			Ca-poor inclusion in feldspar				rim around olivine	Fe-rich core	rim		cpx	rim around olivine
wt %												
SiO ₂	51.21	52.49	51.11	51.09	51.18	50.90	53.36	49.92	50.13	49.16	51.59	51.57
TiO ₂	1.00	0.37	1.34	0.71	0.99	0.75	0.01	0.88	1.00	0.67	0.70	0.06
Al ₂ O ₃	2.34	1.76	3.15	1.27	0.68	2.21	0.51	0.77	0.92	0.65	0.41	0.36
Cr ₂ O ₃	0.04	0.00	0.00	0.04	0.00	0.02	—	—	—	0.00	0.00	0.00
FeO	9.17	9.56	11.79	17.26	12.62	10.89	8.29	18.91	17.54	22.00	17.30	28.81
MnO	0.17	0.29	0.31	0.53	0.28	0.11	0.10	0.48	0.47	0.51	0.53	0.91
MgO	12.67	13.89	16.35	9.54	11.48	12.71	13.95	6.71	8.02	4.23	11.05	17.41
CaO	22.34	20.87	16.18	19.01	21.35	21.01	22.46	21.50	21.35	21.07	18.19	1.39
Na ₂ O	0.73	0.56	0.43	0.49	0.42	0.52	0.54	0.40	0.36	0.87	0.32	0.01
Total	99.66	99.80	100.65	99.93	99.01	99.11	99.37	99.58	99.79	99.15	100.08	100.52
Formulae based on 4 cations and 6 oxygens												
Si	1.92	1.96	1.88	1.97	1.96	1.93	1.99	1.97	1.95	1.97	1.98	1.98
Al	0.10	0.08	0.14	0.06	0.03	0.10	0.02	0.04	0.04	0.03	0.02	0.02
Ti	0.03	0.01	0.04	0.02	0.03	0.02	0.00	0.03	0.03	0.02	0.02	0.00
Cr	0.00	0.00	0.00	0.00	0.00	0.00	—	—	—	0.00	0.00	0.00
Fe ³⁺	0.06	0.03	0.05	0.00	0.02	0.05	0.04	0.01	0.02	0.06	0.00	0.03
Mg	0.71	0.77	0.90	0.55	0.66	0.72	0.78	0.39	0.47	0.25	0.63	0.99
Fe ²⁺	0.23	0.27	0.31	0.56	0.38	0.30	0.22	0.61	0.56	0.68	0.56	0.89
Mn	0.01	0.01	0.01	0.02	0.01	0.00	0.00	0.02	0.02	0.02	0.02	0.03
Ca	0.90	0.83	0.64	0.79	0.88	0.85	0.90	0.91	0.89	0.90	0.75	0.06
Na	0.05	0.04	0.03	0.04	0.03	0.04	0.04	0.03	0.03	0.07	0.02	0.00
Total	4.00	4.00	4.00	4.00	4.00	4.00	4.00	4.00	4.00	4.00	4.00	4.00
X _{Wo}	0.462	0.420	0.314	0.393	0.449	0.429	0.461	0.459	0.454	0.481	0.374	0.030
X _{En}	0.406	0.430	0.508	0.301	0.348	0.403	0.419	0.212	0.249	0.141	0.333	0.511
X _{Fs}	0.133	0.151	0.177	0.306	0.203	0.168	0.120	0.330	0.296	0.379	0.292	0.460

— = not determined; na = not analyzed

Table 5: Representative analyses of unexsolved magnetite and ilmenite, exsolved magnetite and ilmenite and calculated bulk compositions

Dike Sample	BFD 4 GD 39		Larvikite GM 1684		BFD 1 GM 1680			GD 3, gabbro GM1762			GD 3, gabbro GM1762		
	mag unexs.	ilm unexs.	mag unexs.	ilm unexs.	mag exs.	ilm exs.	bulk calc.	mag exs.	ilm exs.	bulk calc.	mag exs.	ilm exs.	bulk calc.
Texture													
wt. %													
SiO ₂	0.02	0.00	0.05	0.00	0.00	0.00	0.00	0.00	0.00	0.00	0.03	0.02	0.02
TiO ₂	25.07	51.98	7.36	50.15	15.42	53.21	26.44	15.44	51.80	32.95	11.34	51.77	25.12
Al ₂ O ₃	2.52	0.12	1.35	0.02	1.05	0.01	0.74	2.20	0.01	1.15	2.35	0.02	1.56
Cr ₂ O ₃	0.17	0.04	0.18	0.02	0.11	0.06	0.10	0.02	0.00	0.01	0.00	0.00	0.00
ZnO	0.03	0.01	—	—	0.09	0.04	0.07	0.10	0.00	0.05	0.19	0.00	0.12
FeO	68.22	44.47	84.98	47.19	78.81	45.07	68.97	77.56	46.51	62.61	80.77	46.49	69.09
MnO	0.90	0.68	0.45	1.96	0.74	2.28	1.19	0.43	1.39	0.89	0.36	1.42	0.72
MgO	1.05	2.30	0.00	0.00	0.00	0.00	0.00	0.00	0.00	0.00	0.00	0.00	0.00
CaO	0.05	0.03	—	—	0.00	0.00	0.00	0.03	0.03	0.03	0.18	0.04	0.14
Total	98.02	99.63	94.37	99.33	96.22	100.67	97.51	95.77	99.74	97.65	95.22	99.76	96.63
Formulae based on 3 (2) cations and 4 (3) oxygens for mag (ilm)													
Si	0.00	0.00	0.00	0.00	0.00	0.00	0.00	0.00	0.00	0.00	0.00	0.00	0.00
Al	0.11	0.00	0.06	0.00	0.05	0.00	0.03	0.10	0.00	0.05	0.10	0.00	0.07
Ti	0.69	0.97	0.21	0.95	0.44	1.00	0.75	0.44	0.99	0.94	0.32	0.98	0.71
Cr	0.01	0.00	0.01	0.00	0.00	0.00	0.00	0.00	0.00	0.00	0.00	0.00	0.00
Fe ³⁺	0.49	0.05	1.51	0.09	1.08	0.00	0.46	1.03	0.03	0.07	1.25	0.03	0.50
Mg	0.06	0.09	0.00	0.00	0.00	0.00	0.00	0.00	0.00	0.00	0.00	0.00	0.00
Fe ²⁺	1.61	0.87	1.20	0.91	1.41	0.95	1.71	1.42	0.95	1.91	1.30	0.95	1.68
Mn	0.03	0.01	0.01	0.04	0.02	0.05	0.04	0.01	0.03	0.03	0.01	0.03	0.02
Zn	0.00	0.00	—	—	0.00	0.00	0.00	0.00	0.00	0.00	0.01	0.00	0.00
Ca	0.00	0.00	—	—	0.00	0.00	0.00	0.00	0.00	0.00	0.01	0.00	0.01
Sum	3.00	2.00	3.00	2.00	3.00	2.00	3.00	3.00	2.00	3.00	3.00	2.00	3.00
mol%													
Usp/Ilm	0.70	0.97	0.21	0.96	0.44	1.00	0.75	0.44	0.99	0.94	0.32	0.99	0.71
Mag/Hem	0.25	0.03	0.76	0.04	0.54	0.00	0.23	0.51	0.01	0.04	0.63	0.01	0.25
Sp	0.05		0.03		0.02		0.02	0.05		0.03	0.05		0.03
For QUILF													
NTi/NHem	0.697	0.026	0.211	0.043	0.438	0.000	0.751	0.439	0.014	0.938	0.323	0.015	0.716
NMg/NGk	0.056	0.085	0.000	0.000	0.000	0.000	0.000	0.000	0.000	0.000	0.000	0.000	0.000
NMn/NPy	0.028	0.014	0.015	0.042	0.024	0.049	0.038	0.014	0.030	0.029	0.012	0.030	0.023

unexs. = unexsolved, exs. = exsolved, calc. = calculated; NTi, NMn, NMg and NHem, NPy, NGk are QUILF-specific parameters for magnetite and ilmenite, respectively (see Andersen *et al.*, 1993); — = not determined.

Table 6: Average Laser-ICP-MS analyses of REEs in clinopyroxene from Isortoq dike rocks

Dike	Olivine-gabbro	BFD 1	BFD 1	BFD 1	BFD 1	BFD 1	BFD 1	BFD 1	BFD 1	BFD 3	GD 1	GD 3	GD 3	Larvikite
Sample	GM 1803	GM 1680	GM 1729	GM 1735	GM 1681 matrix	GM 1681 high-Ca inclusions	GM 1681 low-Ca inclusions	GM 1682	GM 1805	GM 1712	GM 1760	GM 1772	GM 1684	
No. of cpx analysed	n = 7	n = 3	n = 3	n = 6	n = 2	n = 4	n = 3	n = 4	n = 4	n = 3	n = 11	n = 11	n = 4	
<i>REE concentrations in ppm:</i>														
La	7.58	5.60	6.43	8.02	16.53	10.28	2.59	4.18	10.90	10.25	11.55	18.46	13.38	
Ce	32.65	27.72	27.30	32.46	64.06	37.77	12.30	16.84	39.26	38.52	42.36	59.64	52.13	
Pr	6.28	4.70	5.30	6.07	12.93	6.99	2.93	3.44	7.58	7.78	8.02	11.14	9.50	
Nd	34.60	27.53	29.36	38.96	74.00	40.49	18.40	20.40	45.97	43.07	45.54	59.32	56.88	
Sm	10.93	8.29	8.20	11.67	18.27	11.63	6.57	7.04	13.39	13.44	13.44	16.15	14.89	
Eu	2.60	2.73	2.75	3.54	4.70	3.39	2.16	2.46	3.90	2.72	3.43	1.85	3.41	
Gd	11.61	8.27	7.76	12.06	12.40	11.03	8.11	7.73	12.50	13.35	13.35	14.01	12.70	
Tb	1.83	1.30	1.25	1.86	1.76	1.96	1.29	1.08	2.17	2.50	2.12	2.31	1.92	
Dy	10.81	7.56	7.22	10.87	11.09	11.07	7.95	5.83	11.94	13.72	12.02	13.17	10.63	
Ho	2.05	1.42	1.47	2.12	2.22	2.22	1.63	1.19	2.17	2.78	2.46	2.71	2.01	
Er	5.67	3.39	3.54	5.17	6.26	5.85	4.19	2.75	5.55	7.09	6.18	7.19	5.48	
Tm	0.78	0.47	0.52	0.74	1.17	0.88	0.66	0.55	0.80	0.94	0.92	1.10	0.77	
Yb	5.75	3.43	3.25	5.03	9.31	5.84	4.04	2.78	5.72	7.03	6.18	8.99	5.83	
Lu	0.86	0.45	0.49	0.72	1.82	0.92	0.74	0.49	0.76	1.03	0.96	1.80	0.84	
La _N /Yb _N	0.89	1.10	1.33	1.07	1.20	1.19	0.43	1.01	1.28	0.98	1.26	1.38	1.55	
Eu/Eu*	0.70	1.00	1.07	0.92	0.98	0.92	0.91	1.02	0.93	0.65	0.81	0.41	0.89	
Eu/Eu* _{max}	0.74	1.04	1.13	0.98	1.06	0.93	1.13	1.08	1.16	0.80	0.96	0.78	1.20	

Eu/Eu* = Eu_N/(Sm_N x Gd_N)^{0.5}; Eu/Eu*_{max} is the maximum value of Eu/Eu* in an individual clinopyroxene of the respective sample.

Table 7: XRF whole-rock analyses of Isortoq dike rocks

Dike	Olivine-gabbro	BFD 1	BFD 1 anorthosite xenolith	BFD 2	BFD 3	BFD 4	GD 1 syeno- gabbro	GD 3 gabbro	GD 3 syenite	GD 3 syenite	Larvikite	Hbl.- syenite
Sample	GM 1803	GM 1735	GM 1682	GM 1750	GM 1805	GD 39	GM 1712	GM 1760	GM 1772	GM 1778	GM 1684	GD 38
Major elements (wt.%)												
SiO ₂	44.57	46.46	51.86	53.05	49.88	46.73	47.83	41.69	55.17	55.93	56.34	53.91
TiO ₂	2.95	2.25	1.76	1.83	1.93	2.67	2.12	4.19	1.55	1.55	1.28	0.97
Al ₂ O ₃	16.79	16.62	19.32	17.56	15.83	16.03	18.54	14.09	15.41	15.37	16.87	16.62
Fe ₂ O ₃	15.90	14.11	8.82	9.81	12.92	14.92	12.30	17.03	10.50	10.91	8.50	8.57
MnO	0.19	0.17	0.12	0.15	0.17	0.19	0.16	0.22	0.20	0.20	0.14	0.13
MgO	5.08	5.54	2.12	2.17	4.34	5.72	2.59	4.71	1.10	0.99	2.35	4.06
CaO	7.68	7.40	7.62	6.12	6.72	7.77	7.26	8.22	4.16	3.67	4.82	6.11
Na ₂ O	3.69	3.68	4.58	4.40	4.41	3.74	4.46	3.69	5.18	5.86	4.75	4.01
K ₂ O	1.12	1.25	1.63	2.78	1.48	1.18	1.89	1.79	4.03	3.34	3.26	2.48
P ₂ O ₅	0.48	0.47	0.45	0.68	0.40	0.56	0.47	2.48	0.44	0.40	0.33	0.43
LOI	0.67	0.64	0.88	0.56	0.66	-0.43	2.09	0.84	0.64	0.86	0.67	1.91
Total	99.12	98.59	99.16	99.11	98.74	99.08	99.71	98.95	98.38	99.08	99.31	99.20
Mg#*	43.2	48.3	36.4	34.5	44.4	47.7	33.4	39.7	19.9	17.7	39.7	53.0
Trace elements (ppm)												
Sc	17	21	15	18	20	20	14	17	13	10	16	20
V	173	193	86	83	174	162	96	107	6	3	78	155
Cr	36	54	2	4	44	70	n.d.	n.d.	n.d.	n.d.	29	45
Co	62	78	18	22	60	84	40	47	6	7	55	60
Ni	53	87	11	14	60	71	29	n.d.	3	n.d.	34	33
Cu	37	61	10	12	67	47	26	27	n.d.	n.d.	46	46
Zn	92	105	76	85	109	104	86	96	130	124	101	102
Ga	18	20	20	19	21	19	21	15	19	22	23	19
Rb	19	17	15	35	25	14	33	18	32	36	33	60
Sr	411	629	753	563	510	454	558	421	417	265	535	817
Y	30	24	25	32	31	34	42	39	45	51	27	27
Zr	172	140	137	215	221	171	245	150	271	367	245	163
Nb	12	14	11	14	14	12	18	12	22	25	16	14
Ba	463	750	1022	1740	936	649	899	718	2981	2131	2513	972
Pb	4	5	7	9	7	4	15	7	8	11	15	8
La	—	—	24	41	—	16	—	—	38	42	—	35
Ce	—	—	62	95	—	65	—	—	96	101	—	93
Pr	—	—	4	8	—	6	—	—	9	7	—	7
Nd	—	—	31	52	—	32	—	—	51	49	—	44
Sm	—	—	4	9	—	10	—	—	5	8	—	8
Characteristic normative minerals**												
	<i>ne+ol</i>	<i>ne+ol</i>	<i>hy+ol</i>	<i>hy+ol</i>	<i>hy+ol</i>	<i>ne+ol</i>	<i>ne+ol</i>	<i>ne+ol</i>	<i>ne+ol</i>	<i>hy+ol</i>	<i>q+hy</i>	<i>q+hy</i>

* Mg# = 100[Mg/(Mg + Fe²⁺)] with Fe₂O₃/FeO = 0.2; ** Calculation of normative mineral composition according to the CIPW norm; n.d. = not detected; — = not determined;

Table 8: Sr, Nd and O isotopic composition of Isortoq dike rocks and adjacent Ketilidian basement rocks

Rock type	Sample	Material	Sr (ppm)	Rb (ppm)	$^{87}\text{Rb}/^{86}\text{Sr}$	$^{87}\text{Sr}/^{86}\text{Sr}$	$^{87}\text{Sr}/^{86}\text{Sr}$ (i)	Sm (ppm)	Nd (ppm)	$^{147}\text{Sm}/^{144}\text{Nd}$	$^{143}\text{Nd}/^{144}\text{Nd}$	$\epsilon_{\text{Nd}}(\text{i})$	$\delta^{18}\text{O}$ (V-SMOW)
<i>Isortoq dikes:</i>													
BFD 1, anorthosite xenolith	GM 1682	cpx	41.60	0.800	0.0556	0.704454 ± 10	0.70351	13.56	47.42	0.1728	0.512165 ± 09	-5.6	5.73
Larvikite	GM 1684	cpx	52.31	1.087	0.0601	0.705016 ± 10	0.70399	14.35	53.20	0.1631	0.511830 ± 10	-10.7	6.20
GD 1, gabbro	GM 1712	cpx	56.42	0.361	0.0185	0.703728 ± 10	0.70341	19.94	66.67	0.1808	0.512484 ± 10	-0.6	5.30
BFD 1	GM 1735	cpx	61.40	3.085	0.1453	0.705773 ± 10	0.70330	16.16	58.51	0.1670	0.512223 ± 10	-3.6	5.72 ± 0.07
BFD 1	GM 1735	whole-rock						5.64	26.06	0.1308	0.511922 ± 10	-3.9	
BFD 1	GM 1735	plagioclase						2.14	11.74	0.1100	0.511780 ± 10	-3.5	6.61 ± 0.08
BFD 2	GM 1750	cpx	51.41	7.337	0.4130	0.709994 ± 10	0.70296	19.03	74.61	0.1542	0.511902 ± 09	-7.9	5.93
GD 3, gabbro	GM 1760	cpx	44.96	0.739	0.0475	0.704151 ± 10	0.70334	14.80	51.87	0.1725	0.512357 ± 10	-1.8	5.62
GD 3, syenite	GM 1772	cpx	44.92	0.973	0.0627	0.704572 ± 10	0.70350	22.06	91.46	0.1458	0.512146 ± 14	-1.8	5.41
GD 3, syenite	GM 1778	cpx	32.87	1.128	0.0993	0.704920 ± 09	0.70323	20.03	82.24	0.1472	0.512163 ± 10	-1.7	
Olivine-gabbro	GM 1803	cpx	49.32	1.177	0.0690	0.704069 ± 10	0.70289	21.09	73.19	0.1742	0.512475 ± 10	0.3	5.54
BFD 3	GM 1805	cpx	58.67	1.399	0.0690	0.704794 ± 09	0.70362	13.45	47.63	0.1706	0.512079 ± 10	-6.9	5.59
Brown Dike (BD ₀)	GD 37	cpx	44.61	0.218	0.0141	0.703721 ± 09	0.70346	5.79	16.65	0.2103	0.512619 ± 10	-2.6	
Hornblende-syenite	GD 38	amph	101.10	5.863	0.1677	0.707176 ± 10	0.70432	18.99	83.46	0.1376	0.511959 ± 10	-4.2	5.21
BFD 4	GD 39	cpx	67.57	0.391	0.0167	0.703431 ± 09	0.70315	12.62	41.66	0.1831	0.512479 ± 10	-1.0	
<i>Ketilidian basement:</i>													
Granitoid	BT 03	whole-rock	70.58	186.9	7.8080	0.901275 ± 09	0.76821	8.25	54.67	0.0913	0.511341 ± 10	-9.3	8.2
Granitoid	BT 05	whole-rock	946.4	31.96	0.0977	0.704834 ± 16	0.70317	1.94	10.16	0.1154	0.511785 ± 10	-4.3	7.2
Granitoid	BT 06	whole-rock	422.1	109.2	0.7494	0.721722 ± 10	0.70895	6.45	39.03	0.0999	0.511516 ± 10	-7.2	7.9

$^{87}\text{Sr}/^{86}\text{Sr}$ and $^{143}\text{Nd}/^{144}\text{Nd}$ initial ratios were calculated for $T = 1.19$ Ga except for the BD₀ dike (GD 37) for which an age of 1.28 Ga (Upton *et al.*, 2003) was assumed. Standard deviations for $\delta^{18}\text{O}$ are given for samples which were analysed twice.

Table 9: Os isotope data of Isortoq dike rocks, Eriksfjord Formation basalts and Ilímaussaq syenites

Rock type	Sample	Age (Ma)*	Re (ng/g)	Os (ng/g)	Re/Os	$^{187}\text{Re}/^{188}\text{Os}$	$^{187}\text{Os}/^{188}\text{Os}$	$(^{187}\text{Os}/^{188}\text{Os})_i$
Isortoq dikes								
BFD 1	GM 1735	1190	0.353	0.0153	23.13	176.44	4.6635 ± 89	1.131
GD 3, gabbro	GM 1760	1190	0.479	0.0070	68.74	4775.09	103.58 ± 16	7.967
Olivine-gabbro	GM 1803	1190	0.153	0.0021	71.71	2237.83	42.381 ± 58	-2.428
BFD 4	GD 39	1190	0.388	0.0144	26.86	213.58	5.181 ± 11	0.905
Eriksfjord Formation basalts								
Basalt, Mussartût group	EF 024	1200	0.362	0.1490	2.43	11.60	0.10690 ± 1	-0.127
Basalt, Ulukasik group	EF 072	1200	0.343	0.0132	25.94	192.34	4.3238 ± 85	0.440
Basalt, Ilímaussaq group	EF 174	1200	0.207	0.0094	22.13	197.13	6.709 ± 21	2.729
Basalt, Ilímaussaq group	EF 168	1200	0.177	0.0123	14.45	93.49	2.8124 ± 61	0.925
Ilímaussaq intrusion								
Augite-syenite (center)	GM 1857	1160	0.013	0.0041	3.23	17.20	0.9751 ± 24	0.639
Augite-syenite (border)	GM 1858	1160	0.0026	0.00023	11.28	68.22	2.1395 ± 32	0.808

* Age determinations from Paslick *et al.* (1993) for the Eriksfjord Formation basalts and Waight *et al.* (2002) for the Ilímaussaq intrusion.

Table 10: Parameters used in energy-constrained assimilation-fractional crystallization (EC-AFC) modeling

Thermal parameters:

Liquidus temperature of magma	1190 °C
Initial temperature of magma	1140 °C
Solidus temperature	850 °C
Temperature of equilibration	900 °C

Compositional parameters:

	Sr	Nd
Magma initial concentration (ppm)	411	32
Magma isotope ratio	0.70289	0.51111
Magma trace element distribution coefficient	1.5	0.25
Upper crustal assimilant initial concentration (ppm)	480	35
Upper crustal assimilant isotope ratio	0.70806	0.51069
Lower crustal assimilant initial concentration (ppm)	747	63
Lower crustal assimilant isotope ratio	0.70670	0.5099
Assimilant trace element distribution coefficient	1.5	0.25

For the upper and lower crustal assimilants, the thermal parameters for the “standard“ upper-crustal and the “standard“ lower-crustal case, respectively, were taken from Bohrsen & Spera (2001).

Fig. 1

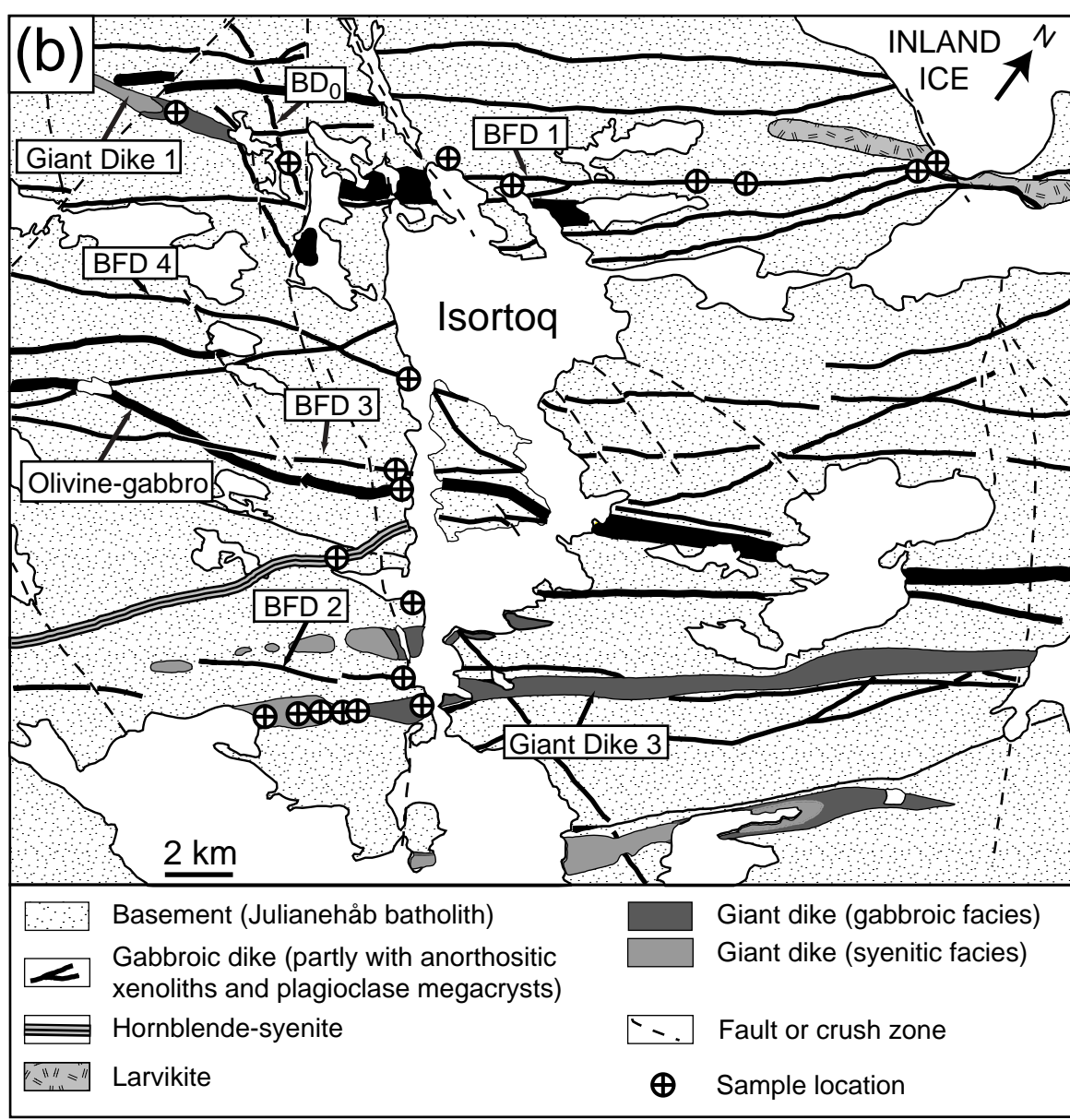
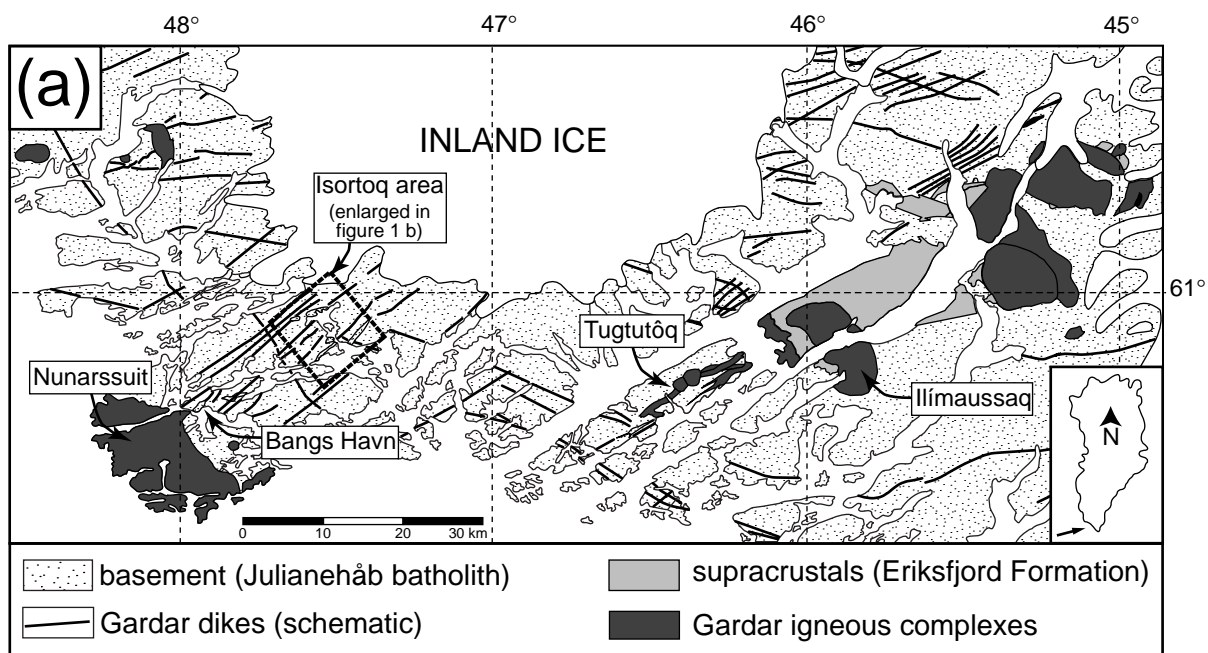


Fig. 2

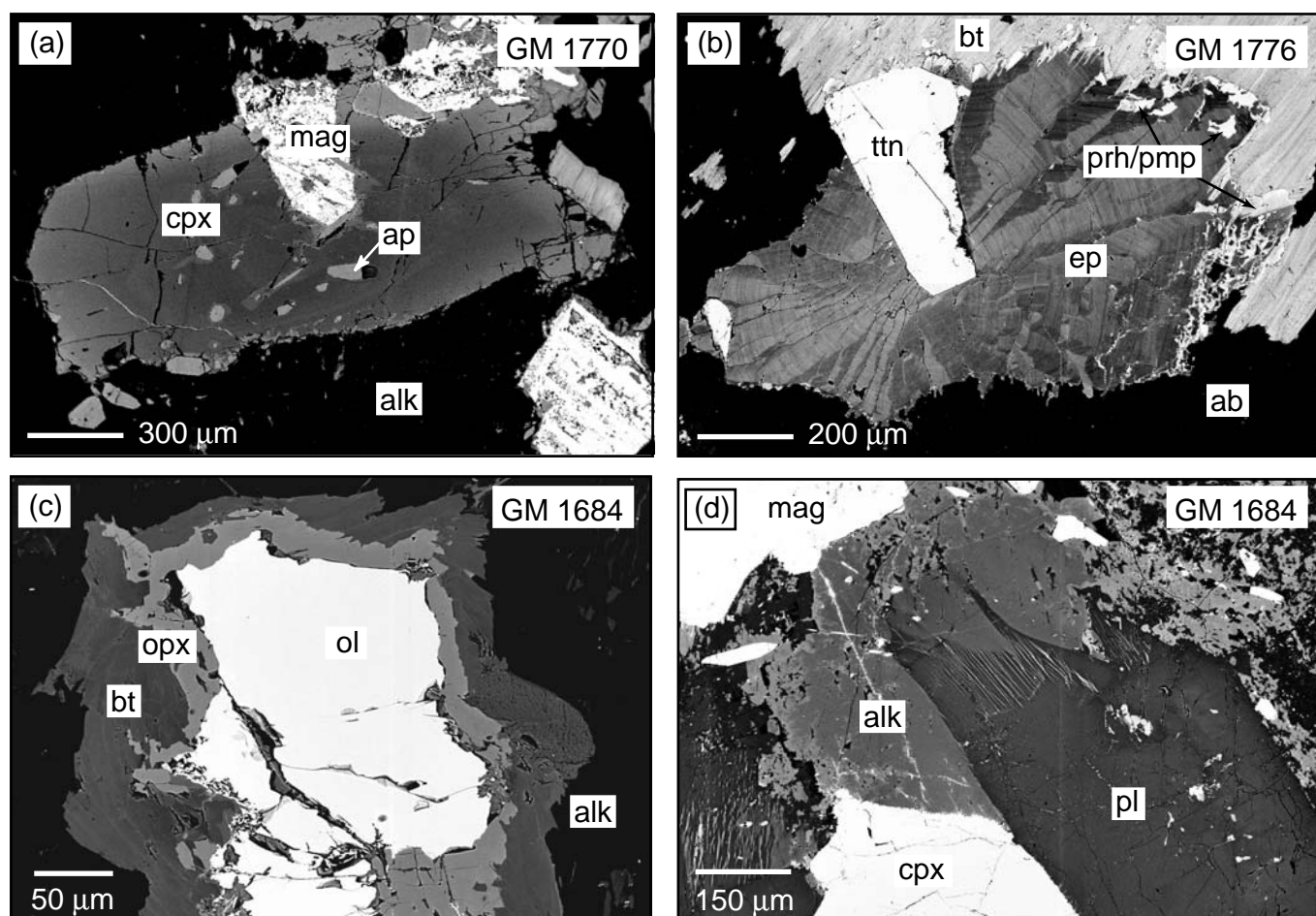


Fig. 3

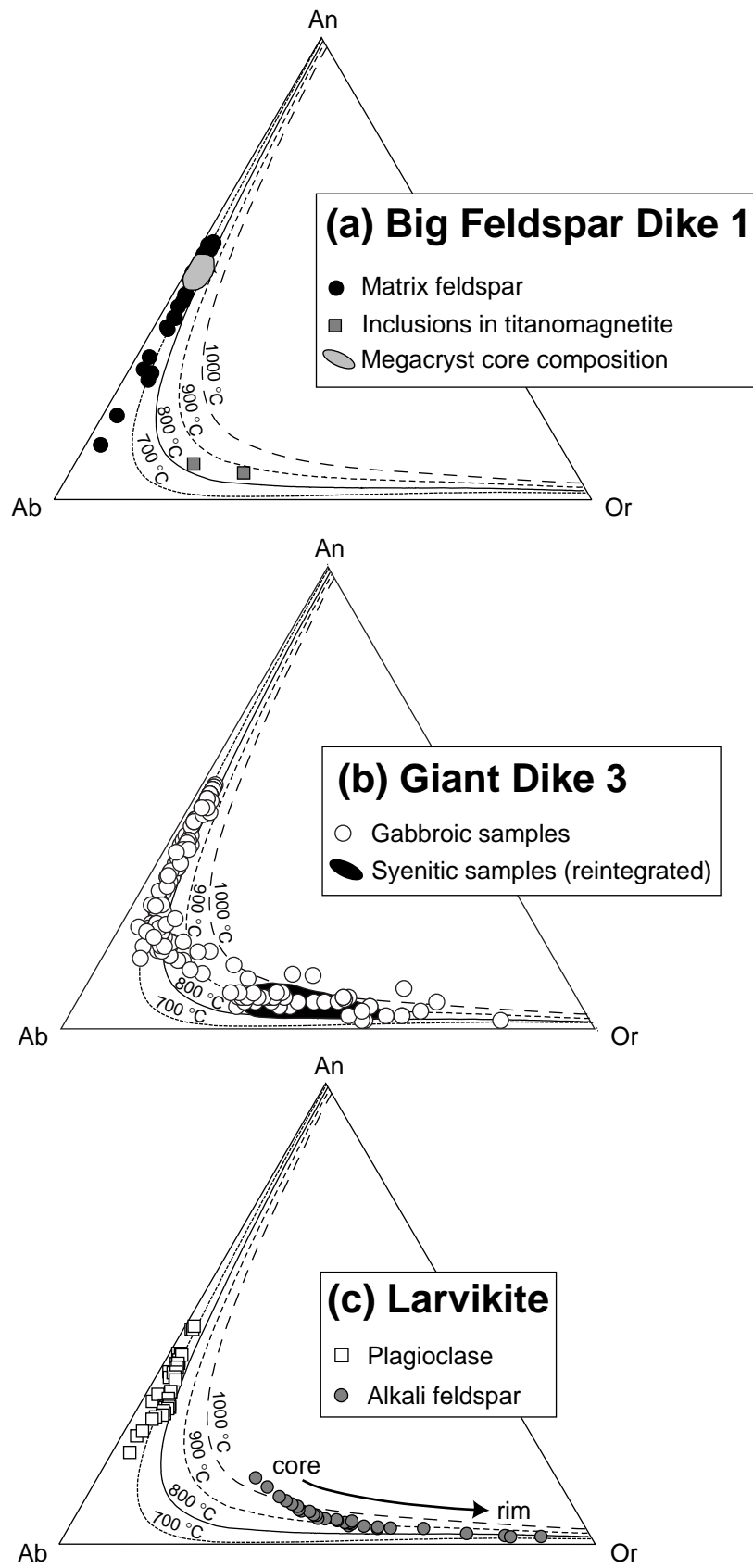
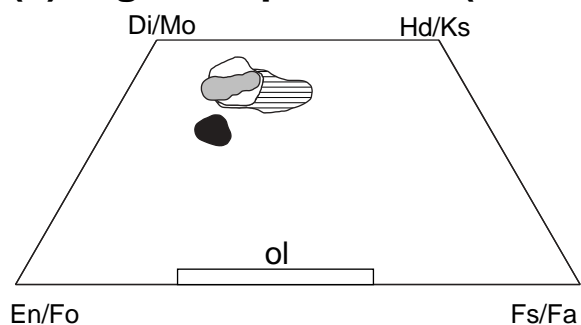


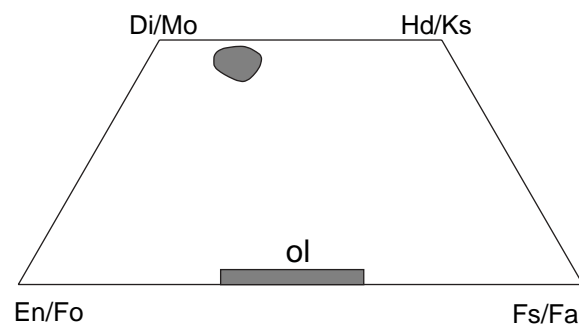
Fig. 4

(a) Big Feldspar Dikes (BFDs)

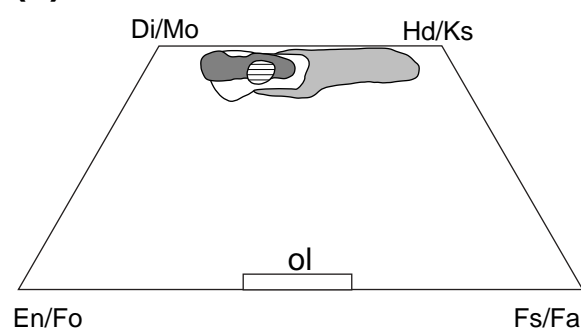


- BFD 1, 3 & 4
- ⊖ BFD 2
- Anorthosite xenolith (GM1682) in BFD 1
- Ca-poor inclusions in feldspar megacryst in BFD 1 (GM1681)

(b) Olivine-gabbro



(c) Giant Dikes 1 & 3



- ⊖ Giant Dike 1 (GM 1712)
- Giant Dike 3
- Gabbroic samples
- Rims around olivine (GM 1761 & 1762)
- Syenitic samples

(d) Larvikite

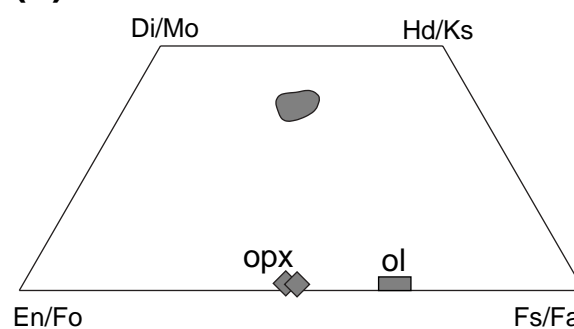


Fig. 5

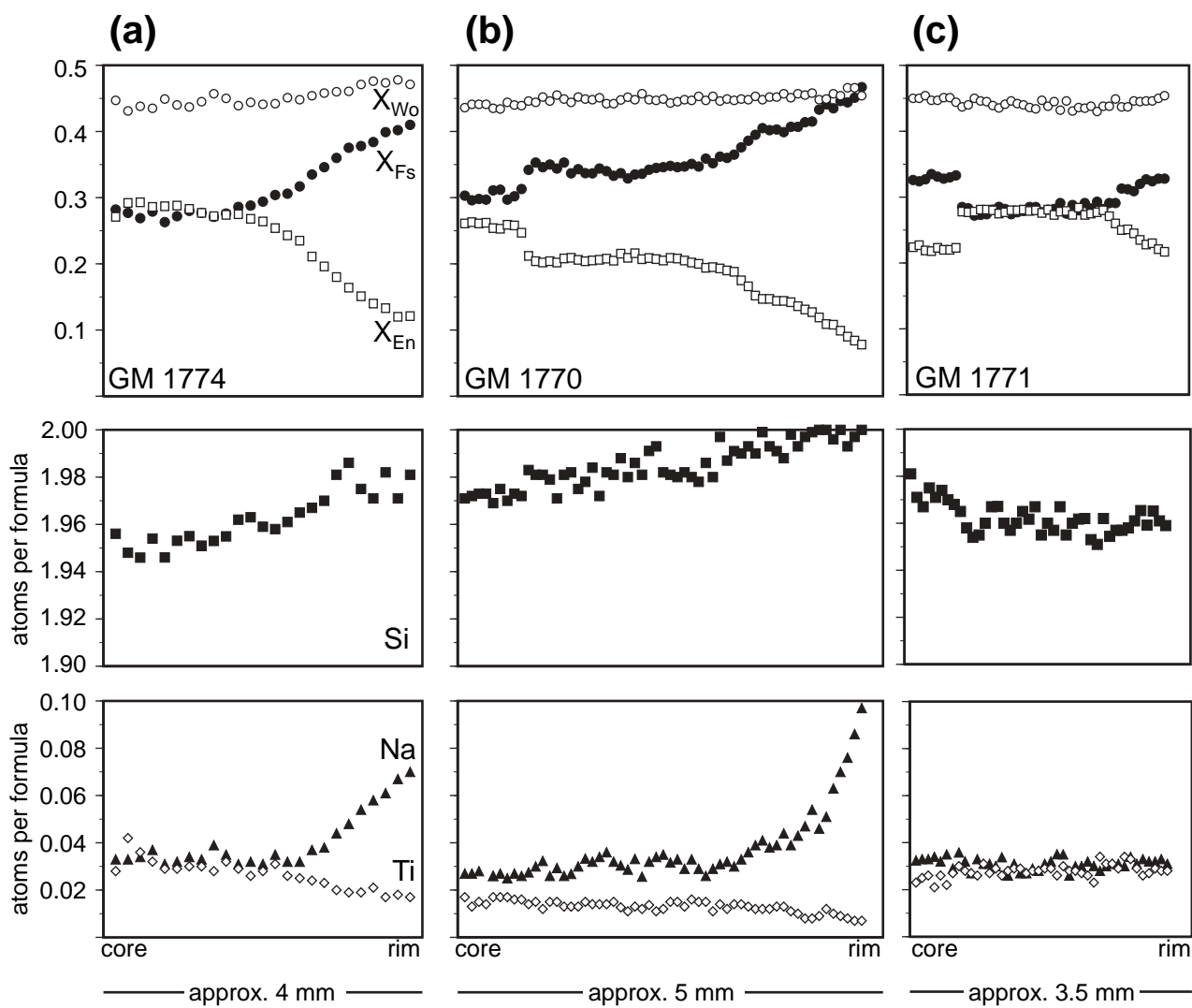


Fig. 6

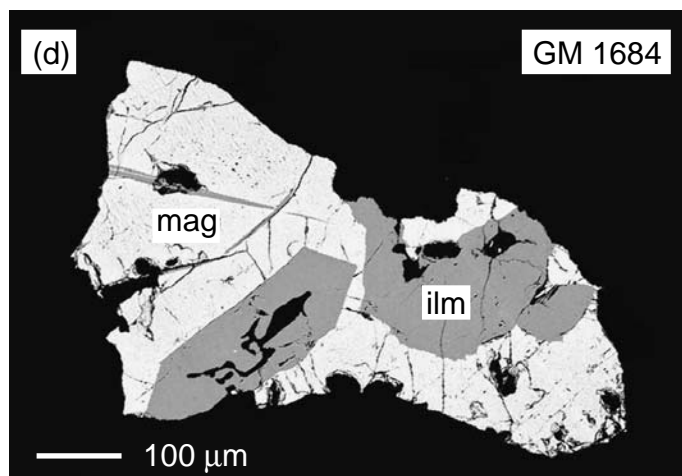
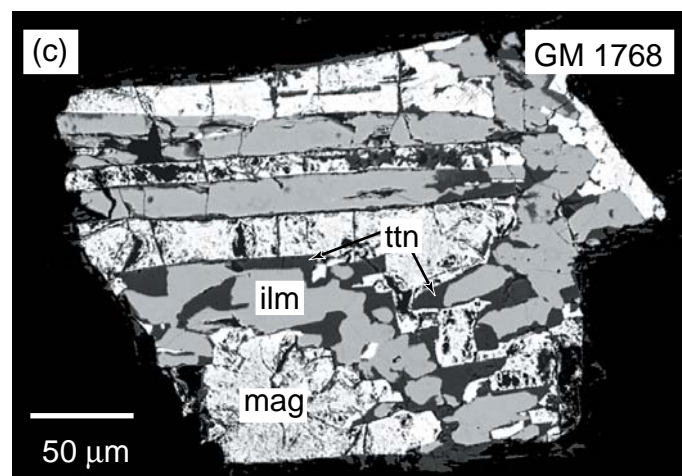
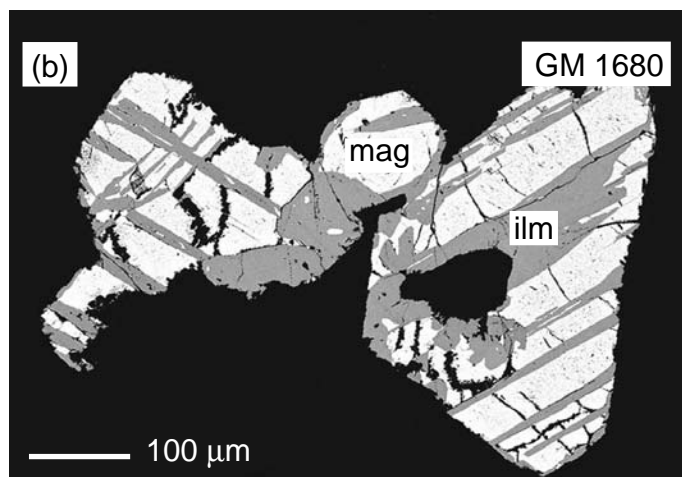
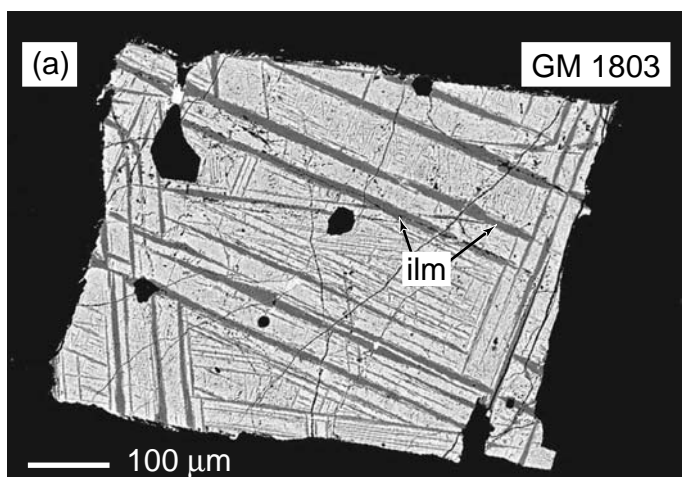


Fig. 7

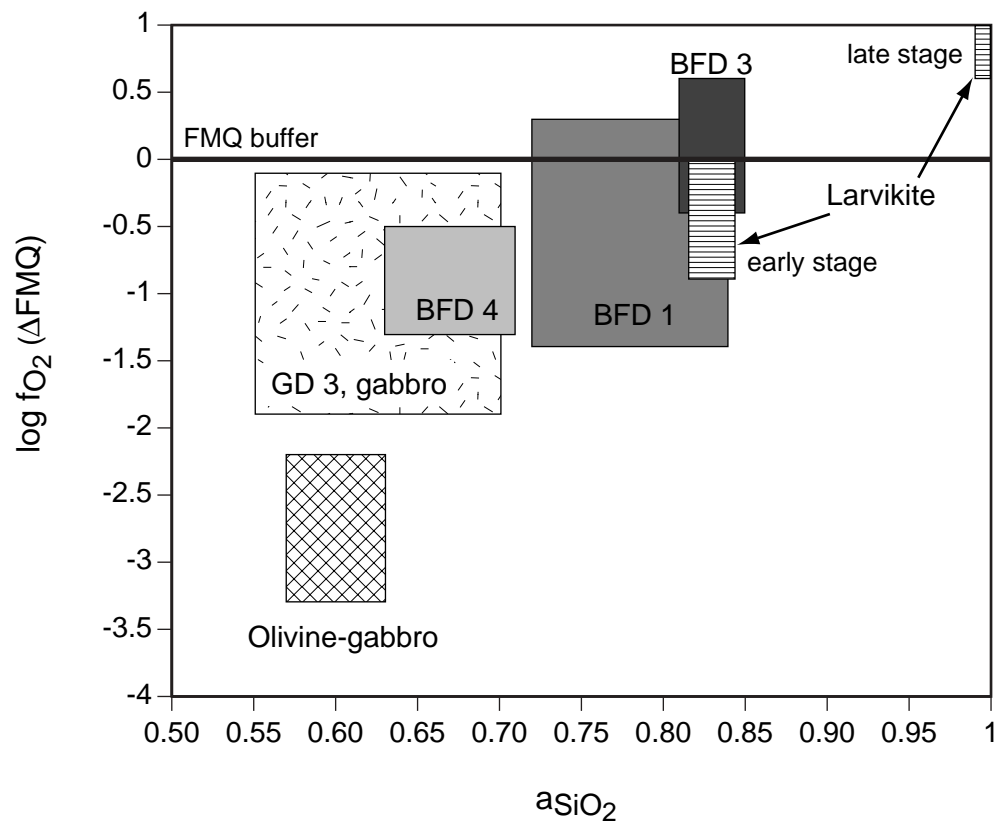


Fig. 8

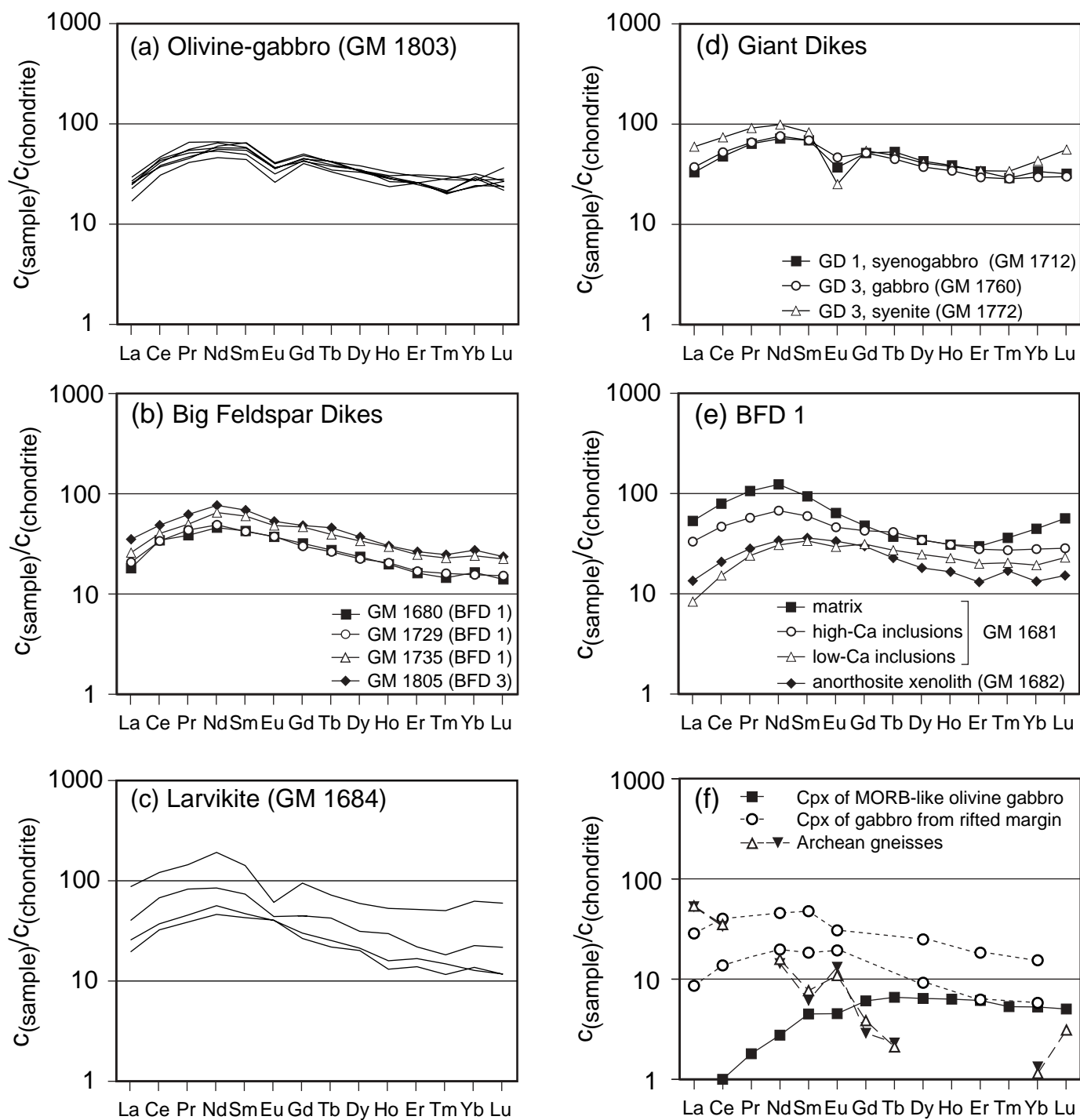


Fig. 9

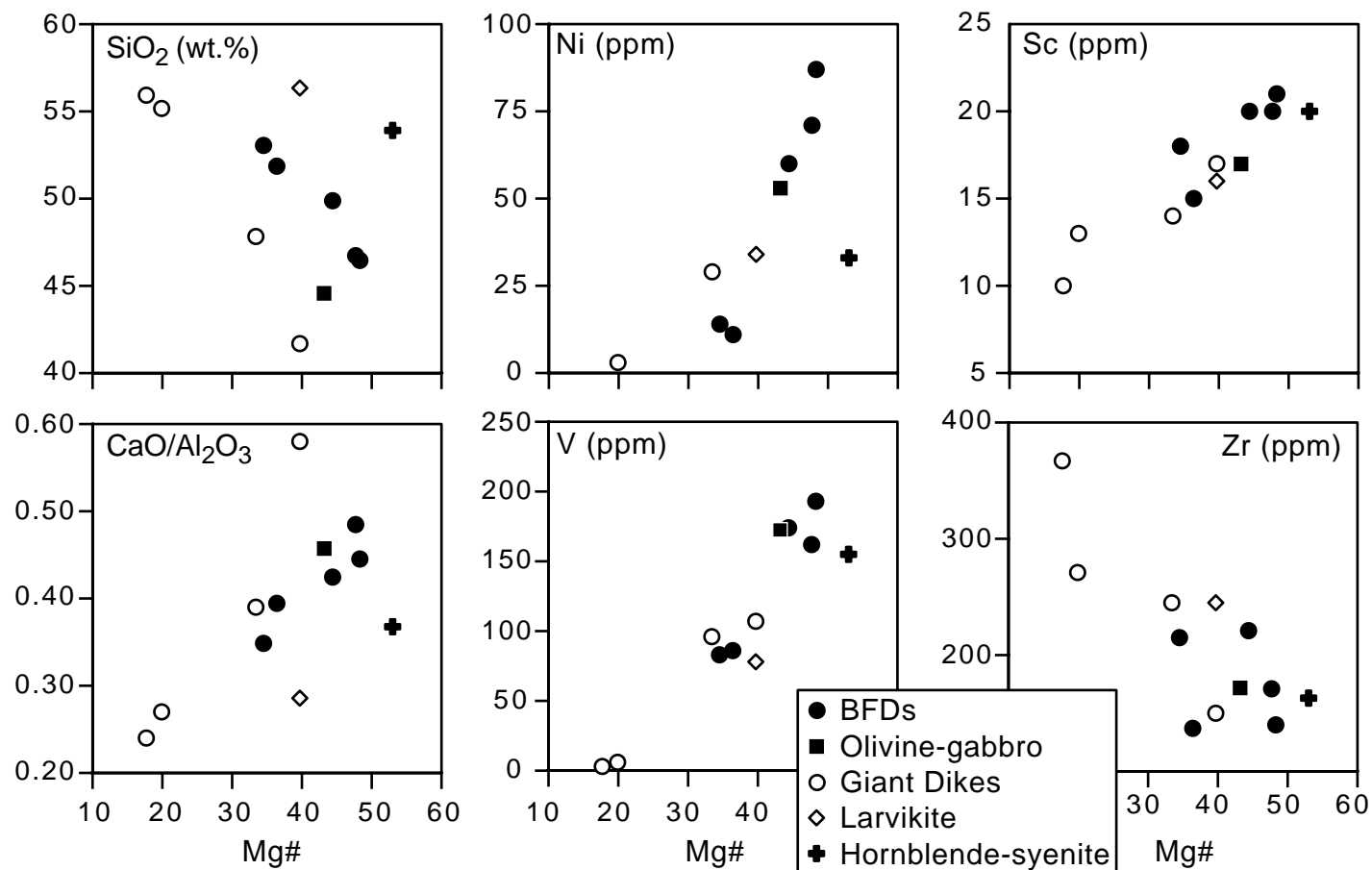


Fig. 10

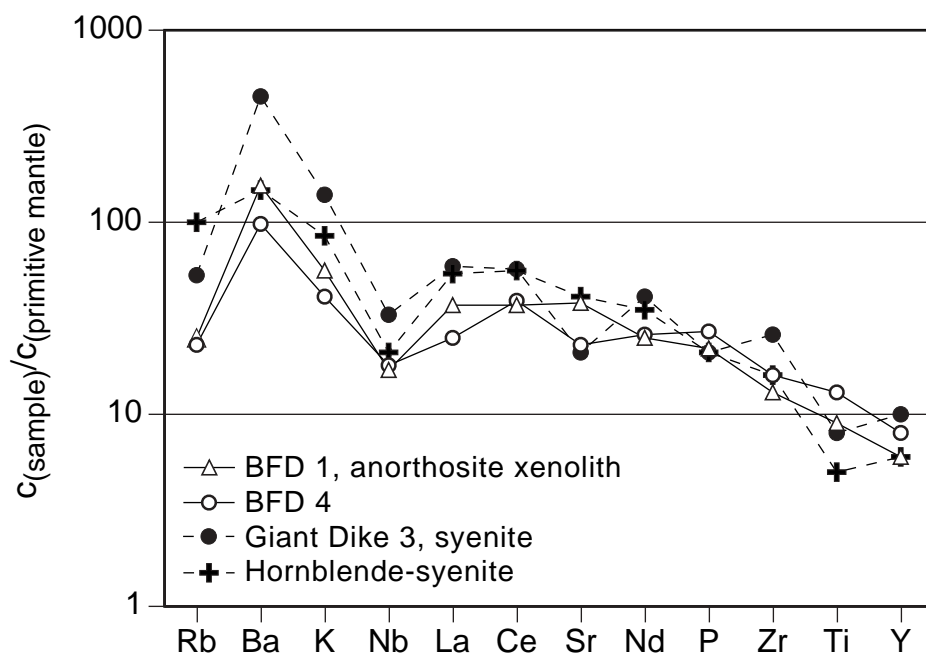


Fig. 11

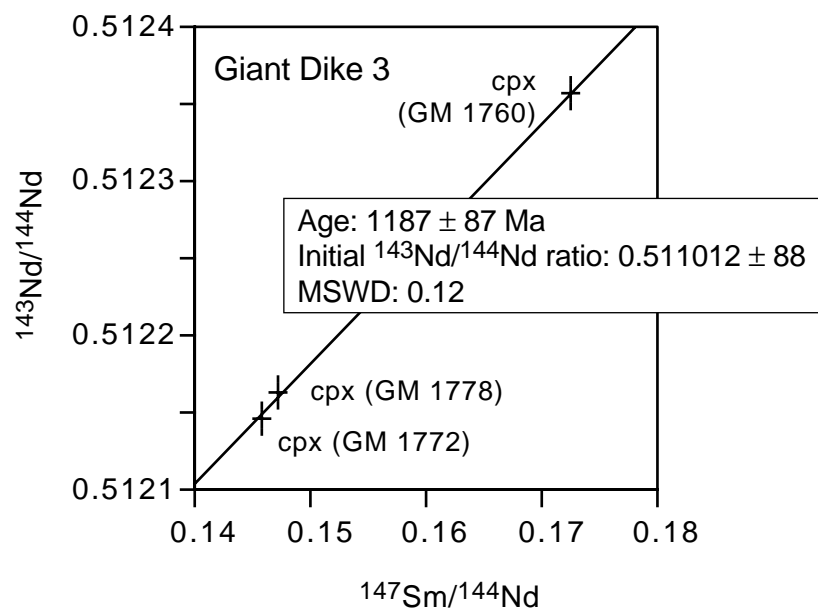
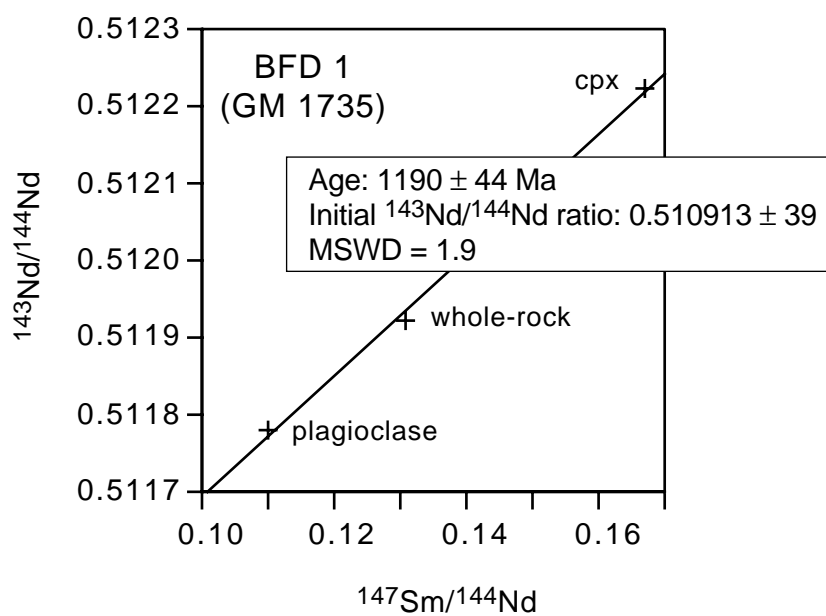
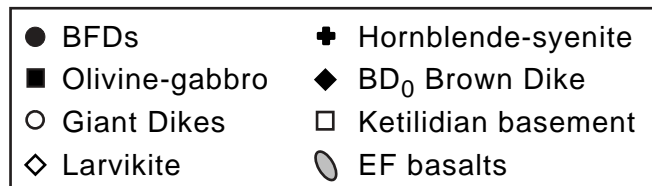
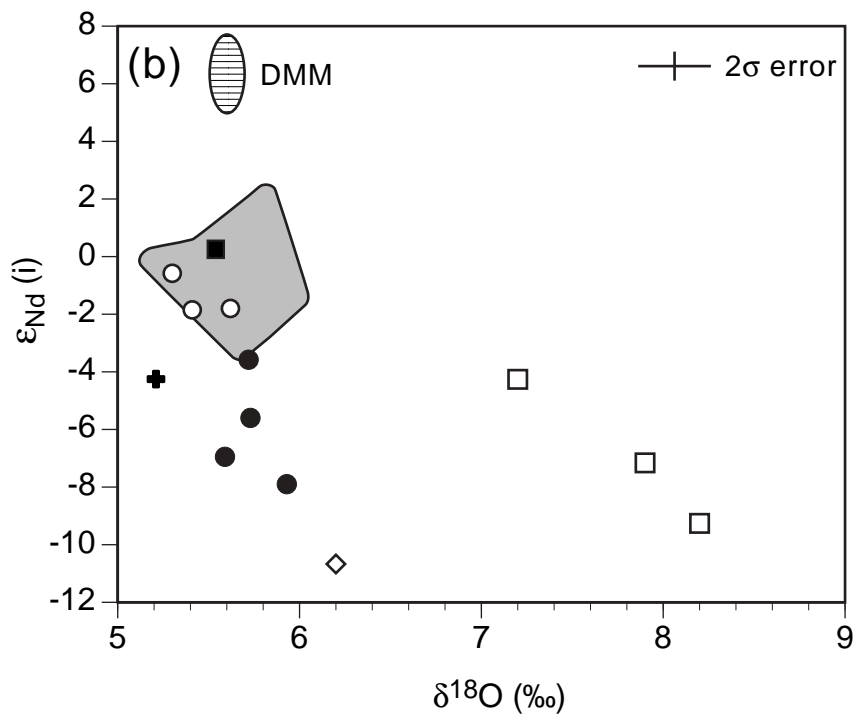
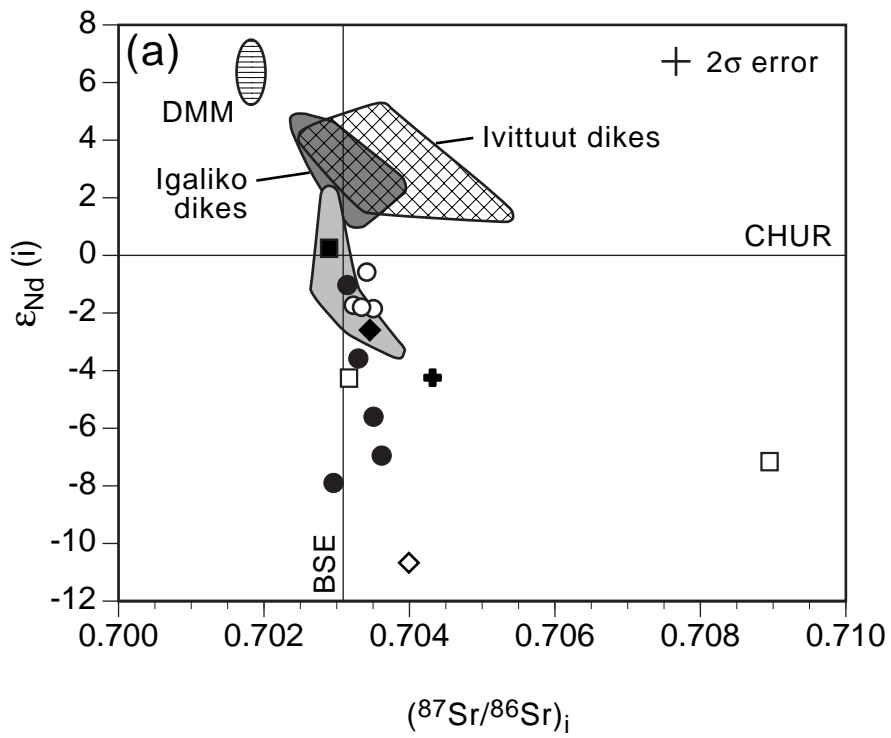


Fig. 12



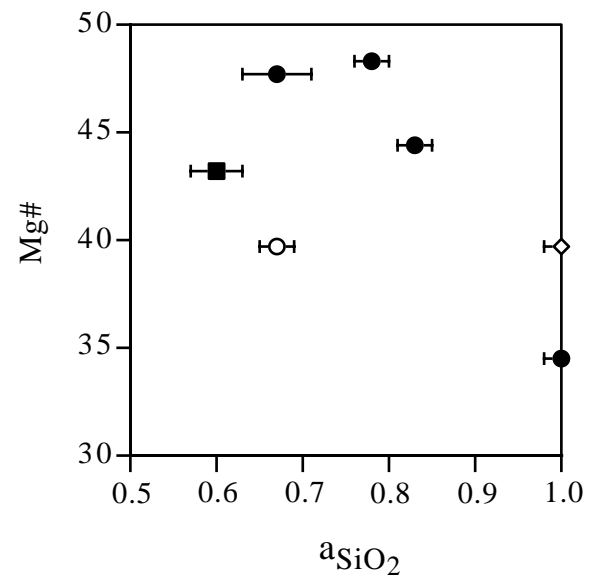
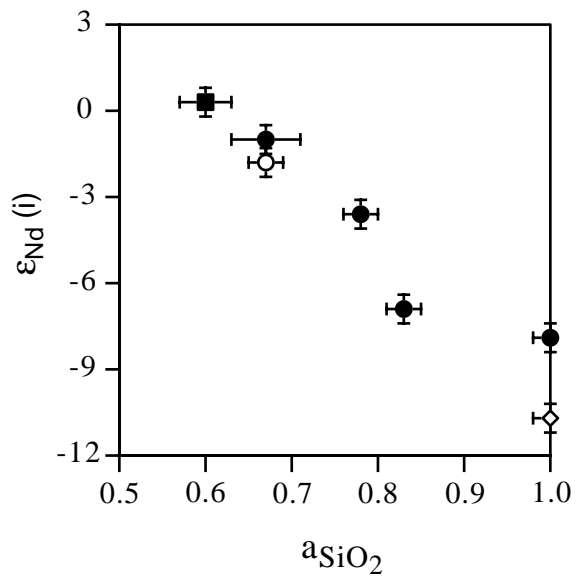
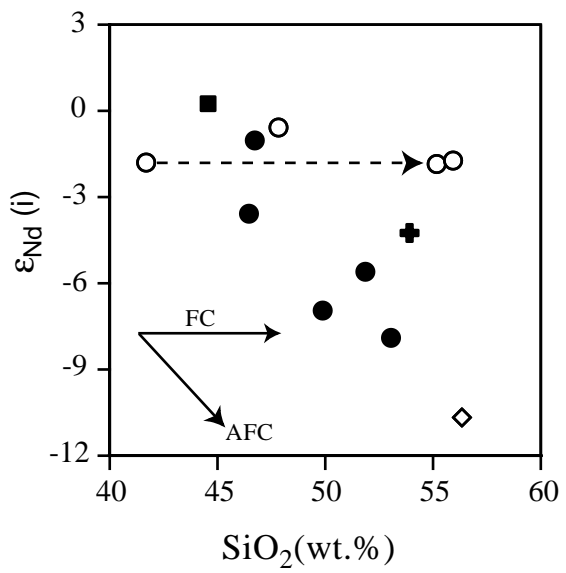


Fig. 13

Fig. 14

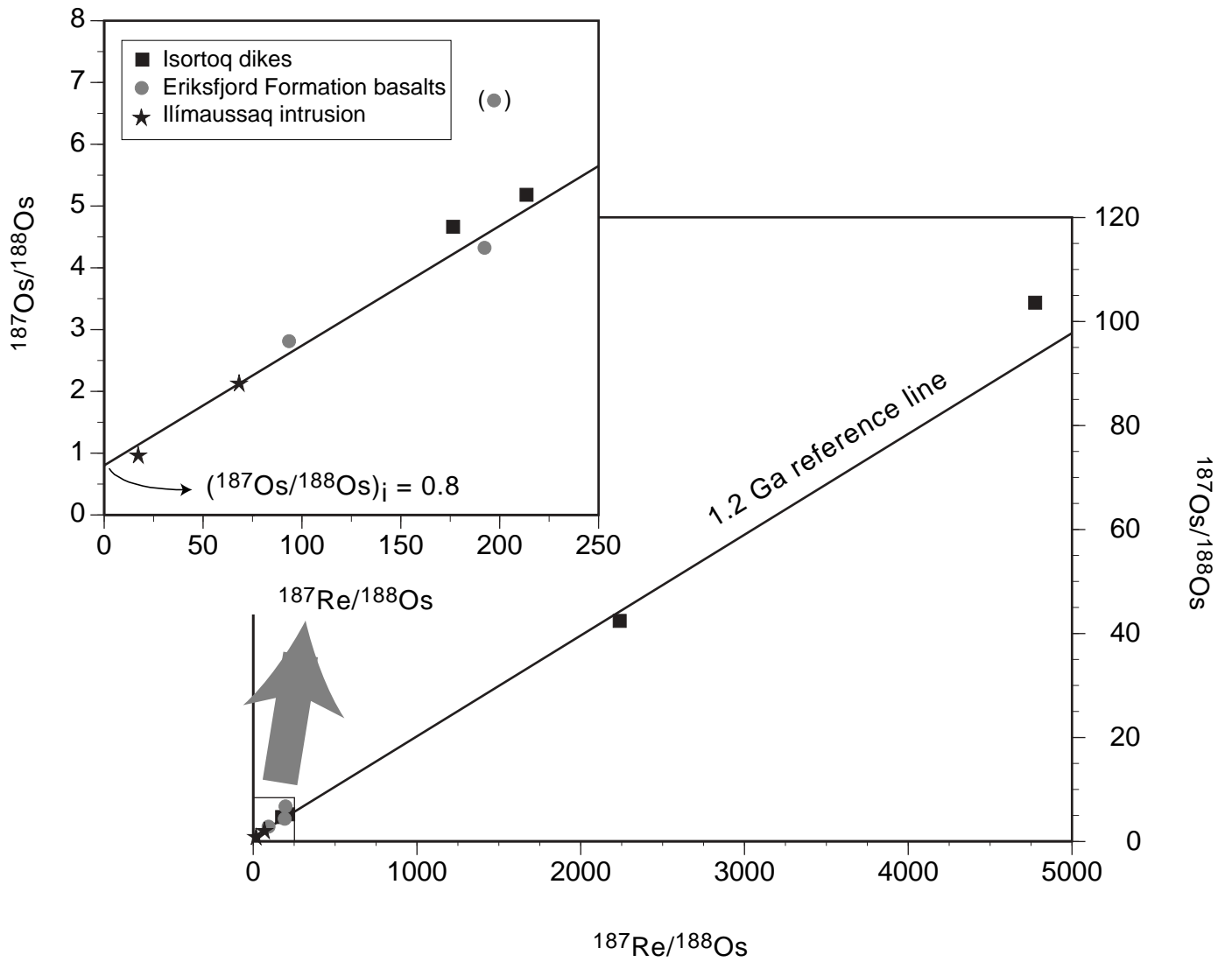


Fig. 15

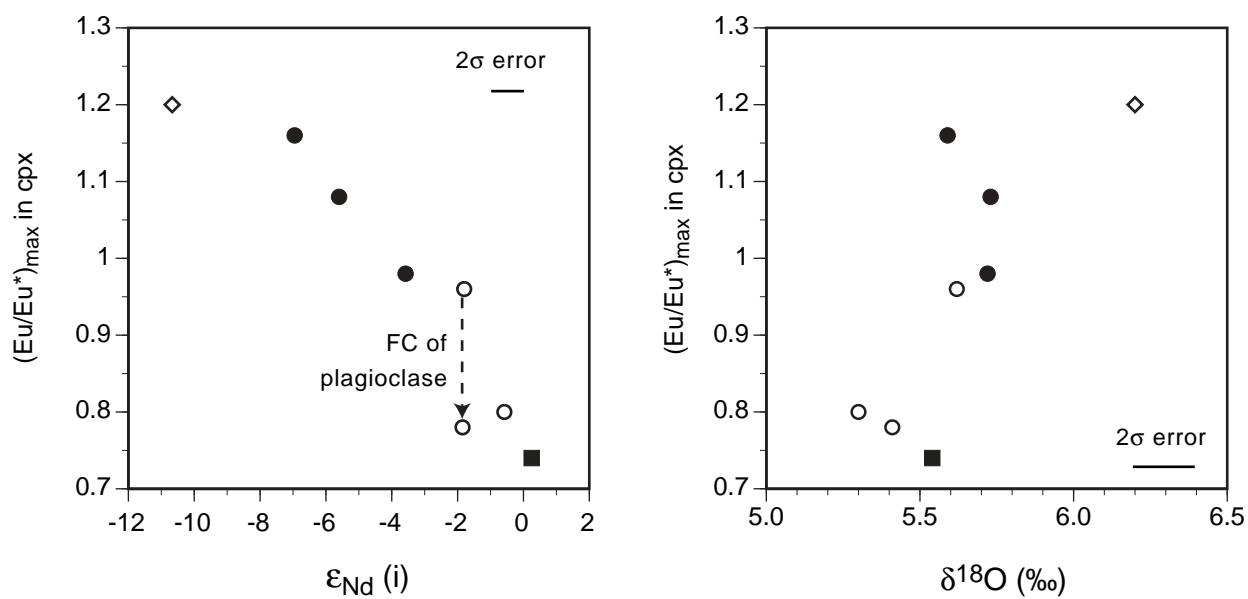
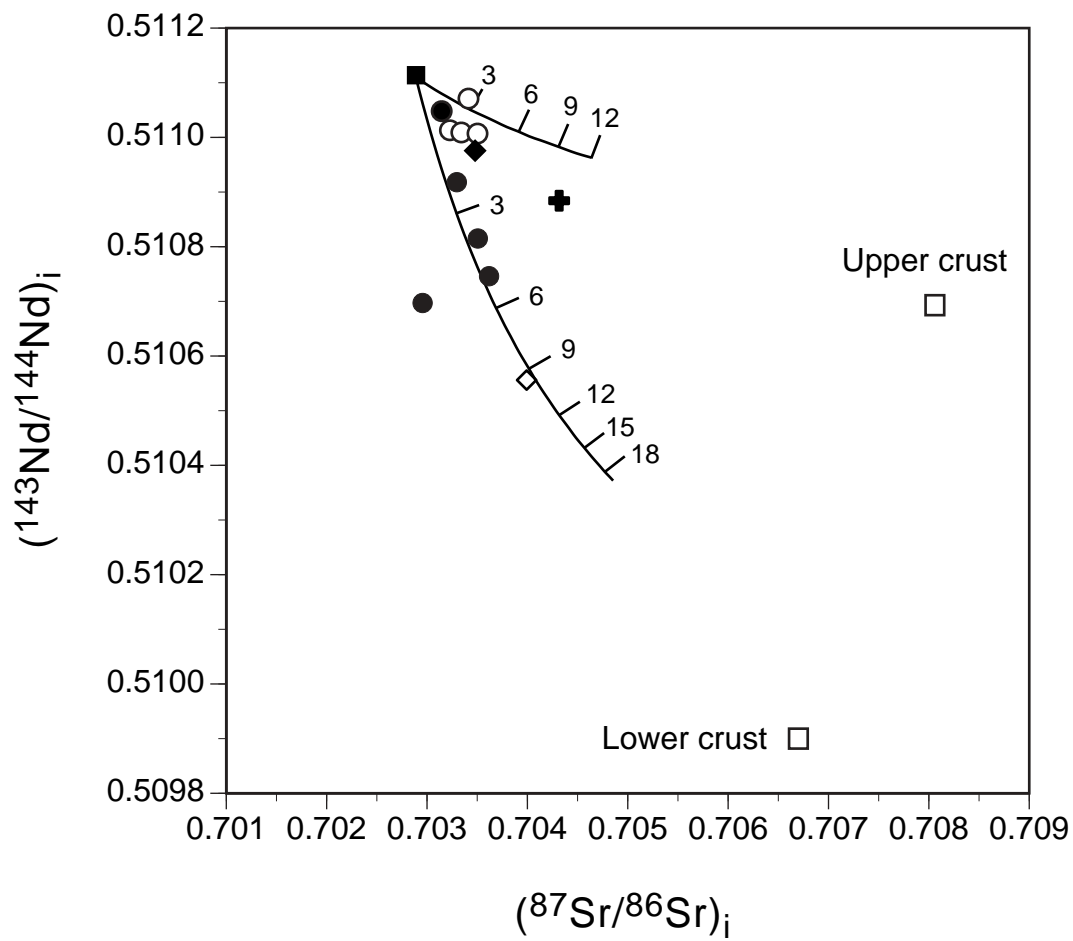


Fig. 16



Kapitel 3:

Geochemische und isotopengeochemische Untersuchungen an Plagioklas-Megakristallen aus gabbroischen Ganggesteinen und Anorthositxenolithen des Isortoq-Gangschwarms

Manuskript-Titel:

Geochemical and isotopic zoning patterns of plagioclase megacrysts in gabbroic dykes from the Gardar Province, South Greenland: implications for crystallisation processes in anorthositic magmas.

Autoren:

Ralf Halama¹, Tod Waight², Gregor Markl¹

¹ Institut für Geowissenschaften, Eberhard-Karls-Universität Tübingen,
Wilhelmstr. 56, D-72074 Tübingen

² Danish Lithosphere Centre, Øster Voldgade 10 L, DK-1350 Kopenhagen,
Dänemark

Veröffentlicht bei:

Contributions to Mineralogy and Petrology 144: 109-127 (2002)

Gutachter:

William Brown (Nancy), Brian G.J. Upton (Edinburgh), Jochen Hoefs (Göttingen)

Eigenanteile:

- | | |
|----------------------------------|-----|
| a) Idee | 40% |
| b) Datenbeschaffung | 80% |
| c) Auswertung und Interpretation | 80% |
| d) Ausarbeitung der Publikation | 90% |

Abstract

Chemical and Sr isotopic zoning patterns in plagioclase megacrysts from gabbroic dykes in the Gardar Province can be used to elucidate magma chamber and emplacement processes. The megacrysts occur either as single crystals or assembled as anorthosite xenoliths. The size of the megacrysts varies from < 1 cm to up to 1 m. They consist of a large core with variable zonation (An_{58-39}) and a relatively small (< 600 μm), normally zoned rim (An_{62-27}). The contact between core and rim is sharp and marked by a sudden increase in anorthite content, which can reach up to 11 mol% An. This gap is interpreted as having formed during dyke emplacement due to a sudden pressure release. Some of the megacryst cores show a fairly constant composition whereas others exhibit an unusual wavy-oscillatory zoning that has not been reported elsewhere to our knowledge. The oscillatory zoning has wavelengths of up to 2500 μm and a maximum amplitude of 7 mol% An. It is interpreted as reflecting movements of the crystals in the magma reservoir. The Sr isotopic composition of one crystal shows a radiogenic inner core [$(^{87}\text{Sr}/^{86}\text{Sr})_i = 0.7044$] and a less radiogenic outer core [$(^{87}\text{Sr}/^{86}\text{Sr})_i = 0.7039-0.7036$]. The lack of a significant change between outer core and rim [$(^{87}\text{Sr}/^{86}\text{Sr})_i = 0.7037$] is consistent with formation of the more An-rich rim due to pressure release. Variations in the core might be related to movements of the crystal and/or magma mixing. A trace-element profile across a megacryst shows a small increase in Sr and a small decrease in Ba and La contents of the recalculated melt composition across the core-rim boundary, while P, Ce, Nd and Eu remain constant. Melt compositional changes upon emplacement are therefore considered to be of minor importance. Constant ratios of incompatible trace-elements in the megacryst cores indicate a dominant influence of a lower crustal source on trace-element budgets.

Introduction

Massif-type anorthosites (MTAs) are large intrusive bodies (up to 17000 km²) mainly restricted to the middle Proterozoic (1.6 - 1.1 Ga) that contain vast accumulations of plagioclase (An_{50±10}) with subordinate mafic minerals (Ashwal 1993 and references therein). They represent the most voluminous anorthosite type on Earth and their relatively sodic plagioclase makes them distinct from other anorthositic rocks (Ashwal 1993). Various mechanisms have been proposed to explain the presence of such plagioclase-rich rocks, including the formation of plagioclase cumulates from basaltic magmas (e.g. Morse 1982), resorption and remelting of plagioclase (Wiebe 1990), delayed nucleation of plagioclase in mafic melts with the formation of "hyperfeldspathic" liquids (Morse 1982) and interaction between aluminous crust and basaltic magma (e.g. Dempster *et al.* 1999). The composition of the melts parental to anorthosites is thought to be broadly basaltic (e.g. Bowen 1917, Emslie 1978, Scoates 2000) or jotunitic (e.g. Vander Auwera *et al.* 1998, Owens and Dymek 2001), but those melt compositions are usually not preserved due to crystal fractionation and accumulation processes.

The ultimate source of the magmas from which the anorthosites crystallised is still much debated, with two principal schools of thought: magmas sourced a) from the mantle (e.g. Emslie 1978, Wiebe 1992, Mitchell *et al.* 1995, Markl and Frost 1999) or b) from the lower crust (e.g. Longhi *et al.* 1999, Schiellerup *et al.* 2000, Bédard 2001). Most authors believe in some sort of interaction between mantle-derived and crustal material during anorthosite genesis, either via crustal contamination of mantle-derived magmas (e.g. Scoates and Frost 1996) or contamination of remobilised crust by basalt (Bédard 2001).

In the Gardar Province, gabbroic "Big Feldspar Dykes" contain both numerous single plagioclase megacrysts and anorthosite xenoliths, and are interpreted to record the formation of anorthositic bodies at depth (Bridgwater 1967, Bridgwater and Harry 1968). Bridgwater (1967) has shown that the feldspathic material in the dykes is genetically linked to the present host, although it did not crystallise in place. Since the Precambrian of Greenland is a continuation of the Canadian Shield, with similar tectonic divisions and orogenic activities at approximately the same time, a close link between the Gardar anorthosite inclusions and the MTAs of the Canadian Shield has been

postulated (Bridgwater 1967). The fact that emplacement ages of the Gardar dykes (~ 1.15 - 1.25 Ma) overlap with ages obtained for Canadian anorthosites (e.g. Higgins and van Breemen 1992, Owens *et al.* 1994) further suggests a genetic relationship between the provinces. Additionally, the Gardar feldspathic material has X_{An} values within the range typical of plagioclase from these anorthosite massifs.

For the Canadian anorthosites, pressure estimates, assumed to represent the final level of emplacement, vary from 3-5 kbar (Fuhrmann *et al.* 1988, Kolker and Lindsley 1989), whereas the Gardar rocks show emplacement depths of 3-4 km corresponding to a pressure of ~ 1 kbar, based on fluid-inclusion data from Ilímaussaq (Konnerup-Madsen and Rose-Hansen 1984). The Gardar dykes with their numerous feldspathic inclusions most likely represent a higher level of exposure of an anorthosite province that is similar to, or even the continuation of, the Canadian Shield. Therefore, a study of the BFDs offers a unique opportunity to reveal details and independent constraints on magma-chamber and emplacement processes at depth during anorthosite genesis.

Examining the "Big Feldspar Dykes" as whole rocks is not useful in the present context because the rocks contain variable amounts of plagioclase megacrysts and do not represent true liquids. Single crystals, however, should preserve information on magma compositions and processes during anorthosite genesis. Investigations on single feldspar crystals have been very successful in elucidating the temporal record of magma chamber dynamics (e.g. Singer *et al.* 1995, Tepley *et al.* 1999) and the liquidus chemistry of magmas (e.g. Blundy and Wood 1991, Bindeman *et al.* 1999). Due to the very low diffusivities of major and trace-element cations (Giletti 1994, Giletti and Shanahan 1997) and high closure temperatures (Cherniak and Watson 1992, Cherniak 1995) in plagioclase, it can be assumed that plagioclase preserves its original composition during cooling, down to a scale of micrometers. Compositional and textural zoning should reflect processes during growth because the diffusive exchange CaAl - NaSi in plagioclase is slow (Grove *et al.* 1984).

Based on major- and trace-element compositional zoning and/or Sr and Nd isotopic zoning in feldspar, evidence for magma recharge (e.g. Tepley *et al.* 2000, Davidson *et al.* 2001), assimilation (e.g. Knesel *et al.* 1999), magma mixing and mingling (Waight *et al.* 2000, Waight *et al.* 2001), convection (Loomis and Welber 1982) and fractional crystallisation processes (Brophy *et al.* 1996)

has been presented in different contexts. Many of those studies concentrated on silicic volcanic and plutonic rocks or on the interplay between the respective magmas, but few dealt with basaltic systems (e.g. Pringle *et al.* 1974, Kuritani 1998, Bindeman *et al.* 1999) or anorthositic rocks (e.g. Wiebe 1992).

The present study investigates chemical and isotopic zoning in single plagioclase megacrysts from two BFDs of the Gardar Province that have the potential to constrain certain aspects of parental-melt compositions and to record information about dynamics and processes recorded within an anorthositic magma chamber.

Geological Background

The Gardar Province of South Greenland represents a mid-Proterozoic rift province with abundant alkaline magmatism lasting from about 1.30 to 1.12 Ga (Emeleus and Upton 1976, Upton and Emeleus 1987). It encompasses about ten igneous complexes, numerous dykes of variable chemical composition and a sequence of interlayered lavas and sediments (Eriksfjord Formation). During the late Gardar period (~1.20-1.12 Ga), several generations of gabbroic and intermediate dykes were emplaced along WSW-ENE to SW-NE trends, concentrated in two main zones (Upton and Emeleus 1987). The emplacement time of the more northerly Nunarssuit-Isortoq swarm is poorly constrained, but demonstrably younger than 1250 Ma (Patchett *et al.* 1978) and post-dating the early "brown dykes" (BD_{0s}) dated at 1282 ± 5 Ma (Upton, pers. comm.). The swarm predates the Nunarssuit syenite for which an U/Pb date is 1171 ± 5 Ma (Finch *et al.* 2001). This is confirmed by a Sm-Nd cpx-plag-whole rock isochron for a dyke from this region that yielded an age of 1190 ± 44 Ma (Halama, unpublished data). Many of the dykes contain abundant anorthosite xenoliths and plagioclase megacrysts and are therefore informally named "Big Feldspar Dykes". The feldspathic material is considered as evidence for an anorthosite body underlying South Greenland (Bridgwater 1967). The megacrysts are interpreted to have formed as unconsolidated roof material in a magma chamber, either as free-floating suspended crystals or derived from overlying anorthosite (Bridgwater and Harry 1968). Large, euhedral crystals have never accumulated to form solid anorthosite. They represent an endmember in a continuous textural series from single plagioclase

crystals to massive plagioclase rock. Bridgwater (1967) emphasised the genetic connection between host rocks and inclusions and inferred that the megacrysts are not true xenocrysts. The basic magmas that carried up the megacrysts were evolved magmas with low Ni contents, low Mg# and high Al/Ca ratios (Upton 1996).

Since the Gardar Province has been tectonically quiet after magmatic activity ceased and no metamorphic events affected the rocks, it is well suited for a study on magmatic processes based on mineral textures and analyses of primary magmatic phases.

Field observations and petrography

Ubiquitous gabbroic "Big Feldspar Dykes" (BFDs) occur in the Isortoq region in the western part of the Gardar province (Fig. 1). They belong to the Nunarssuit-Isortoq dyke swarm that covers an area of roughly 50 x 25 km and were emplaced into granitic basement of the Proterozoic Ketilidian mobile belt (Allaart 1976). The BFDs vary in width from a few metres to up to 100 m. A detailed account of the field relationships has been given by Bridgwater and Harry (1968).

The major matrix mineral phases of the gabbroic BFDs are plagioclase, olivine, clinopyroxene and titanomagnetite. Minor phases are apatite and biotite; pyrrhotite, chalcopyrite, sphalerite and baddeleyite occur as accessory minerals. Additionally, amphibole has been found in the anorthosite xenolith sample. Euhedral matrix plagioclase (width < 300 μm) is normally zoned and represents an early liquidus phase, followed by olivine and clinopyroxene. Biotite occurs either as fringes around Fe-Ti oxides or as euhedral grains.

The characteristic feature of the BFDs is their high content of feldspathic material, varying from single feldspar crystals (< 1 cm up to 1 m in size) to anorthositic bodies up to 30 m length (Fig. 2). These bodies may vary in composition from leucogabbroic to anorthositic and are not true xenoliths, but the term "anorthosite xenolith" is maintained here to remain consistent with previous publications. The boundary between feldspathic inclusions and a megacryst-free dyke matrix can be relatively sharp or gradual with a continuous decrease in feldspar megacryst concentration towards the matrix (Fig. 3a/b). The distribution of megacrysts within the BFDs is mostly random, but at some localities the plagioclase megacrysts are concentrated at the dyke centres (Fig. 3c). The distribution of plagioclase megacrysts can vary within a single dyke and from dyke to dyke.

Occasionally, xenoliths of granitic wall-rock up to several dm in size can be found in the dykes close to their margins.

Several megacrysts from two different BFDs have been investigated in this study. BFD 1 is on average 50-70 m wide and samples were taken from locations distributed over a length of ~ 8 km (Fig. 1). With the notable exception of the anorthosite xenolith sample GM 1682, the dyke matrix is olivine-bearing and quartz-free. Samples from BFD 2 were taken from a 12 m wide dyke section at the shoreline. The matrix of BFD 2 is olivine-free and contains late interstitial quartz.

Analytical methods

Electron microprobe measurements

Mineral compositions were determined using a JEOL 8900 electron microprobe at the Earth Science Department at the University of Tübingen, Germany. An internal $\phi\rho Z$ correction of the raw data was applied (Armstrong 1991). Both natural and synthetic standards were used for major and minor elements. Measuring times were 16 s and 30 s on the peak positions for major and minor elements, respectively. The emission current was 15 nA and the acceleration voltage 15 kV. For all feldspar analyses, a beam diameter of 5 μm was used to avoid errors resulting from diffusion of Na.

Strontium isotope measurements

Drilled feldspar samples for Sr isotopic analyses were collected from polished mineral surfaces using diamond-coated dentist drills with variable diameters (< 1mm) using methods described by Waight *et al.* (2000). The small amounts of feldspar powder from the shallow drill pits (\ll 1 mm) were collected as a slurry, then dried and weighed to determine sample weight. Samples were spiked with an enriched ^{84}Sr - ^{87}Rb mixed tracer and then dissolved in small amounts of HF, HNO_3 and HCl. Rb and Sr were separated using a single pass over a small bed of AG50-X12 resin with HCl elution, followed by clean up of both the Rb and Sr cuts using Sr specific resin. Sr isotopic values were determined using a VG Axiom MC-ICPMS at the Danish Lithosphere Centre, Copenhagen. Sample introduction was carried out using a Micromist nebuliser with Ar as both carrier and nebuliser gas. Mass fractionation during the Rb analyses was monitored using admixed

Zr, and during the Sr runs was corrected using $^{84}\text{Sr}/^{86}\text{Sr} = 0.1194$. Further details of analytical procedures are outlined in Waight *et al.* (2002). Analyses of SRM 987 over the period of this study gave $^{87}\text{Sr}/^{86}\text{Sr} = 0.71025 \pm 3$ (2 SD, $n = 5$). Errors for Sr drill samples are assumed to be $\pm 0.015\%$ which is slightly higher than the precision for whole-rock samples due to difficulties in obtaining an accurate sample weight on such small samples due to static charge effects on Teflon beakers. However, errors in elemental concentrations do not affect elemental ratios and $^{87}\text{Rb}/^{86}\text{Sr}$ ratios are expected to be correct within 0.5%. All initial Sr isotopic ratios have been corrected for radiogenic growth to an age of 1.19 Ga - which is the emplacement age of the dyke (Halama, unpublished data) - using $\lambda = 1.42 * 10^{-11} \text{ a}^{-1}$ (Steiger and Jäger 1977). Despite the possibility that the megacrysts might have grown earlier and the uncertainty in the age determination (error = ± 44 Ma), errors in age correction are insignificant due to the very low Rb/Sr ratios in all samples except the rim sample, which has larger errors due to a higher Rb content coupled with smaller sample size (Table 4). However, extrapolation of age errors for this sample results in a calculated error of 0.70371 ± 18 which does not affect the conclusions of this study.

Trace-element measurements

In-situ laser ablation inductively coupled plasma-mass spectrometer (LA-ICP-MS) trace-element analyses were performed at the EU Large-Scale Geochemical Facility (University of Bristol) using a VG Elemental PlasmaQuad 3 + S-Option ICP-MS equipped with a 266 nm Nd-YAG laser (VG MicroProbe II). The laser beam diameter at the sample surface was approximately 20 μm for all analyses and the laser repetition rate was 6 Hz. Helium gas and then an argon/helium mixture carried the ablated material from the sample cell to the plasma torch. All measurements were made using Thermo Elemental PlasmaLab "time-resolved analysis" (TRA) data acquisition software with a total acquisition time of 100 s per analysis, allowing about 40 s for background followed by 50 s for laser ablation. NIST 610 glass was used for instrument calibration, and NIST 612 was used as a secondary standard. Ca was used as an internal standard to correct the ablation yield differences between and during individual analyses on both standards and samples. To avoid analytical uncertainties due to variations in the concentrations of the internal standard, Ca concentrations were quantitatively measured within 20 μm of the laser ablation pits using a JEOL 8900 electron

microprobe (EMP) at Tübingen University (see above). The precision of trace-element concentrations, based on repeat analyses of standards, is approximately $\pm 5\%$ for element concentrations >10 ppm and $\pm 10\%$ for concentrations <10 ppm. Data processing was carried out off-line using the same PlasmaLab software used for data collection and various custom-designed Excel spreadsheets. The limits of detection are defined as 3.28 standard deviations above the background level, which equates to a 95% confidence that the measured signal is significantly above background. Typical detection limits during this study were 0.1-1 ppm for Sr, Y, Sn, Pb and the REE, 0.5-10 ppm for V, Zn, Ga, Ge, Rb, Cs and Ba and >10 ppm for P.

Results

Major-element zoning in plagioclase

The chemical intercrystal variation of fourteen plagioclase megacrysts and of matrix plagioclase from two BFDs has been studied. The most distinctive features of matrix plagioclases compared to megacrysts is their strong normal zoning (An_{62-27}) and their considerably smaller grain size (width generally $< 300 \mu\text{m}$). Most megacrysts consist of a homogeneous or weakly oscillatory zoned core which dominates the crystal and a relatively narrow ($< 600 \mu\text{m}$), normally zoned rim (Figs. 4, 5). Four crystals with several distinctive features will be described in detail, followed by a comparison of the various megacrysts within a single dyke and observed differences between the two dykes. Representative microprobe analyses of both megacrysts and matrix plagioclase are presented in Table 1.

GM 1680, f 6 (BFD 1) [width ≈ 8 mm]:

This sample contains only a few megacrysts in a medium-grained matrix. The core of the investigated megacryst (f 6) shows a true but weak oscillatory pattern for both An and Ab content (Fig. 4a). The amplitude between the An peak at $750 \mu\text{m}$ ($X_{An} \approx 50.5$) and the An trough at $1950 \mu\text{m}$ ($X_{An} \approx 46.5$) is roughly 4 mol% An. Although a complete period is cut short by the rim growth, $\lambda/2$ can be determined to be $1200 \mu\text{m}$ and a wavelength λ of $2400\text{-}2500 \mu\text{m}$ is indicated. The Or content stays constant at about 2.5 to 3.5 mol% throughout the core and does not show any

oscillatory zoning. The sudden increase in An content at the core-rim boundary amounts to 11 mol%, which is the highest in all crystals studied. The boundary between core and rim is highly irregular, with many areas of An-rich composition within the core and apparent remnants of core composition within the rim zone (Fig. 6). In addition, an alignment of small inclusions ($< 100 \mu\text{m}$) occurs in the core-rim boundary zone. These inclusions consist of clinoamphibole, clinopyroxene, K-feldspar and titanite. The normal zoning trend in the rim, from An_{62} to An_{53} , is smoothly continuous at the beginning, but then passes over into a fine-scale oscillatory pattern with amplitudes of several mol% An. The Or content in the rim is significantly lower than in the core, on average about 1.4 mol% Or.

GM 1729, f 4 (BFD 1) [width $\approx 4 \text{ mm}$]:

In this sample, plagioclase megacrysts of variable size make up 20-40 % of the rock volume. In megacryst f 4, the An content remains relatively constant at approximately $\text{An}_{56\pm 1}$ for the first 900 μm (Fig. 4b). Then, X_{An} starts to oscillate slowly over the next 1100 μm , matched by variations in Ab content. $\lambda/2$ within this period of growth is $\approx 500 \mu\text{m}$, less than half the value of 1200 μm estimated for GM 1680. The crystal rim is marked by a sudden An increase of 8 mol%, combined with a decrease of Or content of roughly 1 mol%. X_{An} decreases smoothly in the inner rim, but drops sharply in the outer 80 μm to An_{29} . Once the An content has dropped below 50 mol%, the Or content increases from ~ 1.5 to ~ 3 mol%. In the core, however, Or content remains constant despite the large variations in An content.

GM 1682, f 3 (BFD 1) [width $\approx 11 \text{ mm}$]:

This sample was taken from the large anorthosite xenolith shown in Fig. 2b. The remarkably constant core composition of $\text{An}_{51\pm 1}$ is only interrupted by a few outliers that are probably related to alteration along cracks and/or small inclusions. The core-rim boundary is different from those of the two previously described crystals (Fig. 5a): The increase in An content is more continuous and less pronounced ($\Delta\text{An} = 5 \text{ mol\%}$) and a significant drop in Or content is lacking. In the rim, the decrease of X_{An} is relatively steep from An_{58} to An_{27} .

GM 1750, f 1 (BFD 2) [width \approx 3 mm]:

This sample is similar to GM 1729 with plagioclase megacrysts of variable size in a fine- to medium-grained matrix. The core composition of crystal f 1 is very constant with An content \approx 41 ± 1 and Or content \approx 6 ± 1 (Fig. 5b). Δ An at the core-rim boundary is 9 mol% (jumping from An₄₃ to An₅₂) with Or content dropping about 2 mol% from 5 to 3. The rim initially has a composition at about An₅₂, followed by a decrease to An₃₇.

The matrix plagioclases of samples GM 1680, GM 1729 and GM 1750 are all normally zoned and show a variation in X_{An} similar to that observed in megacryst rims. However, the highest An content in the matrix plagioclases is usually slightly less than the highest An content in the megacryst rims (Table 2).

To investigate similarities and differences between plagioclase megacrysts within a single dyke and between the two dykes, the average An content of the megacryst core region has been calculated and plotted against the maximum An content in the core (Fig. 7). As expected, $X_{An_{max}}$ and $X_{An_{avg}}$ correlate quite well. The key observations, however, which should be incorporated into any model explaining the petrogenesis of the megacrysts and anorthosite xenoliths, are:

- There are significant differences in $X_{An_{avg}}$ between various megacrysts in a single dyke.
- The range of X_{An} in any single crystal that has a wavy-oscillatory zonation can be as large as the range in $X_{An_{avg}}$ of all the crystals in one particular dyke, but the two ranges may be different.
- With only one exception (GM 1750 f 2), megacrysts from BFD 1 have significantly higher $X_{An_{avg}}$ and $X_{An_{max}}$ values than megacrysts from BFD 2 (Fig. 7).

The main features of all megacrysts analysed are summarised in Table 3. The magnitude of the jump in X_{An} at the core-rim boundary is quite variable and some megacrysts do not show a distinct rim at all. Megacrysts with lower X_{An} in the core also have lower X_{An} in the rim. None of the megacryst rims from BFD 2 crystals reaches values of $X_{An} \approx 0.6$ that are typically observed in BFD 1 megacrysts and matrix plagioclases.

Strontium isotopic zoning in plagioclase

One megacryst (GM 1680 f 6) was selected for Sr isotopic analysis (Fig. 8, Table 4). Based on the initial $^{87}\text{Sr}/^{86}\text{Sr}$ ratios, one can distinguish between an inner core (points 1 and 2) with a relatively high Sr_i of 0.7044, and an outer core (points 3-6) with Sr_i values between 0.7036 and 0.7039 (Fig. 9). The decrease in Sr_i from inner to outer core ($\Delta\text{Sr}_i = 0.0005$) appears to be quite sudden and is outside analytical uncertainty. The Sr_i isotopic composition within the outer core remains constant within analytical uncertainty and the rim is very similar to the outer core in terms of its Sr_i composition of 0.7037 (Table 4, Fig. 9). However, there is a difference in the $^{87}\text{Rb}/^{86}\text{Sr}$ ratio of more than one order of magnitude between the rim analysis and all core analyses. Overall, the data reveal significant within-core isotopic compositional variations but these variations are not related to the core-rim boundary determined by microprobe.

$^{87}\text{Sr}/^{86}\text{Sr}$ initial ratios of BFDs in the Isortoq region, determined on clinopyroxene separates, vary between 0.7030 and 0.7038 at 1.19 Ga (Halama, unpublished data). Thus, the Sr initial ratios of clinopyroxenes from BFDs overlap with values from both megacryst rim and outer core, but are considerably smaller than values from the inner core (Fig. 9).

Trace-element concentrations

Representative trace-element compositions of six plagioclase cores from four different BFD 1 samples are shown in Table 5. The comparison focuses on two main aspects; firstly, the variation of trace-element contents with X_{An} of the plagioclases (Fig. 10) and secondly, inter-trace-element variations (Fig. 11). In general, there is no correlation between trace-element content and X_{An} in individual crystals and between samples. Trace-element contents of Ba, Ga and Ce (Fig. 10) and Sr, Y, La and Nd (not shown) are variable, but apparently independent of X_{An} . The relatively large spread can be attributed mainly to differences of trace-element concentrations between individual crystals with similar An contents, especially for $X_{\text{An}} > 0.5$. Many of the trace-elements measured in the megacryst cores show a positive correlation, e.g. Sr-Ba, Sr-Ga, Sr-Y, Sr-REE, Ba-Ga and Ba-REE. Accordingly, ratios of various trace-elements are relatively constant (Fig. 11).

Calculation of parental melt composition

In addition to the measurements from various crystal cores dealt with above, one trace-element profile across megacryst f 6 from sample GM 1680 was obtained (Fig. 12). To investigate the processes that contributed to the sharp discontinuity between core and rim, trace-element concentrations in the crystal have been recalculated to concentrations in the original melt, using partition coefficients between plagioclase and melt for the respective element determined by Bindeman *et al.* (1998). Partition coefficients between plagioclase and melt for various elements have been also published by Simmons and Hanson (1978), Morse (1988), Blundy and Wood (1991) and Vander Auwera *et al.* (2000), but the data from Bindeman *et al.* (1998) have been chosen in this study because they provide a consistent data set for the elements analysed (Table 6).

Trace-element incorporation into plagioclase depends, among other things, on the major-element crystal chemistry. Since core and rim of the megacryst show considerable differences in X_{An} , measured trace-element concentrations partly reflect the major-element crystal composition and not necessarily differences in the melt from which they crystallised. Therefore, the recalculation of the trace-element contents in the melt allows us to constrain chemical differences in the melt much better than a comparison of the measured concentrations in the crystal.

The distribution of trace-elements between crystal and coexisting melt is given by the partition coefficient D_i that is defined as

$D_i = \text{concentration of element } i \text{ in crystal} / \text{concentration of element } i \text{ in melt.}$

Partition coefficients may vary with pressure, temperature, composition of the melt and crystal composition (Blundy and Wood 1991). For plagioclase, crystal composition, represented by mol% An, is considered to be the most important parameter in controlling D_i (Blundy and Wood 1991). According to Bindeman *et al.* (1998), partition coefficients between plagioclase ($0.4 < X_{An} < 0.8$) and melt can be expressed by the general formula

$$RT \ln D_i = a_i X_{An} + b_i,$$

where R is the gas constant, T is the temperature in K and a_i and b_i are constants determined experimentally specific to each element (Bindeman *et al.* 1998, Table 4).

In their partition experiments, Bindeman *et al.* (1998) used a basaltic melt chemically similar to the gabbroic dykes investigated in this study and therefore their D_i values can be used here with confidence. X_{An} at the laser spots was measured by EMP and then used for the calculations of the D_i values. We performed our calculations at constant P and T because the pressure dependence of $D_i^{plag-melt}$ values has not been determined for most elements except Sr (Vander Auwera *et al.* 2000). Sr increase per kbar pressure increase in the calculated melt is less than 1 % of the Sr concentration in the melt and therefore, a correction for pressure variations is considered to be unnecessary in the present study.

The temperature dependence of D_i values is more important and changes in T may produce changes in D_i values. However, magmatic temperature variations of 100 °C produce a less than 10% effect on $RT \ln D_i$ values, which is within the natural and analytical dispersion (Bindeman *et al.* 1998). Quantitative information on the crystallisation temperature for the megacrysts is lacking, but Markl *et al.* (1998) calculated crystallisation temperatures of 1100 - 1185°C at pressures between 4 and 9 kbar for anorthosites from the Lofoten Islands. Therefore, a constant temperature of $T = 1150^\circ\text{C}$, which is in the middle of the temperature range determined by Markl *et al.* (1998), has been chosen for our calculations.

The calculated Sr content of the melt from which the megacryst crystallised is very constant at roughly 410 ± 20 ppm (Fig. 12). Sr melt concentrations calculated from megacryst rims are initially higher (460 - 540 ppm) and decrease as the outermost part of the crystal grew. Calculated Ba contents in the parental melts show fairly constant values during core growth, but slightly lower values with some scatter during crystallisation of the rim. Calculated P, Ce and Nd concentrations in the original melt exhibit a wide range, which leads to a wide overlap between melt compositions calculated from core and rim concentrations. As for the other REE, calculated La concentrations exhibit a relatively large scatter, but rim values are a somewhat lower than core values. For Ga, adequately determined partition coefficients are lacking and therefore Ga concentrations as

measured in the crystal have been plotted. Ga contents in the rim are about 5-10 ppm lower than in the crystal core.

A comparison of the calculated trace-element concentrations in the melt during rim crystallisation with BFD whole-rock XRF analyses (Halama, unpublished data) shows an overlap for Ba and Sr contents (Table 6). P contents in the calculated melt, however, are significantly above the values determined by XRF.

Discussion

Zoning patterns in plagioclase megacryst cores

Oscillatory zoning in plagioclase is a widespread phenomenon observed in volcanic and subvolcanic environments (e.g. Anderson 1984, Pearce 1994, Kuritani 1998, Ginibre *et al.* 2002). These zoning patterns are typically characterised by small-scale oscillations $\leq 10 \mu\text{m}$ which have been subdivided by Ginibre *et al.* (2002) into saw-tooth zones with dissolution surfaces (5-10 μm) resulting from magma-chamber dynamics and small-scale oscillations ($\leq 1-3 \mu\text{m}$) caused by kinetic effects. However, none of those oscillations is comparable to the large-scale, wavy-oscillatory patterns in the cores of a number of megacrysts observed here. Accordingly, none of the numerous theoretical and numerical models developed (e.g. Allègre *et al.* 1981, Lasaga 1982, L'Heureux and Fowler 1994, 1996) may be applicable to explain these zonations.

As a first step to evaluate the influence of various parameters on the oscillatory zoning, it is important to determine whether the core grew under near-equilibrium or disequilibrium conditions. To assess equilibrium versus non-equilibrium partitioning behaviour, Brophy *et al.* (1996) compared major- and trace-element abundances of two different crystals from the same sample and concluded from the similar absolute concentrations that partitioning occurred under near-equilibrium conditions. Megacrysts in the BFDs are possibly picked up from different areas in the source volume, so this approach might not give unequivocal results. However, a comparison of two megacrysts from sample GM 1729 yields very similar and constant Fe, Ti, Mg, Ba and Sr concentrations. Molar proportions of An, Ab and Or are also similar and show the same wavy pattern in the core next to the core-rim boundary. The generally smooth megacryst core zoning

profiles and the lack of dissolution surfaces within all cores studied (resorption only occurs at the core-rim boundary) are further indications that growth occurred under near-equilibrium conditions. Under near-equilibrium conditions, small changes in T and water content do not have a major effect on plagioclase composition (Loomis and Welber 1982). The effect of pressure on the zoning patterns can be evaluated using the experimental data from Longhi *et al.* (1993). The variation of 2-4 mol% An content would correspond to pressure differences of 2-4 kbar or a crustal thickness of roughly 6-12 km. A crystal travelling up and down through a magma reservoir of this depth is geologically unreasonable. Therefore, a change in melt composition remains as a possible factor. Most likely, this change occurs when the crystal is moving around in the magma chamber to compositionally different areas, driven by convective currents (Upton 1996). Phenocrysts in the magma can avoid capture by the advancing solidification front through floating or settling (Marsh 1996). The smooth changes in X_{An} indicate a rather slow and not a turbulent motion. Mechanisms thought to cause repeated compositional changes in the environment of a growing crystal include magma replenishment (Marsh 1996) and movement of the crystal along thermal and compositional gradients (Marsh 1989). The concept of gradual magma mixing is in accordance with the available data. It can explain wavy-oscillatory major-element zonation and is consistent with some variation in the trace-element contents. If the mixing process is slow, resorption surfaces are not likely to develop.

Given their slow isotopic equilibration rates with respect to Sr, plagioclase crystals should retain magmatic Sr isotopic compositions and are therefore useful as recorders of changing isotopic composition in a magma (Cherniak and Watson 1992, Giletti and Casserly 1994). Therefore, it can be assumed that the Sr isotopic ratios of the plagioclase crystals reflect isotopic ratios in the magma. The variation of the initial $^{87}Sr/^{86}Sr$ ratios within the megacryst core of GM 1680 is consistent with an initially xenocrystic or mixing origin early in its crystallisation history. The high $(^{87}Sr/^{86}Sr)_i$ part of the crystal might have been derived from a lower crustal country rock, but the smooth major-element profiles and the petrographic observations do not support such an origin. Hence, an origin involving the assimilation of crustal material is more likely and consistent with the concept of gradual magma mixing. The plagioclase crystal could initially have crystallised in a magma severely contaminated by crustal melts, e.g. at the wall of the magma chamber or in a first magma

batch that reacted with the country rocks. Later, when the crystal was detached from the magma chamber wall or when the magma conduit was sealed off from the surrounding crustal rocks, it was incorporated into magma with a less radiogenic initial Sr ratio.

In summary, the zoning patterns in the megacryst cores are thought to be related to movement of particular crystals within a magma reservoir where they encountered melt of variable composition. Those megacryst cores with \pm constant X_{An} indicate stable physicochemical conditions during growth.

Significance of the core-rim boundary in plagioclase megacrysts

The core-rim boundary in the plagioclase megacrysts represents a major resorption surface and is characterised by a sudden increase in X_{An} and a concentration of inclusions (Fig. 6). Major resorption surfaces with abrupt changes in anorthite content are generally attributed to changes in P, T, melt composition or water content of the magma (Singer *et al.* 1995, Davidson and Tepley 1997), but the ultimate reason for the resorption might be controversial.

As discussed above, it is likely that megacryst cores grew under near-equilibrium conditions, where changes in water content or temperature should not have large effects on the plagioclase composition (Loomis and Welber 1982). However, a short discussion of the less likely case of disequilibrium growth is included here. During disequilibrium growth, increasing temperature or increasing water content in the melt have been invoked to explain resorption and sharp increases in X_{An} (e.g. Loomis and Welber 1982, Anderson 1984). Components other than H₂O are not considered to play a major role in determining the degree of undercooling and thereby the composition of the crystallising plagioclase (Smith and Brown 1988). A sudden water ingress can be envisaged in a subvolcanic environment, but is more difficult to reconcile with a magma reservoir in mid- to lower crustal depths or close to the crust-mantle boundary such as is proposed for anorthosite genesis (Ashwal 1993). Sudden changes in temperature are hard to achieve in large volumes of magma due to the low thermal conductivity (Smith and Brown 1988). Therefore, the bulk of evidence indicates that an increase in H₂O content or temperature were not the major factors for the prominent resorption surface between core and rim, so that melt composition and pressure remain as variables responsible for the increase in X_{An} and the resorption.

With the Sr initial isotopic ratios (Fig. 9) and the trace-element profiles (Fig. 12), it can be checked independently whether a compositional change in the melt between core and rim crystallisation occurred and if so, of what kind. The initial $^{87}\text{Sr}/^{86}\text{Sr}$ ratios do not show a significant variation between rim and adjacent core values, indicating that the magmas from which core and rim of the megacryst crystallised were isotopically similar. However, this would be expected if both magmas were derived from the same type of reservoir. Additionally, if an enriched mantle source is assumed for the Gardar magmas (Upton and Emeleus 1987), contamination by lower crustal material with similar Sr isotopic characteristics might not be detected by the Sr isotopes at all. Although the calculated melt-composition trace-element profiles have considerable scatter, minor differences in Sr, Ba and La concentration between core and adjacent rim indicate that a small change in melt composition took place between growth of core and rim. The melt from which the rim grew appears to be slightly more primitive with lower concentrations of Ba and La than the melt calculated from the core compositions. The higher Sr concentrations in the melt calculated from the rim are possibly reinforced by the pressure dependence of D_{Sr} (Vander Auwera *et al.* 2000). D_{Sr} decreases with increasing pressure which means that calculated Sr contents in the melt increase when assuming higher pressures. For Ga, it is not clear whether the drop of Ga contents in the rim is due to a real change in melt composition or is an artefact of a supposed change in partition coefficients with crystal chemistry. The overlap of calculated Ce, Nd, Eu and P concentrations between rim and core shows that the compositional change was relatively small. In summary, the compositional change of the magma between core and rim crystallisation is not likely to be responsible for the major resorption surface.

A decrease in pressure has been invoked by Pringle *et al.* (1974) to explain a sharp boundary between plagioclase core and calcic rim. Subsequent experimental work at anhydrous conditions has shown that there is a general increase in albite content of near-liquidus plagioclase with increasing pressure for a compositional range of starting materials (Greene 1969, Thy 1991, Fram and Longhi 1992, Longhi *et al.* 1993). Longhi *et al.* (1993) quantified the shift in plagioclase composition to be ~ 1 mol%/kbar for anorthosite and somewhat higher for mafic compositions. Decreasing pressure leads to a lowering of the melting temperature of plagioclase in the system An-Ab (Smith and Brown 1988), which in turn leads to resorption of the plagioclase, followed by

growth of more An-rich zones under the new pressure conditions. The observed resorption of older plagioclase (core of megacrysts) along cracks and at the former crystal edges is consistent with resorption due to pressure decrease. The concentration of inclusions at, or close to, the core-rim boundary can be explained by a period of rapid crystal growth where melt droplets (now partly recrystallised to secondary minerals) and crystals from the melt have been included.

The megacryst rims with their linear normal zoning patterns and occasionally superimposed oscillations and minor resorption surfaces indicate rapid cooling and simultaneous crystallisation of other phases (Smith and Brown 1988). The rim patterns are comparable to those obtained in experiments (Smith and Lofgren 1983) and numerical simulations (Loomis 1982) with rapid cooling. The similarity of the mineral chemistry between megacryst rims and matrix plagioclases and the textural evidence suggest that their crystallisation occurred contemporaneously (Table 2). Kinetically favoured growth on pre-existing plagioclase crystals, where plagioclase could crystallise before matrix crystals started growing, is thought to be the reason that megacryst rims have slightly higher X_{An} values than matrix plagioclase. The overlap of Ba and Sr concentrations of BFD whole rock XRF analyses with calculated concentrations during rim growth (Fig. 12, Table 6) and the overlap between $^{87}Sr/^{86}Sr$ initial values of the megacryst rim and the BFDs (Fig. 9) also indicate that rim and dyke matrix crystallisation were contemporaneous. The difference in calculated and measured P contents is probably due to the fact that the whole-rock samples do not represent true liquid compositions and some apatite might have been removed by fractional crystallisation. A detailed analysis of the features in the plagioclase rims is beyond the scope of this paper, but it can be concluded that rim growth took place simultaneously with growth of matrix phases at the emplacement level of the dykes.

Following the arguments presented above, an abrupt decrease in pressure as the main reason for the resorption surface is consistent with the available data, possibly accompanied by minor changes in melt composition. Since the increase in X_{An} at the rim occurs in both BFD 1 and BFD 2 megacrysts, it appears that the crystal transport from greater depth to upper crustal levels was a widespread process and the pressure decrease an important factor attending their ascent. The suddenness of the

X_{An} increase may indicate that magma ascent was relatively rapid, possibly supported by crack propagation in the crust. Faulting was a significant process in the Gardar events and many dykes inherited their strike direction from earlier structures (Emeleus and Upton 1976). Therefore, it is probable that the magma ascent was associated with tectonic activity, either reactivation of earlier faults or renewed crustal dislocation.

Pressure estimates of megacryst crystallisation

Microprobe profiles with a step size $\leq 20 \mu\text{m}$ can be taken to yield accurately determined values of $\Delta X_{An}^{\text{core-rim}}$. Assuming, for simplicity, that $\Delta X_{An}^{\text{core-rim}}$ is only caused by pressure decrease, we can apply the results from Longhi and co-workers to estimate the pressure difference between core and rim growth. $\Delta X_{An}^{\text{core-rim}}$ is determined by the adjacent values of X_{An} in the core and in the rim, both of which are variable in the different megacrysts. Using the relation that 1 kbar P decrease leads to 1 mol% An increase (Longhi *et al.*, 1993), the maximum $\Delta X_{An}^{\text{core-rim}}$ values of 11.0 mol% in BFD 1 and 9.2 mol% in BFD 2 yield maximum pressure differences of 11 and 9 kbar, respectively. As the emplacement level of the BFDs is ~ 1 kbar, the calculations indicate that the megacrysts grew at maximum pressures between 10-12 kbar, which is close to the continental crust-mantle boundary. Lower $\Delta X_{An}^{\text{core-rim}}$ values might be explained by crystal growth at higher crustal levels or by growth in suspensions where the change in X_{An} due to pressure changes can be less pronounced because of a complex interplay of tie-line rotations and mass-balance constraints (Longhi *et al.*, 1993).

Chemical and isotopic constraints on "Big Feldspar Dyke" genesis

The most prominent feature of the BFDs are the variously zoned feldspar megacrysts, and any explanation of BFD genesis must first address the formation of these feldspars and their diversity in X_{An} . Processes contributing to variable plagioclase compositions include

- changes in P and T,
- fractional crystallisation,
- assimilation of crustal material and
- changes in the degree of partial melting.

Pressure differences might be responsible for variable anorthite contents of megacryst cores since the albite content of plagioclase increases with increasing pressure (Longhi *et al.* 1993). This scenario would be in agreement with Marsh's (1996) concept of crystals derived from any depth in the lithosphere - in the case of the plagioclase megacrysts from any crustal depth - that may become entrained and reworked. Taking the two BFDs together, megacryst cores show a compositional difference of 19 mol% An (An_{58} to An_{39}) corresponding to a pressure difference of 19 kbar at constant melt composition. A single magma conduit of such a size is geologically unlikely and it is concluded that pressure differences alone cannot account for the diversity of X_{An} values. However, the entrainment of crystals at various crustal levels might be a viable mechanism in the BFD genesis and some variation in X_{An} might be attributable to crystallisation at different pressures.

Variations in crystallisation temperature for the various megacrysts are difficult to constrain. Principally, megacryst crystallisation temperatures were probably similar, but it appears likely that minor variations in temperature occurred and affected the plagioclase chemistry.

Fractional crystallisation during core growth appears not to have occurred on a major scale because of the lack of correlation between incompatible trace-element contents and X_{An} (Fig. 10). If the megacrysts were related to each other by fractional crystallisation processes, one would expect a negative correlation between contents of incompatible trace-elements (e.g. Ba, REE) and X_{An} , which is not the case. Additionally, the wavy-oscillatory major-element patterns with variably increasing and decreasing X_{An} values indicate that fractional crystallisation did not play a major role during core growth.

As argued above, the variation of the initial $^{87}\text{Sr}/^{86}\text{Sr}$ ratios within the megacryst core of GM 1680 is consistent with a mixing origin involving the assimilation of crustal material. Interaction of the magma with refractory lower crust is also indicated by the initial ϵ_{Nd} value of - 3.7 of BFD 1 derived from the isochron (Halama, unpublished data). It seems likely that the incorporation of chemically diverse crustal material led to variable X_{An} contents, maybe to the degree that the chemistry reflects the degree of mixing between mantle and crust (Dempster *et al.* 1999). This is in agreement with the trace-element data, since the incompatible trace-element budgets during crust-mantle interaction are likely to be dominated by the crustal source (Bédard 2001) and constant ratios can therefore be expected (Fig. 11). The wide range of trace-element concentrations (Fig. 10)

is consistent with variable crustal assimilation as well, but could also have been caused by a variable degree of partial melting.

Summary and Conclusions

Petrogenetic model

A preliminary model of BFD petrogenesis is presented below, based on data presented here and also taking into account and combining many ideas of previous workers.

An important aspect of BFD petrogenesis is the intimate relation between megacryst composition and dyke matrix. Bridgwater (1967) noted that X_{An} in megacrysts decreases as the host rocks become more alkaline. This is true for BFD 1 and BFD 2, where the former contains the high- X_{An} megacrysts and olivine but no quartz, while the latter bears relatively low- X_{An} megacrysts, no olivine but late interstitial quartz. Bridgwater and Harry (1968) attributed the compositional changes of the dykes to successive tapping of lower levels in a fractionated magma at depth. Marsh (1996) notes that in a rising magma column, magma is flow differentiated and sorted with heavy crystals moving to the centre and downward due to gravity and grain dispersive pressures. Evidence for flow differentiation occurs in many of the dykes where xenoliths and megacrysts are concentrated in the dyke centre (Fig. 3c). Accordingly, BFD 2 could represent a higher part of a solidified magma column than BFD 1. The lighter, relatively Ab-rich megacrysts are therefore predominant in BFD 2 whereas more An-rich, denser megacrysts occur primarily in BFD 1 (Fig. 7). The generation of the mafic BFD magmas started with minor mantle upwelling (Upton 1996) which supplied heat for melting of lithospheric mantle and/or lower crustal rocks. The maximum pressure derived from the gap in anorthite content at the core-rim boundary of megacrysts (10-12 kbar) indicates that some megacrysts could have originated at considerable depth. Although there is no independent evidence on the crustal thickness in this region now or in the Proterozoic, it seems a reasonable assumption that 10-12 kbars could correspond to the crust-mantle boundary. Other megacrysts with a less pronounced gap might have crystallised in overlying lower crustal regions. Some might have grown in a stagnant crystal mush (Wiebe 1992) whereas others moved around in

the magma chamber. Because of tectonic stresses acting on the pre-Gardar basement, cracks propagated through the crust and enabled the magmas to rise rapidly.

Although melt composition was crucial in fixing an average X_{An} value in the megacryst cores, sudden changes in X_{An} at the core-rim boundary are independent from core composition. During ascent, megacrysts were probably picked up from various regions of the magma reservoir, possibly throughout the crust that acted as a "gravel pile" of crystals (Marsh 1996). At mid-crustal levels, massif-type anorthositic bodies might have formed (Bridgwater 1967). Single megacrysts and xenoliths derived from the anorthosites were transported in suspension in feldspathic magmas (Scoates 2000) and redistributed after they stopped growing (Winther 1992). Upon emplacement, flow differentiation led to a concentration of megacrysts mainly in the dyke centres, as can be seen from field evidence (Figs. 2, 3).

Bearing on massif-type anorthosite petrogenesis

Since the BFDs are intimately related to Proterozoic massif-type anorthosites (Bridgwater 1967), their occurrence in the Gardar province and their genesis is thought to hold clues to the formation of anorthositic plutonic complexes in general. The anorthite content in BFD megacrysts is variable, but within the range typical of massif-type anorthosites. The occurrence of anorthosite xenoliths in the BFDs implies that massif-type anorthosites (MTAs) could have formed at depth, although these complexes remain unexposed in the Isortoq region. However, in pre-Atlantic plate-tectonic reconstructions, the Gardar Province is a continuation of the Canadian Shield which contains huge amounts of MTAs of 1.0 to 1.4 Ga age (e.g. Higgins and van Breemen 1992, Owens *et al.* 1994). They were emplaced at pressures between 3-5 kbar (Fuhrmann *et al.* 1988, Kolker and Lindsley 1989). The Gardar BFDs, emplaced at roughly 1 kbar, are therefore interpreted to represent a higher crustal level above MTA plutons comparable to the Canadian anorthosites. Our investigations and results offer an unique view upon MTA genesis from a crustal level above these complexes and can be compared with previously proposed models for their petrogenesis.

Ashwal (1993) proposed a two-stage model of MTA genesis based on the work of many previous authors (e.g. Bowen 1917, Emslie 1978). In this model, mantle-derived mafic melts are ponded at the crust-mantle boundary, where mafic silicates crystallise and sink and the residual melts become

enriched in aluminium. When plagioclase crystallises, it floats and forms anorthositic cumulates at the top of the magma chamber. Gravitationally unstable plagioclase-rich mushes rise through the crust and form anorthositic massifs in the upper crust. During all stages, heat from the crystallising magmas causes crustal anatexis.

The large-scale major-element oscillatory patterns in plagioclase megacrysts, to our knowledge not described from anywhere else, are thought to be related to movements of the crystals in compositionally diverse magma reservoirs. These magma chambers can be envisaged both at the crust-mantle boundary and/or within the crust. The trace-element and Sr isotope data show that a crustal contribution to the anorthositic magmas was probably important. In accordance with Ashwal's model, crustal contamination is likely in various stages of the magma ascent and could have taken place both by infiltration of crustal melts or by direct assimilation of country rocks (Ashwal 1993).

The major resorption surfaces combined with increases of X_{An} of up to 11 mol% are attributed to a sudden pressure release of up to 11 kbar. This fairly crude estimate of pressure decrease in the plagioclase megacrysts yields crystallisation pressures close to the continental crust-mantle boundary, which is considered to be the place where plagioclase first starts to crystallise in the MTA model (Emslie 1978, Ashwal 1993). Some of the megacrysts from the Gardar province may represent an initial crystallisation at or near the crust-mantle boundary whereas others might have crystallised during magma ascent. Therefore, our data support the view that the initial crystallisation of MTAs could have started at roughly 30-35 km depth.

The sudden increase in X_{An} at the core-rim resorption surface in the megacrysts also indicates a relatively rapid magma ascent from close to the crust-mantle boundary to upper crustal levels. Magma batches with entrapped megacrysts must have been able to travel through the crust without being trapped in anorthositic massifs. This seems to be inconsistent with Ashwal's model, but may be explained by the tectonic environment of the Gardar Rift Province, in which extensional stresses and the development of cracks could have facilitated magma ascent during rifting periods when the BFDs were emplaced. In tectonically more quiet times, plagioclase mushes could have formed and ascended more slowly to mid-crustal levels (~9-15 km depth) below the BFD emplacement levels, where we would expect to find MTA bodies like those present in Canada. Remnants of both

processes can be found today in the "Big Feldspar Dykes": They contain both single plagioclase megacrysts and anorthosite xenoliths derived from massif plutonic masses.

In the Gardar Province, the BFDs are associated with a variety of other alkaline igneous rocks, including carbonatites (Grønnedal-Ika), agpaitic rocks (Ilímaussaq) and peralkaline granites (Puklen) (Upton and Emeleus 1987). The same is true for the Canadian Shield, where occurrences of mid-Proterozoic alkali granites (Strange Lake Complex, e.g. Boily and Williams-Jones 1994), agpaitic alkalic rocks (Red Wine Intrusion, e.g. Curtis and Gittins 1979), syenites (Kipawa Complex, e.g. Currie and van Breemen 1996) and carbonatites (Seabrook Lake Carbonatite, e.g. Cullers and Medaris 1977) have been reported. Given this similarity between Gardar and Canadian rocks, it is tempting to speculate if this association of alkaline igneous rocks might be typical for certain MTA provinces in general. Many geochemical features considered to be characteristic for granitoids associated with MTAs, like high Na + K contents, high Fe/Mg ratios, high REE and halogen contents, very Fe-rich mafic silicates (Ashwal 1993), are strikingly similar to those the rift-related Gardar rocks exhibit.

A plausible model that accounts for the production of a large variety of magmatic rocks in connection with the genesis of massif anorthosites is the "crustal tongue melting model", where underthrusting of a lower crustal mafic tongue is followed by thermal relaxation, asthenospheric uprise and melting of the crustal tongue (Duchesne et al. 1999). In this model, alkaline magmas can be created by contributions from the asthenosphere. Magma uprise takes place along lithospheric discontinuities, which could be much older than the anorthosite emplacement (Duchesne et al. 1999). Such structures are present in the Ketilidian Basement of the Gardar rocks (Alaart 1976) and their reactivation during Gardar times makes the model compatible with the well-established rift setting of the Gardar Province (Upton and Emeleus 1987). However, it remains speculative if this model is applicable to the Gardar Province and perhaps to the Grenville anorthosites as well.

Acknowledgements

We are grateful that we were able to carry out Laser ICP-MS measurements at the Large-Scale Geochemical Facility supported by the European Community - Access to Research Infrastructure action of the Improving Human Potential Programme, contract number HPRI-CT-1999-00008 awarded to Prof. B. J. Wood (University of Bristol). B. Paterson provided invaluable help during those measurements. M. Westphal is thanked for his help with the microprobe and M. Marks for company during fieldwork and many thoughtful comments. Very constructive reviews provided in an exceptionally short time by W. Brown and B. Upton helped to improve the manuscript. Financial funding of this work by the Deutsche Forschungsgemeinschaft (grant Ma-2135/1-2) and the Dansk Grundforskningsfond is gratefully acknowledged.

References

- Allaart JH (1976) Ketilidian mobile belt in South Greenland. In: Escher A, Watt WS (eds) *Geology of Greenland. Grønlands Geologiske Undersøgelse*, pp 121-151
- Allègre CJ, Provost A, Jaupart C (1981) Oscillatory zoning: a pathological case of crystal growth. *Nature* 294:223-228
- Anderson AT (1984) Probable relations between plagioclase zoning and magma dynamics, Fuego Volcano, Guatemala. *Am Mineral* 69:660-676
- Armstrong JT (1991) Quantitative elemental analysis of individual microparticles with electron beam instruments. In: Heinrich, KFJ, Newbury DE (eds) *Electron Probe Quantitation*. Plenum Press, pp 261-315
- Ashwal LD (1993) *Anorthosites*. Springer, Berlin Heidelberg
- Bédard JH (2001) Parental magmas of the Nain Plutonic Suite anorthosites and mafic cumulates: a trace-element modelling approach. *Contrib Mineral Petrol* 141:747-771
- Bindeman IN, Davis AM, Drake MJ (1998) Ion microprobe study of plagioclase-basalt partition experiments at natural concentration levels of trace-elements. *Geochim Cosmochim Acta* 62:1175-1193
- Bindeman IN, Davis AM, Wickham SM (1999) 400 my of Basic Magmatism in a Single Lithospheric Block during Cratonization: Ion Microprobe Study of Plagioclase Megacrysts in Mafic Rocks from Transbaikalia, Russia. *J Petrol* 40:807-830
- Blundy JD, Wood BJ (1991) Crystal-chemical controls on the partitioning of Sr and Ba between plagioclase feldspar, silicate melts, and hydrothermal solutions. *Geochim Cosmochim Acta* 55:193-209
- Boily M, Williams-Jones AE (1994) The role of magmatic and hydrothermal processes in the chemical evolution of the Strange Lake plutonic complex, Quebec-Labrador. *Contrib Mineral Petrol* 118:33-47
- Bowen NL (1917) The problem of the anorthosites. *J Geol* 25: 209-243.
- Bridgwater D (1967) Feldspathic inclusions in the Gardar igneous rocks of South Greenland and their relevance to the formation of major Anorthosites in the Canadian Shield. *Can J Earth Sci* 4:995-1014
- Bridgwater D, Coe K (1970) The role of stoping in the emplacement of the giant dykes of Isortoq, South Greenland. *Geol J, Special issue* 2:67-78
- Bridgwater D, Harry WT (1968) Anorthosite xenoliths and plagioclase megacrysts in Precambrian intrusions of South Greenland. *Meddr Grønland* 185, 243 pp
- Brophy JG, Dorais MJ, Donnelly-Nolan J, Singer BS (1996) Plagioclase zonation styles in hornblende gabbro inclusions from Little Glass Mountain, Medicine Lake volcano, California: implications for fractionation mechanisms and the formation of composition gaps. *Contrib Mineral Petrol* 126:121-136
- Cherniak DJ (1995) Diffusion of lead in plagioclase and K-feldspar: an investigation using Rutherford backscattering and resonant nuclear reaction analysis. *Contrib Mineral Petrol* 120:358-371
- Cherniak DJ, Watson EB (1992) A study of Sr diffusion in K-feldspar, Na-K feldspar and anorthite using Rutherford backscattering spectroscopy. *Earth Planet Sci Lett* 113:411-425
- Cullers RL, Medaris G (1977) Rare earth elements in carbonatite and cogenetic alkaline rocks; examples from Seabrook Lake and Callander Bay, Ontario. *Contrib Mineral Petrol* 65:143-153.
- Currie KL, van Breemen O (1996) The origin of rare minerals in the Kipawa Syenite Complex, Western Quebec. *Can Mineral* 34:435-451
- Curtis LW, Gittins J (1979) Aluminous and titaniferous clinopyroxenes from regionally metamorphosed apaitic rocks in central Labrador. *J Petrol* 20:165-186.
- Davidson JP, Tepley FJ (1997) Recharge in volcanic systems: evidence from isotope profiles of phenocrysts. *Science* 275:826-829
- Davidson JP, Tepley FJ, Palazc Z, Meffan-Main S (2001) Magma recharge, contamination and residence times revealed by in situ laser ablation isotopic analysis of feldspar in volcanic rocks. *Earth Planet Sci Lett* 184:427-442
- Dempster TJ, Preston RJ, Bell BR (1999) The origin of Proterozoic massif-type anorthosites: evidence from interactions between crustal xenoliths and basaltic magma. *J Geol Soc Lond* 156:41-46
- Duchesne JC, Liégeois JP, Vander Auwera J, Longhi J (1999) The crustal tongue melting model and the origin of massive anorthosites. *Terra Nova* 11:100-105
- Emeleus CH, Upton BGJ (1976) The Gardar period in southern Greenland. In: Escher A, Watt WS (eds), *Geology of Greenland*, Copenhagen: Geological Survey of Greenland, pp 152-181
- Emslie RF (1978) Anorthosite massifs, rapakivi granites, and late Proterozoic rifting of North America. *Precambrian*

Res 7:61-98

- Finch AA, Mansfeld J, Andersen T (2001): U-Pb radiometric age of Nunarssuit pegmatite, Greenland: constraints on the timing of Gardar magmatism. *Bull Geol Soc Denmark* 48: 1-7
- Fram MS, Longhi J (1992) Phase equilibria of dykes associated with Proterozoic anorthosite complexes. *Am Mineral* 77:605-616
- Fuhrman ML, Frost BR, Lindsley DH (1988) Crystallization conditions of the Sybille Monzosyenite, Laramie Anorthosite Complex, Wyoming. *J Petrol* 29:699-729
- Giletti BJ (1994) Isotopic equilibrium/disequilibrium and diffusion kinetics in feldspars. In: Parsons, I. (ed.), *Feldspars and their Reactions*, NATO ASI Series 421, Boston: Kluwer Academic, pp 351-382
- Giletti BJ, Casserly JED (1994) Strontium diffusion kinetics in plagioclase feldspars. *Geochim Cosmochim Acta* 58:3758-3793
- Giletti BJ, Shanahan TM (1997) Alkali diffusion in plagioclase feldspar. *Chem Geol* 139:3-20
- Ginibre C, Kronz A, Wörner G (2002) High-resolution quantitative imaging of plagioclase composition using accumulated backscattered electron images: new constraints on oscillatory zoning. *Contrib Mineral Petrol* 142:436-448
- Green TH (1969) High-pressure experimental studies on the origin of anorthosites. *Can J Earth Sci* 6:427-440
- Grove TL, Baker MB, Kinzler RJ (1984) Coupled CaAl-NaSi diffusion in plagioclase feldspar: experiments and application to cooling rate speedometry. *Geochim Cosmochim Acta* 58:2113-2121
- Higgins MD, van Breemen O (1992) The age of the Lac-Saint-Jean anorthosite complex and associated mafic rocks, Grenville Province, Canada. *Can J Earth Sci* 29: 1412-1423.
- Knesel KM, Davidson JP, Duffield WA (1999) Evolution of silicic magma through Assimilation and Subsequent Recharge: Evidence from Sr Isotopes in Sanidine Phenocrysts, Taylor Creek Rhyolite, N.M. *J Petrol* 40:773-786
- Kolker A, Lindsley DH (1989) Geochemical evolution of the Maloin Ranch pluton, Laramie Anorthosite Complex, Wyoming: petrology and mixing relations. *Am Mineral* 74:307-324
- Konnerup-Madsen J, Rose-Hansen J (1984) Composition and significance of fluid inclusions in the Ilimaussaq peralkaline granite, South Greenland. *Bull Minéral* 107:317-326
- Kuritani T (1998) Boundary Layer Crystallization in a Basaltic Magma Chamber: Evidence from Rishiri Volcano, Northern Japan. *J Petrol* 39:1619-1640
- L'Heureux I, Fowler AD (1994) A nonlinear dynamical model of oscillatory zoning in plagioclase. *Am Mineral* 79:885-891
- L'Heureux I, Fowler AD (1996) Isothermal constitutive undercooling as a model for oscillatory zoning in plagioclase. *Can Mineral* 34:1137-1147
- Lasaga AC (1982) Toward a master equation in crystal growth. *Am J Sci* 282:1264-1288
- Longhi J, Fram MS, Vander Auwera J, Montieth JN (1993) Pressure effects, kinetics, and rheology of anorthositic and related magmas. *Am Mineral* 78:1016-1030
- Longhi J, Vander Auwera J, Fram MS, Duchesne J-C (1999) Some Phase Equilibrium Constraints on the Origin of Proterozoic (Massif) Anorthosites and Related Rocks. *J Petrol* 40:339-362
- Loomis TP (1982) Numerical Simulations of Crystallization Processes of Plagioclase in Complex Melts: the Origin of Major and Oscillatory Zoning in Plagioclase. *Contrib Mineral Petrol* 81:219-229
- Loomis TP, Welber PW (1982) Crystallization processes in the Rocky Hill Granodiorite Pluton, California: An interpretation based on compositional zoning of plagioclase. *Contrib Mineral Petrol* 81:230-239
- Markl G, Frost BR (1999) The Origin of Anorthosites and Related Rocks from the Lofoten Islands, Northern Norway: II. Calculation of Parental Liquid Compositions for Anorthosites. *J Petrol* 40:61-77
- Markl G, Frost BR, Bucher K (1998) The origin of Anorthosites and related rocks from the Lofoten islands, Northern Norway: I. Field relations and estimation of intrinsic variables. *J Petrol* 39:1425-1452
- Marsh BD (1989) Magma Chambers. *Ann Rev Earth Planet Sci* 17:439-474
- Marsh BD (1996) Solidification fronts and magmatic evolution. *Mineral Mag* 60:5-40
- Mitchell JN, Scoates JS, Frost CD (1995) High-Al gabbros in the Laramie Anorthosite Complex, Wyoming: Implications for the composition of melts parental to Proterozoic anorthosite. *Contrib Mineral Petrol* 119:166-180
- Morse SA (1982) A partisan review of Proterozoic anorthosites. *Am Mineral* 67:1087-1100
- Morse SA (1988) Partition coefficients for anorthosites. *Chem Geol* 70:154
- Owens BE, Dymek RF (2001) Petrogenesis of the Labrieville Alkalic Anorthosite Massif, Grenville Province, Quebec.

- J Petrol 42: 1519-1546.
- Owens BE, Dymek RF, Tucker RD, Brannon JC, Podosek FA (1994) Age and radiogenic isotopic composition of a late- to post-tectonic anorthosite in the Grenville Province: the Labrieville massif, Quebec. *Lithos* 31: 189-206.
- Patchett PJ, Bylund G, Upton BGJ (1978) Palaeomagnetism and the Grenville orogeny: new Rb-Sr ages from dolerites in Canada and Greenland. *Earth Planet Sci Lett* 40:349-364
- Pearce TH (1994) Recent work on oscillatory zoning in plagioclase. In: Parsons, I. (ed.), *Feldspars and their reactions*. Kluwer, Dordrecht 313-349
- Pringle GJ, Trembath LT, Pajari GE (1974) Crystallization history of a zoned plagioclase. *Mineral Mag* 39:867-877
- Schiellerup H, Lambert DD, Prestvik T, Robins B, McBride JS, Larsen RB (2000) Re-Os isotopic evidence for a lower crustal origin of massif-type anorthosites. *Nature* 405:781-784
- Scoates JS (2000) The Plagioclase-Magma Density Paradox re-examined and the Crystallization of Proterozoic Anorthosites. *J Petrol* 41:627-649
- Scoates JS, Frost CD (1996) A strontium and neodymium isotopic investigation of the Laramie anorthosites, Wyoming, USA: Implications for magma chamber processes and the evolution of magma conduits in Proterozoic anorthosites. *Geochim Cosmochim Acta* 60:95-107
- Simmons EC, Hanson GN (1978) Geochemistry and origin of massif-type anorthosites. *Contrib Mineral Petrol* 66:119-135
- Singer B, Dungan MA, Layne GD (1995) Textures and Sr, Ba, Mg, Fe, K, and Ti compositional profiles in volcanic plagioclase: clues to the dynamics of calc-alkaline magma chambers. *Am Mineral* 80:776-798
- Smith J, Brown WL (1988) *Feldspar minerals 1. Crystal structures, physical, chemical and microtextural properties*, 2nd edn., Springer, Berlin Heidelberg.
- Smith RK, Lofgren GE (1983) An analytical experimental study of zoning in plagioclase. *Lithos* 16:153-168
- Steiger RH, Jäger E (1977) Subcommittee on geochronology: convention of the use of decay constants in geo- and cosmochronology. *Earth Planet Sci Lett* 36:359-362
- Tepley FJ, Davidson JP, Clynne MA (1999) Magmatic interactions as recorded in Plagioclase Phenocrysts of Chaos Crags, Lassen Volcanic Center, California. *J Petrol* 40:787-806
- Tepley FJ, Davidson JP, Tilling RI, Arth JG (2000) Magma mixing, recharge and eruption histories recorded in plagioclase phenocrysts from El Chicón Volcano, Mexico. *J Petrol* 41:1397-1411
- Thy P (1991) High and low phase equilibria of a mildly alkalic lava from the 1965 Surtsey eruption. *Experimental results*. *Lithos* 26:223-243
- Upton BGJ (1996) Anorthosites and troctolites of the Gardar Magmatic Province. In: Demaiffe, D. (ed.), *Petrology and Geochemistry of magmatic suites of rocks in the continental and oceanic crusts. A volume dedicated to Professor Jean Michot, Université Libre de Bruxelles, Royal Museum for Central Africa (Tervuren)*, pp 19-34
- Upton BGJ, Emeleus CH (1987) Mid-Proterozoic alkaline magmatism in southern Greenland: the Gardar province. In: Fitton JG, Upton BGJ (eds), *The Alkaline Rocks*, Boston: Blackwell Scientific 30, pp 449-471
- Vander Auwera J, Longhi J, Duchesne JC (1998) A liquid line of descent of the jotunitic (hypersthene monzodiorite) suite. *J Petrol* 39: 439-468
- Vander Auwera J, Longhi J, Duchesne JC (2000) The effect of pressure on D_{Sr} (plag/melt) and D_{Cr} (opx/melt): implications for anorthosite petrogenesis. *Earth Planet Sci Lett* 178:303-314
- Waight T, Baker J, Willigers B (2002) Rb isotope dilution analyses by MC-ICPMS using Zr to correct for mass fractionation: towards improved Rb-Sr geochronology? *Chem Geol* 186: 99-116
- Waight TE, Maas R, Nicholls IA (2000) Fingerprinting feldspar phenocrysts using crystal isotopic composition stratigraphy: implications for crystal transfer and magma mingling in S-type granites. *Contrib Mineral Petrol* 139:227-239
- Waight TE, Wiebe RA, Krogstad EJ, Walker RJ (2001) Isotopic responses to basaltic injections into silicic magma chambers: a whole-rock and microsampling study of macrorhythmic units in the Pleasant Bay layered gabbro-diorite complex, Maine, USA. *Contrib Mineral Petrol* 142:323-335
- Wiebe RA (1990) Evidence for unusually feldspathic liquids in the Nain complex, Labrador. *Am Mineral* 75:1-12
- Wiebe RA (1992) Proterozoic Anorthosite Complexes. In: Condie, K.C. (ed.), *Proterozoic crustal evolution*, Elsevier, Amsterdam, pp 215-261
- Winther KT (1992) Feldspar megacryst and anorthosite xenolith-bearing dykes in the Narssarssuaq area, South Greenland. *Rapp Grønland Geol Unders* 154:49-59

Figure captions

Fig. 1: Geological map of the Isortoq region after Bridgwater & Coe (1970).

Fig. 2 a/b: Occurrences of feldspathic inclusions in the "Big Feldspar Dykes" of Isortoq. **a** Euhedral feldspar megacryst, length about 40 cm. **b** Anorthositic xenolith in fine-grained dyke matrix, total length of xenolith is about 20 m.

Fig. 3 a-c: Field relationships between feldspathic inclusions and dykes (length of hammer is 60 cm). **a** Gradual transition from feldspar-rich zone to relatively feldspar-poor host dyke matrix. **b** Sharp contact between feldspar-rich and feldspar-poor areas of the dyke. **c** Small dyke showing a concentration of feldspar megacrysts in the dyke centre. Dyke margins are virtually megacryst-free.

Fig. 4 a/b: Microprobe profiles through two plagioclase megacrysts with wavy-oscillatory pattern and normally zoned rims. **a** Wavy-oscillatory pattern throughout the core of the megacryst, followed by a sudden increase in X_{An} at the rim. **b** Initially constant X_{An} , followed by a wavy-oscillatory pattern and a sudden increase in X_{An} at the rim.

Fig. 5 a/b: Microprobe profiles through two plagioclase megacrysts with constant X_{An} in the core and normally zoned rims. **a** X_{An} shows a slight tendency to decrease towards the rim and increases smoothly at the core-rim boundary, before dropping almost 30 mol% in the rim. **b** Within the core, X_{An} has a slight tendency to increase towards the rim before suddenly increasing at the core-rim boundary. X_{An} shows normal zoning in the rim.

Fig. 6: Back-scattered electron images from the core-rim boundary of the analysed megacryst GM 1680 f 6. **a** gives an overview, with various matrix minerals in the lower left corner (ol = olivine, cpx = clinopyroxene, plag = plagioclase). The core-rim boundary is marked by a colour difference in the BSE image and a trail of relatively light inclusions. The microprobe traverse extends for further 2200 μm into the core of the crystal. **b** shows details of the core-rim boundary. Note the various embayments and laths of rim-plagioclase within the core and the concentration of inclusions at the boundary (amph = amphibole, tit = titanite).

Fig. 7: Comparison of X_{An} values from the cores of various megacrysts in BFD 1 and 2. The circle shows the average core composition and the error bars indicate the maximum and minimum X_{An} values found in the respective cores.

Fig. 8: Photographic image of megacryst GM 1680 f 6, showing location of Sr isotopic composition profile. Circles approximate the size of the drill samples collected and sample names correspond to Table 4.

Fig. 9: Sr isotopic composition profile of sample GM 1680 f 6. The rim region is equivalent to the rim detected by microprobe.

Fig. 10: Plots of Ba, Ga and Ce contents vs. X_{An} in plagioclase from various megacrysts. Trace-element concentrations are apparently unrelated to the major-element composition of the crystal.

Fig. 11: Plots of La/Ba vs. Ba and Ga/Sr vs. Sr from various megacrysts of BFD 1. Trace-element ratios are relatively constant throughout the range of trace-element concentrations.

Fig. 12: Laser ICP-MS profile through megacryst GM 1680 f 6. Traverse with 22 spots is shown at the top. Recalculated trace-element concentrations in the melt are shown below, except for Ga where the concentrations measured in the crystal are given.

Table 1: Representative microprobe analyses of plagioclase

Sample	GM 1680	GM 1680	GM 1680	GM 1680	GM 1681	GM 1682	GM 1682	GM 1729	GM 1729	GM 1729	GM 1750	GM 1755
Fsp. no.	1	6	6	6	1	3	4	3	4	5	1	1
	matrix	MC rim	MC rim	MC core	MC core	MC core	MC core	matrix	MC core	MC core	MC core	MC core
SiO ₂	54.50	54.20	53.75	56.22	55.82	56.49	55.70	58.70	54.64	55.16	58.13	58.59
TiO ₂	0.14	0.08	0.09	0.03	0.17	0.15	0.15	0.10	0.03	0.13	0.10	0.08
Al ₂ O ₃	28.16	28.35	28.93	26.55	27.39	26.65	26.55	24.82	27.52	27.01	25.34	25.19
FeO	0.59	0.43	0.38	0.43	0.30	0.47	0.53	0.48	0.55	0.60	0.46	0.53
MnO	0.01	0.01	0.00	0.03	0.00	0.00	0.00	0.00	0.00	0.01	0.01	0.01
MgO	0.08	0.08	0.08	0.08	0.08	0.08	0.07	0.05	0.07	0.06	0.07	0.06
BaO	0.33	0.26	0.28	0.29	0.00	0.08	0.09	0.17	0.00	0.10	0.28	0.27
SrO	0.07	0.00	0.03	0.00	0.26	0.28	0.31	0.25	0.28	0.31	0.02	0.11
CaO	11.49	11.91	12.22	10.09	10.51	9.56	9.75	7.40	10.54	10.17	8.45	8.03
Na ₂ O	4.76	4.61	4.20	5.44	5.13	5.54	5.51	6.62	5.01	5.26	6.15	5.99
K ₂ O	0.37	0.33	0.27	0.62	0.41	0.61	0.59	0.95	0.59	0.59	0.95	1.15
Total	100.50	100.26	100.22	99.78	100.08	99.91	99.25	99.54	99.23	99.40	99.96	100.02
<i>Formulae based on 8 oxygens</i>												
Si	2.46	2.45	2.43	2.55	2.52	2.55	2.54	2.65	2.49	2.52	2.62	2.64
Ti	0.00	0.00	0.00	0.00	0.01	0.01	0.01	0.00	0.00	0.00	0.00	0.00
Al	1.50	1.51	1.54	1.42	1.46	1.42	1.43	1.32	1.48	1.45	1.35	1.34
Fe ²⁺	0.02	0.02	0.01	0.02	0.01	0.02	0.02	0.02	0.02	0.02	0.02	0.02
Mn	0.00	0.00	0.00	0.00	0.00	0.00	0.00	0.00	0.00	0.00	0.00	0.00
Mg	0.01	0.01	0.01	0.01	0.01	0.01	0.00	0.00	0.00	0.00	0.01	0.00
Ba	0.00	0.00	0.00	0.00	0.00	0.00	0.00	0.00	0.00	0.00	0.01	0.01
Sr	0.01	0.01	0.01	0.01	0.01	0.01	0.01	0.01	0.01	0.01	0.00	0.00
Ca	0.56	0.58	0.59	0.49	0.51	0.46	0.48	0.36	0.52	0.50	0.41	0.39
Na	0.42	0.40	0.37	0.48	0.45	0.49	0.49	0.58	0.44	0.47	0.54	0.52
K	0.02	0.02	0.02	0.04	0.02	0.04	0.03	0.05	0.03	0.03	0.05	0.07
Total	5.00	5.00	4.98	5.00	4.98	4.99	5.00	5.00	5.00	5.00	5.00	4.99
X _{An}	0.56	0.58	0.61	0.49	0.52	0.47	0.48	0.36	0.52	0.50	0.41	0.41
X _{Ab}	0.42	0.40	0.38	0.48	0.46	0.49	0.49	0.58	0.45	0.47	0.54	0.54
X _{Or}	0.02	0.02	0.02	0.04	0.02	0.04	0.03	0.06	0.03	0.03	0.05	0.05

MC = megacryst

Table 2: Comparison of matrix plagioclase and megacryst rim compositions

Sample		An_{\max}	An_{\min}
<i>GM 1680</i>	Matrix plagioclase	$An_{55}Ab_{43}Or_2$	$An_{37}Ab_{61}Or_2$
	Megacryst rim	$An_{62}Ab_{37}Or_1$	$An_{37}Ab_{59}Or_4$
<i>GM 1729</i>	Matrix plagioclase	$An_{59}Ab_{39}Or_2$	$An_{32}Ab_{66}Or_2$
	Megacryst rim	$An_{58}Ab_{41}Or_1$	$An_{29}Ab_{68}Or_3$
<i>GM 1750</i>	Matrix plagioclase	$An_{48}Ab_{48}Or_4$	$An_{19}Ab_{69}Or_{12}$
	Megacryst rim	$An_{53}Ab_{44}Or_3$	$An_{37}Ab_{59}Or_4$

Table 3: Key features of all megacrysts analysed

BFD No.	Sample	Step size (μm)	Profile length (μm)	No. of analyses (total/core)	Core An_{max}	Core An_{min}	Core $\text{An}_{\text{avg}} \pm 1\sigma$	$\Delta\text{An} = \text{An}_{\text{core}} - \text{An}_{\text{rim}}$ (mol %)	Major-element pattern (core)	Core-rim transition
1	GM 1680, f 6	20	3820	192/160	51.0	46.4	48.9 ± 1.2	+ 11.0	osc.	sudden
1	GM 1681, f 1	500	16 500	34/34	55.2	52.2	53.7 ± 0.8	-	osc.	-
1	GM 1682, f 2	50	600	13/6	51.6	50.5	51.2 ± 0.7	+ 5.2	const.	x
1	GM 1682, f 3	20	3460	174/152	53.1	48.8	51.8 ± 0.9	+ 4.8	const.	smooth
1	GM 1699, f 1	500	13 500	28/27	58.0	54.8	55.9 ± 0.6	+ 5.6	const.	x
1	GM 1729, f 1	100	1400	15/11	53.6	51.6	52.5 ± 0.6	+ 8.7	const.	x
1	GM 1729, f 4	10	2290	230/199	56.3	48.4	53.7 ± 2.0	+ 7.9	const. + osc.	sudden
1	GM 1729, f 5	10	430	44/33	53.0	49.4	51.1 ± 1.2	+ 5.3	const. + osc.	sudden
1	GM 1733, f 1	500	22 000	45/45	52.6	49.7	51.3 ± 0.8	-	const.	-
2	GM 1750, f 1	10	810	82/69	43.2	40.1	41.3 ± 0.6	+ 9.2	const.	sudden
2	GM 1750, f 7	20	980	50/47	50.0	43.3	47.8 ± 1.3	-	osc.	-
2	GM 1753, f 7	10	430	44/43	45.1	42.0	43.9 ± 0.5	- 9.8	const.	sudden
2	GM 1755, f 1	10	760	77/56	41.7	39.2	40.8 ± 0.6	+ 9.0	const.	inhomogeneous
2	GM 1755, f 2	10	370	38/35	43.6	41.2	42.1 ± 0.5	+ 3.3	const.	sudden

osc. = oscillating, const. = constant, x = not described accurately due to large step size;

Table 4: Isotopic data of drill samples from megacryst GM 1680 f 6

Sample	Rb (ppm)	Sr (ppm)	$^{87}\text{Rb}/^{86}\text{Sr}$	$^{87}\text{Sr}/^{86}\text{Sr}$	$^{87}\text{Sr}/^{86}\text{Sr}$ (i) T = 1.19 Ga
GM 1680-1-Core	0.578	266.37	0.0063	0.704510 ± 34	0.704403
GM 1680-2-Core	0.182	130.39	0.0040	0.704485 ± 28	0.704416
GM 1680-3-Core	0.239	274.70	0.0025	0.703929 ± 17	0.703886
GM 1680-4-Core	0.645	782.24	0.0024	0.703690 ± 20	0.703649
GM 1680-5-Core	1.035	1060.58	0.0028	0.703860 ± 27	0.703812
GM 1680-6-Core	0.658	331.06	0.0056	0.703910 ± 11	0.703815
GM 1680-8-Rim	3.919	97.86	0.1158	0.705684 ± 110	0.703711

Table 5: Representative Laser ICP-MS analyses of plagioclase

Sample	GM 1680	GM 1680	GM 1680	GM 1680	GM 1681	GM 1682	GM 1682	GM 1729	GM 1729	GM 1729
Fsp. no.	1	6	6	6	1	3	4	3	4	5
	matrix	MC rim	MC rim	MC core	MC core	MC core	MC core	matrix	MC core	MC core
P	trace	186	trace	266	123	312	272	267	trace	392
Sc	trace	trace	trace	27	n.d.	57	50	61	trace	93
V	3.0	2.1	2.8	2.4	1.7	3.3	2.8	3.3	3.2	4.4
Zn	6.7	8.6	6.2	10.7	trace	19.6	23.3	17.4	16.4	30.9
Ga	40	35	37	46	24	39	39	40	27	58
Ge	trace	8	9	11	n.d.	24	27	trace	n.d.	30
Rb	n.d.	n.d.	n.d.	n.d.	trace	5.7	5.5	trace	n.d.	trace
Sr	1138	1277	1274	1331	893	1388	1356	776	1112	1920
Y	0.3	0.2	0.2	0.3	0.3	0.4	0.3	0.2	0.3	0.6
Sn	0.5	1.8	1.9	2.8	2.0	3.5	2.7	1.4	2.1	1.6
Cs	n.d.	n.d.	n.d.	n.d.	n.d.	1.9	trace	n.d.	n.d.	n.d.
Ba	370	360	367	654	243	624	703	723	445	952
La	2.32	2.03	2.05	3.25	1.18	4.11	3.87	1.75	2.12	6.18
Ce	3.96	3.48	3.45	5.40	2.40	5.94	7.57	2.87	3.78	7.89
Pr	0.38	0.41	0.36	0.51	0.23	0.76	0.80	0.27	0.38	0.81
Nd	1.32	1.58	1.05	1.81	1.01	2.33	3.53	1.02	1.34	3.77
Sm	trace	n.d.	0.31	0.33	n.d.	n.d.	0.65	n.d.	trace	0.74
Eu	0.72	0.72	0.86	0.75	0.59	1.14	0.92	1.17	0.58	1.15
Gd	trace	0.50	n.d.	0.49	trace	0.92	0.77	0.48	trace	0.74
Tb	n.d.	n.d.	trace	0.06	n.d.	0.15	0.13	trace	n.d.	trace
Dy	n.d.	trace	trace	trace	trace	0.71	0.37	trace	0.35	n.d.
Ho	trace	0.05	n.d.	trace	n.d.	0.12	0.13	n.d.	n.d.	trace
Er	n.d.	trace	n.d.	n.d.	n.d.	0.63	trace	trace	n.d.	trace
Tm	n.d.	n.d.	n.d.	trace	n.d.	0.10	n.d.	trace	n.d.	0.07
Yb	n.d.	n.d.	n.d.	n.d.	n.d.	n.d.	n.d.	n.d.	n.d.	n.d.
Lu	n.d.	n.d.	trace	n.d.	n.d.	0.14	n.d.	trace	n.d.	0.06
Pb	n.d.	n.d.	n.d.	trace	0.53	2.28	2.19	1.26	1.56	2.21

MC = megacryst; n.d. = not detected; trace = concentration is between lower limit of decision (2 standard deviations above background) and lower limit of detection (3.28 standard deviations above background)

Table 6: Exemplified calculations of partition coefficients and original melt compositions from selected plagioclase analyses

Sample	GM 1680 f 6u core	GM 1680 f 6n core	GM 1680 f 6h core	GM 1680 f 6g rim	GM 1680 f 6c rim	Range of melt compositions calculated from the rim	For comparison: Range of BFD whole-rock XRF analyses
X_{An} (mol%)	0.487	0.478	0.496	0.578	0.586		
Trace element concentrations in the crystal (ppm):							
P	268	248	289	182	182		
Sr	1305	1344	1243	1235	1220		
Ba	644	671	586	354	344		
La	2.73	3.02	3.33	2.39	2.01		
Ce	4.58	4.99	5.28	4.36	3.57		
Nd	2.07	2.09	1.97	1.85	1.41		
Eu	0.84	0.84	0.77	0.73	0.71		
Partition coefficients, calculated following the equations from Bindeman et al. (1998) with constant T = 1150 °C:							
D_P	0.10	0.10	0.10	0.08	0.08		
D_{Sr}	3.18	3.26	3.11	2.52	2.46		
D_{Ba}	0.52	0.54	0.50	0.34	0.33		
D_{La}	0.22	0.23	0.22	0.21	0.21		
D_{Ce}	0.17	0.17	0.17	0.15	0.15		
D_{Nd}	0.20	0.20	0.20	0.17	0.17		
D_{Eu}	0.16	0.16	0.15	0.14	0.14		
Trace element concentrations in the original melt (ppm):							
P	2639	2388	2909	2271	2315	1742 - 2599	873 - 1026
Sr	410	413	399	490	495	354 - 544	510 - 629
Ba	1232	1233	1169	1033	1047	897 - 1227	750 - 936
La	12.1	13.3	14.9	11.6	9.8	9.1 - 11.6	
Ce	26.8	28.8	31.3	29.3	24.2	21.7 - 29.3	
Nd	10.4	10.4	10.0	10.8	8.4	6.5 - 10.8	
Eu	5.4	5.3	5.0	5.3	5.2	4.3 - 6.5	

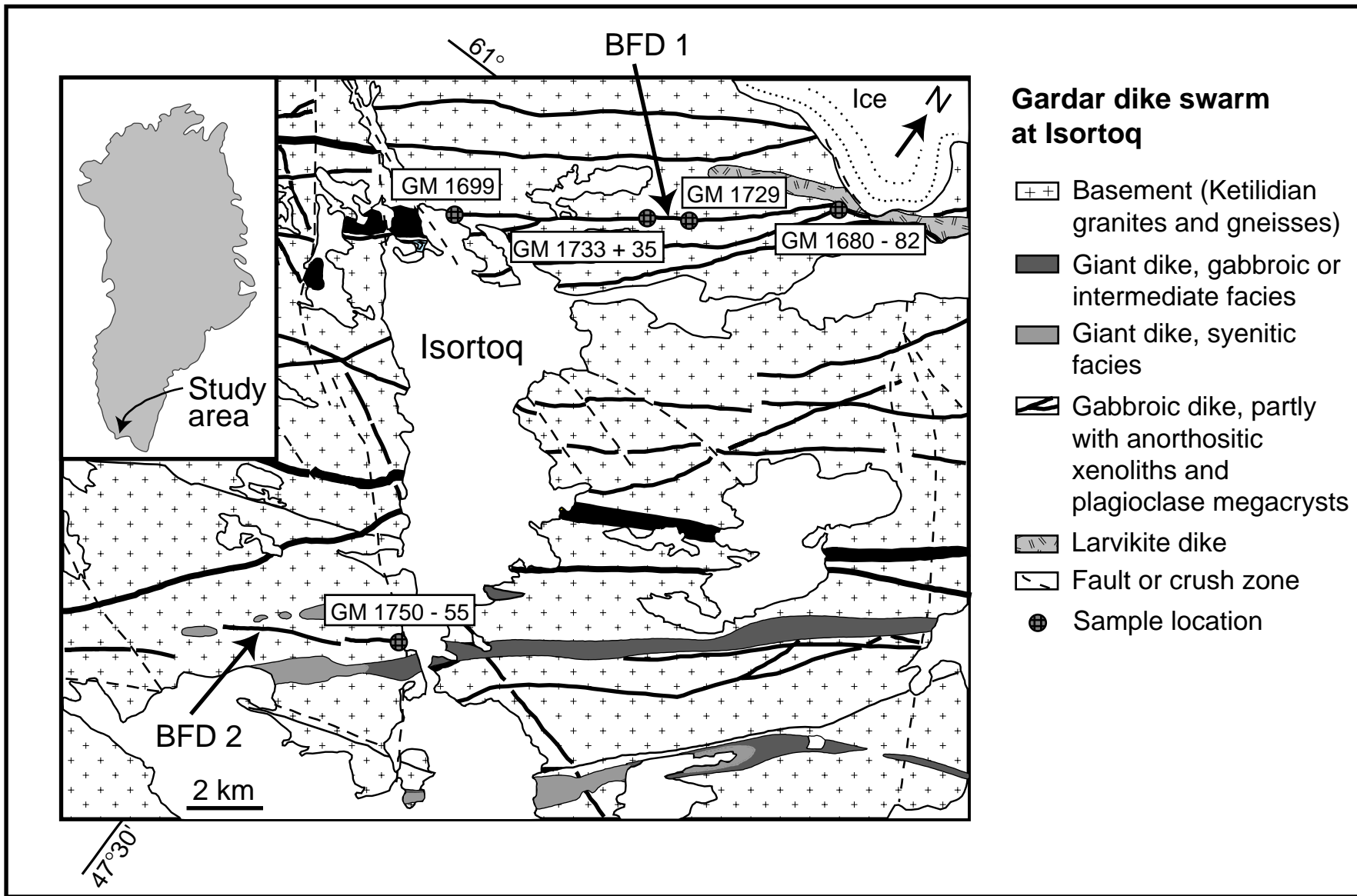
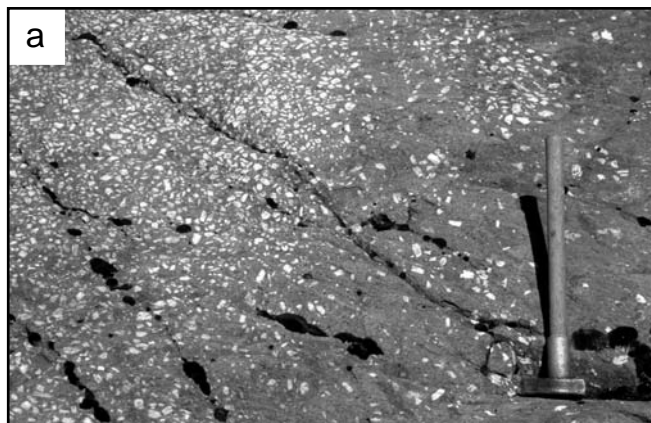


Fig. 1

Fig. 2



Fig. 3



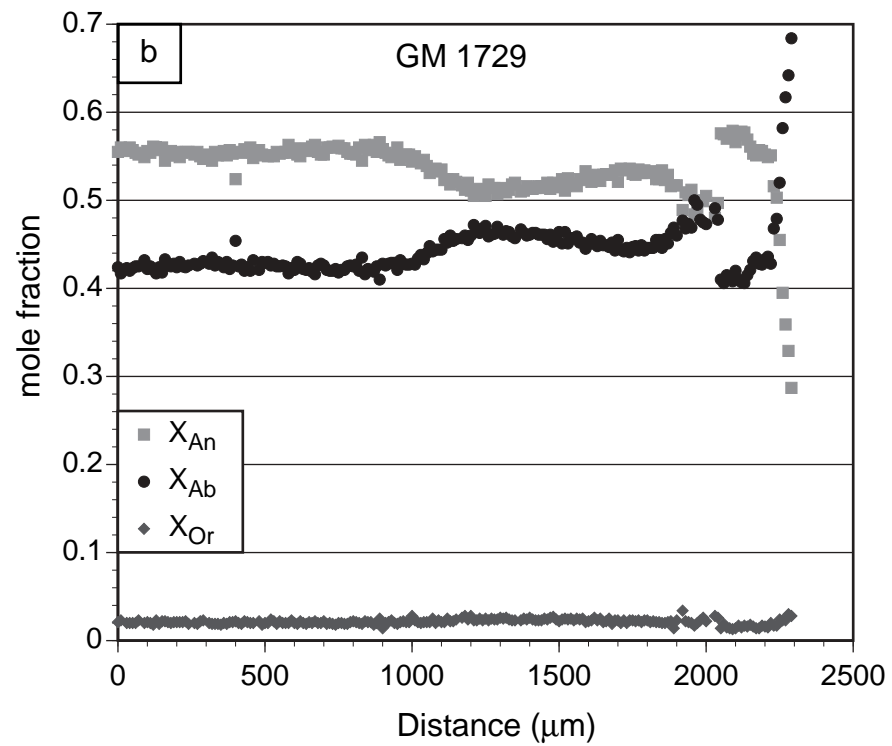
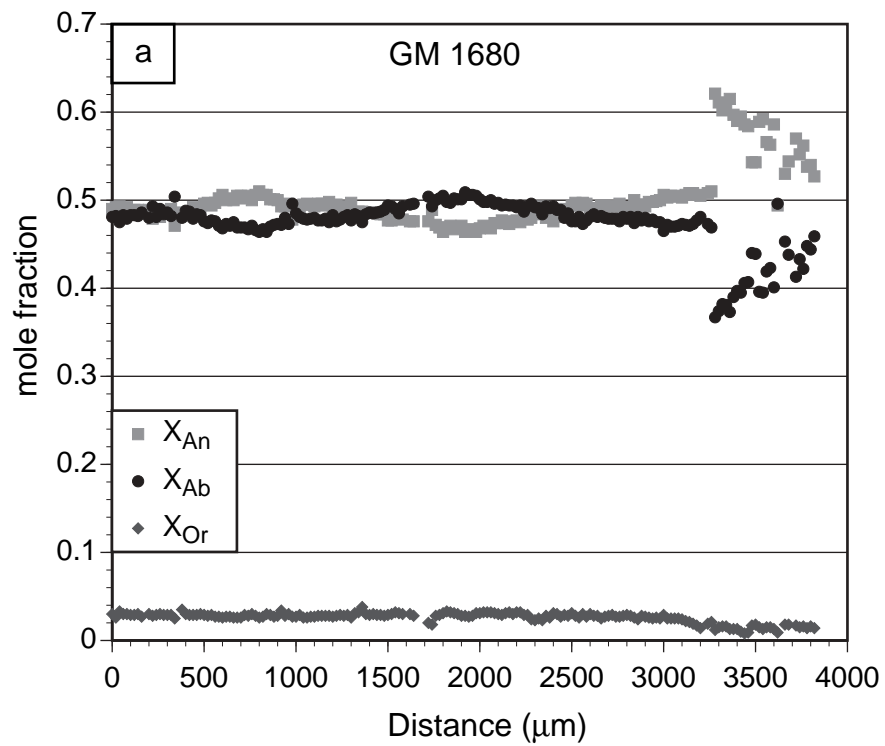


Fig. 4

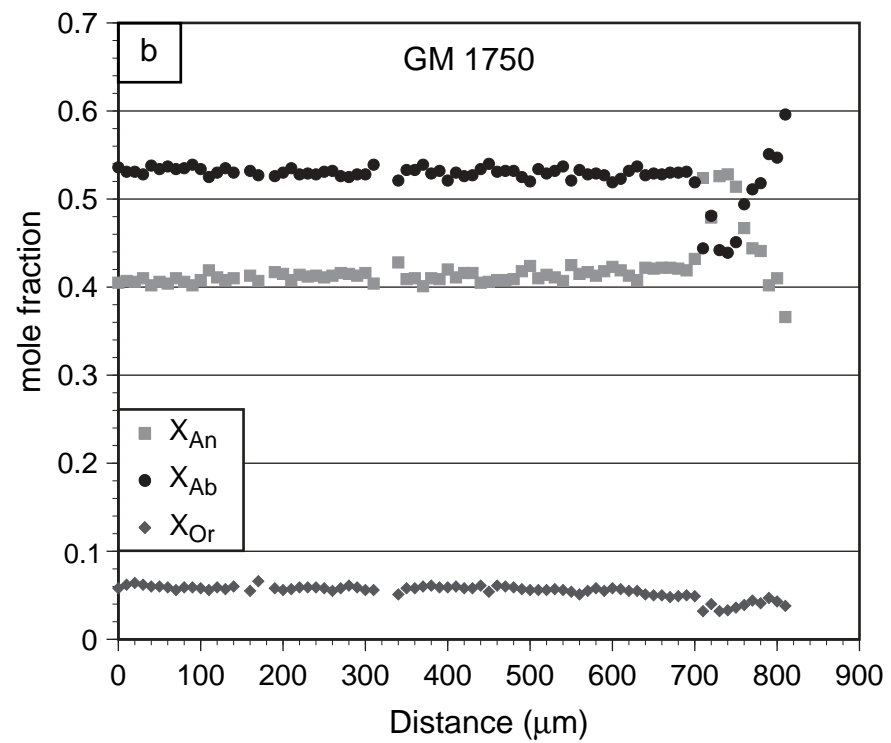
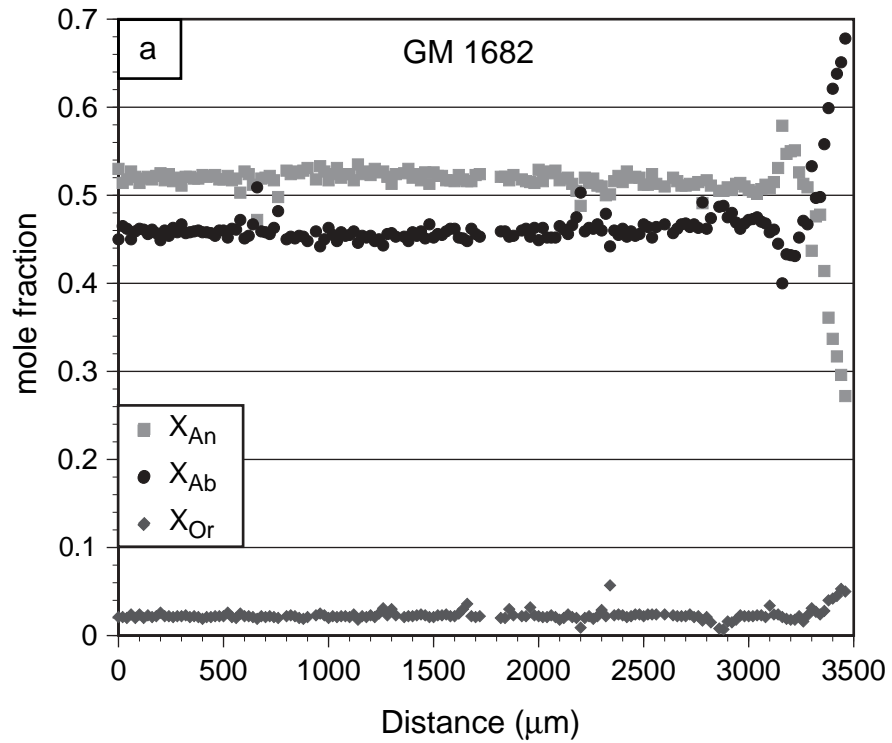
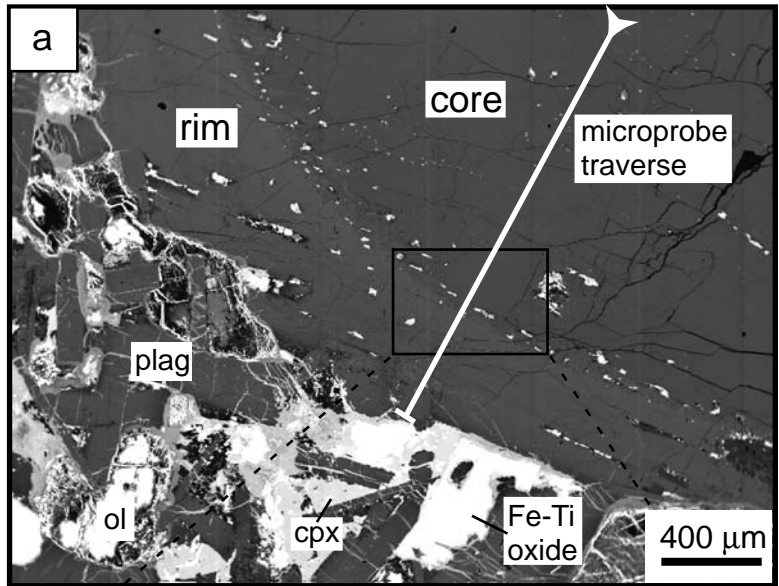
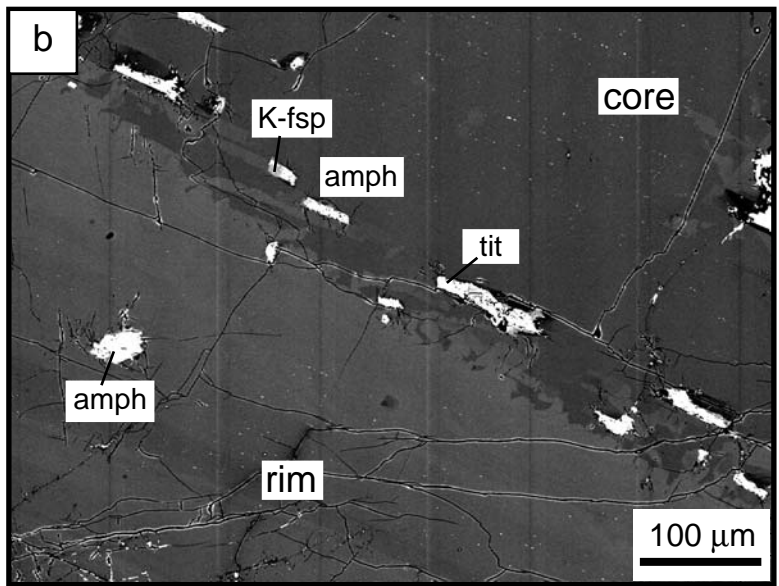


Fig. 5

Fig. 6



GM 1680 f 6



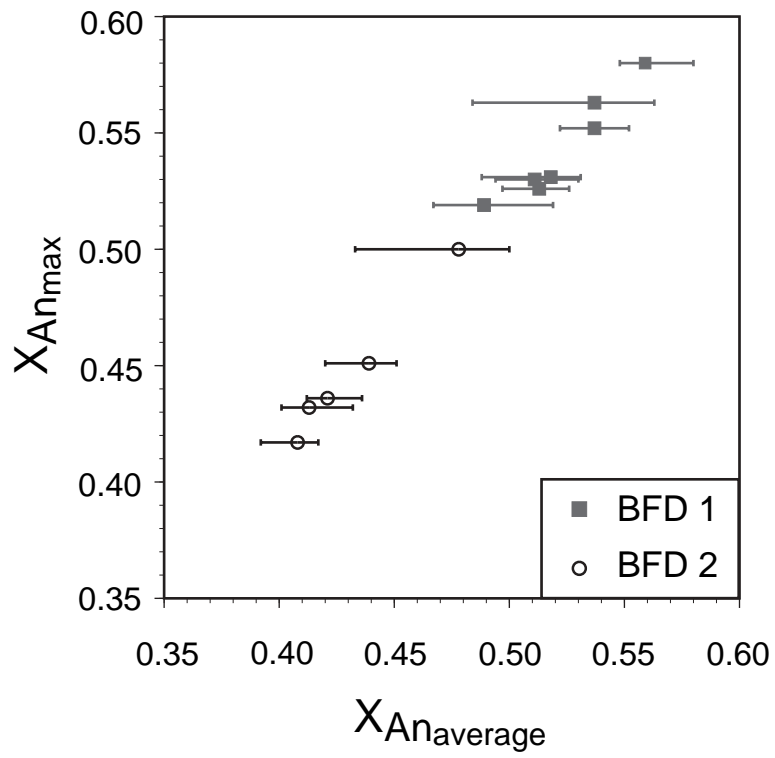


Fig. 7

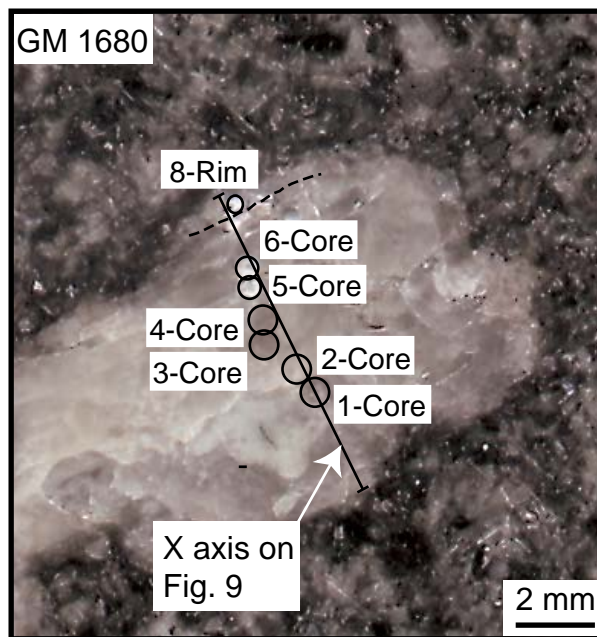


Fig. 8

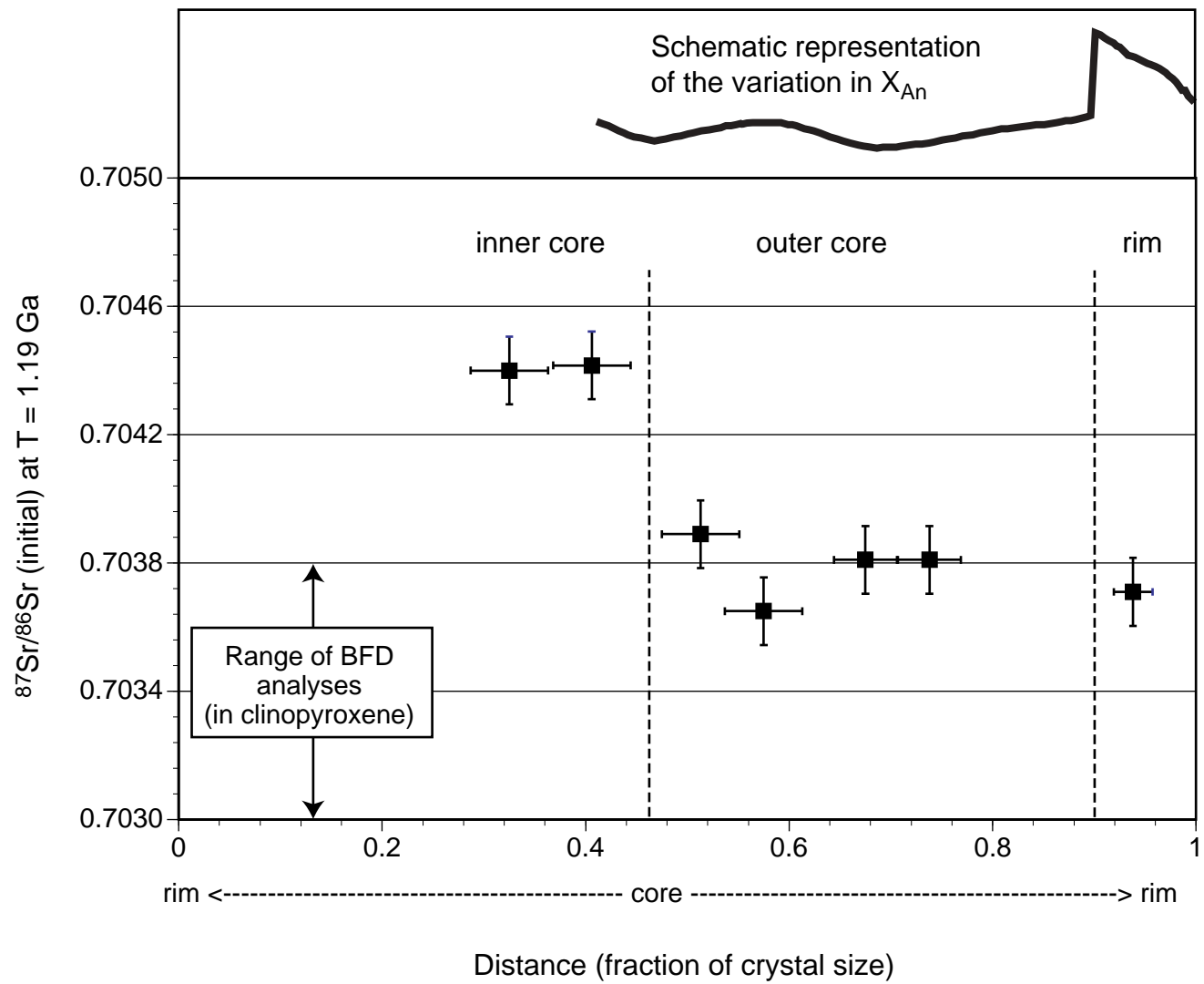


Fig. 9

Fig. 10

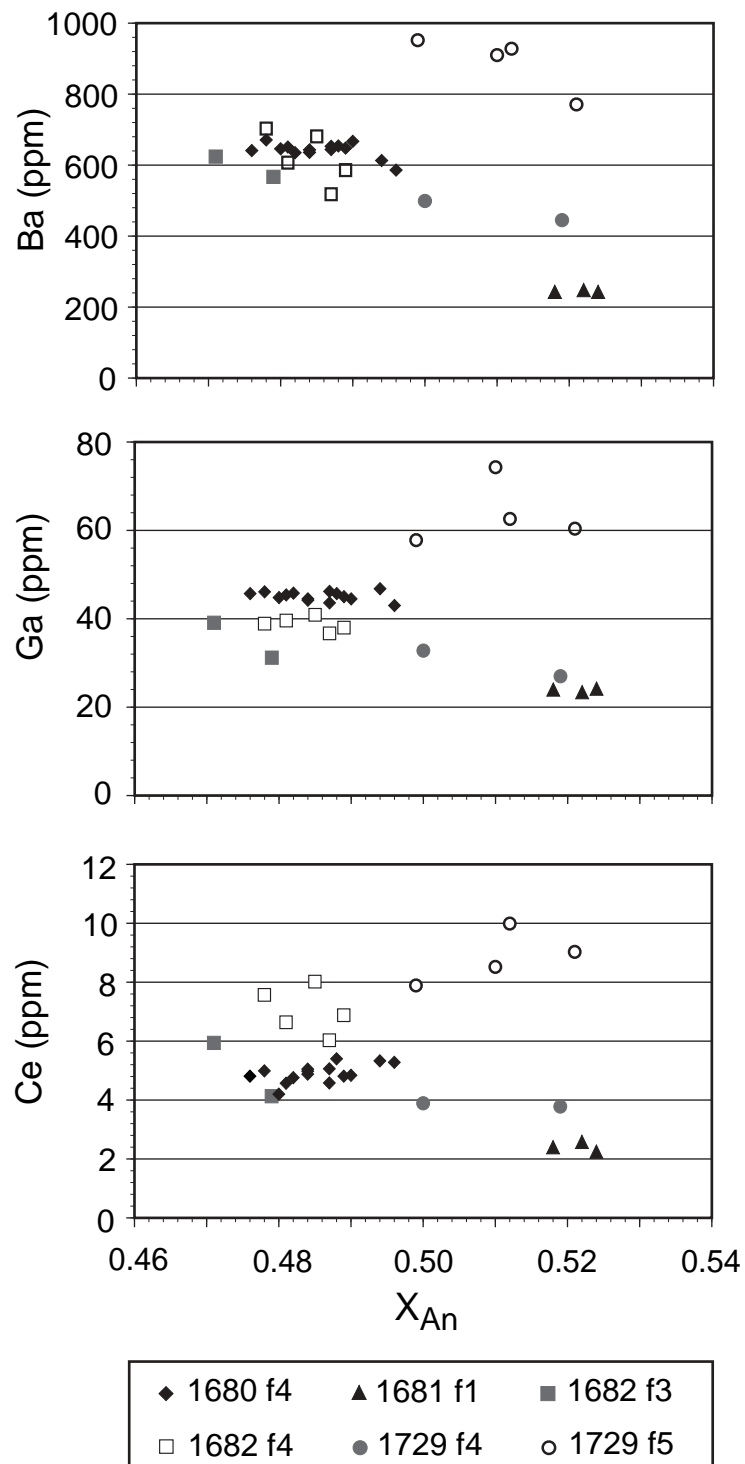


Fig. 11

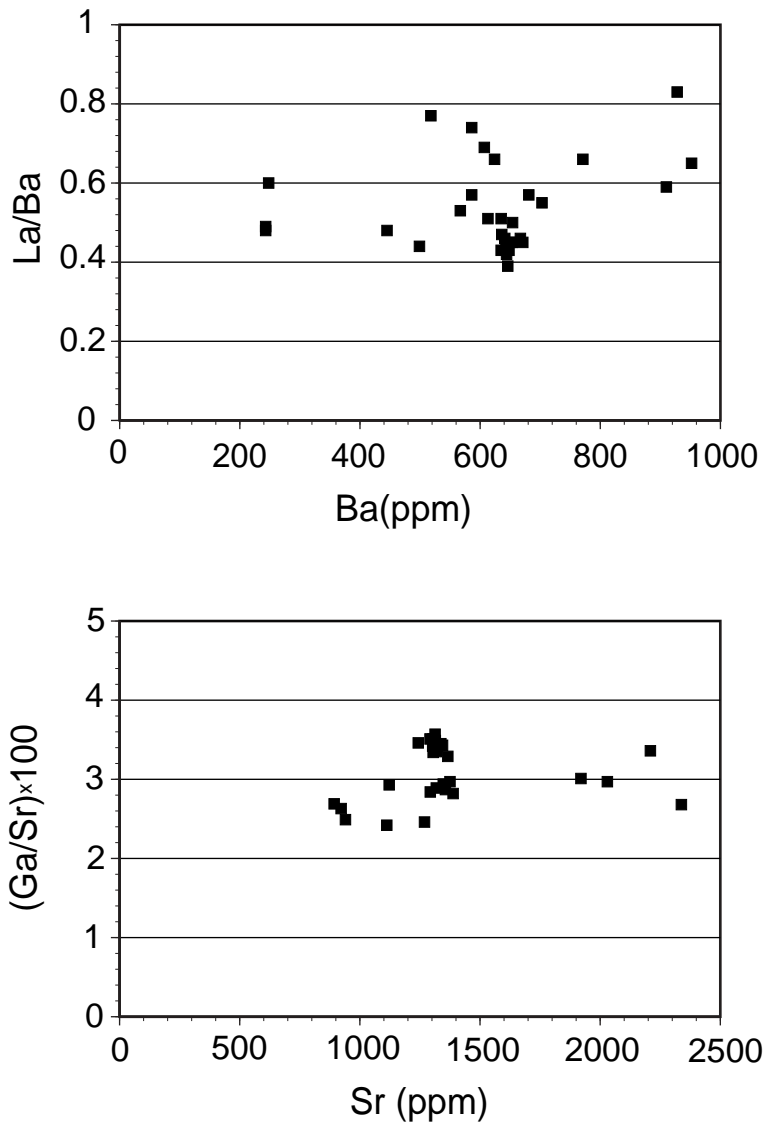
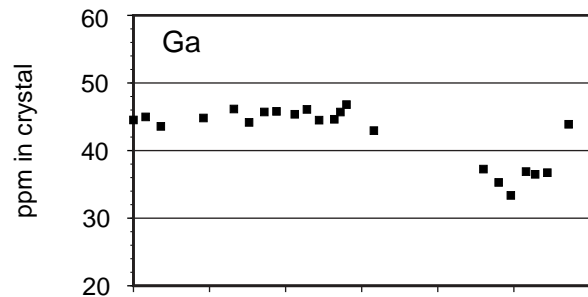
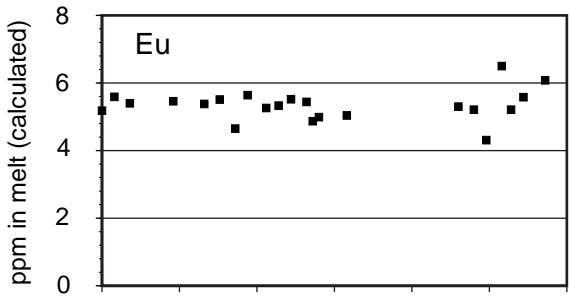
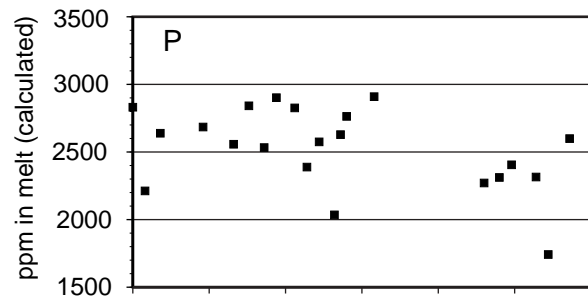
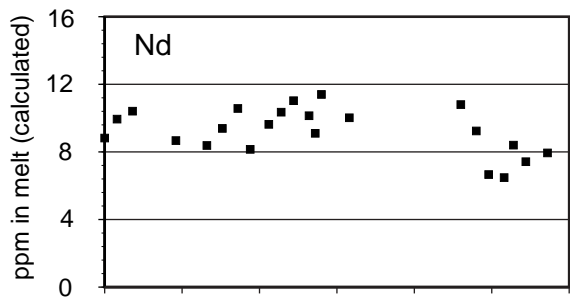
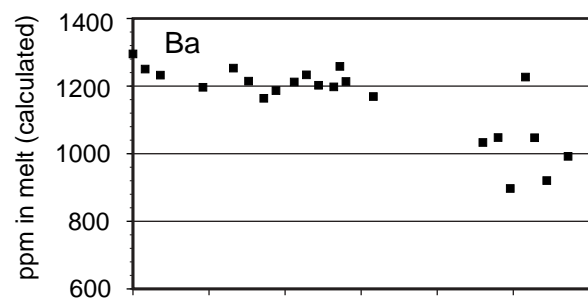
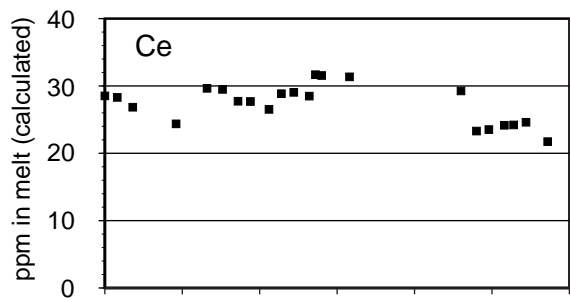
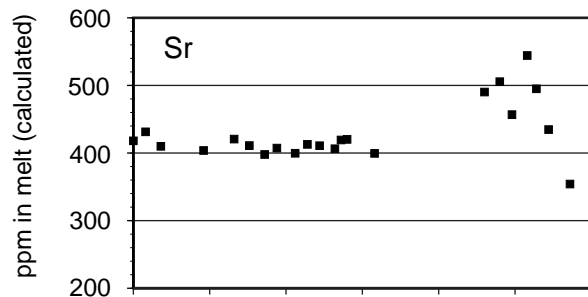
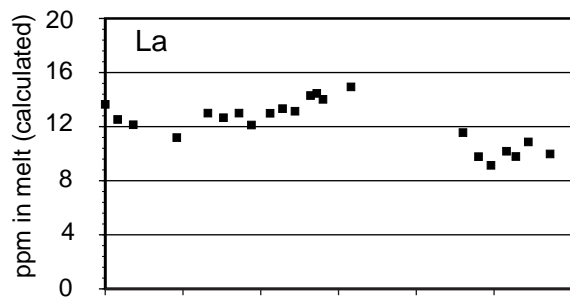
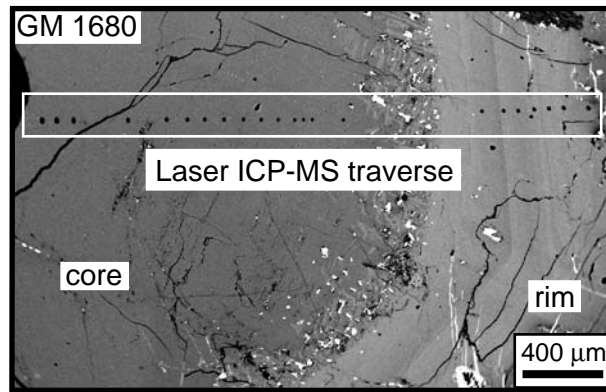


Fig. 12



Kapitel 4:

Petrologische und geochemische Untersuchungen an dem Karbonatit – Nephelin-Syenit Komplex von Grønnedal-Ika

Manuskript-Titel:

The Grønnedal-Ika carbonatite-syenite complex, South Greenland: An origin involving liquid immiscibility

Autoren:

Ralf Halama¹, Torsten Vennemann², Wolfgang Siebel¹, Gregor Markl¹

¹ Institut für Geowissenschaften, Eberhard-Karls-Universität Tübingen,
Wilhelmstr. 56, D-72074 Tübingen

² Institut de Minéralogie et Géochemie, Université de Lausanne, BFSH-2, CH-
1015 Lausanne, Schweiz

Eingereicht bei:

Journal of Petrology

Eigenanteile:

a) Idee	60%
b) Datenbeschaffung	100%
c) Auswertung und Interpretation	80%
d) Ausarbeitung der Publikation	80%

ABSTRACT

The geochemistry and petrogenesis of the bimodal Grønnedal-Ika carbonatite-syenite complex from the Gardar Province, South Greenland, has been investigated in order to explore its magma source and evolution. The Grønnedal-Ika complex is dominated by layered nepheline-syenites, in which aegirine-augite, alkali feldspar and nepheline are the major mineral phases. On the basis of mineral equilibria, temperatures of 680-910 °C and silica activities of 0.28-0.43 were determined for the crystallization of the syenites. Oxygen fugacities, estimated using titanomagnetite compositions, fall between 2 and 5 log units above the fayalite-magnetite-quartz buffer during the magmatic stage and trend towards more oxidizing values above the hematite-magnetite buffer in the late- to post-magmatic stage. Chondrite-normalized REE patterns of apparently unaltered magmatic calcite in carbonatites and syenites are characterized by a general REE enrichment and a steep negative slope ($\text{La}_{\text{CN}}/\text{Yb}_{\text{CN}} = 10\text{-}70$). Calcite from the carbonatites has higher Ba (~ 5490 ppm) and lower HREE concentrations than calcite from the syenites (54-106 ppm Ba). This is consistent with the behavior of these elements during separation of immiscible silicate-carbonate liquid pairs. In the xenolithic porphyritic syenite unit, differences in trace-element compositions between relatively Mg-rich clinopyroxene cores and more Na-rich rims include higher absolute Zr, Hf, Sn, and HREE contents in the rims. These might reflect crystal-chemical controls on trace-element partitioning, but higher Zr/Hf ratios in the rims ($\text{Zr}/\text{Hf} = 45.7 - 58.8$) compared to the cores ($\text{Zr}/\text{Hf} = 31.5 - 42.1$) are interpreted to result from coexistence of a CO_2 -rich fluid/melt during rim growth.

$\epsilon_{\text{Nd}}(\text{T} = 1.30 \text{ Ga})$ values of clinopyroxene from syenites varies between +1.8 and +2.8, and $\epsilon_{\text{Nd}}(\text{T})$ values of whole-rock carbonatites range from +2.4 to +2.8. Calcite from the carbonatites has $\delta^{18}\text{O}$ values of 7.8 ‰ to 8.6 ‰ and $\delta^{13}\text{C}$ values of -3.9 ‰ to -4.6 ‰. $\delta^{18}\text{O}$ values of clinopyroxene separates from the nepheline syenites range between 4.2 ‰ and 4.9 ‰. The average oxygen isotopic composition of the nepheline syenitic melt was calculated to be 5.7 ± 0.4 ‰. Nd and C-O isotope data are typical for mantle-derived rocks and do not indicate significant crustal assimilation for syenites and carbonatites. The difference in $\delta^{18}\text{O}$ between calculated syenitic melts and carbonatites and the overlap in ϵ_{Nd} values between carbonatites and syenites are consistent with a derivation of the carbonatites from the syenites via liquid immiscibility.

INTRODUCTION

Carbonatites typically occur in close association with alkaline silicate igneous rocks, either in individual complexes or in regional association within magmatic provinces (e.g. Harmer, 1999). However, the relationship between carbonatites and their associated silicate rocks are complex and not completely understood (e.g. Bell, 1998; Bell *et al.*, 1998). Proposed models for the generation of carbonatites include direct melting of a carbonate-bearing mantle source (e.g. Wyllie & Huang, 1976; Dalton & Presnall, 1998; Harmer & Gittins, 1998; Moore & Wood, 1998), derivation by immiscible separation from carbonated silicate melts (e.g. Koster van Groos & Wyllie, 1963; Freestone & Hamilton, 1980; Kjarsgaard & Hamilton 1988; Brooker, 1998; Kjarsgaard, 1998; Bühn & Trumbull, 2003) and crystal fractionation of a carbonated alkali silicate melt (e.g. Lee & Wyllie, 1994; Korobeinikov *et al.*, 1998; Veksler *et al.*, 1998a). For the origin of the associated silicate rocks, proposed models include low degrees of partial melting of a metasomatized mantle (e.g. Varne, 1968; Olafsson & Eggler, 1983) and crystallization from a liquid generated by melting of fenitized country-rocks (e.g. Woolley, 1987; Kramm, 1994). Clearly, each carbonatite-syenite complex should be evaluated on its own merits (Bell *et al.* 1998), but there is still a lack of robust criteria that can be used to distinguish carbonatitic melts directly derived from the mantle from those produced by differentiation of a parent silicate melt (Bell, 1998). In this study, we apply criteria discussed in the literature and evaluate new geochemical and petrologic data in order to investigate the petrogenesis of the Grønnedal-Ika nepheline syenite – carbonatite complex in the Gardar Province, South Greenland. Furthermore, data from the Grønnedal syenites will be compared to other well-studied igneous rocks of the Gardar Province that are not associated with carbonatites in order to determine which parameters were important for the carbonatites to develop. In particular, these include silica-undersaturated rocks of the Ilímaussaq complex (Larsen, 1976; Marks & Markl, 2001; Markl *et al.*, 2001), silica-oversaturated rocks of the Puklen intrusion (Marks *et al.*, 2003), and the Eriksfjord Formation (EF) basalts (Halama *et al.*, 2003).

PREVIOUS WORK AND GEOLOGICAL SETTING

The first detailed account on the Grønnedal-Ika complex was given by Callisen (1943), who established the intrusive character of the alkaline rocks. Emeleus (1964) reconstructed the history of

the complex based on detailed mapping and petrographic observations. Later, Gill (1972a,b) and Bedford (1989) obtained numerous geochemical data on minerals and whole-rocks of the complex and associated phonolite dykes. Mainly on the basis of whole-rock REE and other trace-element data, Bedford (1989) proposed an origin of the Grønnedal carbonatites via liquid immiscibility from a conjugate nepheline syenitic liquid. Pearce *et al.* (1997) published C, O and Sr whole-rock isotope data from Grønnedal and concluded that the syenites and carbonatites are unrelated due to differences in C and O isotopic compositions.

The Grønnedal-Ika intrusion (Fig. 1) is 8 x 3 km large and consists predominantly of layered nepheline syenites which were intruded by a xenolithic syenite and a plug of carbonatite (Emeleus, 1964). The complex was emplaced into the border zone between the Ketilidian mobile belt to the south and the Archean block to the north. Country rocks comprise quartzo-feldspathic gneisses and occasional amphibolites (Bedford, 1989). Based on Rb-Sr isotope data, the Grønnedal-Ika complex was dated at 1299 ± 17 Ma (Blaxland *et al.*, 1978), which is consistent with field observations indicating that the emplacement of the complex precedes the suite of olivine dolerite dykes (“Brown Dikes”) for which an U-Pb age is 1280 ± 5 Ma (Upton *et al.*, 2003). Marginal syenites show complex field relations and grade inwards to laminated nepheline syenites (Pearce *et al.*, 1997). The layered and laminated syenites formed part of a layered intrusion and mainly consolidated by bottom accumulation and adhesion to steep-sided cooling surfaces (Emeleus, 1964). The original structure of the intrusion comprises two series of layered syenites, the Lower Series and the Upper Series, which are separated by a raft of gneiss (Emeleus, 1964). In the Lower Series syenites, xenoliths of broadly gabbroic composition were found. Porphyritic microsyenites (PMS) occur as dykes and cut across earlier units of the complex. The xenolithic porphyritic syenite (XPS) is the youngest of the intrusive syenites at Grønnedal-Ika. It contains abundant xenoliths of earlier syenites, trachytes, gneisses and amphibolites and according to Bedford (1989) it represents the conjugate silicate liquid in a possible carbonate-silicate liquid immiscibility process. Finally, a central plug of calciocarbonatite was emplaced (Emeleus, 1964; Pearce *et al.*, 1997). There are three major and several smaller outcrops of carbonatite within the nepheline syenites, thought to have belonged to one central plug (Emeleus, 1964). The carbonatite is xenolithic with fragments of syenites and other rocks and invades the surrounding syenites as dykes, sheets or irregular bodies.

Towards the centre of the carbonatite, the amount of siderite increases. Large amounts of magnetite occur where mafic dykes cut the siderite-rich part of the carbonatite (Emeleus, 1964). The syenites in the invaded zones are altered and impregnated by calcite. Sodalite veins occur in various units of the complex, most likely derived from an orthomagmatic carbonatitic Na- and Cl-rich fluid as commonly present in other carbonatite complexes (Bühn *et al.*, 2002). There is no field evidence for a significant time gap between the emplacement of the syenites and the carbonatite. The last magmatic activity at about 1280 Ma is represented by a variety of dykes, including lamprophyres, porphyritic dolerites and several large olivine dolerites, which intrude the complex. Trachytic, phonolitic and other alkaline dykes were emplaced during renewed magmatic activity at later Gardar times. Intense faulting took place largely following but in part contemporaneous with the intrusion of these dikes (Emeleus, 1964).

The carbonatites of Grønnedal represent the most significant single occurrence of this rock-type in the Gardar province. Other major carbonatite occurrences in the province are carbonatitic dykes associated with nepheline syenites at Igaliko (Pearce & Leng, 1996) and volcanic carbonatites at Qassiarsuk (Andersen, 1997).

PETROGRAPHY

Syenites

The syenites of the Grønnedal-Ika complex are petrographically variable and several distinct intrusive phases can be distinguished (Emeleus, 1964). However, gradational relationships between different rock types within intrusive units are common (Callisen, 1943; Emeleus, 1964) and for the purpose of this study, a division into three main units (Lower Series, Upper Series and Late Syenites) is considered to be sufficient. The Late Syenites comprise the porphyritic microsyenite and the xenolithic porphyritic syenite. For a detailed description of the syenitic rock types, the reader is referred to the excellent work of Emeleus (1964) and Bedford (1989).

The major mafic silicate in the syenites is euhedral to subhedral or poikilitic clinopyroxene. In the XPS, clinopyroxene phenocrysts reach up to 2 mm in length and show a marked discontinuous zoning, whereas matrix clinopyroxene grains are considerably smaller (< 200 µm) and optically unzoned (Fig. 2a,b). Clinopyroxenes in the layered syenites may occur as accumulations and are

commonly rimmed by intercumulus biotite (Fig. 2c). Amphiboles are very scarce in the syenites of Grønnedal-Ika (Bedford, 1989), but they occasionally occur as poikilitic or as subhedral intercumulus grains. Only one sample (GM 1531) was investigated where poikilitic amphibole is the dominant mafic silicate phase (Fig. 2d).

All syenites of the Grønnedal-Ika complex are nepheline-bearing (Emeleus, 1964), and nepheline usually occurs as euhedral prisms (Fig. 2a-c). It is often replaced by the alteration products “gieseckite” (fibrous, micaceous aggregates) and cancrinite (Fig. 2e). Cancrinite also occurs as individual grains apparently not related to nepheline. The abundant platy crystals of alkali feldspar frequently show perthitic exsolution. Alkali feldspar phenocrysts up to 1 cm in length occur in the PMS and the XPS (Fig. 2a). Primary magmatic titanomagnetite is relatively rare, but biotite is usually interspersed with presumably late- to post-magmatic hematite. Minor phases present include short prismatic apatite (Fig. 2c), zircon, blue sodalite, analcite, calcite and fluorite. Calcite appears to be a primary magmatic or late magmatic interstitial phase and not an alteration product (Fig. 2e). Sodalite can occur as small, interstitial grains, partly associated with cancrinite (Bedford, 1989), or as larger aggregates in almost pure sodalite veins.

Carbonatites

The carbonatites consist essentially of varying amounts of calcite, siderite and magnetite. Magnetite is thought to be secondary after original siderite as a result of decarbonation and oxidation in the vicinity of the dolerite dykes (Bedford, 1989). In places, anhedral to subhedral calcite crystals form almost 100% of the rock (Fig. 2f). Individual calcite crystals are 50-500 μm in diameter and commonly show prominent twinning. Siderite occurs as euhedral rhombs or as minute grains and is commonly rusty-brown due to alteration to iron oxides. In the siderite-bearing samples, calcite grains tend to have a cloudy appearance. Minor quantities of apatite, sphalerite, pyrite, strontianite, monazite, pyrochlore, feldspar and alkali amphibole are also present in some samples (Emeleus, 1964; Bedford, 1989; Bondam, 1992). The Grønnedal-Ika carbonatite is poor in U-Th-Nb-REE minerals compared to other carbonatites of the world. It can be classified as calcite carbonatite and calcite-siderite carbonatite (Woolley & Kempe, 1989) or, on the basis of whole-rock geochemical

data with a maximum of 23.1 wt.% Fe₂O₃ (Bedford, 1989), as calciocarbonatite and ferrocronatite (Woolley, 1982).

ANALYTICAL METHODS

Electron microprobe analysis

Mineral compositions were determined using a JEOL 8900 electron microprobe (EMP) at the Institut für Geowissenschaften, Universität Tübingen, Germany. An internal $\phi\rho z$ correction of the raw data was applied (Armstrong, 1991). Both natural and synthetic standards were used for major and minor elements. Measuring times were 16 s and 30 s on the peak positions for major and minor elements, respectively. The emission current was 15 nA and the acceleration voltage 15 kV. For nepheline analyses, a beam diameter of 5 μm was used to avoid errors resulting from diffusion of Na. Feldspars with microperthitic exsolution were measured with a 20 μm wide beam and an average of 2-4 analyses was taken as representative for the respective grain. The bulk compositions of oxy-exsolved titanomagnetite grains were reconstructed by combining image processing (NIH Image software) of back-scattered electron images of the exsolved grains with point analyses of exsolved ilmenite and magnetite according to the method described in Marks & Markl (2001).

Laser ICP-MS *in situ* trace-element measurements

In situ laser ablation inductively coupled plasma-mass spectrometer (LA-ICP-MS) trace-element analyses on ~ 150 μm thick polished sections were performed at the EU Large-Scale Geochemical Facility (University of Bristol) using a VG Elemental PlasmaQuad 3 + S-Option ICP-MS equipped with a 266 nm Nd-YAG laser (VG MicroProbe II). The laser beam diameter at the sample surface was approximately 20 μm . Analyses of calcite were carried out in a beam rastering mode since ablation of calcite proceeded rapidly. Details of the data acquisition are described elsewhere (Halama *et al.*, 2002). The precision of trace-element concentrations, based on repeated analyses of standards, is approximately $\pm 5\%$ for element concentrations >10 ppm and $\pm 10\%$ for concentrations <10 ppm. Typical detection limits for most trace-elements in this study were 0.1 - 1 ppm, except for

Sc, Co and Zn with detection limits in the range of 1-5 ppm. For the REE, detection limits were generally < 0.5 ppm.

Oxygen and carbon isotope analysis

The oxygen isotope composition of hand-picked clinopyroxene separates was measured using a method similar to that described by Sharp (1990) and Rumble and Hoering (1994). 1 - 2 mg of hand-picked clinopyroxene were loaded onto a Pt-sample holder. The sample chamber was pumped out to a vacuum of about 10^{-6} mbar and pre-fluorinated overnight. Samples were then heated with a CO₂-laser in an atmosphere of 50 mbars of pure F₂. Excess F₂ is separated from O₂ by conversion to Cl₂ using KCl held at 150°C. The extracted O₂ is collected on a molecular sieve (13X). Oxygen isotopic compositions were measured on a Finnigan MAT 252 mass spectrometer at the Institut für Geowissenschaften, Universität Tübingen. The results are reported as the per mil deviation from Vienna Standard Mean Ocean Water (V-SMOW) in the standard δ -notation. Replicate oxygen isotope analyses of the NBS-28 quartz standard had an average precision of $\pm 0.1\%$ for $\delta^{18}\text{O}$ values. In each run, standards were analyzed at the beginning and the end of the sample set. A correction was applied to the data equal to the average of the difference between the mean measured value and the accepted value for the standard (9.64 ‰).

The carbon and oxygen isotope composition of the carbonates were measured in automated fashion using a GasBench from ThermoFinnigan connected directly to a Finnigan MAT 252 mass spectrometer. The method is described in detail in Spötl & Vennemann (2003). About 200-400 μg of sample material was recovered as powder by micro-drilling into the calcite. CO₂ obtained by reaction of the carbonates with several drops of 100% orthophosphoric acid is carried via a He-stream over traps to remove water vapors and a GC-column to separate CO₂ from possible interfering gases before it is passed into the mass spectrometer for isotopic analyses. The C- and O-isotope composition is reported in the standard δ -values, relative to PDB and V-SMOW, respectively, with standard analytical errors of $\pm 0.1 \%$ (1 σ) for C and O.

Nd isotope analysis

For Nd isotope analyses, 15-20 mg of hand-picked clinopyroxene, 5-8 mg of carbonatite and 40 mg of basement whole-rock powder were used. Details of the analytical procedures are described elsewhere (Halama *et al.*, 2003). $^{143}\text{Nd}/^{144}\text{Nd}$ ratios were normalized for mass fractionation to $^{146}\text{Nd}/^{144}\text{Nd} = 0.7219$. The average $^{143}\text{Nd}/^{144}\text{Nd}$ ratio obtained for the Ames Nd-standard (Geological Survey of Canada, Roddick *et al.*, 1992) was 0.512119 ± 10 ($n = 42$) during the course of this study. $^{143}\text{Nd}/^{144}\text{Nd}$ ratios have been cross-checked with the La Jolla Nd-standard which gave 0.511831 ± 30 ($n = 12$). The total procedural blank (chemistry and loading) was < 100 pg for Nd.

RESULTS

Mineral chemistry

A comprehensive database on mineral compositions of Grønnedal-Ika is given by Bedford (1989), and is augmented below by the new data on selected minerals relevant to the present work.

Feldspar

Typical feldspar analyses of syenitic rocks are summarized in Table 1. Most feldspars show coarse perthitic exsolution into almost pure albite and orthoclase. Some samples contain feldspar with exsolution on the μm -scale so that the original composition could be obtained using a defocused beam. These compositions are fairly homogeneous throughout the different rock types and vary in the range $\text{An}_{0.1-0.9}\text{Ab}_{38.9-53.6}\text{Or}_{46.1-60.2}$.

Nepheline

Nepheline is chemically unzoned and its composition is fairly homogeneous within the specific samples and also within the whole sample suite, including the PMS and the XPS (Table 1). There are also no significant compositional differences between phenocrysts and matrix nephelines. The compositional variability of nepheline covers the range $\text{Ne}_{73-68}\text{Ks}_{20-15}\text{Qz}_{7-16}$. FeO and CaO contents in nepheline of all rock types is invariably < 1 wt.% and < 0.1 wt.%, respectively.

Clinopyroxene

Typical clinopyroxene compositions are summarized in Table 2 and compositional trends are shown in Fig. 3a-c. In some samples, clinopyroxene shows a weak, patchy zonation with a fairly restricted compositional variability. Other samples contain clinopyroxenes with a marked growth zonation and the compositional range can be as large as in the whole sample suite. The clinopyroxene phenocrysts in the XPS are characterized by a relatively Mg-rich core overgrown by a distinctly more Na-rich rim with a compositional gap in between (Fig. 3c). In general, most clinopyroxenes can be classified as aegirine-augites (Morimoto *et al.*, 1988), but relatively Mg-rich diopside and Na-rich aegirine also occur. In the layered syenites of the Lower and Upper Series, compositions vary between $\text{Di}_{56}\text{Hed}_{34}\text{Aeg}_{10}$ and $\text{Di}_3\text{Hed}_2\text{Aeg}_{95}$. The most primitive core compositions in the XPS reach values of $\text{Di}_{57}\text{Hed}_{29}\text{Aeg}_{14}$, whereas the most evolved rims are of the composition $\text{Di}_7\text{Hed}_{22}\text{Aeg}_{71}$. Matrix clinopyroxene compositions in the XPS overlap with more evolved phenocryst rim compositions. In the gabbroic xenolith, clinopyroxene compositions show a small range of $\text{Di}_{65-59}\text{Hed}_{30-36}\text{Aeg}_5$. In comparison with compositional trends from other alkaline complexes of the Gardar Province (Fig. 3d), the extreme enrichment in Fe^{2+} at low values of Na, as seen in Ilímaussaq (Larsen, 1976) and Igdlarfígssalik (Powell, 1978), is lacking in Grønnedal. However, alkaline rocks from Uganda (Tyler & King, 1967) and Brazil (Gomes *et al.*, 1970) show enrichment in Na and Fe^{3+} starting at even lower levels of Fe^{2+} -enrichment (Fig. 3d).

Two typical core-to-rim zoning profiles of clinopyroxene phenocrysts from the XPS are shown in Fig. 4. In both profiles, the core composition remains constant for all major elements, except for some Na-enrichments along cracks. At the core-rim boundary, there is a significant decrease of Ca, Mg and Al, whereas Na and Fe^{3+} concentrations increase. The rim compositions are more variable, but nevertheless some general trends can be detected. Towards the edge of the crystal, Na and Fe^{3+} continuously increase, whereas Al stays constant. Both Mg and Ca decrease outwards in the rim of crystal 1 (GM 1496; Fig. 4c), whereas there is an only slight decrease in Ca at almost constant Mg in the rim of crystal 2 (GR 51; Fig. 4d).

Amphibole

Amphiboles in the syenites belong to the sodic-calcic group with compositions between taramite and katophorite (nomenclature after Leake *et al.*, 1997). Two typical analyses are reported in Table 2. The F content in the amphibole reaches up to 1.2 wt.%, whereas the Cl content does not exceed 0.04 wt.%. Amphibole separated from sample GM 1531 for isotope analysis has katophoritic composition.

Fe-Ti oxides

Primary magmatic titanomagnetite is characterized by a trellis-type oxy-exsolution texture (terminology after Buddington & Lindsley, 1964) into magnetite and lamellae of the hematite-ilmenite-pyrophanite solid solution series (Fig. 5a,b). The compositional variation in the lamellae ($\text{Ilm}_5\text{Pyr}_{93}\text{Hem}_2 - \text{Ilm}_{56}\text{Pyr}_{23}\text{Hem}_{21}$) is in contrast to the constant composition of the magnetite ($\text{Mag}_{98.99}\text{Usp}_{1.2}$). Reintegrated oxide compositions vary from $\text{Mag}_{61}\text{Usp}_{39}$ to $\text{Mag}_{72}\text{Usp}_{28}$ (Table 3). Except for MnO contents of up to 11.3 wt.%, concentrations of minor elements in the reintegrated oxides are low ($\text{Al}_2\text{O}_3 \leq 0.12$ wt.%, $\text{MgO} \leq 0.03$ wt.%, $\text{ZnO} \leq 0.24$ wt.%). Late- to post-magmatic hematite associated with biotite has almost a pure hematite endmember composition (Table 3, Fig. 5c).

Other minerals

Chemical characteristics of other minerals relevant to the present study are shortly summarised here from Bedford (1989). Sodalite contains around 8 wt.% Cl and only minor amounts (< 0.3 wt.%) of S. Cancrinite (Fig. 5d), with the ideal structural formula (Sirbescu & Jenkins, 1999) $\text{Na}_6\text{Ca}_2[\text{Al}_6\text{Si}_6\text{O}_{24}](\text{CO}_3)_2+n\text{H}_2\text{O}$, has also very low (< 0.15 wt.%) concentrations of S and shows some exchange of Ca for Na. Calcite in the syenites is almost pure CaCO_3 .

Trace-elements

Calcite

Chondrite-normalized REE patterns of calcites are shown in Fig. 6a. Three different patterns can be distinguished in the calcites from the carbonatites. One sample (GM 1502) contains calcite

characterized by a steep REE pattern with high LREE abundances (type A). The overall REE enrichment of this sample is within the lower range of whole-rock analyses from the Grønnedal carbonatite and typical of carbonatites in general (Woolley & Kempe, 1989). There is a slight positive Eu anomaly present ($\text{Eu}/\text{Eu}^* = 1.25$) and the degree of LREE enrichment relative to the HREE expressed as $\text{La}_{\text{CN}}/\text{Yb}_{\text{CN}}$ is ~ 69 . Two distinct types of REE patterns occur in calcite of the other sample (GM 1498), and both show a depletion in LREE relative to the pattern of sample GM 1502 (Fig. 6a). The main characteristic of the type B REE pattern is a convex-upward shape. In contrast, calcite type C has about one order of magnitude lower normalised LREE and MREE abundances and an almost continuous increase from very low LREE abundances towards the HREE. Interstitial calcite from two syenitic samples shows LREE-enriched patterns similar to type A, but with slight negative Eu anomalies ($\text{Eu}/\text{Eu}^* = 0.66$) and a flatter slope ($\text{La}_{\text{CN}}/\text{Yb}_{\text{CN}} = 10.5 - 26.3$). In a similar fashion, the slope of the XPS matrix is flatter than the one of whole-rock carbonatites (Fig. 6a). Trace-element data reveal that Sr, Ba, Pb, Y and Ga occur in significant amounts in the calcites (Table 4). The presumably altered calcites show marked peaks in Pb and Sr. Compared to the calcites from the syenites, calcite type A (GM 1502) is characterized by a relative enrichment of Ba, Sr, Eu and Ga (Fig. 7a). All calcites have very low concentrations of the HFSE, mostly below the detection limits.

Clinopyroxene

Some REE and trace-element abundances in clinopyroxene and amphibole of Grønnedal-Ika are reported by Marks *et al.* (in preparation), who show that the crystal chemistry of an individual clinopyroxene plays a major role in determining the relative trace-element abundances. In this study, we concentrate on additional data of clinopyroxene phenocrysts from the XPS to evaluate whether certain features in trace-element abundances characteristic of a silicate-carbonate liquid immiscibility process can be detected. Typical trace-element concentrations of cores and rims are summarized in Table 4. Chondrite-normalized REE diagrams (Fig. 6b) indicate some distinct differences between core and rim compositions. Core patterns are characterized by a smooth increase in normalized abundances from La to Nd and a smooth decrease from Nd to Tm or Yb that is completed by a slight increase towards Lu. $\text{La}_{\text{CN}}/\text{Yb}_{\text{CN}}$ ratios in the core range from 4.7 to 6.9 and

Eu anomalies are slightly positive with values between 1.02 and 1.37. In the Na-rich phenocryst rims, REE patterns are sinusoidal with generally lower LREE and higher HREE abundances than in the cores (Fig. 6b). $\text{La}_{\text{CN}}/\text{Yb}_{\text{CN}}$ range between 0.32 and 0.75. Eu anomalies in the rims are not significantly different from those in the cores and vary from 0.99 to 1.24.

Trace-element patterns of clinopyroxene cores and rims normalized to primitive mantle values (McDonough & Sun, 1995) are shown in Fig. 7b. A principal feature of all patterns are strong negative Pb and Ti spikes and a depletion in Ba, Sc, V, and Co. Negative Sr spikes are present in all patterns except for two phenocryst cores. These two are also characterized by the lowest Zr and Hf values. All rim compositions have strong positive Zr, Hf, and Sn, but negative Li anomalies. In comparison with the core compositions, rims are also enriched in Zn, but depleted in Rb, Co, and Sc. All rim patterns are very similar to those of aegirine-augites from the layered syenites both in enrichment level and shape (Fig. 7b). Aegirines from the Ilímaussaq intrusion have much lower absolute trace-element concentrations, but their pattern shape has a striking similarity to the one of the phenocryst rims, except for Li.

Ratios of geochemical twin elements were investigated in order to identify characteristic differences between the growth of clinopyroxene cores and rims (Fig. 8). Zr/Hf ratios in the cores vary between 31.5 and 42.1, i.e. they scatter around the primitive mantle value of 37.1 (McDonough & Sun, 1995). In the rims, however, Zr/Hf ratios are higher than in the cores with values ranging from 45.7 to 58.8. In contrast, Y/Ho ratios in each individual phenocryst are slightly higher in the cores (Y/Ho = 19.6 – 22.7) compared to the rims (Y/Ho = 16.8 – 20.5). Nb/Ta ratios scatter a lot and there is no consistent relation between core and rim compositions.

Carbon and oxygen isotope analyses

Pearce *et al.* (1997), Goodenough (1997) and Taubald *et al.* (submitted) presented C and O isotopic data from Grønnedal which are augmented by data of this study (Table 5). In the present suite of samples, oxygen isotope composition of calcite ranges from 7.8 ‰ to 8.6 ‰ and carbon isotope composition varies between – 3.9 ‰ and – 4.7 ‰. Our data overlap with the data from the literature. They are shown in Fig. 9, together with the field of primary, unaltered carbonatites as

proposed by Taylor *et al.* (1967). The C and O isotopic data of Grønnedal carbonates are within the upper half of the primary carbonatite field of Taylor *et al.* (1967).

Recent oxygen isotope studies have shown that individual coarse-grained minerals are less sensitive to low-T alteration and secondary water take-up than whole-rock samples (e.g. Vroon *et al.*, 2001). Extensive studies of mineral separates from ocean island basalts (Eiler *et al.*, 1997) and oceanic-arc lavas (Eiler *et al.*, 2000a) demonstrated that analyses of mineral separates consistently span a narrower range than comparable whole-rock data. At Grønnedal, whole-rock oxygen and carbon isotope data were used as an argument against liquid immiscibility between syenites and carbonatites because of distinct differences in $\delta^{18}\text{O}_{\text{V-SMOW}}$ and $\delta^{13}\text{C}_{\text{PDB}}$ (Pearce *et al.*, 1997). To evaluate this argument in the view of mineral data, the oxygen isotope compositions of fresh magmatic clinopyroxene and amphibole in the syenites were measured (Table 5).

The oxygen isotopic composition of clinopyroxene from the syenites varies from 4.2 ‰ to 4.9 ‰ and that of amphibole ($\delta^{18}\text{O} = 4.7$ ‰) is within this range. The average $\delta^{18}\text{O}$ value of clinopyroxene from the layered syenites is $4.6 \text{ ‰} \pm 0.2 \text{ ‰}$ (1σ). There is no significant isotopic compositional difference between the layered syenites and the late syenites. It was not possible to analyse core and rim compositions in the clinopyroxenes from the XPS separately, but from petrographic observations the proportion of rim composition in the clinopyroxene population should be relatively small compared to the core composition. $\delta^{18}\text{O}$ values of clinopyroxene from the XPS are in the lower range of the entire data set. With $\delta^{18}\text{O} = 5.1$ ‰, clinopyroxene from the gabbroic xenolith is slightly, but significantly higher than in the syenites.

Nd isotope analyses

Nd isotopic analyses of mineral separates and whole-rock samples are presented in Table 6. $\epsilon_{\text{Nd}}(\text{T})$ values were calculated for $\text{T} = 1300$ Ma which is the age of the complex derived from a Rb-Sr isochron (Blaxland *et al.*, 1978). They range from +1.8 to +2.8 for the syenites and from +2.4 to +2.8 for the carbonatites. The average $\epsilon_{\text{Nd}}(\text{T})$ of the carbonatites (2.59 ± 0.20) is slightly higher, but not significantly different from the average of the syenites (2.36 ± 0.40). Thus, the Nd isotopic composition of the Grønnedal-Ika complex appears to be very homogeneous. Plotted in a Sm-Nd

isochron diagram (Fig. 10), all analyses of the mafic minerals and the carbonatites scatter closely around the 1300 Ma reference line. A distinctly lower $\epsilon_{\text{Nd}}(\text{T})$ value than those typical for the syenites was obtained for clinopyroxene from the gabbroic xenolith ($\epsilon_{\text{Nd}}(\text{T}) = -1.7$). A whole-rock sample of macroscopically relatively unaltered basement gneiss has $\epsilon_{\text{Nd}}(\text{T}) = -13.3$.

CALCULATION OF PHYSICO-CHEMICAL PARAMETERS

Temperature, silica activity and oxygen fugacity in the nepheline syenites

The quantification of intensive crystallization parameters can be used to distinguish separate phases in the evolution of complex or individual units. Furthermore, the determination of equilibration temperatures is important for obtaining accurate estimates of the oxygen isotope composition of the melt from mineral data because mineral-melt isotopic exchange is temperature dependent. The quantification of silica activities and oxygen fugacities is relevant for the comparison with other Gardar complexes to evaluate the possible influence of these parameters on the origin of the carbonatite.

Nepheline geothermometry after Hamilton (1961) reveals fairly homogeneous temperatures between 700-850 °C (Fig. 11). Only a few nepheline analyses poor in SiO₂ indicate temperatures as low as 500 °C, suggestive of prolonged re-equilibration (Powell, 1978).

Equilibria among Ne, Ab and Jd components in nepheline, alkali feldspar and clinopyroxene solid solutions, respectively, provide a means to estimate temperatures and silica activities in the nepheline syenites (Markl *et al.*, 2001). These equilibria are believed to reflect the conditions during formation of the last mineral in a specific assemblage (Markl *et al.*, 2001). In the absence of a reliable estimate, pressure was fixed to 1 kbar for all calculations. This value is an estimate from the Ilímaussaq intrusion further south in the Gardar Province based on fluid inclusion studies (Konnerup-Madsen & Rose-Hansen, 1984). For the nepheline syenites of Grønnedal, the following three equilibria are relevant:



Following the approach of Markl *et al.* (2001), equilibration of the magmatic mineral assemblage as long as melt is in contact with the minerals in the absence of growth zonation (feldspars and nephelines) is assumed. Accordingly, zoned clinopyroxene crystals record various stages of crystallization and the increase in Na^+ and Fe^{3+} in clinopyroxene rims and along cracks may also be influenced by oxidizing residual melt or fluid phases (Marks *et al.*, 2003). Therefore, in order to obtain reliable estimates of early magmatic T and a_{SiO_2} conditions, those clinopyroxene compositions that presumably reflect early crystallization, i.e. the most diopside-rich compositions, were used in the calculations. Activities of jadeite in clinopyroxene (a_{Jd}) were calculated after Holland (1990) at temperatures of 800, 900, and 1000 °C. For feldspars, the complete range of compositions measured was used to determine activities of albite (a_{Ab}) after Fuhrmann & Lindsley (1988), again at 800, 900, and 1000 °C. Nepheline activities (a_{Neph}) were calculated after a mixing on site model and do not show a large variation neither between nor within samples. Therefore, an average a_{Neph} for each sample was used. Input parameters and results are summarized in Table 7. The calculations with minimum and maximum values for a_{Jd} and a_{Ab} resulted in four invariant points that form a parallelogram-shaped field in the $T - a_{\text{SiO}_2}$ space (Fig. 12). These fields are considered to represent the equilibration conditions of the assemblage.

For the layered syenites and the PMS, equilibrium conditions vary from 680 to 850°C and a_{SiO_2} values of 0.28 to 0.41 (Table 7). Temperatures agree well with those obtained by nepheline geothermometry after Hamilton (1961). For the XPS, calculations were performed with clinopyroxene compositions from phenocryst cores, phenocryst rims and matrix grains, as it is not clear from petrographic observations which clinopyroxene equilibrated with nepheline and feldspar. Calculations with the most Mg-rich matrix cpx compositions indicate temperatures of 710-775 °C and silica activities of 0.28-0.36. Equilibria with Mg-rich rim compositions yield similar but slightly elevated values of a_{SiO_2} (0.32-0.43) and temperatures of 785-910°C. For both matrix and phenocryst rim compositions, calculated values of T and a_{SiO_2} overlap with the intensive parameters determined for the layered syenites. However, equilibria with typical phenocryst core compositions ($a_{\text{Jd}} = 0.08-0.12$) yield temperatures $< 550^\circ\text{C}$ at silica activities < 0.25 . It is highly unlikely that the cores grew at such low temperatures so that most probably the clinopyroxene core compositions were not in equilibrium with nepheline and alkali feldspar during growth. On the other hand, it can

be speculated that they did equilibrate with feldspar and nepheline phenocrysts as present in the rock at temperatures that must have been higher than matrix equilibration temperatures, i.e. > 900 °C. If T is fixed at 900-1000 °C, the invariant point is displaced due to the high a_{Jd} values of the core compositions towards pressures of 6.5 – 11 kbar and a high-P origin of the clinopyroxene cores might be indicated. Thus, the clinopyroxene phenocryst cores of the XPS appear to have crystallized at a distinct earlier event in the magmatic history, possibly as the only crystallizing phase or at higher P.

Oxygen fugacities in the nepheline syenites were estimated on the basis of the chemical compositions of reintegrated titanomagnetites and the independent temperature determination from Ne-Ab-Jd equilibria. In Fig. 13, theoretical buffer curves are plotted together with displaced buffer curves adjusted to the activities determined from mineral analyses. FMQ* marks the absolute minimum oxygen fugacities in the nepheline syenites since this is the position of the buffer curve if olivine with $a_{\text{Fa}} = 1$ would have been present. Additionally, the projections of tie lines connecting conjugate magnetite-ulvöspinel_{SS} and hematite-ilmenite_{SS} pairs after Buddington & Lindsley (1964) are shown for the magnetite compositions typical of the Grønnedal samples. Buddington & Lindsley (1964) note that at high temperatures Fe-Ti oxides are in equilibrium with a fluid phase due their fast reaction kinetics in hydrothermal experiments. They conclude that at a given temperature and for a known magnetite-ulvöspinel_{SS}, f_{O_2} of the fluid can be read from the graph in the f_{O_2} -T space (Buddington & Lindsley, 1964). Since this fluid phase, in turn, determines the f_{O_2} of the rock (Buddington & Lindsley, 1964), we can estimate the oxygen fugacities of the nepheline syenitic melts at their equilibration temperatures of 710-910 °C with the typical oxide compositions $\text{Mag}_{60-70}\text{Usp}_{30-20}$. They fall between +2 and +5 log units above the FMQ buffer (Fig. 13). This result agrees well with the position of the FsMQ* buffer at very low a_{Fs} values (≤ 0.01) that correspond to the virtually absent ferrosilite component in the aegirine-augites. The occurrence of presumably late-to post-magmatic hematite indicates that oxygen fugacities increased to values > 1 log unit above the HM buffer during the later magmatic evolution.

Stable isotope composition of the Grønnedal melts

Oxygen isotopes in nepheline syenites

Oxygen isotope data of mineral separates from Grønnedal-Ika and other Gardar igneous rocks (Marks *et al.*, 2003; Halama *et al.*, 2003) are plotted in Fig. 14a, together with the respective $\epsilon_{\text{Nd}}(\text{T})$ values. Compared to the EF basalts and MORB, samples from Grønnedal-Ika have slightly lower $\delta^{18}\text{O}$ values at slightly higher values of $\epsilon_{\text{Nd}}(\text{T})$. Clinopyroxene from the gabbroic xenolith overlaps with the EF basalt samples. In contrast, most mineral analyses from the silica-oversaturated rocks from the Puklen intrusion tend towards lower $\delta^{18}\text{O}$ values. In combination with the strongly negative $\epsilon_{\text{Nd}}(\text{T})$ values, the Puklen data were interpreted to reflect the prominent influence of open-system late-stage magmatic processes and assimilation of crustal material (Marks *et al.*, 2003). These factors do not seem to have affected the Grønnedal-Ika rocks. However, not only the oxygen isotopic composition of the melt, but also temperature, chemical composition of the minerals as well as the amount of crustal contamination influence $\delta^{18}\text{O}_{\text{mineral}}$ values. Therefore, it is useful to calculate $\delta^{18}\text{O}_{\text{melt}}$ from the mineral data. $\delta^{18}\text{O}_{\text{melt}}$ values can also be compared to whole-rock data because there is no oxygen isotope fractionation between whole-rocks and melts (Zhao & Zheng, 2003), given that the whole rocks are representative of melt compositions, i.e. no cumulates.

The calculation of the oxygen isotopic composition of melts from mineral data is relatively straightforward for basaltic rocks (Kalamarides, 1986), but less so for the Grønnedal samples because of lower equilibration temperatures and the formation of diopside-aegirine solid solutions. The approach taken to determine $\delta^{18}\text{O}_{\text{melt}}$ values from the mineral data is briefly described below.

Based on the nepheline-albite-jadeite equilibria, we assume that the equilibration temperature (T_{eq}) for all nepheline syenitic samples is ~ 800 °C. In a first step, the mineral-water oxygen isotope fractionation was calculated after Zheng (1993a,b) at T_{eq} . For this purpose, a typical aegirine-augite composition of $\text{Di}_{30}\text{Hd}_{40}\text{Aeg}_{30}$ was used. Secondly, the rock-water oxygen isotope fractionation of a typical nepheline syenite at T_{eq} was determined after Zhao & Zheng (2003). The two fractionation factors were then combined to derive a value for the mineral-rock oxygen isotope fractionation. For nepheline syenites at 800 °C, this value is -1.1‰ . To evaluate the error introduced by variations in mineral composition, mineral-rock fractionations were also calculated with $\text{Di}_{55}\text{Hd}_{35}\text{Aeg}_{10}$ and $\text{Di}_{15}\text{Hd}_{35}\text{Aeg}_{50}$. Resulting errors are $+0.23\text{‰}$ and -0.25‰ at 800 °C. The uncertainty in T_{eq}

introduces an additional error, which was evaluated by performing the calculations at 700 and 900 °C for a fixed $\text{Di}_{30}\text{Hd}_{40}\text{Aeg}_{30}$ composition. These errors are -0.15 ‰ and +0.11 ‰, respectively. Consequently, the overall error introduced by uncertainties in mineral composition and T_{eq} is likely to be < 0.4 ‰ and does not affect the conclusions. $\delta^{18}\text{O}_{\text{melt}}$ for the gabbroic xenolith was calculated using $\Delta_{\text{diopside-rock}} = -0.7$ ‰, based on the gabbro-water fractionation of Zhao & Zheng (2003) at 1000 °C. The $\delta^{18}\text{O}_{\text{melt}}$ values of the EF basalts were taken from Halama *et al.* (in press) who used $\Delta_{\text{clinopyroxene-rock}} = -0.3$ based on Kalamarides' (1986) approach.

Results for the syenitic melts yield an average $\delta^{18}\text{O}$ value of 5.72 ± 0.28 ‰ with a range from 5.3 ‰ to 6.3 ‰ and 5.83 ‰ for the gabbroic xenolith (Fig. 14b). These values are indistinguishable from melt compositions calculated for the EF basalts (5.5-6.3 ‰; Halama *et al.*, 2003), typical MORB glass compositions (5.37-5.81 ‰; Eiler *et al.*, 2000b) or unaltered whole-rock MORBs (5.7 ± 0.2 ‰; Harmon & Hoefs, 1995) and indicate a mantle derivation of the nepheline syenites (Table 5, Fig. 14b). In comparison with $\delta^{18}\text{O}_{\text{whole-rock}}$ data from Grønnedal syenites, the calculated $\delta^{18}\text{O}_{\text{melt}}$ values are significantly lower and more homogeneous than the data range of 8.3-15.1 ‰ given by Pearce *et al.* (1997). By comparison to $\delta^{18}\text{O}_{\text{whole-rock}}$ data from lamprophyres of the Igaliko dyke swarm (8.1-11.1 ‰; Pearce & Leng, 1996), calculated $\delta^{18}\text{O}_{\text{melt}}$ compositions are considerably lower. Finally, the position of the basaltic melt calculated from the gabbroic xenolith falls within the field defined by the EF basalts for $\delta^{18}\text{O}$.

Carbon and oxygen isotopes in carbonatites

By detecting only very small differences between whole-rock C- and O isotope values and carbonate phenocrysts at the Oldoinyo Lengai volcano, Keller & Hoefs (1995) concluded that the isotopic fractionation between carbonate phenocrysts and residual melt is very small. Therefore, we assume that $\delta^{13}\text{C}$ and $\delta^{18}\text{O}$ values in calcite are roughly equal to those in the carbonatite melt and also comparable to whole-rock data. This is confirmed by the overlap of calcite data with whole-rock data (Fig. 9). The C- and O isotope data are compatible with a primary magmatic, mantle-derived carbon and oxygen isotope composition (Fig. 9), i.e. unaffected by surficial secondary processes, although some minor late- to post-magmatic alteration was also postulated (Taubald *et al.*, submitted). The limited variation of $\delta^{18}\text{O}$ and $\delta^{13}\text{C}$ values in the Grønnedal carbonatites might be

explained in a similar way as data from Brazilian carbonatites, where variations in $\delta^{18}\text{O}$ and $\delta^{13}\text{C}$ are caused by isotopic exchange between carbonate rocks and $\text{H}_2\text{O}-\text{CO}_2$ fluids at different T with different $\text{H}_2\text{O}/\text{CO}_2$ ratios (Santos & Clayton, 1995). Alternatively, slightly elevated $\delta^{18}\text{O}$ can occur in carbonates if there is fractionation between carbonates and silicates at low T in a closed system. Carbonatitic dykes from the Igaliko dyke swarm have $\delta^{18}\text{O}$ in the same range (2.5 to 9.2 ‰; Pearce & Leng, 1996) as the Grønnedal carbonatites. However, the average of 4.7 ± 1.5 ‰ and the $\delta^{18}\text{O}$ values of those samples for which ϵ_{Nd} values are available are significantly lower, possibly due to a high-T meteoric water influence (Fig. 14b). $\delta^{13}\text{C}$ in the Igaliko carbonatites (−4.9 to −7.9 ‰) partly overlaps with the Grønnedal data.

DISCUSSION

Crystallization of the nepheline-syenites

Disseminated sodalite in the nepheline-syenites might have crystallized from the silica-undersaturated magmas at high temperature (Sharp *et al.*, 1989), but the presence of sodalite veins suggests derivation from Cl-bearing orthomagmatic carbonatitic fluids. Similarly, the abundant occurrence of cancrinite (Fig. 5d) in the nepheline-syenites suggests the interaction with a late-stage CO_2 - H_2O -bearing fluid (Sirbescu & Jenkins, 1999). Primary fluid inclusion homogenization temperatures indicate that cancrinite crystallizes at 450-650 °C at 1.1-1.5 kbar (Sobolev *et al.*, 1974). Also, experimental work also suggests that cancrinite is a moderately high-temperature mineral (Edgar, 1963). $\text{H}_2\text{O}-\text{CO}_2$ -Cl-bearing fluids have been reported from carbonatites (Bühn & Rankin, 1999), so that the fluid responsible for the precipitation of sodalite veins and cancrinite can reasonably be connected to the carbonatite. Therefore, the presence of late-magmatic cancrinite in the syenites suggests that there was no significant time gap between the emplacement of the syenites and the carbonatites.

In general, the layered syenites, the PMS and the matrix of the XPS equilibrated under very similar T- a_{SiO_2} conditions. The calculated silica activities of the Grønnedal syenites are distinctly lower than in the early augite syenite unit of Ilímaussaq ($a_{\text{SiO}_2} = 0.9 - 0.4$; Marks & Markl, 2001) and the syenitic rocks of Puklen ($a_{\text{SiO}_2} = 0.7 - 1$; Marks *et al.*, 2003). Oxygen fugacities during the early

magmatic stage appear to be distinctly higher in Grønnedal than in both the syenitic rocks from Ilímaussaq (1-5 log units below FMQ; Marks & Markl, 2001) and Puklen (1-3 log units below FMQ; Marks *et al.*, 2003). The absence of olivine and aenigmatite, which frequently occur in other Gardar complexes, is probably also related to differences in oxygen fugacity (Bedford, 1989). In the Ilímaussaq augite-syenite, there is also no indication of more oxidizing conditions during late-magmatic stages (Fig. 13). However, f_{O_2} increases during cooling relative to the FMQ buffer curve towards values above the HM buffer in the agpaiteic magmas of Ilímaussaq (Markl *et al.*, 2001) as well as in syenitic and granitic magmas of Puklen (Marks *et al.*, 2003). These trends are similar to the one observed in the Grønnedal syenites.

Based on the argument that the silica-undersaturated character of mafic alkaline lavas can be attributed to low degrees of partial melting under CO_2 -rich conditions (Mysen & Boettcher, 1975; Wyllie & Huang, 1976; Gerlach *et al.*, 1988), the very low silica activities of the Grønnedal syenites may indicate a high CO_2 content in the melt during melting and fractionation. A build-up of CO_2 is also indicated by the occurrence of calcite in the nepheline syenites. Further constraints on f_{CO_2} can be derived from the equilibrium $CH_4 + 2 O_2 = CO_2 + 2 H_2O$ at variable f_{CH_4}/f_{CO_2} ratios in the T- f_{O_2} space (Fig. 13). At an arbitrarily fixed C:H ratio of 1:2, only for $f_{CH_4}/f_{CO_2} < 0.1$ will the reaction curve approach the conditions estimated for the Grønnedal syenites from the titanomagnetite compositions. This is consistent with the commonly observed dominance of CO_2 - H_2O fluid inclusions in carbonatites (Andersen, 1986; Samson *et al.*, 1995; Bühn & Rankin, 1999). On the other hand, high f_{CH_4}/f_{CO_2} ratios > 0.9 are indicated for Ilímaussaq rocks, which is consistent with the presence of methane-bearing fluid inclusions with low CO_2 contents (Konnerup-Madsen & Rose-Hansen, 1982). The high fugacity of CO_2 would be an important prerequisite for the carbonatite formation at Grønnedal-Ika and a different f_{CO_2} in the Grønnedal parental melt could be the most important difference to the Ilímaussaq parental melt.

Criteria for carbonatite petrogenesis applied to Grønnedal-Ika

Many discussions on carbonatite petrogenesis in the literature lead to certain aspects that might be used to constrain the petrogenesis of an individual complex, and these criteria will be evaluated in this section.

Experimental investigations showed that calciocarbonatites can be produced by wallrock reaction of primary carbonate melts with harzburgitic mantle at $P < 25$ kbar (Dalton & Wood, 1993) and several alkaline complexes were interpreted to contain these so-called primary carbonatites (Harmer & Gittins, 1998). The term primary carbonatites covers carbonatites derived from little or non-fractionated carbonatitic melts in equilibrium with peridotitic mantle (Eggler, 1989). Other studies revealed that primary carbonatites are characterized by elevated Mg-numbers (Sweeney, 1994) and must have compositions dominated by calcic dolomite (Lee & Wyllie, 1998), which basically excludes calciocarbonatites as candidates for primary carbonatitic magmas. Additionally, field relations of many carbonatites, including Grønnedal-Ika, show that very often a small body of carbonatite is associated with a much larger volume of silicate rocks, which is more consistent with formation of carbonatites as residual magmas derived from associated silicate rocks (Barker, 1989). Eggler (1989) provides a set of specific criteria that could be used to recognize primary carbonatites, such as high (Mg+Fe)/Ca ratios, high Mg-numbers, moderate amounts of alkalis and a finite, not too low amount of silicate components. The whole-rock carbonatite data of Pearce *et al.* (1997) suggest that none of the Grønnedal samples satisfy these criteria because they are characterized by low amounts of MgO (< 0.8 wt.%), alkalis (< 0.5 wt.%) and silica (< 1.7 wt.% SiO₂). Thus, the bulk of evidence does not favor a primary, unfractionated origin for the Grønnedal carbonatites. Additionally, the syenites do not reflect primary mantle melt compositions, but indicate differentiation processes at crustal levels (Halama *et al.*, 2002; Bühn & Trumbull, 2003). Some experimental data (e.g. Lee & Wyllie, 1994) support a crystal fractionation model for the genesis of carbonatites, and the generation of calciocarbonatites by fractional crystallisation from ultramafic silicate – calciocarbonatite pairs was also demonstrated (Kjaarsgaard, 1998; Korobeinikov *et al.*, 1998). However, residual liquids of carbonated alkali silicate melts in experimental runs were fairly silica-rich and not carbonatitic in composition, indicating that fractionation is not a feasible mechanism for generating carbonatites from alkali silicate melts at low pressures of 0.2 and 0.5 GPa (Kjaarsgaard, 1998). It was also argued that it is unlikely that a carbonated nephelinitic magma contains enough CO₂ to allow abundant crystallization of carbonate (Gittins, 1989), although minor amounts of primary magmatic, sub-liquidus calcite can be precipitated from alkali silicate melts (Kjaarsgaard, 1998). Furthermore, fractionation cannot

generate the Nb and REE concentrations characteristic of carbonatites (Srivastava, 1997). At Grønnedal, clinopyroxene as principal mafic mineral in the syenites is bound to reduce the CaO content in the remaining melt and thus its fractionation is likely to prohibit the formation of large amounts of calcite. There is also a suspicious lack of mineralogical and chemical continuity between syenites and carbonatites at Grønnedal, something which would be expected if a fractional crystallization relationship would exist (Le Bas, 1989). Although the lack of rocks transitional in composition between carbonatites and nephelinites was generally explained by the very small P-T region in which intermediate melts are stable and their relatively high viscosity (Moore & Wood, 1998), more arguments speak against an origin of the Grønnedal carbonatites solely by fractional crystallization than for it.

Immiscible carbonate-rich magmas separated from silicate magmas tend to be concentrated near calciocarbonatite compositions (Lee & Wyllie, 1998), and liquid immiscibility is not restricted to shallow levels, but can also occur at mantle pressures of 2.5 GPa (Brooker, 1998). The strongly SiO₂-undersaturated, peralkaline character of the nepheline syenites resembles silicate liquids in some early liquid immiscibility experiments (Koster van Groos & Wyllie, 1973). Based on the higher melt-solid interfacial energy of an immiscible carbonate melt compared to the coexisting silicate melt and the resulting restricted migration capability, Minarik (1998) argues that the carbonatite should be latest in the time development of a complex, which is clearly the case in Grønnedal. Further support for liquid immiscibility comes from the overlap in $\epsilon_{Nd}(T)$ values between syenites and carbonatites (Table 6, Fig. 14) that provides evidence for a common source of these two melts. This is in agreement with published Sr isotope data, which also show similar initial $^{87}Sr/^{86}Sr$ ratios for the two rock types (Pearce *et al.*, 1997). Significant contamination with crustal material seems unlikely, as the country rock, represented by an Archean gneiss, has strongly negative $\epsilon_{Nd}(T)$ values that would cause a shift towards lower ϵ_{Nd} . The Nd isotope data show that the Grønnedal rocks are derived either from an isotopically slightly depleted, homogeneous mantle source or a mixture of at least two mantle end-members, one isotopically depleted and one less depleted or enriched. The identical $\epsilon_{Nd}(T)$ values of carbonatites and syenites would require melting of similar mantle end-members in the same proportions by different melting events, which is rather unlikely. Thus, the simplest explanation of the Nd isotope data is one involving magma

differentiation. In summary, there are a number of aspects that favor a liquid immiscibility origin for the Grønnedal carbonatites. In the following sections, it will be evaluated whether trace-element and oxygen isotope data are compatible with this hypothesis.

Evaluation of trace-element characteristics

Whole-rock trace-element data of syenites and carbonatites are consistent with a petrogenetic origin involving liquid immiscibility (Bedford, 1989; Pearce *et al.*, 1997). Experimental data on the partitioning of trace-elements between immiscible carbonate and silicate liquids at 0.8 and 0.9 kbar (Veksler *et al.*, 1998b) will be used to evaluate how certain trace-element characteristics of calcite and clinopyroxenes can be explained by this process.

Comparison of REE and other trace-element abundances of carbonatitic and syenitic calcite

The similar patterns and relative enrichment levels of calcite from sample GM 1502 and whole-rock carbonatites suggests that the relative enrichment of REE in the Grønnedal carbonatites is controlled by calcite (Fig. 6a). Since calcite phenocrysts from carbonatites have low REE abundances and almost flat patterns (Ionov & Harmer, 2002), this suggests that the Grønnedal carbonatites precipitated from residual liquids. The type B and C patterns from sample GM 1498 appear to be variably affected by postmagmatic loss of LREE due to fluid controlled recrystallization and remobilization of carbonate phases (Bau, 1991; Bau & Möller, 1992). Especially the unaltered calcite from sample GM 1502 is rich in Sr, Ba and P. These compositional features were also found in experimentally obtained immiscible carbonatite liquids at low P (≤ 0.5 kbar) by Kjaarsgaard (1998), suggesting a similar origin for the Grønnedal carbonatites. These liquids were considered as good analogue for calciocarbonatites (Kjaarsgaard, 1998) since they were also high in CaO and low in alkalis. The relatively high Ba contents of the carbonatitic calcite compared to calcite from the syenites is in agreement with experimental partitioning data between silicate liquid and carbonate that show a strong preference of Ba for the carbonate liquid liquids (Veksler *et al.*, 1998b). Negative Eu anomalies and lower Sr contents in calcite from the syenites are likely due to feldspar precipitation. The experimental data also indicate a relative preference of the LREE over the HREE for the carbonate liquid, which is qualitatively consistent with the higher

La_{CN}/Yb_{CN} ratios in calcite from the carbonatite compared to calcite from the syenites. However, the high absolute REE concentrations in the carbonatites cannot be explained by the data from liquid immiscibility experiments which show for most REE a preference for the silicate liquid. On the other hand, it was argued that REE favor carbonate liquids because REE are preferentially transported by $(CO_3)^{2-}$ - and F-complexes that are more easily formed in carbonatitic liquids (Cullers & Medaris, 1977; Möller *et al.*, 1980), and it might be possible that the experimental conditions did not reflect natural conditions in this respect.

Controlling parameters in trace-element partitioning for clinopyroxenes

A qualitative assessment of the trace-element patterns in the Grønnedal clinopyroxenes by comparison to clinopyroxenes from other Gardar complexes not associated with carbonatite reveals that there are no significant differences in trace-element contents or patterns (Fig. 7b and Marks *et al.*, in preparation). There are also no significant differences between clinopyroxene phenocryst core and rim patterns for Ba, Sr, Ti, Nb, Ta and the LREE (Figs. 6 + 7), which cannot be explained by diffusional compensation because diffusivities in clinopyroxene are generally low (Cherniak, 2001; Van Orman *et al.*, 2001). Additionally, there are also no significant differences between chemically similar phenocryst rims and other Grønnedal aegirine-augites from the layered syenites (Fig. 7). It is therefore suggested that crystal-chemical effects are dominating the trace-element partitioning behavior in these clinopyroxenes (Wood & Blundy, 1997; Blundy & Wood, 2003). Other effects, like temperature and melt chemistry, may play a subordinate role. Possible effects of a liquid immiscibility process are likely to be masked by these parameters.

Ratios of geochemical twin elements as petrogenetic indicators

Ratios of geochemical twin elements, such as Zr-Hf and Y-Ho, are used as petrogenetic indicators for comparing intrusions with and without associated carbonatites (Bühn & Trumbull, 2003). Buhn and Trumbull (2003) found, for instance, significantly higher Zr/Hf ratios in syenitic rocks associated with carbonatite compared to ones without and related these differences to the ability of CO_2 -rich fluids to fractionate Zr from Hf (Dupuy *et al.*, 1992; Irber, 1999). The Zr/Hf ratios in the clinopyroxene cores of the XPS overlap with those of the other nepheline syenites (Zr/Hf = 31-43)

and those from augite syenitic units at Ilímaussaq (Zr/Hf = 29-34) and Puklen (Zr/Hf = 30-36). Theoretically, higher Zr/Hf ratios might be due to fractionation of clinopyroxene because this mineral, like most other ferromagnesian minerals, prefers Hf over Zr (David *et al.*, 2000). However, the higher Zr/Hf ratios in the phenocryst rims are not likely due to fractionation of clinopyroxene, since both elements are mildly incompatible and effect on Zr/Hf fractionation is negligible when only one ferromagnesian mineral is present (Linnen & Keppler, 2002). Experimental evidence also shows that there is little or no Zr/Hf fractionation in alkaline depolymerized melts (Linnen & Keppler, 2002). The lower Y/Ho ratios in phenocryst rims (Fig. 8) are consistent with exsolution of a CO₂-dominated fluid, which would leave melts with successively decreasing Y/Ho ratios (Bühn & Trumbull 2003). These differences in Zr/Hf and Y/Ho ratios suggest that cores might have grown before and rims during or after the separation of a CO₂-rich fluid. A pure crystal-chemical control on these trends seems unlikely because major element compositions of clinopyroxene rims in the XPS and matrix clinopyroxene from the layered syenites are very similar.

Implications of stable isotope data on liquid immiscibility

The oxygen isotopic fractionation between immiscible silicate and carbonate melts is thought to be close to the fractionation between, for example, pyroxene and calcite (Santos & Clayton, 1995). At temperatures between 800 and 900 °C, $\Delta_{\text{calcite-cpx}}$ varies between 1.0 for aegirine and 2.1 for diopside (Chiba *et al.*, 1989; Zheng, 1993a). Using these values and following the arguments above, we can roughly estimate the oxygen isotopic composition of the immiscible carbonatite melt from the calculated nepheline-syenitic melt composition of 5.7 ‰. It should be between 6.7 ‰ and 7.8 ‰, right within the middle of the available $\delta^{18}\text{O}_{\text{carbonatite melt}}$ data (Fig. 14b). Thus, the oxygen isotope data are consistent with a petrogenetic origin of the carbonatites involving liquid immiscibility. This is in contrast to the conclusion of Pearce *et al.* (1997), who argued that the difference in $\delta^{18}\text{O}$ values between carbonatites and whole-rock syenitic samples contradicts a liquid immiscibility origin. In our view, the small scatter of the mineral oxygen isotope data compared to the whole-rock data suggest that the isotopic signatures are primary, whereas the whole-rock data are suspect of having suffered late- to post-magmatic alteration.

SUMMARY AND CONCLUSIONS

The aim of the present study was to investigate the carbonatite-syenite complex of Grønnedal-Ika in order to identify specific geochemical characteristics that allow distinguishing between the three possible modes of origin proposed for such complexes (e.g. Bell *et al.*, 1998). Certain criteria that support an origin of the carbonatite via liquid immiscibility from a conjugate silicate liquid at Grønnedal-Ika are summarized below:

- Field and petrographic evidence suggests that there was no significant time gap between the emplacement of the silicate rocks and the carbonatites.
- Whole-rock and mineral geochemical fractionation indices such as Mg# and $(\text{Mg}+\text{Fe}^{2+})/\text{Ca}$ confirm that the carbonatites do not represent unfractionated mantle melts. Clearly, the syenitic silicate rocks are also derived from fractionated melts.
- Radiogenic isotope compositions (Sr, Nd) are similar for silicate rocks and carbonatites
- Oxygen isotope ratios for syenitic melts, determined from a set of mafic mineral data using appropriate fractionation factors between minerals and whole-rocks (Zhao & Zheng, 2003) are in the range of typical mantle values ($\delta^{18}\text{O} = 5.7 \text{ ‰}$) and roughly 2 ‰ below the carbonatite melt values. Whole-rock oxygen isotope data for silicate rocks in those alkaline complexes should be evaluated with great caution.
- $\delta^{13}\text{C}$ values of calcite in syenites overlap with $\delta^{13}\text{C}$ values of carbonatitic calcites (Taubald *et al.*, submitted).
- In agreement with liquid immiscibility experiments (Veksler *et al.*, 1998b), the normalized REE patterns of calcite from carbonatites have steeper slopes than calcite from the associated silicate rocks. The same is true for carbonatite whole-rocks compared to the syenites. Other trace-element data from calcite exhibit features that agree well with experimental data, too.
- The precipitation of aegirine-augitic clinopyroxene in the XPS with elevated Zr/Hf and lower Y/Ho ratios indicate the exsolution of a CO_2 -rich fluid. This process is possibly related to the separation of the carbonate melt and would then support the idea that the XPS represents the conjugate silicate liquid in an immiscibility process.
- The silicate rocks associated with the carbonatites are strongly silica-undersaturated.

- The discreteness of occurrence favors liquid immiscibility rather than a fractional crystallization relationship where continuous series of silicate to carbonate rocks would be expected (Le Bas, 1989).
- The carbonatites represent the latest phase in the complex (Minarik, 1998)

Although a comparison of world-wide occurrences of carbonatite-syenite associations is beyond the scope of this study, these criteria might also be applied in general to other associations of carbonatite and silicate rocks. We conclude that the Grønnedal carbonatites are related via liquid immiscibility to the associated syenites. Some of the data suggest that the xenolithic porphyritic syenite represents the conjugate silicate liquid. A possible scenario of the carbonatite genesis would then be similar to the ideas of Lee & Wyllie (1998): From a parent magma, which later crystallized as the layered syenites, separated a carbonate-rich magma that cooled, reached the carbonate-silicate field boundary and then precipitated cumulus carbonatite.

ACKNOWLEDGEMENTS

We would like to thank Bruce Paterson who provided invaluable help during Laser ICP-MS measurements at the Large-Scale Geochemical Facility supported by the European Community - Access to Research Infrastructure action of the Improving Human Potential Programme, contract number HPRI-CT-1999-00008 awarded to Prof. B.J. Wood (University of Bristol). Thanks to the courtesy of Kathryn Goodenough, Chris Bedford and Heinrich Taubald, we were able to include some of their unpublished data into this work. Henry Emeleus is thanked for some thoughtful comments on the data and for lending his copy of Chris Bedford's voluminous Ph.D. thesis to the first author for many months. Gabi Stoschek, Bernd Steinhilber and Elmar Reitter expertly assisted with stable and radiogenic isotope measurements. Thanks to Thomas Wenzel for his help with microprobe measurements and his critical comments that helped to improve the manuscript. Michael Marks is thanked for his pleasant company during fieldwork. The naval station at Grønnedal provided valuable logistical support. Financial funding of this work by the Deutsche Forschungsgemeinschaft (grant Ma-2135/1-2) is gratefully acknowledged.

REFERENCES

- Andersen, T. (1986). Magmatic fluids in the Fen carbonatite complex, S.E. Norway: Evidence of mid-crustal fractionation from solid and fluid inclusions in apatite. *Contributions to Mineralogy and Petrology* **93**, 491-503.
- Andersen, T. (1997). Age and petrogenesis of the Qassarsuk carbonatite-alkaline silicate volcanic complex in the Gardar rift, South Greenland. *Mineralogical Magazine* **61**, 499-513.
- Armstrong, J.T. (1991). Quantitative elemental analysis of individual microparticles with electron beam instruments. In: Heinrich, K.F.J. & Newbury, D.E. (eds.) *Electron Probe Quantitation*. New York & London: Plenum Press, 261-315.
- Bau, M. (1991). Rare-earth element mobility during hydrothermal and metamorphic fluid-rock interaction and the significance of the oxidation state of europium. *Chemical Geology* **93**, 219-230.
- Bau, M. (1996). Controls on the fractionation of isoivalent trace elements in magmatic and aqueous systems: evidence from Y/Ho, Zr/Hf, and lanthanide tetrad effect. *Contributions to Mineralogy and Petrology* **123**, 323-333.
- Bau, M. & Möller, P. (1992). Rare Earth Element Fractionation in Metamorphogenic Hydrothermal Calcite, Magnesite and Siderite. *Mineralogy and Petrology* **45**, 231-246.
- Barker, D.S. (1989). Field relations of carbonatites. In: Bell, K. (ed.) *Carbonatites*. London: Unwin Hyman, 38-69.
- Bedford, C.M. (1989). The mineralogy, geochemistry and petrogenesis of the Grønnedal-Ika complex, south west Greenland. Ph.D. thesis, University of Durham.
- Bell, K. (1998). Radiogenic Isotope Constraints on Relationships between Carbonatites and Associated Silicate Rocks - a Brief Review. *Journal of Petrology* **39**, 1987-1996.
- Bell, K., Kjarsgaard, B.A., & Simonetti, A. (1998). Carbonatites-Into The Twenty-First Century. *Journal of Petrology* **39**, 1839-1845.
- Berman, R.G., Brown, T.H., & Perkins, E.H. (1987). GEO-CALC: software for calculation and display of pressure-temperature-composition phase diagrams. *American Mineralogist* **72**, 861-862.
- Blaxland, A.B., van Breemen, O., Emeleus, C.H., & Anderson, J.G. (1978). Age and origin of the major syenite centers in the Gardar province of south Greenland: Rb-Sr studies. *Bulletin of the Geological Society of America* **89**, 231-244.
- Blundy, J. & Wood, B. (2003). Partitioning of trace elements between crystals and melts. *Earth and Planetary Science Letters* **210**, 383-397.
- Bondam, J. (1992). The Grønnedal-Ika alkaline complex in South Greenland. Review of geoscientific data relevant to exploration. *Grønlands Geologiske Undersøgelse, Open File Series* **92**.
- Boynnton, W.V. (1984). Geochemistry of the rare earth elements: meteorite studies. In: Henderson, P. (ed.) *Rare earth element geochemistry*. Amsterdam: Elsevier, 63-114.
- Brooker, R. (1998). The effect of CO₂ saturation on immiscibility between silicate and carbonate liquids: an experimental study. *Journal of Petrology* **39**, 1905-1915.
- Buddington, A.F. & Lindsley, D.H. (1964). Iron-titanium oxide minerals and synthetic equivalents. *Journal of Petrology* **5**, 310-357.
- Bühn, B. & Rankin, A.H. (1999). Composition of natural, volatile-rich Na-Ca-REE-Sr carbonatitic fluids trapped in fluid inclusions. *Geochimica et Cosmochimica Acta* **63**, 3781-3797.
- Bühn, B. & Trumbull, R.B. (2003). Comparison of petrogenetic signatures between mantle-derived alkali silicate intrusives with and without associated carbonatite, Namibia. *Lithos*, **66**, 201-221.
- Bühn, B., Rankin, A.H., Schneider, J., & Dulski, P. (2002). The nature of orthomagmatic, carbonatitic fluids precipitating REE, Sr-rich fluorite: fluid-inclusion evidence from the Okorusu fluorite deposit, Namibia. *Chemical Geology* **186**, 75-98.
- Callisen, K. (1943). Igneous rocks of the Ivigtut region, Greenland; Part 1, The nepheline syenites of the Grønnedal-Ika area. *Meddelelser om Grønland* **22**.
- Cherniak, D.J. (2001). Pb diffusion in Cr diopside, augite, and enstatite, and consideration of the dependence of cation diffusion in pyroxene on oxygen fugacity. *Chemical Geology* **177**, 381-397.
- Chiba, H., Chacko, T., Clayton, R.N. & Goldsmith, J.R. (1989). Oxygen isotope fractionations involving diopside, forsterite, magnetite, and calcite: Application to geothermometry. *Geochimica et Cosmochimica Acta* **53**, 2985-2995.
- Cullers, R.L. & Medaris, G.Jr. (1977). Rare earth elements in carbonatite and cogenetic alkaline rocks; examples from

- Seabrook Lake and Callander Bay, Ontario. *Contributions to Mineralogy and Petrology* **65**, 143-153.
- Dalton, J.A. & Presnall, D.C. (1998). The continuum of primary carbonatitic-kimberlitic melt compositions in equilibrium with lherzolite: data from the system CaO-MgO-Al₂O₃-SiO₂-CO₂ at 6 GPa. *Journal of Petrology* **39**, 1953-1964.
- Dalton, J.A. & Wood, B.J. (1993). The compositions of primary carbonate melts and their evolution through wallrock reaction in the mantle. *Earth and Planetary Science Letters* **119**, 511-525.
- David, K., Schiano, P., & Allègre, C.J. (2000). Assessment of the Zr/Hf fractionation in oceanic basalts and continental materials during petrogenetic processes. *Earth and Planetary Science Letters* **178**, 285-301.
- Deines, P. (1989). Stable isotope variations in carbonatites. in: Bell, K. (ed.), 1989, *Carbonatites*, Unwin Hyman, London, 301-359.
- Demény, A., Ahijado, A., Casillas, R., & Vennemann, T.W. (1998). Crustal contamination and fluid/rock interaction in the carbonatites of Fuerteventura (Canary Islands, Spain): a C, O, H isotope study. *Lithos* **44**, 101-115.
- DePaolo, D.J. (1981). Trace element and isotopic effects of combined wallrock assimilation and fractional crystallisation. *Earth and Planetary Science Letters* **53**, 189-202.
- Dupuy, C., Liotard, J.M., & Dostal, J. (1992). Zr/Hf fractionation in intraplate basaltic rocks: carbonate metasomatism in the mantle source. *Geochimica et Cosmochimica Acta* **56**, 2417-2423.
- Edgar, A.D. (1964). Studies on cancrinites: II. Stability fields and cell dimensions of calcium and potassium-rich cancrinites. *Canadian mineralogist* **8**, 53-67.
- Eggler, D.H. (1989). Carbonatites, Primary Melts, and Mantle Dynamics. In: Bell, K. (ed.) *Carbonatites*. London: Unwin Hyman, 561-579.
- Eiler, J.M., Farley, K.A., Valley, J.W., Hauri, E., Craig, H., Hart, S.R., & Stolper, E.M. (1997). Oxygen isotope variations in ocean island basalt phenocrysts. *Geochimica et Cosmochimica Acta* **61**, 2281-2293.
- Eiler, J.M., Crawford, A., Elliot, T., Farley, K.A., Valley, J.W., & Stolper, E.M. (2000a). Oxygen isotope geochemistry of oceanic-arc lavas. *Journal of Petrology* **41**, 229-256.
- Eiler, J.M., Schiano, P., Kitchen, N., & Stolper, E.M. (2000b). Oxygen-isotope evidence for recycled crust in the sources of mid-ocean-ridge basalts. *Nature* **403**, 530-534.
- Emeleus, C.H. (1964). The Grønnedal-Ika alkaline complex, South Greenland. The structure and geological history of the complex. *Meddelelser om Grønland* **172**, 1-75.
- Freestone, I.C. & Hamilton, D.L. (1980). The role of liquid immiscibility in the genesis of carbonatites - an experimental study. *Contributions to Mineralogy and Petrology* **73**, 105-117.
- Fuhrman, M.L. & Lindsley, D.H. (1988). Ternary-feldspar modeling and thermometry. *American Mineralogist*, **73**, 201-205.
- Gerlach, D.C., Cliff, R.A., Davies, G.R., Norry, M., & Hodgson, N. (1988). Magma sources of the Cape Verdes archipelago: isotopic and trace element constraints. *Geochimica et Cosmochimica Acta* **52**, 2979-2992.
- Gill, R.C.O. (1972a). Chemistry of peralkaline phonolite dykes from the Grønnedal-Ika area, South Greenland. *Contributions to Mineralogy and Petrology* **34**, 87-100.
- Gill, R.C.O. (1972b). The geochemistry of the Grønnedal-Ika alkaline complex, South Greenland. Ph.D. thesis, University of Durham.
- Gittins, J. (1989). The origin and evolution of carbonatite magmas. In: Bell, K. (ed.) *Carbonatites*. London: Unwin Hyman, 580-600.
- Goldstein, S.L., O'Nions, R.K., & Hamilton, P.J. (1984). A Sm-Nd isotopic study of the atmospheric dust and particulates from major river systems. *Earth and Planetary Science Letters* **70**, 221-236.
- Gomes, C.d.B., Moro, S.L., & Dutra, C.V. (1970). Pyroxenes from the alkaline rocks of Itapirapuã, São Paulo, Brazil. *American Mineralogist* **55**, 224-230.
- Goodenough, K.M. (1997). Geochemistry of Gardar intrusions in the Ivigtut area, South Greenland. Ph.D. thesis, University of Edinburgh.
- Halama, R., Waight, T., & Markl, G. (2002). Geochemical and isotopic zoning patterns of plagioclase megacrysts in gabbroic dykes from the Gardar Province, South Greenland: implications for crystallisation processes in anorthositic magmas. *Contributions to Mineralogy and Petrology* **144**, 109-127.
- Halama, R., Wenzel, T., Upton, B.G.J., Siebel, W., & Markl, G. (2003). A geochemical and Sr-Nd-O isotopic study of the Proterozoic Eriksfjord Basalts, Gardar Province, South Greenland: Reconstruction of an OIB signature in crustally contaminated rift-related basalts. *Mineralogical Magazine* **67**, 831-854.

- Hamilton, D.L. (1961). Nephelines as crystallisation temperature indicators. *Journal of Geology* **69**, 321-329.
- Harmer, R.E. (1999). The Petrogenetic Association of Carbonatite and Alkaline Magmatism: Constraints from the Spitskop Complex, South Africa. *Journal of Petrology* **40**, 525-548.
- Harmer, R.E. & Gittins, J. (1998). The Case for Primary, Mantle-derived Carbonatite Magma. *Journal of Petrology* **39**, 1895-1903.
- Harmon, R.S. & Hoefs, J. (1995). Oxygen isotope heterogeneity of the mantle deduced from global ^{18}O systematics of basalts from different geotectonic settings. *Contributions to Mineralogy and Petrology* **120**, 95-114.
- Holland, T.J.B. (1990). Activities of components in omphacitic solid solutions; an application of Landau theory of mixtures. *Contributions to Mineralogy and Petrology*, **105** 446-453.
- Ionov, D. & Harmer, R.E. (2002). Trace element distribution in calcite-dolomite carbonatites from Spitskop: inferences for differentiation of carbonatite magmas and the origin of carbonates in mantle xenoliths. *Earth and Planetary Science Letters* **198**, 495-510.
- Irber, W. (1999). The lanthanide tetrad effect and its correlation with K/Rb, Eu/Eu*, Sr/Eu, Y/Ho, and Zr/Hf of evolving peraluminous granites suites. *Geochimica et Cosmochimica Acta* **63**, 489-508.
- Jones, A.P. (1984). Mafic silicates from the nepheline syenites of the Motzfeldt centre, south Greenland. *Mineralogical Magazine* **48**, 1-12.
- Kalamarides, R.I. (1986). High-temperature oxygen isotope fractionation among the phases of Kiglapait intrusion, Labrador, Canada. *Chemical Geology* **58**, 303-310.
- Keller, J. & Hoefs, J. (1995). Stable isotope characteristics of recent natrocarbonatites from Oldoinyo Lengai. In: Bell, K. & Keller, J. (eds.) *Carbonatite Volcanism: Oldoinyo Lengai and the Petrogenesis of Natrocarbonatites*. Berlin: Springer, 113-123.
- Kjarsgaard, B.A. (1998). Phase relations of a carbonated high-CaO nephelinite at 0.2 and 0.5 GPa. *Journal of Petrology* **39**, 2061-2075.
- Kjarsgaard, B.A. & Hamilton, D.L. (1988). Liquid immiscibility and the origin of alkali-poor carbonatites. *Mineralogical Magazine* **52**, 43-55.
- Konnerup-Madsen, J. & Rose-Hansen, J. (1982). Volatiles associated with alkaline igneous rift activity: Fluid inclusions in the Ilimaussaq intrusion and the Gardar granitic complexes (south Greenland). *Chemical Geology* **37**, 79-93.
- Konnerup-Madsen, J. & Rose-Hansen, J. (1984). Composition and significance of fluid inclusions in the Ilimaussaq peralkaline granite, South Greenland. *Bulletin de Minéralogie* **107**, 317-326.
- Korobeinikov, A.N., Mitrofanov, F.P., Gehör, S., Laajoki, K., Pavlov, V.P., & Mamontov, V.P. (1998). Geology and copper sulphide mineralization of the Salmagorskii Ring Igneous Complex, Kola Peninsula, NW Russia. *Journal of Petrology* **39**, 2033-2041.
- Koster van Groos, A.F. & Wyllie, P.J. (1973). Liquid immiscibility in the join $\text{NaAlSi}_3\text{O}_8$ - $\text{CaAlSi}_2\text{O}_8$ - Na_2CO_3 - H_2O . *American Journal of Science* **273**, 465-487.
- Kramm, U. (1994). Isotope evidence for ijolite formation by fenitization: Sr-Nd data of ijolites from the type locality Iivaara, Finland. *Contributions to Mineralogy and Petrology* **115**, 279-286.
- Larsen, L.M. (1976). Clinopyroxenes and coexisting mafic minerals from the alkaline Ilimaussaq intrusion, south Greenland. *Journal of Petrology* **17**, 258-290.
- Le Bas, M.J. (1989). Diversification of carbonatite. In: Bell, K. (ed.) *Carbonatites*. London: Unwin Hyman, 428-447.
- Leake, B.E., Wooley, A.R., Arps, C.E.S., Birch, W.D., Gilbert, M.C., Grice, J.D., Hawthorne, F.C., Kato, A., Kisch, H.J., Krivovichev, V.G., Linthout, K., Laird, J., Mandarino, J.A., Maresch, W.V., Nickel, E.H., Rock, N.M.S., Schumacher, J.C., Smith, D.C., Stephenson, N.C.N., Ungaretti, L., Whittaker, E.J.W., & Youzhi, G. (1997). Nomenclature of amphiboles: Report of the Subcommittee on Amphiboles of the International Mineralogical Association, Commission on New Minerals and Mineral Names. *American Mineralogist* **82**, 1019-1037.
- Lee, W.-J. & Wyllie, P.J. (1994). Experimental data bearing on liquid immiscibility, crystal fractionation, and the origin of calcicarbonatites and natrocarbonatites. *International Geology Review* **36**, 797-819.
- Lee, W.-J. & Wyllie, P.J. (1998). Petrogenesis of Carbonatite Magmas from Mantle to Crust, constrained by the system CaO - $(\text{MgO}+\text{FeO}^*)$ - $(\text{Na}_2\text{O}+\text{K}_2\text{O})$ - $(\text{SiO}_2+\text{Al}_2\text{O}_3+\text{TiO}_2)$ - CO_2 . *Journal of Petrology* **39**, 495-517.
- Lieberman, J. & Petrakakis, K. (1991). TWEEQU thermobarometry, analysis of uncertainties and applications to granulites from western Alaska. *The Canadian Mineralogist* **29**, 857-887.
- Linnen, R.L. & Keppler, H. (2002). Melt composition control of Zr/Hf fractionation in magmatic processes.

- Geochimica et Cosmochimica Acta* **66**, 3293-3301.
- Markl, G., Marks, M., Schwinn, G., & Sommer, H. (2001). Phase equilibrium constraints on intensive crystallization parameters of the Ilimaussaq Complex, South Greenland. *Journal of Petrology* **42**, 2231-2258.
- Marks, M. & Markl, G. (2001). Fractionation and assimilation processes in the alkaline augite syenite unit of the Ilimaussaq Intrusion, South Greenland, as deduced from phase equilibria. *Journal of Petrology* **42**, 1947-1969.
- Marks, M., Vennemann, T., Siebel, W., & Markl, G. (2003). Quantification of Magmatic and Hydrothermal Processes in a Peralkaline Syenite-Alkali Granite Complex Based on Textures, Phase Equilibria, and Stable and Radiogenic Isotopes. *Journal of Petrology* **44**, 1247-1280.
- Marks, M., Vennemann, T., Siebel, W., Markl, G. (submitted). Decoupling of O and H isotopes in Fe-rich amphiboles and strong D-depletion during magmatic processes: an example from the peralkaline Ilimaussaq Intrusion, South Greenland. *Geochimica et Cosmochimica Acta*.
- Mattey, D., Lowry, D., & Macpherson, C. (1994). Oxygen isotope composition of mantle peridotite. *Earth and Planetary Science Letters* **128**, 231-241.
- McDonough, W.F. & Sun, S.S. (1995). The composition of the Earth. *Chemical Geology* **120**, 223-253.
- Minarik, W.G. (1998). Complications to carbonate melt mobility due to the presence of an immiscible silicate melt. *Journal of Petrology* **39**, 1965-1973.
- Möller, P., Morteaux, G., & Schley, F. (1980). Discussion of REE distribution patterns of carbonatites and alkalic rocks. *Lithos* **13**, 171-179.
- Moore, K.R. & Wood, B.J. (1998). The transition from carbonate to silicate melts in the CaO-MgO-SiO₂-CO₂ system. *Journal of Petrology* **39**, 1943-1951.
- Morimoto, N., Fabrice, J., Ferguson, A.K., Ginzburg, I.V., Ross, M., Seifert, F.A., Zussman, J., Aoki, K., & Gottardi, G. (1988). Nomenclature of pyroxenes. *Mineralogical Magazine* **52**, 535-550.
- Mysen, B.O. & Boettcher, A.L. (1975). Melting of a hydrous mantle; II, Geochemistry of crystals and liquids formed by anatexis of mantle peridotite at high pressures and high temperatures as a function of controlled activities of water, hydrogen, and carbon dioxide. *Journal of Petrology* **16**, 549-593.
- Olafsson, M. & Eggler, D.H. (1983). Phase relations of amphibole, amphibole-carbonate, and phlogopite-carbonate peridotite: petrologic constraints on the asthenosphere. *Earth and Planetary Science Letters* **64**, 305-315.
- Pearce, N.J.G. & Leng, M.J. (1996). The origin of carbonatites and related rocks from the Igaliko Dyke Swarm, Gardar Province, South Greenland: field, geochemical and C-O-Sr-Nd isotope evidence. *Lithos* **39**, 21-40.
- Pearce, N.J.G., Leng, M.J., Emeleus, C.H., & Bedford, C.M. (1997). The origins of carbonatites and related rocks from the Grønnedal-Ika Nepheline Syenite complex, South Greenland: C-O-Sr isotope evidence. *Mineralogical Magazine* **61**, 515-529.
- Powell, M. (1978). The crystallisation history of the Igdlarfigssalik nepheline syenite intrusion, Greenland. *Lithos* **11**, 99-120.
- Robie, R.A. & Hemingway, B.S. (1995). Thermodynamic properties of minerals and related substances at 298.15 K and 1 bar (105 Pascals) pressure and at higher temperatures. *U.S. Geological Survey Bulletin* **2131**, 461pp.
- Roddick, J.C., Sullivan, R.W., & Dudas, F.Ö. (1992). Precise calibration of Nd tracer isotopic composition for Sm-Nd studies. *Chemical Geology* **97**, 1-8.
- Rumble, D. & Hoering, T.C. (1994). Analysis of oxygen and sulfur isotope ratios in oxide and sulfide minerals by spot heating with a carbon dioxide laser in a fluorine atmosphere. *Accounts of Chemical Research* **27**, 237-241.
- Samson, I.M., Williams-Jones, A.E. & Liu, W. (1995). The chemistry of hydrothermal fluids in carbonatites: Evidence from leachate and SEM-decrepitate analysis of fluid inclusions from Oka, Quebec, Canada. *Geochimica et Cosmochimica Acta* **59**, 1979-1989.
- Santos, R.V. & Clayton, R.N. (1995). Variations of oxygen and carbon isotopes in carbonatites: A study of Brazilian alkaline complexes. *Geochimica et Cosmochimica Acta* **59**, 1339-1352.
- Sharp, Z.D. (1990). A laser-based microanalytical method for the in-situ determination of oxygen isotope ratios of silicates and oxides. *Geochimica et Cosmochimica Acta* **54**, 1353-1357.
- Sharp, Z.D., Helffrich, G.R., Bohlen, S.R., Essene, E.J. (1989). The stability of sodalite in the system NaAlSi₃O₈-NaCl. *Geochimica et Cosmochimica Acta* **53**, 1943-1954.
- Sirbescu, M. & Jenkins, D.M. (1999). Experiments on the stability of cancrinite in the system Na₂O-CaO-Al₂O₃-SiO₂-CO₂-H₂O. *American Mineralogist* **84**, 1850-1860.
- Sobolev, V.S., Bazarova, T.Y., & Kostyuk, V.P. (1974). Inclusions in the minerals of some types of alkaline rocks. In:

- Sørensen, H. (ed.) *The Alkaline Rocks*. London: John Wiley & Sons, 389-401.
- Spötl, C. & Vennemann, T.W. (2003). Continuous-flow isotope ratio mass spectrometric analysis of carbonate minerals. *Rapid Communications in Mass Spectrometry* **17**, 1004-1006.
- Srivastava, R.K. (1997). Petrology, geochemistry and genesis of rift-related carbonatites of Ambadungar, India. *Mineralogy and Petrology* **61**, 47-66.
- Stephenson, D. (1973). The petrology and mineralogy of the South Qôroq centre, Igaliko Complex, South Greenland. Ph.D. thesis, University of Durham.
- Sweeney, R.J. (1994). Carbonatite melt compositions in the Earth's mantle. *Earth and Planetary Science Letters* **128**, 259-270.
- Taubald, H., Morteani, G., & Satir, M. (submitted). Geochemical and isotopic (Sr, C, O) data from the alkaline complex of Grønnedal-Ika (South Greenland): evidence for unmixing and crustal contamination. *International Journal of Earth Sciences*.
- Taylor, H.P., Frechen, J., & Degens, E.T. (1967). Oxygen and carbon isotope studies of carbonatites from the Laacher See District, West Germany and the Alnö District, Sweden. *Geochimica et Cosmochimica Acta* **31**, 407-430.
- Tyler, R.C. & King, B.C. (1967). The pyroxenes of the alkaline igneous complexes of eastern Uganda. *Mineralogical Magazine* **36**, 5-22.
- Upton, B.G.J., Emeleus, C.H., Heaman, L.M., Goodenough, K.M., & Finch, A. (2003). Magmatism of the mid-Proterozoic Gardar Province, South Greenland: chronology, petrogenesis and geological setting. *Lithos* **68**, 43-65.
- Van Orman, J.A., Grove, T.L., & Shimizu, N. (2001). Rare earth element diffusion in diopside: influence of temperature, pressure, and ionic radius, and an elastic model for diffusion in silicates. *Contributions to Mineralogy and Petrology* **141**, 687-703.
- Varne, R. (1968). The petrology of Moroto mountain, eastern Uganda, and the origin of nephelinites. *Journal of Petrology* **9**, 169-196.
- Veksler, I.V., Nielsen, T.F.D. & Sokolov, S.V. (1998a). Mineralogy of crystallized melt inclusions from Gardiner and Kovdor ultramafic alkaline complexes: implications for carbonatite genesis. *Journal of Petrology* **39**, 2015-2031.
- Veksler, I.V., Petibon, C., Jenner, G.A., Dorfman, A.M., & Dingwell, D.B. (1998b). Trace Element Partitioning in Immiscible Silicate-Carbonate Liquid Systems: an Initial Experimental Study Using a Centrifuge Autoclave. *Journal of Petrology* **39**, 2095-2104.
- Vroon, P.Z., Lowry, D., Van Bergen, M.J., Boyce, A.J., & Matthey, D.P. (2001). Oxygen isotope systematics of the Banda Arc: Low $\delta^{18}\text{O}$ despite involvement of subducted continental material in magma genesis. *Geochimica et Cosmochimica Acta* **65**, 589-609.
- Wood, B.J. & Blundy, J.D. (1997). A predictive model for rare earth element partitioning between clinopyroxene and anhydrous silicate melt. *Contributions to Mineralogy and Petrology* **129**, 166-181.
- Woolley, A.R. (1982). A discussion of carbonatite evolution and nomenclature, and the generation of sodic and potassic fenites. *Mineralogical Magazine* **46**, 13-17.
- Woolley, A.R. (1987). Lithosphere metasomatism and the petrogenesis of the Chilwa Province of alkaline igneous rocks and carbonatites, Malawi. *Journal of African Earth Sciences* **6**, 891-898.
- Woolley, A.R. & Kempe, D.R.C. (1989). Carbonatites: nomenclature, average chemical compositions, and element distribution. In: Bell, K. (ed.) *Carbonatites*, London: Unwin Hyman, 1-14.
- Wyllie, P.J. & Huang, W.L. (1976). Carbonation and melting relations in the system CaO-MgO-SiO₂-CO₂ at mantle pressures with geophysical and petrological applications. *Contributions to Mineralogy and Petrology* **54**, 79-107.
- Zhao, Z.-F. & Zheng, Y.-F. (2003). Calculation of oxygen isotope fractionation in magmatic rocks. *Chemical Geology* **193**, 59-80.
- Zheng, Y.-F. (1993a). Calculation of oxygen isotope fractionation in anhydrous silicate minerals. *Geochimica et Cosmochimica Acta* **57**, 1079-1091.
- Zheng, Y.-F. (1993b). Calculation of oxygen isotope fractionation in hydroxyl-bearing silicates. *Earth and Planetary Science Letters* **120**, 247-263.

Figure captions

Fig. 1: Map of the Grønnedal-Ika intrusion, simplified after Emeleus (1964) and Pearce *et al.* (1997).

Fig. 2: Photomicrographs (plane-polarized light) of mineral textures from Grønnedal-Ika rocks. Sample numbers appear in the lower right corner. Ne = nepheline, fsp = alkali feldspar, cpx = clinopyroxene, m-cpx = matrix clinopyroxene, bt = biotite, amph = amphibole, ap = apatite, cal = calcite, ccn = cancrinite. a, b) Clinopyroxene phenocrysts in the XPS showing discontinuous zonation into core and rim, together with small matrix clinopyroxenes. Alkali feldspar and nepheline occur as phenocrysts and within the matrix. c) Typical texture of the layered nepheline syenites with an accumulation of clinopyroxene, partly surrounded by biotite and with apatite. d) Large, poikilitic amphibole. e) Interstitial calcite between biotite, clinopyroxene and alkali feldspar. The boundaries of the cancrinite in the upper left corner are outlined to increase its visibility. f) Calcite grains in calcite-carbonatite.

Fig. 3: a) to c) Compositions of clinopyroxenes from Grønnedal-Ika rocks in the diopside-hedenbergite-aegirine (Di-Hd-Aeg) triangle. Endmember components were calculated as follows: Di = Mg, Hd = $Fe^{2+} + Mn$ and Aeg = Na. d) Generalized trends of pyroxene compositions from other alkaline igneous complexes of the Gardar Province (1-4), Uganda (5) and Brazil (6). Data sources: (1) Larsen (1976), (2) Powell (1978), (3) Jones (1984), (4) Stephenson (1973), (5) Tyler & King (1967) (6) Gomes *et al.* (1970).

Fig. 4: Zoning in clinopyroxene phenocrysts from the xenolithic porphyritic syenite. a) + b) BSE images, lines mark the position of the profiles; c) + d) corresponding electron microprobe core to rim zoning profiles through the crystals. Analyses obviously affected by the presence of cracks were omitted for clarity.

Fig. 5: Back-scattered electron (BSE) images Fe-Ti oxides and cancrinite in Grønnedal-Ika syenites. Abbreviations as for Fig. 2, and hem = hematite, ab = albite, or = orthoclase. a, b) Primary magmatic titanomagnetites showing trellis-type oxy-exsolution into magnetite (light) and ilmenite-pyrophanite-hematite_{ss} (dark lamellae). c) Late- to post-magmatic hematite associated with biotite. d) Perthitically exsolved alkali feldspar and cancrinite.

Fig. 6: Chondrite-normalized REE patterns with chondritic values from Boynton (1984). a) calcite from carbonatites and syenites; comparative whole-rock data are from Bedford (1989) and Goodenough (1997). b) clinopyroxene from the xenolithic porphyritic syenite.

Fig. 7: Multi-element diagram of clinopyroxenes from the xenolithic porphyritic syenite, normalized to primitive mantle values (McDonough & Sun, 1995).

Fig. 8: Y/Ho vs. Zr/Hf diagram of clinopyroxenes and amphiboles in syenites from the Grønnedal-Ika, Ilímaussaq and Puklen intrusions (Ilímaussaq and Puklen data from Marks *et al.*, unpublished).

The light grey shaded field defines the Zr/Hf ratios of common igneous rocks crystallising from silica melt systems (Bau, 1996).

Fig. 9: Carbon and oxygen isotope composition of calcite from Grønnedal-Ika carbonatites, together with the field of primary, unaltered carbonatites proposed by Taylor *et al.* (1967). Arrows indicate schematically the main processes responsible for changes in the isotopic compositions (after Deines, 1989, and Demény *et al.*, 1998). Comparative data are from whole-rocks and carbonate separates (Goodenough, 1997; Pearce *et al.*, 1997; Taubald *et al.*, submitted).

Fig. 10: Sm-Nd isochron diagram with analyses of clinopyroxene and amphibole separates from syenites and whole-rock carbonatites of the Grønnedal-Ika complex. The 1300 Ma reference line is based on the Rb-Sr age of 1299 ± 17 Ma (Blaxland *et al.*, 1978). Errors ($\pm 0.5\%$ for $^{147}\text{Sm}/^{144}\text{Nd}$ and $\pm 0.002\%$ for $^{143}\text{Nd}/^{144}\text{Nd}$) are not larger than the symbols.

Fig. 11: Nepheline compositions of syenitic samples in the nepheline-kalsilite-quartz (Ne-Ks-SiO₂) triangle with isotherms at 1 kbar after Hamilton (1961).

Fig. 12: Temperature-silica activity diagrams showing equilibria among Ab, Ne and Jd for syenitic rocks of Grønnedal-Ika. All calculations were performed using an extension of the GEO-CALC software (Berman, 1987; Lieberman & Petrakakis, 1991). Note that the *x*-axis values are based on a log₁₀ scale.

Fig. 13: f_{O_2} -T diagram with estimated formation conditions of early- and late magmatic Fe-Ti oxides in Grønnedal-Ika syenites. FMQ and HM are the fayalite-magnetite-quartz and the hematite-magnetite buffer at unit activities. FMQ* is the displaced FMQ buffer with values typical values for the syenites ($a_{\text{SiO}_2} = 0.37$, $a_{\text{Mag}} = 0.43$). The same activities were used to calculate the position of the displaced buffer reaction $3 \text{ ferrosilite} + \text{O}_2 = 2 \text{ magnetite} + 6 \text{ SiO}_2$ (FsmQ*). HM* shows the displaced position of the HM buffer representative for the syenitic samples with $a_{\text{Hem}} = 0.98$ and $a_{\text{Mag}} = 0.43$. These calculations were performed using an extension of the GEO-CALC software (Berman, 1987; Lieberman & Petrakakis, 1991). Tie line projections of magnetite-ulvöspinel_{SS} connecting conjugate magnetite-ulvöspinel_{SS} and hematite-ilmenite_{SS} pairs after Buddington & Lindsley (1964) are shown for magnetite compositions typical of the Grønnedal samples. They define the dark grey field (see text for discussion). Stippled curves indicate the position of the equilibrium $\text{CH}_4 + 2 \text{ O}_2 = 2 \text{ H}_2\text{O} + \text{CO}_2$ with C:H = 1:2 and variable $f_{\text{CH}_4}/f_{\text{CO}_2}$ ratios (calculations were performed assuming ideal gas behavior and $P_{\text{total}} = 1$ kbar; thermodynamic data from Robie & Hemingway, 1995). The grey arrow shows a possible evolution path of the Grønnedal syenitic magmas. The trend of the augite-syenite unit from the Ilímaussaq intrusion is after Markl *et al.* (2001).

Fig. 14: Oxygen-neodymium isotope correlation diagrams for a) mineral data and b) calculated melt compositions and whole-rock analyses. ϵ_{Nd} (T = 1.3 Ga) values for MORB were calculated after the DMM models of DePaolo (1981) and Goldstein *et al.* (1984). Hypothetical oxygen isotope composition of clinopyroxene in MORB was calculated based on analyses of MORB olivine ($\delta^{18}\text{O}$

= 5.2 ‰; Eiler *et al.* 1997) and the oxygen isotope fractionation between olivine and clinopyroxene ($\Delta_{\text{ol-cpx}} = -0.4$ ‰; Matthey *et al.*, 1994). Comparative mineral data are from Halama *et al.* (in press), Marks *et al.* (2003) and Marks *et al.* (submitted). For calculation of melt compositions see text. MORB glass data are from Eiler *et al.* (2000b), comparative whole-rock data from Gardar rocks were taken from Pearce & Leng (1996). The Grønnedal carbonatite field roughly indicates available oxygen isotope data from various sources (Pearce *et al.*, 1997; Taubald *et al.*, submitted) combined with the Nd isotope data of this study.

Table 1: Typical microprobe analyses of feldspar and nepheline in Grønnedal-Ika syenites

Unit	Upper Series	Upper Series	PMS	XPS	XPS	Lower Series	Upper Series	Upper Series	PMS	XPS
Sample	GR 44	GR 63	GR 27	GM 1496	GM 1496	GR 13	GR 63	GM 1539	GR 27	GM 1496
Mineral	feldspar	feldspar	feldspar	feldspar	feldspar	nepheline	nepheline	nepheline	nepheline	nepheline
<i>wt. %:</i>										
SiO ₂	66.23	66.49	66.09	65.33	66.74	44.89	44.90	43.47	44.29	44.11
TiO ₂	0.02	0.00	0.01	0.03	0.02	0.01	0.00	0.00	0.02	0.00
Al ₂ O ₃	18.40	18.47	18.77	18.54	18.63	31.86	31.79	32.91	32.03	32.12
FeO	0.23	0.16	0.12	0.12	0.19	0.42	0.68	0.29	0.63	0.52
MnO	0.00	0.01	0.00	0.01	0.00	0.02	0.03	0.00	0.01	0.00
MgO	0.01	0.00	0.01	0.00	0.00	0.02	0.00	0.00	0.00	0.00
BaO	0.11	0.15	0.09	0.21	0.13	0.03	0.03	0.00	0.01	0.02
SrO	0.00	0.01	0.00	0.01	0.05	0.00	0.00	0.11	0.00	0.00
CaO	0.04	0.06	0.16	0.18	0.13	0.04	0.00	0.01	0.02	0.01
Na ₂ O	5.05	5.56	5.98	4.47	5.86	16.15	16.22	16.28	16.24	15.94
K ₂ O	9.55	8.56	8.14	10.52	8.26	5.56	5.67	6.58	5.84	6.09
Total	99.63	99.46	99.38	99.42	100.01	99.01	99.31	99.66	99.09	98.80
<i>Oxygens p.f.u.:</i>										
Si	3.01	3.01	2.99	2.99	3.00	8.66	8.64	8.40	8.56	8.55
Al	0.98	0.99	1.00	1.00	0.99	7.24	7.21	7.50	7.30	7.34
Ti	0.00	0.00	0.00	0.00	0.00	0.00	0.00	0.00	0.00	0.00
Mg	0.00	0.00	0.00	0.00	0.00	0.01	0.00	0.00	0.00	0.00
Fe ²⁺	0.01	0.01	0.00	0.00	0.01					
Fe ³⁺						0.07	0.11	0.05	0.10	0.08
Mn	0.00	0.00	0.00	0.00	0.00	0.00	0.00	0.00	0.00	0.00
Ba	0.00	0.00	0.00	0.00	0.00	0.00	0.00	0.00	0.00	0.00
Sr	0.00	0.00	0.00	0.00	0.00	0.00	0.00	0.01	0.00	0.00
Ca	0.00	0.00	0.01	0.01	0.01	0.01	0.00	0.00	0.00	0.00
Na	0.44	0.49	0.52	0.40	0.51	6.04	6.05	6.10	6.09	5.99
K	0.55	0.49	0.47	0.61	0.47	1.37	1.39	1.62	1.44	1.51
Total	5.00	4.99	5.00	5.02	4.99	23.39	23.42	23.69	23.50	23.48
<i>Mol%:</i>										
An	0.8	0.2	0.3	0.9	0.6					
Ab	52.3	44.5	49.5	38.9	51.6					
Or	46.9	55.3	50.2	60.2	47.8					
Ne						69.8	70.0	72.6	71.1	70.1
Ks						15.8	16.1	19.3	16.8	17.6
Qz						14.4	13.8	8.1	12.1	12.3

Mol% calculations for nepheline as in Wilkinson & Hensel (1994); Ne = nepheline, Ks = kalsilite, qz = quartz;

Table 2: Typical analyses of clinopyroxene and amphibole from Grønnedal-Ika syenites

Unit	LS	LS	LS	US	US	US	US	XPS	XPS	PMS	PMS	GX	US	US
Sample	GR 01	GR 36	GR 36	GM 1526	GR 63	GM 1531	GM 1559	GR 51	GR 51	GR 27	GR 27	GR 08	GM 1531	GM 1526
Mineral	Cpx	Cpx	Cpx	Cpx	Cpx	Cpx	Cpx	Cpx	Cpx	Cpx	Cpx	Cpx	Amph	Amph
<i>wt. %:</i>														
SiO ₂	51.44	50.12	52.10	51.68	51.30	51.30	50.82	48.94	50.86	50.11	49.97	50.77	44.96	44.55
TiO ₂	0.20	0.68	0.43	0.19	0.17	0.28	0.19	1.41	0.33	0.22	0.09	1.02	1.11	1.14
Al ₂ O ₃	1.18	2.96	0.76	0.86	1.10	1.11	1.23	4.45	0.85	1.33	1.07	2.50	4.69	5.77
FeO	25.50	13.48	27.51	23.00	21.42	26.44	19.24	12.43	23.98	20.72	24.91	11.82	31.33	27.37
MnO	0.78	0.36	0.33	0.79	0.96	0.55	0.87	0.24	0.84	0.84	0.92	0.26	1.00	1.06
MgO	1.39	9.78	0.67	3.31	4.09	0.84	5.41	9.20	2.43	4.75	2.00	11.23	1.85	4.29
CaO	12.55	21.18	7.59	14.24	16.14	9.13	17.63	20.96	13.19	20.25	16.06	21.52	3.88	6.83
Na ₂ O	6.36	1.08	9.77	5.59	4.35	8.41	3.63	1.79	6.43	1.93	4.40	0.88	6.42	5.02
K ₂ O	0.01	0.01	0.00	0.00	0.00	0.00	0.01	0.02	0.01	0.01	0.00	0.00	1.79	1.69
F													0.01	0.04
Cl													0.68	1.01
Total	99.40	99.65	99.16	99.68	99.54	98.06	99.04	99.44	98.92	100.17	99.42	100.00	97.72	98.76
<i>Formulae based on 4 (16) cations and 6 (23) oxygens for clinopyroxene and amphibole, respectively:</i>														
Si	2.00	1.91	1.99	1.99	1.99	2.00	1.97	1.86	1.97	1.96	1.97	1.91	7.19	7.02
Al	0.05	0.13	0.03	0.04	0.05	0.05	0.06	0.20	0.04	0.06	0.05	0.11	0.88	1.07
Ti	0.01	0.02	0.01	0.01	0.00	0.01	0.01	0.04	0.01	0.01	0.00	0.03	0.13	0.13
Fe ³⁺	0.41	0.09	0.68	0.38	0.29	0.57	0.27	0.14	0.48	0.16	0.35	0.07	0.82	0.50
Mg	0.08	0.56	0.04	0.19	0.24	0.05	0.31	0.52	0.14	0.28	0.12	0.63	0.44	1.01
Fe ²⁺	0.42	0.34	0.20	0.36	0.40	0.29	0.36	0.25	0.30	0.52	0.47	0.31	3.37	3.10
Mn	0.03	0.01	0.01	0.03	0.03	0.02	0.03	0.01	0.03	0.03	0.03	0.01	0.14	0.14
Ca	0.52	0.86	0.31	0.59	0.67	0.38	0.73	0.85	0.55	0.85	0.68	0.87	0.67	1.15
Na	0.48	0.08	0.72	0.42	0.33	0.63	0.27	0.13	0.48	0.15	0.34	0.06	1.99	1.53
K	0.00	0.00	0.00	0.00	0.00	0.00	0.00	0.00	0.00	0.00	0.00	0.00	0.37	0.34
F													0.00	0.01
Cl													0.34	0.50
Total	4.00	4.00	4.00	4.00	4.00	4.00	4.00	4.00	4.00	4.00	4.00	4.00	16.00	16.00
Di	8.0	56.5	3.9	19.2	23.7	4.9	32.2	57.1	14.8	28.5	12.3	62.5		
Hed	44.2	35.4	21.4	38.7	43.5	31.0	39.6	28.4	34.3	56.4	52.6	31.2		
Aeg	47.8	8.1	74.7	42.1	32.8	64.1	28.1	14.5	50.9	15.1	35.1	6.3		

LS = Lower Series, US = Upper Series, GX = Gabbroic xenolith; Calculation of clinopyroxene endmembers: Di = Mg, Hed = Fe²⁺ + Mn, Aeg = Na.

Table 3: Typical microprobe analyses of Fe-Ti oxides in Grønnedal-Ika syenites

Unit Sample	Xenolithic porphyritic syenite GM 1496			Layered syenite, US GM 1539/3			Layered syenite, US GM 1539/5			Layered syenite, US GR 63/5			Layered syenite, US GM 1539
	mag exs.	ilm exs.	bulk calc.	mag exs.	ilm exs.	bulk calc.	mag exs.	ilm exs.	bulk calc.	mag exs.	ilm exs.	bulk calc.	hem assoc. with bt
<i>wt.%</i>													
SiO ₂	0.00	0.01	0.00	0.04	0.01	0.03	0.00	0.01	0.00	0.00	0.01	0.00	0.00
TiO ₂	0.64	51.64	13.51	0.57	50.03	9.55	0.30	49.38	10.15	0.52	40.93	11.83	0.09
Al ₂ O ₃	0.15	0.04	0.12	0.02	0.01	0.02	0.00	0.00	0.00	0.00	0.01	0.00	0.03
Cr ₂ O ₃	0.02	0.00	0.01	0.00	0.02	0.00	0.01	0.03	0.01	0.00	0.01	0.00	0.00
ZnO	0.12	0.06	0.10	0.05	1.10	0.24	0.02	0.31	0.08	0.04	0.49	0.16	0.02
FeO	92.24	4.42	70.07	91.22	31.23	80.32	90.92	27.45	78.19	92.44	44.58	79.04	89.53
MnO	0.40	43.52	11.29	0.06	15.72	2.90	0.11	20.81	4.26	0.09	10.50	3.00	0.07
MgO	0.00	0.00	0.00	0.03	0.02	0.03	0.03	0.02	0.03	0.03	0.05	0.03	0.01
Total	93.56	99.69	95.11	91.99	98.14	93.11	91.39	98.01	92.72	93.11	96.58	94.08	89.75
<i>Formulae based on 3 (2) cations and 4 (3) oxygens for mt (ilm)</i>													
Si	0.00	0.00	0.00	0.00	0.00	0.00	0.00	0.00	0.00	0.00	0.00	0.00	0.00
Al	0.01	0.00	0.01	0.00	0.00	0.00	0.00	0.00	0.00	0.00	0.00	0.00	0.00
Ti	0.02	0.98	0.39	0.02	0.97	0.28	0.01	0.95	0.30	0.02	0.79	0.34	0.00
Cr	0.00	0.00	0.00	0.00	0.00	0.00	0.00	0.00	0.00	0.00	0.00	0.00	0.00
Fe ³⁺	1.96	0.04	1.22	1.96	0.07	1.44	1.98	0.09	1.40	1.97	0.41	1.31	2.00
Mg	0.00	0.00	0.00	0.00	0.00	0.00	0.00	0.00	0.00	0.00	0.00	0.00	0.00
Fe ²⁺	1.00	0.05	1.02	1.01	0.60	1.18	1.00	0.49	1.15	1.01	0.55	1.24	0.00
Mn	0.01	0.93	0.37	0.00	0.34	0.10	0.00	0.45	0.14	0.00	0.23	0.10	0.00
Zn	0.00	0.00	0.00	0.00	0.02	0.01	0.00	0.01	0.00	0.00	0.01	0.00	0.00
Total	3.00	2.00	3.00	3.00	2.00	3.00	3.00	2.00	3.00	3.00	2.00	3.00	2.00
<i>mol%</i>													
Usp	0.02		0.39	0.02		0.28	0.01		0.30	0.02		0.34	
Mag	0.98		0.61	0.98		0.72	0.99		0.70	0.98		0.66	
Ilm		0.05			0.62			0.50			0.56		0.00
Pyr		0.93			0.35			0.46			0.23		0.00
Hem		0.02			0.03			0.05			0.21		1.00
aMag*			0.37			0.52			0.49			0.43	

US = Upper Series, exs. = exsolved, calc. = calculated, assoc. with bt = associated with biotite; * aMag was calculated using an ideal mixing model.

Table 4: Trace element compositions of clinopyroxene and calcite in Grønnedal-Ika rocks determined by Laser ICP-MS

Rock type	XPS	XPS	XPS	XPS	Carbonatite	Carbonatite	Carbonatite	Syenite	Syenite
Sample	GM 1496	GM 1496	GM 1496	GM 1496	GM 1502	GM 1498	GM 1498	GR 44	GR 63
No. of analyses	9	1	3	1	6	2	5	7	5
Mineral	cpx 1 core	cpx 1 rim	cpx 4 core	cpx 4 rim	calcite type A	calcite type B	calcite type C	interstitial calcite	interstitial calcite
<i>ppm:</i>									
Cs	0.27	—	—	—	—	—	—	—	—
Rb	2.98	0.44	9.89	0.45	—	—	—	—	—
Ba	1.34	—	2.21	1.06	5486	76.24	11.96	54.07	105.5
Th	0.08	—	0.11	0.27	0.34	—	—	0.12	0.15
U	0.04	—	0.04	—	—	—	—	—	0.01
Nb	1.93	1.79	2.97	2.47	0.59	—	—	—	—
Ta	0.23	0.11	0.38	0.47	—	—	—	—	—
La	21.90	5.46	10.46	12.00	606.0	8.89	0.53	447.2	429.3
Ce	72.50	22.52	39.13	47.48	1367	30.46	1.61	1091	1081
Pb	0.22	0.25	0.77	0.47	24.25	25.54	51.93	12.80	24.17
Pr	13.37	4.38	7.20	9.63	145.4	7.21	0.35	115.2	121.9
Sr	392.1	281.5	607.3	413.7	15115	6110	5620	8753	6166
Nd	68.45	25.19	42.08	47.87	652.4	57.74	2.02	445.5	507.6
Zr	380.7	5529	236.9	5557	0.35	—	—	0.31	—
Hf	10.33	94.09	7.51	121.5	—	—	—	—	—
Sm	17.52	7.18	11.18	13.31	117.2	34.13	1.16	76.47	97.41
Eu	5.37	2.28	4.28	3.69	40.22	15.90	0.64	15.10	19.93
Ti*	2098	1918	2098	1918	n.a.	n.a.	n.a.	n.a.	n.a.
Sn	2.53	34.58	1.86	36.97	0.76	0.67	0.47	—	—
Gd	12.04	5.10	8.16	9.80	82.13	47.53	1.81	63.10	87.87
Tb	1.75	0.88	1.12	1.69	10.60	8.81	0.64	8.33	12.15
Dy	8.08	5.11	5.15	8.90	48.80	47.31	5.83	42.97	67.53
Li	10.94	—	26.22	2.96	—	—	—	—	—
Y	27.83	19.16	16.83	31.68	160.4	183.7	35.82	191.2	296.6
Ho	1.30	1.09	0.81	1.55	7.20	9.24	1.73	8.03	13.15
Er	2.67	3.70	1.67	5.15	13.46	19.56	6.08	18.94	33.68
Tm	0.35	1.11	0.20	0.92	1.31	1.99	1.13	2.15	4.40
Yb	2.59	11.59	1.19	10.79	5.92	9.71	7.00	11.47	27.68
Lu	0.47	2.11	0.24	2.21	0.58	0.93	0.88	1.16	3.56
Sc	6.51	3.19	5.29	—	1.51	—	1.80	—	—
V	2.16	6.38	82.16	12.07	—	—	—	—	—
Co	19.78	7.38	23.41	9.91	1.85	1.46	1.57	—	1.08
Zn	113.2	403.2	105.4	372.4	7.24	20.00	21.67	1.87	4.83
Ga	12.34	26.27	18.06	14.75	50.89	1.07	—	2.83	5.44
La _{CN} /Yb _{CN}	5.71	0.32	5.91	0.75	68.98	0.62	0.05	26.29	10.46
Eu/Eu*	1.13	1.15	1.37	0.99	1.25	1.21	1.35	0.66	0.66
Zr/Hf	36.9	58.8	31.5	45.7	—	—	—	—	—
Y/Ho	21.41	17.58	20.78	20.44	22.28	19.88	20.71	23.81	22.56

Eu/Eu* = $\text{Eu}_{\text{CN}} / (\text{Sm}_{\text{CN}} \times \text{Gd}_{\text{CN}})^{0.5}$; — = not detected; n.a. = not analysed; * = determined by microprobe.

Table 5: O- and C isotope composition of minerals from the Grønnedal-Ika intrusion

Sample	Sample material	$\delta^{18}\text{O}_{\text{V-SMOW}}$	$\delta^{13}\text{C}_{\text{PDB}}$
Syenites:			
Lower Series:			
GR 01	cpx	4.8 / 4.9	
GR 36	cpx	4.6	
GR 10	cpx	4.8	
GR 13	cpx	4.9 / 4.8	
GM 1554	cpx	4.4	
Upper Series:			
GR 15	cpx	4.8	
GM 1526	cpx	4.7	
GR 44	cpx	4.3	
GM 1559	cpx	4.2	
GM 1531	amph	4.6 / 4.7	
GR 63	cpx	4.8	
GM 1539	cpx	4.6	
Late syenites:			
GR 18 - PMS	cpx	4.8	
GR 27 - PMS	cpx	4.3	
GR 51 - XPS	cpx	4.5	
GM 1496 - XPS	cpx	4.2	
Gabbroic xenolith:			
GR 08	cpx	5.2 / 5.1	
Carbonatites:			
GR 46	calcite	7.9	-4.7
GR 70	calcite	8.6 / 8.6	-4.4 / -4.2
GR 73	calcite	8.4 / 8.2	-4.3 / -4.4
GR 74	calcite	7.9	-4.6
GM 1498	calcite	8.0	-3.9
GM 1502A	calcite	7.9	-3.9
GM 1502B	calcite	7.9	-4.0

PMS = Porphyritic microsyenite; XPS = Xenolithic porphyritic syenite;

Table 6: Mineral separate and whole-rock Nd isotope analyses from Grønnedal-Ika

Sample	Type	Sm (ppm)	Nd (ppm)	$^{147}\text{Sm}/^{144}\text{Nd}$	$^{143}\text{Nd}/^{144}\text{Nd}$	$^{143}\text{Nd}/^{144}\text{Nd}(\text{T})$	$\epsilon_{\text{Nd}}(\text{T})$	$\epsilon_{\text{Nd}}(\text{0})$	T_{DM}^*	T_{CHUR}
Syenites:										
<i>Lower Series:</i>										
GR 01	cpx	17.42	81.65	0.1290	0.512205 ± 10	0.511103	2.8	-8.4	1.60	0.97
GR 13	cpx	27.56	139.29	0.1196	0.512120 ± 10	0.511099	2.7	-10.1	1.58	1.02
<i>Upper Series:</i>										
GR 15	cpx	27.21	133.23	0.1235	0.512120 ± 07	0.511066	2.1	-10.1	1.64	1.08
GR 44	cpx	43.37	243.51	0.1077	0.511971 ± 10	0.511052	1.8	-13.0	1.61	1.14
GR 63	cpx	35.85	179.91	0.1205	0.512081 ± 10	0.511052	1.8	-10.9	1.65	1.11
GM 1531	amph	12.06	71.65	0.1018	0.511969 ± 09	0.511100	2.8	-13.1	1.53	1.07
GM 1559	cpx	32.56	160.78	0.1224	0.512115 ± 10	0.511070	2.2	-10.2	1.63	1.07
<i>Late syenites:</i>										
GR 27 - PMS	cpx	33.79	170.24	0.1200	0.512115 ± 10	0.511091	2.6	-10.2	1.59	1.04
GM 1496 - XPS	cpx	15.72	69.67	0.1364	0.512243 ± 10	0.511078	2.3	-7.7	1.67	1.00
Gabbroic xenolith:										
GR 08	cpx	16.66	63.05	0.1598	0.512236 ± 09	0.510872	-1.7	-7.8	2.34	1.66
Carbonatites:										
GR 46	whole-rock	243.83	1587.0	0.0929	0.511891 ± 10	0.511098	2.7	-14.6	1.52	1.10
GR 70	whole-rock	54.37	374.06	0.0879	0.511852 ± 10	0.511102	2.8	-15.3	1.51	1.10
GR 73	whole-rock	235.97	1260.3	0.1132	0.512049 ± 09	0.511083	2.4	-11.5	1.58	1.07
GR 74	whole-rock	344.58	1915.4	0.1088	0.512010 ± 09	0.511081	2.4	-12.3	1.57	1.09
Basement gneiss:										
GR 78	whole-rock	4.492	20.74	0.1309	0.511399 ± 11	0.510281	-13.3	-24.2	3.01	2.85

* T_{DM} calculated with $(^{147}\text{Sm}/^{144}\text{Nd})_{\text{DM}} = 0.219$ and $(^{143}\text{Nd}/^{144}\text{Nd})_{\text{DM}} = 0.513151$; PMS = Porphyritic microsyenite, XPS = Xenolithic porphyritic syenite; Calculations of $^{143}\text{Nd}/^{144}\text{Nd}(\text{T})$ and $\epsilon_{\text{Nd}}(\text{T})$ for $\text{T} = 1.30$ Ga (Blaxland et al., 1978).

Table 7: Activities used in calculations for jadeite-albite-nepheline equilibria and resulting temperatures and silica activities of syenitic rocks from Grønnedal-Ika

Sample	Comment	a _{Jd}		a _{Ab}		a _{Neph}	Calculated temperatures in °C	Calculated silica activities
		min	max	min	max	average		
<i>Layered syenites</i>								
GR 44		0.038	0.050	0.66	0.79	0.73	680 – 810	0.28 – 0.38
GR 63		0.035	0.042	0.70	0.80	0.74	750 – 850	0.33 – 0.41
GM 1539		0.042	0.046	0.67	0.81	0.74	710 – 780	0.30 – 0.37
GM 1559		0.036	0.047	0.66	0.76	0.74	700 – 830	0.30 – 0.38
<i>Late syenites</i>								
PMS – GR 27		0.042	0.051	0.68	0.79	0.74	680 – 780	0.29 – 0.36
XPS – GM 1496	equilibria with phenocryst cpx rims	0.031	0.035	0.59	0.79	0.74	785 – 910	0.32 – 0.43
XPS – GM 1496	equilibria with matrix cpx	0.042	0.044	0.59	0.79	0.74	710 – 775	0.28 – 0.36

Fig. 1

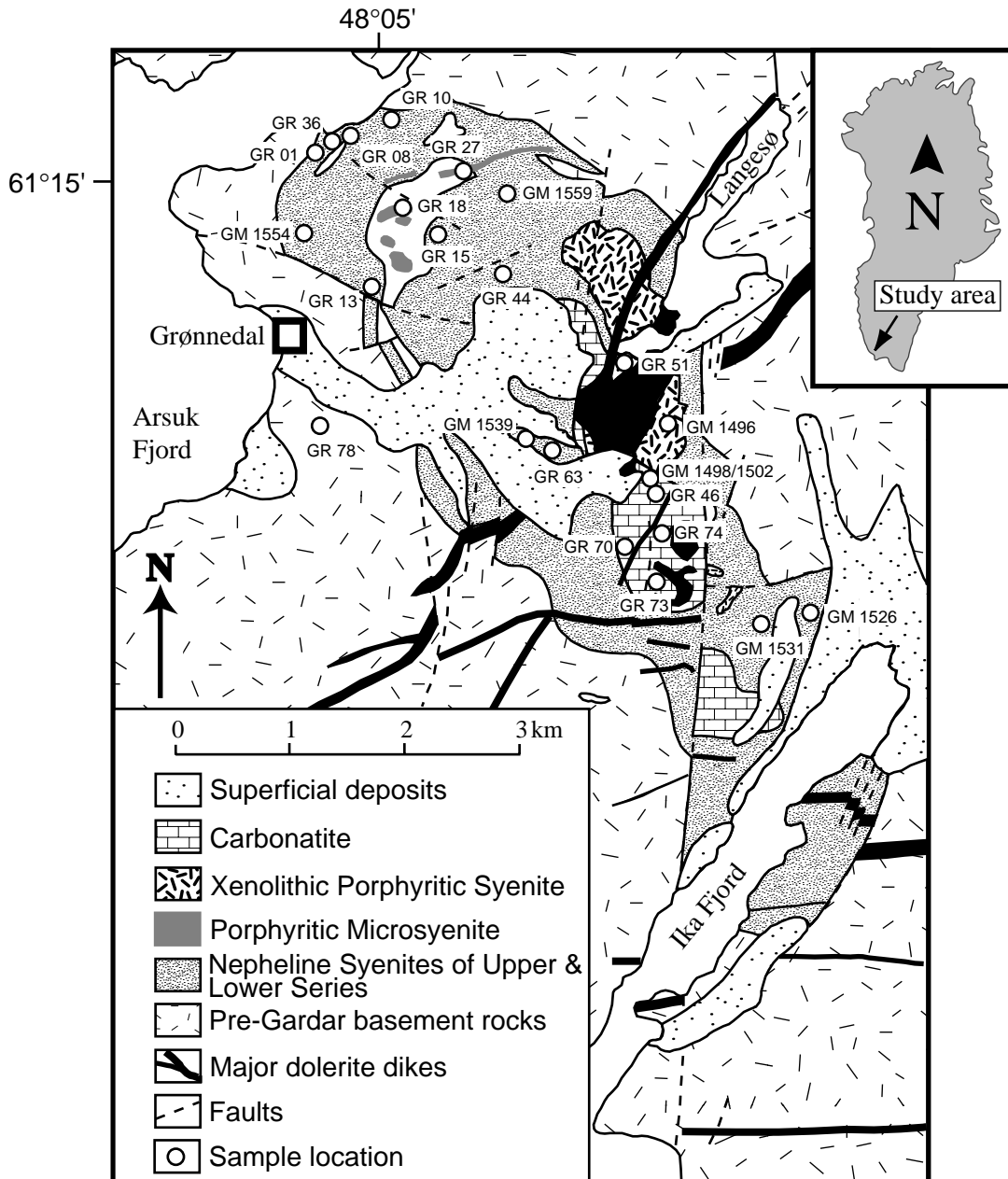


Fig. 2

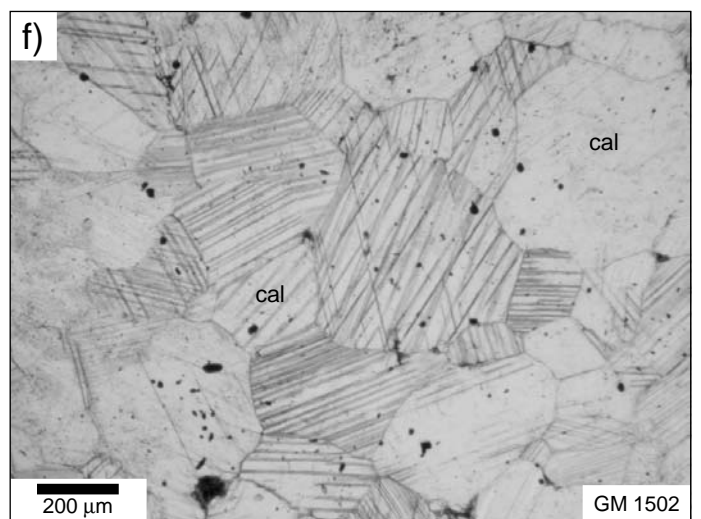
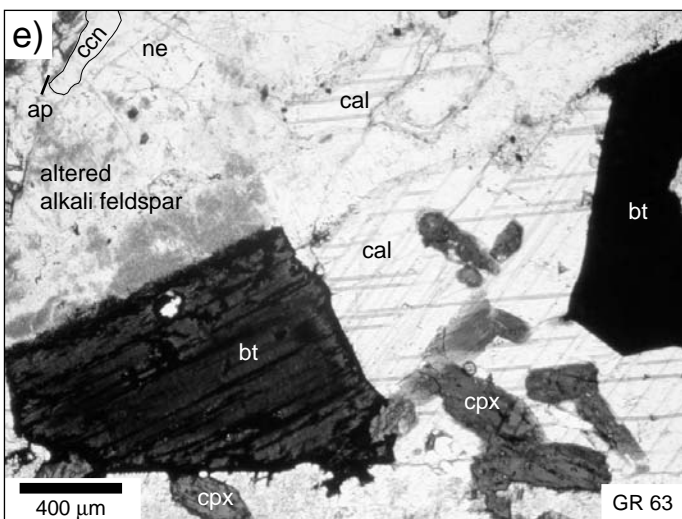
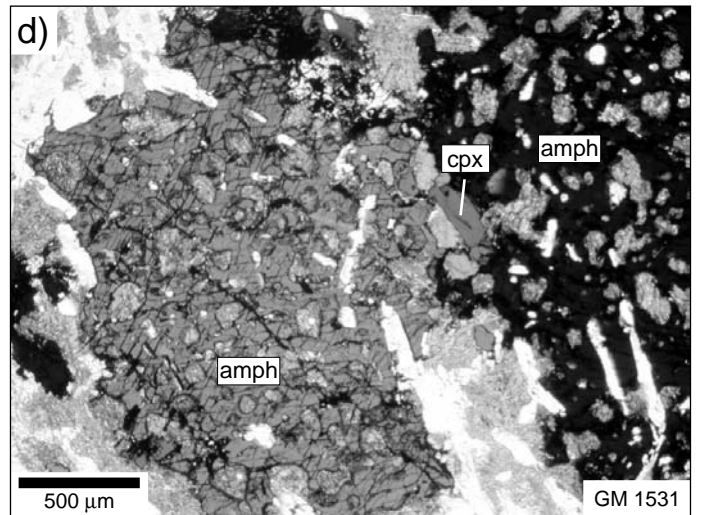
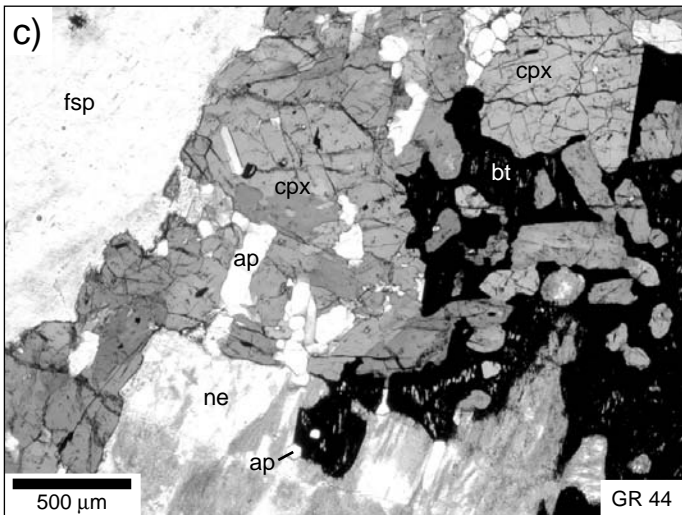
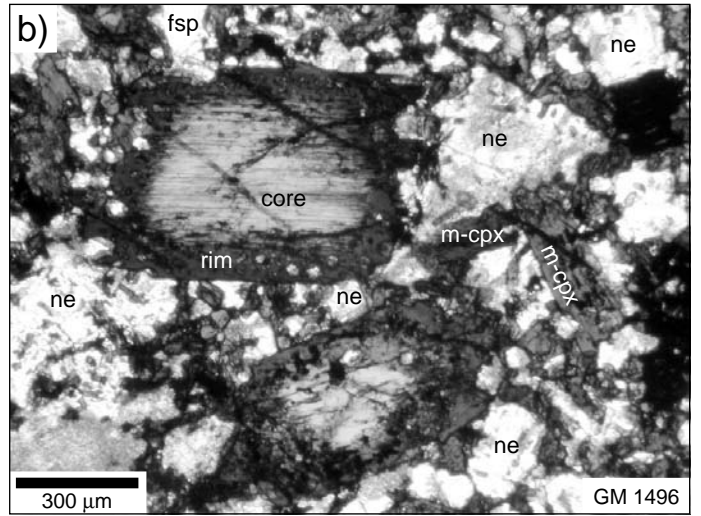
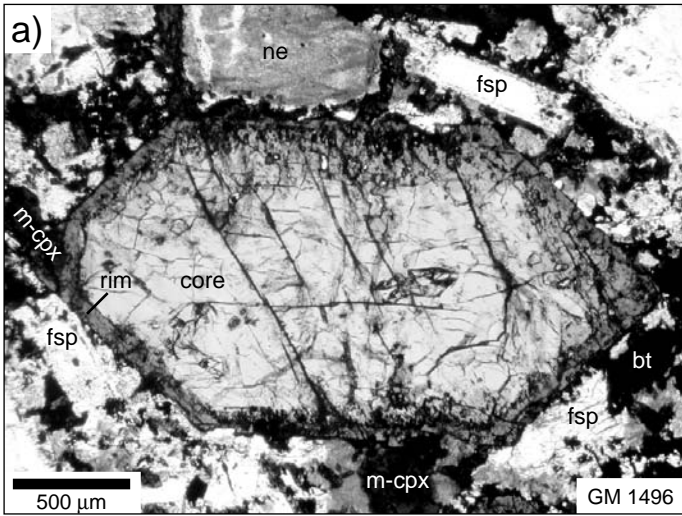
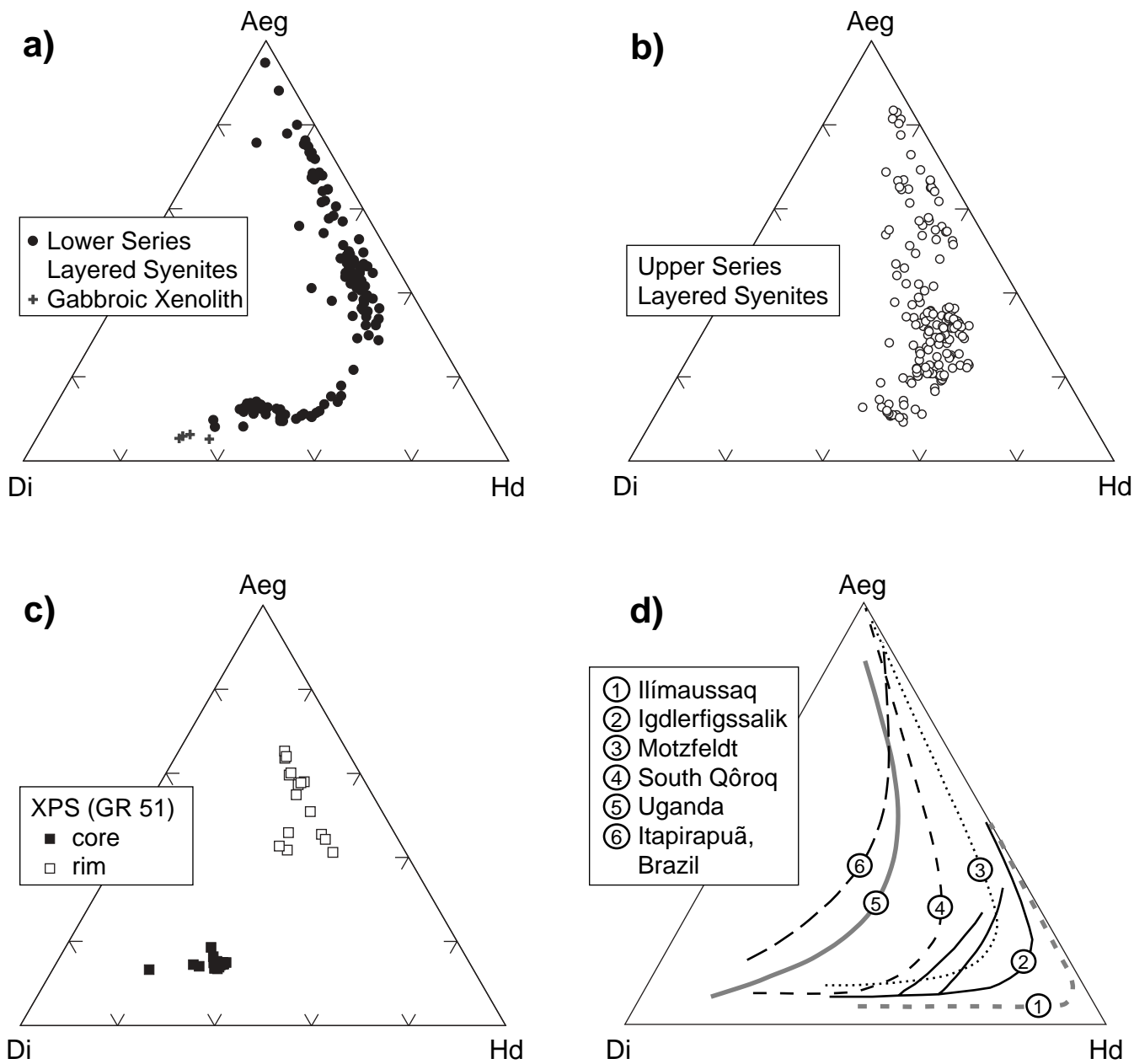


Fig. 3



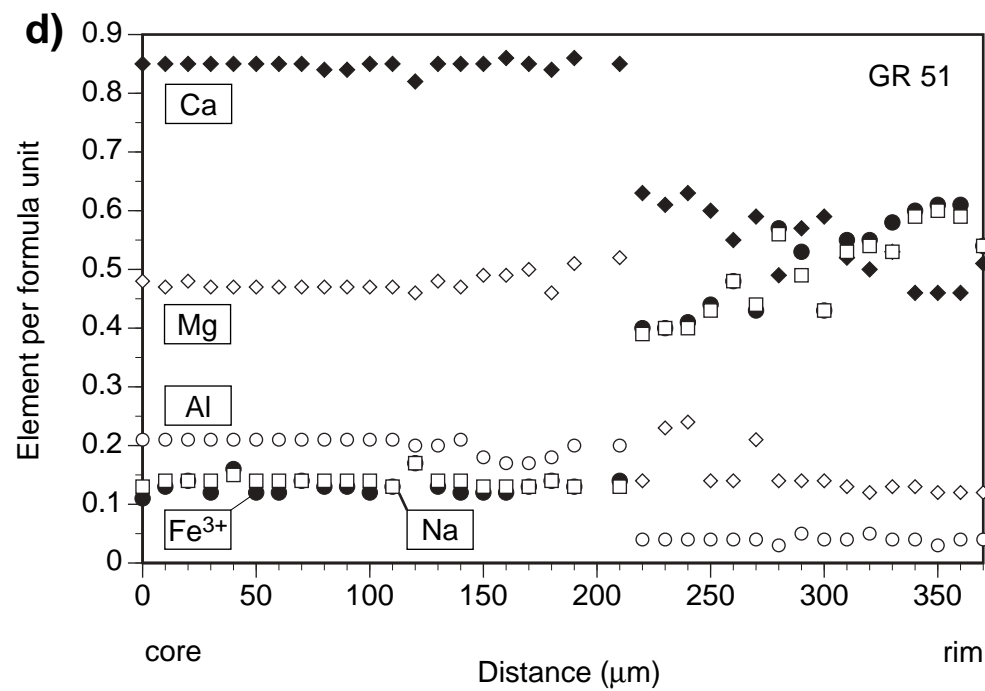
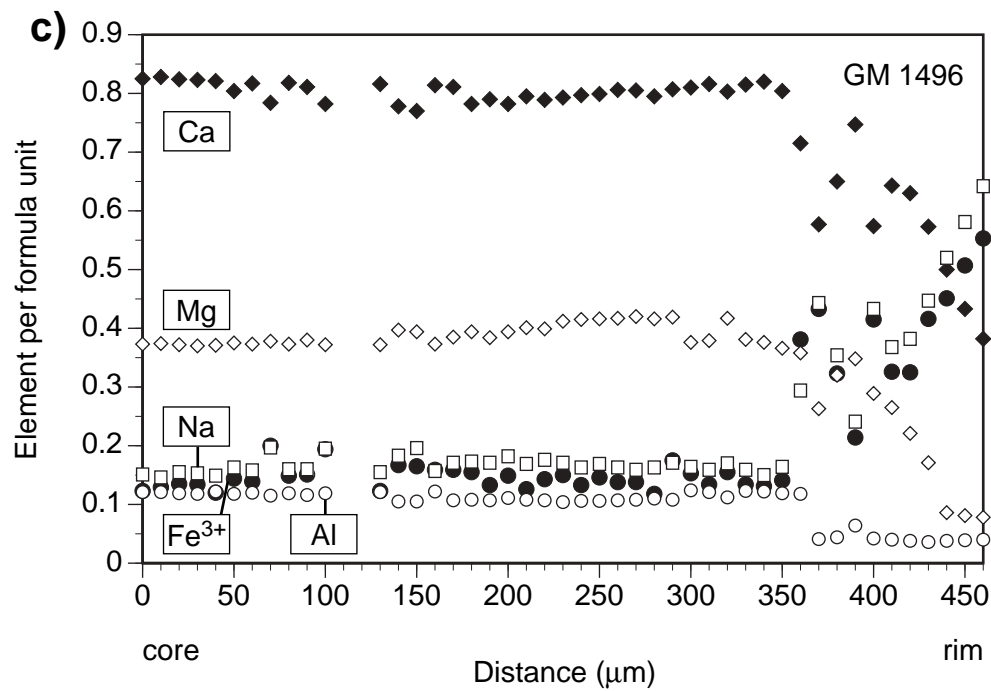
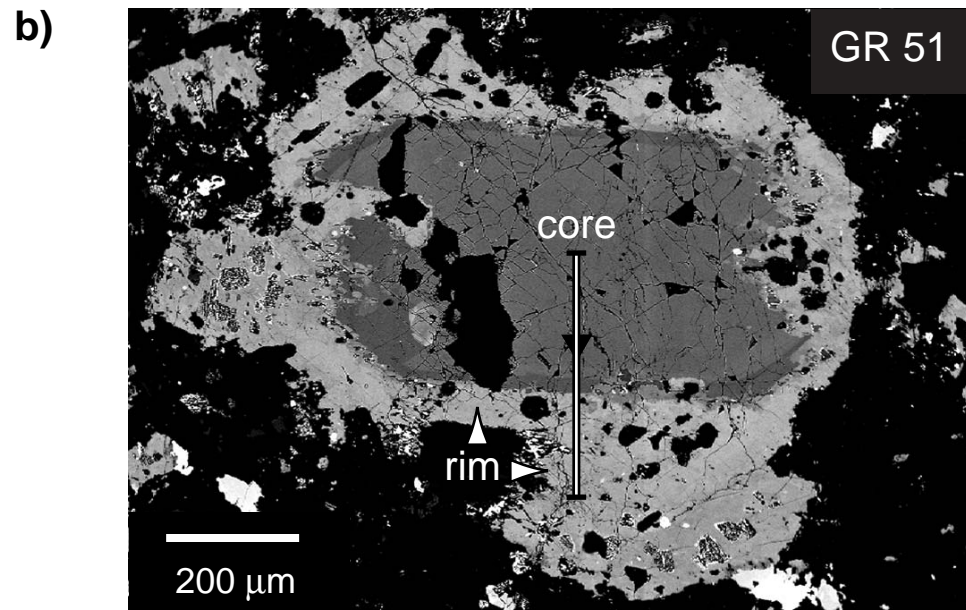
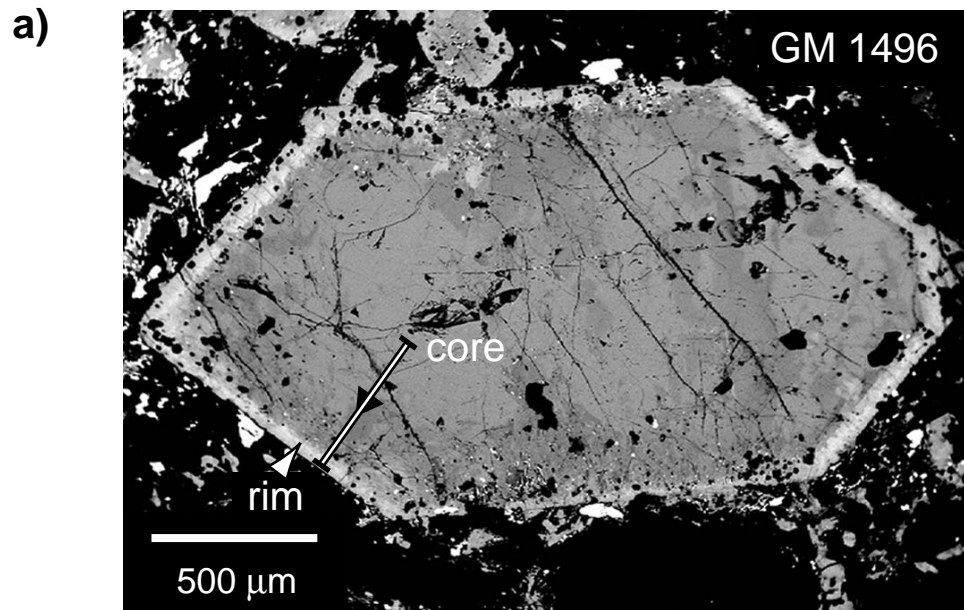


Fig. 5

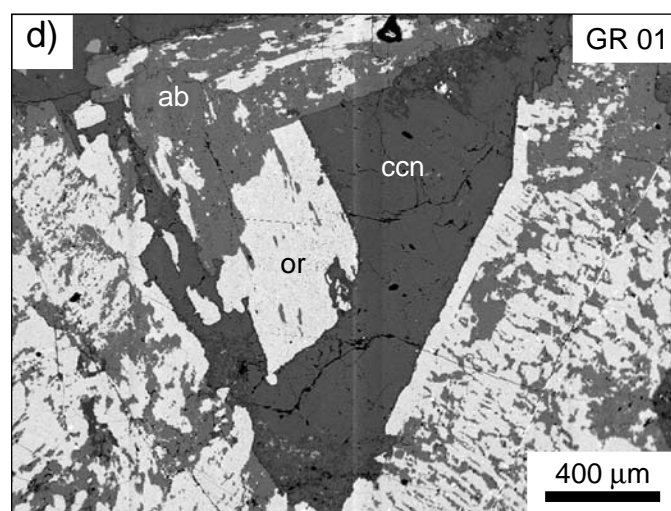
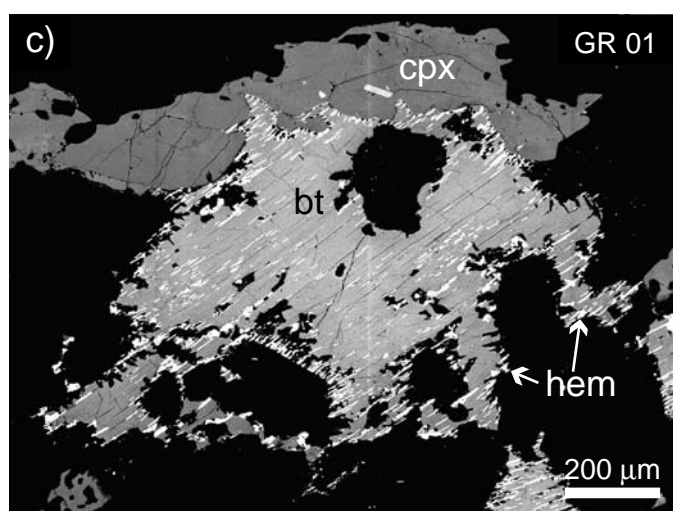
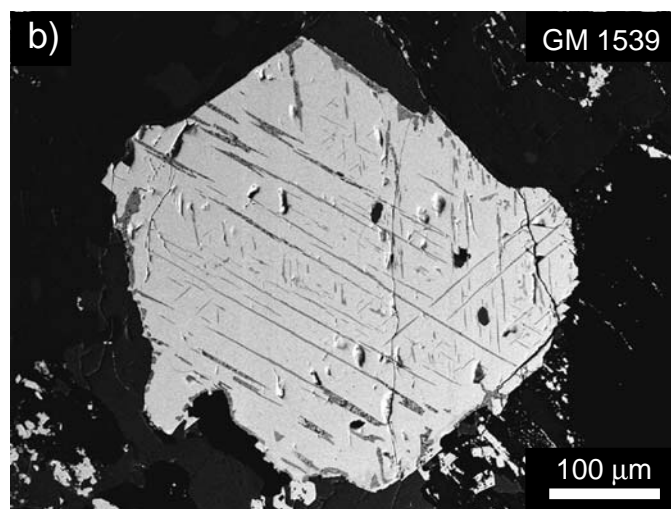
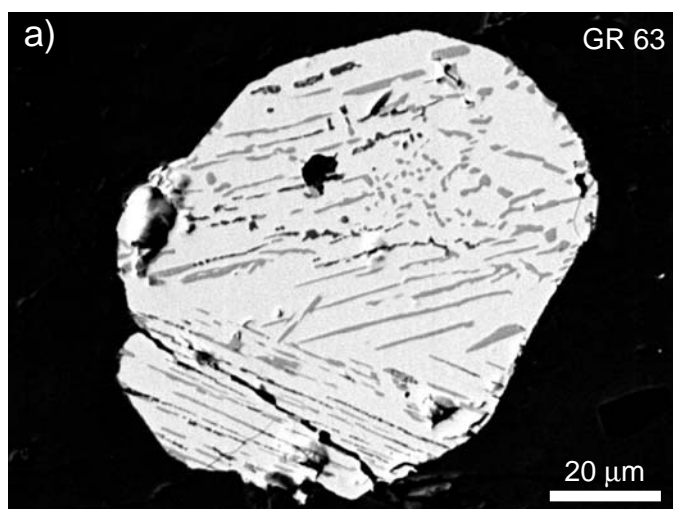
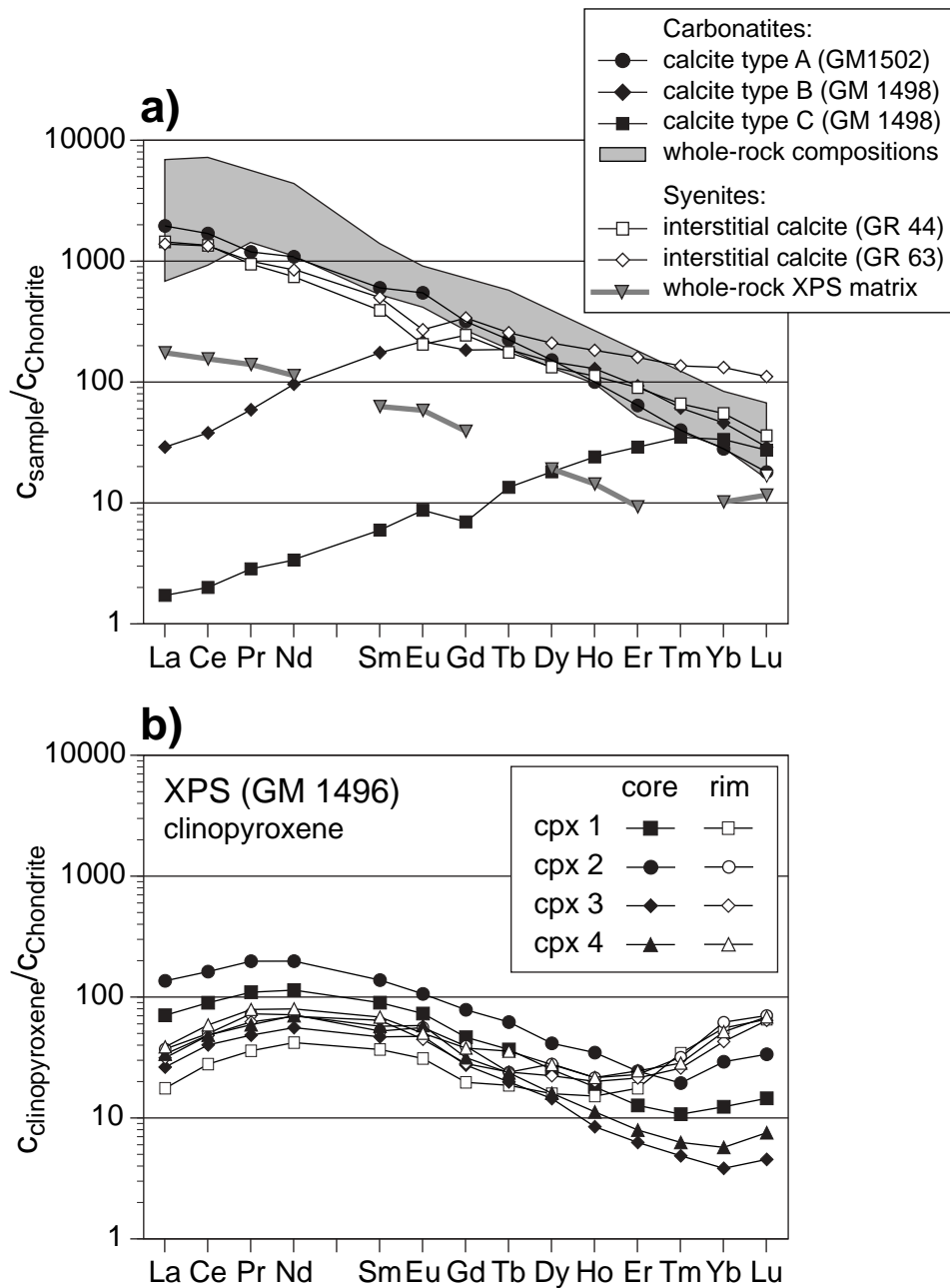


Fig. 6



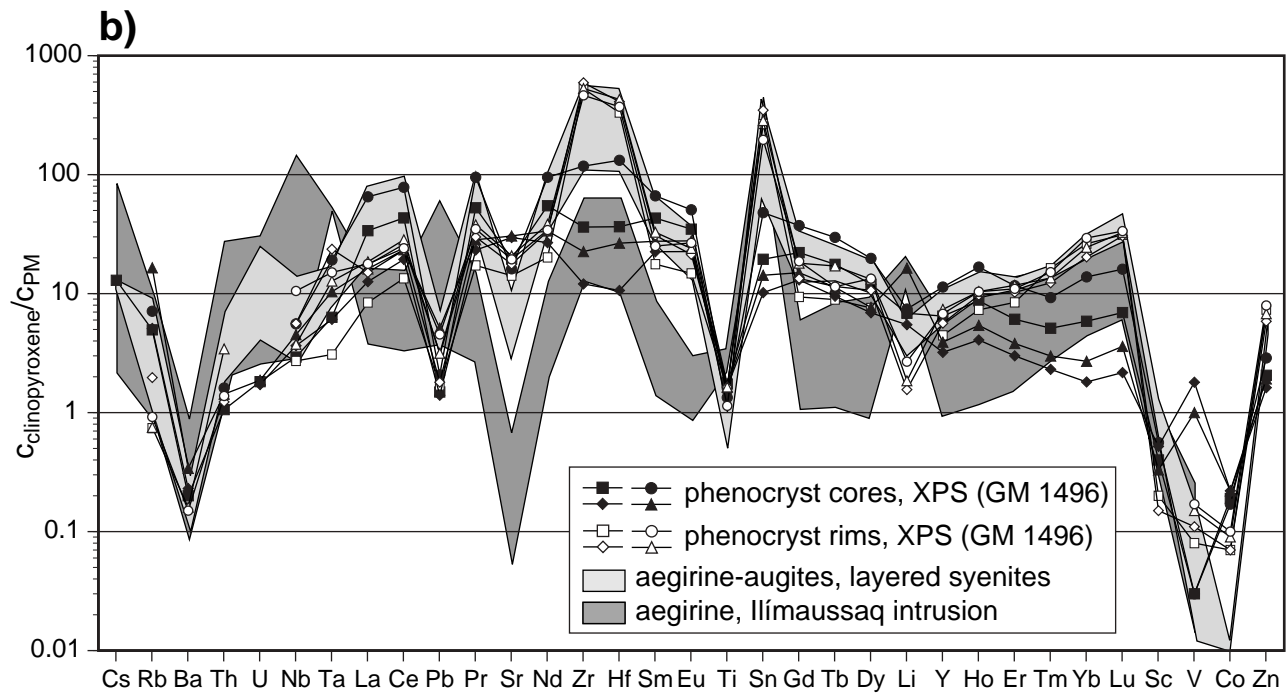
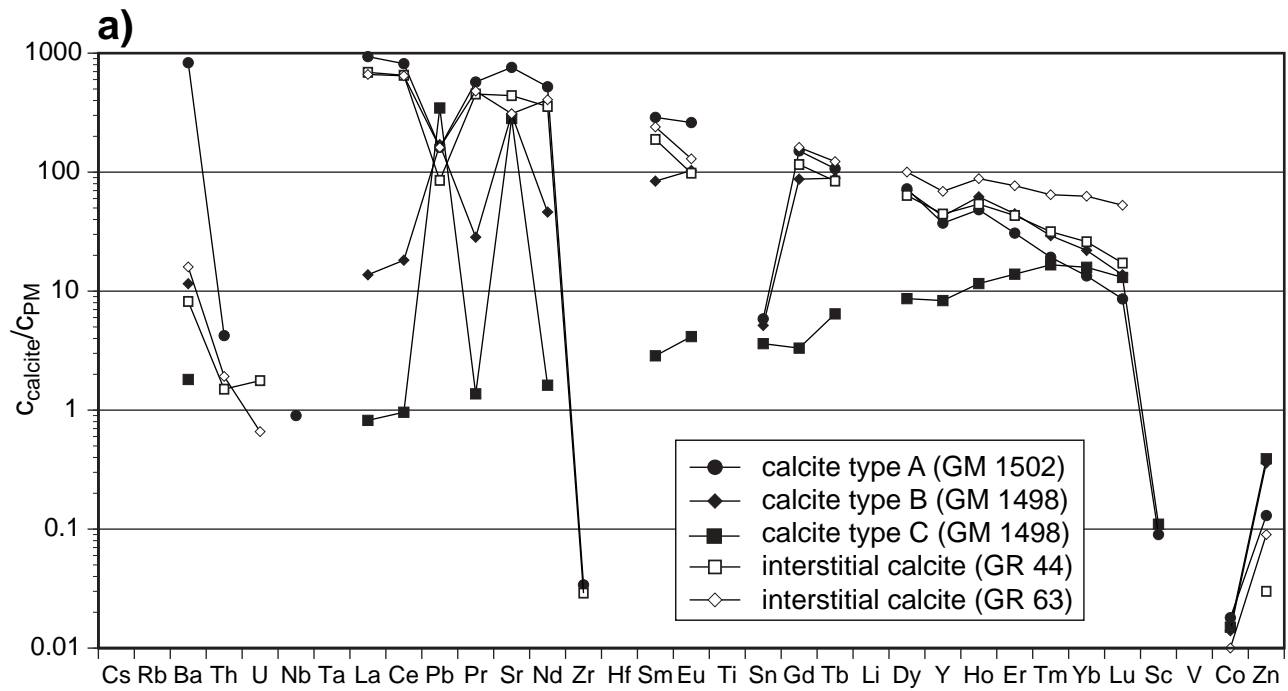


Fig. 7

Fig. 8

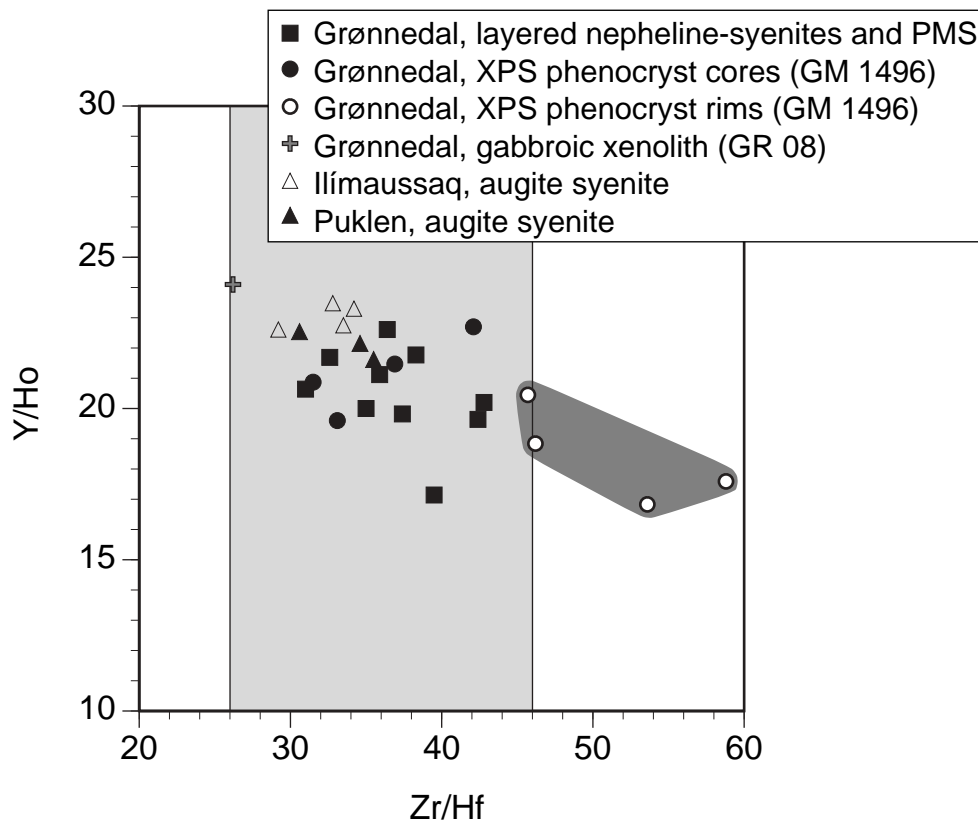
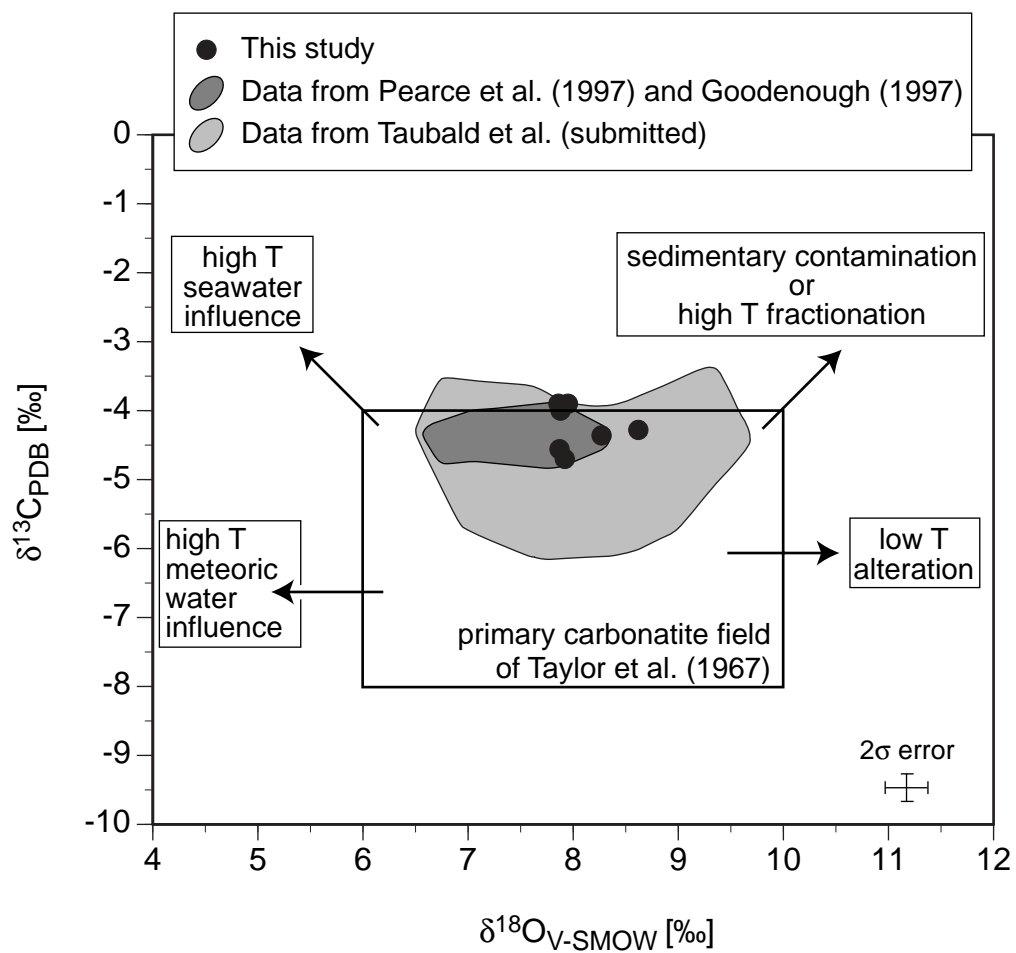


Fig. 9



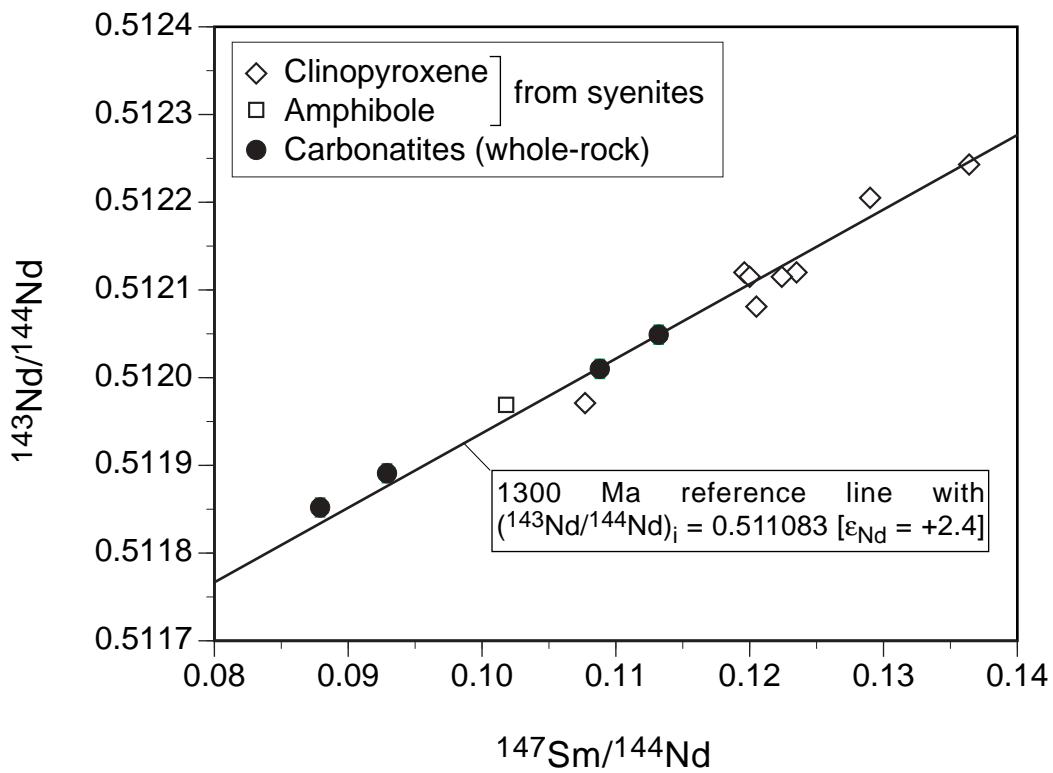


Fig. 10

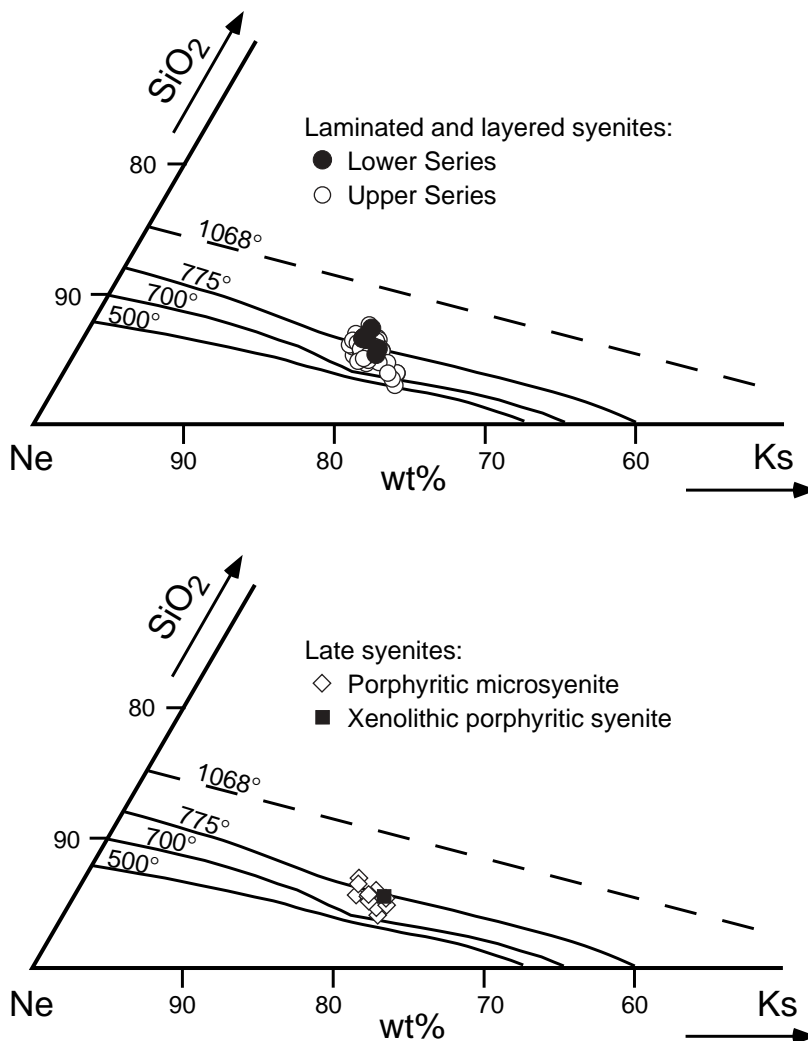


Fig. 11

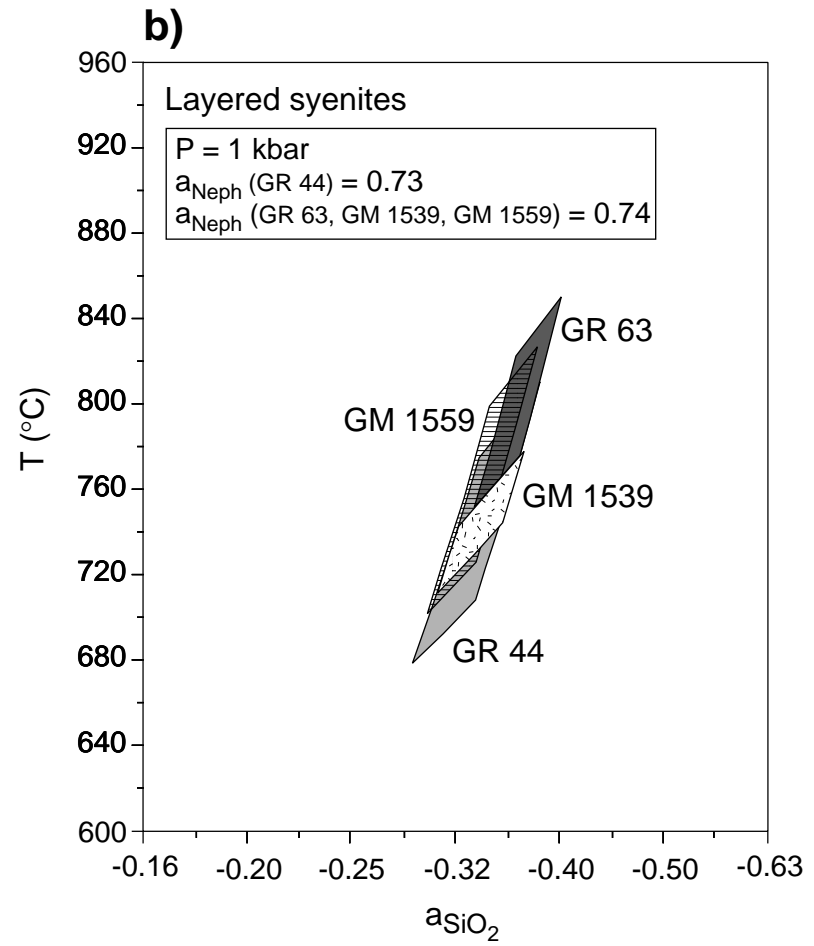
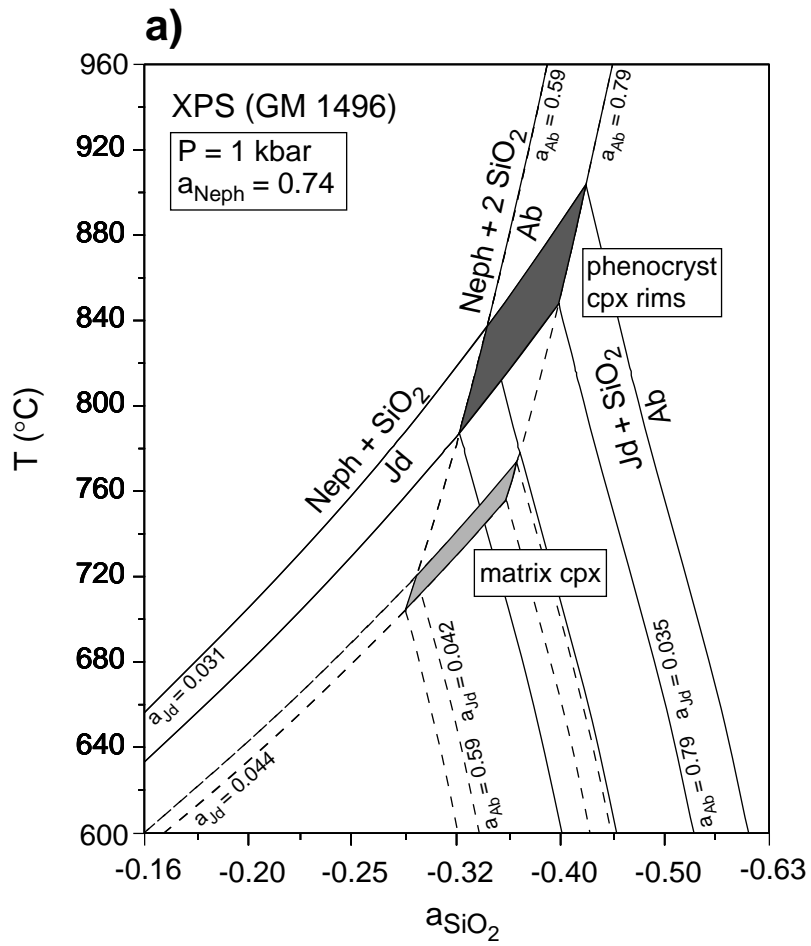


Fig. 12

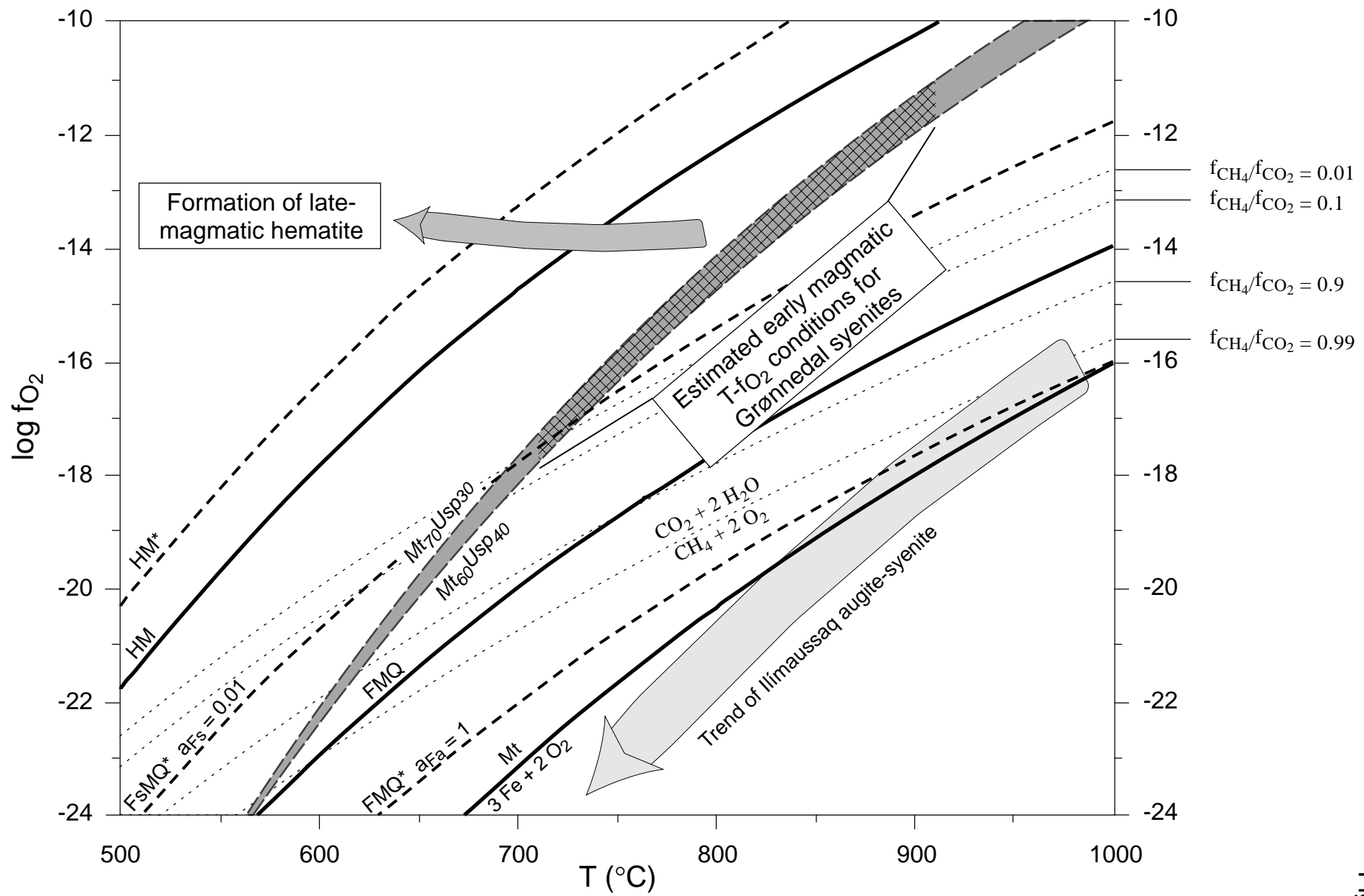
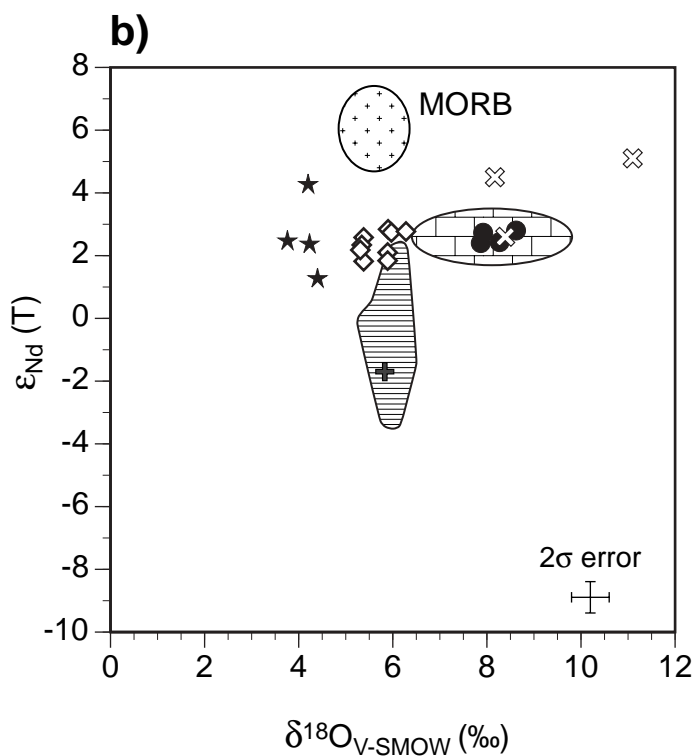
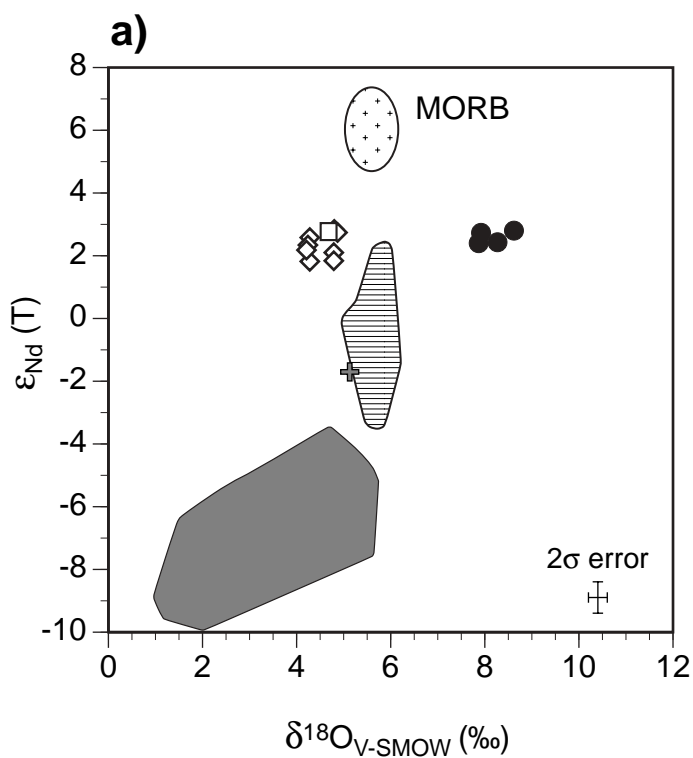


Fig. 13



Grønnedal-Ika rocks:

- calcite from carbonatites
- ◇ clinopyroxene from syenites
- amphibole from syenites
- ⊕ clinopyroxene from gabbroic xenolith

Other rocks:

- hypothetical clinopyroxene in MORB
- ▨ clinopyroxene from the EF basalts
- clinopyroxene and amphibole from the Puklen intrusion

Grønnedal-Ika data:

- ◇ calculated nepheline-syenitic melt
- ⊕ calculated basaltic melt
- carbonatites (this study)
- ⊕ carbonatites (literature data)

Comparative data:

- MORB glass composition
 - ▨ calculated melt of EF basalts
 - ★ carbonatites
 - ⊗ lamprophyres
-] from Igaliko

Kapitel 5:

Spurenelementuntersuchungen an mafischen Mineralen (Klinopyroxen, Amphibol) dreier Alkaligesteinsintrusionen Südgrönlands

Manuskript-Titel:

Trace element variations in clinopyroxene and amphibole from alkaline to peralkaline syenites and granites: Implications for mineral-melt trace-element partitioning

Autoren:

Michael Marks, Ralf Halama, Thomas Wenzel, Gregor Markl

Institut für Geowissenschaften, Eberhard-Karls-Universität Tübingen,
Wilhelmstr. 56, D-72074 Tübingen

Eingereicht bei:

Chemical Geology

Eigenanteile:

- | | |
|----------------------------------|-----|
| a) Idee | 25% |
| b) Datenbeschaffung | 35% |
| c) Auswertung und Interpretation | 30% |
| d) Ausarbeitung der Publikation | 30% |

Abstract

We present a detailed LA-ICP-MS study on trace element compositions of clinopyroxene and amphibole from three rift-related alkaline to peralkaline igneous complexes (syenites and granites) in South Greenland. Investigated clinopyroxenes and amphiboles evolve from Ca-Mg-dominated via intermediate to Na-Fe³⁺-dominated members. Most trace elements are highly enriched compared to primitive mantle values, which is in accordance with the highly fractionated character of the host rocks. High field strength element (HFSE; Ti, Zr, Hf, Sn, Nb, Ta) abundances appear to be mainly controlled by the major element composition of the host crystal that in turn determines the crystal site parameters. A crystal chemical control is also indicated for the REE, since clinopyroxenes and amphiboles show a continuous development from LREE-enriched patterns in the calcic minerals via wave-shaped pattern in the Ca-Na minerals towards a more pronounced HREE enrichment in the most Na-rich minerals. The low absolute abundances of large ion lithophile elements (Ba, Sr, Pb, Eu²⁺) are interpreted to reflect both a crystal-chemical aversion to incorporate these elements and the effect of prolonged feldspar fractionation on the melt composition. Additionally, oxygen fugacity and crustal assimilation affect the incorporation of Eu and Pb, respectively.

The partitioning of most trace elements between clinopyroxene and co-genetic amphibole is fairly independent of melt composition or major element composition of the crystals. Most trace elements show a slight preference for amphibole, which is most pronounced for Nb, Ta, U, Th, Rb, Ba and Li. Exceptions to this general trend occur in rocks affected by late-stage fluid circulation resulting in the re-distribution of some mobile elements.

Calculation of trace-element compositions of melts from the mafic mineral data using published partition coefficients for alkaline systems shows that melt compositions similar to whole-rock compositions are obtained for clinopyroxenes with broadly augitic to diopsidic compositions. There is a considerable mismatch between calculated melt and whole-rock data for various elements, i.e. Zr, Hf and the HREE, when melt compositions are calculated from NaFe³⁺-rich aegirine-augites and aegirines. Melt compositions from amphiboles also show only limited overlap with whole-rock data. The reasons for these differences may include: 1. The crystallization history of the rocks is very complex so that trace element partitioning cannot be expressed with a single partition coefficient. 2. Published mineral-melt partition coefficients cannot generally be applied due to

compositional differences between the alkaline to peralkaline systems of this study and the previous studies. 3. Whole-rocks do not reflect melt compositions.

Using a theoretical model on clinopyroxene-melt trace element partitioning based on the crystal chemistry alone, we show that the relative preference for HREE increases as the crystal becomes more aegirine-rich, which is in qualitative accordance with the observed REE patterns. Absolute values of D_{REE} decrease with progressing crystal chemical evolution, but they increase with falling temperatures. Melts calculated from the theoretically determined partition coefficients show a good overlap with whole-rock data for relatively Fe^{3+} -poor clinopyroxene compositions. Melts calculated from aegirines do not agree with whole-rock compositions, suggesting that the theoretical model needs refinements for the previously not considered incorporation of the $\text{NaFe}^{3+}\text{Si}_2\text{O}_6$ component and/or that the fluid-rich nature of the peralkaline melts has changed the trace-element partitioning behavior.

1. Introduction

Trace element data can be used to model and interpret magmatic processes (e.g. Schiano *et al.*, 1993; Walter *et al.*, 1995; Costa *et al.*, 2003). *In situ* determination of trace elements in minerals from both natural and experimental samples has become increasingly popular and many studies have been published concentrating on basaltic systems (e.g. Jeffries *et al.*, 1995; Benoit *et al.*, 1996; Coogan *et al.*, 2000; Thompson & Malpas, 2000; Tiepolo *et al.*, 2002), on ultramafic mantle rocks and on phases relevant to mantle melting (e.g. Nimis & Vanucci, 1995; Blundy & Dalton, 2000, Grégoire *et al.*, 2000; Tiepolo *et al.*, 2000b). Studies on trace element partitioning and trace element contents in more evolved silicic systems are less frequent (Lemarchand *et al.* 1987; Wood & Trigila, 2001), and especially the trace element concentrations of mineral phases in alkaline silicate plutonic rocks have only been studied in a few cases (Larsen 1979; Wörner *et al.*, 1983; Shearer and Larsen 1994). Recent studies based on theoretical models have shown that the crystal chemistry exerts a major control on trace element partitioning (Blundy & Wood, 1991, 1994; Wood & Blundy, 1997, 2001). The size of ions relative to the site of interest and the charge of ions are critical factors in governing trace element behavior, whereas the melt composition is thought to be of little significance (Blundy & Wood, 2003). Unfortunately, experimental trace element partitioning studies between mafic minerals and alkaline silicate melts are rare. The available data derived from natural rocks (e.g. Larsen, 1979; Wörner *et al.*, 1983) show a scatter, which is surprisingly large even when differences in the mineral compositions are taken into account.

In this study, we compare the trace element contents of mafic minerals from three related, but petrologically different alkaline to peralkaline igneous complexes in order to investigate the partitioning behavior of trace elements in natural alkaline silicate melts. Alkaline plutonic complexes are common in rift-related provinces and they are commonly characterized by an enrichment of rare elements with economic potential (e.g. Kramm & Kogarko, 1994; Panneer Selvam & Suryanarayana Rao 1996; Platt, 1996; Digonnet *et al.*, 2000). Our study is focused on clinopyroxene and amphibole because these two minerals can incorporate large amounts of geochemically relevant trace elements (Wood & Blundy, 1997; Botazzi *et al.*, 1999). The three complexes studied show an almost continuous spectrum in mafic mineral compositions from Ca-Mg-rich and Na-poor to Ca-poor and Na-Fe³⁺-rich. This enables us to relate relative trace element

abundances in the minerals to their crystal chemistry. Furthermore, we determine distribution coefficients between clinopyroxene and amphibole for a wide range of elements in alkaline igneous rocks and compare them with literature data for other rock types. Finally, we use a range of partition coefficients from the literature determined for natural alkaline rocks (Larsen, 1979; Wörner *et al.*, 1983; Lemarchand *et al.*, 1987) to evaluate if they are applicable for the rocks studied here. *In situ* trace element analyses of minerals avoid the problem of whole-rock data from plutonic rocks that are frequently influenced by accumulation of certain minerals and that might represent a mixture of various processes (e.g. Marks *et al.*, 2003).

2. Regional geology

The Gardar Igneous Province (Fig. 1) in South Greenland represents a failed rift structure of Mid-Proterozoic (1.35 – 1.14 Ga) age (Upton & Emeleus, 1987; Upton *et al.*, 2003). It comprises a sequence of interlayered basalts and sandstones (Eriksfjord Formation; Poulsen, 1964), a large number of dike rocks of variable chemical composition and twelve major alkaline to peralkaline igneous complexes. The basement rocks mainly consist of I-type calc-alkaline plutonic rocks (Julianehåb batholith) (van Breemen *et al.*, 1974; Alaart, 1976; Kalsbeek & Taylor, 1985), which were emplaced between 1.85 and 1.80 Ga (Garde *et al.*, 2002). Archaean country rocks occur in the northwestern part of the province.

The igneous complexes are mostly composite and show a range from relatively primitive gabbroic to highly evolved syenitic rocks. Fluid inclusion data (Konnerup-Madsen & Rose-Hansen, 1984) and the preserved contacts between supracrustal rocks and the Ilímaussaq intrusion (Poulsen, 1964) show that the magmas intruded into shallow crustal levels (< 5 km).

For this study, we selected three igneous complexes: 1.) The Puklen complex evolved from silica-saturated syenites to alkali granites and represents a silica-oversaturated fractionation trend (Pulvertaft, 1961; Parsons, 1972; Marks *et al.*, 2003). 2.) The Ilímaussaq complex, evolving from alkaline, SiO₂-saturated syenites towards agpaitic nepheline syenites represents the silica-undersaturated trend (Larsen & Sørensen, 1987; Markl *et al.*, 2001b). 3.) The Grønnedal-Ika complex represents an association of SiO₂-undersaturated syenite with carbonatite (Emeleus, 1964;

Pearce *et al.*, 1997; Halama *et al.*, submitted). In the following, we shortly review the petrogenesis of these three complexes.

2.1 The Puklen complex

The Puklen complex is situated in the western part of the Gardar Province (Fig. 1). The field geology was described in detail by Pulvertaft (1961) and Parsons (1972) and the petrology and geochemistry was investigated by Marks *et al.* (2003). The first magma pulse formed a suite of silica-saturated to oversaturated syenites. In the southern part of the intrusion, a fine-grained and leucocratic granophyre cuts the adjoining syenite. A second pulse of magma produced a homogeneous, coarse-grained peralkaline granite, which grades into, or may be locally intruded by fine-grained and leucocratic microgranite.

The primary mafic minerals in syenites are augite \pm olivine + Fe-Ti oxide + calcic to sodic-calcic amphibole I. Secondary calcic amphibole II formed by late-stage autometamorphic reactions. In the granites, the primary mafic minerals are ilmenite and sodic amphibole, the latter is overgrown by late-stage aegirine. Detailed isotopic work (Marks *et al.*, 2003) showed that the Puklen melts were primarily derived from a mantle source with variable amounts of crustal assimilation.

2.2 The Ilímaussaq complex

The formation of the Ilímaussaq complex (Fig. 1) involved three magma batches (Larsen & Sørensen, 1987; Konnerup-Madsen & Rose-Hansen, 1984). The earliest melt batch is represented by a shell of augite syenite, which was later intruded by a sheet of alkali granite in the north of the complex. The third intrusive phase comprises the major part of the complex and consists of different varieties and partly layered agpaitic nepheline syenites (Ferguson, 1964). The major mafic minerals in the augite syenite are augite + olivine + Fe-Ti oxide + calcic amphibole (Larsen 1976, 1977, 1981; Markl *et al.*, 2001a+b; Marks & Markl, 2001). In the alkali granite and in the agpaites, sodic amphibole and aegirine occur in addition to high amounts of eudialyte (REE-rich Zr-silicate). Homogeneous oxygen and neodymium isotope compositions of mineral separates from the augite syenite and the agpaitic nepheline syenites indicate a closed system evolution of the complex and support a mantle derivation of the magma (Marks *et al.*, submitted). The only exception is the alkali

granite, which can be explained by higher amounts of crustal contamination compared to the other rock types (Marks *et al.*, submitted).

2.3 The Grønnedal-Ika complex

The Grønnedal-Ika complex consists of partly layered silica-undersaturated nepheline syenites, which were intruded by a central plug of calcio-carbonatite (Emeleus, 1964; Bedford, 1989; Pearce *et al.*, 1997). The major mafic mineral in the nepheline syenites is clinopyroxene, amphibole is very scarce (Bedford, 1989). The nepheline syenitic magmas of the Grønnedal-Ika intrusion are thought to be produced by fractional crystallisation of mafic magmas. Sr and Nd isotopic data indicate a fairly homogeneous mantle source for the syenitic and carbonatitic magmas. Crustal rocks were not significantly assimilated (Pearce *et al.*, 1997; Halama *et al.*, submitted).

3. Sample material and analytical methods

Several representative samples from each rock type of each of the three intrusions were selected for this study. Most of the analysed samples have been part of previous petrological and geochemical studies on the respective igneous complexes (Markl *et al.*, 2001b; Marks & Markl, 2001; Markl & Baumgartner, 2002; Marks *et al.*, 2003; Halama *et al.*, submitted). Selected samples and minerals analysed are summarised in Table 1.

In situ laser ablation inductively coupled plasma-mass spectrometer (LA-ICP-MS) analyses of REE and other trace elements were performed at the EU Large-Scale Geochemical Facility (University of Bristol) using a VG Elemental PlasmaQuad 3 + S-Option ICP-MS equipped with a 266 nm Nd-YAG laser (VG MicroProbe II). The laser beam diameter at the sample surface was approximately 20 μm . All measurements were made using Thermo Elemental PlasmaLab "time-resolved analysis" (TRA) data acquisition software with a total acquisition time of 100 s per analysis, allowing about 40 s for background followed by 50 s for laser ablation. NIST 610 glass was used for instrument calibration, and NIST 612 was used as a secondary standard. Si was used as an internal standard to correct the ablation yield differences between and during individual analyses on both standards and samples. To avoid analytical uncertainties due to variations in the concentrations of the internal standard, Si concentrations were quantitatively measured within 20 μm of the laser ablation pits

using a JEOL 8900 electron microprobe (EMP) at the Universität Tübingen (see below). The precision of trace element concentrations, based on repeated analyses of standards, is approximately $\pm 5\%$ for element concentrations >10 ppm and $\pm 10\%$ for concentrations <10 ppm. Data processing was carried out offline using the same PlasmaLab software used for data collection and various custom-designed Excel spreadsheets. The limits of detection are defined as 3.28 standard deviations above background level, which equates to a 95% confidence that the measured signal is significantly above background. Typical detection limits are 1 - 20 ppm for Sc, V, Co, Cu, Zn, Ga, Rb and Ba, 0.2 - 1 ppm for Sr, Y, Zr, Nb, Sn, Cs, Hf and Pb and 0.05 – 0.6 ppm for the REE, U, Th and Ta. Detection limits for Li are highly variable between 2 and 80 ppm depending on the specific setting during measurements.

Major element composition of minerals was determined using a JEOL 8900 electron microprobe at the Institut für Geowissenschaften at the Universität Tübingen, Germany. Both natural and synthetic standards were used for calibration. The beam current was 15 nA and the acceleration voltage was 15 kV. The counting time on the peak was 16 s for major elements, and 30-60 s for minor elements (Mn, Ti, Zr, F, Cl). Background counting times were half peak counting times. The peak overlap between the Fe $L\beta$ and F $K\alpha$ lines was corrected for. Data reduction was performed using the internal $\phi\rho Z$ procedures of JEOL (Armstrong, 1991).

4. Major element compositional trends of clinopyroxene and amphibole from the three investigated complexes

4.1 Clinopyroxene

The pyroxene trends observed in the three investigated intrusive complexes are shown in Fig. 2. In all three complexes, the most primitive pyroxenes (in terms of X_{Fe}) are diopsidic with low Na contents (< 0.1 a.p.f.u.). During fractionation, pyroxene composition gets more Fe- and Na-rich, reaching almost end-member aegirine composition in Puklen and Ilímaussaq (Larsen, 1976; Marks & Markl, 2001; Markl *et al.*, 2001b; Marks *et al.*, 2003). Differences in the degree and timing of Na- and Fe^{3+} -enrichment can be attributed to oxygen fugacity during crystallization: The strongly reducing conditions (below the FMQ buffer) in the Ilímaussaq complex and in most of the Puklen

samples allow a strong Fe-enrichment, but still low Na contents during fractionation (e.g. Larsen, 1976). In contrast, more oxidized conditions in the Grønnedal-Ika complex (Pearce *et al.*, 1997; Halama *et al.*, submitted) result in relatively high Na- and Fe³⁺-contents at intermediate Fe/Mg ratios. A similar compositional trend found in the Puklen complex is the result of more oxidized ($\Delta\text{FMQ} = +1$) conditions during late-magmatic autometasomatism (Marks *et al.*, 2003).

4.2 Amphibole

Figure 3 shows the amphibole trends observed in the three investigated intrusive complexes in the Ca_B vs Si diagram after Mitchell (1990). The Puklen and Ilímaussaq trends are typical of magmatic alkaline to peralkaline rocks. Primary amphibole ranges in composition from almost pure Ca-amphibole (ferro-edenite, ferro-pargasite, hastingsite) with relatively high Al-contents in the early rock types and evolves via Na-Ca amphibole (katophorite, ferro-richterite) to Na-amphibole (nyböite, arfvedsonite, leakeite) in the most evolved rocks. Secondary amphibole in the Puklen rocks evolves from ferro-edenite towards ferro-actinolite, which is known only from silica-oversaturated alkaline complexes (Mitchell, 1990). Amphiboles in the Grønnedal-Ika syenites are mainly sodic-calcic katophorites, sodic and calcic amphiboles are very scarce (Bedford, 1989).

5. Trace element compositions

Overall, more than 230 trace element analyses of clinopyroxene and 150 analyses of amphibole were performed. In order to present a good overview of the whole data set, we present the averages of analyses from the respective minerals of each sample studied. In cases of significant chemical zoning with respect to major and trace element composition within individual grains, representative zoning profiles are shown. Typical analyses of clinopyroxene and amphibole from the three investigated igneous complexes are summarized in Tables 2 and 3. All rare earth element (REE) and trace element (TE) patterns are normalized to primitive mantle values of McDonough & Sun (1995). The order of presentation for both clinopyroxenes and amphiboles follows the above-described major element trends starting with the Ca-rich endmembers.

5.1 Clinopyroxene

5.1.1 Augites of Puklen and Ilímaussaq

Figures 4 a & b show average REE and TE patterns from augites of Puklen and Ilímaussaq, which are characterized by low Na/Ca ratios < 0.15 . Normalized REE concentrations for all augites are 10 to 200 times enriched relative to primitive mantle values. The patterns are sinuoidal and show strongly developed negative Eu anomalies ($\text{Eu}/\text{Eu}^* = 0.12 - 0.38$ for Puklen and 0.31 and 0.42 for Ilímaussaq). La_N/Yb_N values vary between 1.5 and 3.7 (Puklen) and between 2.1 and 2.3 (Ilímaussaq).

Most other incompatible elements are enriched by a factor of about ten to hundred compared to primitive mantle values. For all augites, relative depletions can be detected for the HFSE (Ti, Zr, Hf, Nb). For the large ion lithophile elements (LILE), strong negative peaks are observed for Ba and Sr and also for Pb except for three Puklen samples. The transitional metals Sc, V, Co and Zn are generally less enriched (Sc and Zn) or even depleted (V and Co). Principally, the REE and TE patterns for augites from Puklen and Ilímaussaq are very similar. However, the negative peaks for Pb and Sr are stronger developed in the Ilímaussaq augites and those of Zr, Hf and Ti appear to be weaker than in Puklen augites. In augites from Puklen, a slightly positive anomaly of Li can be detected, which is less pronounced in the Ilímaussaq augites.

Fig. 5 shows representative zoning profiles (Na p.f.u., X_{Fe} and selected trace element contents) across an augite from Puklen (Fig. 5a) and Ilímaussaq (Fig. 5b), respectively. Both profiles show similar characteristics. With increasing fractionation (increase of X_{Fe} and Na content from core to rim), Sc decreases and Zn, Zr and the REE increase. Whereas the amount of enrichment of Zn is more or less equal in both augites, the enrichment of Zr and REE_{tot} is much more extensive in the Ilímaussaq than in the Puklen augite.

5.1.2 Aegirine-augites of Grønnedal-Ika

REE and TE patterns for aegirine-augites of Grønnedal-Ika are shown in Fig. 6. Their Na/Ca ratios vary between 0.2 and 2. The enrichment levels for REE and most other TE are in a similar range compared to augites. Besides the lack of a significant Eu anomaly ($\text{Eu}/\text{Eu}^* = 0.69 - 1.16$) and

stronger enrichment in Tm-Lu, the shape of the REE patterns is rather similar to that of augites (Fig. 6a). La_N/Yb_N ratios are quite variable with a range from 0.6 to 6.5.

As for augites, negative peaks are detected for some LILE (Ba, Pb, Sr), Ti and the transitional elements (Sc, V, Co). In contrast to augites, positive peaks for Zr, Hf and Sn and a negative Li anomaly are developed.

In most samples, aegirine-augites are fairly homogeneous. However, in one sample (GM1496), aegirine-augite with a relatively low Na/Ca ratio of about 0.2 shows a thin rim of distinctly more Na-rich compositions (Na/Ca ratio \sim 0.7). Mantle-normalized REE patterns and TE patterns of core and rim compositions for a typical crystal of this sample are shown in Fig. 6b. The core pattern is parallel to that of the rim from La to Gd but shows a strong decrease towards Lu. Furthermore, rim compositions are enriched in Zr, Hf, Sn and Zn but depleted in Li, Sc, V and Co compared to the core and are generally similar to the patterns of the other aegirine-augites (Fig. 6a).

5.1.3 Aegirines of Puklen and Ilímaussaq

Average mantle-normalized REE patterns for aegirines (Figs. 7) are rather variable in their level of enrichment, their extent of negative Eu anomalies ($\text{Eu}/\text{Eu}^* = 0.16 - 0.63$) and their shape, especially for the Puklen aegirines. With the exception of one sample, all Puklen aegirines show a more or less pronounced enrichment of HREE, whereas all Ilímaussaq aegirines are enriched in both LREE and HREE. This results in a V-shaped pattern, which seems to be typical of aegirines (Larsen, 1976; Shearer & Larsen, 1994; Piilonen *et al.*, 1998). La_N/Yb_N ratios are typically lower than in augites and aegirine-augites and vary from 0.1 to 2.9.

As for augites and aegirine-augites, multi-element diagrams for aegirines show more or less pronounced negative peaks for Ba, Sr, V and Co (Fig. 7). In contrast, normalized Pb concentrations are variable with some aegirines having a clear positive and some a slightly negative Pb peak. As in aegirine-augites, positive peaks for Zr, Hf and Sn are present, whereas the negative Ti peak has disappeared in the aegirines. A positive Li anomaly can be found in most aegirines similar to most augites, but unlike the aegirine-augites.

5.2 Amphibole

5.2.1 Ca and Na-Ca-amphiboles of Puklen, Ilímaussaq and Grønnedal-Ika

Average REE patterns of Ca- and Ca-Na-amphiboles are shown in Figs. 8 and 9. The Puklen amphiboles have strongly developed negative Eu anomalies ($\text{Eu}/\text{Eu}^* = 0.06 - 0.29$), but two different patterns can be distinguished: Ferro-richterites show pronounced HREE-enrichment with La_N/Yb_N ratios between 0.47 and 0.45. In contrast, ferro-edenites are characterised by variably developed LREE-enrichment and a flat HREE section resulting in La_N/Yb_N ratios between 1.5 and 2.5. Secondary ferro-actinolites from Puklen syenites are heterogeneous in terms of enrichment level and shape with La_N/Yb_N ratios between 0.7 and 1.1. REE patterns of Ilímaussaq ferro-pargasites from the augite syenite are characterized by significant negative Eu-anomalies ($\text{Eu}/\text{Eu}^* = 0.26$ and 0.30), a LREE enrichment and a smooth decrease from Gd to Lu. La_N/Yb_N ratios vary from 5.3 to 8.6. The Grønnedal-Ika katophorites lack a significant Eu anomaly ($\text{Eu}/\text{Eu}^* = 0.70 - 0.71$). They show slight enrichments in LREE and the heaviest REE ($\text{La}_N/\text{Yb}_N = 4.4$ and 7.1).

Most trace elements in Ca- and Ca-Na amphiboles are 5-300 times enriched compared to primitive mantle values. Characteristic features of most samples are negative anomalies for Ba, Sr, V and Co and positive ones for Sn and Li. Strong negative Pb anomalies are only present in amphiboles from Ilímaussaq and Grønnedal. Positive Zr-Hf peaks do not occur in the Ca-amphiboles, but in the Ca-Na amphiboles of Grønnedal.

Figure 10 shows a representative zoning profile from core to rim of a Ca-Na amphibole crystal from a Puklen syenite (GM1615). The contents of Zr, Zn and REE increase from core to rim. With increasing fractionation (increase in X_{Fe} and Na/Ca ratio), LREE (La as example) slightly decrease and HREE (Yb as example) strongly increase resulting in a decrease of the La_N/Yb_N ratio from about 1.2 - 1.3 in the core regions to about 0.13 at the rim of crystals. However, the Eu/Eu^* value remains relatively constant at about 0.25.

5.2.2 Na-amphiboles of Puklen and Ilímaussaq

REE and TE spectra of arfvedsonites are shown in Fig. 11. Eu anomalies are strongly negative in the Puklen arfvedsonites ($\text{Eu}/\text{Eu}^* = 0.04$ and 0.19), but more variable in Ilímaussaq arfvedsonites ($\text{Eu}/\text{Eu}^* = 0.26 - 0.92$). The enrichment of LREE and HREE is highly variable developed with

La_N/Yb_N ratios < 1 to 4. TE patterns of arfvedsonites are highly heterogeneous within and among the Puklen and Ilímaussaq rocks. Highly variable concentrations can be observed for Th, U, Pb, Zr and Hf. Most Ilímaussaq Na-amphiboles have positive anomalies of Zr, Hf, Nb, Sn and Li, which are much less prominent in Puklen.

Principally, zoning profiles of arfvedsonite from Puklen and Ilímaussaq (Fig. 12) show similar characteristics as the profiles of Ca-amphiboles (Fig. 10) and augites (Fig. 5), except for the REE. Zn and Zr increase from core to rim and Sc decreases. However, the total content of REE decreases with fractionation, which is in contrast to the behaviour of augites and Ca-amphiboles. The behaviour of LREE and HREE in the two amphibole types is different: In Na-amphiboles, LREE and HREE have similar concentrations in the core regions. During fractionation, HREE contents remain fairly constant, whereas LREE concentrations strongly decrease. This is in contrast to Ca-amphiboles, where LREE contents slightly decrease and HREE strongly increase during fractionation. Both processes result in a decrease of the La_N/Yb_N ratio with increasing fractionation.

6. Discussion

In principle, relative trace element abundances in minerals can reflect the influence of two factors: First, the composition and structure of the melts or fluid phases they crystallized from (e.g. Adam & Green, 2003) and second, the control by crystal-chemical effects (e.g. Blundy & Wood, 1994). The latter implies that the major element composition of the crystals dominates the incorporation of the trace elements (e.g. Blundy & Wood, 1991; Wood & Blundy, 1997). Additional parameters that influence trace-element partitioning to a lesser extent are P, T and f_{O_2} .

Absolute trace-element abundances in melts may depend on the fractionation of minerals that preferentially incorporate certain trace-elements and on assimilation of crustal material. In the Gardar Province, early plagioclase fractionation is indicated by the abundant occurrence of anorthosite xenoliths (Bridgwater, 1967; Bridgwater & Harry, 1968; Halama *et al.*, 2002) and strongly negative Eu anomalies in whole-rock samples of the earliest intrusive units from Ilímaussaq (Bailey *et al.*, 2001). Furthermore, fractionation of alkali feldspar is seen in the investigated complexes. Since negative Eu anomalies are mostly controlled by feldspar fractionation (Drake & Weill, 1975) and Ba, Sr, Eu^{2+} and to a lesser extent Pb are compatible in

alkali feldspar in silicic magmas (Nash and Crecraft, 1985; White, 2003) the absolute concentrations of these are likely to be generally diminished in the residual Gardar magmas from which the complexes crystallized. The lack of significant negative Eu anomalies in the Grønneidal samples is probably related to the more oxidized conditions (Bedford, 1989; Pearce *et al.*, 1997) leading to the stabilization of Eu^{3+} , which is incompatible in feldspar. Low concentrations of Co and V in the investigated mafic minerals might be attributed to early precipitation of olivine and spinel because both are compatible in olivine and/or spinel (Arth, 1976) and the presence of mafic cumulates underneath the exposed alkaline complexes is required by the low whole-rock Ni contents and confirmed by large positive gravity and magnetic anomalies centered on the Ilímaussaq area (Blundell, 1978; Forsberg & Rasmussen, 1978). The systematic decrease of Sc concentrations from calcic to sodic clinopyroxenes and amphiboles and within a growing augite (Fig. 5) indicates that fractionation of clinopyroxene was important, as Sc is compatible in clinopyroxene and amphibole within a large range of magma compositions (e.g., Arth, 1976; Mahood & Hildreth, 1983). In Ilímaussaq, amphiboles and clinopyroxenes show an evolution from a pronounced LREE enrichment in the most Ca-rich minerals towards roughly an order of magnitude lower values in the Na-rich compositions, contrary to the trend expected for incompatible trace elements. The same trend can be seen in single minerals, as exemplified in a representative zoning profile of a Na-amphibole from Ilímaussaq (Fig. 12). This feature is best explained by the fractionation of eudialyte, which is a REE-bearing mineral with highly enriched LREE contents compared to HREE (Bailey *et al.*, 2001) and which is ubiquitous in the agpaitic Ilímaussaq rocks.

6.1 Crystal chemical controls on trace-element partitioning

Both clinopyroxenes and chemically corresponding amphiboles show a continuous development from from LREE-enriched patterns in the calcic minerals via wave-shaped pattern in the Ca-Na minerals towards a more pronounced HREE enrichment in the most Na-rich minerals (Fig. 11). These principal changes point towards a crystal chemical control on trace-element partitioning because of the following arguments:

- The enrichment of HREE in Ca-Na- and especially Na-rich mafic silicates might partly reflect a general preference for trivalent REE as the incorporation of Na⁺ requires charge balance with a trivalent ion, following the coupled substitution $\text{Na} + \text{REE} \rightleftharpoons 2 \text{Ca}$ on the M2 site as proposed for REE partitioning in clinopyroxene (Wood & Blundy, 1997). However, this process should also affect the LREE, which do not show significant enrichment in the Na-rich minerals. Therefore, it seems more likely that there is a particular site preference of the HREE with smaller ionic radii into the optimal sites available in the more Na-rich minerals. HREE were also shown to be compatible in Na-bearing clinopyroxene on the spinel-lherzolite solidus (Blundy *et al.*, 1998).
- For amphiboles, there are multiple crystal-chemical mechanisms for REE³⁺ incorporation and REE are distributed over more than one structural site (Botazzi *et al.*, 1999). Additionally, it is known that the REE site-preference is mainly a function of major-element composition of the B-group sites in amphiboles (Tiepolo *et al.*, 2000a). This is in agreement with our data, where we observe distinct changes in REE patterns from calcic amphiboles (2 Ca²⁺ on B-site) via sodic-calcic amphiboles (B-site occupied by one Ca²⁺ and one Na⁺) towards sodic amphiboles (2 Na⁺ on B-site).

Similarly to the REE, Ti, Zr, Hf and Sn show a systematic behavior in terms of their normalized concentrations in the various pyroxene types. Their normalized concentrations relative to the neighboring elements increase with increasing Na-content in the host mineral. This increase is most pronounced for Zr, Hf and Sn and weaker for Ti. In amphiboles, similar systematics for Zr, Hf and Sn can be observed, whereas Ti remains fairly constant and relatively less depleted throughout the amphibole series from calcic to sodic varieties. The overall similar geochemical behavior of these elements is probably related to their similar ionic radii and charges (Shannon, 1976). The general increase of Zr, Hf and Sn during fractionation within one single pluton can to a certain extent be attributed to enrichment of incompatible elements during closed system fractional crystallization. However, several arguments indicate a major element crystal-chemical control on the contents of these trace element as well:

- In two of the investigated complexes, significant amounts of Ti-rich magnetite and/or ilmenite crystallized early in their evolution (Larsen, 1976; Marks & Markl, 2001; Marks *et al.*, 2003) and thus, probably much of the Ti initially present was incorporated into these minerals, causing a strong depletion of Ti in the evolving melt. However, in the Ilímaussaq clinopyroxenes, the resulting effect on Ti content in clinopyroxene is surprisingly small: Early augites contain only slightly more Ti (up to 5200 ppm) than later aegirines (up to 4200 ppm) and in the Puklen rocks, early augites are even poorer in Ti (maximum of 5200 ppm) than late-stage aegirines (up to 10500 ppm). Despite presumably decreasing Ti contents in the melt, Ti contents in the precipitated mafic silicates increase with fractionation.
- Ti-rich aegirines have been described from a number of peralkaline igneous rocks of the Gardar province (Larsen, 1976; Jones & Peckett, 1980; Shearer & Larsen, 1994; Ranløv & Dymek, 1991) and elsewhere (Nielsen, 1979; Piilonen *et al.*, 1998; Njonfang & Nono, 2003). In contrast, Ti-rich augites in more primitive alkali basaltic lavas of the Gardar Province have not been reported so far despite relatively high whole-rock TiO₂ contents of 1.7-3.0 wt.% (Halama *et al.*, 2003) compared to the typically low TiO₂ contents (< 0.7 wt.%) in the highly fractionated agpaitic rocks of Ilímaussaq (Bailey *et al.*, 2001).
- For an optimal site of about 0.70 Å in pyroxenes and amphiboles (Jensen, 1973; Bailey *et al.*, 2001), Zr⁴⁺ (0.72 Å), Hf⁴⁺ (0.71 Å) and Sn⁴⁺ (0.69 Å) fit fairly well, whereas Ti⁴⁺ (0.61 Å) is considerably smaller (Shannon, 1976). This relatively large mismatch of Ti might contribute to the rather weak increase in Ti contents during fractionation compared to Zr, Hf and Sn.
- Positive Zr-Hf anomalies are only present in Ca-Na- and Na-dominated clinopyroxenes and amphiboles, but not in the calcic varieties, again suggesting a crystal-chemical control. An enrichment of Zr and Hf due to prolonged fractional crystallization alone is not a viable explanation since the neighboring elements do not show such an extreme enrichment.
- In the Ilímaussaq intrusion, late-stage hydrothermal mineralizations containing rare Sn silicates like sørensenite (Na₄SnBe₂(OH)₄Si₆O₁₆) are well known (Semenov *et al.*, 1965). Thus, one can argue, that the high Sn contents in late aegirines compared to earlier augites are an effect of fractionation and enrichment of Sn. However, the relatively high Sn contents and strikingly

positive Sn anomalies in the Grønnedal aegirine-augites argue against this, since these pyroxenes are invariably early magmatic phases.

Among the transition metals, Zn^{2+} has an ionic radius of 0.74 Å in six-fold coordination, which is very similar to the ionic radius of Sc^{3+} (0.745 Å) (Shannon, 1976). Since the compatibility of Sc in clinopyroxene and amphibole is well-known, it is likely that the Zn^{2+} ion with a similar ionic radius may have a similar degree of compatibility, which can explain the enrichment in normalized Zn contents in both clinopyroxene and amphibole compared to primitive mantle.

6.2.1 Lithium: Influence of the melt composition

In the clinopyroxenes, Li behaves quite variable with flat patterns or small positive peaks in the mantle-normalized augite patterns, negative peaks in the aegirine-augites and positive peaks in the aegirines. The enrichment level is also quite different, depending on the complex: Clinopyroxenes from Ilímaussaq have medium values of ~ 20-40x, from Puklen ~ 100x and from Grønnedal < 7x primitive mantle values, apparently independent of the mineral composition. This indicates that Li contents in the clinopyroxenes are mainly dependent on the melt composition. The Puklen melts were relatively most enriched in Li, whereas the Grønnedal melts had relatively low Li contents. The generally positive Li peaks in amphiboles, however, particularly in the sodic members, are clearly an effect of preferential partitioning of Li into amphibole and it was shown by Hawthorne *et al.* (1993, 1994) that Li could be a major component in Na-amphiboles from peralkaline igneous rocks.

6.2.2 Crustal contamination

It has been shown that crustal assimilation is of only minor importance for the evolution of the Ilímaussaq and Grønnedal complexes (Marks *et al.*, 2003; Halama *et al.*, submitted). This is in contrast to the Puklen samples, where crustal contamination plays a major role (Marks *et al.*, 2003). By using Nd isotopic data as indicators for crustal contamination (Marks *et al.*, 2003) we will discuss in the following how crustal assimilation influences the incorporation of specific elements into clinopyroxene and amphibole.

Syenites show a range of ϵ_{Nd} values between -3.8 and -7.2 , and alkali granites vary between -5.9 and -9.6 . Within the syenites, samples GM1593 ($\epsilon_{\text{Nd}} = -7.2$) and GM1600 ($\epsilon_{\text{Nd}} = -6.4$) are the most contaminated ones. Augites of these two samples have the highest contents in U, Pb, V and Zn but the lowest concentrations of Ti, Zr, and Hf. This is consistent with assimilation of crustal rocks, which have high contents of U, Pb, V and Zn and low contents of Ti, Zr and Hf compared to the primitive mantle (Rudnick & Fountain, 1995; McDonough & Sun, 1995). These two samples are also those with positive Pb anomalies (Fig. 4). We defined a Pb/Pb* value, which was calculated similar to Eu/Eu* as the geometric mean $Pb/Pb^* = Pb_N \sqrt{(Ce_N \cdot Pr_N)}$. This should be a useful parameter, since Ce and Pr normally have similar normalized values. The significant correlation between Pb/Pb* and ϵ_{Nd} values in Fig. 13 confirms the influence of crustal contamination on this parameter and provides evidence of a relation between trace element composition in minerals and assimilation processes during the magmatic evolution of an alkaline complex. The same argument may also hold for the differences in primary Li melt contents discussed above.

6.3 Partitioning of trace elements between coexisting clinopyroxene and amphibole

To establish meaningful inter-mineral partition coefficients, chemical equilibrium is required. However, chemical equilibrium is often difficult to evaluate (e.g. Chazot *et al.*, 1996). We calculated clinopyroxene-amphibole trace element abundance ratios for selected samples where textural and isotopic criteria (Markl *et al.*, 2001b; Marks *et al.*, 2003) indicate equilibrium conditions (Figs. 14a-d, Table 4). These values might not strictly be interpreted as partition coefficients but can be used as useful guides for trace element partitioning during petrogenesis also of other alkaline magmatic rocks and will be used here as an approximation for equilibrium partition coefficients.

Calculated clinopyroxene-amphibole partition coefficients ($D_{\text{cpx-amph}}$) for the majority of trace elements vary for the Ilímaussaq augite syenites (Fig. 14a) between 0.1 and 0.6. In the Puklen syenites (Fig. 14b), they are slightly higher (between 0.6 and 1.7). In the Na-Ca system of Grønneidal (Fig. 14c), a larger range between 0.3 and 2.7 is observed. Finally, in the Na-dominated system of Ilímaussaq (Fig. 14d) they vary between 0.07 and 0.9. For a specific element, the determined $D_{\text{cpx-amph}}$ values for the whole sample suite vary within about one order of magnitude.

However, samples with similar major element chemical composition show similar patterns, despite certain differences in the absolute D values. This points to the reasonable assumption of chemical equilibrium between the respective mineral pairs. Thus, clinopyroxene-amphibole partition coefficients seem to be relatively independent of major element mineral compositions and no systematic variation of D values with increasing Na-content of clinopyroxene and amphibole can be observed. This provides an interesting tool to assess equilibration of clinopyroxene, amphibole and melt in magmatic systems. Some elements exhibit noteworthy features:

- Nb and Ta have always a strong preference for amphibole, which is in accordance with previous studies on mantle minerals (e.g., Witt-Eickschen & Harte, 1994; Chazot *et al.*, 1996) and andesitic melts (Brenan *et al.*, 1995). U and Th are also preferentially incorporated into amphibole except for the Puklen samples.
- Rb and Ba are apparently less compatible in clinopyroxene than in amphibole, which is consistent with previous studies (e.g., Brenan *et al.*, 1995; Chazot *et al.*, 1996). This is caused by a strong preference of these two elements for the A-site in amphibole (e.g. Dalpé & Baker, 2000), which has no equivalent position in pyroxene. As for U and Th, Rb and Ba in the Puklen syenites have significantly higher $D_{\text{cpx-amph}}$ values. This might be caused by secondary fluid circulation, which was shown to disturb the Rb/Sr isotopic system in the Puklen minerals (Marks *et al.*, 2003).
- $D_{\text{cpx-amph}}$ values for Sr are characterized by small positive peaks in the Ca-rich system, but slight depressions in the Na-rich system. The two Puklen samples behave variable, which may be an effect of secondary metasomatism, as mentioned above (Marks *et al.*, 2003).
- Zr, Hf and Sn develop a preference for clinopyroxene as the system evolves towards Ca-Na and Na-rich compositions, but absolute D_{Zr} and D_{Hf} values > 1 only occur in the Ca-Na system (Grønnedal). For Zr and Hf, literature data are contradictory, indicating similar compatibilities in andesitic rocks (Brenan *et al.*, 1995), variable behavior (Vannucci *et al.*, 1991) or a preference for amphibole (Chazot *et al.*, 1996) in ultramafic rocks.
- The $D_{\text{cpx-amph}}$ values of the REE are continuously increasing from the LREE towards the HREE in the Ilímaussaq and Grønnedal rocks. However, whereas in Ilímaussaq, all D_{REE} are < 1 , D_{REE} values in Grønnedal increase from $D_{\text{La}} = 0.2$ towards $D_{\text{Lu}} = 2.7$, i.e. the LREE partition

preferentially into amphibole, but the HREE do not. In contrast, D_{REE} values for Puklen syenites are fairly constant. For the REE, Klein *et al.* (1997) assumed that as a consequence of nearly identical values of Young's moduli and lattice site geometries of M4- and M2-sites in amphibole and clinopyroxene, respectively, $D_{\text{cpx-amph}}$ should be identical for all REE and consequently, REE patterns of clinopyroxenes and amphiboles should be subparallel. Measured REE partition coefficients between clinopyroxene and amphibole in mantle rocks (Witt-Eickschen & Harte, 1994; Chazot *et al.*, 1996) partly confirm this assumption as our data for the Puklen syenites do (Figs. 4a, 8a and 14b). However, Witt-Eickschen and Harte (1994) also found a slight tendency of increase of $D_{\text{cpx-amph}}$ for the REE with increasing Na-content, which is not confirmed by our data. The tendency of increase of $D_{\text{cpx-amph}}$ values from La to Lu found by Witt-Eickschen and Harte (1994) in mantle rocks and by Irving and Frey (1984) for basaltic rocks is in accordance with our results for the Ilímaussaq and Grønneidal rocks, but not for the Puklen syenites.

Figure 15 compares clinopyroxene-amphibole partition coefficients of selected elements in different rock types and synthetic melts from the literature with our data. Most data are available for ultramafic (Vannucci *et al.*, 1991; Chazot *et al.*, 1996; Grégoire *et al.*, 2000) and basaltic compositions (Irving and Frey, 1984; Adam and Green, 1994), but data for more evolved compositions are scarce (Villemant *et al.*, 1981; Wörner *et al.*, 1983; Lemarchand *et al.*, 1987). Overall, the literature data span a comparable range from ~0.1 to ~10 in calculated $D_{\text{cpx-amph}}$ values as our data for alkaline igneous rocks do. Furthermore, there are no systematic changes in absolute $D_{\text{cpx-amph}}$ values with SiO_2 content or alkalinity (Fig. 15). This indicates that trace element partitioning between clinopyroxene and amphibole is not significantly influenced by the melt composition. Obviously, melt compositional and thus melt structural effects influencing the partitioning of trace elements between mafic silicates and silicic melts have similar influence on clinopyroxene and amphibole. This is interpreted to be due to the principally similar crystal structures and cation sites of these two minerals.

6.4 Evaluation of mineral-melt partition coefficients for alkaline systems

Generally, the mismatch between whole-rock composition and calculated melt composition may have two reasons: First, the whole-rock composition does not represent a melt and second, the partition coefficient data are not applicable to the minerals investigated. The latter factor can be caused by differences in crystal and/or melt chemistry between the system under investigation and the reference system or by changes in crystallization parameters during the evolution of the complex which lead to changes in the partition coefficients. It is very likely that all of these reasons apply to some degree on the alkaline plutonic rocks investigated here and they might also be related to the large range in partition coefficients determined in natural rocks (Table 5). It is also known that processes of chemical differentiation are polythermal and often polybaric and thus, partition coefficients can vary for a single phase in the course of crystallization (Blundy and Wood, 2003). Large crystallization intervals were for instance reported in Ilímaussaq (Markl *et al.*, 2001) and the occurrence of chemically distinct clinopyroxene cores in Grønnedal might be related to pressure differences during crystallization (Halama *et al.*, submitted). Further complexities in the rocks studied might arise due to the influence of late magmatic and/or meteoric fluids (Puklen: Marks *et al.*, 2003) or liquid immiscibility (Grønnedal: Bedford, 1989; Halama *et al.*, submitted). Properties of the melt phase may also influence partition coefficients independently of mineral composition and crystal-chemical effects (e.g. Adam and Green, 2003).

To investigate the applicability of published partition coefficients for alkaline systems, melt compositions were calculated from the mineral data with minimum and maximum mineral-melt partition coefficients listed in Table 5 (Larsen, 1979; Wörner *et al.*, 1983; Lemarchand *et al.*, 1987). These data are derived from bulk mineral separate analyses, where mineral zoning or the incorporation of accessory phases enriched in certain trace elements might have contributed to some of the considerable variation. To evaluate the accuracy of the partition coefficients, knowledge of the trace element composition of the melt is required. Whole-rock compositions of the intrusive rocks of the investigated complexes are unlikely to represent melts due to accumulation processes. Nevertheless, we used the compositions of fine-grained dike rocks that are considered by the authors (Larsen, 1979; Upton *et al.*, 1985) as possible initial melt compositions (Table 5). One is an aphyric marginal facies sample from an alkali olivine basalt of the older giant dyke complex

(OGDC) of Tugtutôq (Upton *et al.*, 1985), close to the Ilímaussaq complex, which might resemble an initial melt of the augite-syenite. The other is a peralkaline dike rock that resemble peralkaline Ilímaussaq magmas (Larsen, 1979). The range of calculated melt compositions is additionally compared to whole-rock data from the augite-syenite (Ilímaussaq; Bailey *et al.*, 2001) and various nepheline-syenites (Grønnedal-Ika; Pearce *et al.*, 1997). The Puklen complex is not investigated here because of the very limited set of available whole-rock trace element data and the known multiphase evolution (Marks *et al.*, 2003).

By comparing the assumed OGDC initial melt composition with the augite-syenite, we note that the trace element patterns are very similar except for Sr (Fig. 16 a/b). This can be interpreted in two ways: Either the OGDC sample is also influenced by accumulation processes that are not detectable by optical means or the trace element contents of the augite-syenite whole-rocks are in fact similar to the OGDC initial melt compositions except for Sr that might have been removed by plagioclase fractionation. Ba, Sr and Eu in the Ilímaussaq calculated melts tend to show marked negative spikes and lower concentrations than the whole-rocks. This can partly be attributed to accumulation of feldspar, which can be observed both in Grønnedal and Ilímaussaq. Additionally, relatively high detection limits for Ba and Sr in the previous studies did not allow to extrapolate the range of distribution coefficients to lower values (e.g. Wörner *et al.*, 1983), and we will therefore not investigate elements compatible in feldspar (Ba, Sr, Eu^{2+} , Pb) further.

However, other element concentrations in the calculated melts might be compared to the whole-rocks with more reliability. It has then to be considered whether the calculated concentrations and the shape of the trace element patterns agree with the whole-rock data. For Ilímaussaq, melt compositions calculated from augites show a good agreement with whole-rock data for most elements except Cs, U and Zr (Fig. 16a). Positive deviations in the melt calculated from amphibole compared to the whole-rock values occur for Th, U, L, Ce, Nd, Zr, Hf, Yb and Lu (Fig. 16b). In Grønnedal, melts were calculated from diopsidic to aegirine-augitic clinopyroxene phenocryst cores ($\text{melt}^{\text{cpx-core}}$) and from an average aegirine-augite ($\text{melt}^{\text{cpx-matrix}}$). $\text{Melt}^{\text{cpx-core}}$ trace element concentrations and patterns show a fairly good agreement with the whole-rock data. By comparison with $\text{melt}^{\text{cpx-matrix}}$, the overlap of $\text{melt}^{\text{cpx-core}}$ is markedly better for Zr, Hf, Yb and Lu (Fig. 16c). Melt compositions calculated from the Grønnedal amphiboles ($\text{melt}^{\text{amph}}$) are similarly characterized by

positive deviations in Zr, Hf, Yb and Lu and, in contrast to the Ilímaussaq data, by lower Th and U contents compared to the whole-rocks. Additionally, there are significant differences between both melt compositions calculated from clinopyroxenes and the whole-rock data for Cs and Ta and between melt^{amph} and whole-rocks for Sm, Eu and Tb (Fig. 16c,d).

The discrepancy between melt^{cpx-matrix} and melt^{cpx-core} suggests that the known partition coefficients for these elements are not suitable in a more evolved Ca-Na system where aegirine-augite is precipitated. This is supported by the positive Zr-Hf peaks and HREE-enrichments in the aegirines (Fig. 7) that indicate that the partition coefficients for Zr, Hf and the HREE increase as the pyroxene becomes more Na-rich. A crystal-chemical control is also suggested when the broadly augitic clinopyroxene compositions with relatively low Na contents used in the previous studies (Larsen, 1979; Wörner *et al.*, 1983; Lemarchand *et al.*, 1987) are considered in comparison to the Na-rich aegirine. In summary, partition coefficients derived from natural samples can be used for calculating melt compositions from clinopyroxenes with low Na-Fe³⁺-contents, but they do not yield reliable melt compositions when Na-Fe³⁺-rich clinopyroxene or amphibole data are taken.

To evaluate the crystal-chemical control on REE partitioning more quantitatively, we calculated partition coefficients for the REE (D_{REE}) from known clinopyroxene crystal compositions after the model of Wood and Blundy (1997) (WB97 model). Examples of the calculated D_{REE} values are listed in Table 6 and the results are shown graphically in Fig. 17. Calculations at 800 °C and 1 kbar (Fig. 17a) show that the apex of the parabolic curve trends towards smaller ionic radii as the clinopyroxene becomes more Na-Fe³⁺-rich. This means that the HREE become more compatible relative to the LREE, which can also be seen in the decreasing $D_{\text{La}}/D_{\text{Lu}}$ ratios (Table 6) and which is in qualitative agreement with the observed increase in HREE concentrations in aegirine-augites and aegirines (Figs. 6, 7). Calculated D_{REE} for augite and Mg-rich aegirine-augitic clinopyroxene cores where Fe²⁺ dominates over Fe³⁺ (Table 6) agree fairly well with data from natural samples. The calculated D_{REE} for aegirine-augite rims and aegirines at 800 °C tend to be lower than the range of measured values. However, aegirine formation temperatures are considered to be around 350-550 °C in Ilímaussaq (Markl *et al.*, 2001). Therefore, D_{REE} of a representative aegirine were calculated at temperatures between 800 and 350 °C (Table 6). There is a significant increase in D_{REE} and a decrease in the $D_{\text{La}}/D_{\text{Lu}}$ ratio as the temperature decreases (Fig. 17b).

Melt compositions calculated using the D_{REE} determined from the Wood and Blundy (1997) model and using the D_{REE} derived from natural samples are compared to whole-rock data and possible melt compositions from Ilímaussaq (Fig. 18). For the augite-syenite, the melts calculated after the WB97 model show a good overlap with the whole-rock data, except for Eu. This confirms the applicability of the theoretical model to augitic clinopyroxenes in alkaline systems. Melts calculated from a typical aegirine composition are compared to an assumed initial peralkaline melt composition derived from a dike rock from Ilímaussaq (Larsen, 1979) and agpaitic whole-rock compositions (Bailey *et al.*, 2001). As before, we note that the possible melt composition has similar REE contents as the whole-rocks. All melt compositions calculated after the WB97 model have lower REE contents than the whole-rocks, and the most significant deviations occur when the lowest aegirine formation temperatures are assumed. There is a reasonable overlap between the WB97 model melts and melts calculated with the D_{REE} from natural samples, but the WB97 model melts tend to higher LREE and lower HREE concentrations. Despite the consideration of crystal-chemical effects, the partition coefficients calculated after the WB97 model appear not to be suitable to calculate melt compositions from aegirines. One reason could be, that aegirines are often late-stage and secondary minerals that may have crystallized from an aqueous fluid rather than from a melt (e.g. Marks *et al.*, 2003), but petrographic evidence suggests a primary origin for the aegirine in the investigated sample (GM 1334), so that we assume that the aegirine crystallized from a melt. However, agpaitic Ilímaussaq melts are known to be fluid-rich (e.g. Larsen and Sørensen, 1987; Bailey *et al.*, 2001) and it is possible that the fluid-rich nature of the melt has affected the partitioning behavior of the REE. On the other hand, the theoretical model was based on clinopyroxenes with Mg numbers from 0.63 to 1 in anhydrous systems (Wood and Blundy, 1997), which does not apply to the formation of Mg-poor aegirine in the Ilímaussaq peralkaline rocks where ubiquitous amphibole indicates a hydrous magma. Wood and Blundy (1997) also note that compositions containing substantial amounts of the $\text{NaFe}^{3+}\text{Si}_2\text{O}_6$ component deviate from the simple activity-composition relationship used in their model and deviations from the model were for instance reported for Na –and Al-rich low-degree mantle melts (Blundy *et al.*, 1998). Therefore, experimental data on trace element partitioning in alkaline Fe^{3+} -rich systems would be highly

desirable to improve the theoretical model and obtain more accurate partition coefficients for those systems.

7. Summary and concluding remarks

This comparative study on trace element contents in mafic minerals of three alkaline igneous complexes confirms that trace element contents of amphiboles and clinopyroxenes are mainly influenced by two factors: Whereas the major element composition of the host mineral exerts the dominant control on the partitioning behavior of the trace elements (e.g. Blundy and Wood, 2003), changes of the melt composition during magmatic processes such as fluid interaction, fractionation or crustal assimilation naturally influence the absolute and/or relative concentrations. We show that clinopyroxenes and amphiboles show a continuous development from LREE-enriched patterns in the calcic minerals via wave-shaped pattern in the Ca-Na minerals towards a more pronounced HREE enrichment in the most Na-rich minerals and an increase in Zr, Hf, Sn and HREE concentrations with increasing Na/Ca ratio. These features appear to be related to an increasing preference of these elements for the mineral structure as the magmatic evolution proceeds. Calculations of clinopyroxene-melt partition coefficients based on a theoretical model after Wood and Blundy (1997) show that HREE relative to LREE are more easily incorporated into the crystal structure as the system becomes more Na-Fe³⁺-rich, which is in qualitative agreement with the observed REE concentrations.

The partitioning of most trace elements between clinopyroxene and co-genetic amphibole seems to be fairly independent of melt composition or major element composition of the host crystals. Most trace elements show a slight preference for amphibole, which is most pronounced for Nb, Ta, U, Th, Rb, Ba and Li. However, in Puklen samples U, Th, Rb and Ba have significantly higher $D_{\text{cpx-amph}}$ values up to about 20, which might be explained by secondary fluid circulation and late-stage autometasomatism resulting in the re-distribution of these elements in the Puklen rocks. In contrast, Zr, Hf and Sn develop a preference for clinopyroxene relative to the neighboring elements, as the system evolves from a Ca-dominated to a Na-dominated one. In comparison with literature data, no major differences or systematic changes in $D_{\text{cpx-amph}}$ values from ultramafic via basanitic to the highly fractionated rocks studied here can be observed.

In evolved magmatic systems like the alkaline complexes of the Gardar Province, the calculation of trace element compositions of melts from mineral data needs to be evaluated for each element and in dependence of the mineral composition. Published clinopyroxene-melt partition coefficients for alkaline systems from the literature may be used with some confidence only if the clinopyroxene has a similar crystal composition, i.e. if it is broadly diopsidic to augitic. Partition coefficients based on the theoretical model of Wood and Blundy (1997) are also applicable for clinopyroxenes in alkaline systems, but only if the mineral is relatively poor in Fe^{3+} . For clinopyroxenes containing considerable amounts of $\text{NaFe}^{3+}\text{Si}_2\text{O}_6$, neither the published partition coefficients nor partition calculated on the basis of the crystal chemistry (Wood and Blundy, 1997) appear to be adequate. Possible reasons include the fluid-rich nature of the late peralkaline melts and possible deviations of systems with considerable amounts of the $\text{NaFe}^{3+}\text{Si}_2\text{O}_6$ component from the simple activity-composition relationship used in the model. For amphiboles, calculated melt compositions show poor overlap with whole-rock data, which is possibly related to their late magmatic formation under more hydrous conditions.

Acknowledgements

Laser ICP-MS measurements were carried out at the Large Scale Geochemical Facility supported by the European Community - Access to Research Infrastructure action of the Improving Human Potential Programme, contract number HPRI-CT-1999-00008 awarded to Prof. B. J. Wood (University of Bristol) which is gratefully acknowledged. Bruce Paterson provided invaluable help during these measurements. Financial support for this work was granted by the Deutsche Forschungsgemeinschaft (grant Ma-2135/1-2).

References

- Adam, J., Green, T. H., 1994. The effects of pressure and temperature on the partitioning of Ti, Sr and REE between amphibole, clinopyroxene and basanitic melts. *Chem. Geol.* 117, 219-233.
- Adam, J., Green, T., 2003. The influence of pressure, mineral composition and water on trace element partitioning between clinopyroxene, amphibole and basanitic melts. *Eur. J. Mineral.* 15, 831-841.
- Allaart, J. H., 1976. Ketilidian mobile belt in South Greenland. In: Escher, A., Watt, W.S. (Eds.), *Geology of Greenland*, Grønlands Geologiske Undersøgelse, pp. 121-151.
- Armstrong, J. T., 1991. Quantitative elemental analysis of individual microparticles with electron beam instruments. In: Heinrich, K.F.J., Newbury, D.E. (Eds.), *Electron Probe Quantitation*. Plenum Press, New York & London, pp. 261-315.
- Arth, J. G., 1976. Behaviour of trace elements during magmatic processes—a summary of theoretical models and their applications. *Journal of Research of the U.S. Geological Survey* 4, 41-47.
- Bailey, J. C., Gwozdz, R., Rose-Hansen, J., Sørensen, H., 2001. Geochemical overview of the Ilimaussaq alkaline complex, South Greenland. *Geology of Greenland Survey Bulletin* 190, 35-53.
- Bedford, C. M., 1989. The mineralogy, geochemistry and petrogenesis of the Grønnedal-Ika complex, south west Greenland. Unpublished PhD thesis, University of Durham
- Benoit, M., Polvé, M., Ceuleneer, G., 1996. Trace element and isotopic characterization of mafic cumulates in a fossil mantle diapir (Oman ophiolite). *Chem. Geol.* 134, 199-214.
- Blundell, D. J., 1978. A gravity survey across the Gardar Igneous Province, SW Greenland. *J. Geol. Soc. London* 135, 545-554.
- Blundy, J. D., Wood, B. J., 1991. Crystal-chemical controls on the partitioning of Sr and Ba between plagioclase feldspar, silicate melts, and hydrothermal solutions. *Geochim. Cosmochim. Acta* 55, 193-209.
- Blundy, J., Wood, B., 1994. Prediction of crystal-melt partition coefficients from elastic moduli. *Nature* 372, 452-454.
- Blundy, J., Dalton, J., 2000. Experimental comparison of trace element partitioning between clinopyroxene and melt in carbonate and silicate systems, and implications for mantle metasomatism. *Contrib. Mineral. Petrol.* 139, 356-371.
- Blundy, J., Wood, B., 2003. Partitioning of trace elements between crystals and melts. *Earth Planet. Sci. Lett.* 210, 383-397.
- Blundy, J. D., Robinson, J. A. C., Wood, B. J., 1998. Heavy REE are compatible in clinopyroxene on the spinel lherzolite solidus. *Earth Planet. Sci. Lett.* 160, 493-504.
- Bottazzi, P., Tiepolo, M., Vannucci, R., Zanetti, A., Brum, R., Foley, S. F., Oberti, R., 1999. Distinct site preferences for heavy and light REE in amphibole and the prediction of $D_{\text{REE}}^{\text{Amph/L}}$. *Contrib. Mineral. Petrol.* 137, 36-45.
- Brenan, J. M., Shaw, H. F., Ryerson, F. J., Phinney, D. L., 1995. Experimental determination of trace-element partitioning between pargasite and a synthetic hydrous andesitic melt. *Earth Planet. Sci. Lett.* 135, 1-11.
- Bridgwater, D., 1967. Feldspathic inclusions in the Gardar igneous rocks of South Greenland and their relevance to the formation of major Anorthosites in the Canadian Shield. *Canadian J. Earth Sci.* 4, 995-1014.
- Bridgwater, D., Harry, W. T., 1968. Anorthosite xenoliths and plagioclase megacrysts in Precambrian intrusions of South Greenland. *Meddelelser om Grønland* 185, 243 pp.
- Chazot, G., Menzies, M., Harte, B., 1996. Determination of partition coefficients between apatite, clinopyroxene, amphibole, and melt in natural spinel lherzolites from Yemen: Implications for wet melting of the lithospheric mantle. *Geochim. Cosmochim. Acta* 60, 423-437.
- Coogan, L. A., Kempton, P. D., Saunders, A. D., Norry, M. J., 2000. Melt aggregation within the crust

- beneath the Mid-Atlantic Ridge: evidence from plagioclase and clinopyroxene major and trace element compositions. *Earth Planet. Sci. Lett.* 176, 245-257.
- Costa, F., Chakraborty, S., Dohmen, R., 2003. Diffusion coupling between trace and major elements and a model for calculation of magma residence times using plagioclase. *Geochim. Cosmochim. Acta* 67, 2189-2200.
- Dalpe, C., Baker, D. R., 2000. Experimental investigation of large-ion-lithophile-element-, high-field-strength-element- and rare-earth-element-partitioning between calcic amphibole and basaltic melt: the effects of pressure and oxygen fugacity. *Contrib. Mineral. Petrol.* 140, 223-250.
- Digonnet, S., Goulet, N., Bourne, J., Stevenson, R., Archibald, D., 2000. Petrology of the Abloviak aillikite dykes, New Quebec; evidence for a Cambrian diamondiferous alkaline province in northeastern North America. *Canadian J. Earth Sci.* 37, 517-533.
- Drake, M. J., Weill, D. F., 1975. Partitioning of Sr, Ba, Ca, Y, Eu^{2+} , Eu^{3+} and other REE between plagioclase feldspar and magmatic liquid: an experimental study. *Geochim. Cosmochim. Acta* 39, 689-712.
- Emeleus, C. H., 1964. The Grønnedal-Ika alkaline complex, South Greenland. The structure and geological history of the complex. *Meddelelser om Grønland* 172, 75 pp.
- Escher, A., Watt, W. S., 1976. *Geology of Greenland*. Copenhagen, Geological Survey of Greenland, 603 pp.
- Ferguson, J., 1964. *Geology of the Ilimaussaq alkaline intrusion, South Greenland*. Bulletin Grønlands Geologiske Undersøgelse 39, 82 pp.
- Forsberg, R., Rasmussen, K. L., 1978. Gravity and rock densities in the Ilimaussaq area, South Greenland. *Rapport Grønlands Geologiske Undersøgelse* 90, 81-84.
- Gaetani, G. A., Grove, T. L., 1995. Partitioning of rare earth elements between clinopyroxene and silicate melt: Crystal-chemical controls. *Geochim. Cosmochim. Acta* 59, 1951-1962.
- Garde, A. A., Hamilton, M. A., Chadwick, B., Grocott, J., McCaffrey, K. J. W., 2002. The Ketilidian orogen of South Greenland: geochronology, tectonics, magmatism, and fore-arc accretion during Palaeoproterozoic oblique convergence. *Canadian J. Earth Sci.* 39, 765-793.
- Grégoire, M., Moine, B. N., O'Reilly, S. Y., Cottin, J. Y., Giret, A., 2000. Trace element residence and partitioning in mantle xenoliths metasomatized by highly alkaline, silicate- and carbonate-rich melts (Kerguelen Islands, Indian Ocean). *J. Petrol.* 41, 477-509.
- Halama, R., Waight, T., Markl, G., 2002. Geochemical and isotopic zoning patterns of plagioclase megacrysts in gabbroic dykes from the Gardar Province, South Greenland: implications for crystallisation processes in anorthositic magmas. *Contrib. Mineral. Petrol.* 144, 109-127.
- Halama, R., Wenzel, T., Upton, B. G. J., Siebel, W., Markl, G., 2003. A geochemical and Sr-Nd-O isotopic study of the Proterozoic Eriksfjord Basalts, Gardar Province, South Greenland: Reconstruction of an OIB-signature in crustally contaminated rift-related basalts. *Min. Mag.* 67, 831-854.
- Halama, R., Vennemann, T., Siebel, W., Markl, G., submitted. The Grønnedal-Ika carbonatite-syenite complex, South Greenland: An origin involving liquid immiscibility. *J. Petrol.*
- Hawthorne, F. C., Ungaretti, L., Oberti, R., Bottazzi, P., 1993. Li: An important component in igneous alkali amphiboles. *Am. Mineral.* 78, 733-745.
- Hawthorne, F. C., Ungaretti, L., Oberti, R., Cannillo, E., 1994. The mechanisms of $[\text{6}]\text{Li}$ incorporation in amphiboles. *Am. Mineral.* 79, 443-451.
- Irving, A. J., Frey, F. A., 1984. Trace element abundances in megacrysts and their host basalts: Constraints on partition coefficients and megacryst genesis. *Geochim. Cosmochim. Acta* 48, 1201-1221.
- Jeffries, T. E., Perkins, W. T., Pearce, N. J. G., 1995. Measurements of trace elements in basalts and their phenocrysts by laser probe microanalysis inductively coupled plasma mass spectrometry (LPMA-ICP-MS). *Chem. Geol.* 121, 131-144.
- Jensen, B. B., 1973. Patterns of trace element partitioning. *Geochim. Cosmochim. Acta* 37, 2227-2242.
- Jones, A. P., Peckett, A., 1980. Zirconium-bearing aegirines from Motzfeldt, South Greenland. *Contrib.*

- Mineral. Petrol. 75, 251-255.
- Kalsbeek, F., Taylor, P. N., 1985. Isotopic and chemical variation in granites across a Proterozoic continental margin—the Ketilidian mobile belt of South Greenland. *Earth Planet. Sci. Lett.* 73, 65-80.
- Klein, M., Stosch, H.-G., Seck, H. A., 1997. Partitioning of high field-strength and rare-earth elements between amphibole and quartz-dioritic to tonalitic melts: an experimental study. *Chem. Geol.* 138, 257-271.
- Konnerup-Madsen, J., Rose-Hansen, J., 1984. Composition and significance of fluid inclusions in the Ilimaussaq peralkaline granite, South Greenland. *Bull. Minéral.* 107, 317-326.
- Kramm, U., Kogarko, L. N., 1994. Nd and Sr isotope signatures of the Khibina and Lovozero agpaitic centres, Kola Province, Russia. *Lithos* 32, 225-242.
- Larsen, L. M., 1976. Clinopyroxenes and coexisting mafic minerals from the alkaline Ilimaussaq intrusion, south Greenland. *J. Petrol.* 17, 258-290.
- Larsen, L. M., 1977. Aenigmatites from the Ilimaussaq intrusion, south Greenland: Chemistry and petrological implications. *Lithos* 10, 257-270.
- Larsen, L. M., 1979. Distribution of REE and other trace elements between phenocrysts and peralkaline undersaturated magmas, exemplified by rocks from the Gardar igneous province, South Greenland. *Lithos* 12, 303-315.
- Larsen, L. M., 1981. Chemistry of feldspars in the Ilimaussaq augite syenite with additional data on some other minerals. *Rapport Grønlands Geologiske Undersøgelse* 103, 31-37.
- Larsen, L. M., Sørensen, H., 1987. The Ilimaussaq intrusion—progressive crystallization and formation of layering in an agpaitic magma. In: Fitton, J.G., Upton, B.G.J. (Eds.), *Alkaline Igneous Rocks*. Geological Society Special Publication 30, 473-488.
- Lemarchand, F., Villemant, B., Calas, G., 1987. Trace element distribution coefficients in alkaline series. *Geochim. Cosmochim. Acta* 51, 1071-1081.
- Mahood, G., Hildreth, W., 1983. Large partition coefficients for trace elements in high-silica rhyolites. *Geochim. Cosmochim. Acta* 47, 11-30.
- Markl, G., Baumgartner, L., 2002. pH changes in peralkaline late-magmatic fluids. *Contrib. Mineral. Petrol.* 144, 31-346.
- Markl, G., Marks, M., Wirth, R., 2001a. The influence of T, aSiO₂, fO₂ on exsolution textures in Fe-Mg olivine: an example from augite syenite of the Ilimaussaq Intrusion, South Greenland. *Am. Mineral.* 86, 36-46.
- Markl, G., Marks, M., Schwinn, G., Sommer, H., 2001b. Phase equilibrium constraints on intensive crystallization parameters of the Ilimaussaq Complex, South Greenland. *J. Petrol.* 42, 2231-2258.
- Marks, M., Markl, G., 2001. Fractionation and assimilation processes in the alkaline augite syenite unit of the Ilimaussaq Intrusion, South Greenland, as deduced from phase equilibria. *J. Petrol.* 42, 1947-1969.
- Marks, M., Vennemann, T. W., Siebel, W., Markl, G., 2003. Quantification of magmatic and hydrothermal processes in a peralkaline syenite-alkali granite complex based on textures, phase equilibria, and stable and radiogenic isotopes. *J. Petrol.* 44, 1247-1280.
- Marks, M., Vennemann, T., Siebel, W., Markl, G., submitted. Decoupling of O and H isotopes in Fe-rich amphiboles and strong D-depletion during magmatic processes: an example from the peralkaline Ilimaussaq Intrusion, South Greenland. *Geochim. Cosmochim. Acta*.
- McDonough, W. F., Sun, S. S., 1995. The composition of the Earth. *Chem. Geol.* 120, 223-253.
- Mitchell, R.H., 1990. A review of the compositional variation of amphiboles in alkaline plutonic complexes. *Lithos* 26, 135-156.
- Nash, W. P., Crecraft, H. R., 1985. Partition coefficients for trace elements in silicic magmas. *Geochim. Cosmochim. Acta* 49, 2309-2322.
- Nielsen, T. F. D., 1979. The occurrence and formation of Ti-aegirines in peralkaline syenites; an example

- from the Tertiary ultramafic alkaline Gardiner complex, East Greenland. *Contrib. Mineral. Petrol.* 69, 235-244.
- Nimis, P., Vannucci, R., 1995. An ion microprobe study of clinopyroxenes in websteritic and megacrystic xenoliths from Hyblean Plateau (SE Sicily, Italy): constraints on HFSE/REE/Sr fractionation at mantle depth. *Chem. Geol.* 124, 185-197.
- Njonfang, E., Nono, A., 2003. Clinopyroxene from some felsic alkaline rocks of the Cameroon Line, central Africa: petrological implications. *Eur. J. Mineral.* 15, 527-542.
- Panneer Selvam, A., Suryanarayana Rao, S., 1996. Geology and uranium mineralisation of the Proterozoic alkali syenite from Rasimalai, North Arcot Ambedkar District, Tamil Nadu, India Exploration and Research for Atomic Minerals 9, 41-54.
- Parsons, I., 1972. Petrology of the Puklen syenite-alkali granite complex, Nunarssuit, South Greenland. *Meddelelser om Grønland* 195, 73 pp.
- Pearce, N. J. G., Leng, M. J., Emeleus, C. H., Bedford, C. M., 1997. The origins of carbonatites and related rocks from the Grønnedal-Ika Nepheline Syenite complex, South Greenland: C-O-Sr isotope evidence. *Min. Mag.* 61, 515-529.
- Piilonen, P. C., McDonald, A. M., Lalonde, A. E., 1998. The crystal chemistry of aegirine from Mont Saint-Hilaire, Quebec. *Canadian Mineralogist* 36, 779-791.
- Platt, R. G., 1996. Nepheline syenite complexes - an overview. In: R.H. Mitchell (Ed.), *Undersaturated alkaline rocks; mineralogy, petrogenesis, and economic potential*. Mineralogical Association of Canada Short Course Series vol. 24, 63-99.
- Poulsen, V., 1964. The sandstones of the Precambrian Eriksfjord Formation in South Greenland. *Rapport Grønlands Geologiske Undersøgelse* 2, 16 pp.
- Pulvertaft, T. C. R., 1961. The Puklen intrusion, Nunarssuit, SW Greenland. *Meddelelser om Grønland* 123, 35-49.
- Ranløv, J., Dymek, R. F., 1991. Compositional zoning in hydrothermal aegirine from fenites in the Proterozoic Gardar Province, South Greenland. *Eur. J. Mineral.* 3, 837-853.
- Rudnick, R., Fountain, D. M., 1995. Nature and composition of the Continental Crust: A lower crustal perspective. *Reviews of Geophysics* 33, 267-309.
- Schiano, P., Allegre, C.-J., Dupré, B., Lewin, E., Joron, J.-L., 1993. Variability of trace elements in basaltic suites. *Earth Planet. Sci. Lett.* 119, 37-51.
- Semenov, E. I., Gerassimivsky, V. I., Maksimova, N. V., Andersen, S., Peteresen, O. V., 1965. Sørensenite, a new sodium-beryllium-tin-silicate from the Ilimaussaq Intrusion, South Greenland. *Bulletin Grønlands Geologiske Undersøgelse* 61, 19 pp.
- Shannon, R. D., 1976. Revised effective ionic radii and systematic studies of interatomic distances in halides and chalcogenides. *Acta Crystallographica* A32, 751-767.
- Shearer, C. K., Larsen, L. M., 1994. Sector-zoned aegirine from the Ilimaussaq alkaline intrusion, South Greenland: Implications for trace-element behavior in pyroxene. *Am. Mineral.* 79, 340-352.
- Thompson, G. M., Malpas, J., 2000. Mineral/melt partition coefficients of oceanic alkali basalts determined on natural samples using laser ablation-inductively coupled plasma-mass spectrometry (LAM-ICP-MS). *Min. Mag.* 64, 85-94.
- Tiepolo, M., Tribuzio, R., Vannucci, R., 2002. The compositions of mantle-derived melts developed during the Alpine continental collision. *Contrib. Mineral. Petrol.* 144, 1-15.
- Tiepolo, M., Vannucci, R., Bottazzi, P., Oberti, R., Zanetti, A., 2000a. Partitioning of REE, Y, Th, U and Pb between pargasite, kaersutite and basanite to trachyte melts: implications for percolated and veined mantle. *Geochemistry, Geophysics, Geosystems* 1, paper number 2000GC000064.
- Tiepolo, M., Vannucci, R., Oberti, R., Foley, S., Bottazzi, P., Zanetti, A., 2000b. Nb and Ta incorporation and fractionation in titanian pargasite and kaersutite: crystal-chemical constraints and implications for

- natural systems. *Earth Planet. Sci. Lett.* 176, 185-201.
- Upton, B. G. J., Emeleus, C. H., 1987. Mid-Proterozoic alkaline magmatism in southern Greenland: the Gardar province. In: Fitton, J.G. & Upton, B.G.J. (Eds.), *Alkaline Igneous Rocks*. Geological Society Special Publication 30, 449-471.
- Upton, B. G. J., Emeleus, C. H., Heaman, L. M., Goodenough, K. M., Finch, A., 2003. Magmatism of the mid-Proterozoic Gardar Province, South Greenland: chronology, petrogenesis and geological setting. *Lithos* 68, 43-65.
- Upton, B.G.J., Stephenson, D., Martin, A.R., 1985. The Tugtutôq older giant dyke complex: mineralogy and geochemistry of an alkali gabbro-augite-syenite-foyaite association in the Gardar Province of South Greenland. *Min. Mag.* 49, 624-642.
- van Breemen, O., Aftalion, M., Allart, J. H., 1974. Isotopic and Geochronologic Studies on Granites from the Ketilidian Mobile Belt of South Greenland. *Bulletin of the Geological Society of America* 85, 403-412.
- Vannucci, R., Tribuzio, R., Piccardo, G. B., Ottolini, L., Bottazzi, P., 1991. SIMS analysis of REE in pyroxenes and amphiboles from the Proterozoic Ikaaulak intrusive complex (SE Greenland): implications for LREE enrichment processes during post-orogenic plutonism. *Chem. Geol.* 92, 115-133.
- Villemant, B., Jaffrezic, H., Joron, J.-L., Treuil, M., 1981. Distribution coefficients of major and trace elements; fractional crystallization in the alkali basalt series of Chaîne des Puys (Massif Central, France). *Geochim Cosmochim Acta* 45, 1997-2016.
- Walter, A.V., Flicoteaux, R., Parron, C., Loubet, M., Nahon, D., 1995. Rare-earth elements and isotopes (Sr, Nd, O, C) in minerals from the Juquia carbonatite (Brazil); tracers of a multistage evolution. *Chem. Geol.* 120, 27-44.
- White, J. C., 2003. Trace-element partitioning between alkali feldspar and peralkalic quartz trachyte to rhyolite magma. Part II: Empirical equations for calculating trace-element partition coefficients of large-ion lithophile, high field-strength, and rare-earth elements. *Am. Mineral.* 88, 330-337.
- Witt-Eickschen, G., Harte, B., 1994. Distribution of trace elements between amphibole and clinopyroxene from mantle peridotites of the Eifel (western Germany): An ion-microprobe study. *Chem. Geol.* 117, 235-250.
- Wood, B. J., Blundy, J. D., 1997. A predictive model for rare earth element partitioning between clinopyroxene and anhydrous silicate melt. *Contrib. Mineral. Petrol.* 129, 166-181.
- Wood, B. J., Blundy, J. D., 2001. The effect of cation charge on crystal-melt partitioning of trace elements. *Earth Planet. Sci. Lett.* 188, 59-71.
- Wood, B. J., Trigila, R., 2001. Experimental determination of aluminous clinopyroxene-melt partition coefficients for potassic liquids, with application to the evolution of the Roman province potassic magmas. *Chem. Geol.* 172, 213-223.
- Wörner, G., Beusen, J.-M., Duchateau, N., Gijbels, R., Schmincke, H.-U., 1983. Trace element abundances and mineral/melt distribution coefficients in phonolites from the Laacher See Volcano (Germany). *Contrib. Mineral. Petrol.* 84, 152-173.

Figure captions

Fig. 1: Sketch map of the alkaline igneous Gardar Province, South Greenland, with the three igneous complexes Puklen, Ilímaussaq and Grønnedal-Ika (modified after Escher and Watt, 1976).

Fig. 2: Major element compositional trends for clinopyroxenes of the three complexes studied, after data from Larsen (1976), Marks & Markl (2001), Markl *et al.* (2001b), Marks *et al.* (2003) and Halama *et al.* (submitted).

Fig. 3: Major element compositional trends for amphiboles of the three complexes studied, after data from Larsen (1976), Marks & Markl (2001), Markl *et al.* (2001b), Marks *et al.* (2003) and Halama *et al.* (submitted).

Fig. 4: Averaged primitive mantle-normalized REE and TE patterns for augites of (a) Puklen and (b) Ilímaussaq. Normalizing values are after McDonough & Sun (1995).

Fig. 5: Zoning profiles for selected elements and X_{Fe} from core to rim of augite from (a) Puklen and (b) Ilímaussaq.

Fig. 6: (a) Averaged mantle-normalized REE and TE patterns for aegirine-augites of Grønnedal. (b) Mantle-normalized REE patterns and TE patterns of core and rim compositions for an individual aegirine-augite of sample GM 1496.

Fig. 7: Averaged mantle-normalized REE and TE patterns for aegirines of (a) Puklen and (b) Ilímaussaq.

Fig. 8: Averaged mantle-normalized REE and TE patterns for (a) ferro-edenites and ferro-richterites and (b) ferro-actinolites of Puklen.

Fig. 9: Averaged mantle-normalized REE and TE patterns for (a) ferro-pargasites of Ilímaussaq and (b) katophorites of Grønnedal.

Fig. 10: Zoning profile for selected elements, X_{Fe} and Na/Ca ratio from core to rim of ferro-richterite from Puklen.

Fig. 11: Averaged mantle-normalized REE and TE patterns for arfvedsonites of (a) Puklen and (b) Ilímaussaq.

Fig. 12: Zoning profile for selected elements from core to rim of arfvedsonite from Ilímaussaq.

Fig. 13: ϵ_{Nd} versus Pb/Pb* diagram for mineral separates of the Puklen rocks. ϵ_{Nd} data from Marks *et al.* (2003). See text for definition of Pb/Pb*.

Fig. 14: Clinopyroxene/amphibole partition coefficients for (a) Ilímaussaq augite syenites, (b) Puklen syenites, (c) Grønnedal nepheline syenite and (d) Ilímaussaq agpaites.

Fig. 15: Clinopyroxene/amphibole partition coefficients from this study compared to literature data (Villemant *et al.*, 1981; Lemarchand *et al.*, 1987; Adam & Green, 1994; Irving and Frey, 1984; Chazot *et al.*, 1996; Grégoire *et al.*, 2000; Vanucci *et al.*, 1991, Wörner *et al.*, 1983). A.I. is the alkalinity index, i.e. the $(K_2O + Na_2O)/Al_2O_3$ molecular ratio.

Fig. 16: Comparison of melts calculated from the mineral data, using the partition coefficient listed in Table 5, with whole-rock data. (a) + (b) Ilímaussaq; whole-rock augite-syenite data from Bailey *et al.* (2001); initial magma OGDC is an aphyric marginal facies sample from an alkali olivine basalt of the older giant dyke complex (OGDC) of Tugtutôq (Upton *et al.*, 1985) considered to represent the initial magma composition. (c) + (d) Grønnedal-Ika; whole-rock data from various nepheline-syenites (Pearce *et al.*, 1997).

Fig. 17: Clinopyroxene-melt REE partition coefficients calculated from mineral chemical data at $P = 1$ kbar after Wood and Blundy (1997). Dark grey vertical bars mark the position of r_0 (see Table 6 for data and explanations). a) D_{REE} calculated for different representative clinopyroxene compositions at 800 °C. b) D_{REE} calculated for aegirine at different temperatures.

Fig. 18: Primitive mantle-normalized REE plots of calculated melts and comparative whole-rock data from Ilímaussaq. L79, W83 and L87 denote melts calculated with a range of partition coefficients from Larsen (1979), Wörner *et al.* (1983) and Lemarchand *et al.* (1987) listed in Table 5. WB denotes melts calculated with the partition coefficients derived from the theoretical model of Wood and Blundy (1997) listed in Table 6. Whole-rock data are from Bailey *et al.* (2001) (B01), Upton *et al.* (1985) (U85) and Larsen (1979) (L79). a) Augite-syenite and melts calculated from augites b) Agpaitic rocks and melts calculated from aegirines.

Table 1: Summary of samples and minerals analyzed

Rock type	Sample	Analyzed mafic minerals
<i>Ilímaussaq:</i>		
augite syenite	GM1331	augite, calcic amphibole
augite syenite	GM1333	augite, calcic amphibole
alkali granite	GM1303	aegirine, sodic amphibole
agpaite	GM1294	aegirine
agpaite	GM1305	aegirine
agpaite	GM1334	aegirine, sodic amphibole
agpaite	GM1336	aegirine
agpaite	GM1337	aegirine, sodic amphibole
agpaite	GM1344	aegirine
agpaite	GM1347	aegirine, sodic amphibole
agpaite	GM1370	aegirine, sodic amphibole
agpaite	GM1371	aegirine
agpaite	GM1396	sodic amphibole
late-stage vein	GM1401	sodic amphibole
pegmatite	GM1657	sodic amphibole
<i>Puklen:</i>		
syenite	GM1586	augite, calcic amphibole I
syenite	GM1589	calcic amphibole I, calcic amphibole II
syenite	GM1590	augite, calcic amphibole I
syenite	GM1600	augite, calcic amphibole I, calcic amphibole II
syenite	GM1603	augite, calcic amphibole I, calcic amphibole II
syenite	GM1615	augite, sodic-calcic amphibole
syenite	GM1616	augite, sodic-calcic amphibole
syenite	GM1635	augite
granophyre	GM1593	calcic amphibole I, calcic amphibole II
alkali granite	GM1587	aegirine, sodic amphibole
alkali granite	GM1605	aegirine, sodic amphibole
alkali granite	GM1608	aegirine
microgranite	GM1620	aegirine, sodic amphibole
microgranite	GM1627	aegirine, sodic amphibole
<i>Grønnedal-Ika:</i>		
nepheline syenite	GR01	aegirine-augite
nepheline syenite	GR13	aegirine-augite
nepheline syenite	GR15	aegirine-augite
nepheline syenite	GR44	aegirine-augite
nepheline syenite	GR63	aegirine-augite
nepheline syenite	GM1496	aegirine-augite
nepheline syenite	GM1526	aegirine-augite, sodic-calcic amphibole
nepheline syenite	GM1531	sodic-calcic amphibole

Table 2: Average major, minor and trace element contents of clinopyroxenes from Ilímaussaq, Puklen and Grønnedal-Ika

Complex	Ilímaussaq	Puklen	Puklen	Grønnedal-Ika	Grønnedal-Ika	Grønnedal-Ika
Rock type	augite syenite	syenite	syenite	nepheline syenite	nepheline syenite	nepheline syenite
Sample No.	GM1331	GM 1586	GM1600	GR44	GM1526	GM1496
Clinopyroxene type	augite	augite	augite	aegirine-augite	aegirine-augite	aegirine-augite core
No. of analyses	6	14	8	10	10	3
Major and minor elements (wt.%)*						
SiO ₂	50.35	49.53	50.27	50.77	51.80	50.29
TiO ₂	0.91	0.61	0.95	0.20	0.16	0.35
Al ₂ O ₃	1.73	0.53	0.80	1.14	0.99	2.50
FeO	14.17	24.53	20.27	21.53	24.54	17.35
MnO	0.49	0.66	0.50	0.90	0.78	0.38
MgO	10.55	3.46	6.36	4.35	2.08	6.75
CaO	21.06	19.75	19.71	17.93	11.56	19.41
Na ₂ O	0.53	0.82	0.93	3.30	7.17	2.22
K ₂ O	0.01	0.02	0.01	0.00	0.01	0.01
Total	99.81	99.92	99.80	100.12	99.09	99.26
Na/Ca ratio	0.05	0.08	0.08	0.33	1.12	0.21
X _{Fe}	0.43	0.79	0.62	0.64	0.72	0.52
Trace elements (ppm)						
Cs	0.15	0.63	0.95	—	0.25	—
Rb	0.85	3.31	6.41	2.49	2.11	3.06
Ba	1.14	2.14	21.6	0.85	1.89	1.53
Th	0.98	0.26	4.90	0.29	0.19	—
U	0.44	0.36	1.62	0.08	0.08	0.04
Nb	1.01	0.79	8.23	2.96	9.02	2.40
Ta	n.a.	0.14	1.68	0.48	0.91	0.23
La	28.91	32.44	13.4	43.4	11.2	8.17
Ce	104.4	98.11	313	140	42.8	32.5
Pb	0.74	1.71	35.6	0.49	0.46	0.21
Pr	16.45	17.54	45.6	22.9	8.19	5.90
Sr	27.65	5.80	43.2	205	56.9	589
Nd	75.81	92.74	219	106	41.2	33.5
Zr	243.1	199.1	90.3	1127	5721	127
Hf	7.26	6.74	3.98	29.4	145	3.01
Sm	19.42	23.32	53.0	23.1	10.4	9.13
Eu	2.35	1.72	1.93	4.80	2.03	3.48
Sn	1.43	1.95	4.64	8.11	54.7	1.32
Gd	14.97	19.69	44.8	15.6	6.81	7.09
Tb	2.62	3.15	7.63	2.12	1.26	0.94
Dy	15.16	17.67	45.9	11.5	6.91	4.65
Li	32.0	195.0	278	8.47	5.31	8.76
Y	68.90	84.57	228	42.9	23.4	13.8
Ho	3.03	3.70	9.11	1.97	1.37	0.61
Er	7.87	9.52	23.9	5.62	4.76	1.32
Tm	1.17	1.64	3.40	1.03	1.15	0.16
Yb	8.87	14.84	23.4	9.16	13.5	0.80
Lu	1.40	2.83	3.69	1.88	2.78	0.15
Sc	210.3	121.2	118	12.8	13.2	8.50
V	3.99	1.38	196	12.1	4.21	148
Co	n.a.	10.60	111	12.3	6.59	22.8
Zn	199.9	276.4	487	247	306	89.2
Ga	10.63	6.40	7.56	10.5	12.8	12.1

* = analyzed by electron microprobe; n.a. = not analyzed; — = not detected

Table 2 continued

Complex	Grønnedal-Ika	Ilfmaussaq	Ilfmaussaq	Ilfmaussaq	Puklen	Puklen
Rock type	nepheline syenite	alkali granite	agpaite	agpaite	alkali granite	microgranite
Sample No.	GM1496	GM1303	GM1294	GM1334	GM1587	GM1620
Clinopyroxene type	aegirine- augite rim	aegirine	aegirine	aegirine	aegirine	aegirine
No. of analyses	2	8	4	7	8	11
Major and minor elements (wt.%)*						
SiO ₂	51.11	51.89	52.45	52.88	52.48	53.06
TiO ₂	0.32	0.56	0.69	0.59	0.93	0.37
Al ₂ O ₃	1.07	0.13	1.33	1.07	0.31	0.28
FeO	21.45	30.46	28.72	28.24	30.38	27.36
MnO	0.67	0.08	0.08	0.12	0.18	0.56
MgO	3.91	0.08	0.01	0.13	0.04	1.35
CaO	14.05	0.08	0.54	2.27	0.09	4.38
Na ₂ O	5.68	13.14	13.46	12.41	13.35	11.73
K ₂ O	0.05	0.01	0.00	0.02	0.04	0.01
Total	98.32	96.43	97.28	97.73	97.79	99.09
Na/Ca ratio	0.73	297	45	9.9	275	4.8
X _{Fe}	0.57	0.97	1.00	0.91	0.99	0.51
Trace elements (ppm)						
Cs	—	0.31	0.20	0.18	13.1	0.01
Rb	1.18	0.77	0.68	1.04	107	6.60
Ba	—	3.26	0.49	0.37	175	2.52
Th	0.10	1.19	0.49	0.14	15.8	0.35
U	—	0.46	0.14	0.05	14.5	0.23
Nb	3.69	27.0	74.9	4.67	371	48.0
Ta	0.87	1.43	n.a.	n.a.	22.7	1.69
La	9.73	2.41	4.06	5.01	370	39.5
Ce	38.9	7.17	11.4	13.8	622	115
Pb	0.27	25.0	28.8	0.82	1172	2.20
Pr	7.60	1.17	1.82	1.97	76.6	18.2
Sr	352	2.01	2.44	4.62	38.0	6.50
Nd	41.6	5.72	7.89	8.38	368	86.5
Zr	6218	1338	982	1406	2303	234
Hf	116.1	54.2	18.7	29.0	51.1	7.52
Sm	12.5	3.43	1.83	1.48	76.1	19.5
Eu	3.28	0.20	0.20	0.15	3.99	0.99
Sn	45.3	97.3	265	169	125	2.06
Gd	7.29	4.08	1.59	0.99	77.0	15.0
Tb	1.14	1.14	0.30	0.15	11.7	2.48
Dy	7.19	9.11	1.61	0.92	60.3	15.2
Li	2.49	71.0	25.0	29.0	148	176
Y	24.3	35.5	7.62	4.38	429	78.0
Ho	1.44	2.47	0.27	0.21	13.4	3.18
Er	4.49	10.4	0.79	0.77	39.0	10.8
Tm	0.84	2.02	0.20	0.24	6.03	1.88
Yb	8.96	11.5	2.13	3.08	45.4	18.0
Lu	2.06	1.77	0.51	0.79	6.53	3.45
Sc	2.45	2.44	3.44	10.6	7.38	53.0
V	8.99	0.76	0.20	5.73	8.41	3.50
Co	7.85	n.a.	n.a.	n.a.	7.90	5.31
Zn	322	376	61.6	130	1033	385
Ga	19.3	5.66	72.2	40.6	13.7	4.60

* = analyzed by electron microprobe; n.a. = not analyzed; — = not detected

Table 3: Average major, minor and trace element contents of amphiboles from Ilímaussaq, Puklen and Grønnedal-Ika

Complex	Ilímaussaq	Puklen	Puklen	Puklen	Puklen
Rock type	augite syenite	granophyre	syenite	granophyre	syenite
Sample No.	GM1331	GM1593	GM1600	GM1593	GM1615
Amphibole type	calcic ferro-pargasite	calcic I ferro-edenite	calcic I ferro-edenite	calcic II ferro-actinolite	sodic-calcic ferro-richterite
No. of analyses	6	8	9	4	7
Major and minor elements (wt.%)*					
SiO ₂	41.07	44.08	44.98	50.42	48.67
TiO ₂	3.13	0.83	1.25	0.06	1.10
Al ₂ O ₃	9.04	5.00	5.00	0.74	0.82
FeO	19.42	29.51	28.04	33.42	31.53
MnO	0.38	0.34	0.53	0.41	0.74
MgO	8.90	4.03	5.09	2.45	0.62
CaO	10.55	9.62	9.54	10.54	5.60
Na ₂ O	2.71	2.86	2.61	0.85	6.08
K ₂ O	1.49	0.99	0.91	0.26	1.27
Cl	0.13	0.30	0.26	0.01	0.04
F	0.72	1.57	2.33	0.00	0.74
Total	97.55	99.13	100.55	99.16	97.23
Na/Ca ratio	0.46	0.54	0.50	0.15	1.95
X _{Fe}	0.55	0.80	0.76	0.88	0.96
Trace elements (ppm)					
Cs	0.02	1.43	1.01	—	0.39
Rb	19.4	105	12.3	—	28.9
Ba	303	161	13.5	2.90	2.85
Th	23.3	4.31	2.40	3.05	0.35
U	6.61	1.00	0.24	0.32	0.14
Nb	365	303	86.5	10.4	137
Ta	n.a.	7.57	1.93	0.88	2.11
La	253	72.4	109	32.5	42.0
Ce	557	264	407	57.9	103
Pb	5.89	28.5	20.0	9.39	7.41
Pr	168	37.1	57.8	7.47	15.0
Sr	96.6	30.4	25.1	10.7	15.3
Nd	692	155	245	28.7	66.7
Zr	1640	50.9	976	52.6	1087
Hf	49.9	2.92	8.18	4.91	25.4
Sm	134	39.6	61.6	6.11	12.6
Eu	9.65	0.70	1.68	0.37	0.88
Sn	4.50	96.2	14.6	41.8	9.56
Gd	95.4	30.7	46.3	5.67	9.03
Tb	14.0	6.45	8.38	1.11	1.72
Dy	76.1	42.8	50.3	7.21	14.2
Li	29.0	722	167	240	1466
Y	345	250	269	48.5	130
Ho	14.7	9.28	10.0	1.64	4.87
Er	36.7	25.7	26.2	5.95	24.6
Tm	4.89	4.12	3.83	1.63	6.67
Yb	32.4	31.1	29.9	22.7	65.3
Lu	4.38	4.36	4.39	5.81	13.1
Sc	156	83.6	54.6	40.4	48.4
V	1.64	29.0	147	5.77	4.75
Co	n.a.	43.6	29.8	n.a.	17.6
Zn	381	1381	1109	1927	1476
Ga	56.0	45.5	23.5	5.32	13.2

* = analyzed by electron microprobe; n.a. = not analyzed; — = not detected

Table 3 continued

Complex	Grønnedal-Ika	Ílímaussaq	Ílímaussaq	Puklen	Puklen
Rock type	nepheline syenite	alkali granite	agpaite	alkali granite	microgranite
Sample No.	GM1526	GM1303	GM1334	GM1587	GM1620
Amphibole type	sodic-calcic katophorite	sodic arfvedsonite	sodic arfvedsonite	sodic arfvedsonite	sodic arfvedsonite
No. of analyses	1	14	7	7	5
Major and minor elements (wt.%)*					
SiO ₂	44.55	43.66	47.39	51.07	49.59
TiO ₂	1.12	1.10	0.73	1.92	0.69
Al ₂ O ₃	5.65	5.53	2.96	0.53	2.38
FeO	27.59	27.04	33.17	29.90	29.36
MnO	1.10	1.08	0.66	0.84	0.78
MgO	4.18	4.10	0.84	1.14	3.84
CaO	6.47	6.34	2.38	0.24	5.21
Na ₂ O	5.37	5.26	7.71	8.61	5.44
K ₂ O	1.72	1.68	1.74	1.58	0.56
Cl	0.03	0.03	0.00	0.02	0.14
F	1.13	1.11	0.07	2.57	0.13
Total	98.91	96.94	97.66	98.42	98.13
Na/Ca ratio	1.50	44.65	5.88	65.56	1.87
X _{Fe}	0.75	1.00	0.94	0.92	0.81
Trace elements (ppm)					
Cs	—	—	0.20	14.8	0.69
Rb	18.7	53.4	41.3	192	13.2
Ba	3.37	1.20	3.18	79.5	2.17
Th	—	1.48	0.20	154	1.65
U	—	1.33	0.13	9.84	0.93
Nb	517	94.6	132.8	355	36.4
Ta	20.4	1.22	n.a.	11.0	1.06
La	53.9	12.4	17.9	3986	104
Ce	145	44.2	44.1	7791	300
Pb	0.95	15.0	2.55	1260	24.0
Pr	20.1	4.74	5.67	1169	41.1
Sr	93.7	5.99	18.9	726	37.4
Nd	84.1	17.3	21.3	4993	186
Zr	1766	853	1472	1697	576
Hf	50.4	27.2	34.2	39.3	15.5
Sm	15.4	2.98	3.00	771	62.2
Eu	2.56	0.23	1.00	36.0	3.00
Sn	19.1	38.1	39.1	58.9	20.8
Gd	7.79	1.83	1.50	612	43.5
Tb	1.16	0.41	0.51	86.6	6.50
Dy	5.47	3.72	1.90	505	41.6
Li	31.3	756	390	2895	288
Y	18.4	21.6	12.1	2494	177
Ho	0.92	1.49	0.73	122	9.51
Er	2.70	8.77	2.49	298	23.6
Tm	0.53	2.78	0.78	33.7	4.11
Yb	5.17	35.3	8.04	191	38.6
Lu	1.04	7.88	1.58	26.1	7.77
Sc	6.44	8.43	11.7	20.8	42.0
V	1.41	0.89	7.32	32.6	4.20
Co	19.8	3.23	n.a.	13.0	8.80
Zn	592	3287	956	4667	931
Ga	32.3	6.16	36.0	16.2	6.40

* = analyzed by electron microprobe; n.a. = not analyzed; — = not detected

Table 4: Clinopyroxene-amphibole distribution coefficients for alkaline igneous rocks

Complex	Ílímaussaq	Ílímaussaq	Ílímaussaq	Ílímaussaq	Puklen	Puklen	Gronnedal-Ika
Rock type	augite syenite	augite syenite	agpaitite	agpaitite	quartz syenite	quartz syenite	nepheline syenite
Mineral pair	augite - ferro-pargasite	augite - ferro-pargasite	aegirine - arfvedsonite	aegirine - arfvedsonite	augite - ferro-edenite	augite - ferro-edenite	aegirine-augite - katophorite
Sample	GM 1331	GM 1333	GM 1334	GM 1337	GM 1600	GM 1603	GM 1526
Cs	7.50	1.57	0.90	0.25	0.94		
Rb	0.04	0.05	0.03	0.03	0.52	1.08	0.11
Ba	0.004	0.004	0.12	0.04	1.60	3.92	0.56
Th	0.04	0.36	0.70	0.01	2.04	22.10	
U	0.07	0.58	0.38	0.07	6.84	16.92	
Nb	0.003	0.003	0.04	0.01	0.10	0.03	0.02
Ta					0.87	0.04	0.04
La	0.11	0.11	0.28	0.07	1.23	1.55	0.21
Ce	0.19	0.15	0.31	0.12	0.77	1.52	0.29
Pb	0.13	0.30	0.32	0.22	1.78	2.28	0.48
Pr	0.10	0.20	0.35	0.15	0.79	1.59	0.41
Sr	0.29	0.60	0.24	0.11	1.72	0.34	0.61
Nd	0.11	0.26	0.39	0.15	0.90	1.76	0.49
Zr	0.15	0.17	0.96	0.52	0.93	0.76	3.24
Hf	0.15	0.19	0.85	0.80	0.49	0.57	2.88
Sm	0.15	0.33	0.49	0.18	0.86	1.52	0.67
Eu	0.24	0.35	0.15	0.11	1.15	1.48	0.79
Ti	0.28	0.45	0.68	0.66	0.16	0.28	0.14
Sn	0.32	0.05	4.32	1.92	0.32	0.23	2.87
Gd	0.16	0.37	0.66	0.18	0.97	1.52	0.87
Tb	0.19	0.34	0.29	0.15	0.91	1.36	1.09
Dy	0.20	0.35	0.48	0.19	0.91	1.39	1.26
Li	1.10	0.25	0.07	0.06	1.66	0.82	0.17
Y	0.20	0.33	0.36	0.18	0.85	1.46	1.28
Ho	0.21	0.35	0.29	0.12	0.91	1.59	1.49
Er	0.21	0.37	0.31	0.17	0.91	1.52	1.76
Tm	0.24	0.41	0.31	0.20	0.89	1.52	2.19
Yb	0.27	0.46	0.38	0.26	0.78	1.52	2.62
Lu	0.32	0.61	0.50	0.33	0.84	1.66	2.69
Sc	1.35	14.13	0.90	0.50	2.17	2.53	2.05
V	2.43	6.17	0.78	0.48	1.33	0.20	2.99
Co					3.72	1.67	0.33
Zn	0.53	0.50	0.14	0.06	0.44	0.59	0.52

Table 5: Maximum and minimum partition coefficients for alkaline rocks used to calculate melt compositions and “initial magma” compositions

Element	Clinopyroxene		Amphibole		“Initial magmas”	
	D_{\max}	D_{\min}	D_{\max}	D_{\min}	OGDC	Ilímaussaq
					<i>in ppm:</i>	<i>in ppm:</i>
Cs	0.05	0.03				6.99
Rb	0.04	0.02	0.14	0.11	27	360
Ba	0.02	0.01	5.58	0.39	1477	36
Th	0.15	0.01	0.07	0.03		63
U	0.09	0.02	0.45	0.06		29
Nb	0.03	0.03			25	867
Ta	0.50	0.21	1.25	0.85		
La	0.66	0.06	0.99	0.22	39.3	483
Ce	0.96	0.21	2.06	1.05	89.3	845
Pb	0.13	0.10				71
Sr	0.25	0.25	9.77	3.00	1186	50
Nd	2.27	0.49	3.56	2.53	51.9	298
Zr	1.02	0.24	1.77	0.37	136	4231
Hf	1.54	0.40	1.19	0.54		90
Sm	6.18	0.48	7.29	2.12	9.4	39.3
Eu	13.87	0.60	9.39	1.07	3.5	3.40
Tb	8.63	0.60	9.74	1.45		7.64
Tm	0.79	0.35	2.00	0.92		
Yb	2.63	0.40	2.10	0.33	2.2	34.2
Lu	2.06	0.41	2.83	1.08	0.3	
Sc	334	4.05	120.7	0.90	14	

Partition coefficients from Larsen (1979), Wörner et al. (1983) and Lemarchand et al. (1987). “Initial magmas” are a chilled marginal facies sample from an alkali olivine basalt of the OGDC (Upton et al., 1985) and an eudialyte-bearing nepheline-porphyrific phonolitic dike (Larsen, 1979).

Table 6: Selected typical mineral compositions and REE partition coefficients calculated from the crystal chemistry after the theoretical model of Wood and Blundy (1997)

Mineral	Augit	→	Aegirine- augite, core	Aegirine- augite, rim	Aegirine	→	→	→
Intrusion	Ilímaussaq	→	Grønnedal	Grønnedal	Ilímaussaq	→	→	→
Sample	GM 1331	→	GM 1496	GM 1496	GM 1303	→	→	→
Temperature (°C)	900	800	800	800	800	650	500	350
<i>Cations p.f.u.</i>								
Si	1.924	→	1.943	1.984	2.002	→	→	→
Al ^(IV)	0.076	→	0.057	0.016	0.000	→	→	→
Al ^(VI)	0.002	→	0.057	0.033	0.006	→	→	→
Ti	0.026	→	0.010	0.009	0.016	→	→	→
Fe ³⁺	0.062	→	0.145	0.395	0.942	→	→	→
Mg	0.601	→	0.389	0.225	0.004	→	→	→
Fe ²⁺	0.391	→	0.416	0.302	0.041	→	→	→
Mn	0.016	→	0.012	0.022	0.003	→	→	→
Ca	0.862	→	0.804	0.584	0.003	→	→	→
Na	0.039	→	0.166	0.428	0.983	→	→	→
Total	4.000	→	4.000	4.000	4.000	→	→	→
<i>Calculated parameters</i>								
r ₀	1.032	1.032	1.025	1.011	0.974	0.974	0.974	0.974
E _{M2} at P, T	277.1	280.7	280.7	280.7	280.7	286.1	291.5	296.9
Mg# melt	0.22	0.22	0.11	0.05	0.0004	0.0004	0.0004	0.0004
D ₀ ³⁺	1.45	3.41	2.48	1.68	1.30	6.61	63.5	1812
<i>Calculated partition coefficients after Wood& Blundy (1997)</i>								
D _{La}	0.20	0.38	0.22	0.09	0.01	0.03	0.09	0.47
D _{Ce}	0.33	0.66	0.40	0.17	0.03	0.08	0.31	2.13
D _{Pr}	0.51	1.07	0.66	0.31	0.07	0.20	0.88	8.17
D _{Nd}	0.72	1.57	1.00	0.49	0.13	0.43	2.26	26.7
D _{Sm}	1.12	2.57	1.72	0.94	0.33	1.30	8.74	148
D _{Eu}	1.27	2.94	2.01	1.16	0.45	1.91	14.0	269
D _{Gd}	1.38	3.22	2.25	1.35	0.60	2.67	21.0	448
D _{Tb}	1.44	3.38	2.42	1.52	0.76	3.53	29.5	689
D _{Dy}	1.45	3.41	2.48	1.63	0.92	4.42	38.9	975
D _{Ho}	1.41	3.30	2.45	1.68	1.06	5.20	47.4	1253
D _{Er}	1.34	3.12	2.35	1.67	1.16	5.82	54.4	1488
D _{Tm}	1.25	2.88	2.21	1.62	1.24	6.25	59.3	1660
D _{Yb}	1.15	2.64	2.05	1.55	1.28	6.50	62.2	1764
D _{Lu}	1.06	2.40	1.89	1.46	1.30	6.61	63.4	1808
D _{La} /D _{Lu}	0.189	0.112	0.089	0.055	0.015	0.007	0.002	0.0005

All calculations were carried out for 0.1 GPa. r₀ is the radius of the ion that would ideally fit into the crystallographic site of interest, E_{M2} is the Young's Modulus of the M2-site in clinopyroxene and D₀³⁺ is the partition coefficient of the element with the radius r₀. Mg# melt was estimated from the pyroxene composition after Wood & Blundy (1997). The arrow (→) stands for repetition of the information of the previous column.

Fig. 1

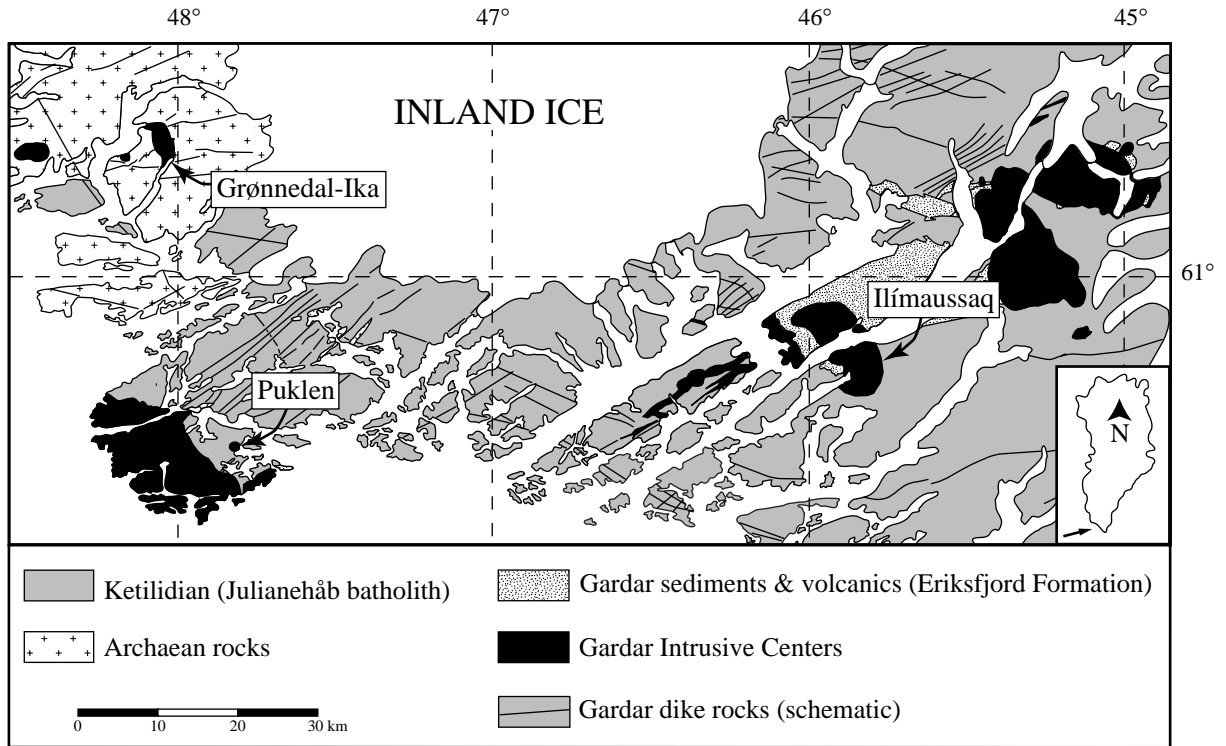


Fig. 2

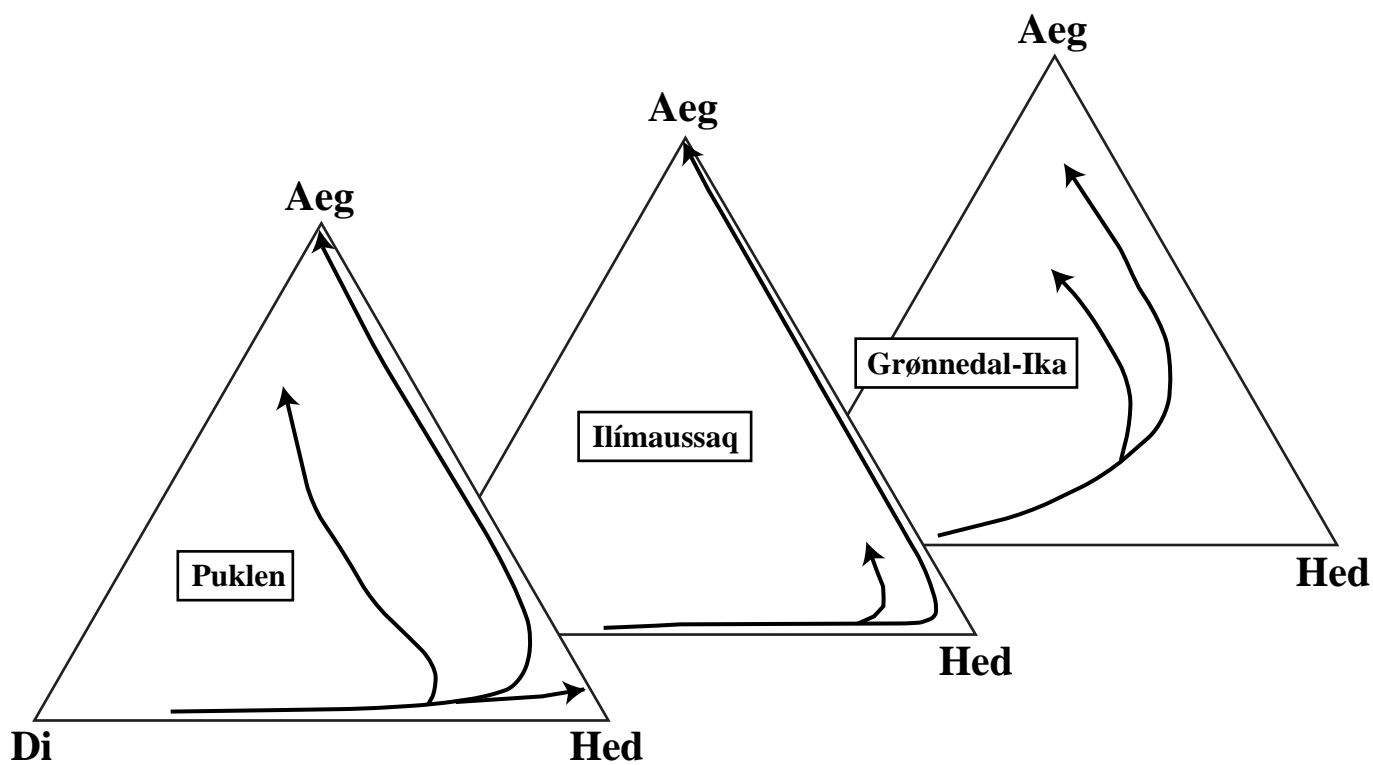
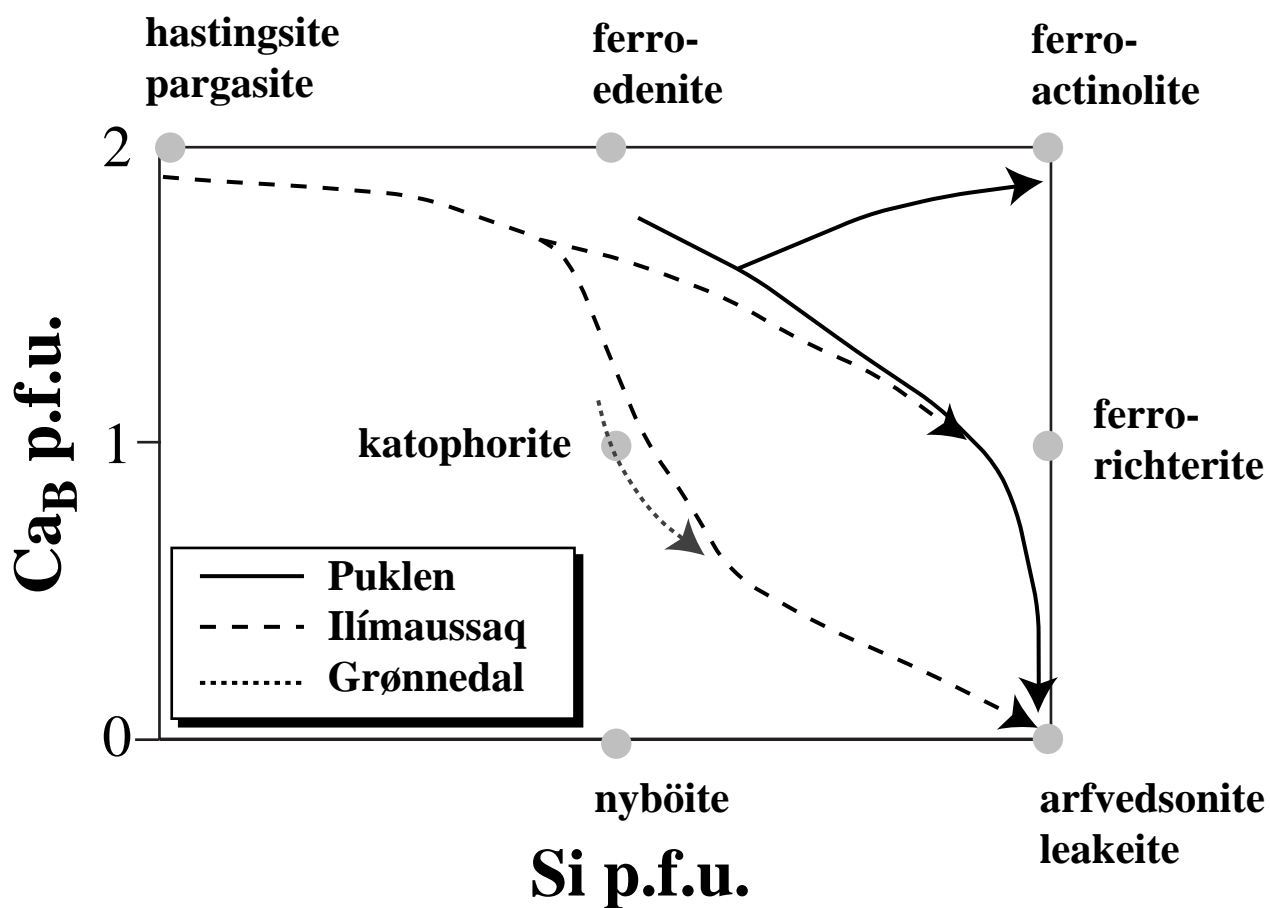
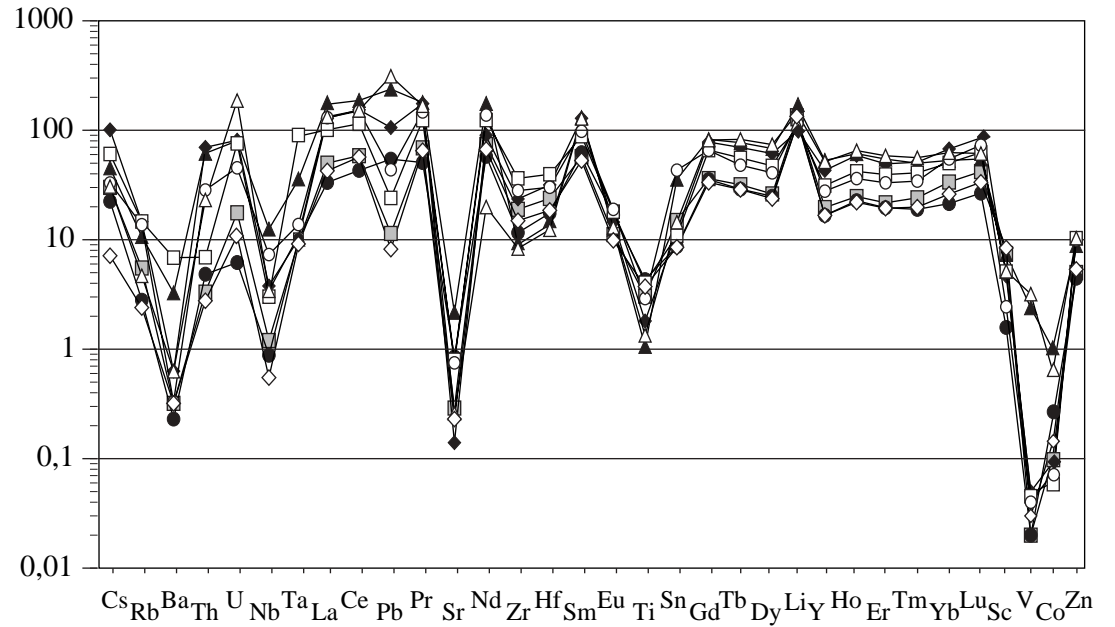
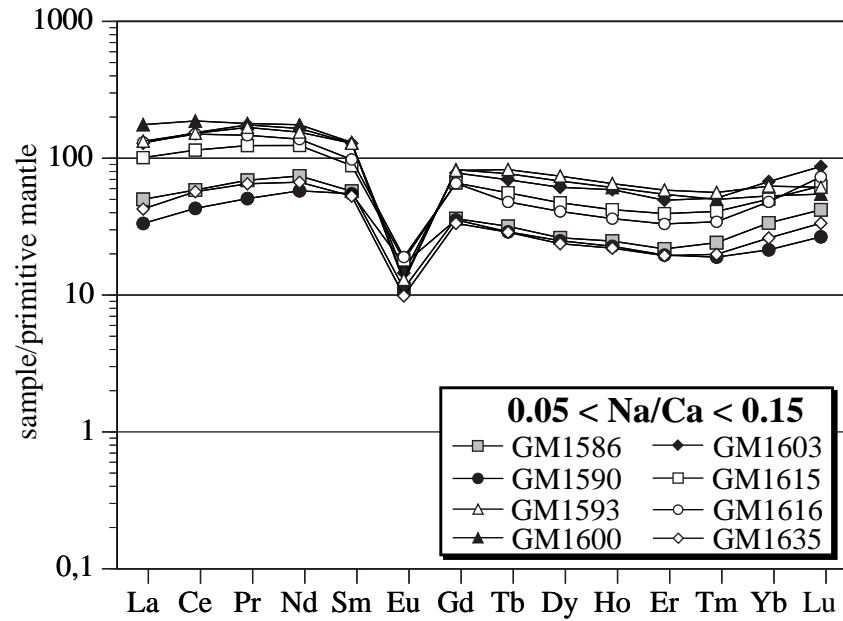


Fig. 3



(a) Puklen augites



(b) Ilímaussaq augites

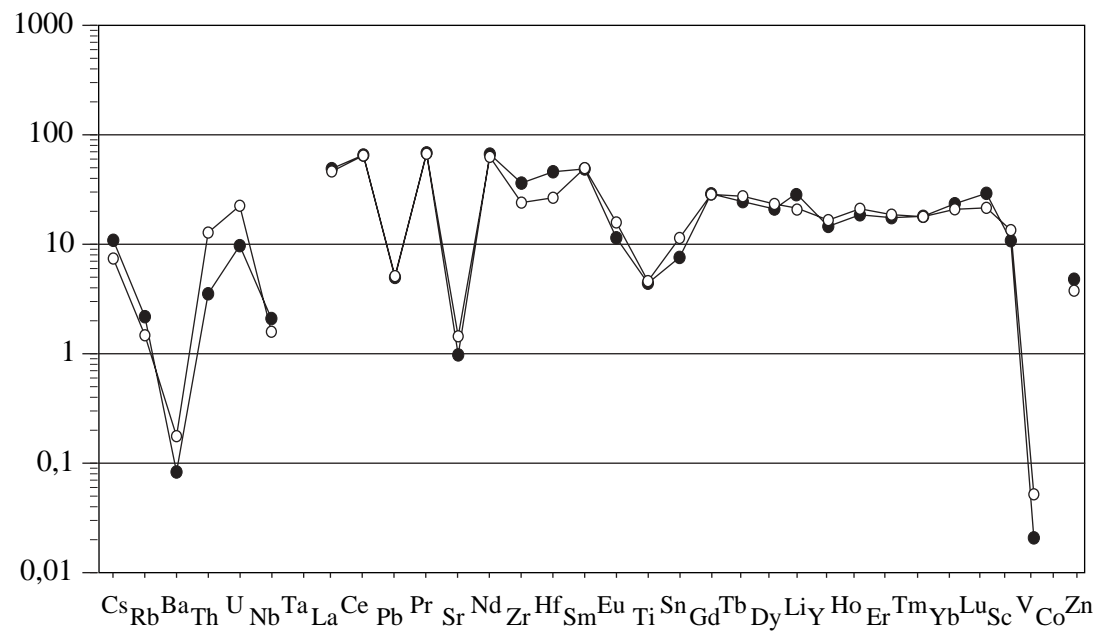
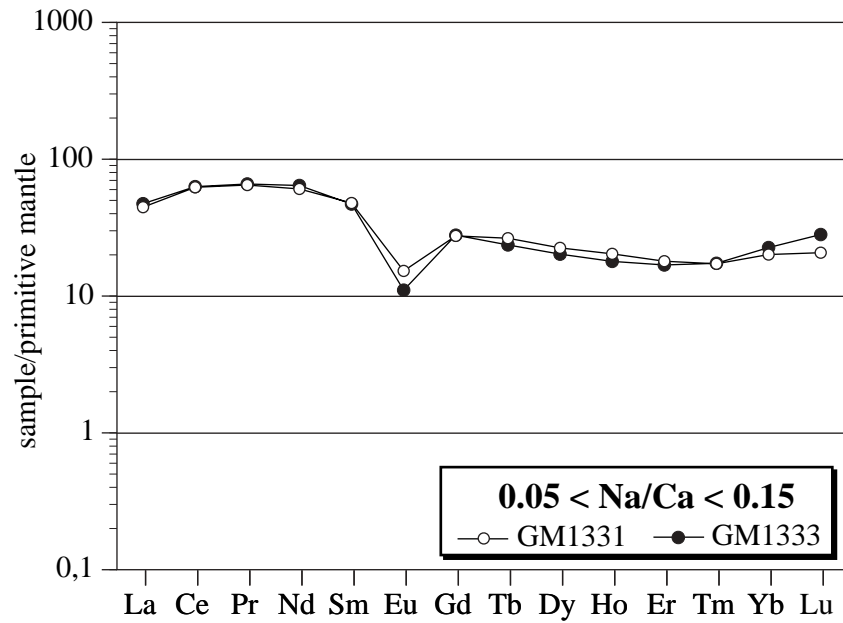
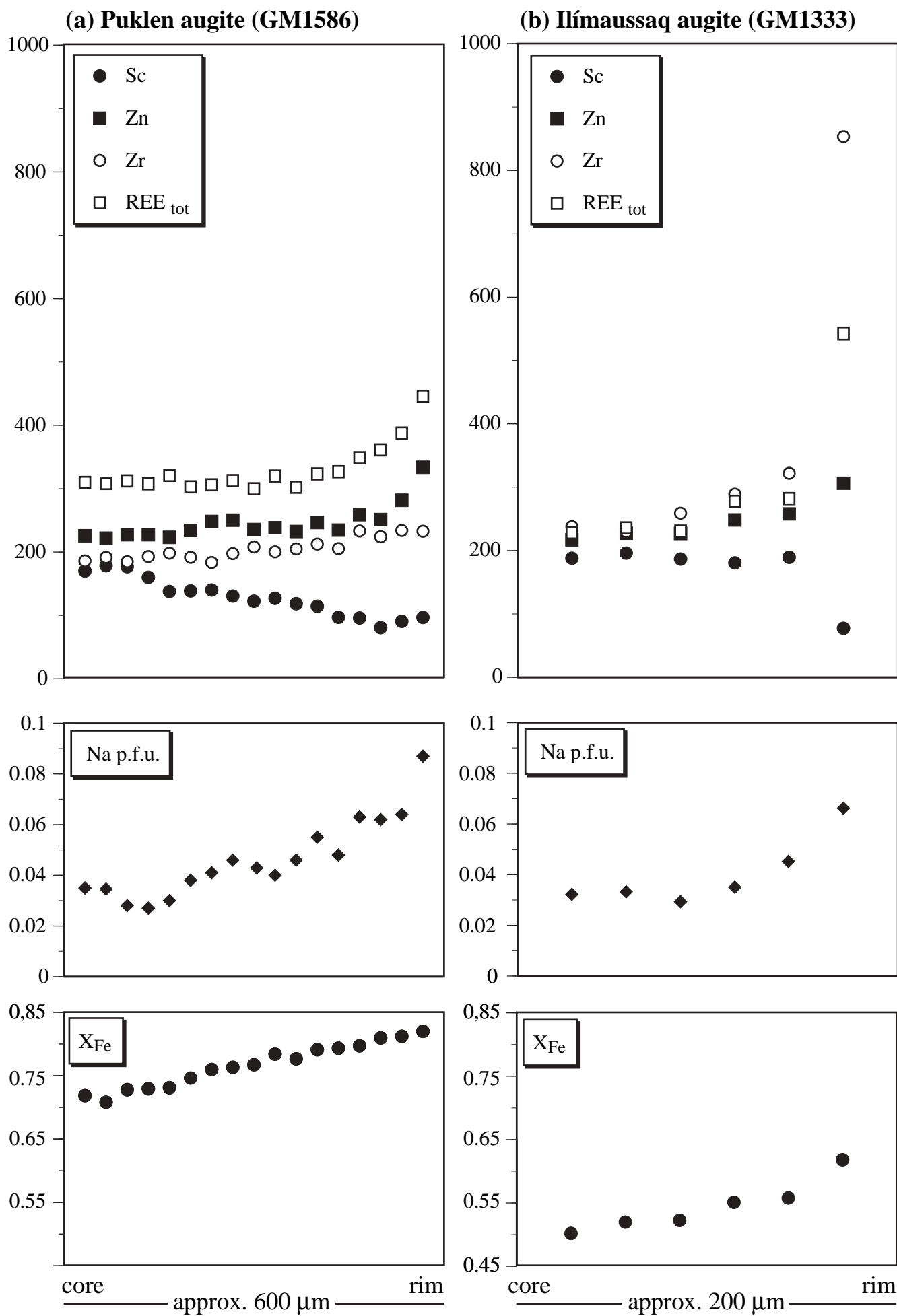
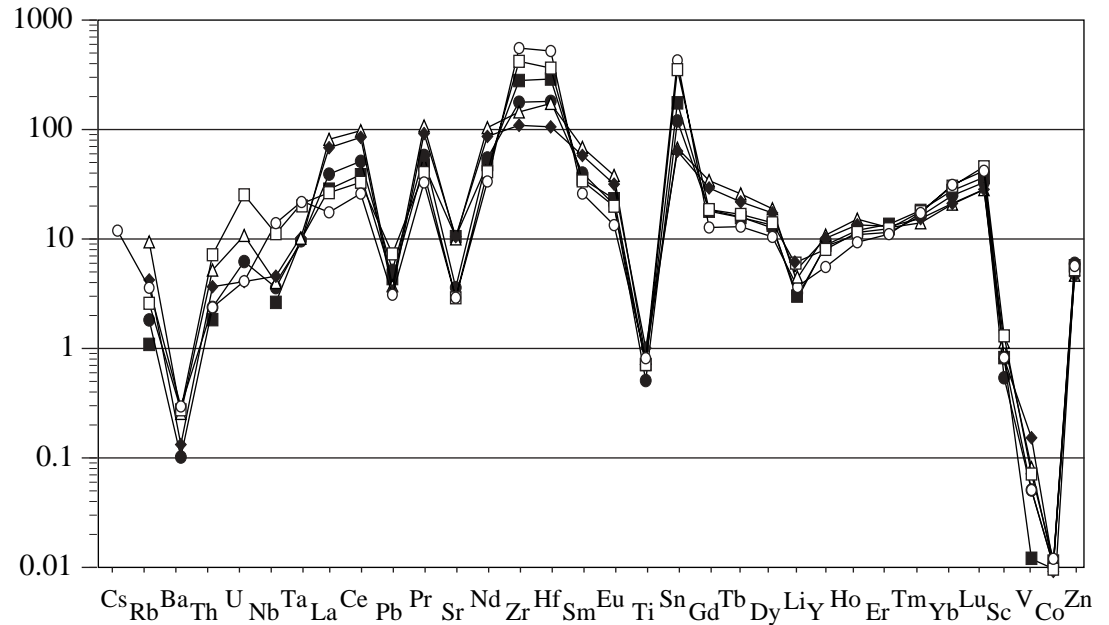
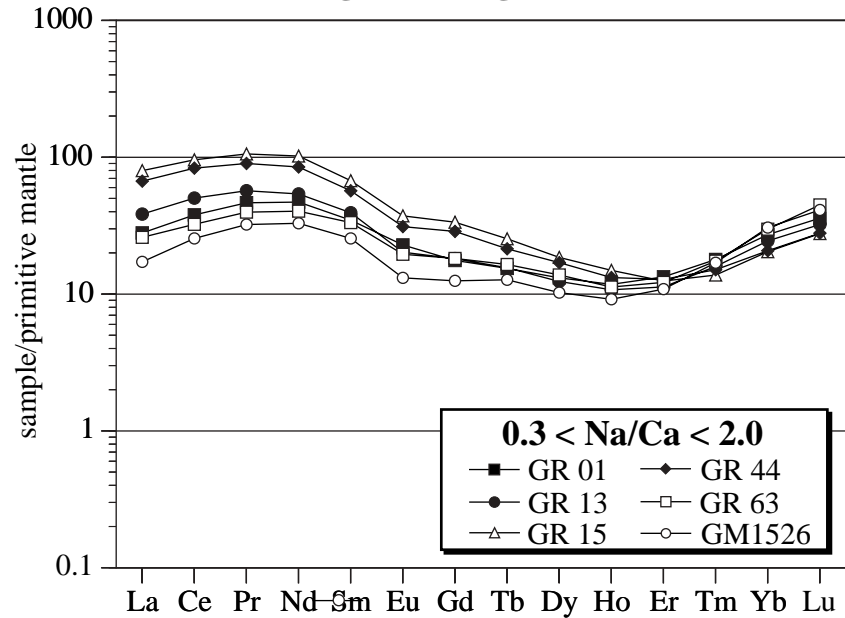


Fig. 4

Fig. 5



(a) Grønnedal-Ika aegirine-augites



(b) Grønnedal-Ika aegirine-augites sample GM1496

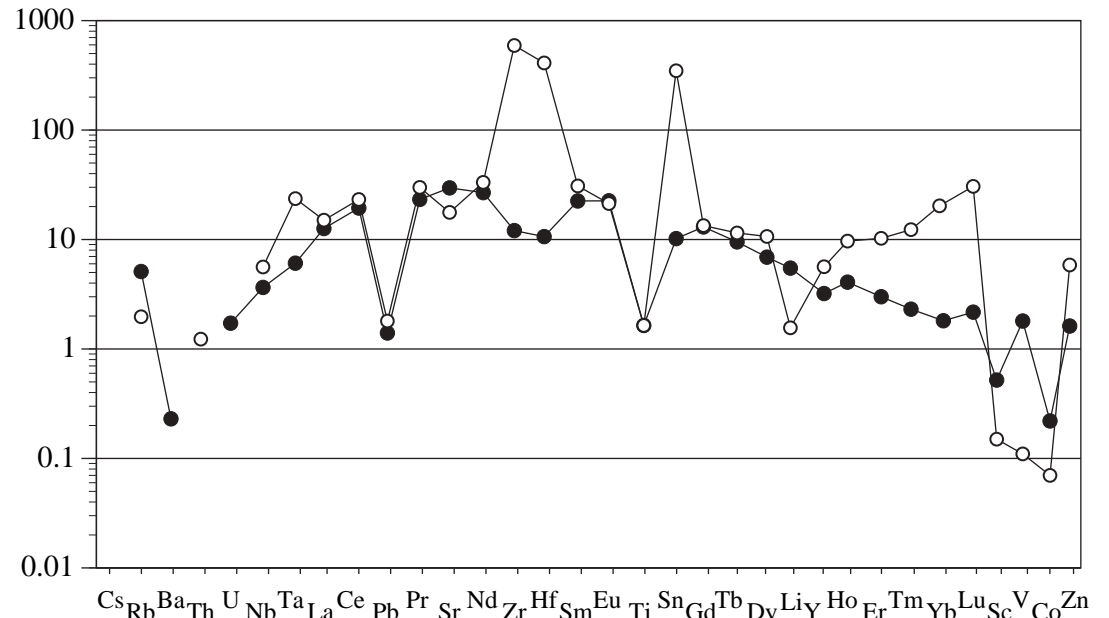
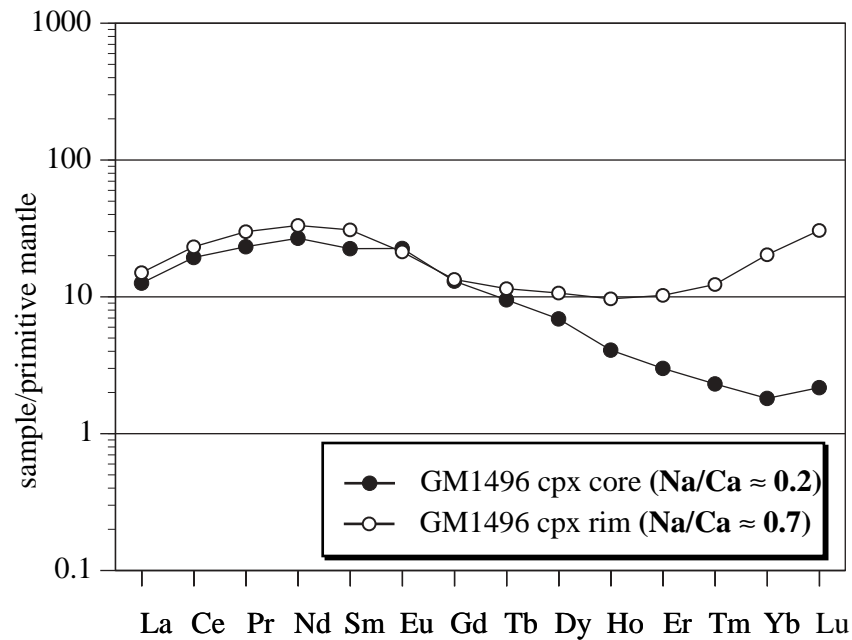
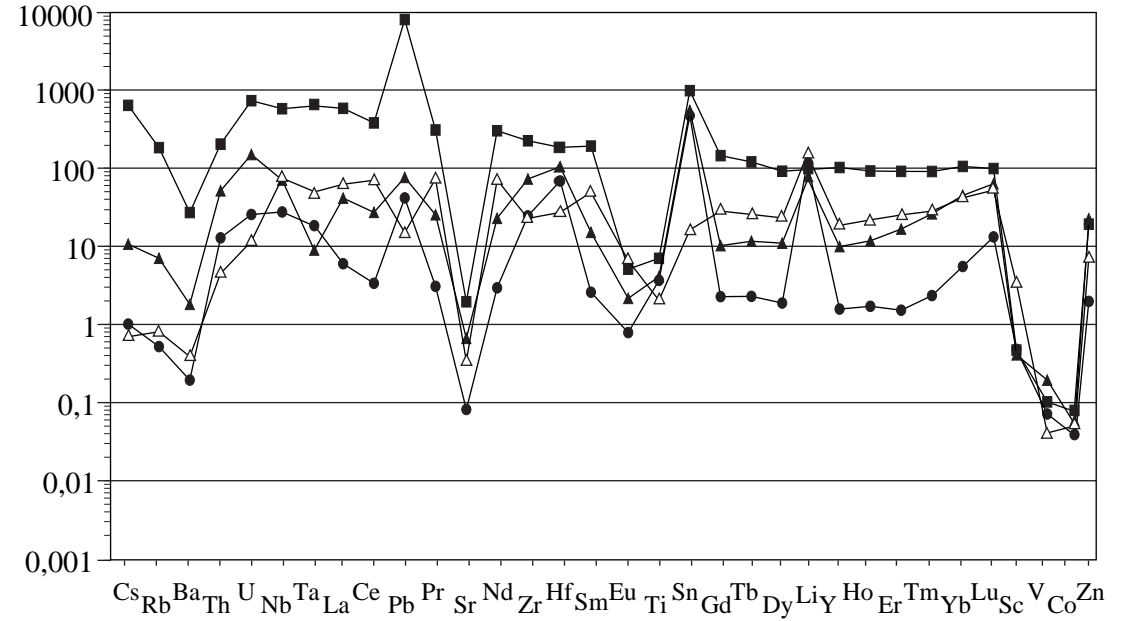
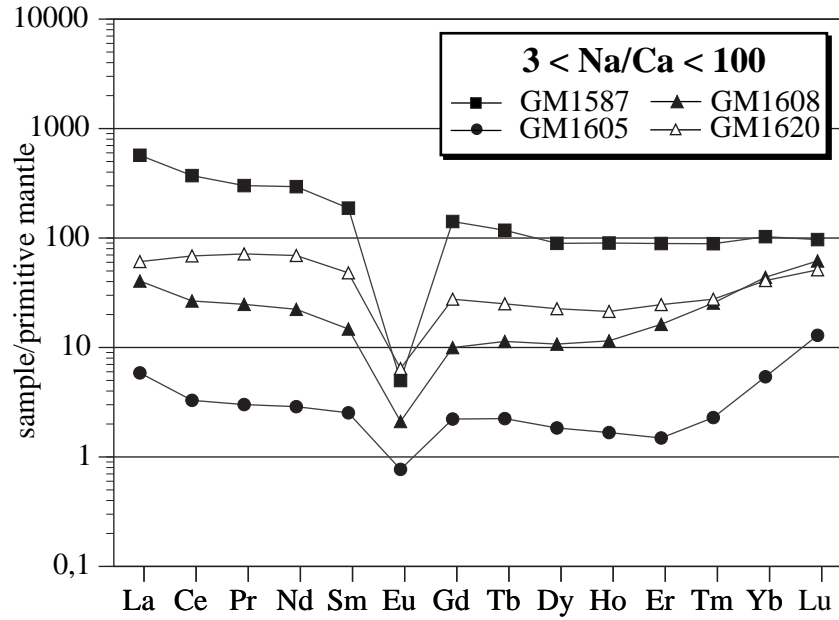


Fig. 6

(a) Puklen aegirines



(b) Ilímaussaq aegirines

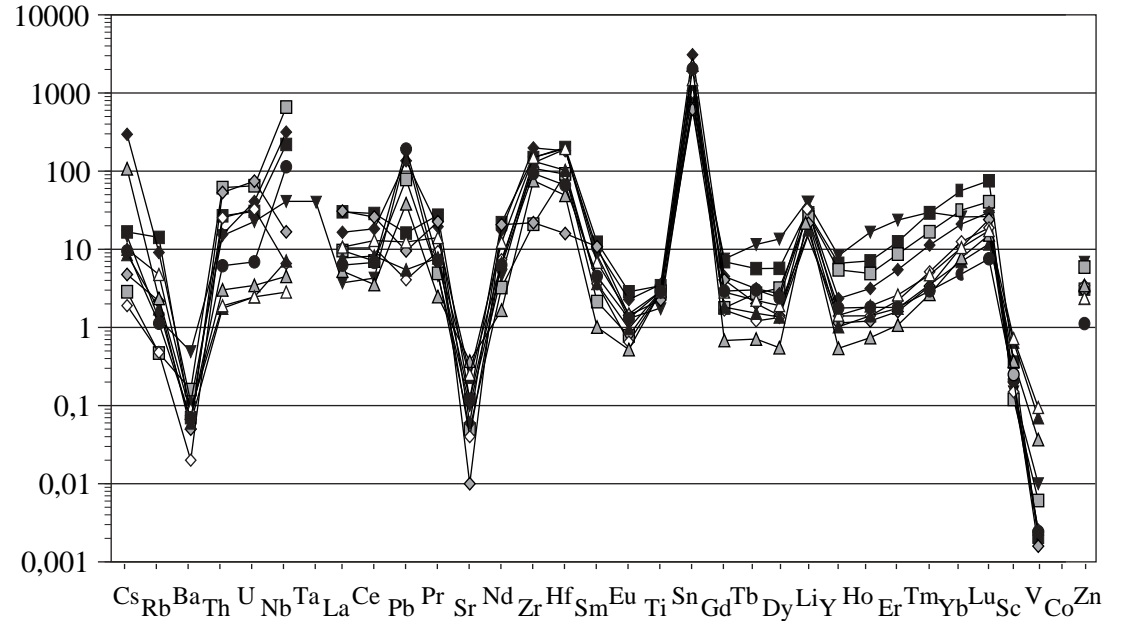
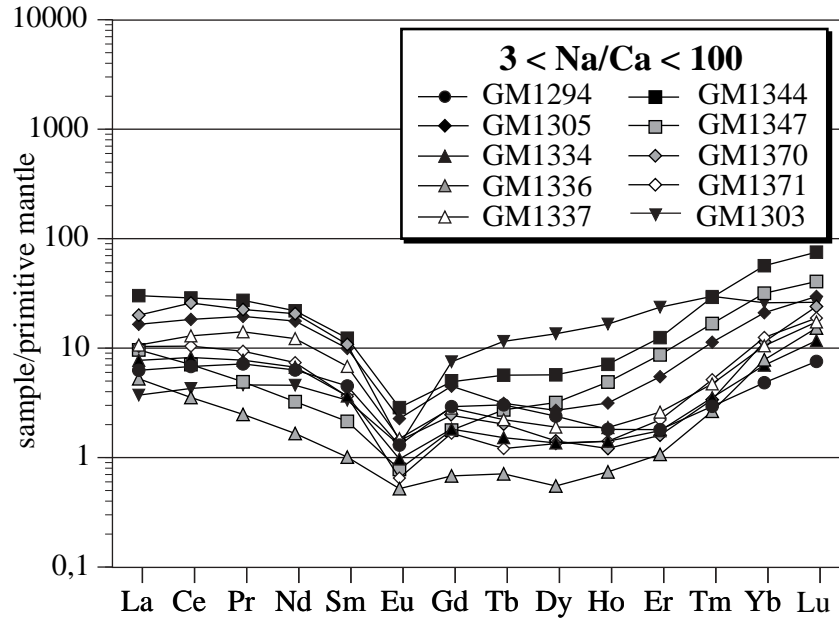
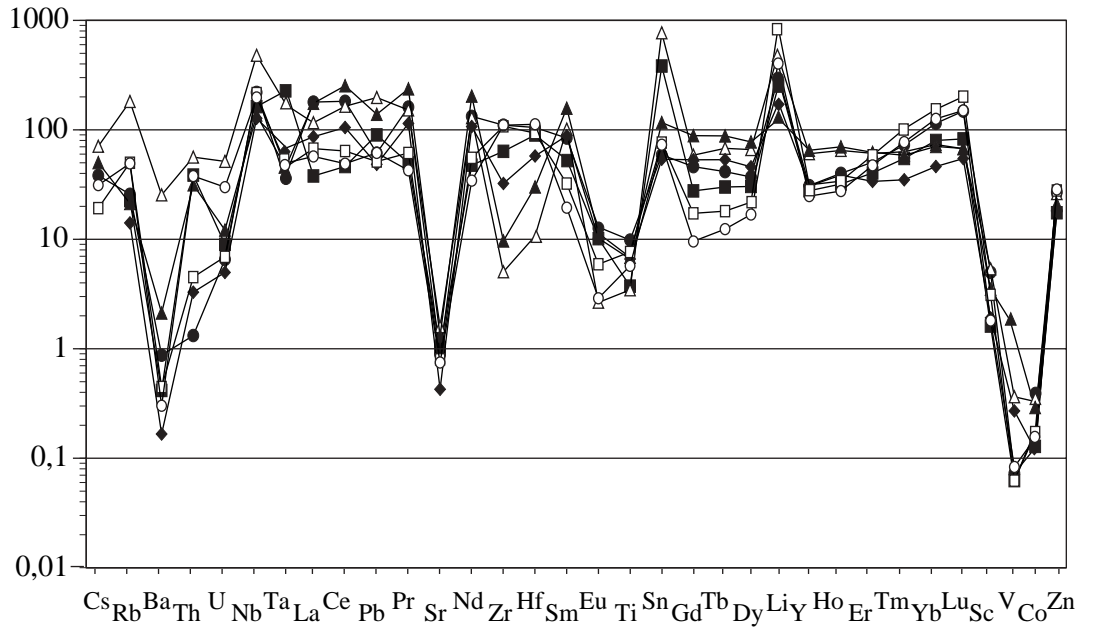
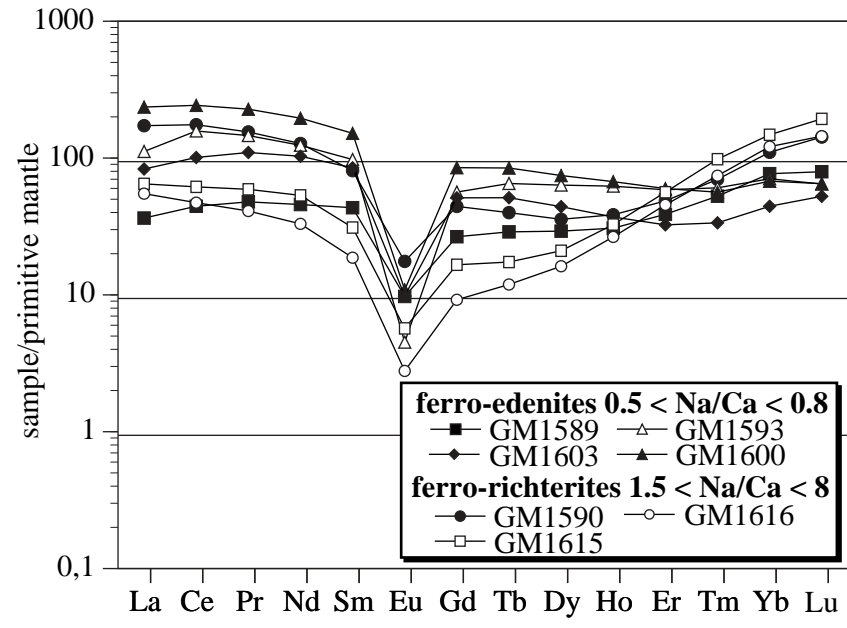


Fig. 7

(a) Puklen primary ferro-edenites and ferro-richterites



(b) Puklen secondary ferro-actinolites

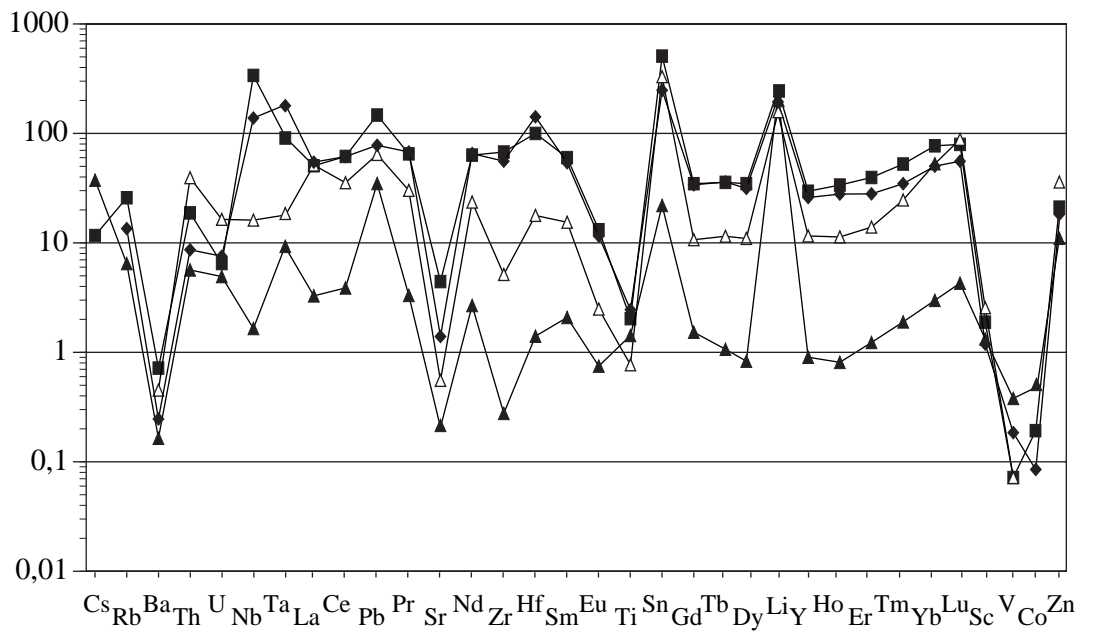
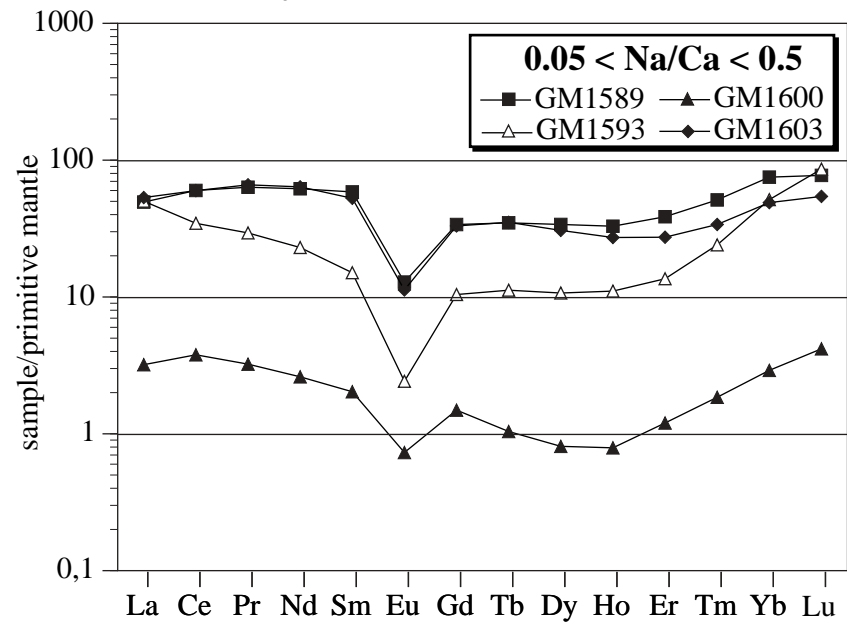
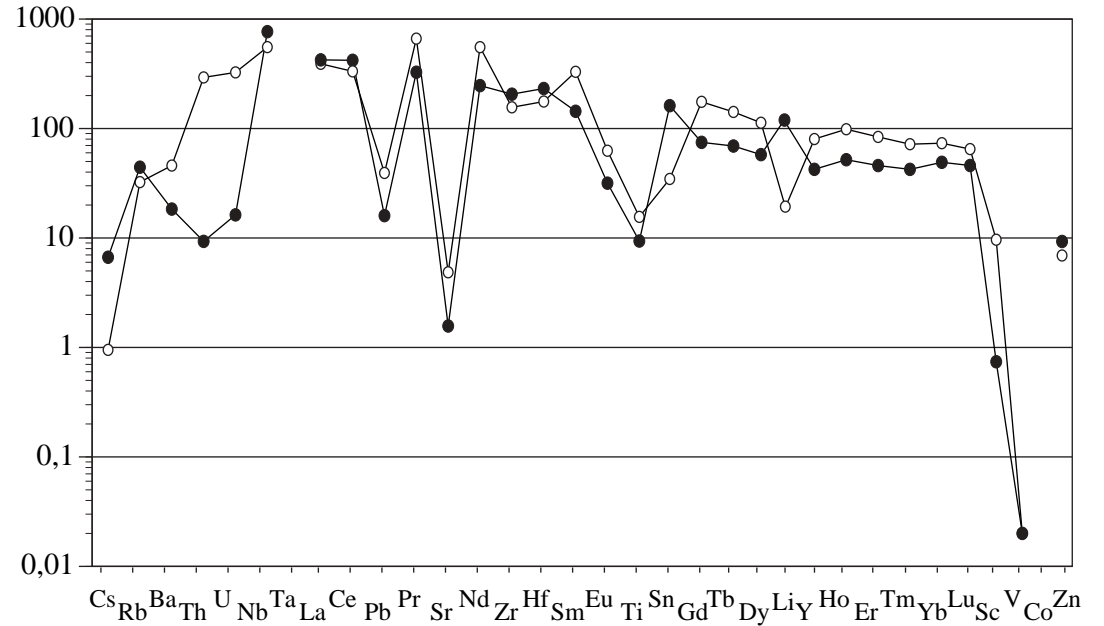
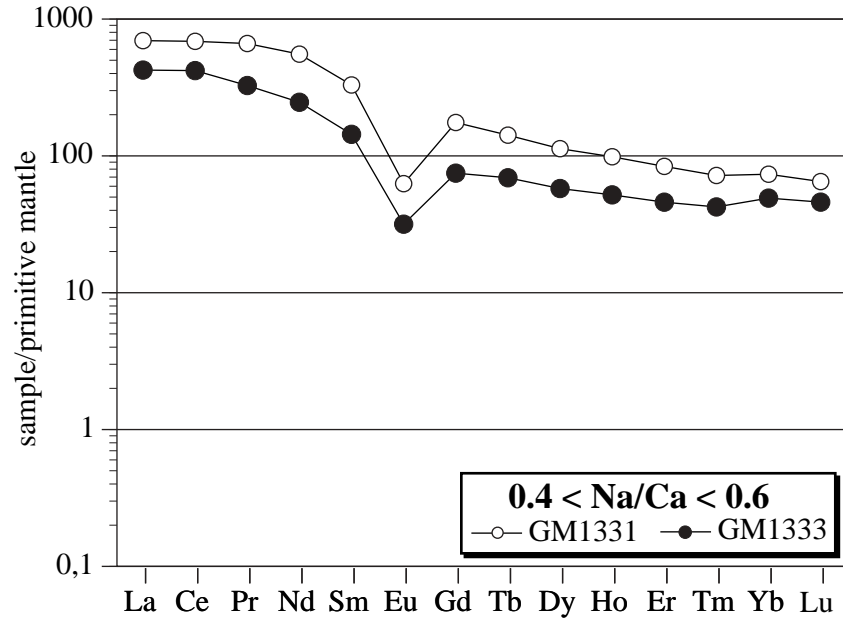


Fig. 8

(a) Ilímaussaq ferro-pargasites



(b) Grønnedal-Ika katophorites

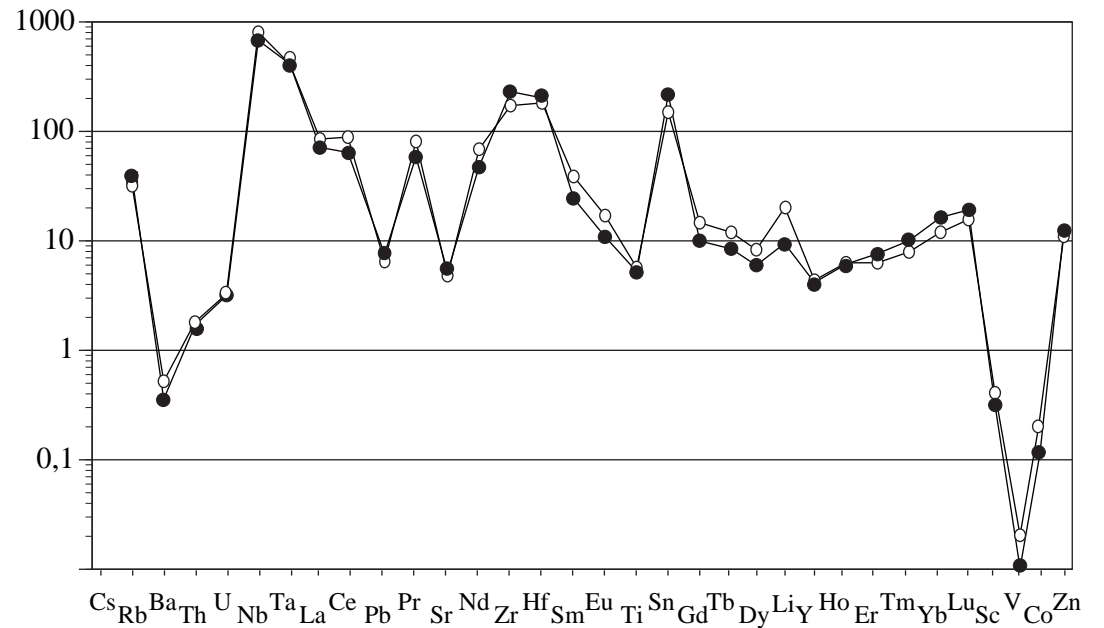
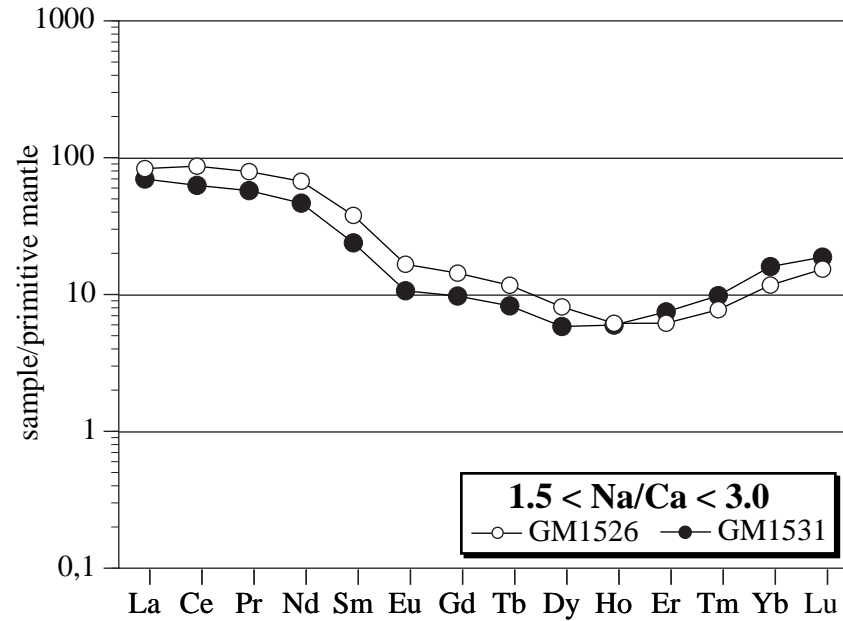
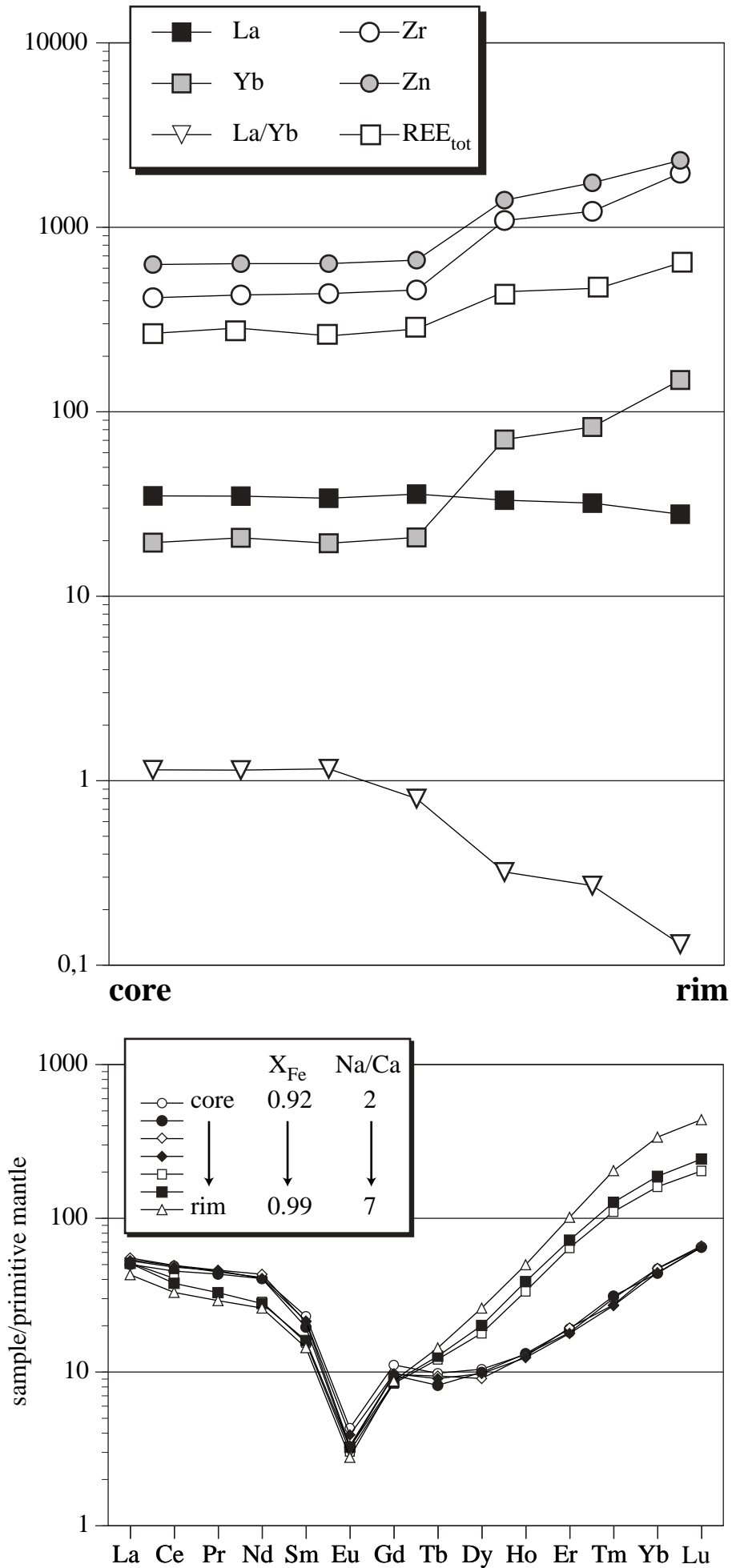


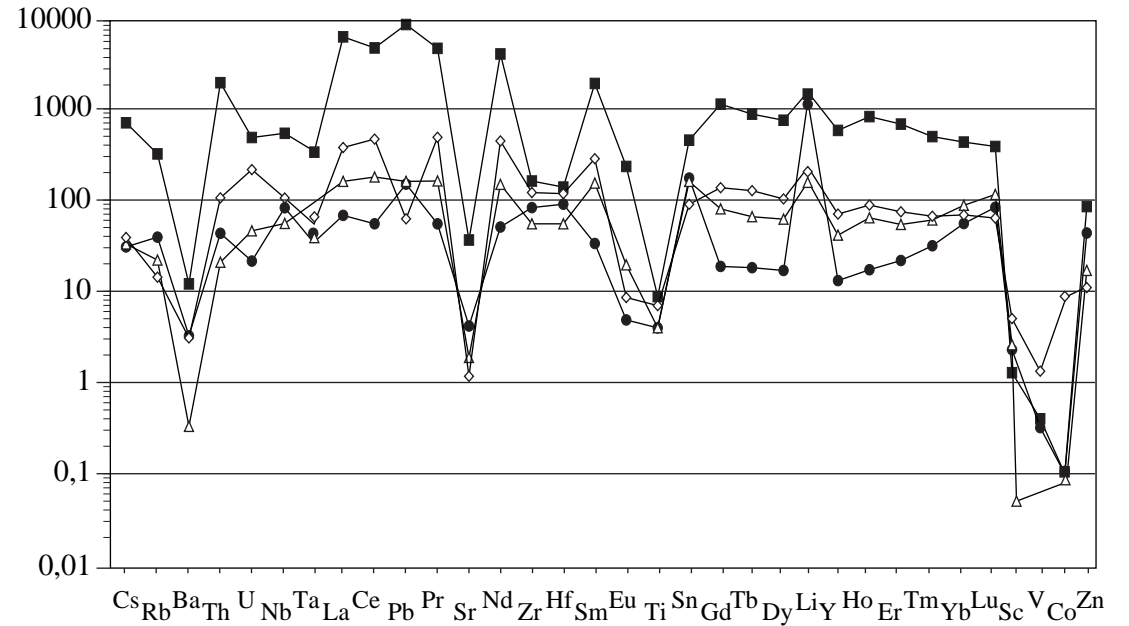
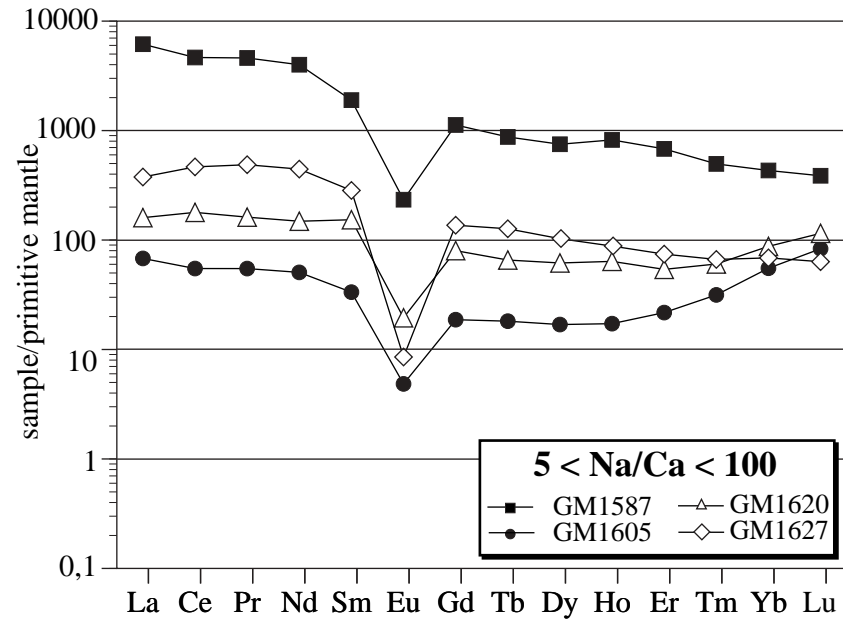
Fig. 9

Puklen ferro-richterite (GM1615)

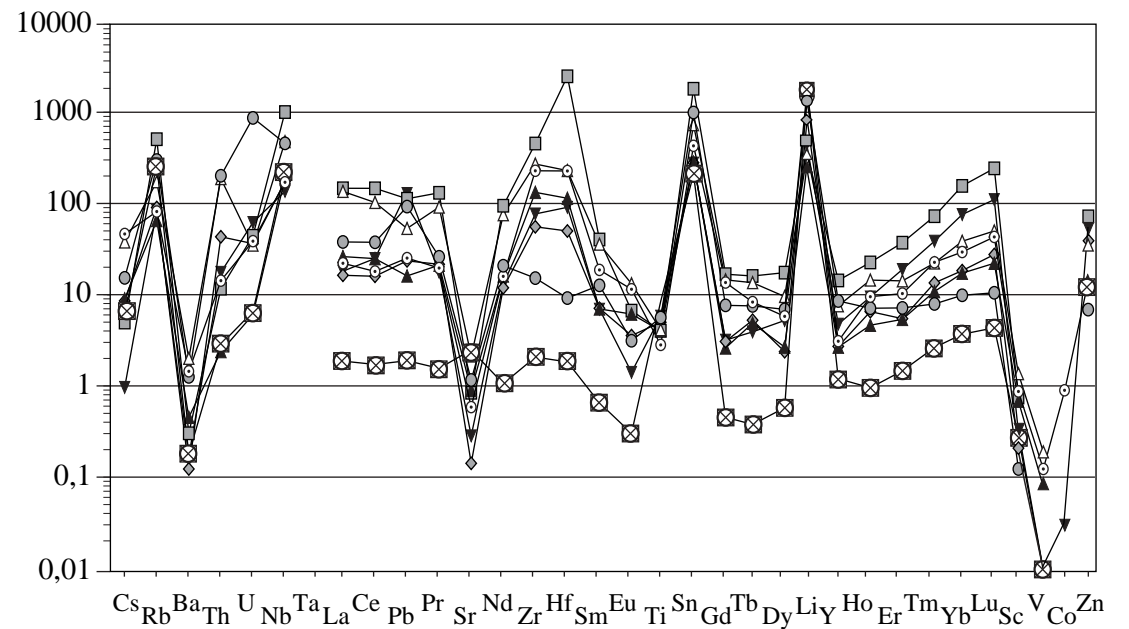
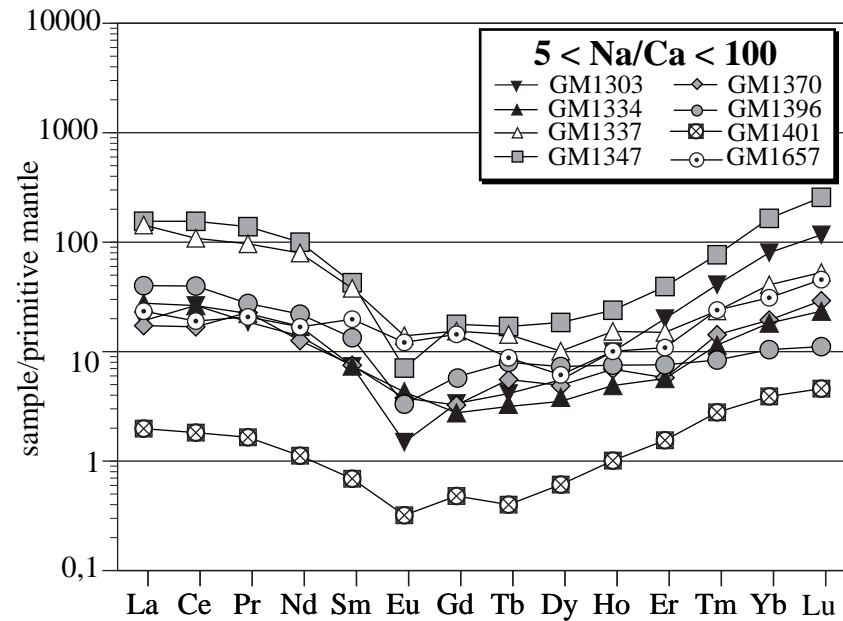
Fig. 10



(a) Puklen arfvedsonites



(b) Ilímaussaq arfvedsonites



Ílímaussaq arfvedsonite (GM1303)

Fig. 12

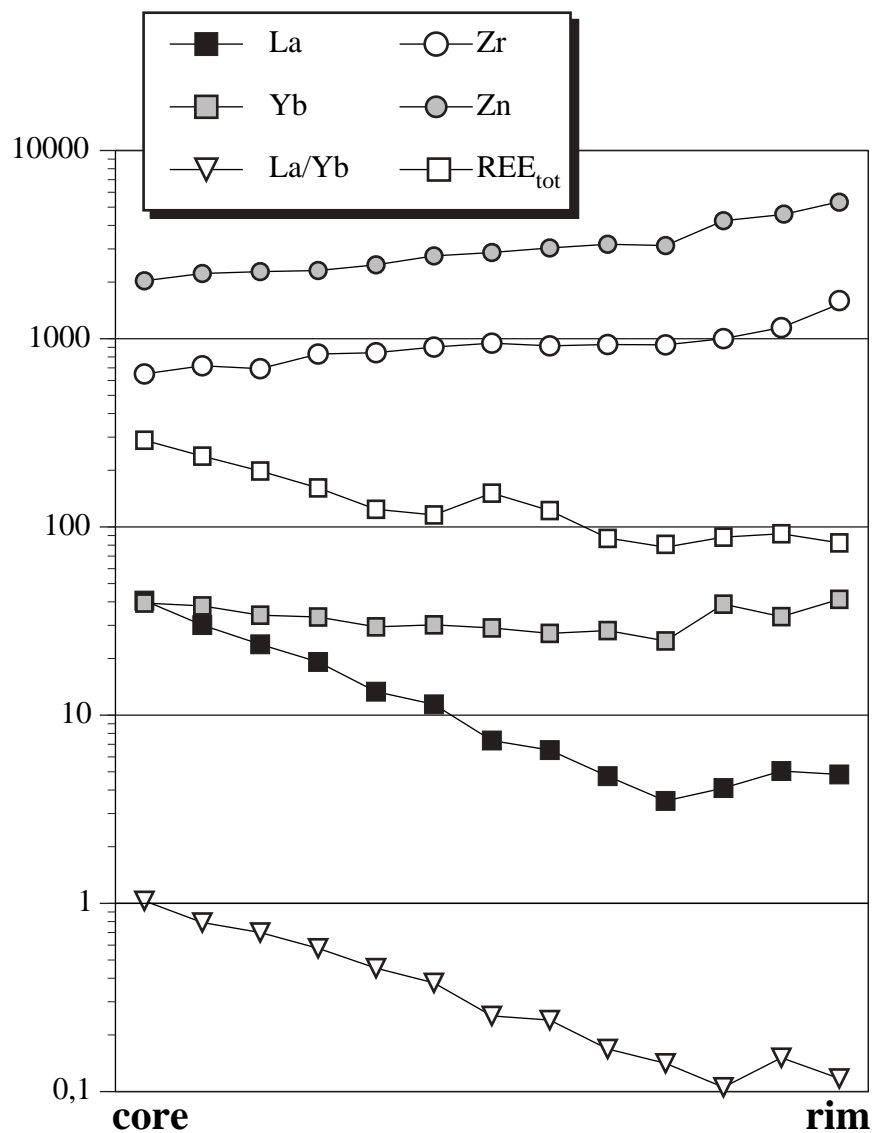
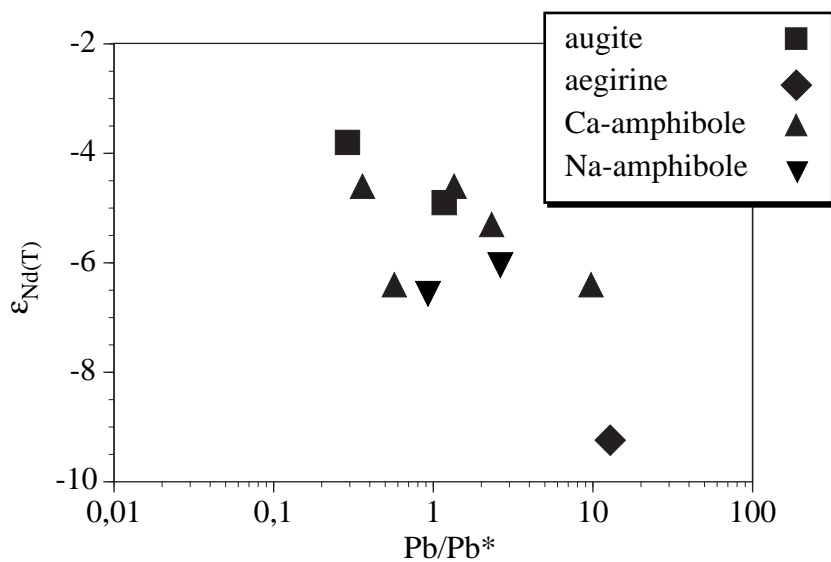


Fig. 13



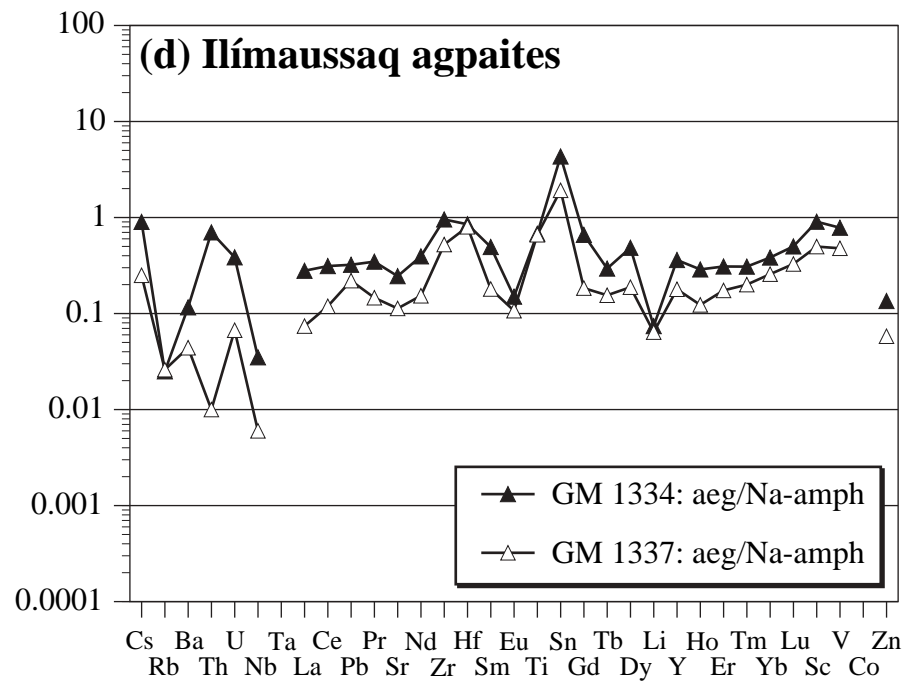
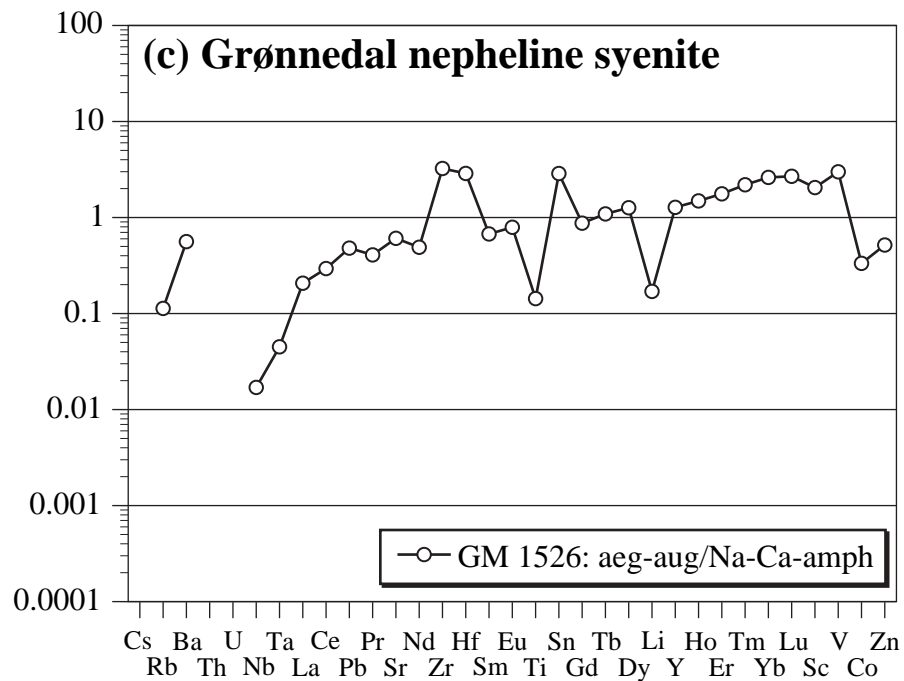
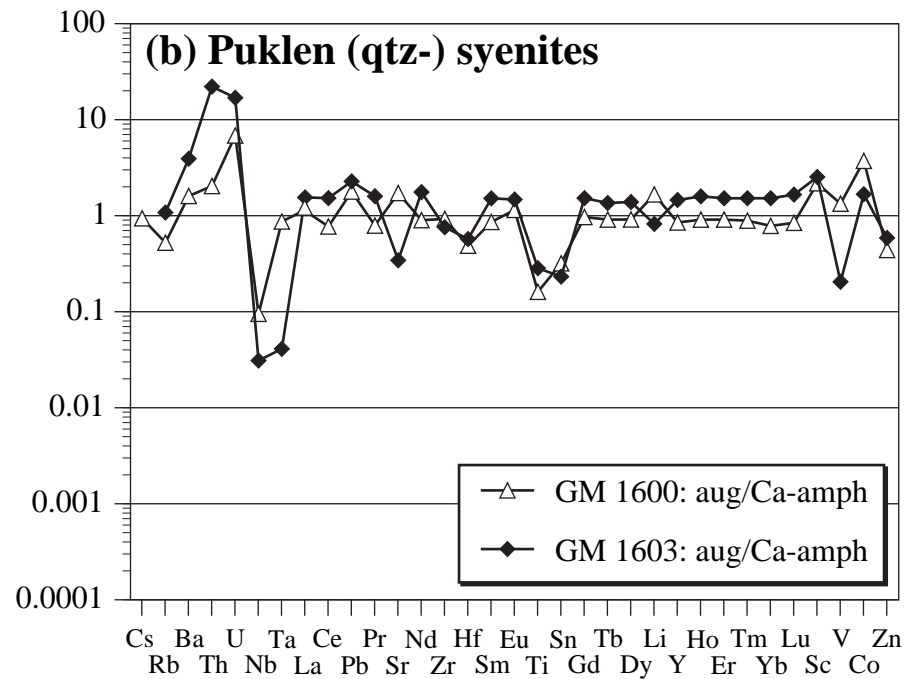
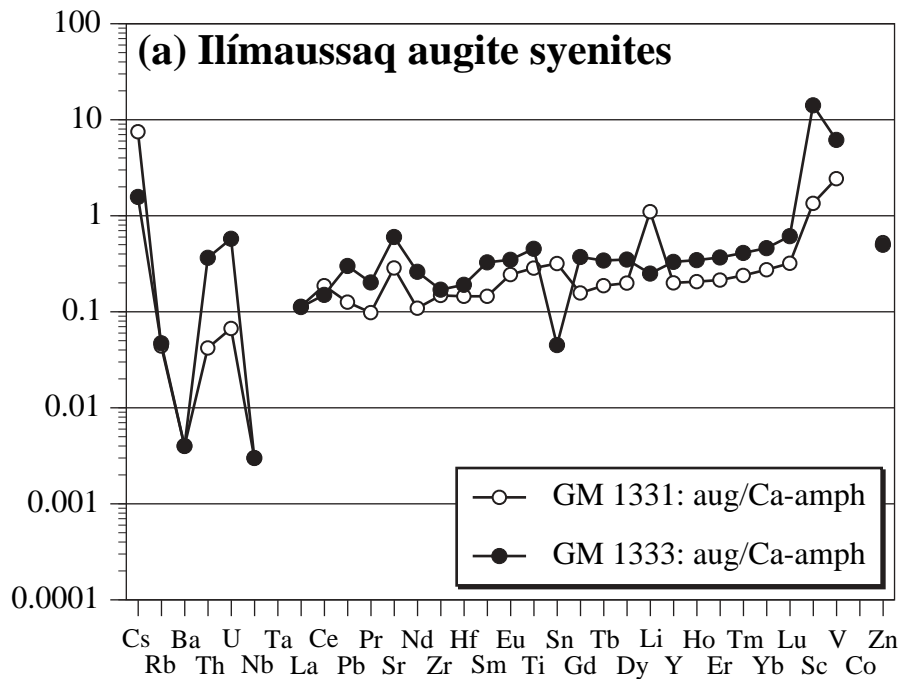
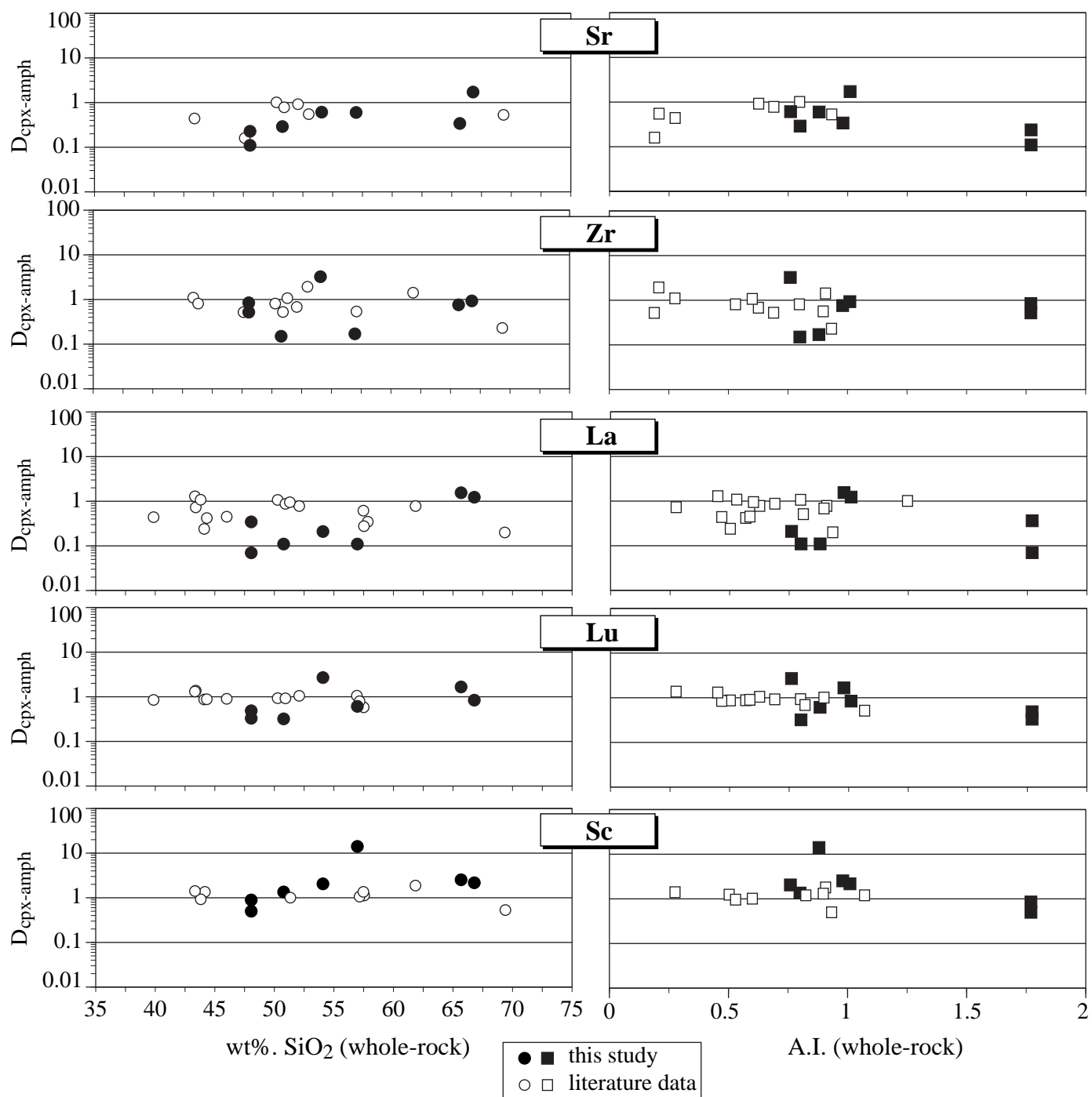


Fig. 14

Fig. 15



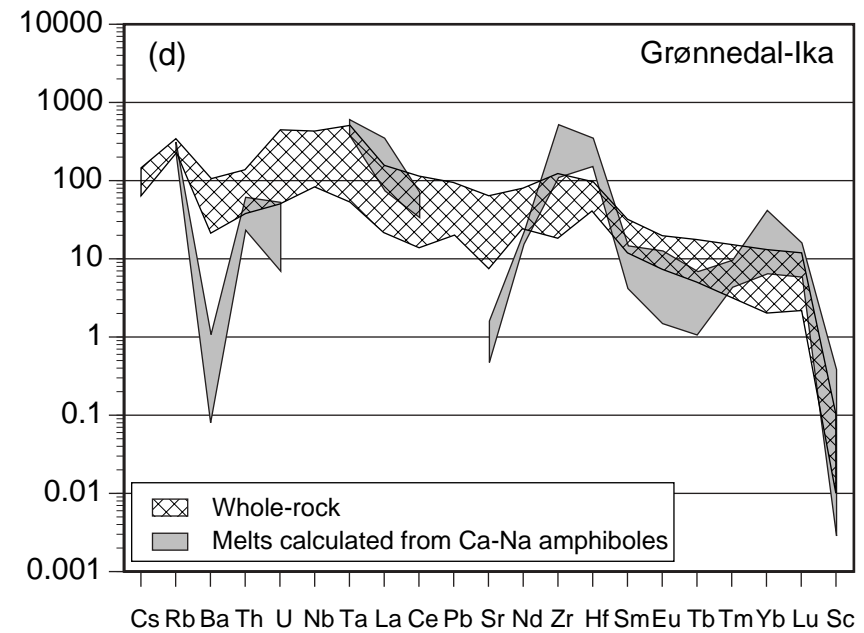
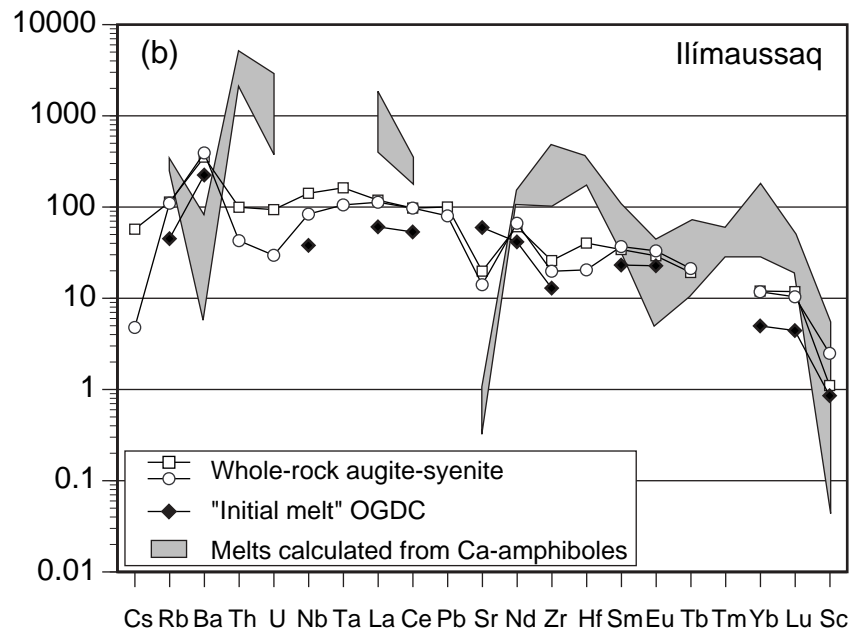
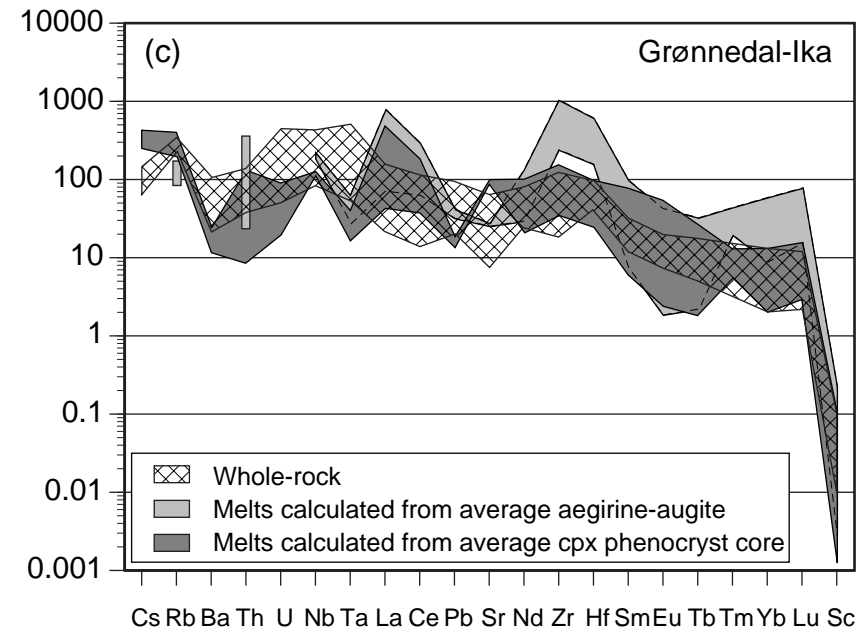
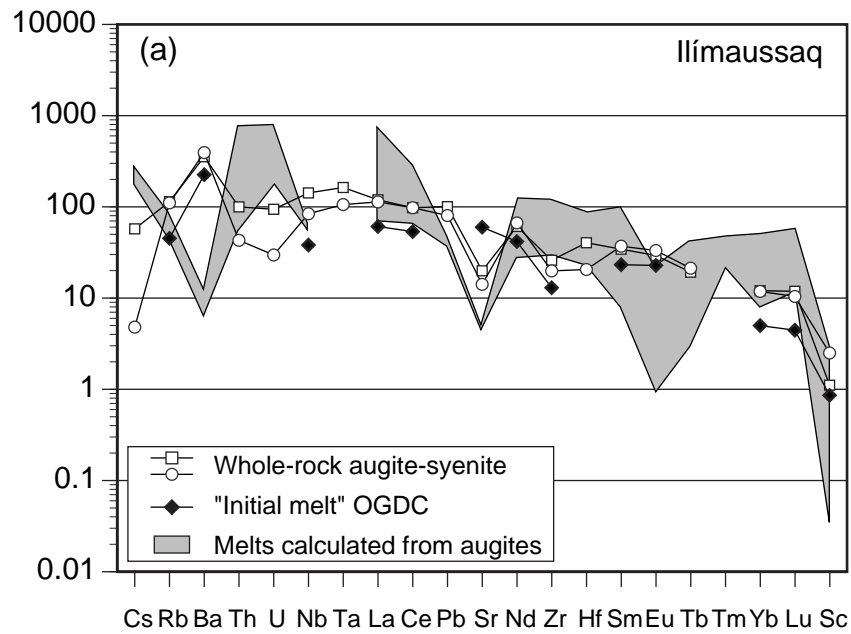


Fig. 16

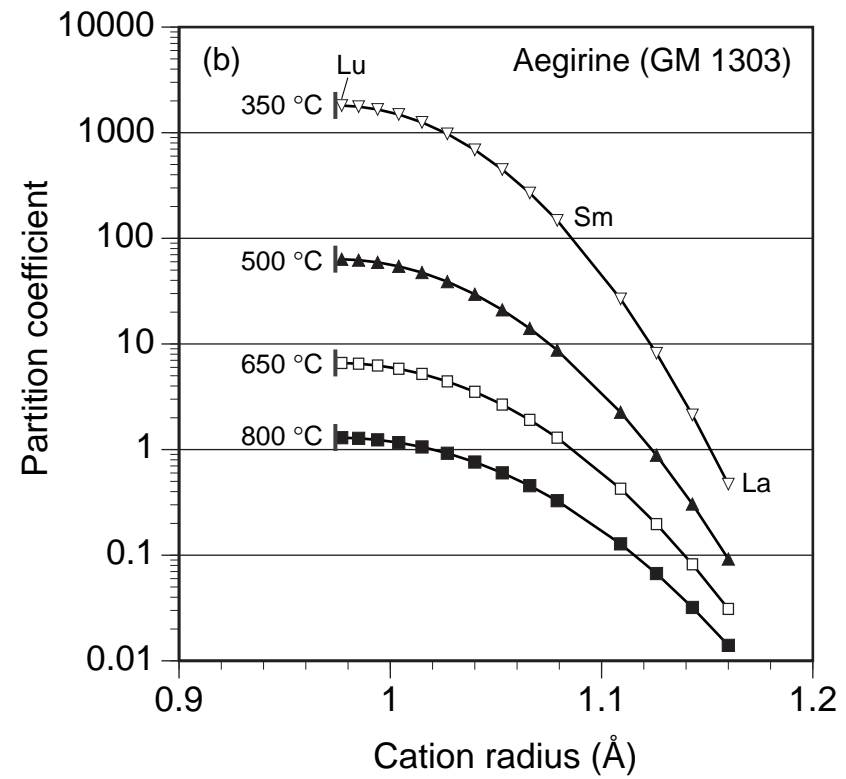
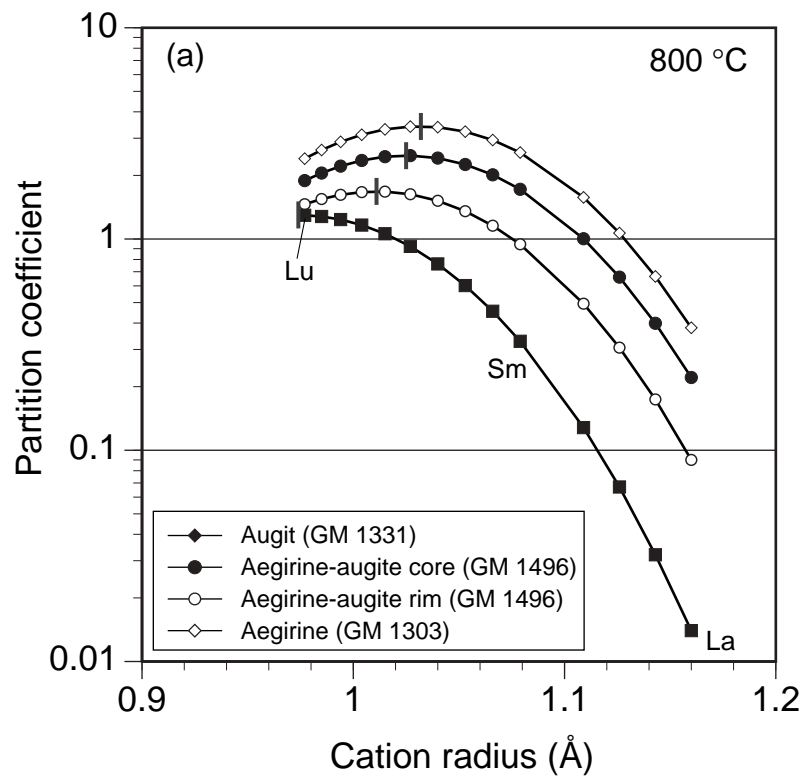
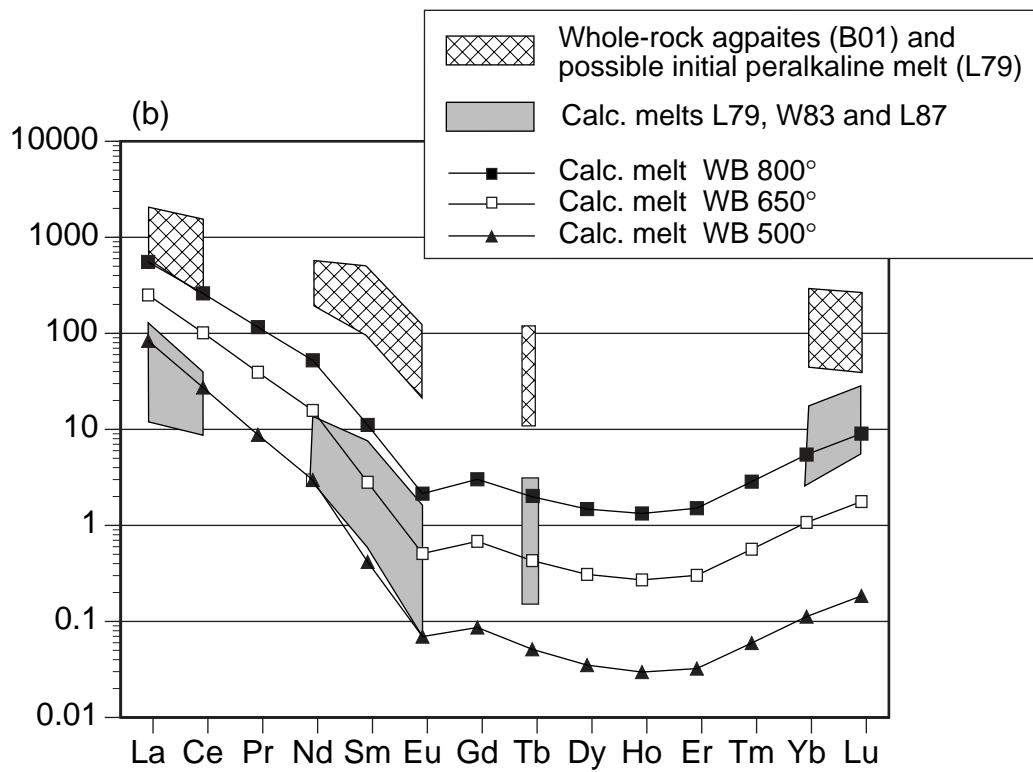
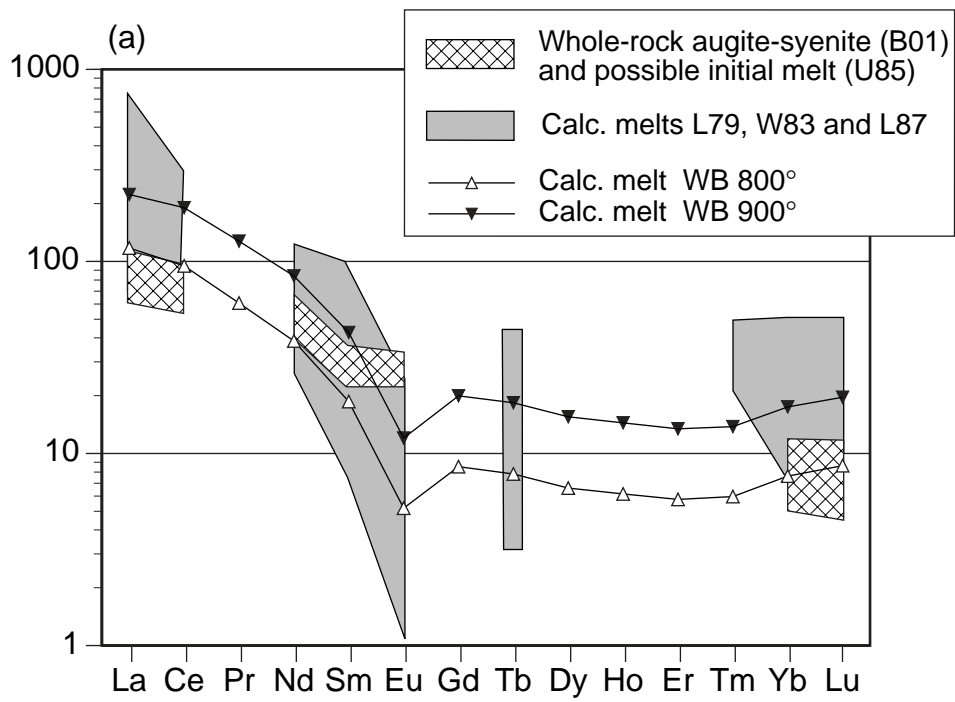


Fig. 17

Fig. 18



BILDUNGSGANG

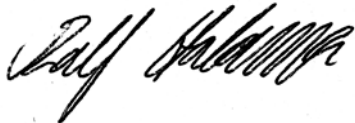
- 23.07.1974 Geburt in Frankenthal/Pfalz
- 1980-1984 Grundschule in Dirmstein
- 1984-1993 Gymnasium in Frankenthal/Pfalz,
Abitur im Juni 1993
- 1994-1996 Grundstudium in Geologie an der Johannes Gutenberg-Universität Mainz,
Diplom-Vorprüfung im September 1996
- 1996-1997 Studium der Geologie an der University of Glasgow, Schottland
- 1997-2000 Hauptstudium in Geologie an der Johannes Gutenberg-Universität Mainz,
Diplomarbeit über Massentransport und Elementmobilität im Caples
Terrane, Neuseeland
Diplom-Hauptprüfung Juli 2000
- Seit 2000 Promotionsstudium an der Eberhard Karls-Universität Tübingen,
Promotion über Petrologie und Geochemie magmatischer Gesteine der
Gardar-Provinz, Südgrönland

EIDESSTATTLICHE VERSICHERUNG

Hiermit erkläre ich, dass ich die vorliegende Arbeit selbstständig verfasst habe und keine anderen als die von mir angegebenen Quellen und Hilfsmittel benutzt habe.

Ferner erkläre ich, dass ich nicht anderweitig mit oder ohne Erfolg versucht habe, eine Dissertation einzureichen.

Tübingen, 7. November 2003

A handwritten signature in black ink, appearing to read 'Ralf Halama', written in a cursive style.

(Ralf Halama)